DOCTOR OF PHILOSOPHY

A comparison between optical properties measured in the field and the laboratory, and the development of an optical model.

Harker, Genevra E. L.

Award date:
1997

Awarding institution:
Bangor University

A Comparison between Optical Properties Measured in the Field and the Laboratory, and the Development of an Optical Model

Genevra E. L. Harker

A thesis submitted to the School of Ocean Sciences,
University of Wales, Bangor,
for the degree of
Doctor of Philosophy

August 1997

SUMMARY

This thesis investigates the consistency of optical properties measured *in situ* and in the laboratory in order to construct a predictive optical model.

Fieldwork was undertaken at several sites which represented different aquatic environments, from clear ocean waters to dynamic estuarine systems. At each, diffuse attenuation and irradiance reflectance measurements were taken. Water samples were also collected for the determination of constituent concentrations and further optical analysis. Spectrophotometric measurements of sample absorption were taken in the laboratory, both from solutions in glass cells and particles on filters, with a comparison of different correction techniques.

Regression analysis was then used to calculate the specific absorption of different constituents and compare these with derived values from the *in situ* measurements. The derived specific absorption curve for phytoplankton was in close agreement with that presented in Gallegos *et al* (1990), while the exponential curve for yellow substance absorption agreed with Tassan (1988). Having derived these specific absorption curves with similar values to those found in the literature, the curve for mineral suspended particles was established as an exponential curve which decayed with wavelength to a constant value in the red. The use of different pathlength amplification factors with the laboratory spectra was used in comparison with the field measurements. A new correction equation was developed for mineral particles which resulted in closer agreement between the laboratory and *in situ* measurements than factors found in the literature.

Using these specific curves as a basis, an optical model was written. This model predicts absorption and scattering from the constituent concentrations and then calculates the resultant diffuse attenuation and reflectance across the spectrum and for PAR. This was found to work well for absorption and diffuse attenuation.

The greatest limitation to the model was the uncertainty in quantifying scatter, particularly in sediment laden waters where scatter will dominate the optical signal. The inability to include particle distribution and incorporate the precise particle characteristics which determine scatter led to a large error in the predictions which was then compounded in the reflectance values.

The relationships between the constituent concentrations and the inherent optical properties can be changed to suit the particular environment if the precise characteristics (such as the dominant phytoplankton absorption spectrum or the size and refractive index of the sediment) are known. This enables the model to be used in a wider context for future studies.

An inversion technique which assumed specific absorption values for each constituent at different wavelengths was then employed to write another model which derives the constituent concentrations from reflectance and diffuse attenuation values. This second model worked well for predicting mineral solid concentrations from an independent survey undertaken in the Menai Strait, but did not extend to other constituents.

It is concluded that for accurate predictive optical models a high degree of local knowledge of particle characteristics is necessary.

CONTENTS

ACKNOWLEDGEMENTS

Many things have helped with the building of this thesis, particularly the patience from family and friends.

However, I must thank G. Thomas for all his boat work and support throughout the surveys, and the conversations on cold winter days when out on the boat with the titbits of advice on practicalities. I would also like to thank Will Bevan who kindly arranged for me to sample at Llyn Cwmystradllyn, and the crew of the HMS Herald who put up with a couple of mad scientists!

The most important thankyou is to my supervisor, Dave Bowers, who has cheerfully seen me through all sorts of dilemmas over the last few years and drawn me back to the issue in hand.

1. INTRODUCTION

People have always wanted to exploit the resources of the ocean and have therefore wanted effective methods for quantifying the various constituents present. Humans rely greatly on sight, and therefore light, everyday - the use of optical measurements to investigate underwater conditions is an extension of this. It is obvious that when water contains may particles the appearance is different to that of a pure water body so the next step is to explain this change and relate the differences to concentrations. As colour, to the human eye, is highly subjective (Smith *et al*, 1995a & b), early methods developed knowledge of the loss of light overall, not the variation with wavelength. The broad band of visible electromagnetic radiation (400-700 nm) is known as Photosynthetically Active Radiation (PAR).

The first widely used tool for measuring light attenuation was the Secchi disk, studied and developed by Angelo Secchi in 1886, who discovered that the depth of disappearance was inversely proportional to the amount of organic and inorganic matter along the path of sight (Preisendorfer, 1986a). Although this disk bears the name of Secchi, it was used many years earlier. The first reported oceanographic cruise where optical measurements were taken was in 1817 (Højerslev, 1994). This was the Rurik Circumnavigational Cruise led by Otto van Kotzebue who used a piece of red cloth lowered on a line to estimate the depth of light penetration. He later refined this method, using a white disk for measurements in the Pacific Ocean. This disk is still widely used today in conjunction with more sophisticated instruments and remains the easiest way to gauge the attenuation of light.

The progression of optical techniques has since relied on technical innovation. The first non-subjective measurements were taken using photographic equipment underwater. The initial study was by Fol and Sarasin in 1885 (Jerlov, 1968) where they lowered photographic plates in the Mediterranean to a depth of several hundred metres (Højerslev, 1994).

In 1890, Forel developed the colour scale (Austin, 1991) which was based on

comparing vials of different coloured mixtures of copper sulphate and potassium chromate (from blue to yellow) with the colour of the submerged white disk. Similar techniques are still used today as an immediate gauge of the water colour, notably the development of colour cards viewed just beneath the water surface (*e.g.* Davies-Colley *et al*, 1988; Davies-Colley & Close, 1990).

Also in 1890, theoretical optics was starting to develop with the paper by Ludwig Valentin Lorenz investigating optical physics. However, this was published in Danish and it was not until 1915 that it was translated into French and became more widely appreciated (Højerslev, 1994).

During the 1920s and 1930s extensive work was done with photoelectric cells by people such as Shelford and Gail (Jerlov, 1968) which led to advances in radiance and irradiance meters including Clarke in 1933 and Pettersson & Landberg in 1934. For greater detail, overviews of this development are given in Jerlov (1974) and Højerslev (1994).

The first beam transmissometer was devised by Pettersson in 1934 (Jerlov, 1968), with Kalle publishing important work on particle scattering in 1939. Kalle's work provided the basic parameters needed for particle distribution meters, which were subsequently developed and are still used today.

At the same time, the theoretical analysis of the light field was progressing through a series of papers by Shuleikin (1923 and 1933), and Gershun (1936 and 1939 - see Jerlov 1968 for details of these), in which he define the 'new' photometric concept of scalar irradiance. Another important paper was published in 1939 by Le Grand (see Jerlov, 1974), analysing the methods used in underwater optics and deducing the fundamental laws.

Since then, observational techniques have improved with the development of the photomultiplier tube in the 1950s and the use of lasers.

On a different scale, remote sensing has broadened the spatial limitation of optics. The realisation that optical remote sensing could be useful occurred when photographs were taken from Sputnik on the Gemini and Apollo Earth orbital missions. These showed that different water masses could be distinguished. Following these photographs, airborne spectroradiometers were successfully used to differentiate water masses from their optical signal (Clarke *et al*, 1970 from Austin, 1991).

In 1978, the first satellite able to measure colour was launched - the Coastal Zone Color Scanner (CZCS) - which operated for 8 years and led to the development of algorithms to derive constituent concentrations. Chlorophyll algorithms were particularly of interest to develop maps for global phytoplankton distributions and primary productivity.

More sophisticated colour satellites are now in orbit, or planned, to extend these optical classifications and derive concentrations with more accuracy. Much work has therefore been done on deriving constituent concentrations from optical properties with mixed success and often limited to the area of study.

The relationships between the inherent and apparent optical properties with the constituent concentrations are complex and all affect the observed water colour (Fig. 1). Thus, for any study concerning water colour, all three factors and their interactions must be considered. There has been a variety of models developed to help understand the links between the different properties (Appendix I), but there is more to be learned about the relationships, particularly for coastal water, and sediment laden areas.

The aim of this thesis is to establish observed relationships between certain optical properties and the constituent concentrations, concentrating on locations where mineral suspensoids dominate the optical signal. The information gained from these observations will then be applied within a predictive model. The chapters therefore progress from field measurements through to the development of an ocean colour model. There is an introduction to the various optical properties, followed by a

description of the instruments used to measure them. The different sites and conditions are described to show the range of locations and the nature of the measurements at each site. This is followed by the methods and results for the field and then the laboratory measurements. The *in situ* and laboratory results are then compared to test their consistency, before being incorporated into a model which predicts absorption, scattering, beam attenuation, diffuse attenuation and reflectance from the constituent concentrations. Finally, an inverse model is developed to derive concentrations from the optical properties.

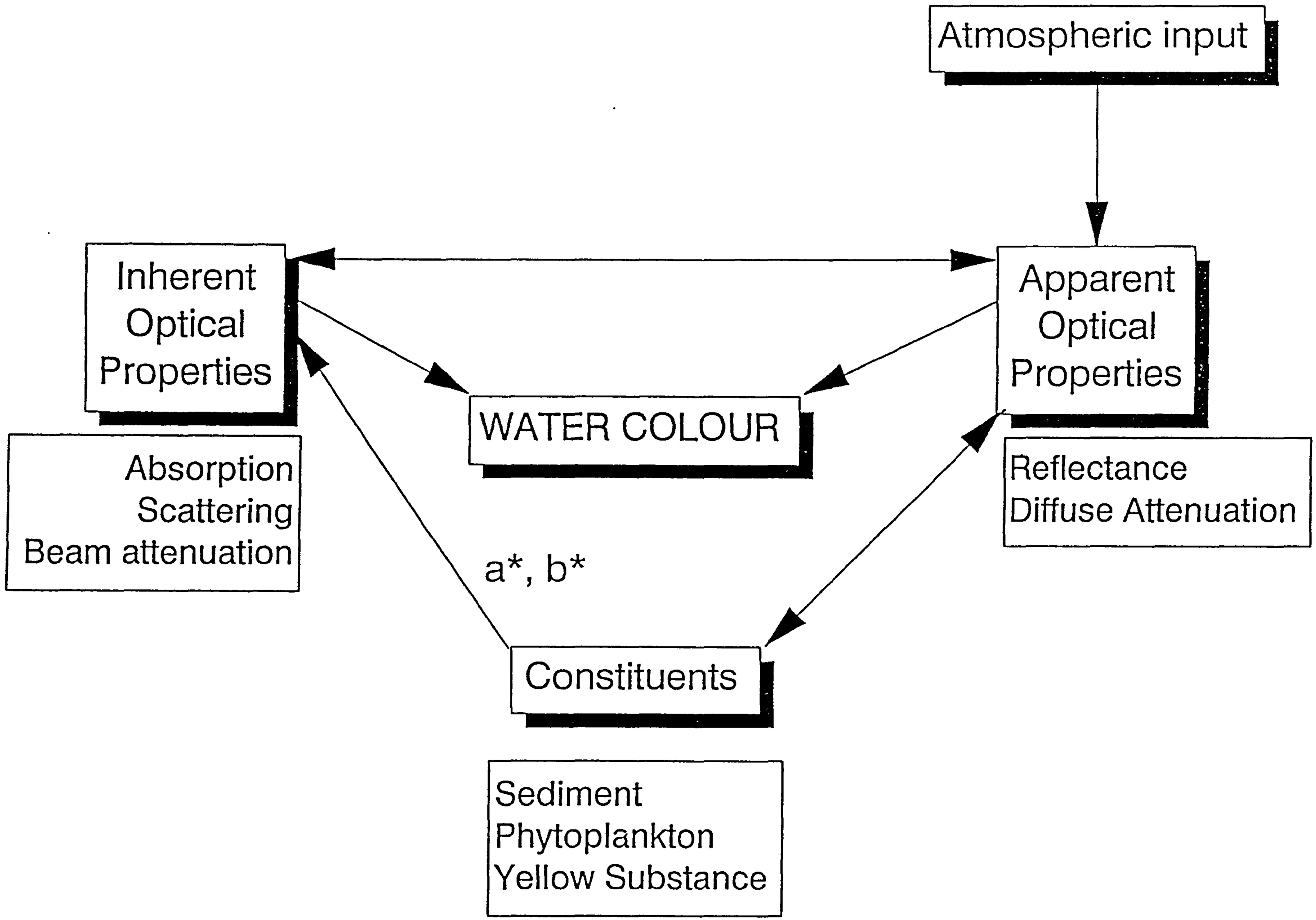

Figure 1.1 Flow diagram of the relationships between optical properties and constituents

2. OPTICAL BACKGROUND

The definitions of basic optical properties which are discussed later in this thesis are given in this chapter. Definitions of further properties, to give a wider context, are presented in Appendix II.

The optical properties of a water mass are determined by the structure of the light field and the nature of the substances within it. Properties which, by definition, are controlled by the light field, and are only indirectly affected by the substances, are known as apparent optical properties, such as diffuse attenuation and reflectance. However, some characteristics are solely governed by the constituents so that any variation is directly caused by a change in the concentrations. These are known as inherent optical properties, and include absorption, scattering, beam attenuation and the volume scattering function.

In order to use colour models for predictive purposes, or for monitoring concentrations, the relationships between the constituents and the inherent optical properties must be understood. This chapter describes the light field (§2.1), the apparent optical properties (§2.2), the inherent optical properties (§2.3) and then examines further relationships which have been described between various optical characteristics (§2.4).

2.1 LIGHT FIELD

2.1.1 Radiance and Irradiance

The light field is usually described through radiance and irradiance. Radiance is defined as "the radiant flux per unit solid angle per unit projected area of a surface":

$$L(\theta,\phi) = \frac{d^2\Phi}{dA\cos\theta\, d\omega}$$

whilst irradiance is defined as "the radiant flux incident on an infinitesimal element

of surface containing the point under consideration, divided by the area of that element" (Jerlov, 1968):

$$E = \frac{d\Phi}{dA}$$

and so describes the light from a hemi-spherical rather than a point source.

2.2 APPARENT OPTICAL PROPERTIES

2.2.1 Diffuse Attenuation

At any particular wavelength, the decrease in irradiance is described:

$$E(z) = E_0 \, e^{-Kz} \qquad eqn. \ 2.1$$

where E is irradiance, E_0 is the irradiance immediately below the surface,
K is the diffuse attenuation and z is depth

so that diffuse attenuation K is defined as "the vertical gradient of the logarithm of the quantity" (either radiance or irradiance):

$$K_x = -\frac{1}{E_x}\frac{dE_x}{dz}$$

where the subscript x represents d or u for downward or upward

The net downward attenuation K_E is therefore defined:

$$K_E = -\frac{1}{E_d - E_u}\frac{d(E_d - E_u)}{dz}$$

PAR attenuation is more rapid as the different wavelengths decrease at different rates, resulting in a steeper decrease near the surface. Most of the work in this thesis considers diffuse attenuation at discrete wavelengths, so that the exponential relationship applies.

The light field can be described in terms of the optical depth ζ, which is a gauge of the level of light compared with the surface. ζ is defined:

$$\zeta = K_d z$$

Optical depths of 2.3 and 4.6 are particularly useful for phytoplankton studies, as these correspond to the mid-point and lower limit of the euphotic zone, where irradiance has decreased to 10% and 1% of the surface value (Kirk, 1994).

2.2.2 Reflectance

Reflectance R is the ratio between upwelling and downwelling irradiance:

$$R(\lambda) = \frac{E_u(\lambda)}{E_d(\lambda)}$$

where λ is wavelength

although it is sometimes used as the equivalent ratio for radiance.

2.3 INHERENT PROPERTIES

When electromagnetic radiation hits a particle the electric field of the incident radiation causes the particle to change its energy level. The excited charges may then change the form of the energy (*e.g.* by converting it to heat) - absorption (Bohran & Huffman, 1980), or reradiate energy - scattering.

2.3.1 Absorption

The absorption coefficient (a) is defined as the absorptance (A - see Appendix II) of an infinitesimally thin layer of the medium normal to the beam, divided by the thickness (Δr) of the layer

$$a = -\frac{\Delta \Phi_a}{\Phi_o} / \Delta r$$

where Φ_a is the radiant flux lost from the beam by absorption, and Φ_o is the incident flux

The absorption coefficients of the different constituents are additive, so that the total absorption of sea water is:

$$a = a_w + a_y + a_p \qquad \textit{eqn. } 2.2$$

a is the absorption coefficient for seawater, a_w is pure water, a_y is yellow substance and a_p is particles

The characteristic shape of absorption curves between 400 and 700 nm for each component is shown in Fig. 2.1. Pure water has a defined absorption spectrum which increases with wavelength, tabulated by Smith & Baker (1981). Yellow substance (or Gelbstoff) absorption decreases exponentially from blue to red (Tassan, 1994):

$$a_y(\lambda) = a(440)\ \exp[-0.014\ (\lambda - 440)]$$

where λ is wavelength in nm

Although Tassan uses an exponent of -0.014, values have been observed between -0.013 and -0.016 (Howard-Williams & Vincent, 1985 in Davies-Colley, 1992). Carder *et al* (1989) noted that a lower exponent indicates a higher contribution from the humic acids relative to the fulvic acids. This was also implied by Blough *et al* (1993) who noted that the exponential slope changed with salinity. Carder *et al* (1989) also found a change in the slope between the ultraviolet-blue range and the longer visible wavelengths.

Zooplankton can cause short term fluctuations in the observed optical signal (Austin 1970), but the biomass is less than 10 % that of phytoplankton (Bukata *et al*, 1981), and is therefore not considered to be a significant contributor to total absorption. Similarly, bacteria are not included in eqn. 2.2 as they do not make a significant contribution to absorption, although they have been studied for their scattering effect (Ulloa *et al*, 1992). Thus, the organic particles are considered to consist of phytoplankton and its detritus only. As the absorption spectrum varies with species and stage of development (*e.g.* Morel & Bricaud, 1981; Hoepffner & Sathyendranath, 1992; Babin *et al*, 1993; Moritorena & Guiliocheau, 1996; Sathyendranath *et al*, 1996) a single characteristic equation is difficult. However, chlorophyll-a is the dominant pigment in most phytoplankton, and is therefore considered representative.

This pigment has a double-peaked absorption curve, with a minimum in the green; the exact position of the peaks and the magnitude are altered slightly with the addition of extra pigments and detrital material. The specific absorption curve (*i.e.* the absorption due to one unit concentration) is multiplied by the concentration to determine the contribution of pigment to overall absorption.

Inorganic particle absorption is less well described in the literature. Kirk (1985) suggested that inorganic particles are pure scatterers and that absorption occurs due to organic material adsorbed on the surface (Bader *et al*, 1960; Davies-Colley, 1983). This conforms to the negative exponential curves which have been used for mineral particles (Gallegos *et al*, 1990). However, other factors have an influence on the absorption, and the exact shape and magnitude of the absorption curve is highly variable being dependent on the surface texture and hardness of the mineral constituents as well (Pak *et al*, 1970; Han & Rundquist, 1994 & 1996).

The theoretical link between irradiance and absorption is described (Voss, 1989):

$$aE_0 = - \text{div } E$$

where E_0 is total scalar irradiance and E is net irradiance

As irradiance is assumed constant horizontally, this simplifies to:

$$a = \frac{1}{E_0}\frac{dE}{dz}$$

The average cosine μ is defined:

$$\bar{\mu} = \frac{E_d - E_u}{E_0}$$

the ratio of net to scalar irradiance

So that,

$$a = -\frac{\mu(z)}{E_0(z)}\frac{dE_0(z)}{dz} - \frac{d\mu(z)}{dz}$$

Alternatively, this can be written (Jerlov, 1976 in Setiapermana, 1990):

$$a = \mu K_E$$

where K_E is the difference in net irradiance between two depths considered

Direct measurement of absorption is difficult, as scattering is often included in any measurements. However, both laboratory and *in situ* instruments are being developed (*e.g.* Fry & Kattawar, 1988; Fry *et al*, 1992) which are based on an integrating sphere to minimize scattering effects. An integrating sphere has a totally reflective internal surface which redirects the light to a single point at which there is a sensor. Thus, all scattered light will eventually be recorded by the measuring sensor, so that any loss must be due to absorption.

When measuring absorption by scanning filters in the laboratory, a pathlength amplification factor (β) is necessary, and is applied before the conversion to the absorption coefficient. This compensates for the effect of multiple scattering on the filter. β is defined as the ratio between the optical pathlength and the geometrical pathlength. To correct for β in phytoplankton cultures, Cleveland & Weidemann (1993) developed the conversion:

$$a(\lambda) = 0.378A(\lambda) + 0.523[A(\lambda)]^2$$

where $a(\lambda)$ is the absorption coefficent, $A(\lambda)$ is the absorbance, or optical density, and λ is wavelength

The effect of this with increasing absorbance is shown in Fig. 2.2. A similar algorithm was developed in 1992, by Hoepffner and Sathyendranath:

$$a(\lambda) = 0.31\,A(\lambda) + 0.57\,[A(\lambda)]^2$$

Both of these corrections were based on measurements of phytoplankton cultures with

$A(\lambda) < 0.4$ and therefore are not ideal for the range of particle absorption studied in the Menai Strait. A more general correction, suitable for high absorbances, is $\beta = 2$ (Bricaud, pers. comm.); this assumes the multiple scattering is independent of wavelength. Alternatively, Balch & Kilpatrick (1992) inversely related β to the optical density.

2.3.2 Scattering

Scattering is harder to quantify. Total scatter can be estimated by using instruments such as a nephelometer (Ganf *et al*, 1989), or an absorbance-scatterance meter (Bricaud *et al*, 1995), but is usually derived from other measurements or determined theoretically.

There are three mechanisms of scatter by a particle (Williams, 1970): i) energy is reflected; ii) energy is refracted or diffracted; iii) energy is absorbed and then reradiated in a different direction but at the same wavelength (electromagnetic scatter). The first two processes are only relevant to particles which have a radius greater than 10 λ (*i.e.* 4-7 μm); the third is therefore the dominant process in the ocean, as most scattering is due to particles with radius less than 1 μm (Kullenberg, 1953; Beardsley *et al*, 1970; Stramski & Kiefer, 1991). In pure water, molecular (or Rayleigh) scattering is most important, involving particles less than or equal in diameter to the wavelength of light. The amount of scatter across the spectrum follows λ^{-4} and leads to Raman emission as light is reradiated at a lower energy level and, therefore, a longer wavelength. Most sea water contains particles with diameter > λ (Kullenberg, 1968), particularly Case 2 waters. As this thesis mainly considers coastal or inland waters, Rayleigh scattering is inappropriate and therefore is not included in the calculations.

When light crosses an interface or hits a particle, the refracted energy continues at a different angle to the incident light. This angle is dependent on the properties of the new medium, in particular the speed of light. The ratio between the incident and refracted angles is determined by the refractive index n, given by Snell's law:

$$n = \frac{\sin i}{\sin j}$$

where i is the angle of incidence and j is the angle of refraction

Sea water has a refractive index of 4/3 relative to air.

Electromagnetic scattering was described by Mie, in 1908, assuming homogeneous, spherical particles. This is not an exact representation of the natural environment but a good approximation (Jerlov, 1968). The theory determines scattering with an efficiency factor K_f:

$$K_f = \frac{4 I_T}{\pi D^2}$$

where I_T is the total scattered radiation and D is the diameter of the particles

As the particle radius increases, K_f oscillates in value until it becomes steady at approximately 2. This occurs at a radius of 3-5 μm (Thompson *et al*, 1979).

The scattering coefficient is related to the efficiency factor, the number of particles per unit volume (N), and the diameter (D) of the particles (assuming a monodisperse system):

$$b = \frac{K_f N \pi D^2}{4}$$

For polydisperse systems (which include particles of various sizes) this becomes:

$$b = \frac{\pi}{4} \sum_{i=1}^{n} K_{fi} N_i D_i^2$$

Thus, if there are only two predominant particle sizes, the overall scatter is calculated as the sum of the two separate scattering distributions, not the scatter calculated for an average size (Zaneveld *et al,* 1974).

The efficiency factor employed here is suitable for particles which are pure scatterers;

when particles also absorb, an imaginary term must be included in the refractive index:

$$m = n - in'$$

where $n' = a\lambda/4\pi$ and a is the absorption coefficient

Consequently, the efficiency factor is lowered resulting in less overall scatter (Voss, 1992). This is confirmed with observations by Bricaud & Morel (1986). An average value of 1.15 for the real term can be used for mineral suspensoids, such as clay and silt (Williams, 1970), whereas n < 1.05 is appropriate for phytoplankton (Jonasz & Prandke, 1986). This illustrates the difference between mineral and organic particles (which absorb more) even when the imaginary term is omitted.

The proportion of light which is scattered backwards is variable. Kirk (1981a) assumed a value of 0.019 in turbid water, although Gallie & Murtha (1992) found a log relationship with suspended mineral concentration. The amount of backscatter can be related to absorption, as both the backscatter ratio and the scattering coefficient are altered by changes in a (Morel and Prieur, 1981). Thus, although a backscatter ratio of 0.019 is assumed for inorganic particles (Kirk 1981a), the value for phytoplankton ranges from 0.0001 to 0.002 (Morel & Bricaud, 1981b). This shows that the contribution by living algae to backscatter is relatively small (Ahn *et al*, 1992).

2.3.3 Volume Scattering Function

The volume scattering function $\beta_v(\theta)$ is a more accurate description of the light distribution, quantifying the proportion of energy scattered in all directions:

$$\beta_v(\theta) = \frac{dI(\theta)}{EdV}$$

where $dI(\theta)$ is the intensity in the direction of the incident beam and dV is the volume element irradiated

Petzold (1977) measured the volume scattering function in different water masses and found that although it varied in magnitude with the nature of the water, it remained approximately the same shape, with 18-28% of the radiation scattered between 0° and

1.0°, 50% within 5° (Di Toro, 1978), and up to 75% scattered within 10°. This tendency towards forward scattering in the natural environment, is due to the presence of particles (Tyler, 1961), as molecular scattering is uniform over all angles. Thus, forward scatter becomes more pronounced in turbid water (Kullenberg, 1974). Even in very clear water a predominance towards forward scattering indicates the presence of small particles (Ochakovsky, 1966). Forward scattering is independent of wavelength but as the angle increases, and molecular scattering becomes relatively more important, the wavelength dependence increases, becoming greater at shorter wavelengths (Kullenberg, 1953; 1968; Kirk & Oliver, 1995). The difference in scattering between mineral and organic particles is also apparent in the volume scattering function. This difference enabled Pak *et al* (1970) to determine the type of particles in the water column from the vector diagram of scattering. They identified predominantly biological particles at the surface through to geological at greater depths. However, below a certain depth, $\beta_v(\theta)$ is less useful as the light becomes totally diffuse (Preisendorfer, 1959).

Although the volume scattering funcction is an important parameter for describing the light field it was not possible to measure this in the field. It has therefore been neglected within the analysis and the variation assumed negligable.

2.3.4 Beam Attenuation

Beam attenuation (c) is the total amount of energy "lost" from a direct path through the water, and is defined as the sum of absorption and scattering. The beam attenuation coefficient is always greater than the diffuse attenuation, and is the equivalent to the radiant flux of K to irradiance:

$$\Phi = \Phi_0 \, e^{-cr}$$

where Φ is the radiant flux, Φ_0 is the initial radiant flux and r is the length considered

As this is the easiest inherent property to measure, using a transmissometer, the relationship between c and suspended solids has been investigated in several studies

(*e.g.* Ivanoff *et al*, 1961; Spinrad *et al*, 1983; Trowbridge *et al*, 1994). It has been found that c is directly related to concentrations of particles of radius < 100 μm (Campbell & Spinrad, 1987).

As discussed in §2.3.1 and §2.3.2, the composition of the particulate matter greatly influences the relative effectiveness of scatter and absorption, and consequently, the beam attenuation. With more particles in the water, the attenuation is higher, while a relative increase in scattering produces an increase in reflectance. It is therefore possible to estimate a depth profile of particle concentrations from the attenuation profile in clear ocean water. On this basis, Jerlov (1968) classified sea water into different types, identified by the attenuation curve. Three of these were for open ocean and nine for coastal regions, the latter type having much higher attenuation values and more complex interactions (Fig. 2.3). Any site could fit a basic profile with a similar magnitude, although Jerlov expected variation within each type at different locations. The aim was to extend these classifications to the properties within the water, and ultimately, the productivity so that nutrient-rich areas could be identified.

2.3.5 Secchi Depth

The Secchi depth z_{SD} is dependent upon both apparent and inherent optical properties but shall be explained here, as it mainly depends on the constituent concentrations. This depth is that at which the white Secchi disk can no longer be seen when lowered into the water. It is measured by markers on the rope and indicates the overall clarity. Consequently, the recorded depth is subjective, and can change with the viewer; it is also dependent on the reflectance and surface area of the disk (Edmondsen, 1980), the amount of shading and the state of the water surface (Tyler, 1968). However, it remains a workable estimate of clarity.

Given these complications, it has been suggested that z_{SD} should only be used as an indication of clarity, or contrast, and not as a quantifiable parameter (Preisendorfer, 1986b).

2.4 RELATIONSHIPS BETWEEN PROPERTIES

2.4.1 Radiance and Irradiance

Both the Satlantic and the PRR600 measure downwelling irradiance E_d and upwelling radiance L_u. These measurements are designed to correspond to satellite observations, but cannot be used to directly calculate subsurface irradiance reflectance. It is therefore necessary to know the relationship between radiance and irradiance. If a Lambertian reflector is assumed, then:

$$E_u = \pi L_u$$

However, water does not usually act as a Lambertian reflector as radiance is not equal at all angles. Kirk (1994) used a Monte Carlo model to estimate the ratio E_d/L_u, with a solar altitude of 45°, and found this to be approximately 5. However, this value does not appear to be constant (Smith, pers. comm.), as the ratio varies with local conditions, so the use of one conversion factor is not appropriate.

2.4.2 Apparent and Inherent Optical Properties

K_d and R can be related to downward backscatter b_{bd} by defining another optical property $\kappa(z)$, which is "the average vertical attenuation coefficient in upward travel from the first point of upward scattering of all upwelling photons at a given depth" (Kirk, 1994). The relationship can then be described:

$$R(z) \simeq \frac{b_{bd}(z)}{K_d(z) + \kappa(z)}$$

Monte Carlo models have shown that κ is approximately proportional to K_d (Kirk, 1994) at the mid point of the euphotic zone (z_m):

$$\kappa(z) \simeq 2.5\ K_d(z)$$

Through the use of radiative transfer theory (Appendix II) a relationship can also be

established between K_d and a. In 1936, Gershun (from Kirk, 1994) derived the relationship:

$$\frac{d\vec{E}}{dz} = -cE_0 + bE_0 = -aE_0$$

where $\bar{E}$ is net downward irradiance

so that:

$$a = K_E \frac{\vec{E}}{E_0}$$

$$a = K_E \bar{\mu}$$

Preisendorfer (1961, from Kirk 1994) derived a relationship with the diffuse absorption and scattering coefficients:

$$K_d(z) = a_d(z) + b_{bd}(z) - b_{bu}(z)R(z)$$

which describes the downward diffuse attenuation as the sum of the downward absorption and backscatter (*i.e.* the loss from the light field), minus the product of upward backscatter and reflectance (which add a component to the level of light and thus decrease the attenuation).

A simplified version of the radiative transfer theory can be used to show that *R(0)*, the reflectance at the surface, is proportional to $b_b / (a+b_b)$, but as b_b is much lower than a is approximately proportional to b_b/a, which leads to (*e.g.* Morel & Prieur, 1981):

$$R(\lambda) = 0.33 \frac{b_b(\lambda)}{a(\lambda)} \qquad \textit{eqn. } 2.3$$

However, this is only an approximation as the constant of proportionality (0.33) is dependent on the solar altitude (Kirk, 1994). Kirk (1985) incorporated the solar variation by changing this constant as μ_0 (the average cosine):

$$R = \left[0.975 - 0.629\mu_0\right] \frac{b_b}{a} \qquad \textit{eqn. 2.4}$$

If the value of 0.85 is assumed for μ_0 the constant becomes 0.44.

Through the use of Monte Carlo models, Kirk (1994) has shown that for K_d at the mid-point of the euphotic zone:

$$K_d(z_m) = (a^2 + Gab)^{1/2} \qquad \textit{eqn. 2.5}$$

For water with the same volume scattering function as San Diego Harbour, Kirk (1994) has calculated that G=0.256. For the average K_d through the whole euphotic zone G=0.231. G determines the proportion of the diffuse attenuation which is 'lost' through scattering. In turbid water, the value of G will be lower as forward scatter will dominate and be backscattered into the path, whereas in clear water, the energy is lost with uniform scatter in all directions.

The above equations can be rearranged to calculate a and b. If the backscatter ratio is assumed to be 0.019 (Kirk, 1994), then

$$\frac{b}{a} = \frac{R}{(0.33.0.019)}$$

while

$$\frac{K_d}{a} = \left[1 + G\frac{b}{a}\right]^{1/2}$$

so

$$a = \frac{(K_d / a)}{K_d}$$

Both reflectance equations were used in the derivation of a and b, as although 0.33 is a general value which does not include the effect of solar altitude, the value of 0.85 for μ_0, based on the optical properties of San Diego Bay (Petzold, 1977), is also unrealistic.

The Secchi depth can be related to both diffuse and beam attenuation. In general, it is not directly related to K_d, although empirical studies have suggested that at 505 nm $K_d = 3.35/z_{SD}$ (Man'kovskiy, 1978) and for PAR, $K_d = 1.44/z_{SD}$ (Holmes, 1970). Tyler (1968) deduced that $(c+K_d) = 8.69/z_{SD}$, while observations by Holmes (1970) suggest $(c+K_d) = 9.42/z_{SD}$. Davies-Colley and Close (1990) simplified the interpretation by taking horizontal clarity measurements with a black disc so that only c is measured. Using this method, Davies-Colley and Smith (1995) measured almost maximum theoretical clarity in a New Zealand freshwater spring - 63 m visibility. This technique also enables measurements in shallow lakes where depth is only one or two attenuation depths.

2.4.3 Apparent Optical Properties and Constituents

Controlled studies, which have increased the level of suspended sediment concentration, have found a non-linear relationship with reflectance (Curran & Novo, 1988), with the correlation improving at higher wavelengths (Han & Rundquist, 1994a). The gradient of the correlation is lower with finer material (Han & Rundquist, 1996). In general, the peak reflectance moves towards higher wavelengths with increased concentration (Tassan, 1988; Gitelson, 1992; Han & Rundquist, 1994b).

Both Novo *et al* (1989) and Bhargava & Mariam (1990) have noted that the reflectance spectrum changed with sediment type as well as concentration. Consequently, the reflectance has been used to identify sediment (Hunt, 1977). The higher the organic content in the sediment the lower the general level of reflectance (Bhargava & Mariam, 1990). In the laboratory, reflectance is most easily measured when the sediment is pulverized (Balsam & Deaton, 1991), with the spectra being used to distinguish different sediments (*e.g.* Hunt & Salisbury, 1976; Hunt & Ashley, 1979) or even different minerals and the water content (Gaffey, 1985; Deaton &

Balsam, 1991; Balsam & Wolhart, 1993). However, although these investigations are used for bed analysis they have not been extended to *in situ* measurement where laboratory procedures are not possible.

In many of these reflectance studies, the derivative of the spectrum is used to highlight the changes in the curve (Goodin *et al*, 1993). This technique has also been used for phytoplankton analysis to distinguish between pigments (Sathyendranath *et al*, 1994).

As attenuation has been used to classify different marine water, so reflectance has been used to classify lakes into 5 categories (Vertucci & Likens, 1989), showing the change from clear water through increasing pigment and yellow substance concentrations (Fig. 2.4).

When observations are taken in water which is not deep enough to eliminate bottom effects, the reflectance value is a function of bottom albedo and depth of the water (Maritorena *et al*, 1994). This is useful for sea bed studies in shallow water as the effects will depend on the nature of the bed (Estep, 1994), but to investigate the constituents in the water column itself deeper water is essential.

In previous studies, yellow substance has been related to salinity; Kalle (1966) found a strong inverse relationship, while Davies-Colley (1992) did not find any link. It is assumed that the freshwater contains a higher concentration of humic acids, so that as the fresh water is diluted, becoming more saline, so the yellow substance concentration decreases. This was used successfully to identify the mixing process with water from the Baltic Sea and from clearer oceanic water (Jerlov, 1968).

2.5 REMOTE SENSING

Airborne or satellite sensors can be used to monitor water quality (McNeil *et al*, 1976; Thomas, 1981), and identify different water masses and events (Topliss *et al*, 1991). Airborne sensors are the most effective method of monitoring, with spectroradiometers used to differentiate different water bodies since Clarke *et al*'s work in 1970 (Austin,

1991). However, this method is expensive and is subject to a greater water surface effect than satellites (van Stokkom *et al*, 1993). There are several satellites carrying visible light sensors which have recently been launched or are planned, with the successful launch of ADEOS in August 1996, and the prospective launches of SeaWiFS and a similar European satellite. These give greater spatial and temporal coverage of the ocean than airborne techniques. Previously, the only sensor designed for ocean colour measurements was the Coastal Zone Color Scanner (CZCS) which operated between 1978 and 1986. The data from this have subsequently been studied in great detail in order to develop workable monitoring algorithms to identify and quantify phytoplankton. The LANDSAT satellites have two visible band sensors - the Thematic Mapper and the Multi-Spectral Scanner - which can be used to observe sediment (indicated by a high overall reflectance signal) and distinguish pollutants (Munday & Alfoldi, 1979; Sydor, 1980; Schiebe *et al*, 1992).

Predominantly, the work on the CZCS data considers ratios of the upwelling light, and how these are related to chlorophyll concentrations from ground truth data. The sensor had four bands of 20 nm bandwidth centred on 443 nm, 520 nm, 550 nm and 670 nm; most ratios involve blue to green comparisons (Gordon *et al*, 1980; Morel, 1980; Neuymin *et al*, 1982; Smith & Baker, 1982; Parslow, 1991; Mittenzwey *et al*, 1992) while some used green to red or a combination of ratios (Bukata *et al*, 1981b). Alternatively, the difference between wavebands may be used (Giannini, 1981). Viollier & Sturm (1984) specified that the constants used for the algorithms would change with phytoplankton type, and between the range of studies undertaken there is a great variation, as shown in Table 2.1. Other studies have quantified the effect of sediment on these ratios (Simpson & Brown, 1987; Brown & Simpson, 1990; Quibell, 1991). The depth of the euphotic zone has been shown to have an effect on the algorithms (Hojerslev, 1980 & 1981), while better agreement has been found when depth-averaged values of chlorophyll were used rather than just the surface value (Anderson *et al*, 1981; Smith, 1981).

Other constituents have been shown to interfere with these algorithms, as Hochman *et al* (1994 & 1995) found that half the supposed chlorophyll signal was due to

dissolved organic matter. There are also algorithms to derive sediment concentrations, but these become less effective when organic concentrations exceed 1 mgl^{-1} (Agnew, 1983), although once the sediment concentration is above 25 mgm^{-3} the chlorophyll signal is much weaker (Holyer, 1978).

A further limitation with satellite measurements is the necessity for good atmospheric algorithms prior to the interpretation of the ocean signal (Viollier *et al*, 1980; Sturm, 1981; Smith & Wilson, 1981).

$\log C = \log a + b \log (Rt) \rightarrow C = a\ Rt^{b}$					
Author	a	b	Rt	r^2	Comments
Gordon *et*	0.505	-1.269	L_w 443/L_w 550		Only applies for
al (1980)	0.843	-3.975	L_w 520/L_w 550		C<0.6 mgm^{-3}
Clark	0.766	-1.329	L_w 443/L_w 550	0.908	Also used by Austin
(1981)	0.518	-1.806	L_w 443/L_w 520	0.874	& Petzold (1981)
	1.694	-4.449	L_w 520/L_w 550	0.913	
	48.853	-1.372	L_w 520/L_w 670	0.876	
Smith &	0.483	-3.08	L_w 443/L_w 520	0.882	Only applies for
Wilson	0.783	-2.12	L_w 443/L_w 550	0.943	0.05<C<5.0 mgm^{-3}
(1981)	2.009	-5.93	L_w 520/L_w 670		
Sturm	0.5	-1.3	L_w 443/L_w 550		After Gordon *et al*
(1981)					(1979) C<1 mgm^{-3}
	0.8	-4.0	L_w 520/L_w 550		After Gordon (1980)
					C>1 mgm^{-3}
	1.5	-2.0	L_w 443/L_w 550		After Morel & Prieur
					(1978)
Topliss *et al*	1.2	-2.7	L_w 443/L_w 550		Average over all
(1991)	2.9	-6.4	L_w 520/L_w 550		concentrations
	0.88	-3.2	L_w 443/L_w 550		Only C<1.5 mgm^{-3}
	3.7	-4.0	L_w 520/L_w 550		Only C>1.5 mgm^{-3}

Table 2.1 Different algorithms derived from CZCS data to extract phytoplankton concentrations

Optical remote sensing is important to give a wide spatial coverage at low cost. Most work has tried to develop algorithms for extracting chlorophyll concentrations in Case 1 waters with the aim of estimating primary productivity. There has been less work with coastal waters where the chlorophyll signal is dominated by that from sediment and yellow substance.

The quantitative use of satellite images is dependent on the development of inverse optical models, deriving the concentrations of phytoplankton, yellow substance and sediment from the upwelling radiance. However, other models which aim to understand the interactions between these constituents and how they effect the reflectance signal aid general interpretation of the images, and can lead to better inversion techniques in the longterm.

2.6 SUMMARY

In order to compare the inherent and apparent properties it is necessary to derive the inherent optical properties of absorption and scattering from the apparent properties measured *in situ* using the equations in §2.4.2. This method rearranges the equations calculated from observations and modelling of a turbid environment described by Kirk (1985). The derived values of the absorption coefficient can then be related to the absorption measured in the laboratory. Consequently, diffuse attenuation and reflectance need to be measured in the field. It is also useful to measure beam attenuation in the field so that scattering can be determined once the absorption coefficent is known. Beam attenuation was the only possible inherent property that could be measured *in situ* with the instrumentation available, but can give a direct field comparison between the inherent and apparent properties using $c=a+b$ with the derived a and b values and is therefore an important parameter. In total, observations were taken of K_d, R and c in the field (plus ambient light measurements), and a in the laboratory, with a experimentation to determine the importance of b.

Figure 2.1 Examples of specific absorption curves for
a) water
b) yellow substance
c) phytoplankton
d) inorganic particles

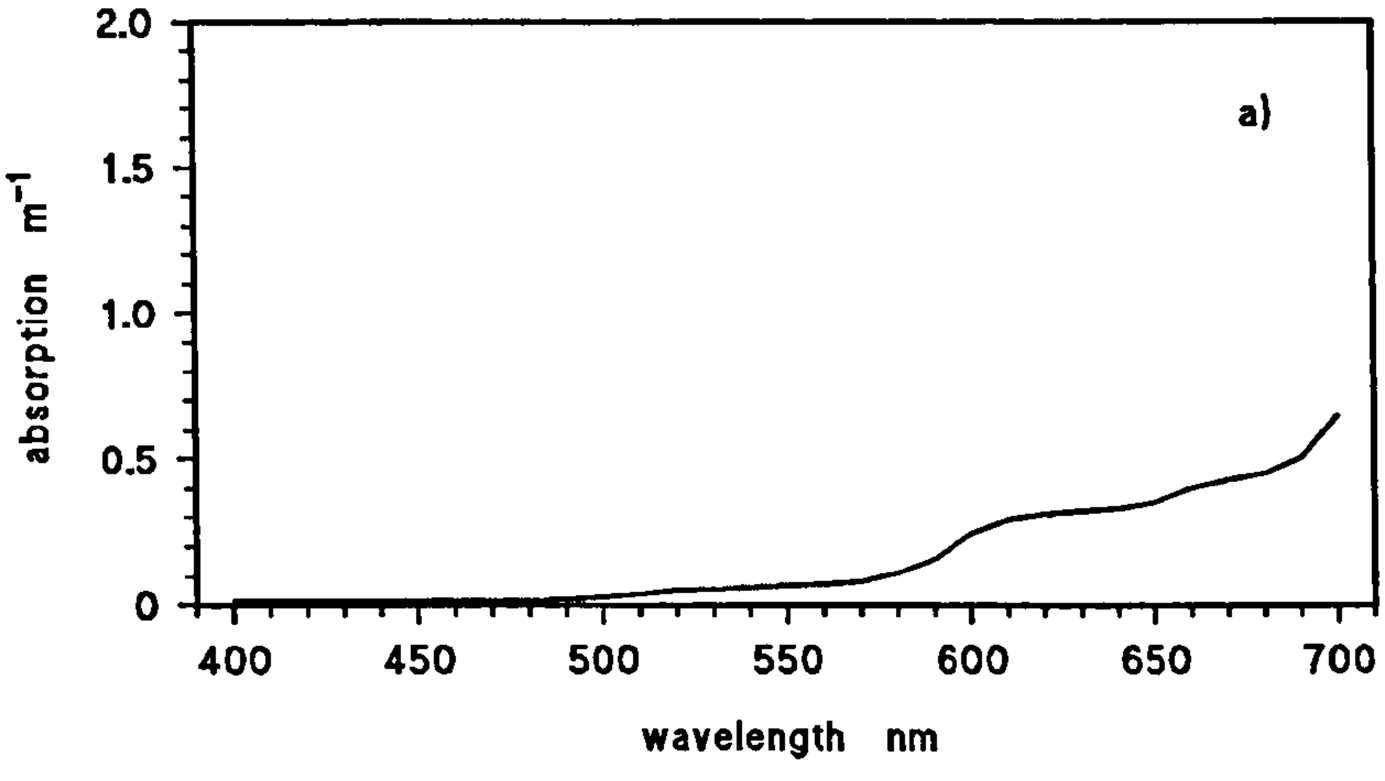
a)
absorption m-1
2.0
1.5
1.0
0.5
0
400
450
500
550
600
650
700
wavelength nm

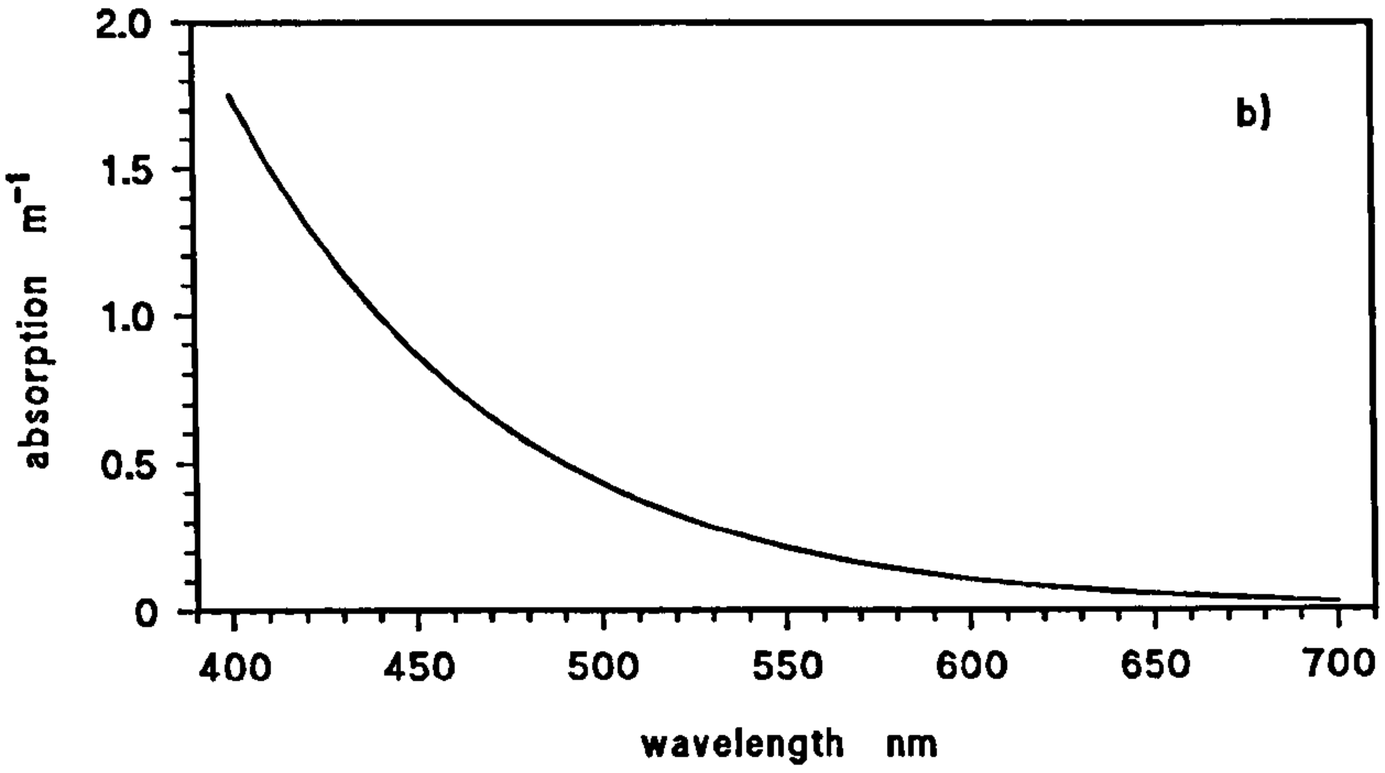
b)
absorption m-1
2.0
1.5
1.0
0.5
0
400
450
500
550
600
650
700
wavelength nm

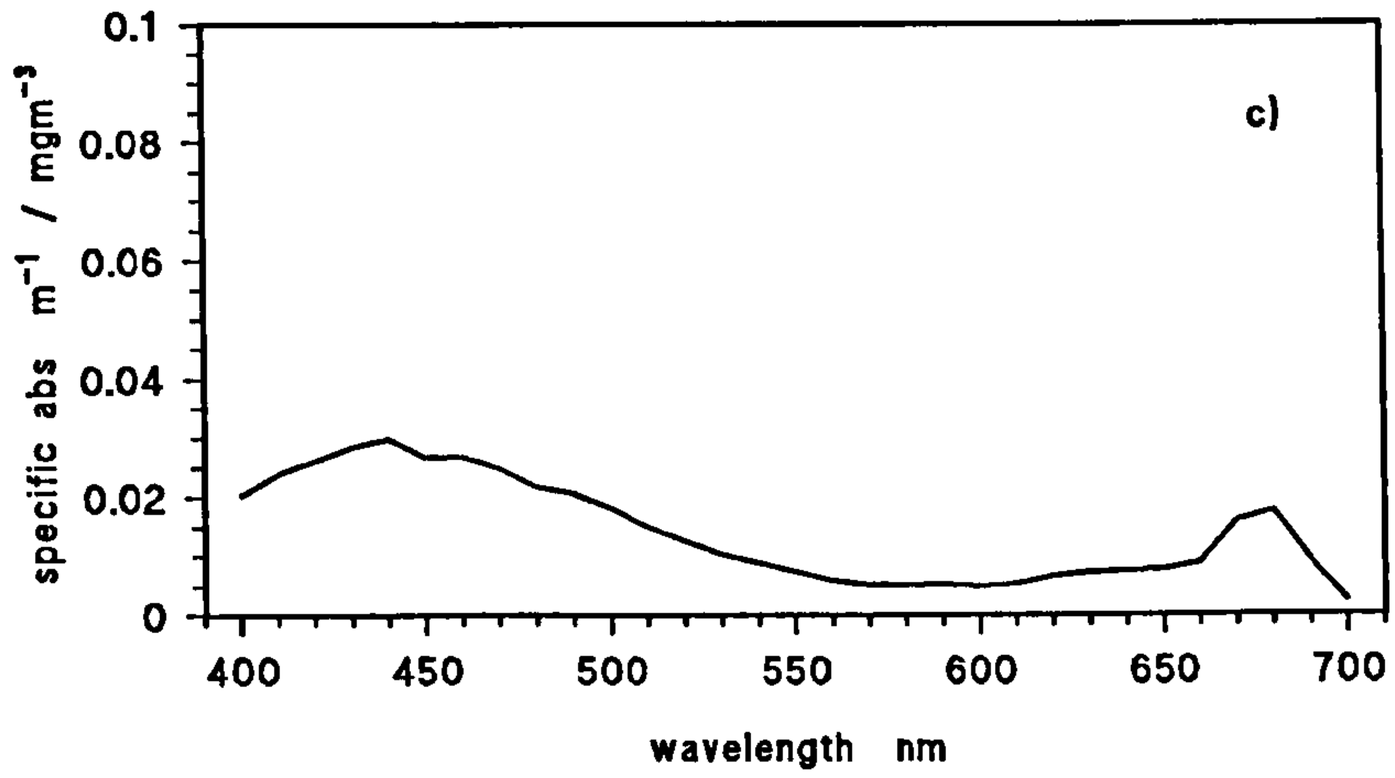
c)
specific abs m-1 / mgm-3
0.1
0.08
0.06
0.04
0.02
0
400
450
500
550
600
650
700
wavelength nm

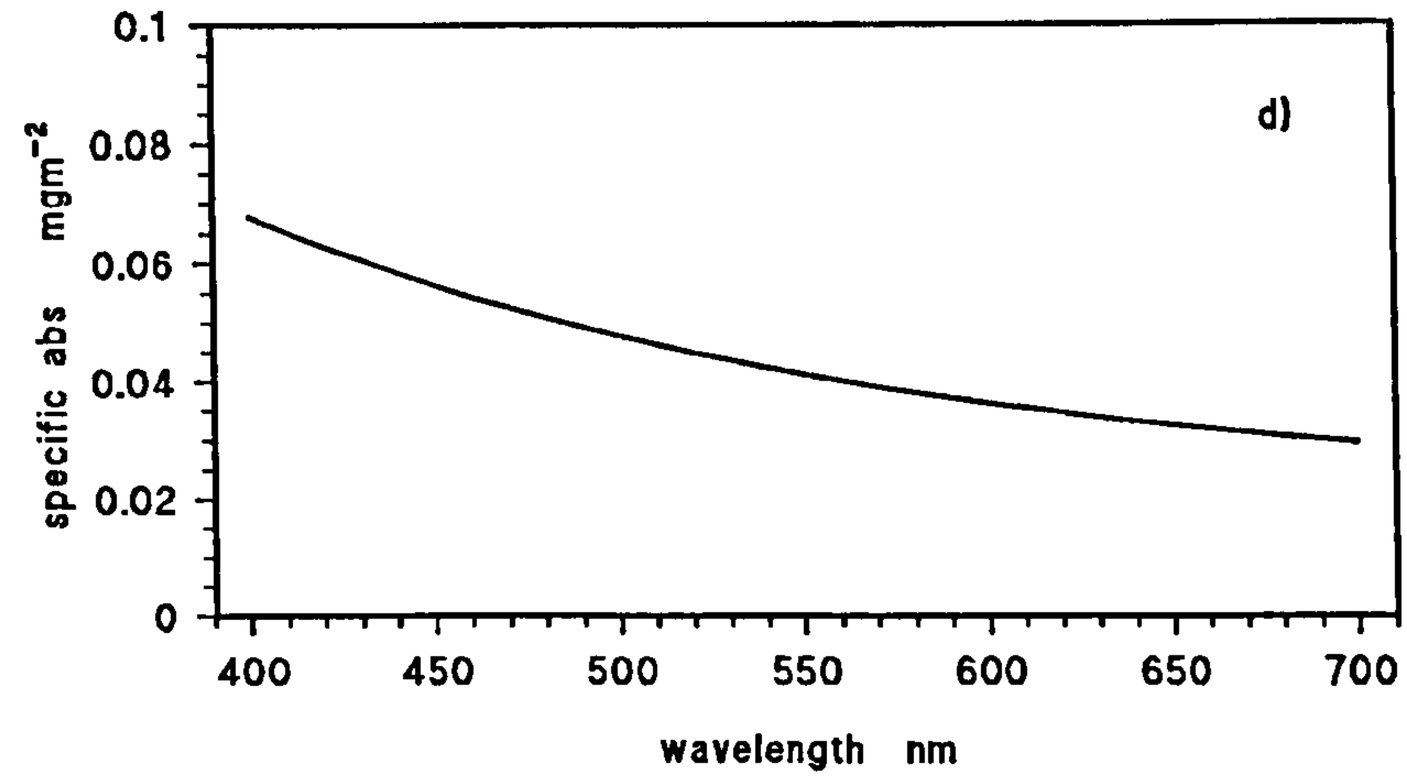
d)
specific abs mgm-2
0.1
0.08
0.06
0.04
0.02
0
400
450
500
550
600
650
700
wavelength nm

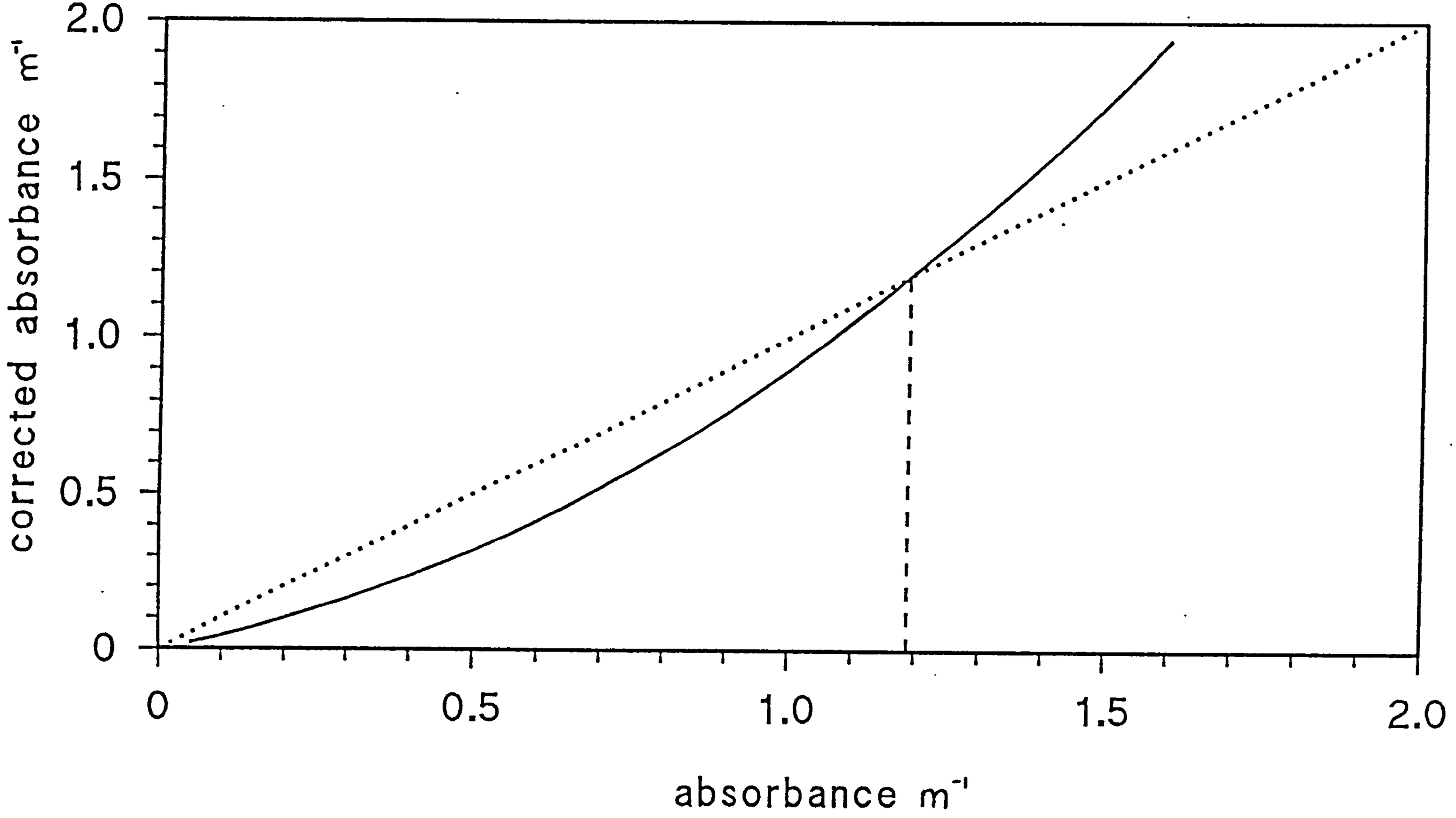

Figure 2.2 Effect of Cleveland & Weidemann (1993) pathlength amplification correction

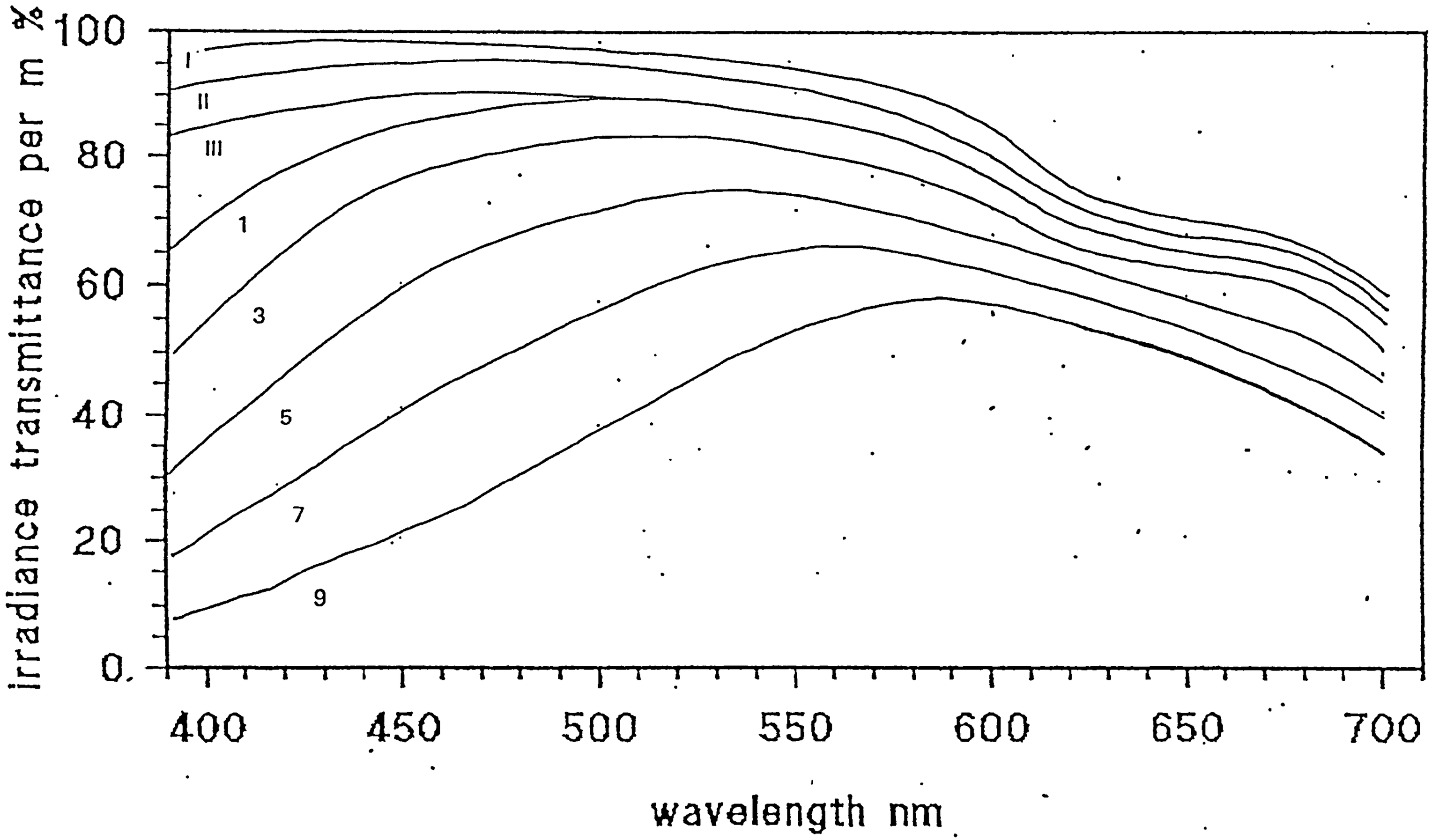

Figure 2.3 Transmittance classification curves for clear ocean water (I-III), and coastal water (1-9). Adapted from Jerlov (1968)

Figure 2.4 Reflectance curves used to classify lakes. Adapted from Vertucci & Likens (1989)

reflectance %
0
1
2
3
4
5
6
400
450
500
550
600
650
700
wavelength nm
Type 1
Type 2
Type 3
Type 4
Type 5

3. INSTRUMENTATION

3.1 FIELD WORK

Seven types of optical sensor were used over the different surveys, including two built by UCNW staff, and five commercially manufactured. To measure vertical attenuation and reflectance the upwelling and downwelling radiance or irradiance must be quantified at different depths. This can either be the absolute or the relative value, as the ratio is needed, not the exact quanta of energy present.

The UCNW instruments were passive sensors which measured relative irradiance at different wavebands, and could be oriented to measure either the upwelling or downwelling signal. Specifications of all instruments are given below:

Secchi Disk

- white disk of 30 cm diameter
- rope marked at 0.5 m for depth measurement

7-Channel (Fig. 3.1) - IRM1

- 5 visible channels, 1 UV and 1 unused
- readings averaged over three seconds
- sequential wavelength readings
- 10 nm bandwidth, centred on 444 nm, 521 nm, 552 nm, 596 nm and 670 nm (response curves are shown in Appendix III)
- pressure sensor, accuracy to 0.1 m
- instrument surrounded by a weighted, protective frame to maintain a vertical orientation in the water, within which the sensor could be turned upside down
- connected by a cable to a deck unit, which was computer driven to store data
- surface cosine collector also connected to deck unit to monitor the ambient light field
- relative calibration

This instrument measured the downwelling light at different depths, being kept at at each level for 20-30 seconds. It was then brought back to the surface and the sensor

inverted to measure upwelling light. A second 'profile' was then done keeping the sensor at each depth for the same amount of time again. This resulted in a time lag of several minutes between the start of the downwelling profile and the end of the upweling profile, although simultaneous surface readings were taken to monitor the changes in ambient light over this period.

4-Channel (Fig. 3.2) - CS2, CS3, CS4, CS23, CS24

- 4 visible channels
- 10 nm bandwidth, centred on 440 nm, 490 nm, 570 nm and 670 nm
- one sensor, CS24, fitted with a pressure sensor, accuracy ± 0.1 m
- internal logging
- relative calibration

The CS24 could be used to measure profiles in a similar manner to the IRM1, as a pressure sensor was fitted. However, the other sensors were used at fixed positions either near the bed looking upwards, when a tide gauge was available, or using floats on the surface looking downwards. These could be configured for different sampling intervals, from 30 seconds to 30 minutes dependent on the nature of the deployment.

The commercial instruments included a Satlantic, PRR-600, transmissometers, and a surface radiometer: Spectron SE590.

Satlantic -

- designed to coincide with the SeaWiFS satellite channels
- one irradiance sensor, usually positioned to measure the downwelling signal:

  7 visible wavebands of 10 nm bandwidth,

  centred on 410 nm, 440 nm, 490 nm, 510 nm, 550 nm, 670 and 700 nm
- one radiance sensor, to measure the upwelling signal:

  7 visible wavebands

  centred on 410 nm, 440 nm, 490 nm, 510 nm, 550 nm, 685 and 700 nm
- pressure sensor
- internal logging

- weighted frame to maintain vertical orientation
- relative calibration

The sampling period could be set to 1 second which enabled profiles to be performed with a smooth lowering of the instrument. This produced more accurate measurements of the vertical attenuation. However, although there were upward and downward looking sensors the reflectance could not be directly calculated as the relationship between radiance and irradiance was unknown. Consequently, the instrument was lowered smoothly through one profile, then brought to the surface and inverted so that the sensors were in the opposite orientation, and a second profile was taken. There was therefore always an error added to the calculation of reflectance either by the conversion of radiance to irradiance or the time lag between profiles.

PRR-600 -

- designed to coincide with the SeaWiFS satellite channels
- one irradiance sensor, usually positioned to measure the downwelling signal:
  6 visible wavebands of 10 nm bandwidth,
  centred on 410 nm, 440 nm, 490 nm, 510 nm, 550 nm and 665 nm
  1 PAR band
- one radiance sensor, to measure the upwelling signal:
  7 visible wavebands
  centred on 410 nm, 440 nm, 490 nm, 510 nm, 550 nm, 665 and 685 nm
- pressure sensor
- temperature sensor
- cable connects the instrument to a computer which logs the data
- relative calibration

This instrument had similar limitations to the Satlantic, having a fast sample rate to enable accurate profiles of radiance and irradiance to be taken, but necessitating the inversion of the whole instrument to calculate reflectance.

Intercomparison of these instruments occurred in the Menai Pier Surveys. The colour sensors were compared in air after the first survey. Although the absolute readings

were different, the ratios between the colour bands were the same and the variations with light level were consistent. It was hoped to compare the CS24, IRM1 and Satlantic in the August 1995 Survey but due to the malfunctionsing of the CS24 and the inability to download the Satlantic on two occasions this opportunity was not realised.

Profiling Transmissometer SBE 19 Seacat Profiler -

- 10 nm band width, centred on 670 nm
- 20 cm pathlength
- attached to a CTD:

  conductivity, which is converted to salinity

  temperature

  pressure

Transmissometer

- 10 nm band width, centred on 670 nm
- 25 cm pathlength

Spectron SE590 -

- one cosine receiver for ambient light
- one spectral sensor with 15° field of view
- 2 m beam to enable deployment out of shadow effects
- total range 368 nm to 1115 nm, measuring at 2 nm intervals within the visible spectrum
- wavelengths measured simultaneously, averaged over four readings
- both sensors attached to a manually controlled deck unit, data written to tape then transferred to ASCII format later

To confirm that the sensors were not drifting, the spectral sensor was directed at a spectralite sheet after every fifth reading. If the reflectance signal was close to 100% across the spectrum when compared with the cosine sensor, this verified that the sensors were performing correctly.

3.2 LABORATORY

Instruments

The laboratory equipment required included spectrophotometers, a Turner fluorometer and balances. Due to problems with various instruments, three spectrophotometers and three balances were used between 1993 and 1996.

3.2.1 Spectrophotometers

1) Hewlett Packard Diode Array

used for Menai Strait Survey November 1993-June 1994, Conwy and Cwmystradllyn, summer 1995

2) SHIMADZU UV-1201 Scanning Spectrophotometer

used for all spectra taken until September 1995 (other than those mentioned above), and inorganic spectra November 1993-June 1994

20 W Halogen lamp

monochrometer: concave holographic grating

detector: silicon diode

wavelength accuracy ± 1.0 nm

photogrammetric range: -0.3 → 3.0 Abs units

accuracy ± 0.005 Abs

repeatability ± 0.002 Abs

3) SHIMADZU UV-1601 Scanning Spectrophotometer

used for all spectra after September 1995, plus the inorganic spectra for Menai Pier Survey August 1995

also used to derive pigments from Cwmystradllyn, Conwy and the Clyde surveys during 1996

3.2.2 Turner Fluorometer

used to measure chlorophyll related pigments for all surveys except Vestfjorden, Cwmystradllyn, Conwy and Clyde Sea surveys in 1996

3.2.3 Balances

All balances were calibrated periodically by NAMAS accredited technicians. For consistency, the balance which was used to pre-weigh filters was used through all stages of the filtering process.

1) *METTLER INSTRUMENTE AG CH-8606*

used for Menai Strait Survey, Cardigan Bay, Clyde Sea

accuracy 10^{-6} g

2) *OERTLING*

Menai Pier Survey 1994

accuracy 10^{-5} g

3) *OHAUS ANALYTICAL Plus DB2*

Vestfjorden, Menai Pier Survey 1995, Conwy, Cwmystradllyn

accuracy 10^{-5} g

Photograph

Figure 3.1 UCNW Irradiance Meter (IRM1)

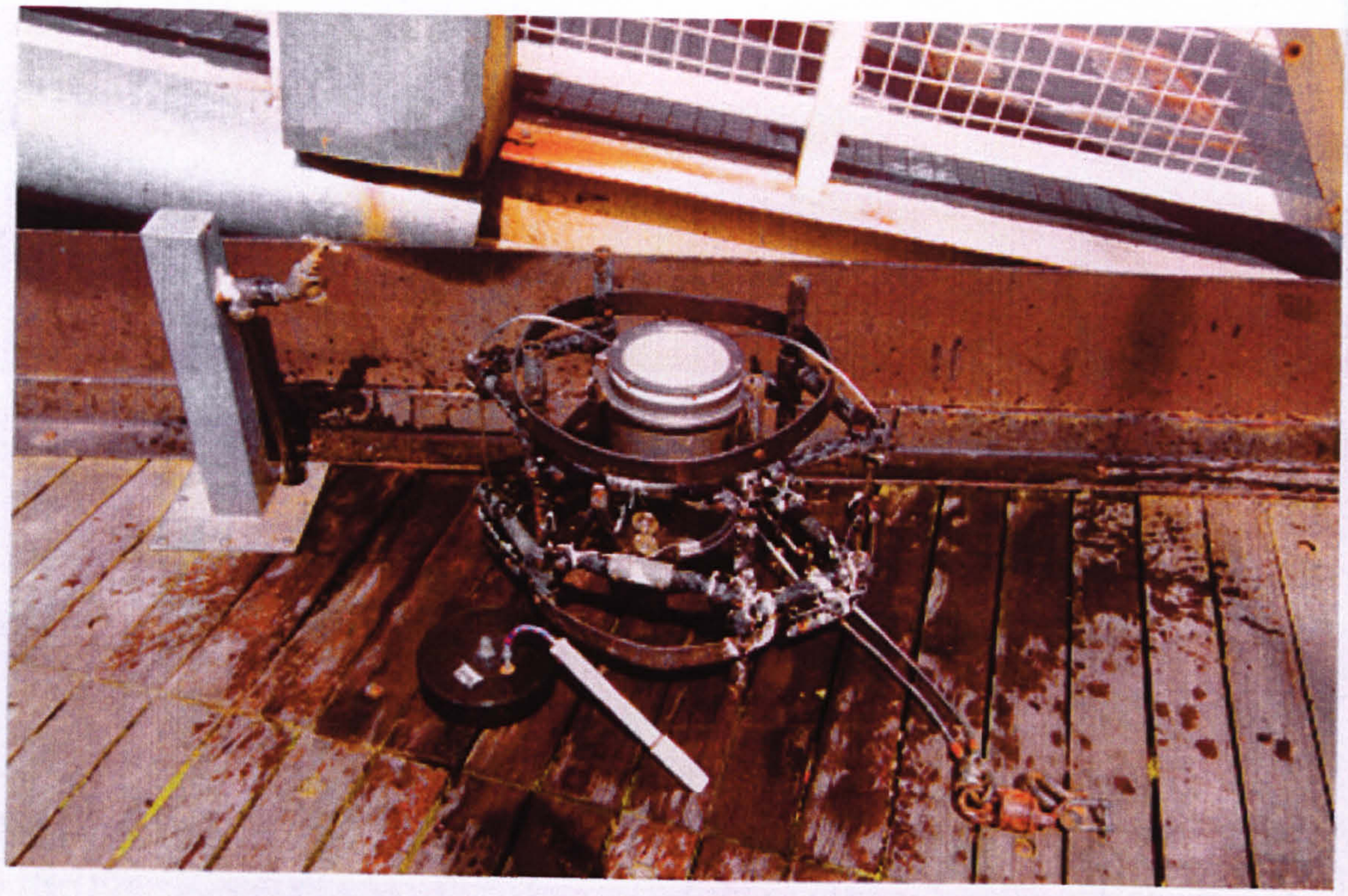

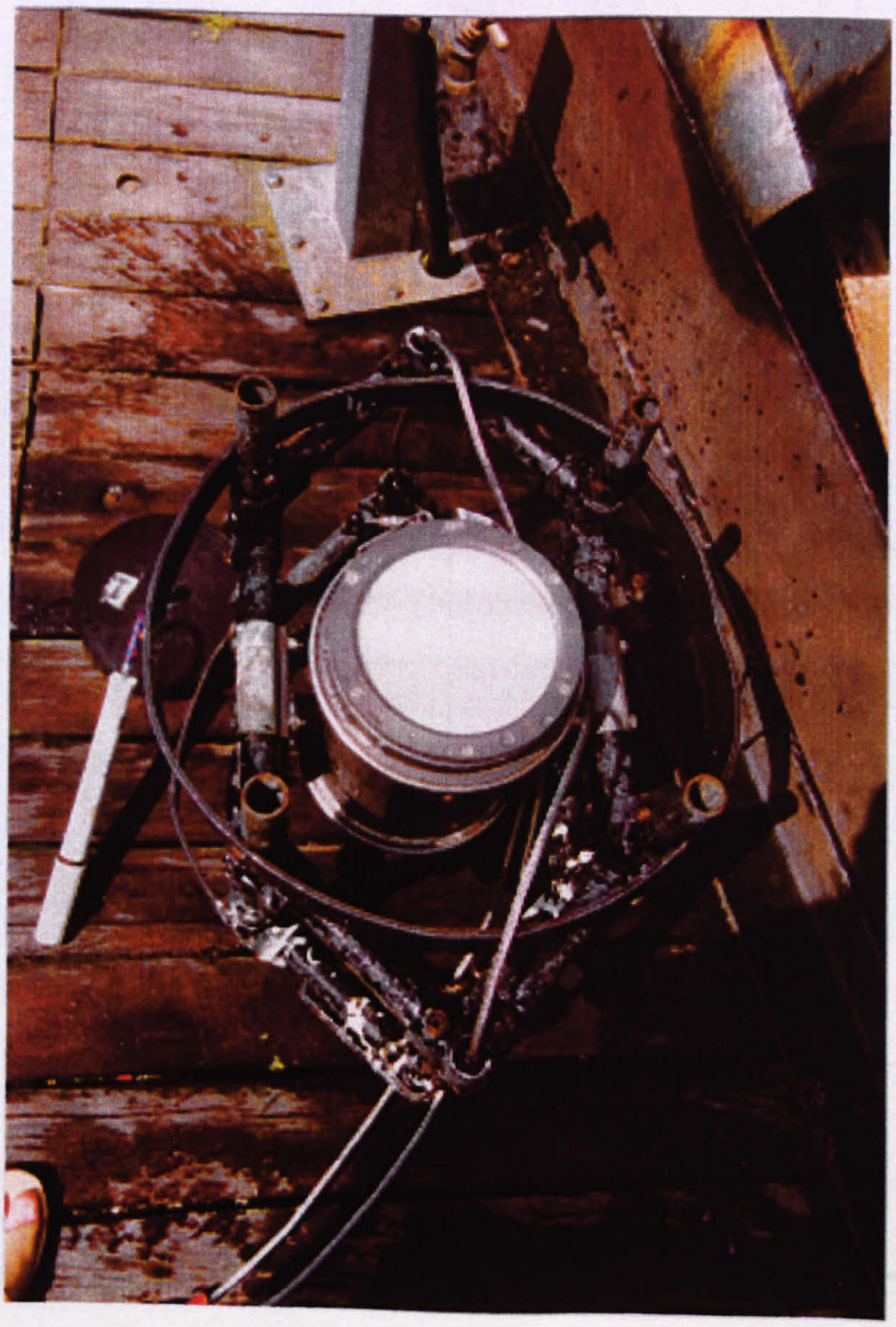

Photograph

Figure 3.2 **UCNW Colour Sensor (CS)**

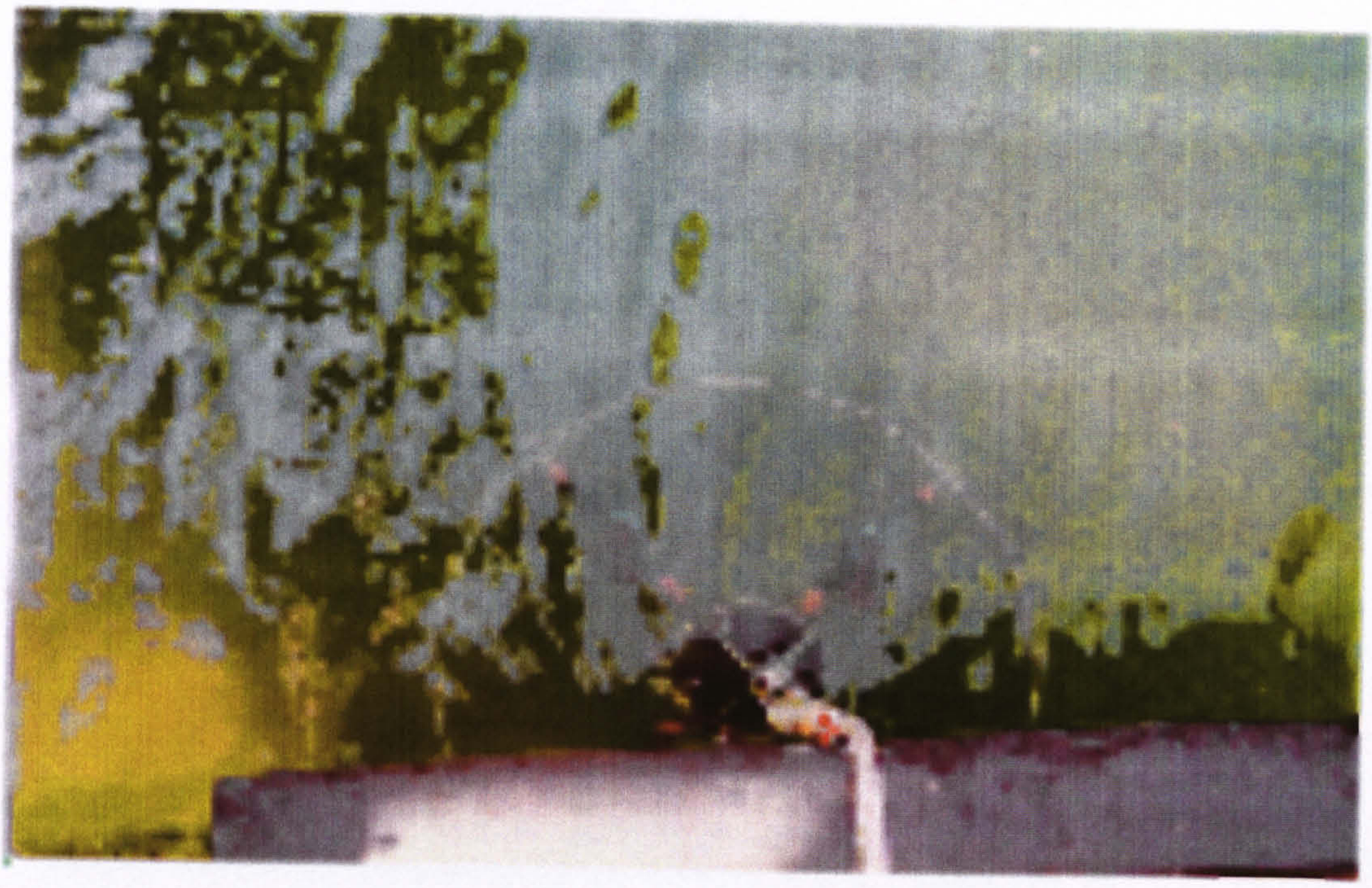

Photograph

Figure 3.3 Satlantic

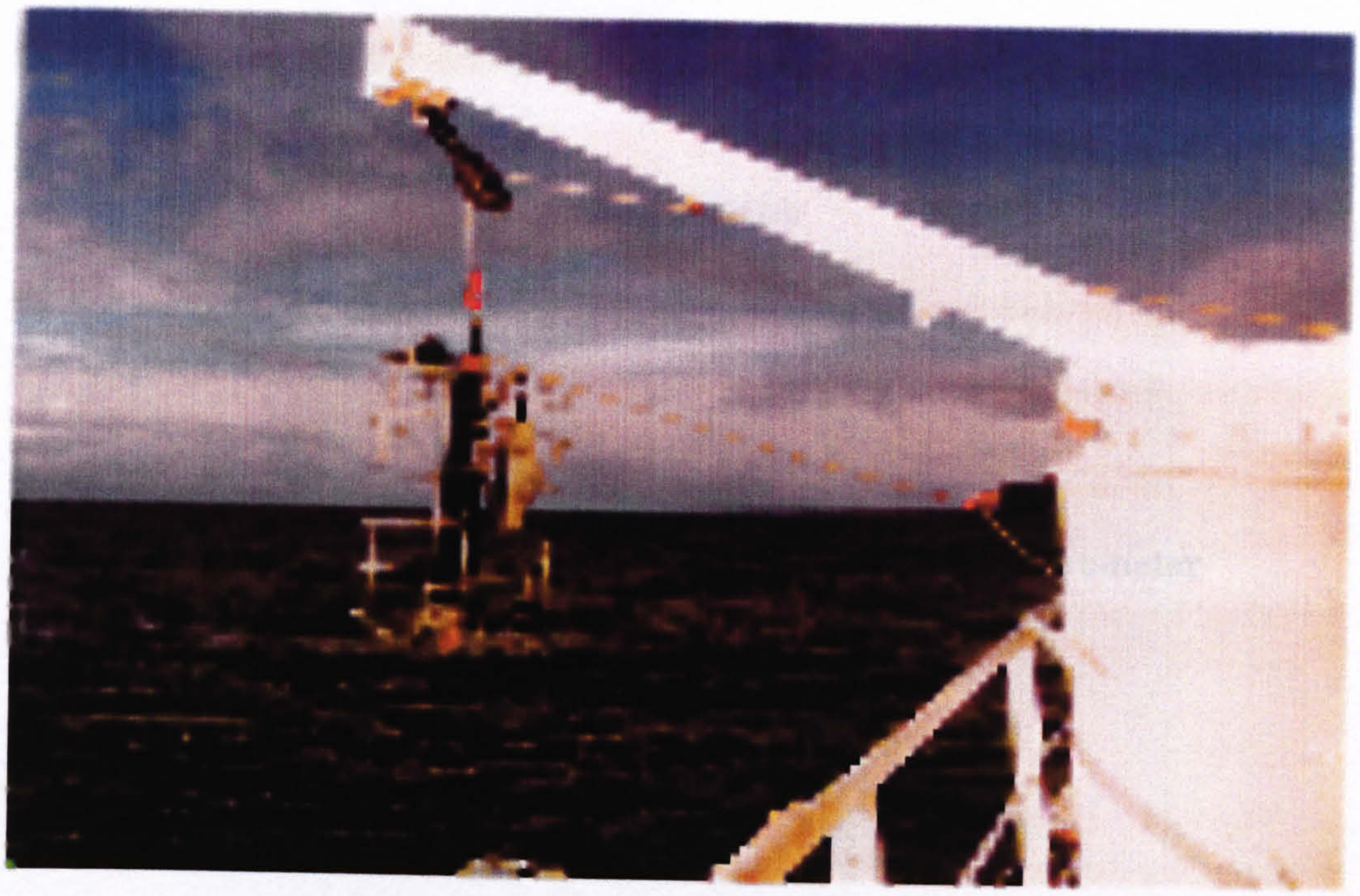

Photograph

Figure 3.4 **PRR-600 and Profiling Fluorometer**

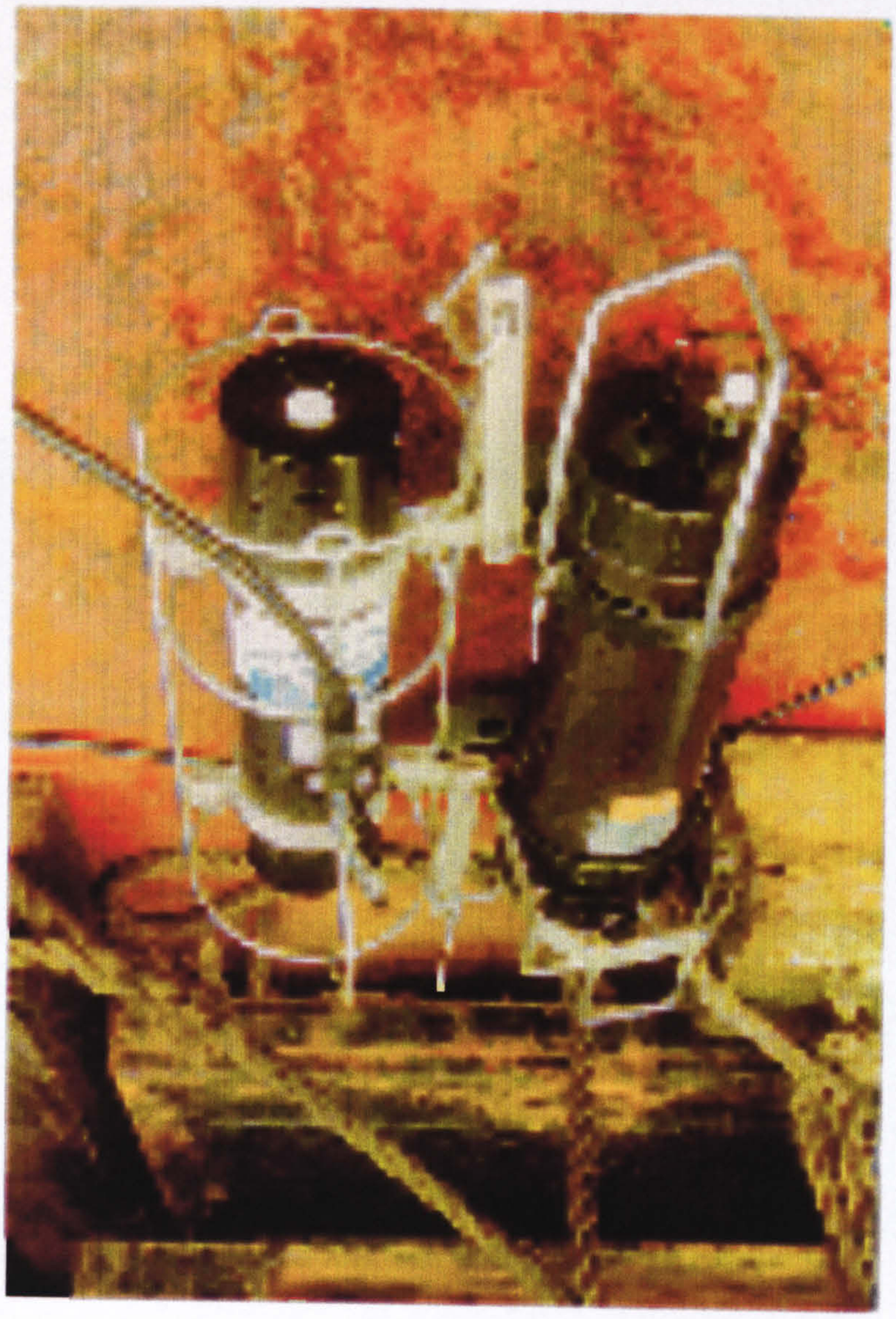

Photograph

Figure 3.5 Spectron SE-590

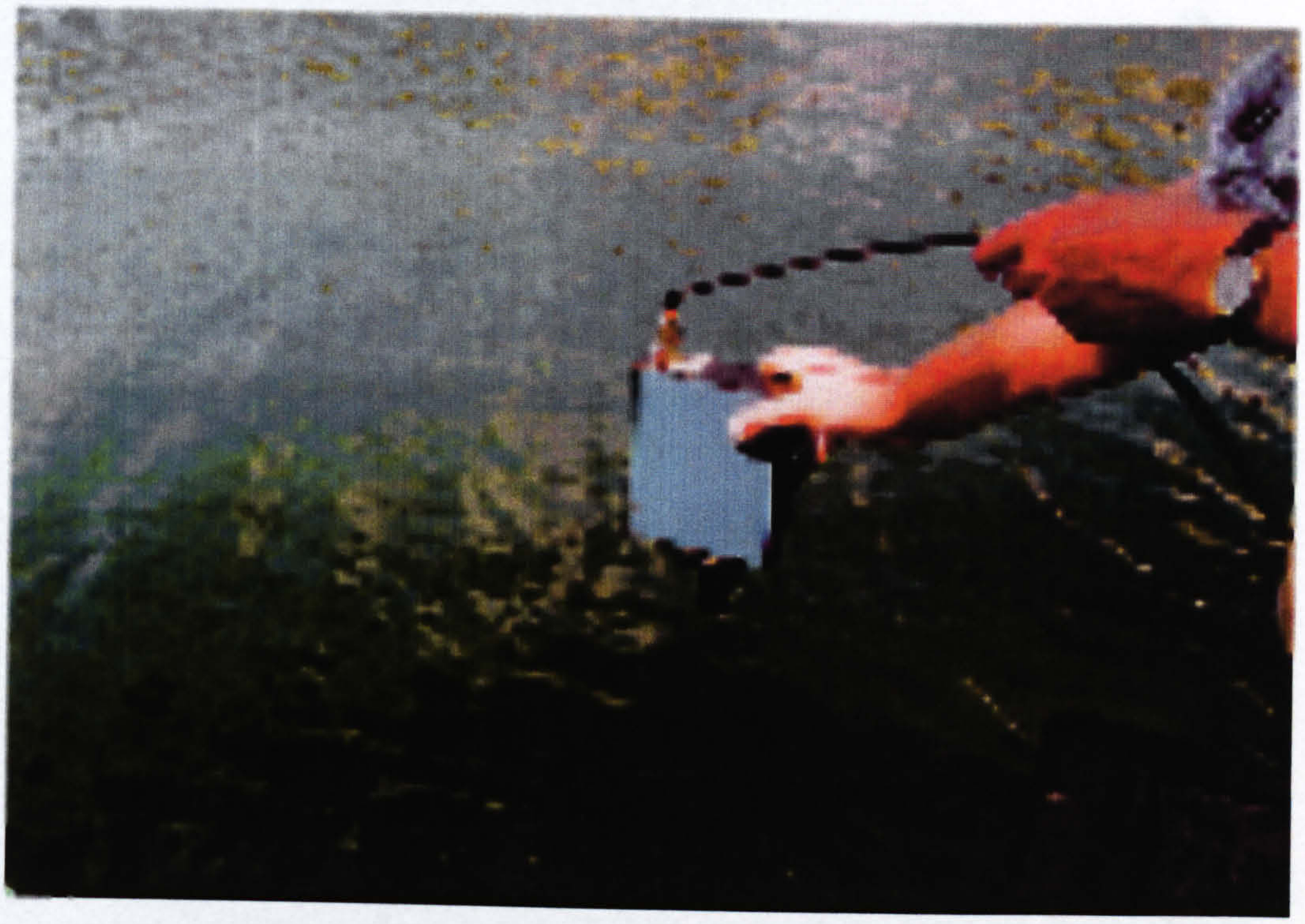

4. FIELD SURVEYS

Surveys were undertaken in a range of water types to distinguish the different optical environments. Most of the data were collected in the Menai Strait, but other marine sites were included, plus estuarine and freshwater locations to provide a contrast. The various sites with the different instruments used are given in Table 4.1 chronologically, with details of the surveys then described below, while standard methods for the field and laboratory measurements are given in chapter 5.

4.1 MENAI STRAIT SURVEY

The Menai Strait separates Anglesey from mainland northwest Wales. In this area, there is a series of northeast-southwest depressions where the drainage has exploited the weaker geology due o faults of Caledonian origin (Asghar, 1992). The Strait formed in such a valley whih was overdeepended during the last glacial maximum, and was finally flooded in the Flandian transgression: 6000-7000 BP (Embleton, 1964). The glacial histor of the region has resulted in a general stratigraphy of Upper Boulder Clay overlying meltwater sands and then Lower Boulder Clay, although the upper layer of this succession has subsequently been eroded within the Strait (Jones, 1978). The sources of sediment include run-off from the land, but mainly consist of sea floor deposits, *i.e.* boulder-clay from the Conwy Bay area, and sand/lag-gravel deposits from the Irish Sea.

Ten sites along the Menai Strait (Fig. 4.1) were visited every month from November 1993 to October 1994, with the exception of April and September. The positions (Table 4.2) were easily identifiable, out of the main current and covered a range of environmental conditions. These were chosen to give a contract of optical conditions due to the different surroundings as described in the comments.

date	site	description	instrumentation
Nov 1993 - Oct 1994	Menai Strait, Wales	Optically dynamic, marine strait	IRM1, Secchi disk
February 1994	Clyde Sea, Scotland	Clear, deep marine	IRM1
April 1994	Loch Striven, Scotland	Phytoplankton bloom sea loch	IRM1, Sechhi disk
June 1994	Cardigan Bay, Wales	Study water either side of salinity front	IRM1, Secchi disk
July 1994	Menai Bridge Pier, Wales	Readings from the floating pier at Menai Bridge	IRM1, Satlantic, Spectron, CS2, CS3, CS4, Secchi disk, fixed transmissometer
September - October 1994	Vestfjorden, Norway	Clear water, less coastal effect, different phytoplankton species	Satlantic, CS2 Secchi disk
July 1995	Dolgarrog, Conwy Estuary, Wales	Turbid estuary with high concentrations and changing salinity	CS23, CS24 SBE 19 transmissometer, Spectron SE 590
August 1995	Llyn Cwmystradllyn Wales	High mountain lake, high YS, low sediment and phytoplankton	CS23, CS24 SBE 19 (did not work), Spectron SE 590
August 1995	Menai Bridge Pier, Wales	as above	IRM1, Satlantic CS24
March 1995	Dolgarrog, Conwy and Llyn Cwmystradllyn Wales	as above	PRR-600, SBE 19 transmissometer
June 1996	Clyde Sea, Clyde Estuary, Scotland	Contrast between clear water and turbid estuary	PRR-600, Secchi disk

Table 4.1 Description of surveys, with optical relevance, and instrumentation used in the field

	latitude °N	longitude °W	comments
1	53°15.62	04°05.23	sandy floor
2	53°15.30	04°06.08	beside sandy spit
3	53°14.59	04°07.61	near concrete slipway
4	53°14.05	04°08.78	near mouth of River Cadnant
5	53°13.47	04°09.51	beside small town
6	53°12.89	04°11.94	at mouth of small river
7	53°12.18	04°12.80	shore reinforced with wall
8	53°11.26	04°12.93	beside mud/sand spit
9	53°10.73	04°13.21	protected bay
10	53°10.35	04°14.54	beside busy sports centre

Table 4.2 Description of sites along the Menai Strait

Throughout the Menai Strait the water is vertically well mixed, confirmed by the transmissometer profile in Fig. 4.2, indicating that surface water samples were representative of the upper 12 m of the water column. The readings were taken at various points in the spring-neap cycle (Fig. 4.3), dependent upon weather conditions.

The UCNW Irradiance meter (IRM1), used to measure *K* and *R*, was lowered from a small powered boat (the *Sandpebbler*). Water depth was measured with the boat's sonar, while ambient light and Secchi depth readings were taken. Downwelling light was measured at approximately 3, 2, 1 and 0.5 m, while upwelling was measured at 1 and 0.5 m. These depths were adjusted according to the water clarity, profiling to a greater depth in clearer water. All sites were visited within a day, except for the November survey when 1-4 were visited on 17 November and 5-10 on the following day. In January and October deteriorating weather conditions prevented data collection at all sites, limiting data to sites 4-8, and 2-10 respectively. A total of 94 stations was taken over the year.

A bucket was lowered over the side to collect water samples, which were stored in plastic bottles in black bags during the day until the boat returned to the laboratory in the late afternoon. 2.5 l of water were collected at each site, 1 l to be filtered for suspended particulate matter (SPM), and 3x250 ml for chlorophyll extraction and yellow substance measurement.

4.2 MENAI PIER SURVEY

In both 1994 and 1995, measurements were made for two weeks at the end of the floating Menai Bridge Pier. Daily samples were taken to determine constituent concentrations, while optical instruments were deployed. Different sensors were used for the two surveys, so they will be described separately.

4.2.1 July 1994

The two week period, 11-25 July, covered a spring-neap-spring cycle, with water samples taken at noon each day. For one 24-hour period (21-22 July), hourly samples were taken to identify any semi-diurnal signal. In addition, seven Spectron measurements, and eight IRM1 profiles were made.

Three 4-channel colour sensors were used: CS2 was positioned on the roof of the Westbury Mount Building, and took one reading every 30 minutes - this was the overall reference to evaluate ambient changes. CS4 was attached to a low strut of the southern tower of the pier, 0.83 m beneath chart datum, measuring downwelling light. CS3 was deployed daily, between 08.00 and 17.30, to measure upwelling light at a depth of 0.5 m. A transmissometer was also attached to the pier, 2 m below the platform.

During the first week the Spectron was used to measure the surface reflectance, and sub-surface reflectance by taking readings through a black pipe (to minimize the surface effect - see §5.1.2 for details). The IRM1 was deployed to identify changes in the radiance profile. These measurements were taken on 11-15, 18-19 and 22 July, to establish independent reflectance and attenuation values.

Each day at noon, a tidal height reading and Secchi depth were taken. 5 l of water were collected and analysed in the laboratory. The concentrations of pigment and SPM (3 replicates for each) were measured, with the filtrate used for yellow substance absorption. One filter was immediately placed in the UV1201 spectrophotometer to measure the 'wet' spectrum, while all were scanned after drying and again after furnacing (refer to §5.2.4.). It was discovered that salt remained on the SPM filters,

enhancing the particle weights. The filters were therefore re-rinsed several weeks later, which increased the uncertainty of the final weights.

Fig. 4.4 shows the points in the tidal cycle at which water samples were taken. It also compares the tidal heights measured at these times with the predicted heights. There seems to be a discrepancy with the height of low tide at neaps. The difference reaches 0.5m, which is greater than variations caused by atmospheric pressure. This has implications for the depths assumed when analysing the colour sensor data (§6.2).

4.2.2 August 1995

This survey covered a neap-spring-neap cycle, 21 August-4 September. The transmissometer was fixed to the southern pier tower below low water (springs), but was the only instrument used for continuous monitoring. The water samples were taken at 14.00 hours to prevent shading from the pier itself, taking surface water to be analysed as before, plus near-bottom samples on four occasions. A total of thirteen water samples was analysed; five CS profiles, and eight Satlantic profiles (five of which could be used for reflectance) were taken.

The optical sensors took profiles through the water column at the same time as sample collection. During the first week, the CS24 measured upwelling and downwelling profiles, recording every 30 seconds, with another sensor measuring the ambient light every minute. There were problems with data logging on the CS24 so it was replaced by the Satlantic on Friday 25 August. The Spectron was used to measure surface and sub-surface reflectance as before, over the entire fortnight; this was prevented on 26 August due to rain.

In the laboratory, 3 x 1 l were filtered for SPM concentrations, 3 x 250 ml for pigment extraction, and 1 x 2 l filtered to measure wet filter absorbance spectra, although this was reduced to 1 l when particle concentrations increased in the middle of the survey. Water was filtered through membrane filters to determine yellow substance using the UV1201 spectrophotometer.

4.3 LOCH STRIVEN 1994

In April 1994, the RV *Prince Madog* undertook a survey in Loch Striven (Fig. 4.5), while two colour sensors and two fluorometers were deployed on a mooring. Loch Striven is a sheltered sea loch to the north of the Clyde Sea, and has been extensively used in phytoplankton studies (Tett, 1990). The instruments recorded data from 19 March until 20 April; they were then downloaded and returned to the mooring until 11 May 1994, with the cruise occurring over the turn around, 18-22 April. From the ship, readings were taken with IRM1 and a profiling fluorometer; the water samples were analysed on board for SPM, chlorophyll concentrations and yellow substance.

4.4 CLYDE SEA 1994 and 1996

The first survey in the Clyde Sea was in February 1994. The Clyde Sea (Fig. 4.5), or the Outer Firth of Clyde, is a fjordic sea loch extending from 55°00′N to 56°15′N, bounded by the Mull of Kintyre to the west, the Ayrshire coast to the east and the North Channel to the southwest. The total surface area is 3000 km^2, fed by a catchment area of 10500 km^2 which provides a total inflow of freshwater of ~ 340 m^3s^{-1}. Thus, the low tidal currents (~0.1 ms^{-1}) result in almost permanent stratification (Walne, 1993).

Two profiles were taken at stations CS6 and CS8, to the east of Arran, with the IRM1, deployed from the RV *Prince Madog*. Water samples were also taken. Weather conditions prevented further data being collected.

The second survey was undertaken in June 1996 (Table 4.3). Optical measurements were taken with a Secchi disk and the PRR-600 while water samples were taken for concentrations and filter spectra. Two deep mooring stations were visited, and then six stations extending into the Clyde River to observe changes associated with salinity variations.

Date	Site	lattitude °N	longitude °W	comments
22/02/94	CS6	55°33'42.0	04°58'34.2	Clyde Sea
24/02/94	CS8	55°44'18.0	05°13'25.8	
18/06/96	CS1	55°09'59.4	05°22'07.2	Clyde Sea
	CS4	55°21'55.8	05°03'54.6	
19/06/96	CE6	55°55'58.9	04°34'12.6	Furthest station in Clyde
	CE5	55°58'09.7	04°45'31.2	Estuary moving towards
	CE4	55°56'07.8	04°53'30.6	Clyde Sea
	CE3	55°51'56.1	04°56'55.8	
20/06/96	LR1	55°56'27.0	05°11'37.8	Loch Ridden
	IW1	55°46'23.4	05°13'49.8	

Table 4.3 Description of Clyde stations in 1994 and 1996 survey

4.5 CARDIGAN BAY 1994

Cardigan Bay (Fig. 4.6) is the largest bay in the British Isles and has a high seasonal influx of cold water from the Snowdonia and Plynlimon Mountains. The bay shoals eastwards and shorewards, with a maximum depth of 50 m. Due to the irregular coastline of the northern shore, the tidal streams are asymmetrical, resulting in the ebb flow lasting 1½ hours longer than the flood (Browne, 1993).

Where the flooding saline water meets the freshwater a front is formed, usually in the vicinity of Hell's Mouth. The aim of this survey was to collect optical data from either side of the marked front. On the first attempt (24 June 1994), poor weather prevented the front from being identified, and data being collected. However, on the way back to Pwllheli, it was possible to take measurements in the lee of St. Tudwal's Islands. Two profiles were taken, plus water samples which were analysed later that day.

On the 30 June, there was a second attempt which proved more successful. Three profiles (with water samples) were taken on either side of the front. Unfortunately, this was starting to break up due to the state of the tide. The water appeared clearer than that studied in the Menai Strait but with higher concentrations of particles than in the Clyde. The instruments used were those employed in the Menai Strait Survey.

4.6 VESTFJORDEN 1994

In September 1994, there was an opportunity to join the HMS *Herald*, on a survey to Vestfjorden, northern Norway. The fjord extends from 67°00′ N to 68°30′ N, and 12° E to 16° E, bounded by the Lofoten Islands to the west and the Norwegian coastline to the east.

The survey positions are as shown on Fig. 4.7, and the sites at which optical measurements were taken are in Table 4.4. While on station, three instruments were deployed over the side of the ship: the Satlantic, a UCNW 4-channel colour sensor (CS2) and a profiling fluorometer. As these measurements were required to fit around the observations taken by the ship's crew the deployment of the optical instruments was not ideal. All sensors were lowered on the port side of the ship, regardless of the position of the sun. The winch for the Satlantic was also located near the bow-thrusters which were necessary to maintain position throughout the cast, consequently the surface layers were usually disrupted by the expulsion of air through these ports. The colour sensor was lowered two metres aft of the Satlantic, and left in the water while the ship was on station to ensure that at least one reading was taken. Unfortunately, this was sometimes affected by discharge from the galley and could not be pushed far from the ship's side as the bow continuously headed into the wind.

For each site, surface water samples were taken by lowering a bucket towards the stern of the ship, away from galley and laundry discharges. Where possible, samples were also taken from a depth of 10m on the ship's rosette sampler. The water samples were immediately taken to the ship's wet lab, where, for the surface water, 2 l were filtered for SPM and 3 x 1 l were filtered for chlorophyll, the filtrate being collected and scanned in a 100 mm cell to measure yellow substance. An unfiltered surface water sample, which included all constituents, was also scanned with the spectrophotometer. The water from the rosette sampler was limited, so that, for the samples at depth, 2 l were filtered for SPM with only 1 l filtered for chlorophyll, and a small sample scanned. The chlorophyll filters were put directly in 90% acetone and left in a dark fridge for 24 hours before the acetone was refiltered and the filtrate scanned against an acetone blank to gauge the chlorophyll concentration. Two drops

of HCl (conc) acid were then added and another spectrum taken. The SPM filters were left to air-dry and then stored until they could be oven dried in the Menai Bridge laboratory and weighed.

date	time GMT	station	latitude °N	longitude °W	cloud cover	wind direction	wind speed	profile no.
29/09/94	08:45	V2121	67.8	13.5	7	035	32	1
	13:20	V2129	67.8	13.4	5	035	20	3
30/09/94	08:05	M1606	66.9	11.6	6	029	5	4
	09:50	M1506	66.7	11.1	6	013	2	5
	11:30	M1406	66.7	10.9	7	019	8	6
01/10/94	07:00	M2506	67.7	13.5	6	004	12	7
	10:30	M2306	67.6	13.3	6	036	11	8
	12:00	M2206	67.4	12.9	5	029	13	9
	13:44	M2106	67.3	12.6	3	029	12	
02/10/94	07:50	M1906	67.1	12.0	5	033	18	10
	11:45	M1906	67.1	12.0	5	033	23	11
03/10/94	08:15	M1906	67.1	12.0	6	028	11	12
	09:40	M1907	67.2	11.8	4	004	5	13
	11:15	M1908	67.3	11.6	5	032	5	14
	12:30	M1909	67.4	11.3	6	032	6	15
	14:00	M1910	67.5	11.1	5	034	9	
01/10/94	09:35	M1914	67.9	10.1	7	031	23	

Table 4.4 Description of Vestfjorden sites

On the first day of analysis on board it was discovered that the 'distilled' water included a sterilising agent which caused a yellow discoloration. From the second day onwards, the water was much improved but still gave unusual peaks in the spectra when used as a blank, so may have been affecting the optical measurements taken.

The first five days of the survey had relatively calm weather, with clear skies and sun on 1-2 October. However, the weather then deteriorated as the ship headed westwards and optical measurements were not possible. Unfortunately, the high swell and winds prevented further observations throughout the final five days of the survey.

4.7 CONWY ESTUARY (DOLGARROG) SURVEY 1995/1996

An estuarine environment was sampled as a contrast to previous sites, the estuary having higher SPM concentrations and varying yellow substance. A pilot study was undertaken to assess the practicability of taking measurements from a bridge, and to monitor the change in yellow substance on the rising tide. This showed a marked change in g440 values and so was considered suitable. The survey itself was carried out at Dolgarrog Bridge (Fig. 4.8) on 27 July 1995.

The instruments deployed were a UCNW 4-channel colour sensor (CS23), attached to a frame with floats so that the sensor pointed downwards at the surface (Fig. 4.9); a transmissometer, with depth sensor; a surface colour sensor (CS24) for ambient light measurement and the Spectron. The CS23 took readings every 30 seconds, with the transmissometer reading every 10 seconds. Both instruments were lowered from the bridge and remained in the water between 11:00 and 14:00 BST. Water samples were taken at half hour intervals between 11:45 and 13:15, in conjunction with Spectron reflectance measurements. This period covered the flood tide, with the change in salinity indicating the influx of sea water.

As the water flowed inland, large quantities of foam and scum were apparent on the surface, possibly scoured from the banks downstream. Debris collected on the frame of the colour sensor, so limiting the downwelling light. It was not possible to remove the scum, so that for readings after 12:00 the sensor was partially obscured by debris on the surface.

The water samples were returned to the laboratory and analysed. Although enough water was collected for triplicate samples of 1 l for SPM, the concentrations were too high for water to pass through the filter - consequently, the volume was decreased to

250 ml. The yellow substance was transported in dark glass bottles and then filtered and measured with the Diode-Array spectrophotometer. The filters for chlorophyll were frozen and analysed three weeks later when the fluorometer was available.

A second survey was undertaken on 26 March 1996, in which the profiling transmissometer was used, plus the PRR-600 - profiling so that attenuation could be calculated. Half hourly samples were taken between 14:00 and 16:00, on the flood tide. However, as the survey was done six days after spring tides the change in salinity was not observed, and the increase in water height was due to the backing of river water. The same laboratory techniques were used as above, except that the pigments were quantified immediately using the spectrophotometer rather than the fluorometer. Also, cell spectra were taken with and without a diffuser to study the particle scattering effects.

4.8 LLYN CWMYSTRADLLYN SURVEY 1995/1996

A mountain lake provided further contrast to the marine surveys. This was expected to have little particulate matter, but some dissolved organics. Dwr Cymru kindly gave permission for surveys in Llyn Cwmystradllyn, a reservoir on the southern flank of Moel Hebog, Snowdonia (Fig. 4.10). Readings were taken from a tower situated 5 m into the reservoir accessed from the dam by a small bridge. Instruments were deployed from this walkway.

The same methods were employed as for the first Conwy survey, with the exception of the CS23. This profiled over 4 m, to calculate the vertical attenuation. On the first survey, 2 August 1995, the transmissometer was deployed but did not work, so there are no beam attenuation values.

Due to the lack of particulate material, over 1 l of water was required for SPM concentrations, limiting the analysis to duplicates rather than triplicates. The chlorophyll filters were frozen until 26 August when the pigment was extracted.

Once again, a second survey was undertaken, on 31 March 1996, following the same

structure as the second Conwy survey. As the water mass does not change in the lake on an hourly timescale, the instrument was turned upside-down to allow comparison between downwelling irradiance and radiance.

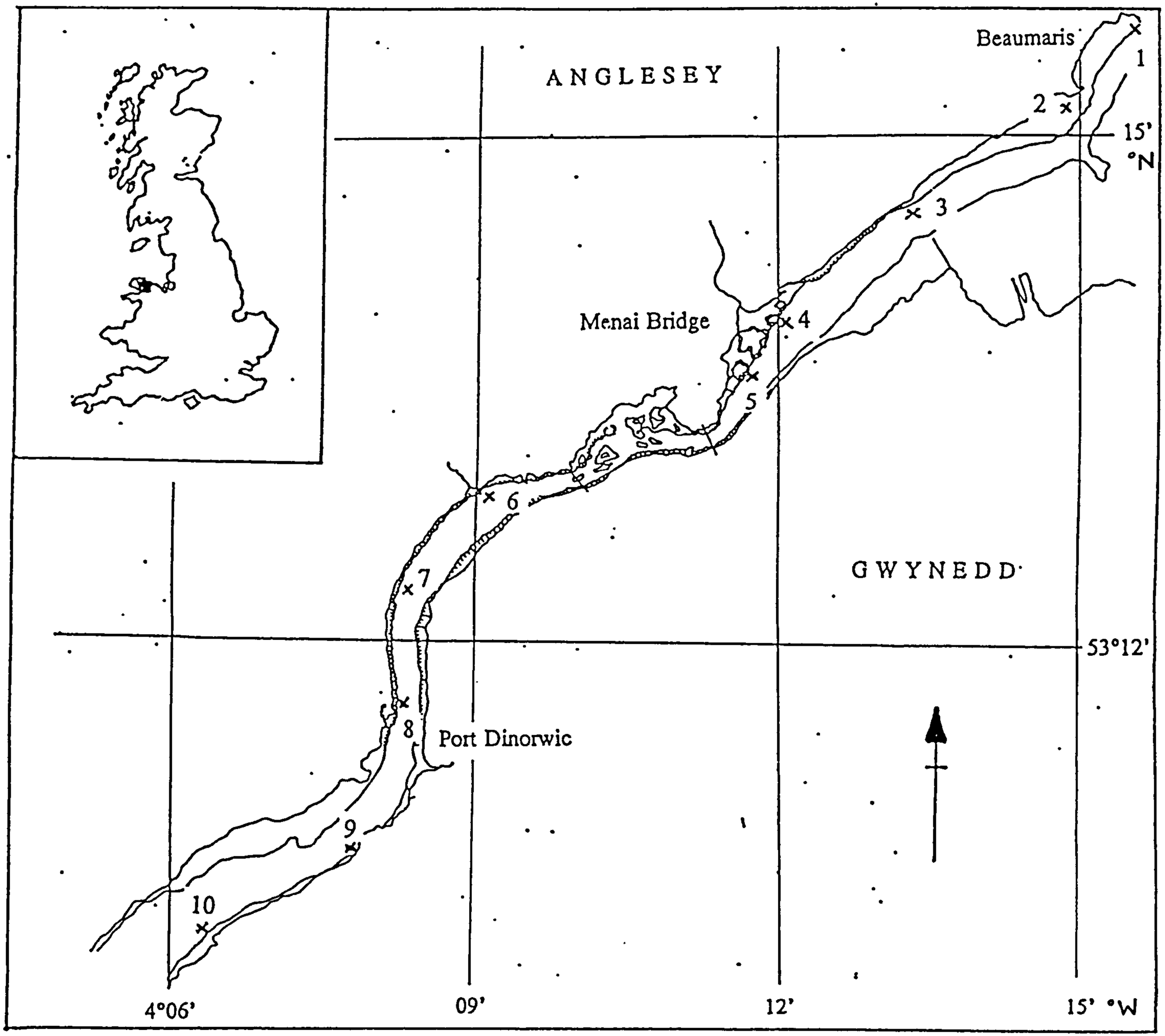

Figure 4.1 Menai Strait, showing 10 sites for survey 1993-1994

Figure 4.2 Profile in Menai Strait 31/03/94

a) Transmittance
b) Salinity
c) Temperature

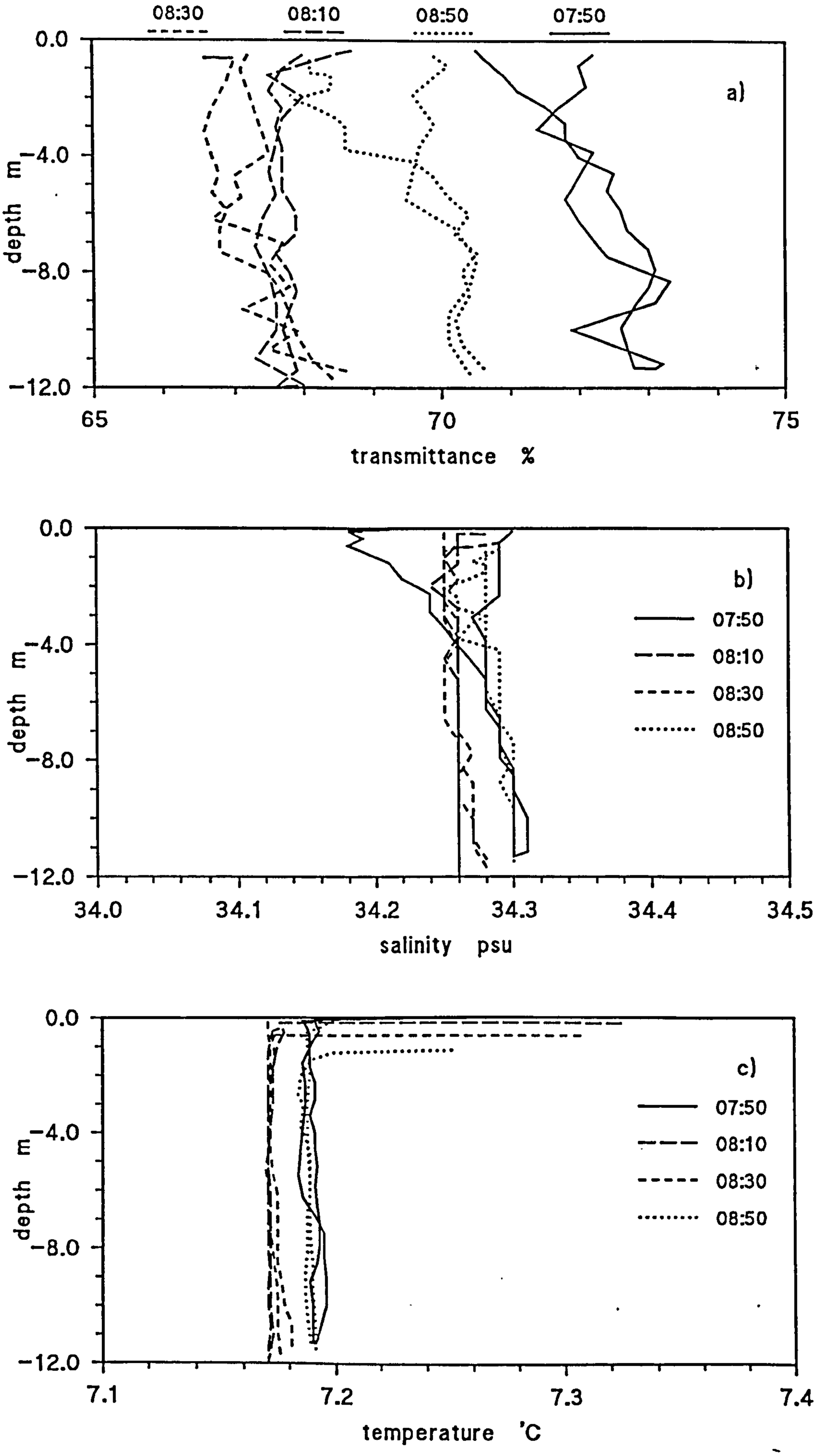
08:30
08:10
08:50
07:50
a)
0.0
−4.0
−8.0
−12.0
depth m
65
70
75
transmittance %
b)
07:50
08:10
08:30
08:50
34.0
34.1
34.2
34.3
34.4
34.5
salinity psu
c)
07:50
08:10
08:30
08:50
7.1
7.2
7.3
7.4
temperature 'C

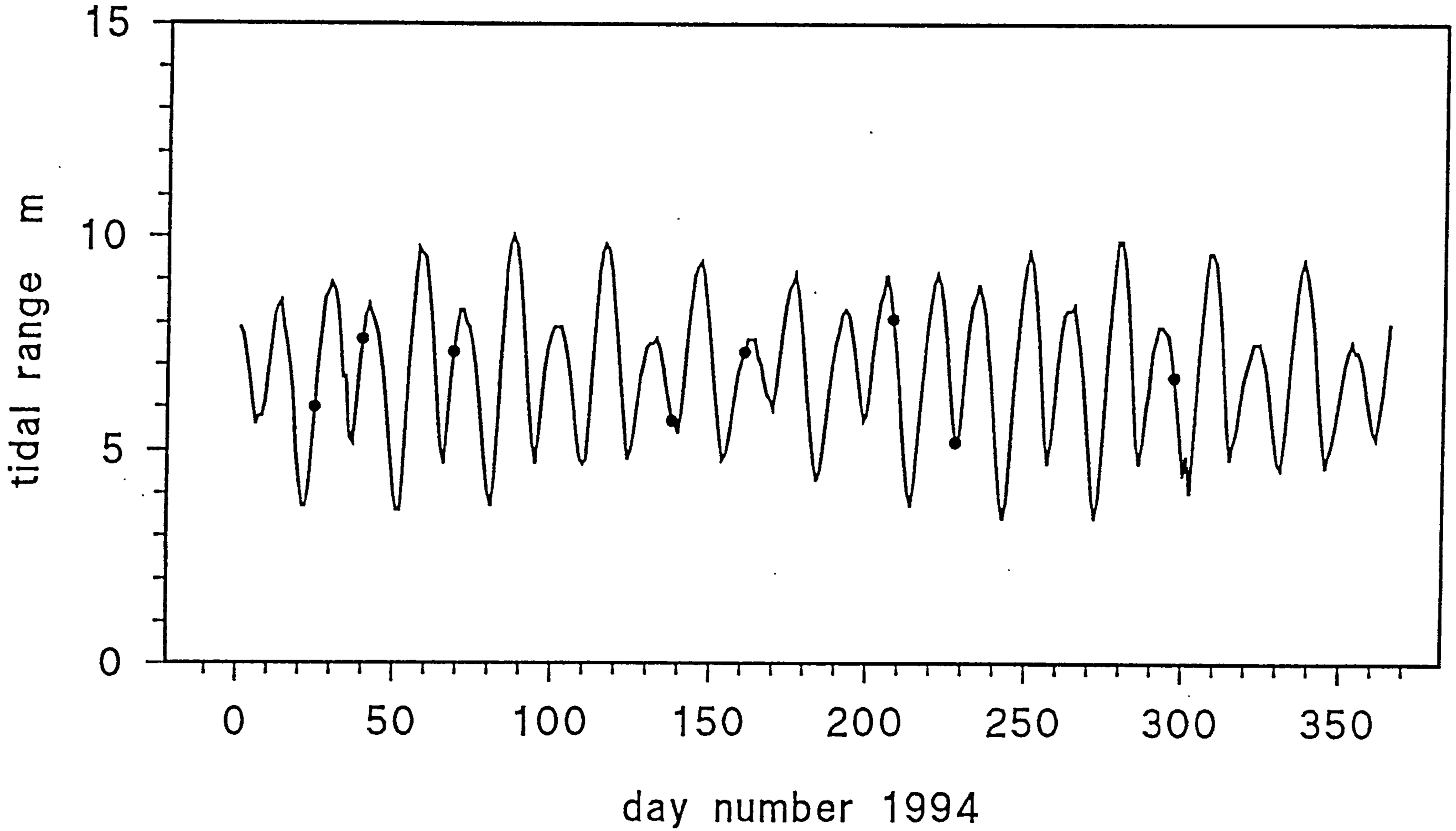

Figure 4.3 Tidal curve, showing spring-neap cycles for Menai Strait with dates of surveys

Figure 4.4 Tidal curve for Pier Surveys

a) July 1994

b) August 1995

The dots show times at which daily samples were taken.

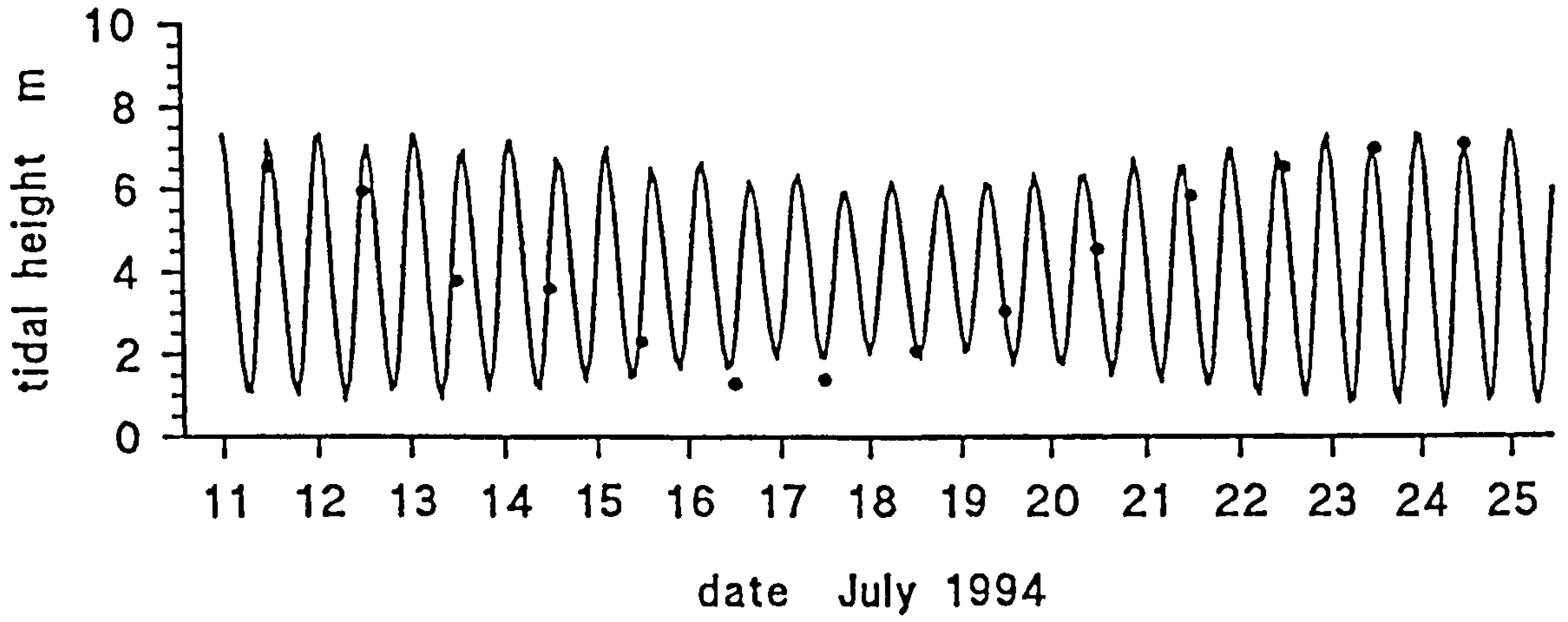
tidal height m
10
8
6
4
2
0
11 12 13 14 15 16 17 18 19 20 21 22 23 24 25
date July 1994

tidal height m
10
8
6
4
2
0
233 235 237 239 241 243 245 247
day number [21 August - 4 September 1995]

Figure 4.5 Clyde Sea and surrounding area, Scotland

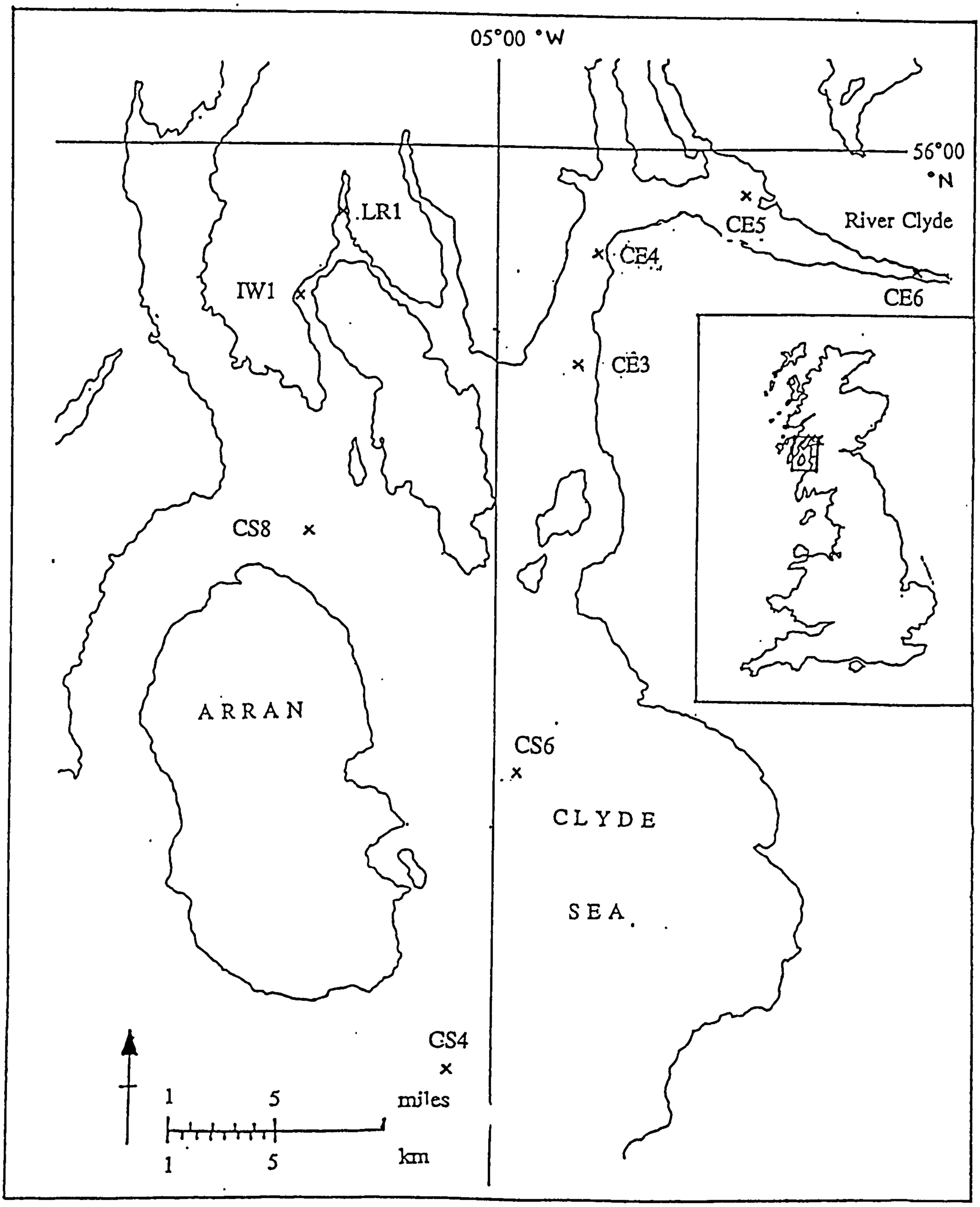
05°00 °W
56°00 °N
LR1
IW1
CS8
ARRAN
CS6
CLYDE
SEA
CS4
CE5
River Clyde
CE4
CE6
CE3
1 5 miles
1 5 km

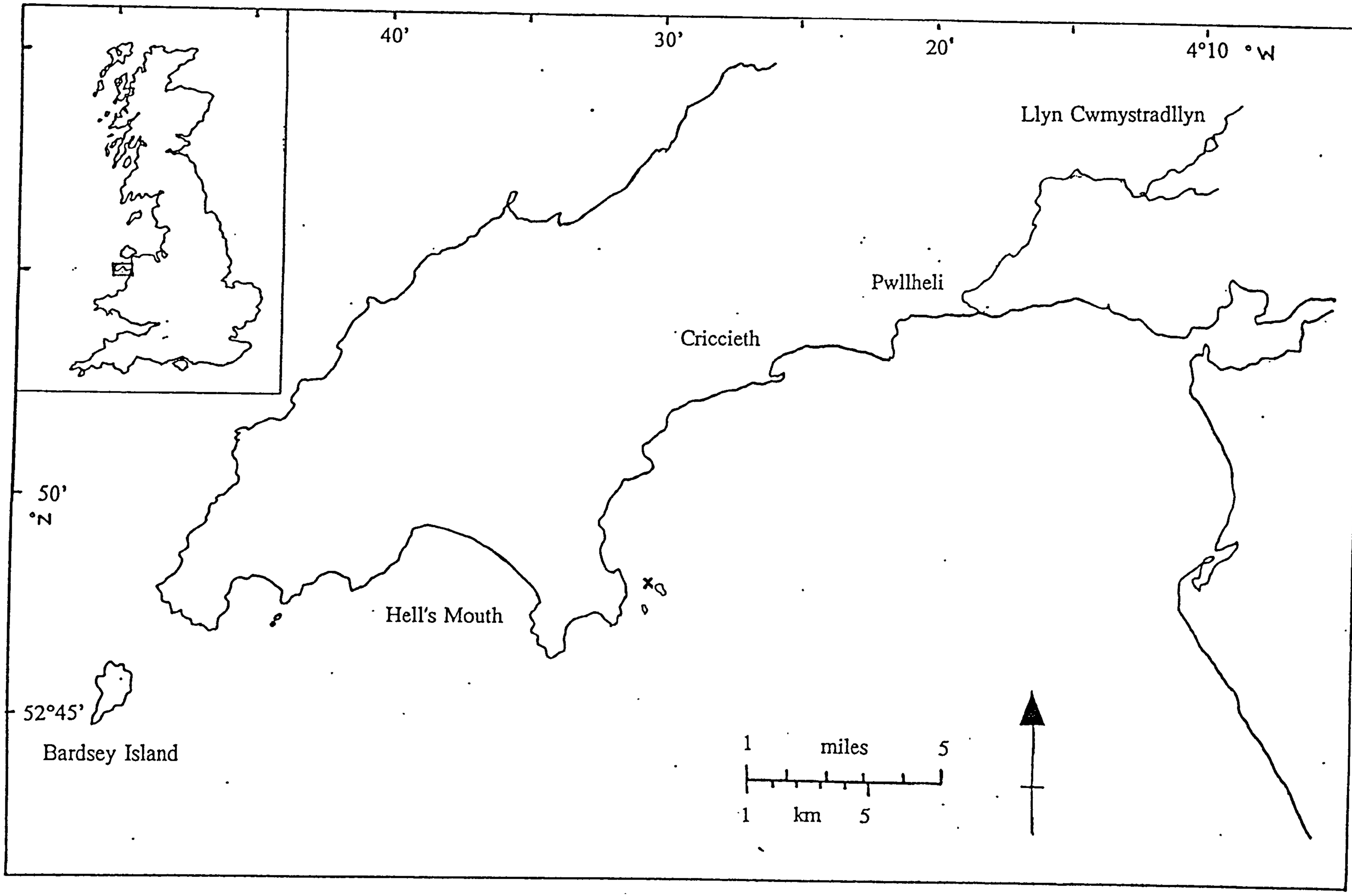

Figure 4.6 Cardigan Bay and Cwmystradllyn, North Wales

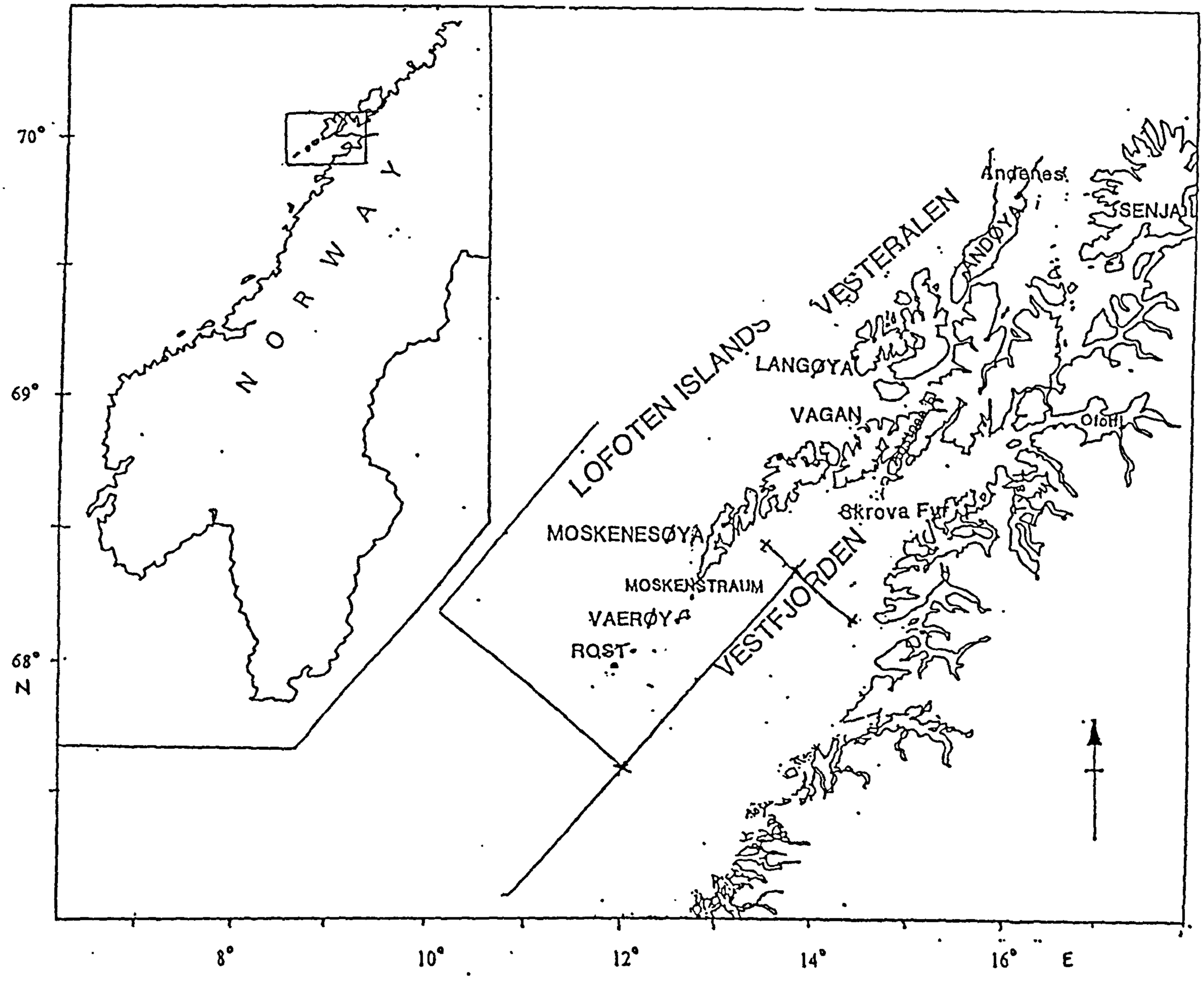

Figure 4.7 Vestfjorden survey route

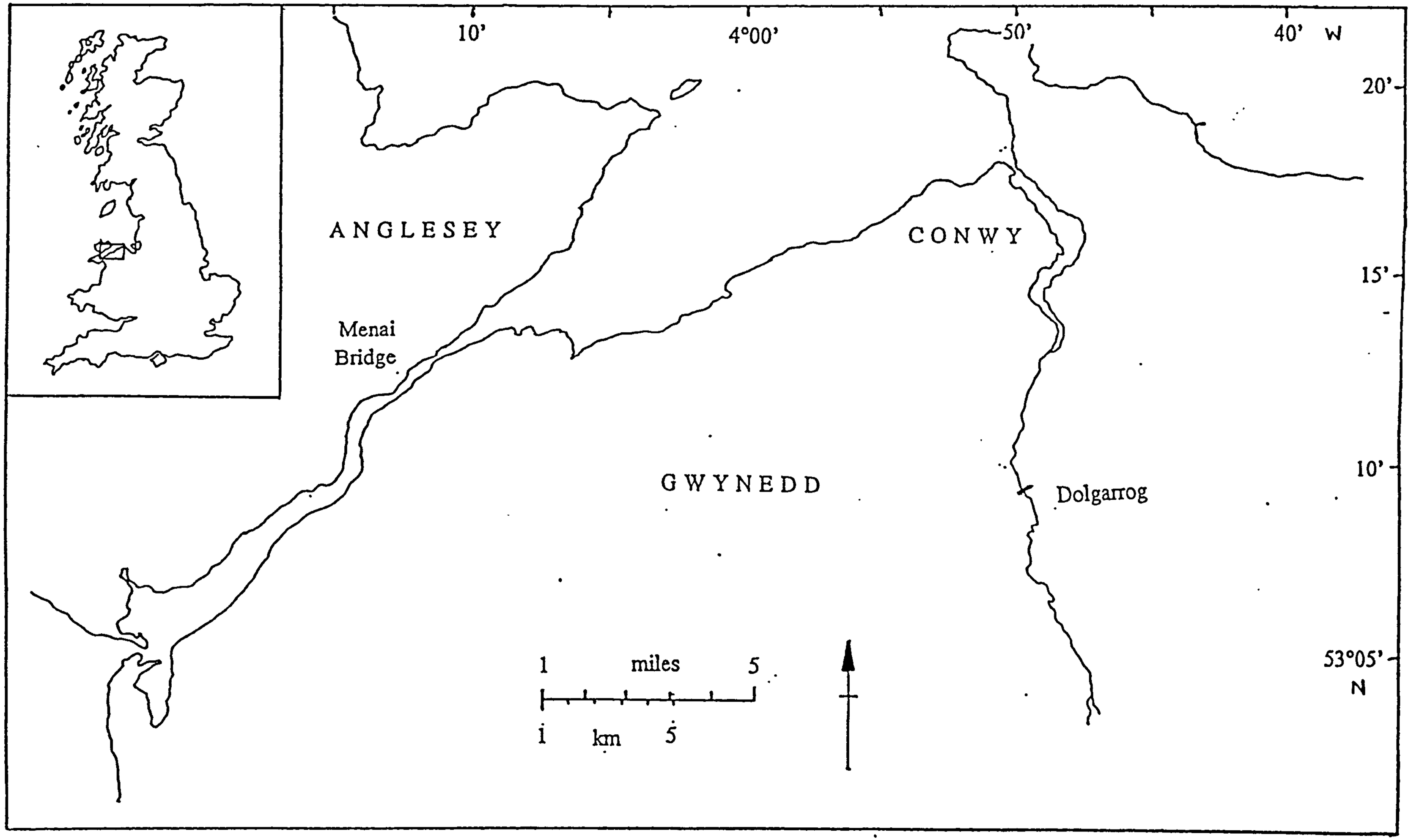

Figure 4.8 Conwy Estuary and River

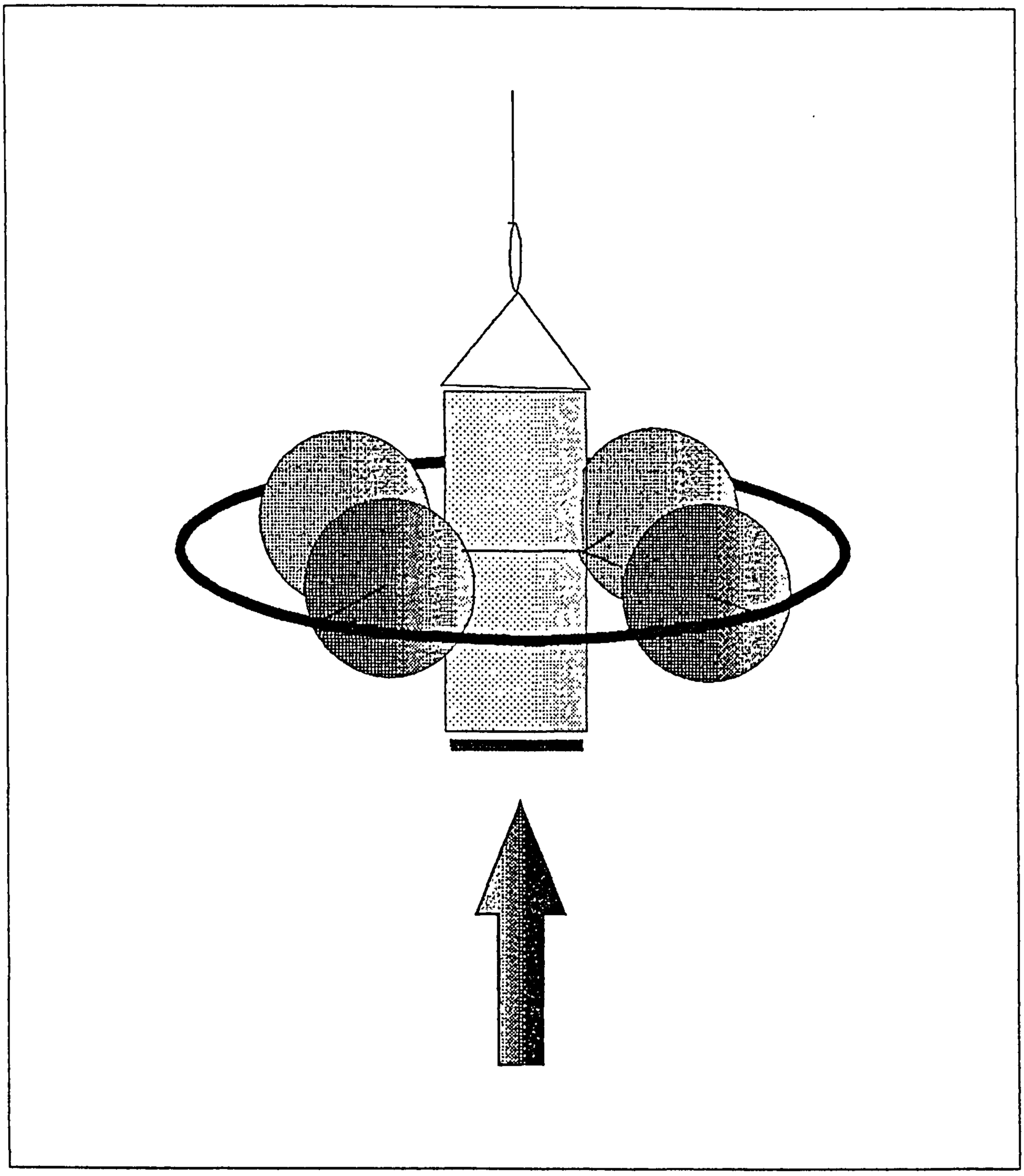

Figure 4.9 Colour sensor with floats

5. TECHNIQUES

5.1 FIELD MEASUREMENTS

In situ measurements were made of diffuse attenuation K, reflectance R and beam attenuation c. These were taken so that Kirk's (1985) algorithms could be used to derive absorption and scattering which could then be compared with the laboratory measurements of absorption. In each survey, K and R were both measured with one of the following instruments: IRM1, the CS instruments, the Satlantic or the PRR600. There were fewer measurements of c as the transmissometer was not deployed in all surveys. Methods for data collection and processing are given below.

5.1.1 Diffuse attenuation

Before deployment a dark reading was taken with each light sensor - the cap remained on, or the sensor was covered to completely exclude the light, so that the background reading of the instrument could be determined. Then, light levels were measured at different depths in the water column to calculate K. The UCNW instruments required up to 2 minutes at each depth to record three readings which could then be averaged for a representative value. The dark readings were subtracted from this measurement to compensate for the baseline value. Simultaneous measurements were taken of the ambient light level which were used to adjust for fluctuations in incident radiation.

The resultant light level ($E(z)$) at each depth was thus:

$$E(z) = \frac{S(z) - S(d)}{S(0^+)}$$

where S() is the sensor reading and z, d and 0^+ represent depth, dark and ambient (surface) readings respectively

As these instruments had a relative calibration rather than an absolute calibration, the value E cannot be given units, but indicates the relative change in irradiance. Therefore K can be calculated:

$$K = -\frac{\ln E_0 - \ln E}{z}$$

The Satlantic and PRR600 can be programmed to take readings more frequently (*e.g.* one per second) and can therefore profile quickly, giving a more continuous record of the light field and thus, a more accurate calculation of *K*. With all instruments, it is necessary to measure the ambient light in order to distinguish between variations due to the loss within the water and differences in incident radiation.

Measurements were taken on the sunny side of the ship/platform to minimise shading. This is particularly important from small boats where the shadow of the boat lowers light levels near the surface, but has no effect at greater depths, resulting in an apparent increase in irradiance with depth. The instrument will create self-shading, but as this is assumed constant throughout, the attenuation measurement will not be affected.

K was calculated as above, being the slope of the natural log of the subsurface measurements, as shown in Fig. 5.1. All values were divided by the relevant ambient reading when taken, but this was not always possible due to the use of different sensors. The near-surface measurements were excluded (for example the top 1.5 m) to prevent bias caused by noisy values due to surface wave disturbance, Fig. 5.2. The exclusion of data points was decided by inspecting the data and judging where error would be added. It was also important not to include readings close to the dark current of the instrument as these lower the attenuation values. These were omitted within the analysis program by setting a limit above the dark readings - this value was 15 for the IRM1 and 50 for the Satlantic and PRR-600.

When the sensor is pointing upwards the downwelling attenuation (K_d) is measured, therefore upwelling (K_u) is recorded by turning the instrument over. *K* is similar for upwelling and downwelling irradiance although the level of light is different. Fig. 5.3 illustrates this in the **Pier Survey 1995.**

The upwelling readings include all scattered and reflected light from objects at a greater depth, it is therefore important to calculate K_u where the influence of the bed or any subsurface structures is negligible - ideally, the depth of water should be greater than 6 attenuation depths [6*($1/K_d$) m (Aiken *et al*, 1995)].

The upwelling signal is also affected by self shading from the instrument itself. It is assumed that self-shading will be constant throughout the profile. However, the effect would be more pronounced near the surface, particularly in turbid water where the upwelling signal is greater due to the high number of particles scattering light back towards the surface. Consequently, the lack of downwelling light due to the sensor would significantly reduce the backscattered light upwards. This is particularly important for reflectance values.

5.1.2 Reflectance

Reflectance values were taken to be the ratio between upwelling and downwelling irradiance immediately below the surface:

$$R = \frac{E_{u0}}{E_{d0}}$$

as discussed in §2.2.2.

Light levels could not be accurately measured at the air-sea interface, so that upward and downward irradiance values were extrapolated from deeper measurements using K as calculated in §5.1.1. The ratio between the extrapolated value for the upwelling and for the downwelling irradiance was then used as reflectance at the surface.

For all readings with IRM1, the downward light was measured at several depths then the instrument was brought to the surface and turned over to measure upward light. This meant there was a slight delay between upward and downward profiles, and an allowance was included for the distance between the light sensor and the depth sensor.

Both the Satlantic and the PRR600 measured downwelling irradiance and upwelling

radiance L_u. These are designed to correspond to satellite observations, but cannot be used to directly calculate subsurface irradiance reflectance, as discussed in §2.2.2. To avoid the unknown conversion factor, the instruments were used in their normal orientation and then inverted to measure upwelling irradiance and downwelling radiance. Although this enables the irradiance reflectance to be calculated, the upwelling values are close to the dark readings of the instrument and so may not be sensitive to changes. Unfortunately, the stronger downwelling radiance values saturated the Satlantic sensor in the surface 5 m. This problem was not encountered with the UCNW instruments which are tolerant to a wider range of irradiance levels.

Above the water surface the Spectron was used to measure reflectance. This is calculated as the ratio between the signal from the surface of the water and the ambient cosine reading. Initially, the surface value was used, holding the Spectron 1 m above the water, but this reading included a high proportion of interface reflectance, which dominated the signal emitted from the water. To eliminate this extra reflectance, the measurement was taken through a black pipe, covered to exlude sunlight, with one end held ~5 cm below the surface (Fig. 5.4). This method excludes the signal from the interface, measuring the upwelling signal within the water. As the pipe was 34 cm long, and the field of view was 15° from nadir, only ~30 % of the signal was from the water; therefore, readings taken through the pipe must be multiplied by 3.33 to calculate the reflectance. Subsequently, measurements with and without the pipe were taken for comparison. The relationship between with and without pipe (see Appendix IV) has thus been calculated as:

$$R_{[no\ pipe]} = 0.36\ R_{[pipe]}$$

5.1.3 Beam attenuation

Two types of transmissometer were used to measure *c*: a profiling instrument in **Conwy** and in the **Menai Strait**, and a fixed instrument in the **Pier Surveys**. Both dark and clear readings must be taken, V_{min} and V_{max} respectively, so that the voltages can be converted to transmittance (T):

$$T = \frac{V - V_{min}}{V_{max} - V_{min}}$$

The beam attenuation is then calculated:

$$c = \frac{\ln T}{l} = a + b$$

where l is the pathlength of the instrument, and a and b are absorption and scattering respectively

It was observed in the **1995 Pier Survey** that when the transmissometer was exposed at low tide, the reading went to V_{min} instead of V_{max} as expected. This was due to water collecting on the ledge in front of the light source, and deflecting the beam away from the receptor (Fig. 5.5). This suggests that transmissometers should always be deployed in a vertical position when there is a possibility of exposure, as regular "clear" readings give a useful gauge of the degree of fouling each day.

5.1.4 Secchi Depth

Secchi disk readings were taken in most surveys. The Secchi depth z_{SD} is that at which the disk can no longer be seen when lowered into the water. At this point, the depth is gauged by markers on the rope. This parameter indicates the overall clarity, but the recorded depth is subjective, and can change with the viewer; it is also dependent on the reflectance and surface area of the disk (Edmondsen, 1980), the amount of shading and the state of the water surface (Tyler, 1968). However, it remains a workable estimate of clarity.

5.2 LABORATORY

Laboratory analysis of the water samples was performed on the day of collection whenever possible. When delay was unavoidable, samples were stored in black bags and refrigerated overnight, or stored in a freezer for longer periods of time. This is not considered to affect the results (Tett, pers. comm.).

5.2.1 Pigment extraction and determination

For each site, three replicates of 250 ml volume were filtered through Whatman GF/F filters (47 mm diam.) having shaken the samples to ensure they were well mixed. The filters were then immersed in 8 ml of 90% acetone in individual plastic centrifuge tubes, and refrigerated, in a black bag, for a minimum of 19 hours (usually 36) to ensure all pigment was extracted. If there was a delay in analysis the filters were desiccated, using silica crystals, and frozen before acetone was added. The tubes were centrifuged at 3000 rpm for 15 minutes, and the solution poured into a glass cell (rinsed with acetone), in which the fluorescence was measured with the Turner Fluorometer (f_o). Two or three drops of 2N (8% by volume concentrated hydrochloric acid) were added for the determination of phaeopigments, and the fluorescence measured again (f_a).

The following algorithms were used to convert the fluorescences to pigment concentrations (Tett, 1990):

$$C = K_f(f_o - f_a).v_e / V \qquad mgm^{-3}$$

$$Ph = K_f(H_f f_a - f_o).v_e / V \qquad mgm^{-3}$$

where K_f and H_f are instrument specific constants, v_e is extract volume and V is the volume of water filtered

For the surveys in 1996, the fluorometer was not available so the pigments were measured with the spectrophotometer. The pigments were extracted in the same way as above, then the solution was poured into a 10 mm cuvette and the spectrum measured against a blank of pure acetone. Drops of acid were added and the spectrum taken again, against a blank of acidified acetone.

The appropriate algorithms for this method are (Parsons *et al*, 1984):

$$\begin{aligned} Chl\text{-}a &= 11.85\,A_{664} - 1.54\,A_{647} - 0.08\,A_{630} \\ Chl\text{-}b &= 21.03\,A_{647} - 5.43\,A_{664} - 2.66\,A_{630} \\ Chl\text{-}c &= 24.52\,A_{630} - 1.67A_{664} - 7.60\,A_{647} \end{aligned}$$

where A is the absorbance at the subscript wavelength minus the absorbance at 750 nm

The chlorophyll concentrations are then calculated:

$$C\ (mg\ Chl\ m^{-3}) \quad = \quad \frac{Chl\ *\ v}{V\ *\ l}$$

where v is the volume of acetone used in ml, V is the volume of seawater in litres and l is the length of the cuvette in cm

Phaeopigments can then be calculated:

$$Ph \quad = \quad \frac{26.7\,[1.7\,(665_a)\ -\ (665_o)]\ *\ v}{V\ *\ l}$$

where the subscripts o and a represent the reading before and after the addition of acid, respectively, absorbances corrected to 750 nm

When in **Vestfjorden,** it was not possible to follow either of these procedures. A litre of water was filtered initially, and the pigments extracted in acetone as before. After the tubes were taken out of the fridge, the filter/acetone was transferred to a clean syringe and the liquid forced through a Whatman GF/C filter. The filtrate was put in a 10 mm cuvette and scanned between 350 and 750 nm in the UV-1201 Spectrophotometer. This was compared with a blank of pure acetone. HCl acid was again added to determine phaeopigments.

5.2.2 Yellow substance

The absorbance of the filtrate (from the above filtration, using GF/F filters) was measured between 300 and 800 nm in a spectrophotometer, against a blank of distilled water. 100 mm cells were necessary to detect the dissolved organic matter/humic acids. Membrane filters could be used instead of GF/F filters to eliminate smaller particles but a comparison showed that GF/F filters were adequate for the levels present during the summer (see Appendix V). A greater difference would be observed during the winter but GF/F filters were nevertheless used for consistency. This also meant that all absorption was measured whereas if membrane (0.2 μm) filters were used, the absorption by particles between 0.2 μm and 0.7 μm would have been omitted. However, when comparing these data with other surveys (some of which use GF/F, and some membrane filters) the particular definition of "yellow substance" must

be considered.

The absorbance value at 750 nm (a750) was taken to represent scattering. This is necessary as water and inorganic particles are the only significant absorbers at 750 nm (Gallegos *et al*, 1990) - the effect of water is removed by use of the blank, and the particles have been removed by the filtering so that any signal is due to scattering by particles small enough to pass through the filter. Thus, a750 is subtracted across the spectrum (assuming the effect of scattering is uniform) before converting absorbance into absorption. The conversion algorithm used to obtain the absorption coefficient from the measured absorbance was:

$$a(\lambda) = \frac{\ln(10).A(\lambda)}{l}$$

where $a(\lambda)$ is absorption, $A(\lambda)$ is absorbance and l is the cell length in m

Yellow substance was then quantified by the absorption value at 440 nm (g440).

5.2.3 Seston

One litre of well mixed water from each site was filtered through pre-rinsed, -ashed and -weighed GF/F filters, followed by 300-500 ml distilled water to remove any salt. The amount of water for rinsing was based upon a comparison of measurements using different volumes of water, and taking the volume which resulted in the lowest weight (Fig. 5.6). The filters were dried overnight at 80°C, and weighed with the same balance that was used initially. This gave the total seston weight and thus concentration. Filters were then furnaced at 500°C for three hours and re-weighed to quantify inorganic particles (Parsons *et al*, 1984).

For several sites, the water was filtered through two filters, one on top of the other, the bottom filter acting as a blank. This underwent the same drying and weighing techniques as the top filter to assess errors within the method. The final weights from these were variable, and although usually below 0.4mg the highest value was 5.5 mg. In general, this error was 10% of the total value; for example, during the **July Pier Survey**, between 16 and 19 July, the total seston on the "top" filters weighed 3.14 mg,

3.76 mg, 3.99 mg and 3.41 mg while the "blank" filters weighed 0.26 mg, 0.48 mg, 0.58 mg and 0.37 mg respectively.

The addition of an extra filter below another meant that the filters were handled more and could lead to greater error. It is therefore preferable to do triplicate samples with a greater volume of water and gauge any measurements error from the variability between these, so using the average for the final value. This technique was used in the later surveys, **Conwy Estuary** and **Llyn Cwmystradllyn**, when three 1 l replicates were filtered for seston. The average value from these gives a more accurate concentration as well as gauging natural variability.

5.2.4 Spectra

Spectra of water samples and particles on filters were taken, using the Hewlett Packard Diode-Array spectrophotometer for **November 1993-June 1994**, and thereafter with the SHIMADZU UV-1201. It was found that there was less "noise" in the SHIMADZU spectra.

In **November 1993**, the range taken was 400-700 nm, but this was extended to 300-800 nm to observe variations due to organics (Bricaud *et al*, 1981) in the ultra-violet and scattering within the near infra-red.

The absorbance spectra of liquids were taken in a 100 mm glass cell, with a distilled water blank. The scan was downloaded onto computer disk. To convert the absorbance measured by the spectrophotometer to absorption, the procedure previously described for yellow substance was followed. Both the spectra of the filtrate and the untreated water samples were measured in this way.

Particles were scanned on GF/F filters (having been filtered as above). These were saturated with distilled water and placed on a glass slide, which was then positioned over the detector (see Appendix VI for a comparison between the filter over detector and source), and scanned between 300 and 800 nm. A clean filter saturated with distilled water was used as a blank. Spectra were taken of 'dried' and furnaced

particles for all surveys, and fresh filters in **January 1994, June 1994,** and the **Menai Pier Surveys.** The absorption coefficient was then calculated:

$$a(\lambda) = \frac{\ln(10).A(\lambda)}{V / area}$$

where V is the volume of water filtered and area is the area of the filter which is covered with particles

Various pathlength amplification factors, as discussed in §2.3.1, were applied to the measurements and then compared.

5.3 SUMMARY

The measurements were thus split into two distinct categories - the observation of apparent properties *in situ* and inherent properties in the laboratory. Consequently, in the field the upwelling and downwelling diffuse attenuation was measured, and then used to calculate the irradiance reflectance at the surface. In some instances, beam attenuation was also measured. Water samples were then taken back to the laboratory in order to measure the spectral absorption due to the water itself, the yellow substance and the particulates.

In the field, error was added by the time lag between the measurement of upwelling and downwelling attenuation, plus instrument shading. In the laboratory, the pathlength amplification factor present in filter measurements added uncertainty to the value of absorption, while solutions allowed particles to settle. To enable the comparison between the field and laboratory measurements, inherent-apparent relationships have been used which were developed by Kirk (1985), but due to the large uncetainties in the applicability of these equations more general relationships were also used, plus various values for the pathlength amplification factor including the variation calculated by Cleveland and Weidemann (1993) and a constant value of 2.

These adjustments were performed to all values to identify if the agreement between the *in situ* and laboratory measurements was improved when a particular combination was used, so confirming the appropriate corrections for that survey.

Figure 5.1 Diffuse attenuation: slope of ln(irradiance) at 555 nm

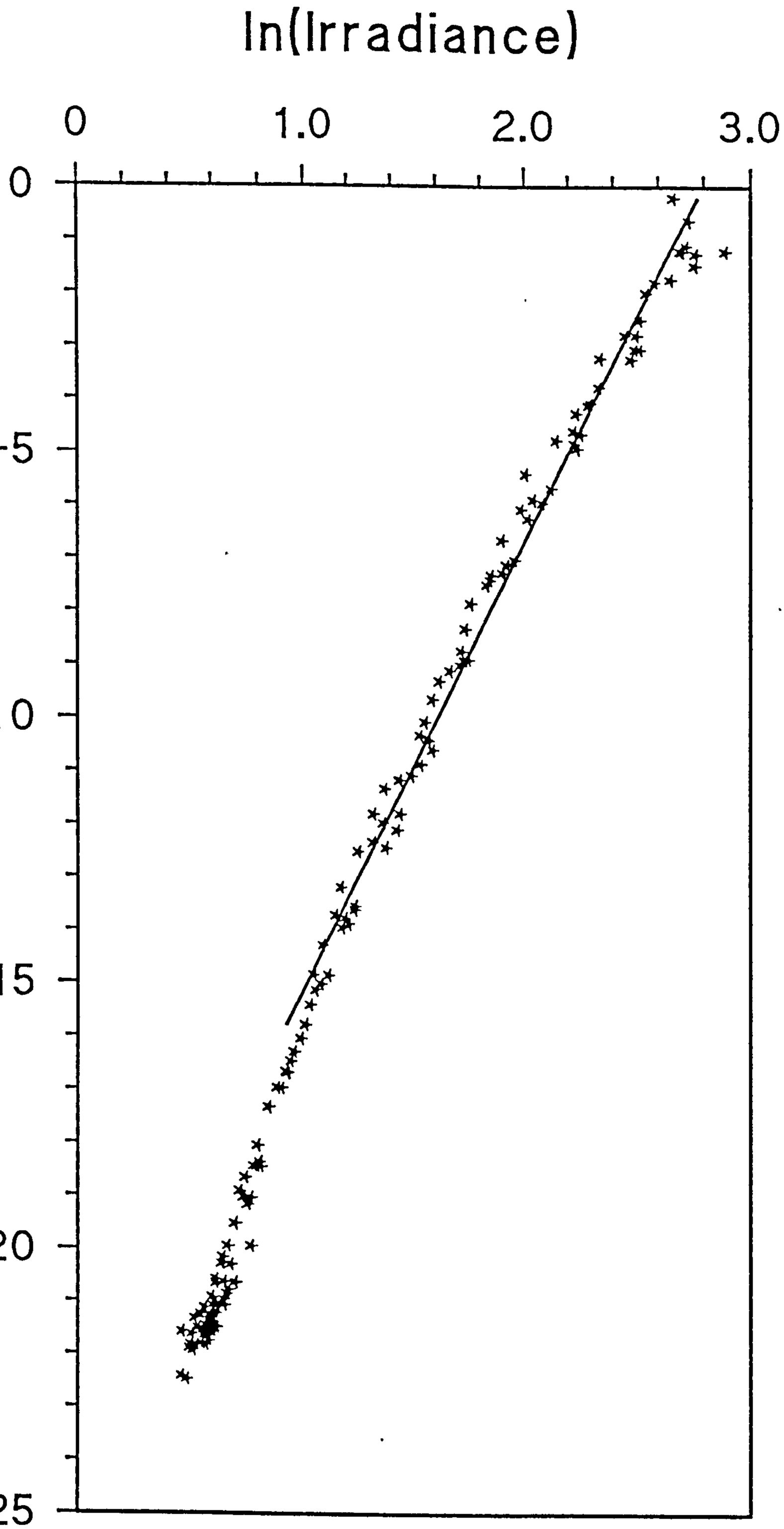
ln(Irradiance)
0
1.0
2.0
3.0
0
−5
−10
−15
−20
−25
depth m

Figure 5.2 Noise near surface in irradiance profile at 555 nm (AMB95)

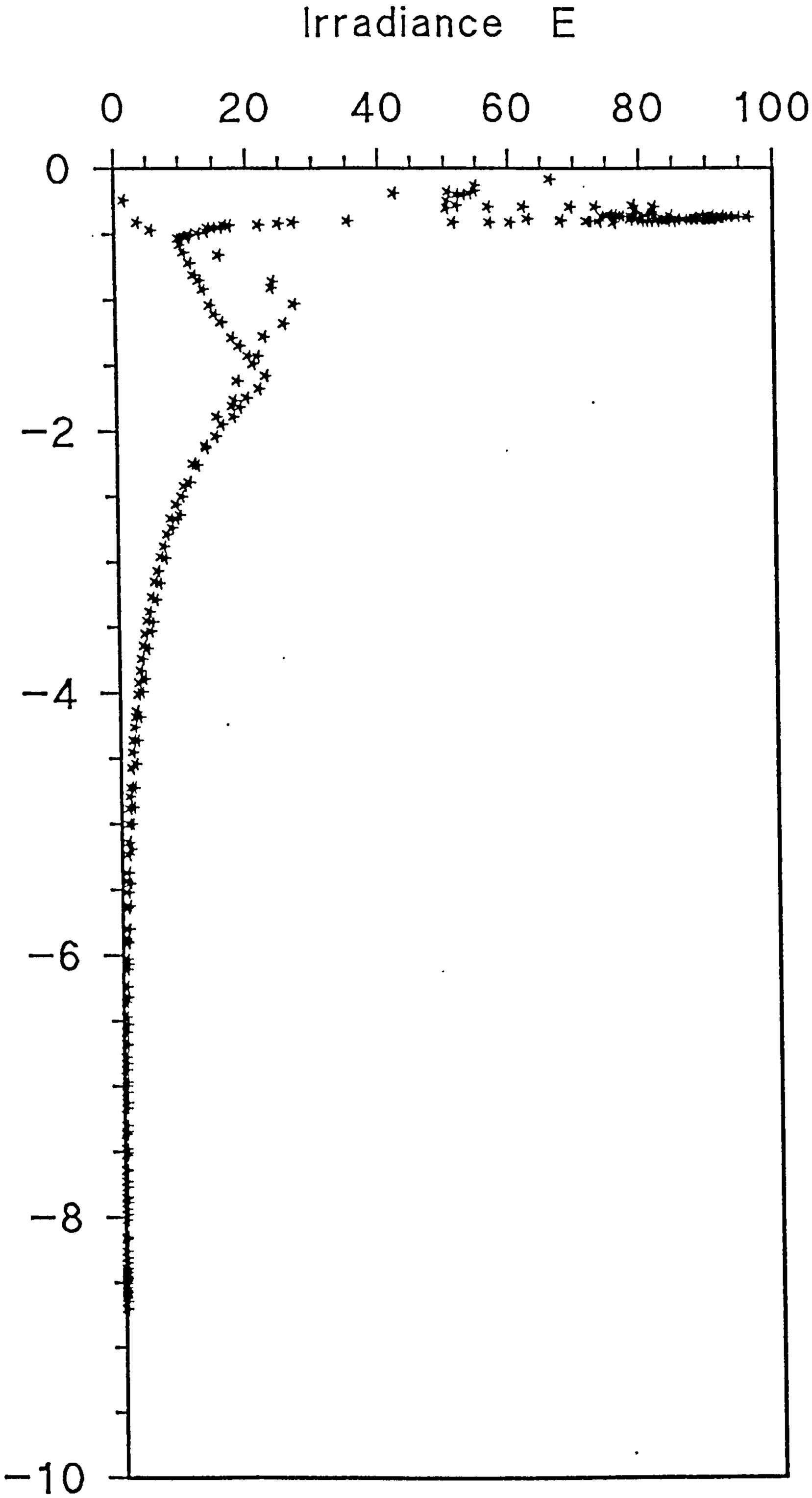
Irradiance E
0
20
40
60
80
100
0
−2
−4
−6
−8
−10
depth · m

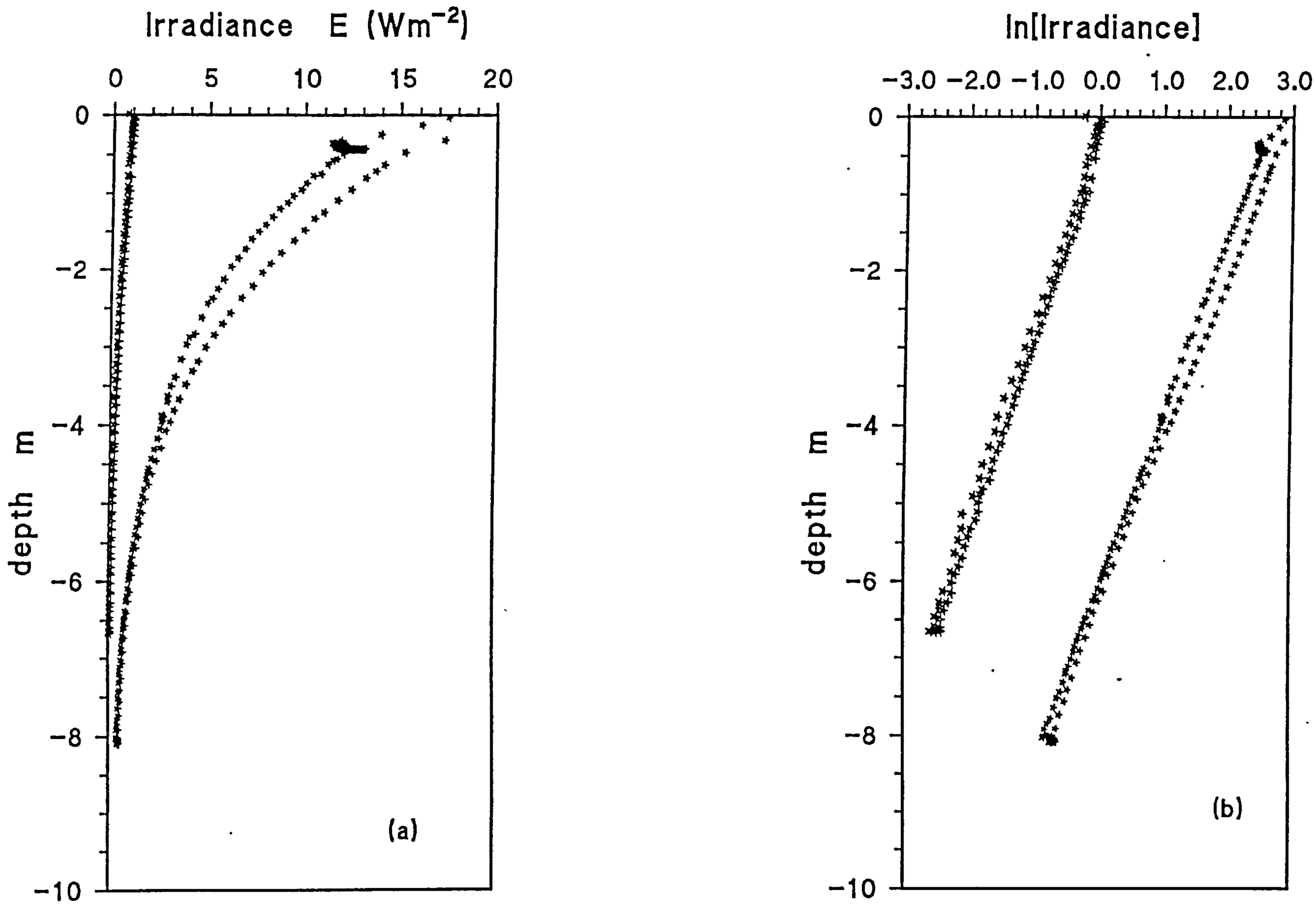

Figure 5.3 Upwelling and downwelling irradiance (a) at 555 nm, with corresponding ln values (b) to calculate K

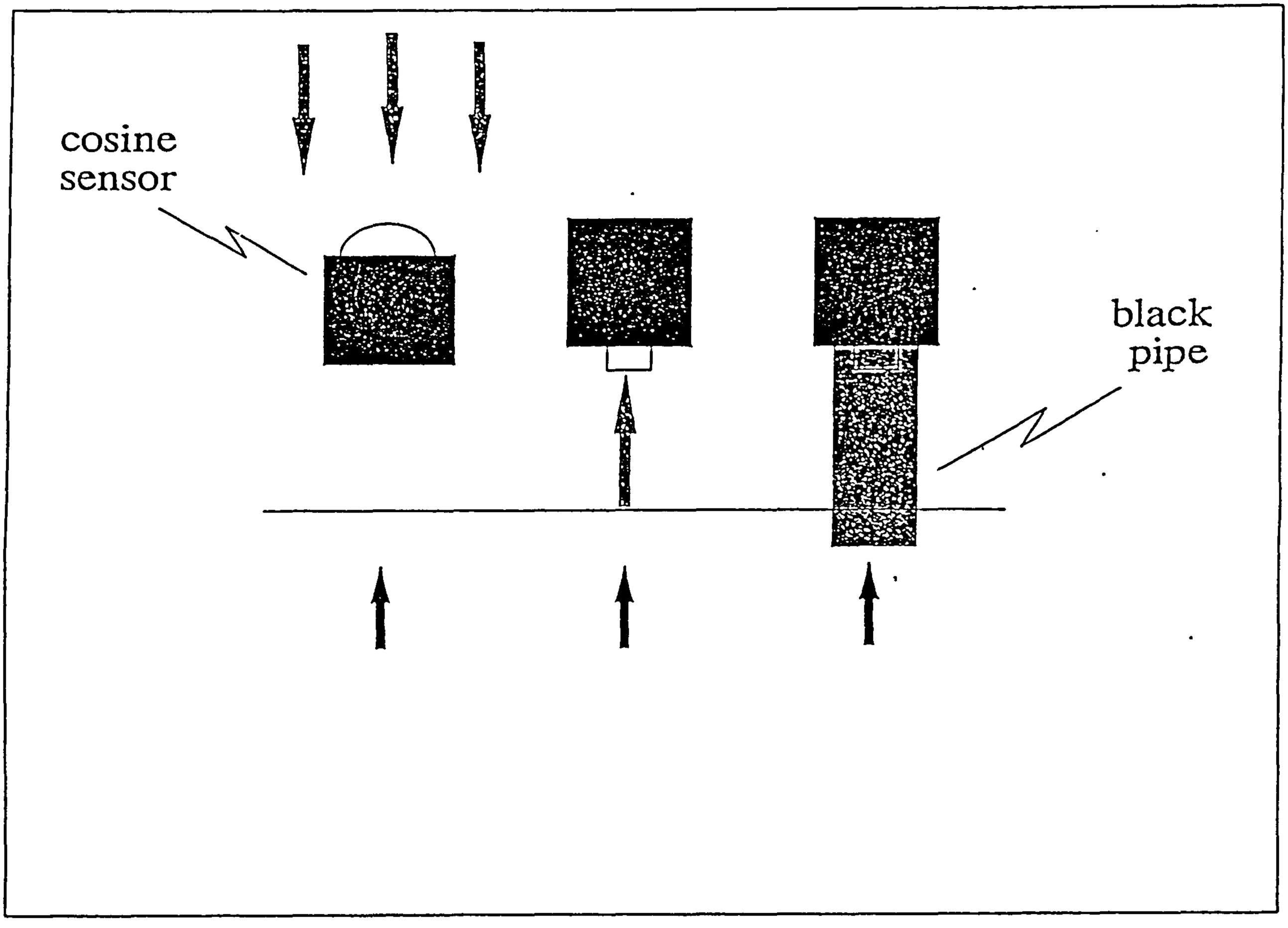

Figure 5.4 Schematic drawing of the Spectron, with cosine receptor

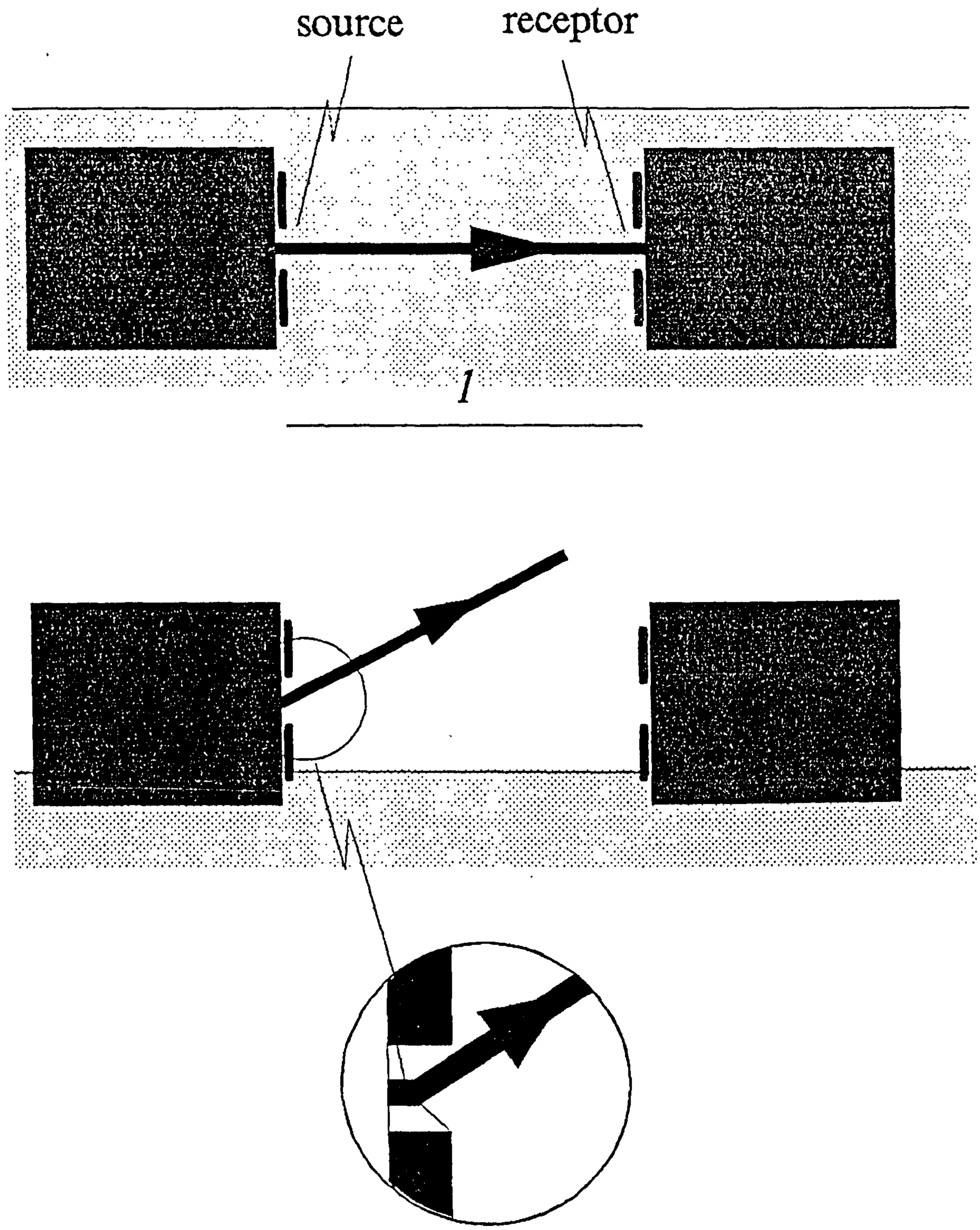

Figure 5.5 Transmissometer, with beam deflected by water on ledge of instrument

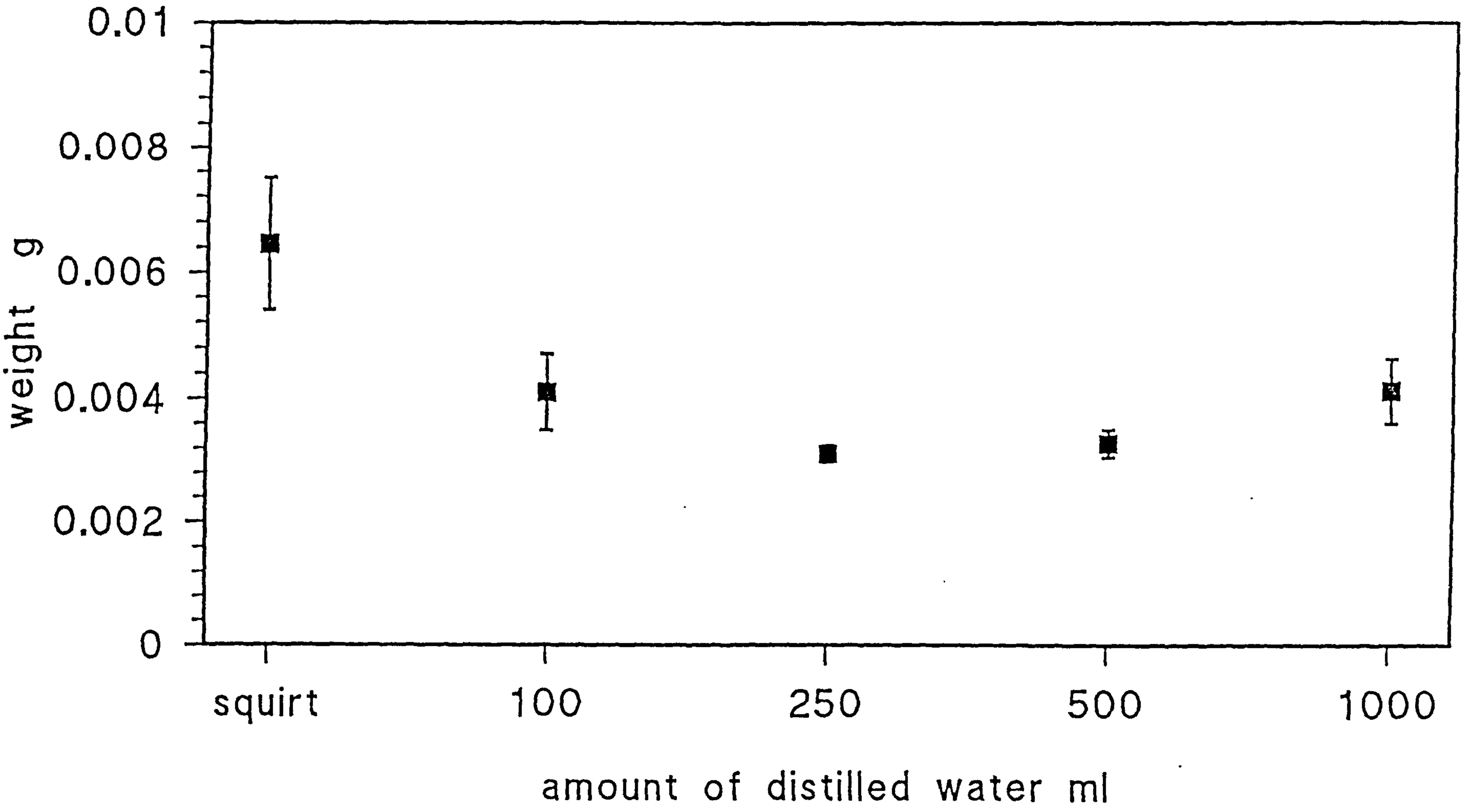

Figure 5.6 Weight when filters rinsed with different volumes of distilled water, n=3 for each point

6. FIELD RESULTS

All results are tabulated in Appendix VII.

6.1 CONSTITUENT CONCENTRATIONS

Both the inorganic solids and the pigment concentrations showed seasonal variation during the **Menai Strait Survey** (Fig. 6.1). Pigment concentration remained below 1.5 mgm^{-3} during the winter, and then peaked in May and June, with 18.7 and 14.1 mgm^{-3} respectively. Conversely, the inorganic particle concentrations were greatest during November and December, reaching 35 mgl^{-1}. This was attributed to increased wind stirring combined with greater mobility of the mineral particles due to decreased binding by organics. Yellow substance did not show any trend in variation, during the **Strait** survey, remaining at ~0.3 m^{-1}.

Vestfjorden had the lowest concentrations, with pigments below 0.2 mgm^{-3} and yellow substance less than 0.35 m^{-1}. The **Clyde Sea** had a similar level of yellow substance (~ 0.35 m^{-1} in 1994) decreasing to 0.089 m^{-1} in 1996 when the membrane technique of measurement was used. Pigment concentrations were still low, varying from 0.8 mgm^{-3} in 1994 to 1.0 mgm^{-3} in 1996, while inorganic concentrations increased from 0.25 mgl^{-1} in 1994 to 2.49 mgl^{-1} in 1996. A significant increase in all constituents was measured within the Clyde Estuary, with maximum concentrations of 1.57 m^{-1} and 4.55 mgl^{-1} for yellow substance and MSS respectively at CE6 (the station furthest inland), and a maximum of 3.15 mgm^{-3} for pigments at CE3.

Yellow substance varied between 0.248 m^{-1} and 0.588 m^{-1} in **Cardigan Bay**, with low pigments (0.09-0.77 mgm^{-3}) but relatively high inorganic concentrations (5.1-9.1 mgl^{-1}). Values for yellow substance were similar in **Llyn Cwmystradllyn** (0.28-0.40 m^{-1}) combined with low pigment and MSS concentrations (1.1-2.2 mgm^{-3} and 1.3-4.0 mgl^{-1} respectively). These concentrations are indicative of the nature of the lake, *i.e.* there is a low contribution from run-off due to the situation in a mountainous area, leading to low levels of particulates and terrestrial humic acid.

In both the **July Pier Survey** and **Loch Striven** a phytoplankton bloom was observed, reaching chlorophyll concentrations of 8.51 and 43.8 mgm^{-3} respectively. The **Loch Striven** data also showed higher values of yellow substance (0.29-0.56 m^{-1}) suggesting that the phytoplankton contributed a detrital component to the humic acids.

In the **August Pier Survey** (1995), the inorganic concentrations followed a spring-neap tidal cycle, being greatest at spring tide (10.25 mgl^{-1}), decreasing to 1.01 mgl^{-1} at neap tide. Although yellow substance varied considerably during this period (0.092-0.405 m^{-1}), the variation did not directly follow the spring-neap cycle.

The highest concentration in all constituents was found in the **Conwy River:** pigments 10.4-56.1 mgm^{-3}, yellow substance 1.7-3.8 m^{-1}, 18-164 mgl^{-1} for TSS, and 12-136 mgl^{-1} for MSS.

6.2 DIFFUSE ATTENUATION

A wide range of K_d values occurred across the various sites (Fig. 6.2). Seasonal variation was again apparent in the **Menai Strait,** resulting in a total range of K_d from 0.4 to 3.5 m^{-1}. **Vestfjorden** was the clearest water body, with values of 0.115-0.272.m^{-1}; this was expected as these sites were in Case 1 waters. However, both the **Cardigan** and **Clyde Sea** results were of a similar magnitude, with K_d less than 0.4 m^{-1} at 443-444 nm. **Loch Striven,** the **Pier Surveys** and the **Strait Survey** all reached higher values, with the upper limit indicating the total amount of seston present (see §5.1.1). Similarly, the maximum value at 440 nm observed in the Clyde Estuary was 2.26 m^{-1} at CE6, corresponding to the higher concentrations of constituents.

The decrease in irradiance observed in **Vestfjorden** illustrates Eqn 2.1 very well, following an exponential curve (Fig. 6.3). The comparison of this decrease across the spectrum shows how the longer wavelengths attenuate faster in clear water (Fig. 6.4).

Fig. 6.5 shows the change in attenuation throughout the year in the **Menai Strait.** The high values in November and December 1993, $1.5 < K_d < 3.5$, decrease through

the spring and summer to K_d ~ 0.5 m^{-1} in August 1994, before increasing in October. The values at 552nm are given in Table 6.1 to show the typical variation at a particular wavelength; as all channels co-varied, these values are representative of the whole spectrum.

Month\stn	1	2	3	4	5	6	7	8	9	10
November	1.59	1.64	2.24	1.95	1.31	1.89	0.89	2.22	2.41	2.42
December	-	2.54	1.32	2.24	2.64	2.56	-	2.29	-	-
January	-	-	-	0.45	0.65	0.51	0.67	0.66	-	-
February	0.82	0.88	0.42	0.47	050	1.22	0.86	0.94	0.96	0.67
March	0.97	0.79	0.61	0.48	0.35	1.14	0.80	1.06	1.06	0.90
May	0.79	0.92	0.65	0.67	0.60	0.61	0.56	0.56	0.57	0.41
June	0.72	0.67	0.47	0.59	0.57	0.57	0.57	0.65	0.52	0.56
July	-	0.42	0.44	0.49	0.52	0.60	0.59	0.88	0.66	0.49
August	0.14	0.47	0.28	0.33	0.39	0.24	0.43	0.30	0.19	0.34
October	-	0.39	0.56	0.67	0.53	0.59	0.50	0.67	0.18	0.80

Table 6.1 K_d (m^{-1}) values at 552 nm for the **Menai Strait Survey** 1993-1994

The consistency of the spectral shape in the **Menai Strait** is illustrated in Fig. 6.6a-d where each channel is compared to the reading at 596 nm (overall minimum). This shows the attenuation at short wavelengths is most variable, although still with a high correlation (r^2 = 0.91). The slope in all four correlations is greater than 1, which indicates that the attenuation at 596 nm will become an increasingly marked minimum as the overall magnitude rises. The negative intercepts for the 521 and 552 nm channels indicate that at low values of K_d (clear water) the minimum will shift to lower wavelengths. A characteristic spectrum for the **Menai Strait** can therefore be derived by normalizing the spectra; this is shown in Fig 6.7.

The attenuation values for the **Pier Surveys** were less accurately determined. In **July 1994,** the IRM1 was used on eight days, although two of these were badly affected

by shadow and were therefore considered void. The CS sensors were deployed throughout this survey, but as readings were only taken every 30 minutes, attenuation could not be calculated over a short period of time. The best estimates needed to use readings over the entire day, which removes any short term variation, $K_d(570)$ increasing from 0.386 m^{-1} on 13/07/94 to 0.874 m^{-1} on 19/07/94, before decreasing again. Fig. 6.8 shows how the values of K_d from the different instruments vary, and the increase in error over shorter periods due to fewer readings.

As the colour sensors were taking measurements over the whole fortnight, they were useful for monitoring changes in the level of irradiance at set positions. The bottom sensor CS4 clearly shows a tidal signal (Fig. 6.9). At neaps there is an increase in irradiance towards the middle of the day, this is due to the increase in ambient irradiance, and also the decrease in tidal height. At spring tides there was a clear duality in the signal, with peaks early in the morning and late in the afternoon; the decrease during the middle of the day is caused by the increased water column above the sensor at high tide (Fig. 6.9). Similarly, the tidal signal can be identified in the 490:570 ratio at the bottom (Fig. 6.10). The ratio decreases as the tidal height increases, as light at 490 nm is attenuated faster than that at 570 nm. The 490:570 ratio remains constant throughout the survey both for the surface sensor and the upwelling light sensor, confirming that this change in signal is due to the height of the water column and not changes in the ambient radiation or constituent concentrations.

The following year, the profiling CS24 was used to measure K_d, recording every 30 seconds. However, due to a malfunction in the pressure sensor the instrument switched itself off at various times under the water, limiting the usefulness of the readings. After five days, this was replaced by the Satlantic, but unfortunately, this would not download on two occasions, giving a total of eight profiles over the survey. In addition, the surface sensor was not sensitive enough, nor recording at short enough intervals to be equivalent to the sub-surface sensors, so that ambient changes could not be removed from the underwater data.

The **August 1995 Pier Survey** shows that K_d at Menai Bridge (Station 5 in the **Strait**

Survey) was similar the next year, 0.4-1.2 m^{-1}, although extending over a wider range than August 1994 as the readings were taken over a full spring-neap cycle. Measurements over the two-week period identified a tidal signal, with K_d being highest at neap tides (Fig. 6.11).

As the water body did not change in **Cwmystradllyn,** it was possible to do a series of profiles over time, showing that the attenuation did not change throughout the day, and studying the relative diminution of different wavelengths with depth. This is clearly shown with the change in the 440:570 ratio in Fig. 6.12, and illustrates the phenomenon observed in the **Pier Survey.**

6.3 REFLECTANCE

No trend was observed in reflectance during the **Menai Strait Survey** (Fig. 6.13). This may be due to the difficulty in measuring upwelling irradiance which is so low that it was near the threshold of the instrument, particularly for the winter readings. The range of ambient light levels is shown in Fig. 6.14, illustrating the marked difference between winter and summer conditions. The blue and red channels were most affected as these had the greatest attenuation values. On inspection of the data, there seemed to be slightly lower values of R during the summer (May-August), but the high variability of the measurements prohibits any clear distinction.

There was a detectable trend in the colour sensor R through the **July Pier Survey** (Fig. 6.15), which does not coincide with the attenuation trend, as the signal continues to increase until 22/07/94, and then remains constant rather than decreasing after 19/07/94 as K_d did. Unfortunately, there were not enough readings with IRM1 to confirm this trend.

The Spectron reflectance values do not show any clear progression through the first week of the **July** survey either. However, in 1995 the Spectron indicated an increase from 7.3 % initially to 26.3 % on 31/08/95. The reflectance calculated from the Spectron and that from the Satlantic (assuming the conversion between L_u and E_u is π) do not correlate well (Fig. 6.16).

The lack of pigment in **Cwmystradllyn** limits the level of reflectance, with only a small peak between 550 and 600 nm (Fig. 6.17). However, as the water body did not change, the lake was used to study the relationship between E_u and L_u (Fig. 6.18). This comparison suggests the relationship:

$$E_u = 3.29\ L_u$$

close to the value of π used for a Lambertian surface (see §2.4.1). This constant implies a lack of directionality in the light field which was confirmed by tilting the sensor and observing only small changes with angle (Fig. 6.19).

There is a marked difference in the shape of the reflectance spectrum at **Cwmystradllyn** and that observed at **Dolgarrog** (Fig. 6.20). The high concentration of sediment in the **Conwy** results in a shift of maximum R to longer wavelengths, giving the water a reddy-brown appearance. This illustrates that the absorption increased at the blue end of the spectrum due to yellow substance and sediment.

This shift in the maximum to longer wavelengths was seen more gradually in the spectra from the **Clyde** (Fig. 6.21) where CS1 and CS4 are in the **Clyde Sea**, with low reflectance, while CE3 and CE5 are taken in the estuary, showing a higher level of reflectance with the peak further towards the red.

The effect of bottom reflectance can be seen in the profiles from **Cwmystradllyn** (Fig. 6.22a and b) and **Dolgarrog** (Fig. 6.22c and d). R is expected to decrease exponentially with depth (Kirk, 1994) whereas in these surveys the reflectance increases near the bottom. This is due to the more penetrating wavelengths being reflected upwards from the bed. This highlights the need for a larger water column to ensure that light is not reaching the bottom.

6.4 SECCHI DEPTH

The Secchi depths (z_{SD}) observed in the **Menai Strait** clearly support the diffuse attenuation data (Fig. 6.23), as the depth increases from 1.6 m in March to 4.25 m in August.

Through the **Pier surveys** a tidal signal was observed. During the **July Survey** (Fig. 6.24) neither the spring-neap nor the diurnal tidal signal were clearly shown in the Secchi depths. However, in **August 1995** the spring-neap cycle is obvious in the observed depths (Fig. 6.25), with values of 4.25 m at neap tides to 1.4 m at springs.

6.5 BEAM ATTENUATION

During the **Menai Strait Survey** a transmissometer was used on only one occasion from the *Sandpebbler*, to confirm that the column was mixed. This was taken on 31/03/94 from 07:30 to 09:00 as the tide turned. The results have already been shown in Fig. 4.3. However, a transmissometer was deployed for both **Pier surveys.**

In **July 1994,** the transmissometer stopped recording after six days limiting the readings to those taken at midday which was noted manually when taking the other optical measurements. However, from 11/07/94 to 17/07/94 the attenuation increased from 1 m^{-1} to 3 m^{-1} corresponding to the development of an algal bloom (Fig. 6.26). On each day a semi-diurnal cycle is apparent, *c* being greatest at high tide, which is superimposed on the general trend. The midday readings for the remainder of the survey confirm the subsequent decline in attenuation to the initial level observed as the phytoplankton concentrations decreased. The tidal signal was not mirrored in the temperature readings, although the increase to 18/08/94 was apparent, suggesting that the phytoplankton bloom dominated the properties of the water column.

There was a greater range in attenuation in **August 1995,** extending from 2 m^{-1} on 21/08/95 to 9 m^{-1} on 29/08/95 on the neap-spring succession (Fig. 6.27), and then declining to ~ 5 m^{-1}. The readings at the end of the deployment were higher than the initial measurements of attenuation due to fouling of the instrument. Once again, the semi-diurnal cycle was apparent.

The highest values of attenuation were observed in the **Conwy,** ~ 50 m^{-1} corresponding to 1 % transmittance. This coincides with the tidal front passing the bridge (Fig. 6.28). The beam attenuation then decreased again after the front had

passed and the salinity of the water increased.

6.6 DERIVATION OF *a* AND *b*

Kirk's algorithms (1985) were applied to K_d and R as described in §2.4.2 to derive a and b. Fig. 6.29 shows the variation over the whole year from the IRM1 data in the **Menai Strait.** Even though R did not show a seasonal trend, the change in K_d resulted in a decrease in b from winter to summer, corresponding to the decrease in TSS (see §5.1). In the **July Pier survey,** the derived absorption follows the trend of diffuse attenuation (Fig. 6.30a and b), with a maximum value on 19/07/94, whereas scattering increases until 22/07/94. This trend is apparent when using values calculated over the whole day or only 2 hours (Fig. 6.30c and d), suggesting that these are real progressions and illustrating the stronger dependences between absorption-attenuation, and scattering-reflectance.

In both **Pier surveys,** $a+b$ can be compared with c to test the validity of the Kirk algorithms in this environment. In July (Fig. 6.31a), both the colour sensors and IRM1 agree in magnitude with the transmissometer, but neither shows the same trend. In **August 1995,** the Satlantic results in values of c which are much lower than that measured with the transmissometer. However, when the Spectron reflectance was used in conjunction with the Satlantic K_d, the agreement was much better (Fig. 6.31b).

6.7 DERIVATION OF *a** AND *b**

To determine the specific values of absorption and scattering for each constituent *in situ*, the derived values of a and b can be regressed on the concentrations. The absorption value for water must first be removed, and then a multiple regression on yellow substance, pigment and inorganic concentrations can be performed. If there are not enough data points for a particular site, and one constituent dominates the signal, an approximate value can be reached by dividing the absorption (minus water) by the concentration.

In the **Menai Strait,** yellow substance did not vary significantly, and therefore cannot be extracted through regression, so must be considered as a constant, giving the

equation:

$$a - a_w = a_{const} + a_c^* C + a_m^* M$$

The absorption and scattering values for sea water at relevant wavelengths are given in Table 6.2.

λ (nm)	410	440	490	510	520	550	570	600	670	700
a (m^{-1})	.0162	.0145	.0196	.0357	.0477	.0638	.0799	.2440	.4300	.65
b (m^{-1})	.0068	.0049	.0031	.0026	.0024	.0019	.0017	.0014	.0008	.0007

Table 6.2 Absorption and scattering coefficients for sea water (Smith & Baker, 1982) at wavelengths which coincide with instrumentation used

The results from a regression of pigment and MSS concentrations on the **Menai Strait** IRM1 a-a_w are given in Table 6.3.

λ (nm)	chl slp	std dev	mss slp	std dev	const	r^2	n
absorption							
444	0.0110	0.021	0.0332	0.018	0.313	0.318	51
521	0.0086	0.014	0.0393	0.012	0.112	0.632	65
552	0.0043	0.014	0.0395	0.011	0.104	0.650	64
596	0.0052	0.012	0.0312	0.010	0.200	0.617	58
670	0.0024	0.012	0.0375	0.009	0.457	0.718	47
scattering							
444	-0.0167	0.088	0.2769	0.078	1.341	0.688	51
521	-0.0425	0.110	0.2762	0.091	1.746	0.631	65
552	-0.0397	0.117	0.2887	0.096	1.763	0.625	64
596	-0.0467	0.106	0.3005	0.083	1.564	0.707	58
670	-0.0360	0.100	0.218	0.077	1.299	0.598	47

Table 6.3 Results from the regression of absorption and scattering on pigment and inorganic concentrations for the **Menai Strait** survey

This regression can be undertaken for each survey. The resultant specific absorption and scattering coefficients are given in Table 6.4 and 6.5 respectively.

λ (nm)	410	440	490	510	520	550	600	670
				a_c^*				
MS	-	0.011	-	-	0.009	0.004	0.005	0.002
MP	0.4125	0.4140	0.2852	0.3288	-	0.3253	-	0.3438
Clyde	0.0569	0.0052	-0.0043	-0.0031	-	-0.0051	-	0.0118
Loch S	-	-0.0032	-	-	0.0055	0.0050	0.0026	0.0026
Card B	-	0.2254	-	-	0.0367	0.0737	0.2318	0.2525
Vestfj	0.377	0.351	0.366	0.344	-	0.322	-	0.269
Cwm	-0.0105	-0.0277	-0.0265	-0.0079	-	-0.0079	-	-0.0290
Conwy	-0.0295	0.0196	-0.0092	-0.0041	-	0.0033	-	0.0022
				a_m^*				
MS	-	0.033	-	-	0.039	0.039	0.031	0.038
MP	0.0084	0.0012	0.0088	-0.0001	-	-0.0071	-	-0.0134
Clyde	0.1111	0.0704	0.0470	0.0356	-	0.0312	-	0.0121
Loch S	-	-0.0112	-	-	-0.0040	-0.0053	0.0003	-0.0146
Card B	-	0.0433	-	-	0.0225	0.0350	0.0404	0.0356
Vestfj	0.0019	0.0009	-0.0030	-0.0012	-	-0.0021	-	0.0120
Cwm	-0.0260	-0.0319	-0.0366	-0.0354	-	-0.0354	-	-0.0272
Conwy	0.0037	-0.0009	0.0021	0.0016	-	0.0004	-	0.0008
				const/a_y*				
MS	-	0.3239	-	-	0.1116	0.1040	0.2003	0.4572
MP	0.0254	-0.1446	-0.1591	-0.1961	-	-0.1998	-	0.0913
Clyde	0.1948	0.1493	0.0832	0.848	-	0.0859	-	0.4064
Loch S	-	0.5314	-	-	0.1948	0.1624	0.2544	0.5884
Card B	-	-0.1403	-	-	0.0078	-0.0632	-0.1233	0.1348
Vestfj	0.1370	0.0935	0.0624	0.0614	-	0.0809	-	0.374
Cwm	0.478	0.324	0.189	0.150	-	0.120	-	0.498
Clyde	0.1948	0.1493	0.0832	0.0848	-	0.0859	-	0.4064

Table 6.4 Specific absorption for each constituent at all sites from the regression of concentrations on derived absorption

λ (nm)	410	440	490	510	520	550	600	670
				b_c^*				
MS	-	0.011	-	-	0.009	0.004	0.005	0.002
MP	-1.1073	-1.4167	-1.589	-1.397	-	-1.3311	-	-1.1749
Clyde	-0.0047	-0.2166	0.0047	-0.0403	-	-0.0416	-	-0.0729
Loch S	-	0.3414	-	-	-0.0004	0.0098	0.0074	-0.0007
CardB	-	0.1823	-	-	-0.0478	0.4807	0.1423	0.0552
Vestfj	0.0462	0.0096	0.0282	0.1094	-	0.0920	-	1.368
Cwm	0.0410	0.0106	-0.0061	-0.0098	-	-0.0295	-	0.0154
Conwy	0.2059	0.2722	-0.0006	-0.1034	-	-0.2631	-	-0.1514
				b_m^*				
MS	-	0.033	-	-	0.039	0.039	0.031	0.038
MP	0.2444	0.2777	0.4082	0.2923	-	0.3433	-	0.2152
Clyde	0.0411	0.2673	0.1659	0.1940	-	0.2217	-	0.1863
Loch S	-	0.6760	-	-	0.0067	0.0119	0.0063	-0.0418
Card B	-	-0.1167	-	-	0.0080	0.1309	-0.1199	-0.0325
Vestfj	-0.0039	-0.0105	-0.0071	-0.0093	-	-0.0087	-	-0.0179
Cwm	-0.3325	-0.2827	-0.2295	-0.2208	-	-0.2329	-	-0.2190
Conwy	-0.0194	-0.0257	-0.0240	-0.0155	-	0.0017	-	-0.0050
				const				
MS	-	1.3408	-	-	1.7459	1.7633	1.5636	1.2987
MP	2.1663	2.7144	3.0573	2.9661	-	2.6836	-	1.7172
Clyde	0.0831	0.3528	0.2569	0.2619	-	0.2161	-	0.2733
Loch S	-	-	-	-	0.7515	0.5366	0.5521	1.104
Card B	-	1.2239	-	-	0.9718	-0.0147	1.1625	0.6136
Vestfj	0.1481	0.1396	0.1204	0.1099	-	0.0906	-	0.0894
Cwm	0.8338	0.7855	0.6698	0.6428	-	0.6647	-	0.5106
Conwy	-0.3039	0.5737	3.581	4.173	-	4.976	-	3.534

Table 6.5 Specific scatter for each constituent at all sites from the regression of concentrations on derived scatter

The great range in coefficients and the presence of negatives show that this regression technique only applies when a greater number of points are included. However, the mixture of concentrations from different locations will be less effective in identifying the characteristic spectra of different water bodies.

6.8 DISCUSSION

The constituent concentrations and the optical properties show similar trends confirming the dependence of the water colour on the constituents. When the mineral solid concentrations are high there is a corresponding increase in diffuse attenuation. The increase in MSS in the winter in the **Menai Strait** indicates that the mineral particles are freer to move around without the organic binding which is present during the warmer months. The higher number of particles results in more photons being intercepted, and thus higher scattering and absorption.

The range of K_d values was shown in Fig. 6.2. The linked increase in particle concentrations and K_d is also apparent in the shape of the attenuation spectra. The spectral shape of K_d changes with overall magnitude (Fig. 6.32). At low values, minimum attenuation occurs between 500 and 550 nm, with a slight increase towards the blue and a much greater increase in the red. As the value of K_d becomes greater, the minimum shifts to longer wavelengths (550-600 nm), while the blue attenuation exceeds the red. This change in shape represents the shift from water dominating the signal with high absorption in the red, through an increase in dissolved organics which absorb in the blue (Fig. 6.33), to particles which absorb more in the blue and increase overall scattering.

It is also apparent that the optical properties covary due to their dependency on the constituents, particularly z_{SD} and K_d. Comparison of z_{SD} with K_d (Fig. 6.34) gives a correlation for the **Menai Strait** survey and **Cardigan Bay** (using K_d at 552 nm) of:

$$\frac{1}{K} = 0.926 z_{SD} - 0.148 \qquad r^2 = 0.636 \qquad n = 80$$

where the constant is significantly different from zero.

If the PAR sensor is considered (used during **AMB95**) the relationship improves to:

$$\frac{1}{K} = 0.588\, z_{SD} + 0.242 \qquad r^2 = 0.804 \qquad n = 11$$

Although there is a strong relationship between K_d and z_{SD} neither of the above regressions agree the relationship discussed in §2.4.2 (Holmes, 1970) of $K_d = 1.44/z_{SD}$.

However, it is possible to compare z with $c+K_d$ (Fig. 6.35), using either the Kirk derived $a+b=c$ or the transmissometer reading for c.

In the **Menai Strait Survey** there is good agreement when using $a+b$ correlating as

$$\frac{1}{(c+K)} = 0.216\, z_{SD} - 0.204 \qquad r^2 = 0.587 \qquad n = 51$$

The relationship is improved when the values for **Cardigan Bay** and the **Clyde** 1996 are included plus the **Pier survey** readings, using the transmissometer c:

$$\frac{1}{(c+K)} = 0.251\, z_{SD} - 0.283 \qquad r^2 = 0.811 \qquad n = 69$$

The correlation improves further when PAR attenuation is used (Fig. 6.36):

$$\frac{1}{(c+K)} = 0.060\, z_{SD} + 0.019 \qquad r^2 = 0.865 \qquad n = 10$$

Again, these show a good correlation between z_{SD} and $(c+K_d)$ but do not agree exactly with the values from the literature discussed in §2.4.2.

In previous studies, yellow substance has been related to salinity (see §2.4.3). This was tested in the **Clyde Sea/Estuary** survey (Table. 6.5). A good correlation was found (Fig. 6.37), even when sites which were beyond the influence of the estuary were included:

$$Sal = 34.95 - 11.977\,YS \qquad r^2 = 0.982$$

which confirms that yellow substance can be used as a conservative tracer in this location.

6.9 SUMMARY

In general, the variation in constituent concentrations and apparent optical properties were related. The spectral shape of K_d changed as the magnitude increased indicating the change in the dominant constituent, with the increase in sediment resulting in an overall higher value and, more specifically, an increase in the blue.

Reflectance was less clearly linked with the constituents but this may be due to errors within the measurement. It was also difficult to derive specific absorption and scattering coefficients for each survey due to the limited number of samples, although for the more intensive surveys such as the **August Pier Survey** and the **Menai Strait Survey** this was possible. For future studies, this would be a good way of distinguishing the dominant optical parameters at any particular location.

A good correlation was found between z_{SD} and $(c+K_d)$, as well as confirmation that yellow substance could be used as a tracer for salinity. The use of optics to monitor salinity variation within estuaries would be a useful progression.

		Yellow Substance m^{-1}	Salinity psu
CS1	0.5	0.089	33.89
	13.0	0.099	34.07
	30.0	0.058	34.79
CS4	0.5	0.115	33.54
	10.7	0.097	33.74
	21.9	0.097	33.76
CE6	0.5	1.57	16.71
	6.0	0.94	22.49
CE5	0.5	0.393	30.53
	7.1	0.138	33.01
	17.0	0.124	33.36
CE4	0.5	0.225	32.32
	8.1	0.067	33.15
	31.2	0.102	33.62
CE3	0.5	0.262	31.58
	14.0	0.127	33.34
	33.6	0.104	34.01
LR1	0.5	0.209	32.45
	9.2	0.145	33.03
	26.1	0.14	33.7
IW1	0.5	0.085	33.18
	16.0	0.087	33.5
	40.0	0.129	33.99
	160.0	0.163	34.39

Table 6.5 Yellow substance concentrations and salinities for stations in the **Clyde Sea**, Estuary and surrounding lochs, 1996

Figure 6.1 Concentrations for Menai Strait Survey

Figure 6.2 Diffuse attenuation ranges at 443-444 nm at different sites

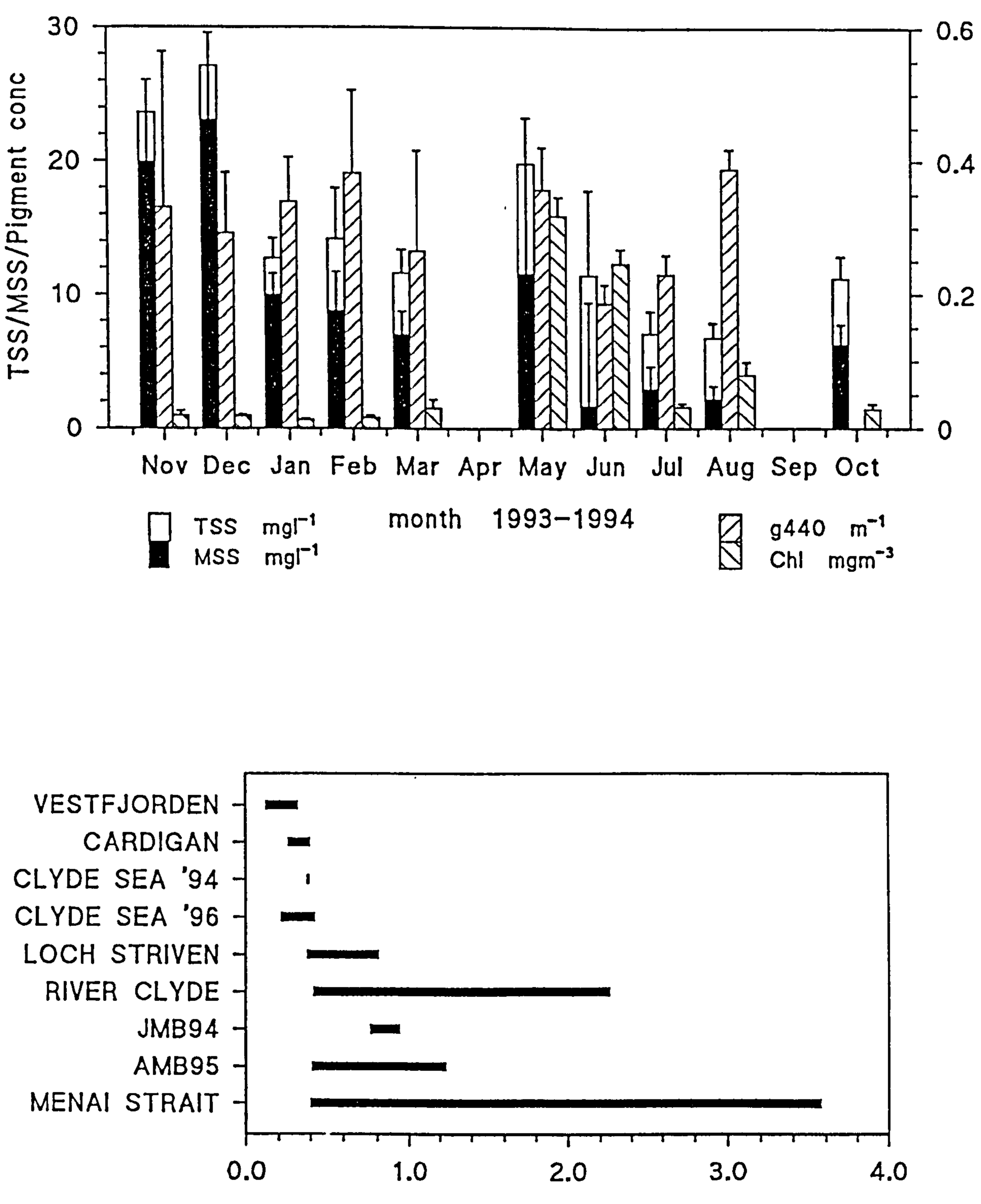
30
20
10
0
TSS/MSS/Pigment conc
0.6
0.4
0.2
0
g440
Nov Dec Jan Feb Mar Apr May Jun Jul Aug Sep Oct
month 1993–1994
TSS mgl⁻¹
MSS mgl⁻¹
g440 m⁻¹
Chl mgm⁻³
VESTFJORDEN
CARDIGAN
CLYDE SEA '94
CLYDE SEA '96
LOCH STRIVEN
RIVER CLYDE
JMB94
AMB95
MENAI STRAIT
0.0
1.0
2.0
3.0
4.0
attenuation m⁻¹

Figure 6.3 Irradiance profile at 555 nm (Vestfjorden)

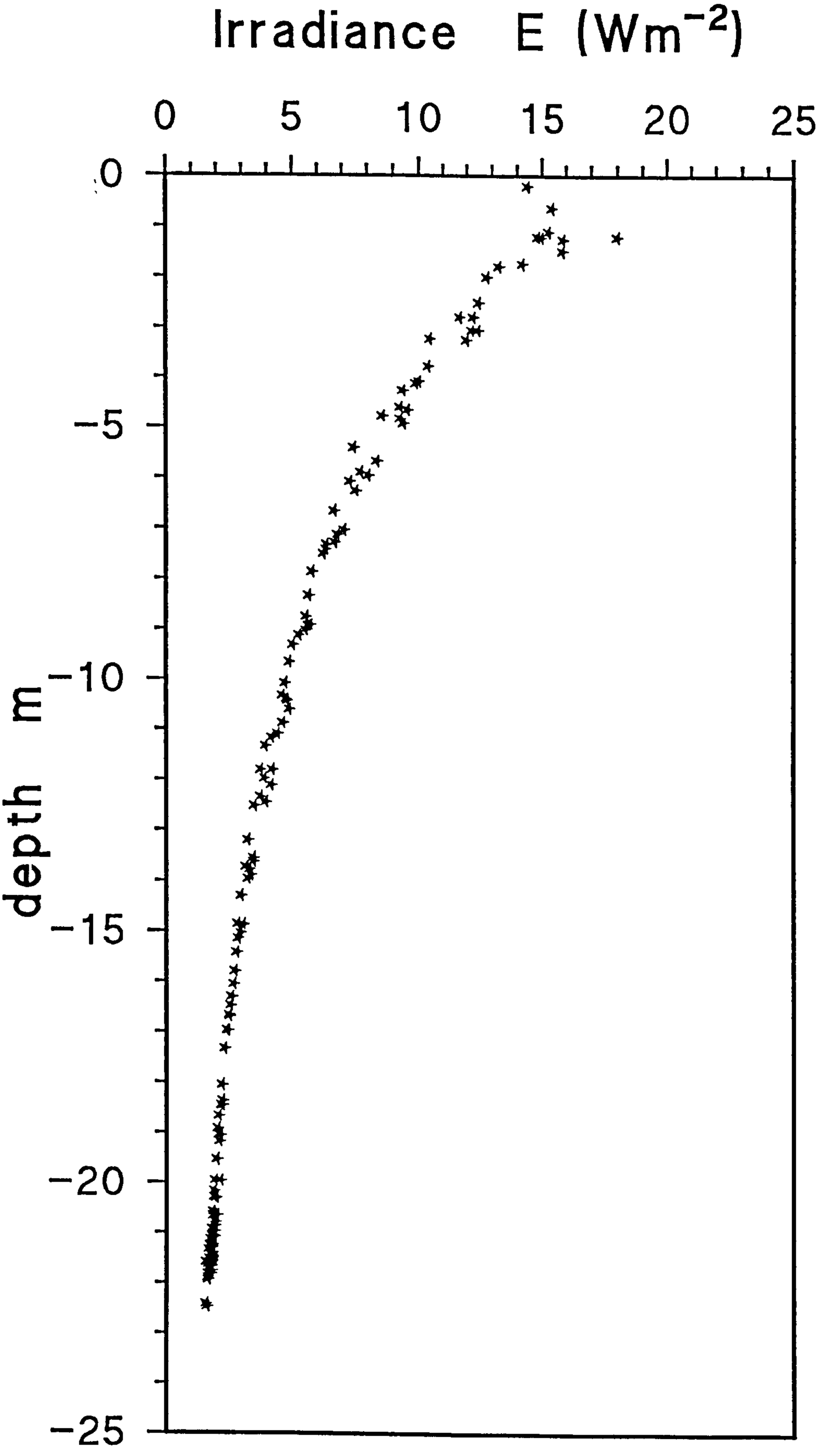
Irradiance E (Wm^{-2})
0
5
10
15
20
25
0
−5
−10
−15
−20
−25
depth m

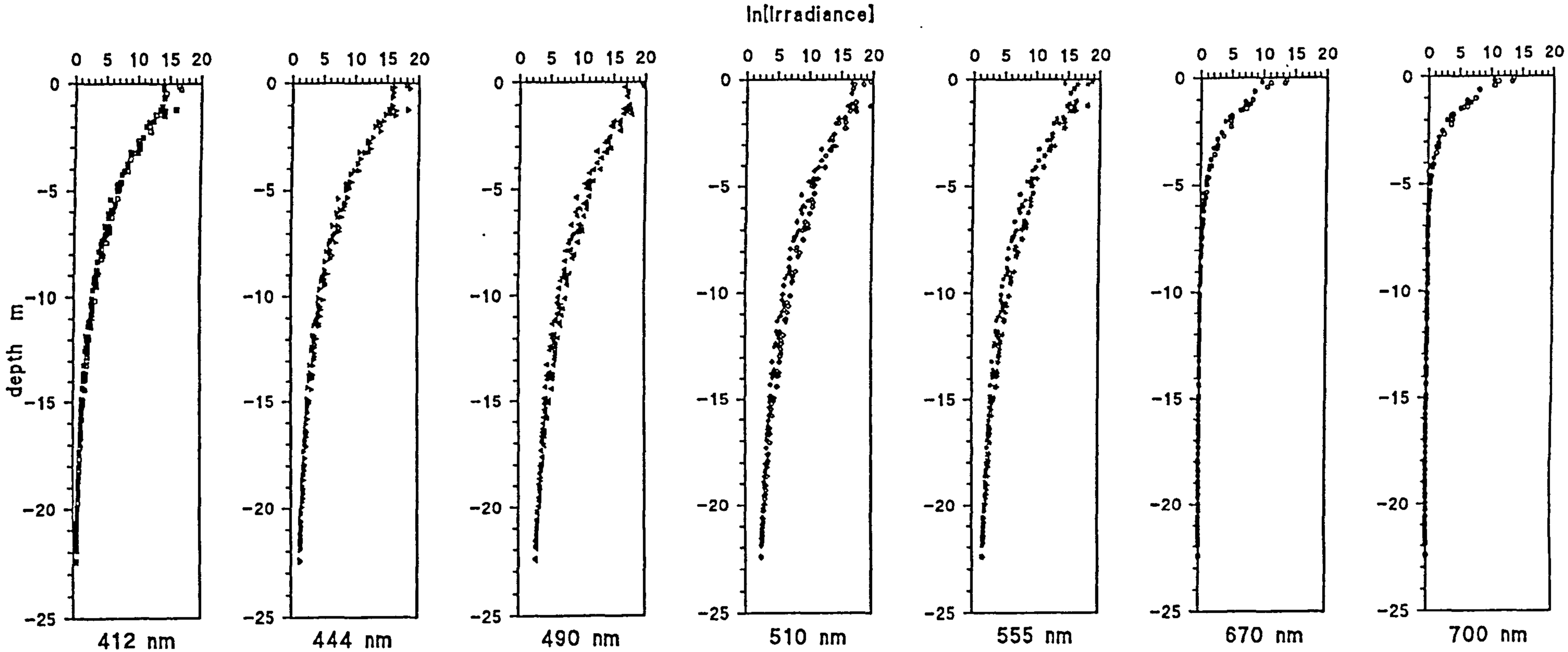

Figure 6.4 Irradiance profiles at 7 wavelengths: 412, 444, 490, 510, 555, 670 and 700 nm (Vestfjorden)

Figure 6.5 Diffuse attenuation at all sites for each month in the Menai Strait Survey

a) 444 nm
b) 521 nm
c) 552 nm
d) 596 nm
e) 670 nm

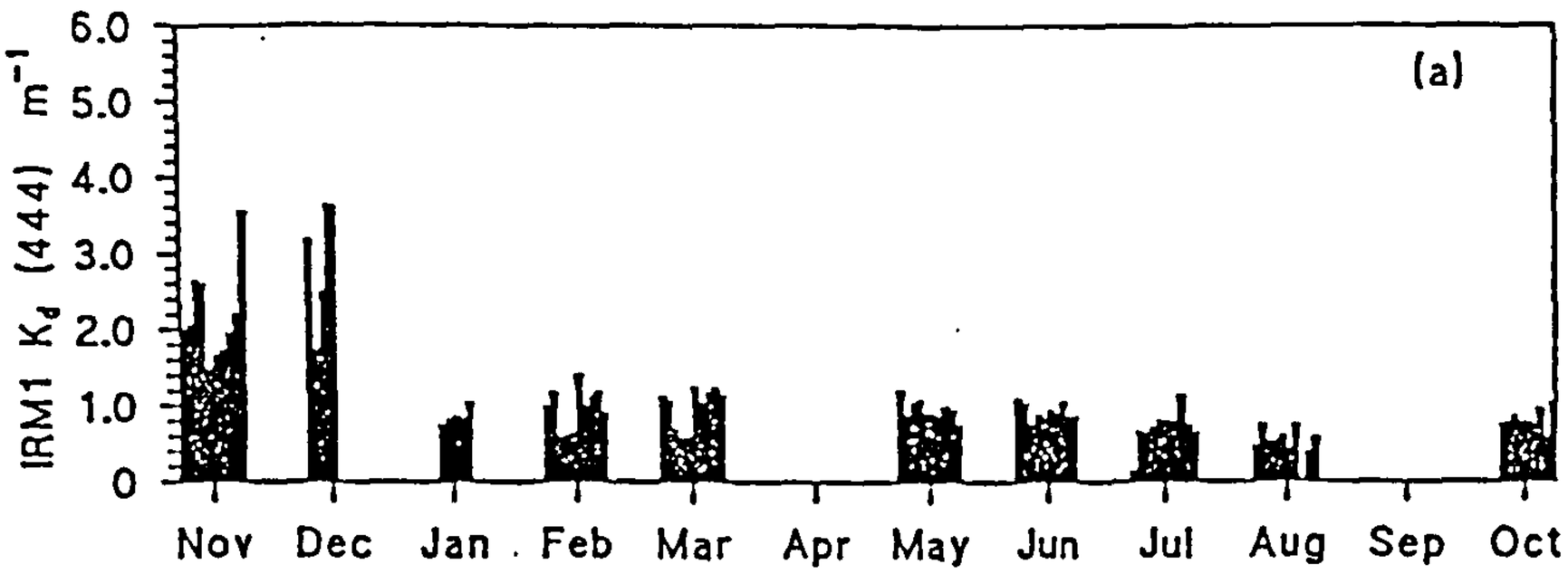
(a)
IRM1 K_d (444) m^{-1}
6.0
5.0
4.0
3.0
2.0
1.0
0
Nov Dec Jan Feb Mar Apr May Jun Jul Aug Sep Oct

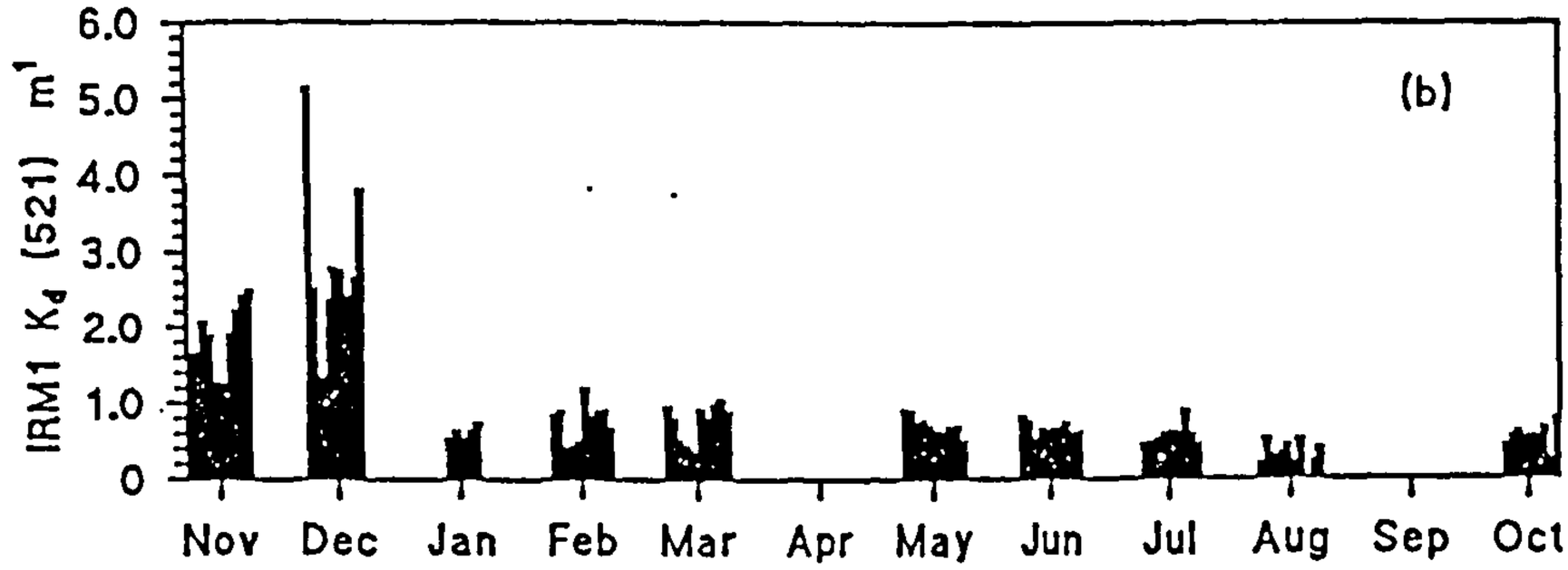
(b)
IRM1 K_d (521) m^{-1}
6.0
5.0
4.0
3.0
2.0
1.0
0
Nov Dec Jan Feb Mar Apr May Jun Jul Aug Sep Oct

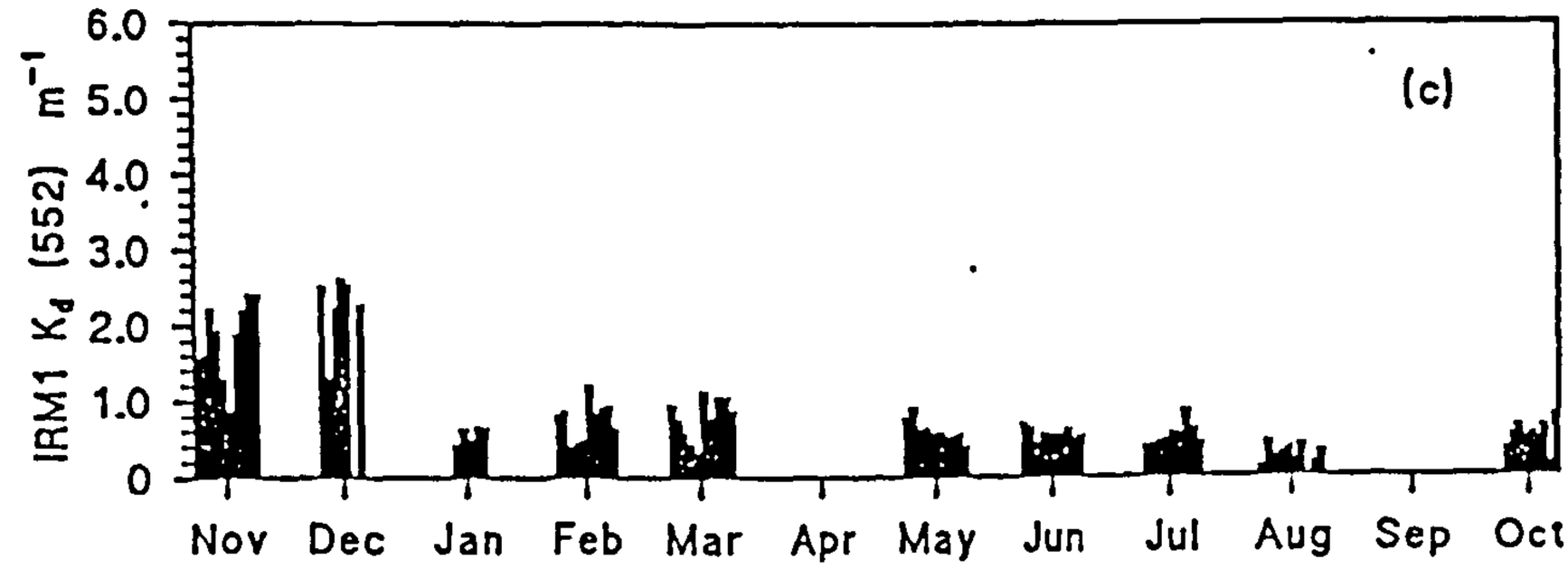
(c)
IRM1 K_d (552) m^{-1}
6.0
5.0
4.0
3.0
2.0
1.0
0
Nov Dec Jan Feb Mar Apr May Jun Jul Aug Sep Oct

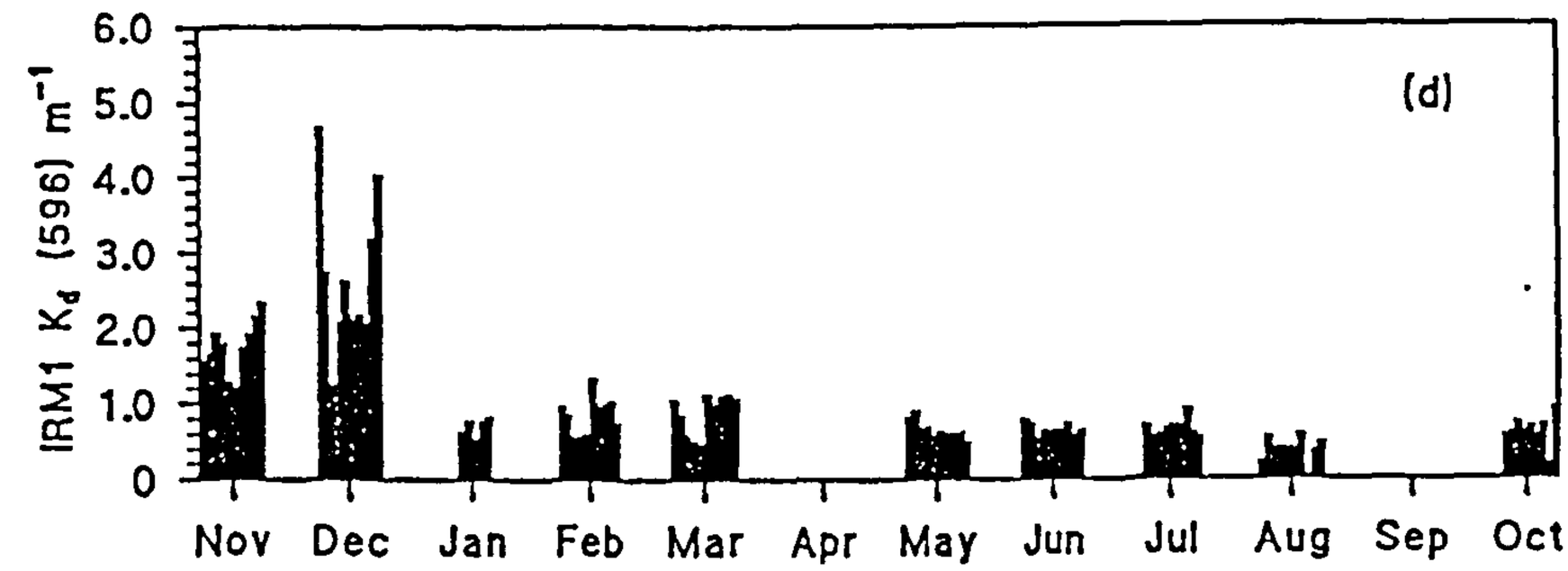
(d)
IRM1 K_d (596) m^{-1}
6.0
5.0
4.0
3.0
2.0
1.0
0
Nov Dec Jan Feb Mar Apr May Jun Jul Aug Sep Oct

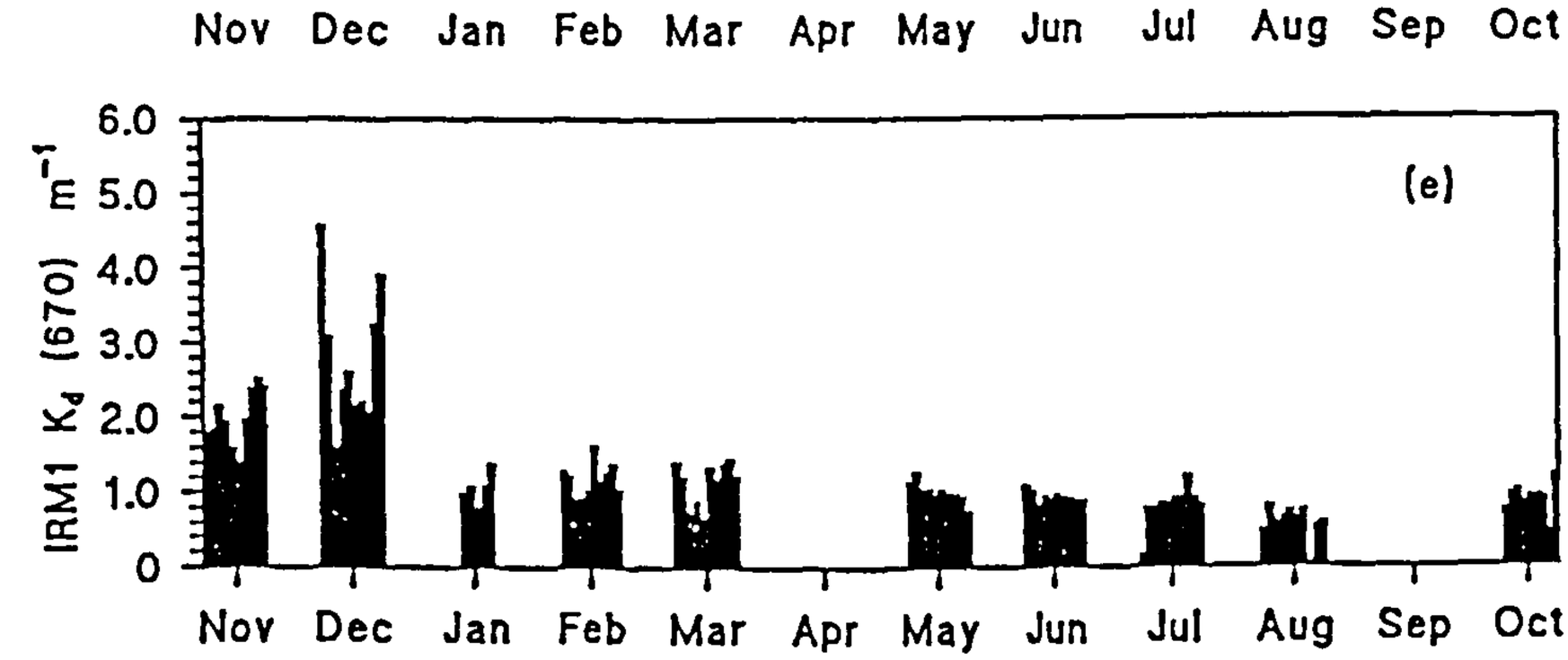
(e)
IRM1 K_d (670) m^{-1}
6.0
5.0
4.0
3.0
2.0
1.0
0
Nov Dec Jan Feb Mar Apr May Jun Jul Aug Sep Oct
month 1993–1994

Figure 6.6 Consistency of spectral shape of K_d in Menai Strait Survey, comparing each IRM1 channel with the value at 596 nm

a) 444 nm against 596 nm
b) 521 nm against 596 nm
c) 552 nm against 596 nm
d) 670 nm against 596 nm

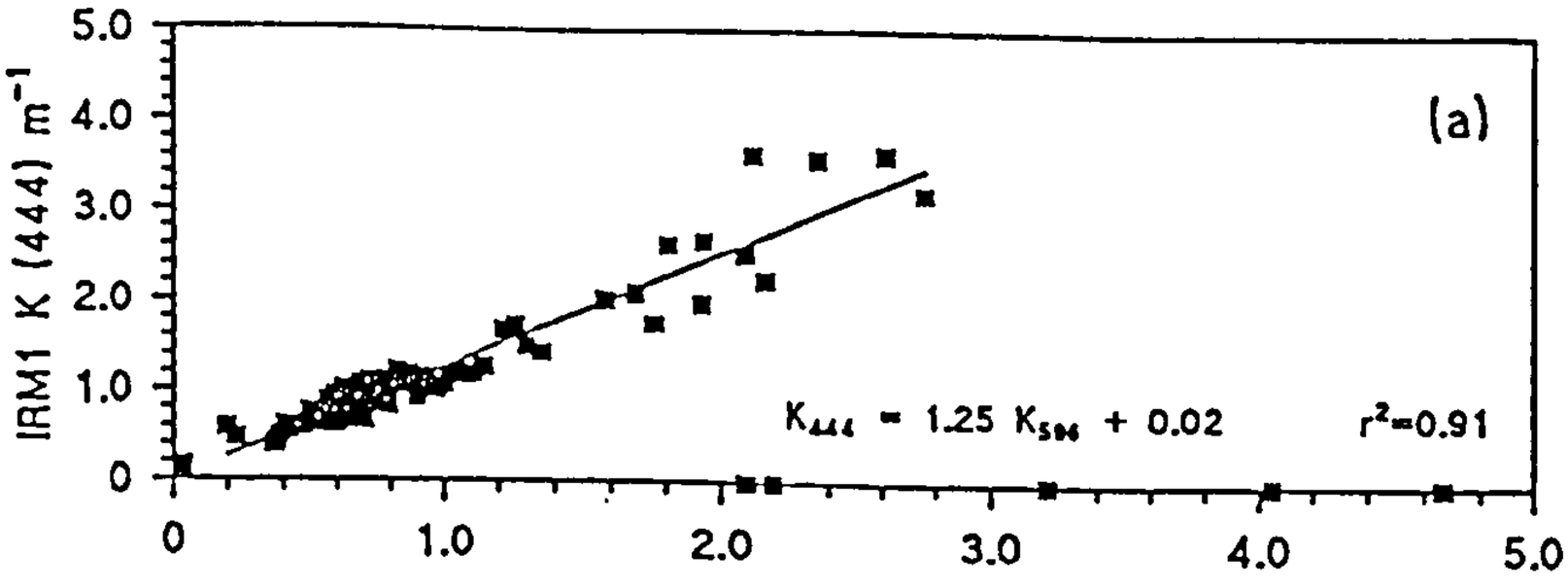
IRM1 K (444) m⁻¹
5.0
4.0
3.0
2.0
1.0
0
(a)
K444 = 1.25 K596 + 0.02
r²=0.91
0
1.0
2.0
3.0
4.0
5.0

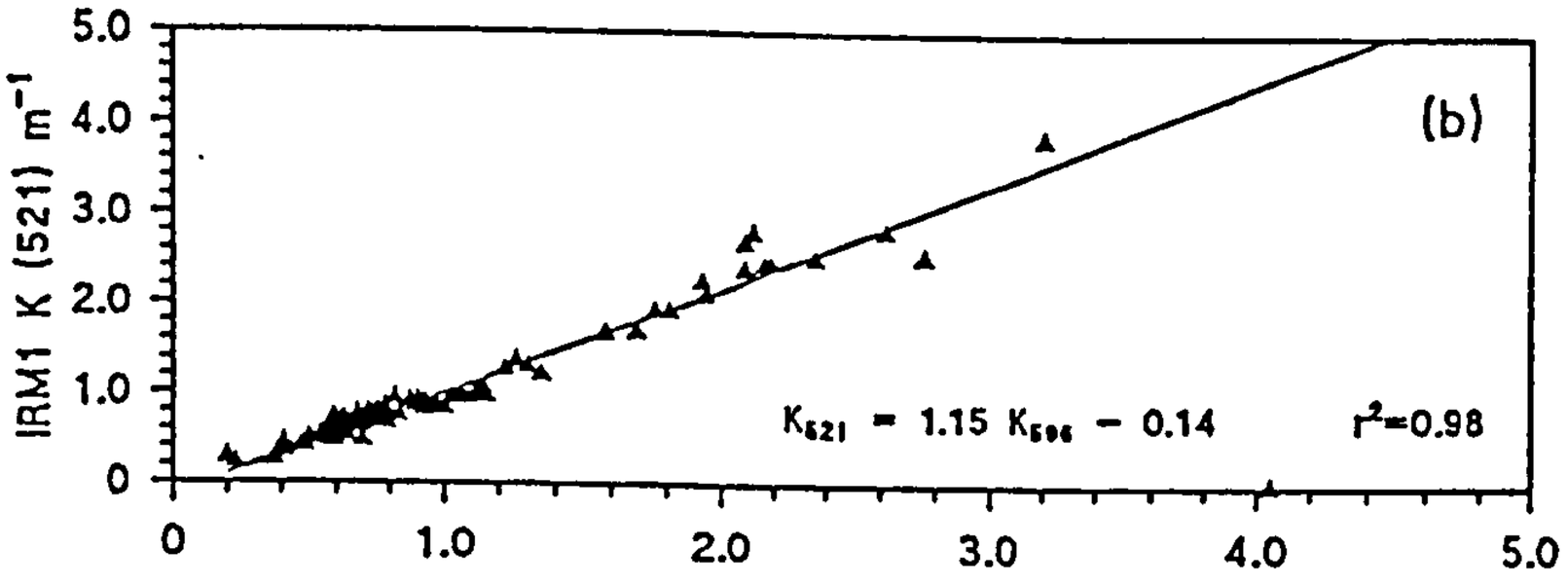
IRM1 K (521) m⁻¹
5.0
4.0
3.0
2.0
1.0
0
(b)
K521 = 1.15 K596 − 0.14
r²=0.98
0
1.0
2.0
3.0
4.0
5.0

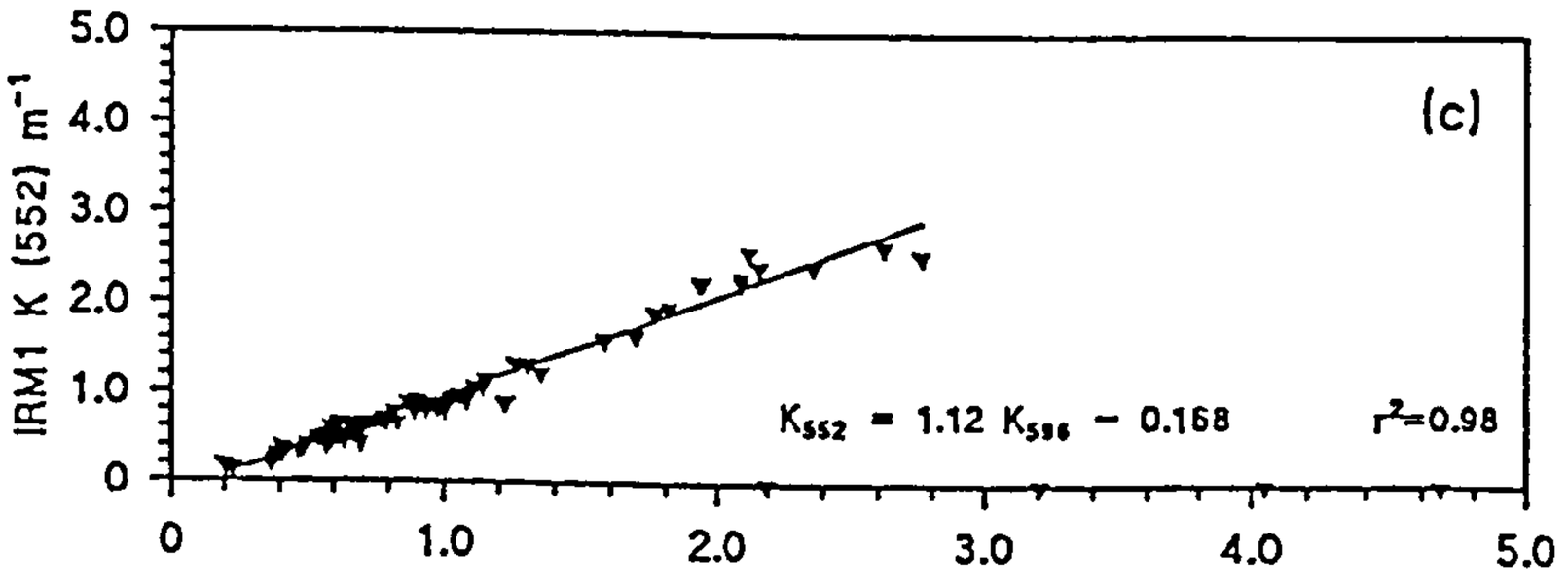
IRM1 K (552) m⁻¹
5.0
4.0
3.0
2.0
1.0
0
(c)
K552 = 1.12 K596 − 0.168
r²=0.98
0
1.0
2.0
3.0
4.0
5.0

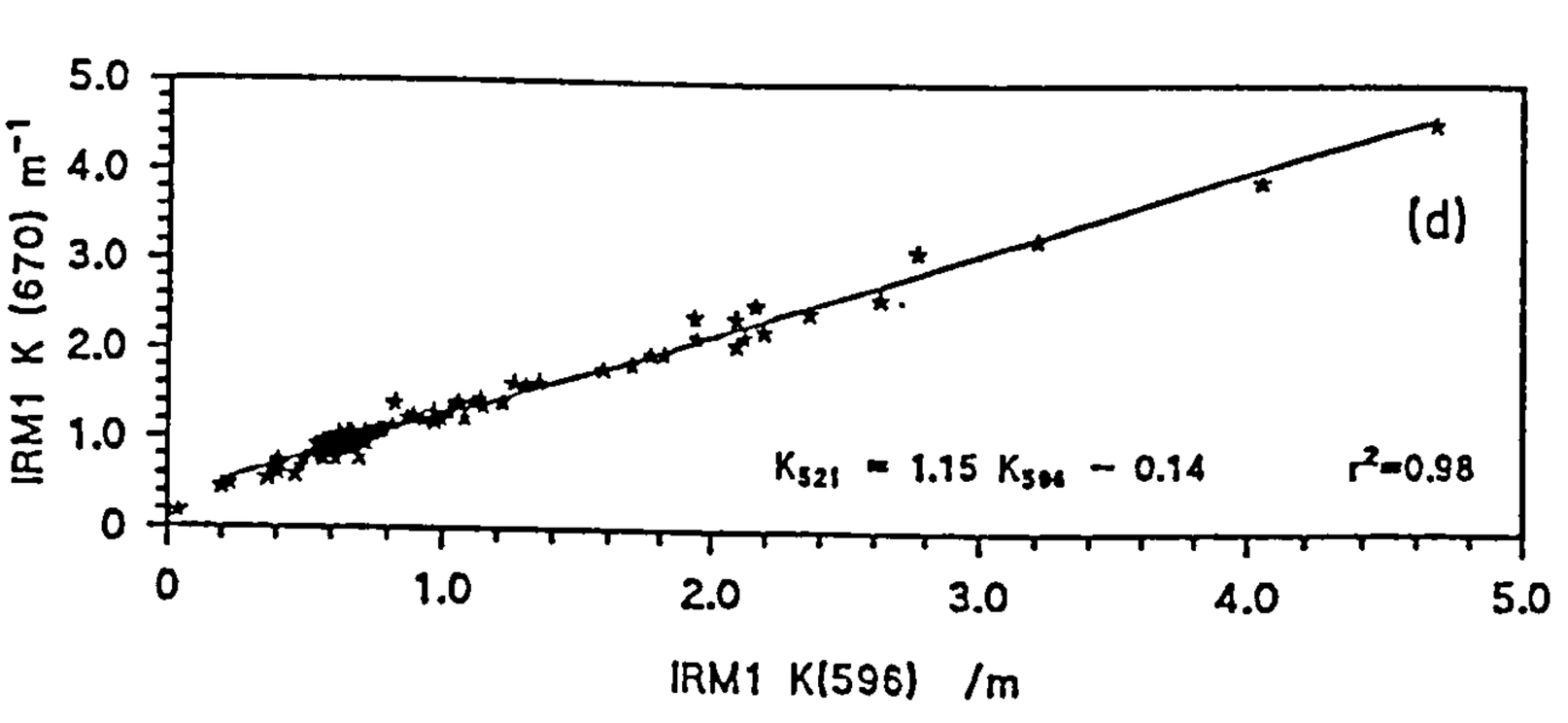
IRM1 K (670) m⁻¹
5.0
4.0
3.0
2.0
1.0
0
(d)
K521 = 1.15 K596 − 0.14
r²=0.98
0
1.0
2.0
3.0
4.0
5.0
IRM1 K(596) /m

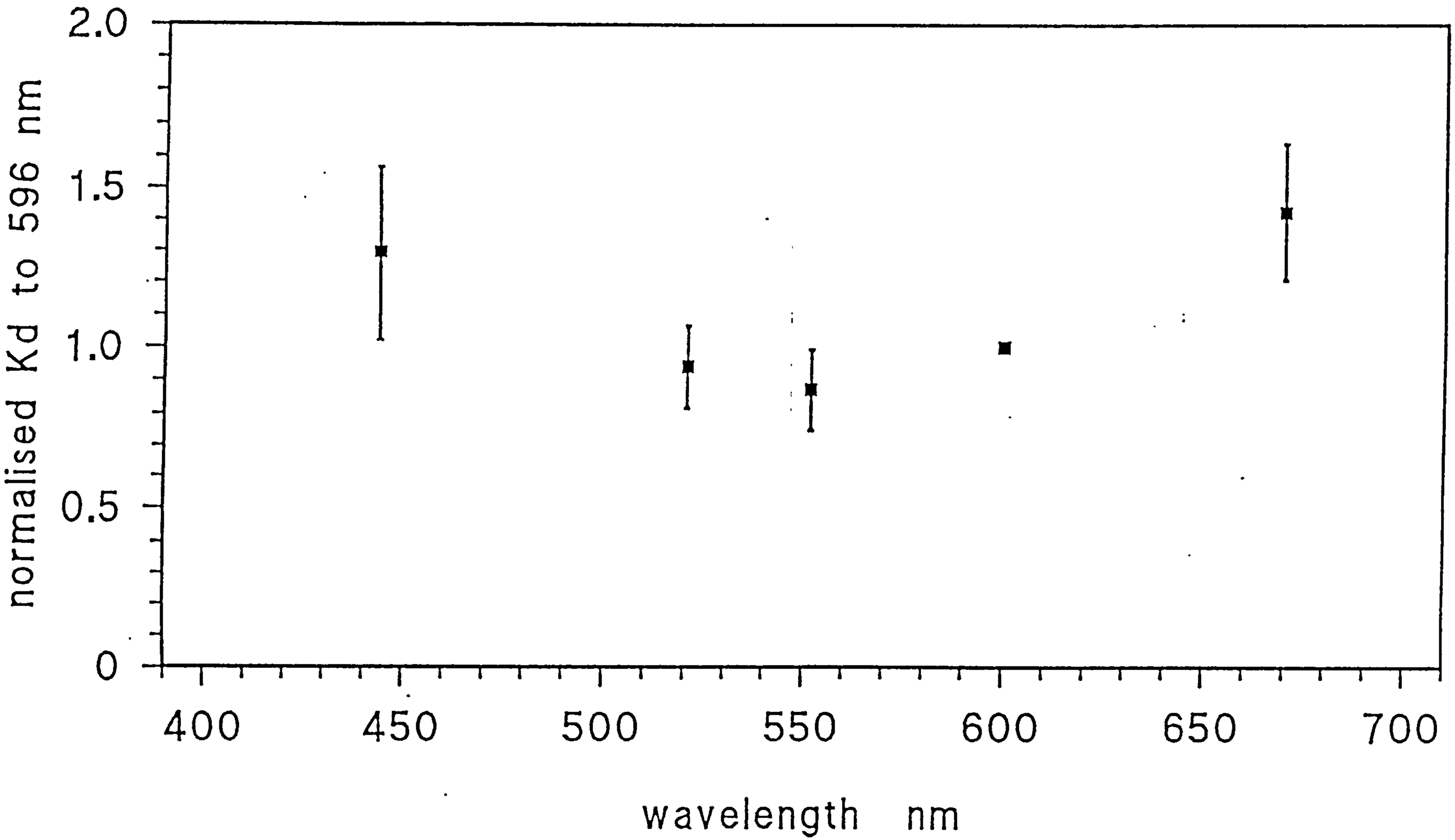

Figure 6.7 Characteristic spectrum for Menai Strait diffuse attenuation

Figure 6.8 K_d for July Pier Survey 1994, calculated from different instruments
a) colour sensor: all readings
b) colour sensor: 12:00-14:00 GMT
c) IRM1

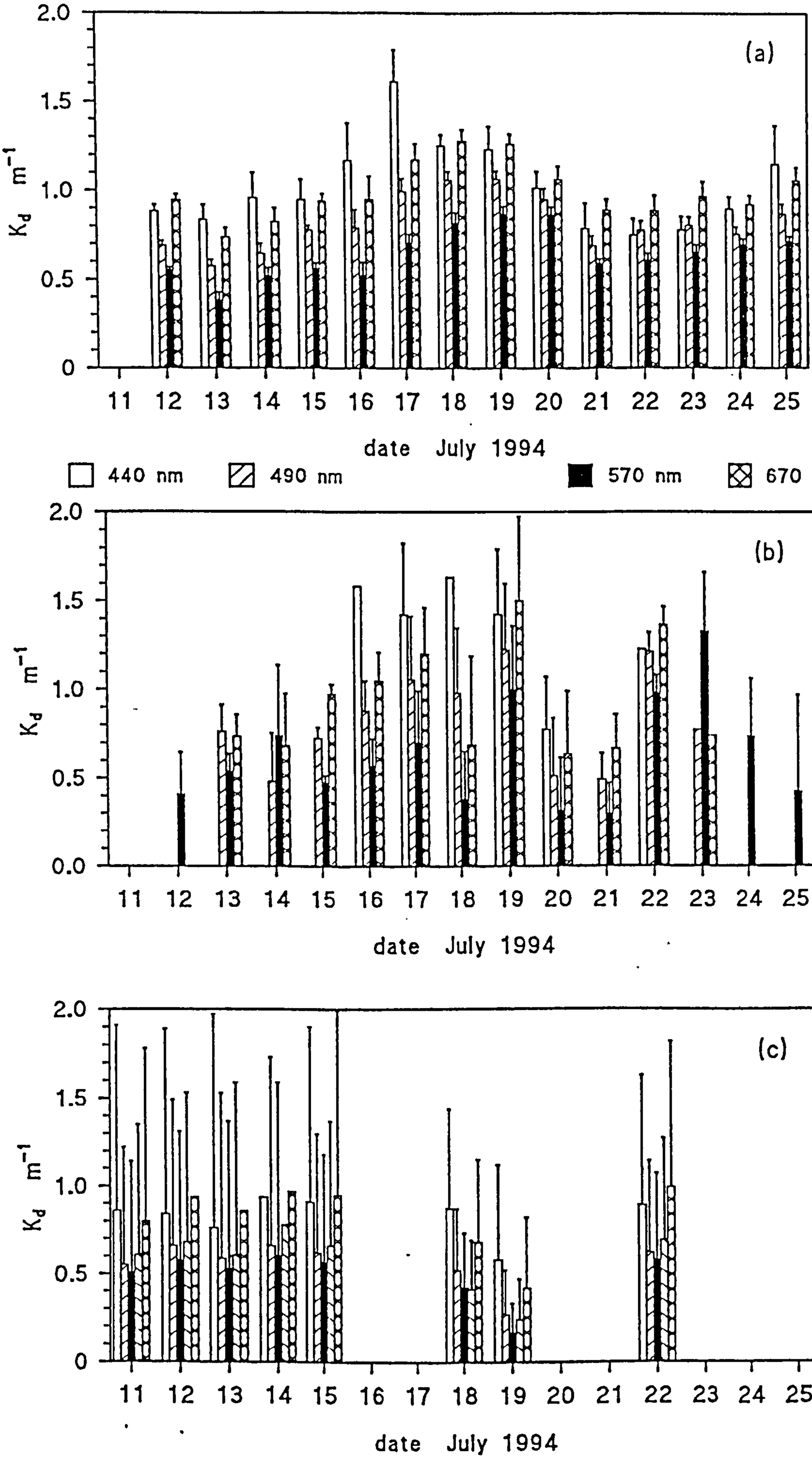
(a)
(b)
(c)
K_d m^{-1}
2.0
1.5
1.0
0.5
0.0
11 12 13 14 15 16 17 18 19 20 21 22 23 24 25
date July 1994
440 nm
490 nm
570 nm
670 nm

Figure 6.9 JMB94 level of light (570 nm) at bottom colour sensor showing variation with height of water column through tide: spring tide 11/07/94, neap 17-18/07/94

a) 12-15 July .
b) 16-18 July
c) 19-21 July
d) 22-25 July

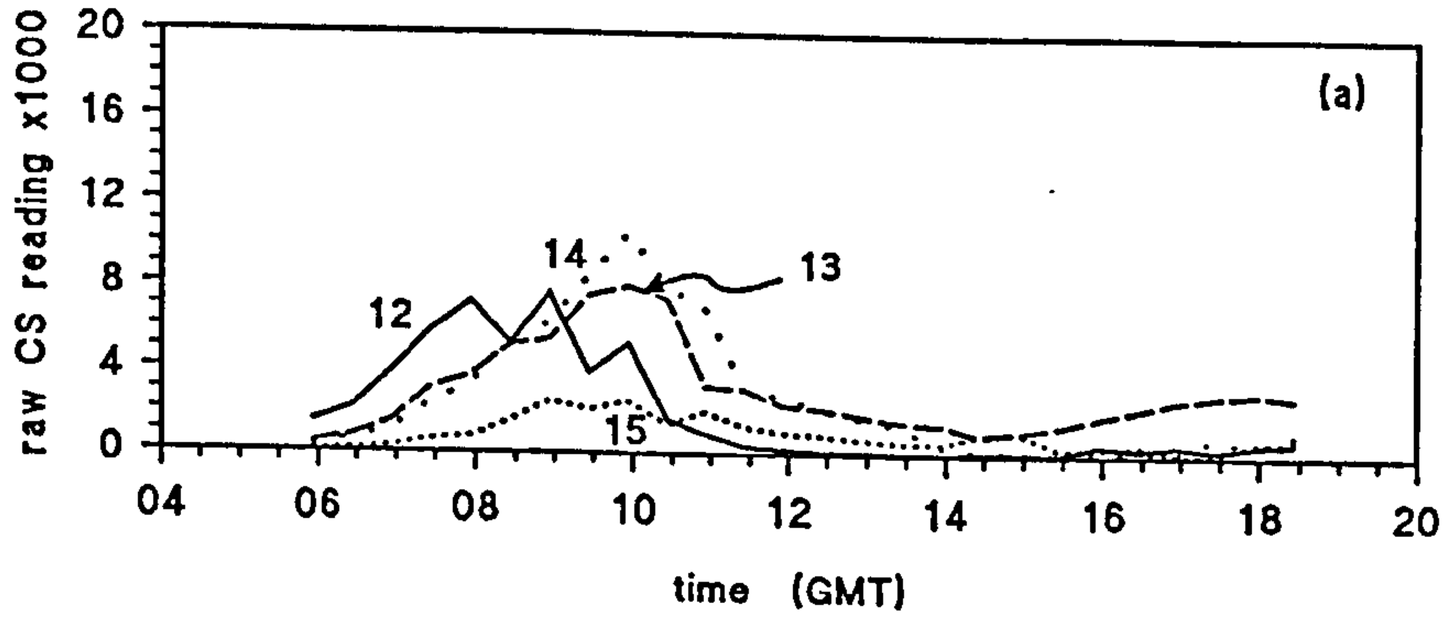
raw CS reading x1000
20
16
12
8
4
0
04
06
08
10
12
14
16
18
20
time (GMT)
(a)
12
13
14
15

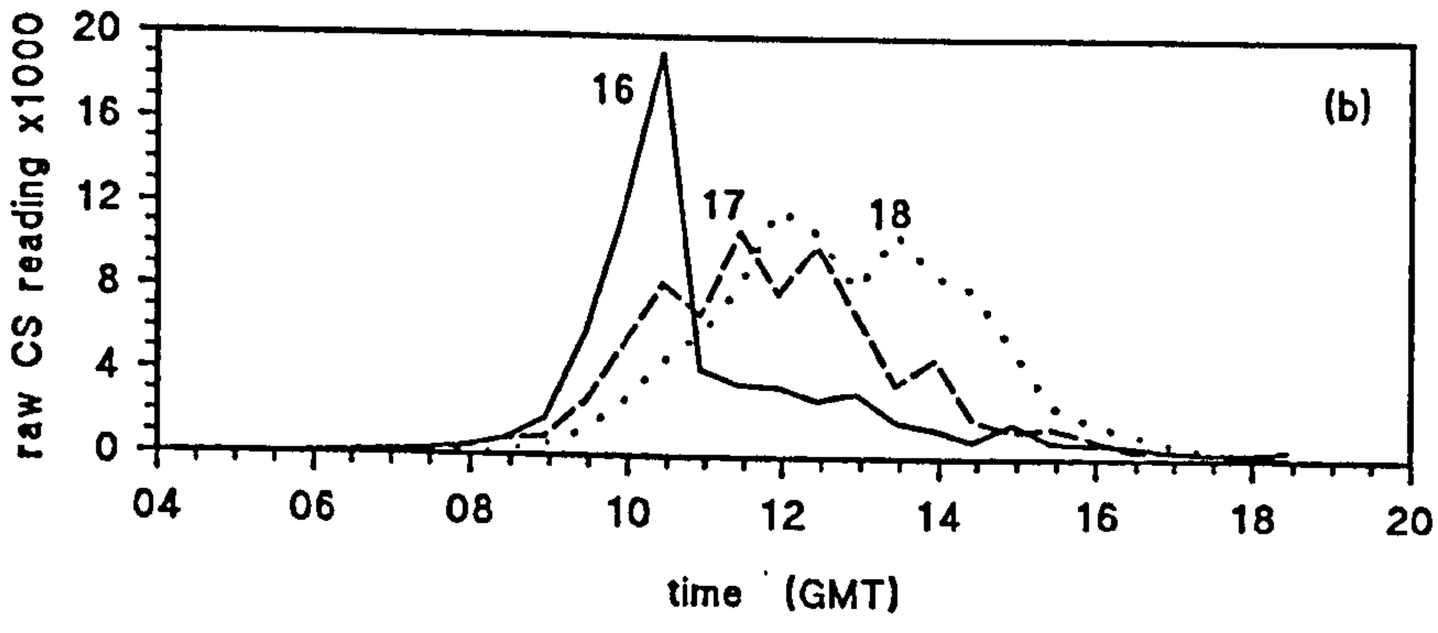
raw CS reading x1000
20
16
12
8
4
0
04
06
08
10
12
14
16
18
20
time (GMT)
(b)
16
17
18

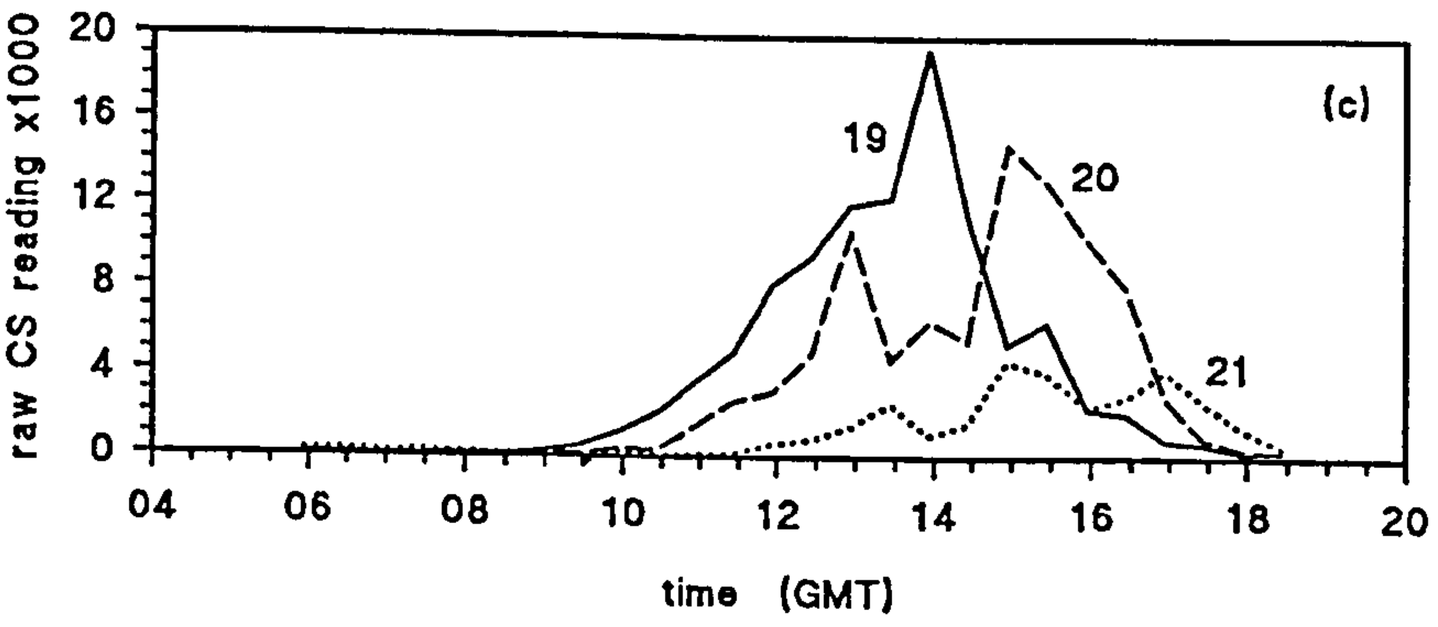
raw CS reading x1000
20
16
12
8
4
0
04
06
08
10
12
14
16
18
20
time (GMT)
(c)
19
20
21

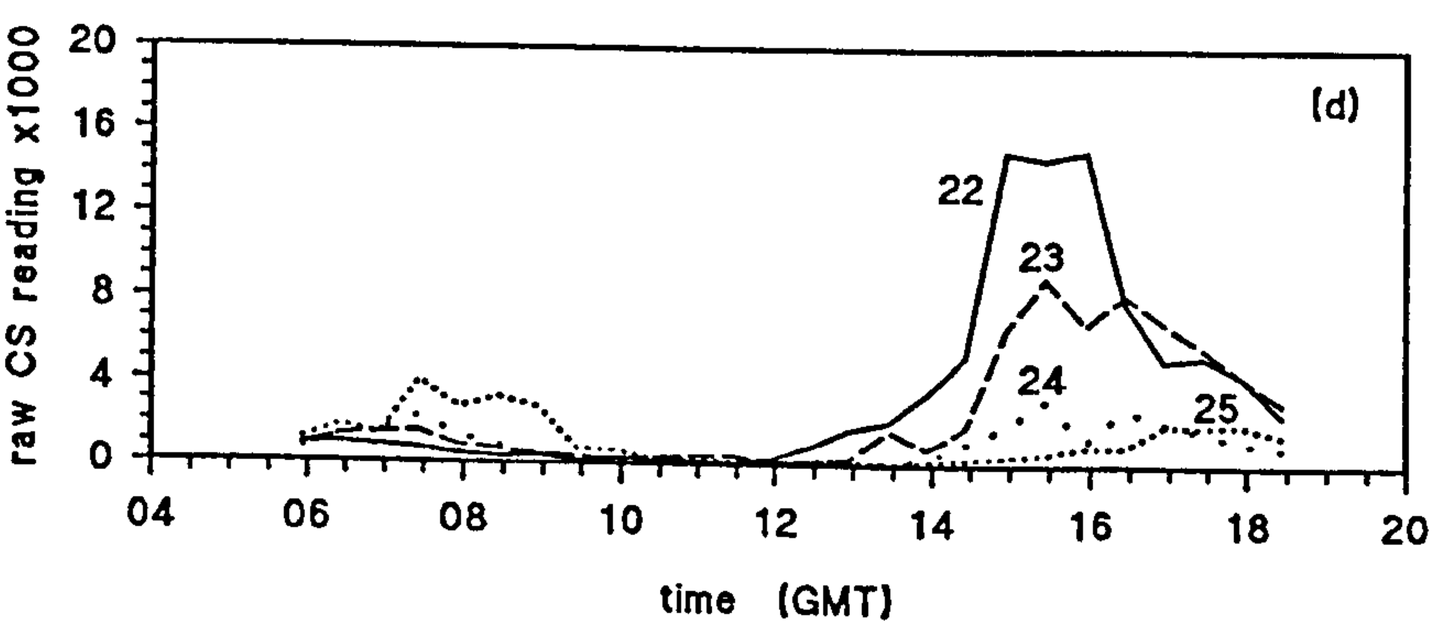
raw CS reading x1000
20
16
12
8
4
0
04
06
08
10
12
14
16
18
20
time (GMT)
(d)
22
23
24
25

Figure 6.10 JMB94 490:570 ratio at bottom sensor showing change with tidal cycle, from low values at midday with spring tides, with a peak at midday for neap tides

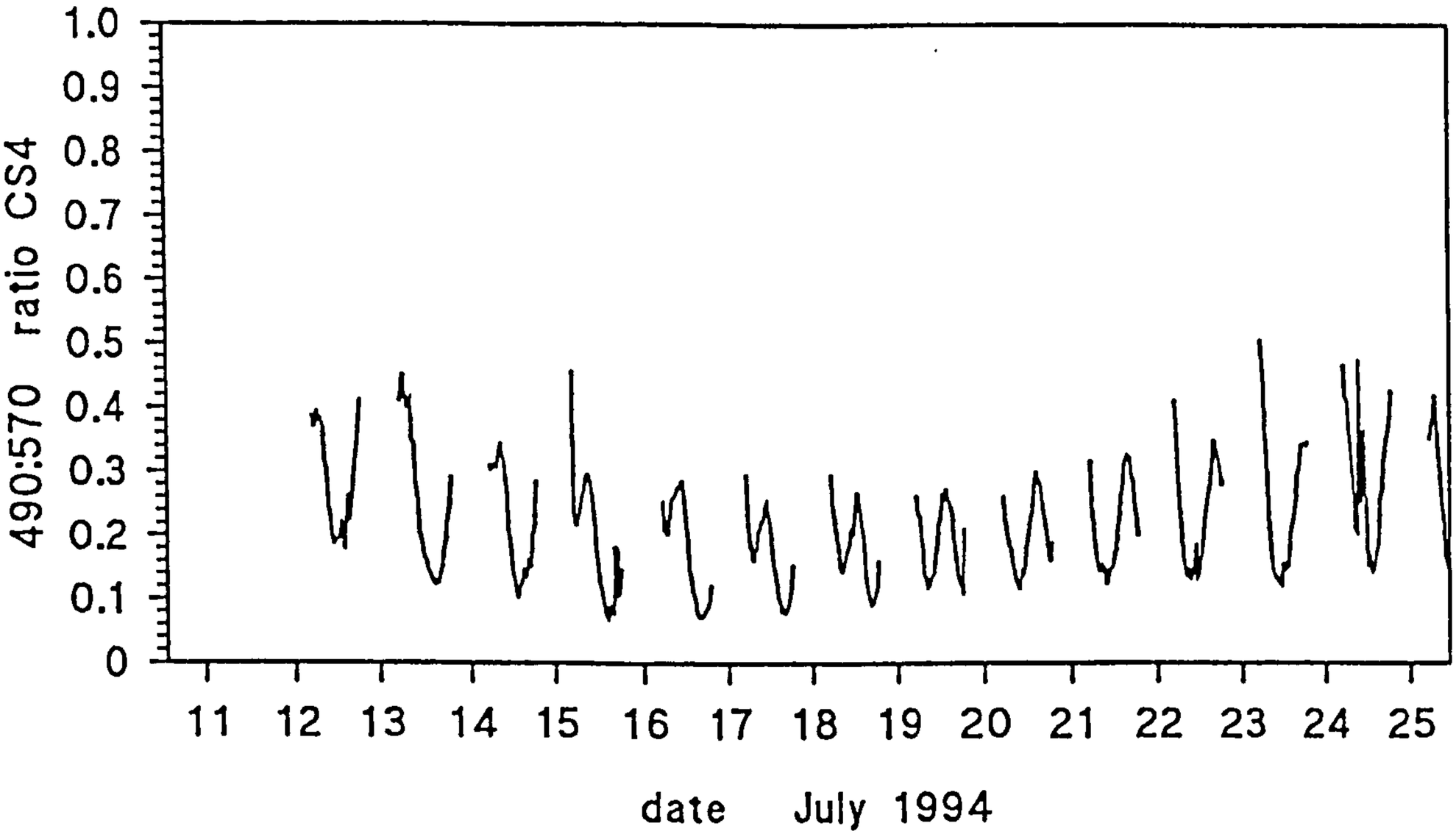
490:570 ratio CS4
1.0
0.9
0.8
0.7
0.6
0.5
0.4
0.3
0.2
0.1
0
11 12 13 14 15 16 17 18 19 20 21 22 23 24 25
date July 1994

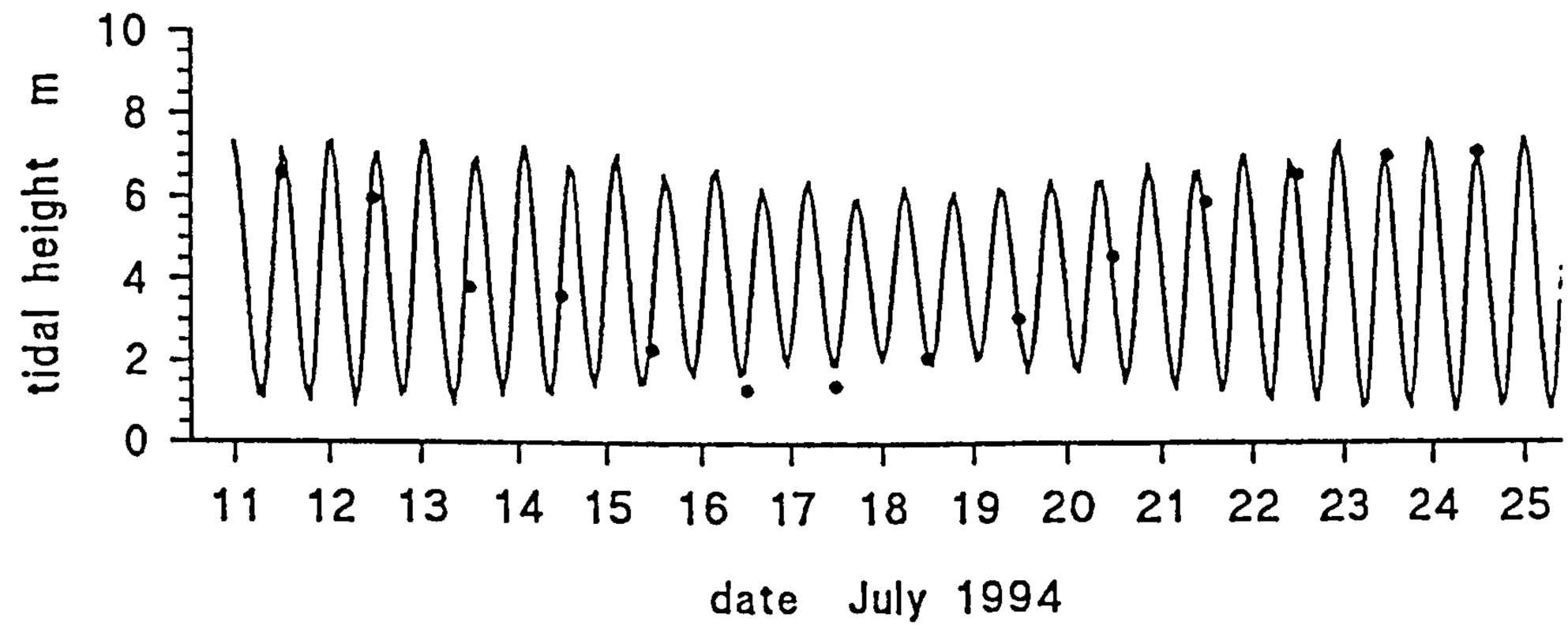
tidal height m
10
8
6
4
2
0
11 12 13 14 15 16 17 18 19 20 21 22 23 24 25
date July 1994

Figure 6.11 July Pier Survey 1994: diffuse attenuation calculated from colour sensor readings for the whole day

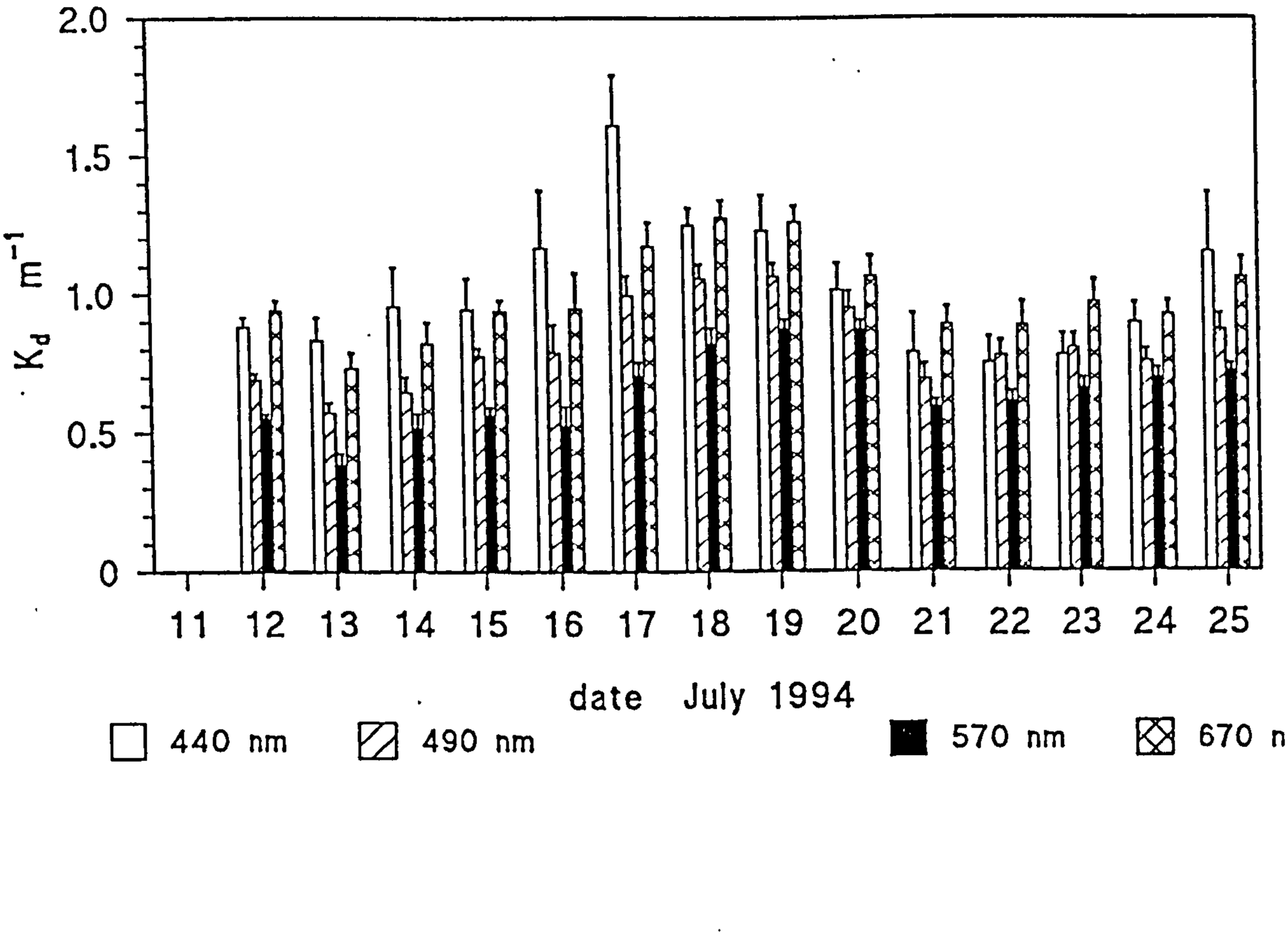
2.0
1.5
1.0
0.5
0
K_d m^{-1}
11 12 13 14 15 16 17 18 19 20 21 22 23 24 25
date July 1994
440 nm
490 nm
570 nm
670 n

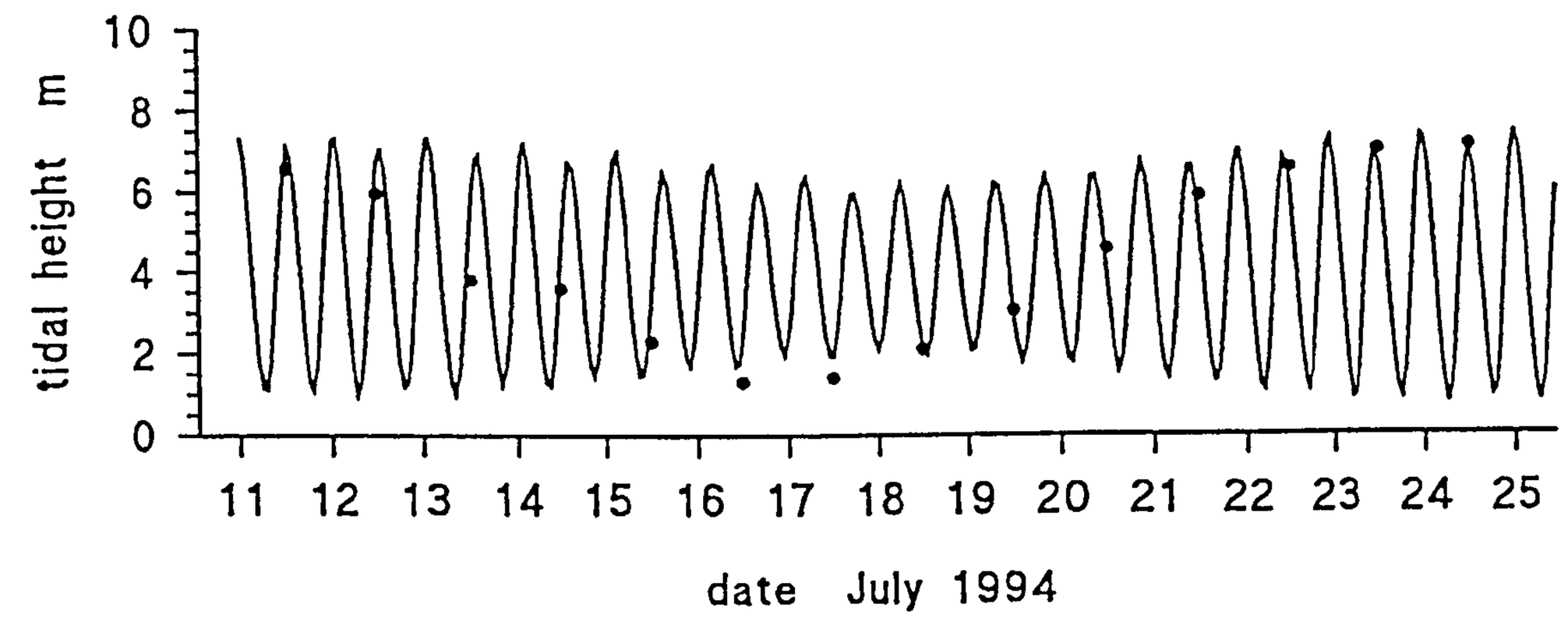
10
8
6
4
2
0
tidal height m
11 12 13 14 15 16 17 18 19 20 21 22 23 24 25
date July 1994

Figure 6.12 Cwmystradllyn [02/08/95] 440:570 variation through water column, indicating relative decrease in blue light to green light

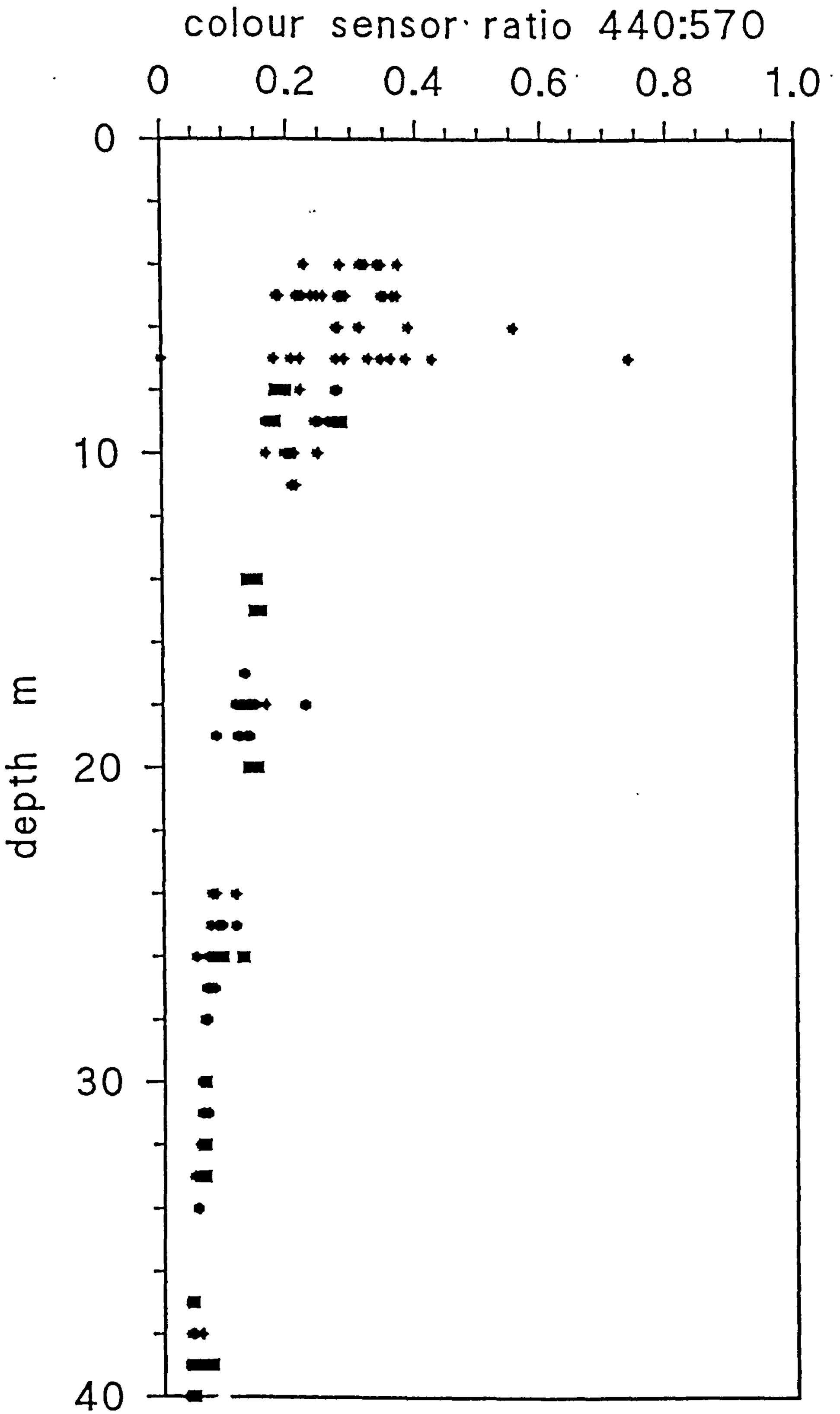
colour sensor ratio 440:570
0
0.2
0.4
0.6
0.8
1.0
0
10
20
30
40
depth m

Figure 6.13 Reflectance values for Menai Strait Survey

a) 444 nm
b) 521 nm
c) 552 nm
d) 596 nm
e) 670 nm

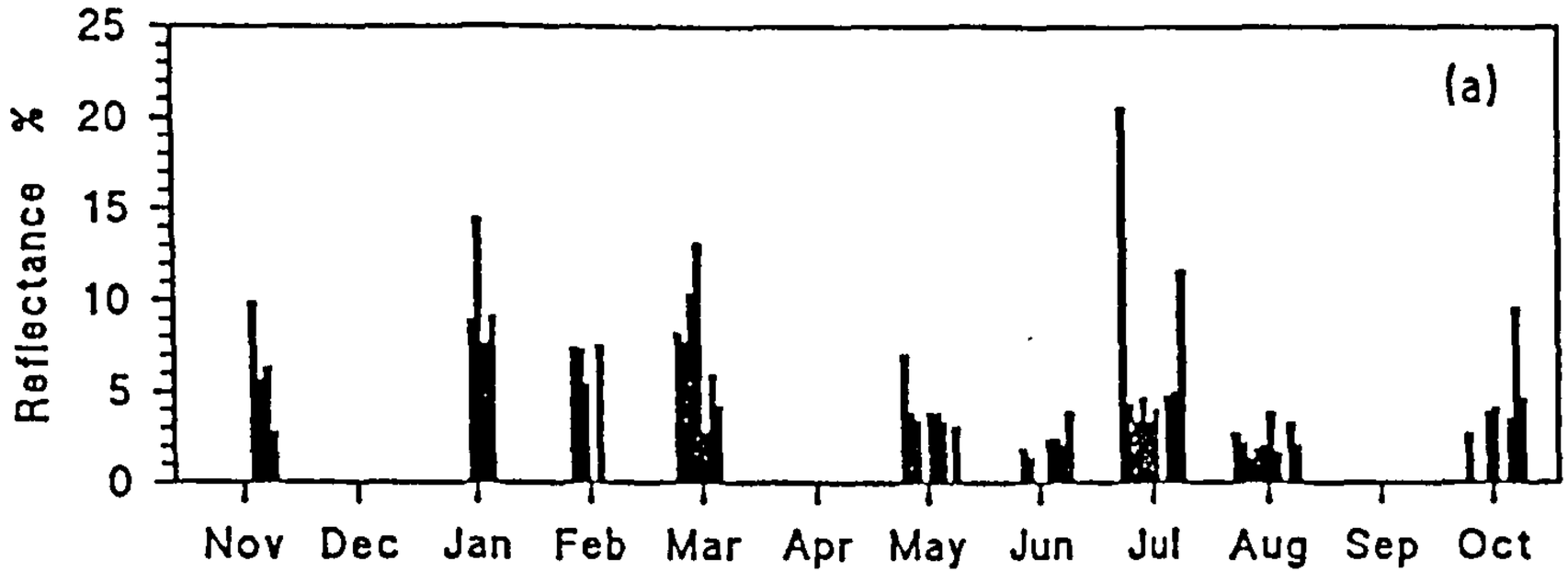
(a)
Reflectance %
25
20
15
10
5
0
Nov Dec Jan Feb Mar Apr May Jun Jul Aug Sep Oct

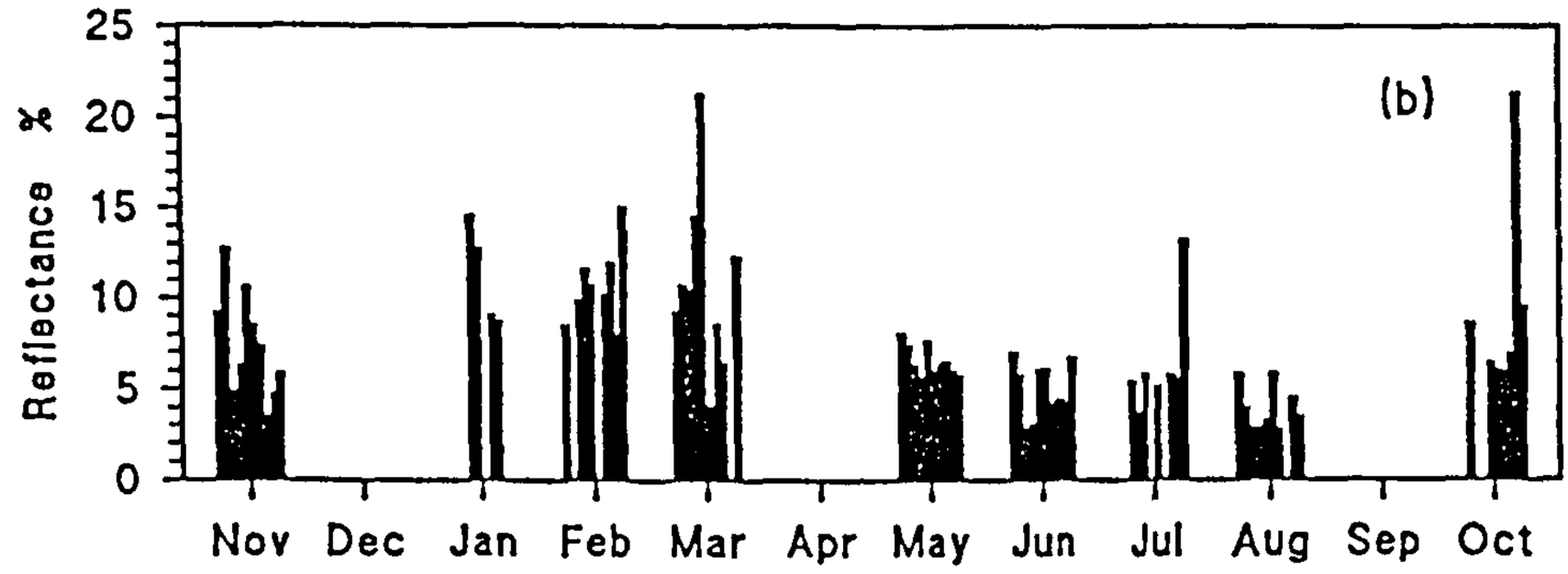
(b)
Reflectance %
25
20
15
10
5
0
Nov Dec Jan Feb Mar Apr May Jun Jul Aug Sep Oct

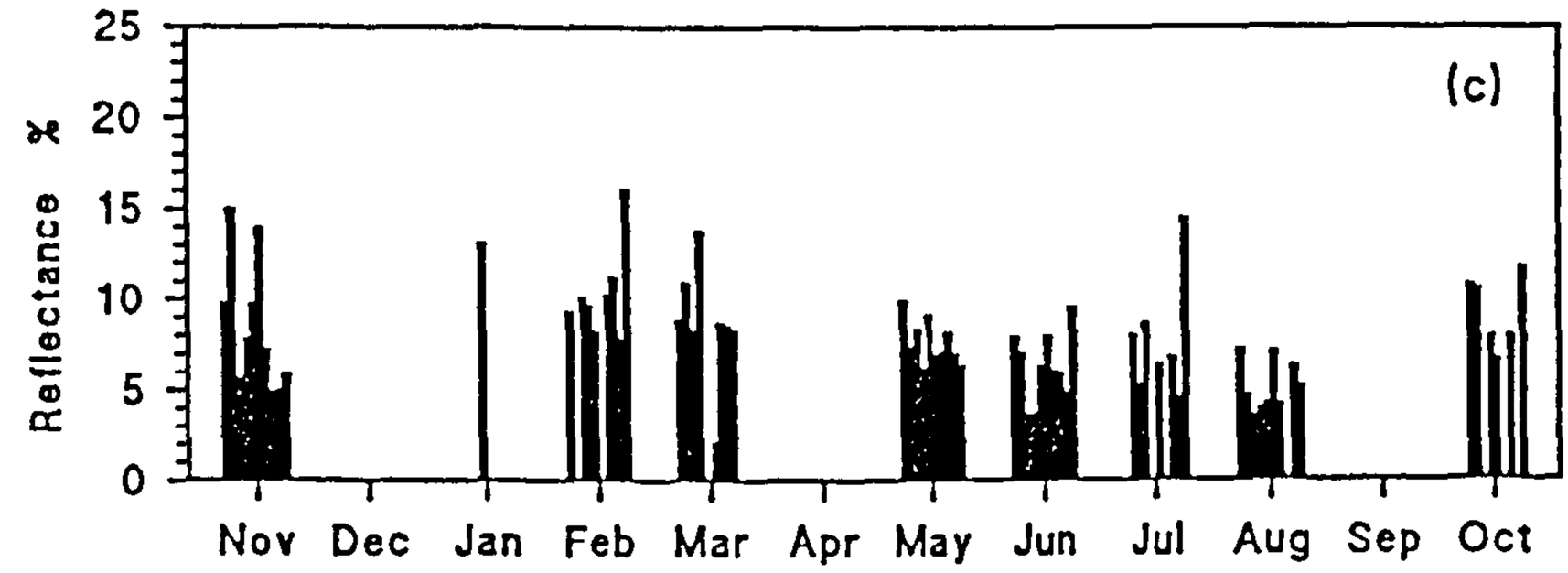
(c)
Reflectance %
25
20
15
10
5
0
Nov Dec Jan Feb Mar Apr May Jun Jul Aug Sep Oct

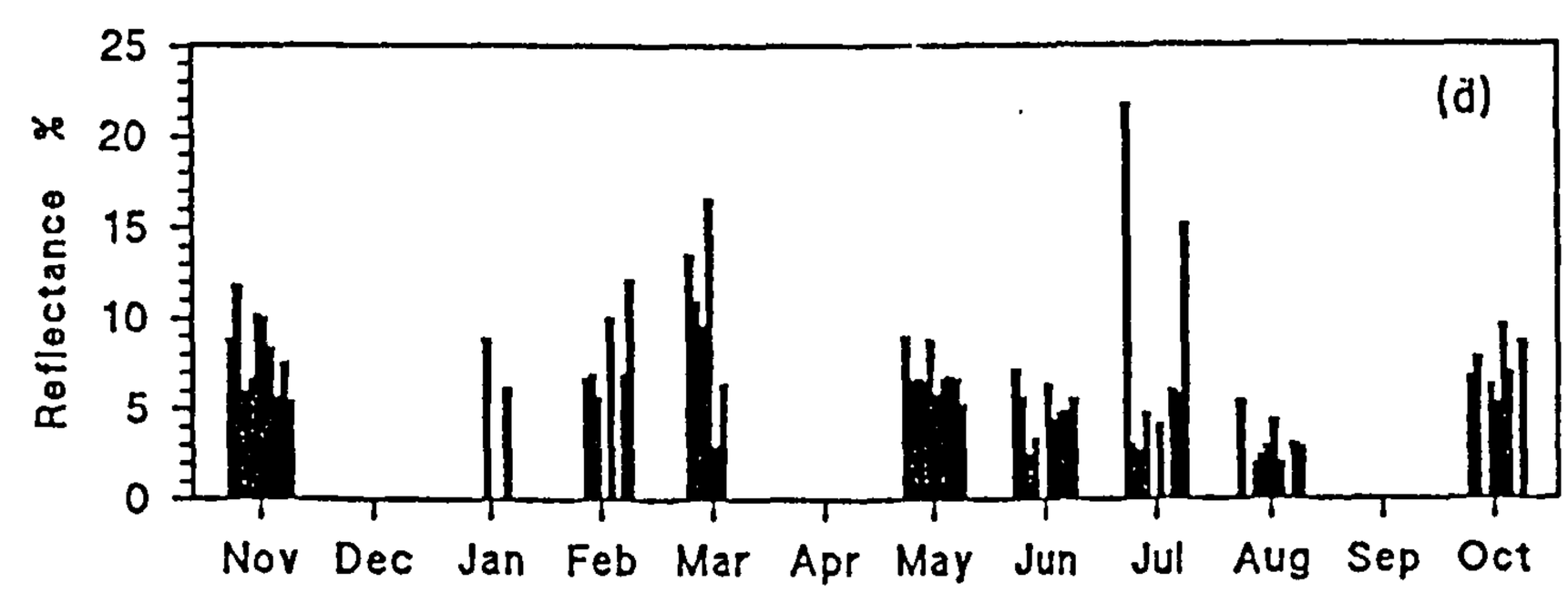
(d)
Reflectance %
25
20
15
10
5
0
Nov Dec Jan Feb Mar Apr May Jun Jul Aug Sep Oct

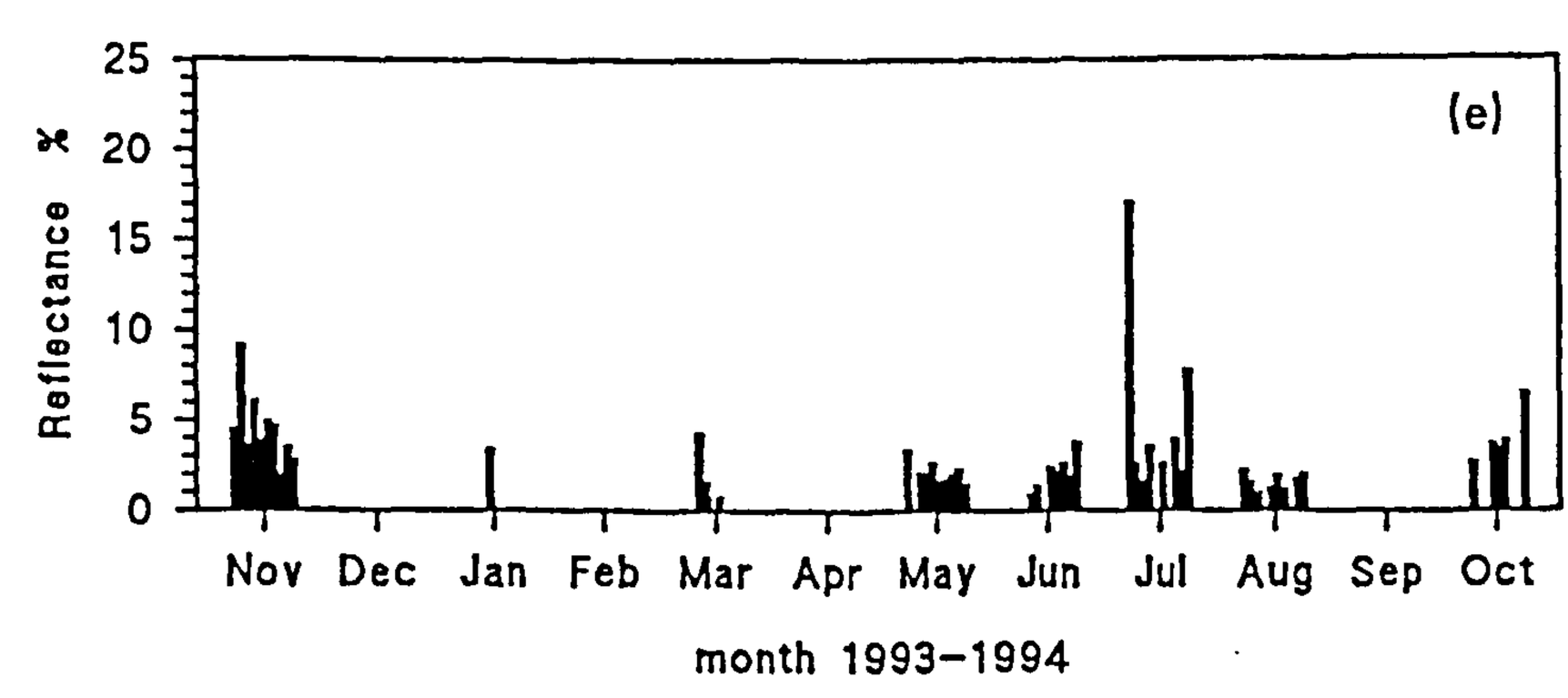
(e)
Reflectance %
25
20
15
10
5
0
Nov Dec Jan Feb Mar Apr May Jun Jul Aug Sep Oct
month 1993–1994

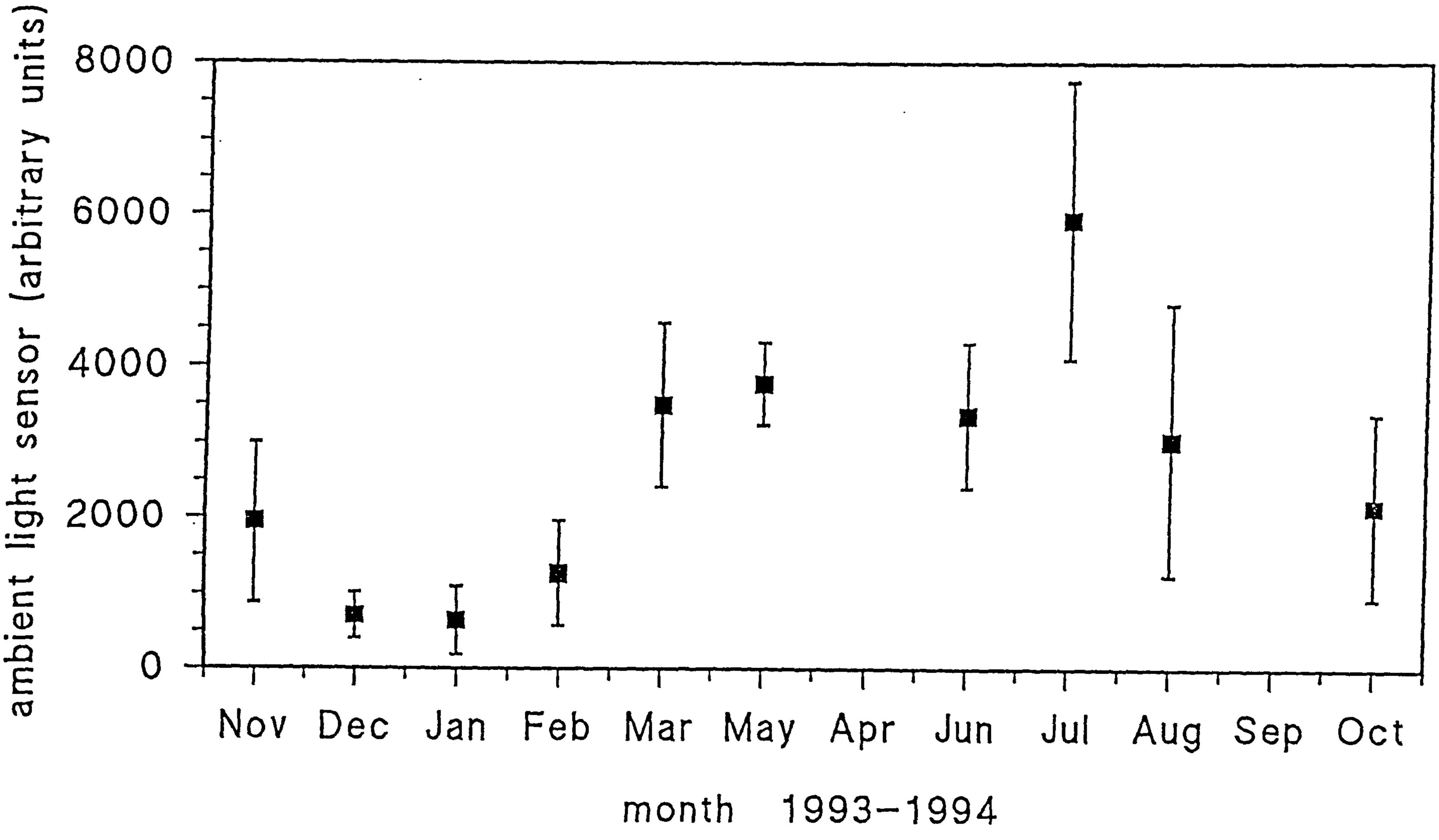

Figure 6.14 Ambient light measured with cosine detector in Menai Strait Survey for 1993-1994, Channel 1: 670 nm

Figure 6.15 Reflectance values for July Pier Survey 1994
a) colour sensor 12:00-14:00 GMT
b) Spectron SE-590 spectra

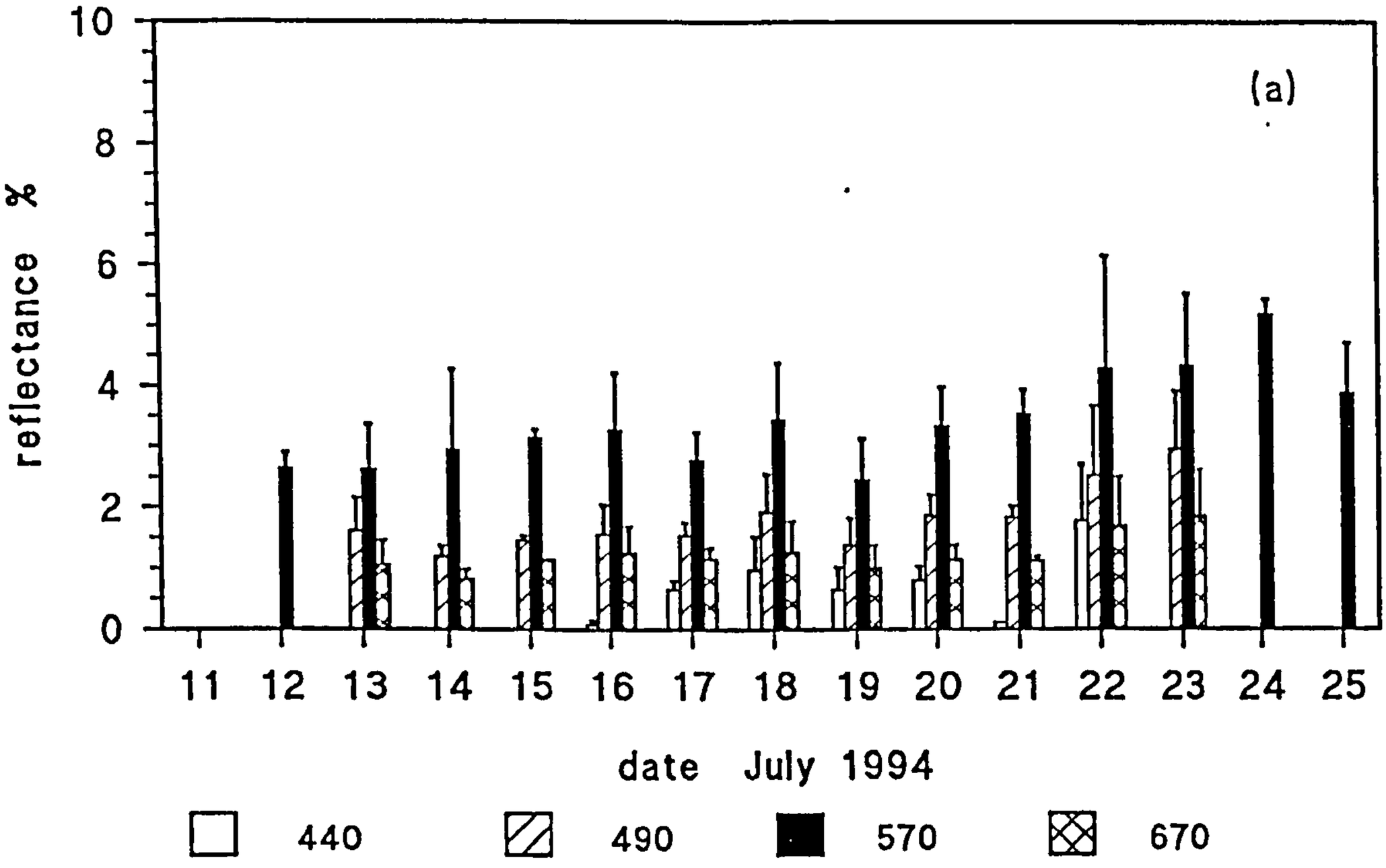
(a)
reflectance %
10
8
6
4
2
0
11 12 13 14 15 16 17 18 19 20 21 22 23 24 25
date July 1994
440
490
570
670

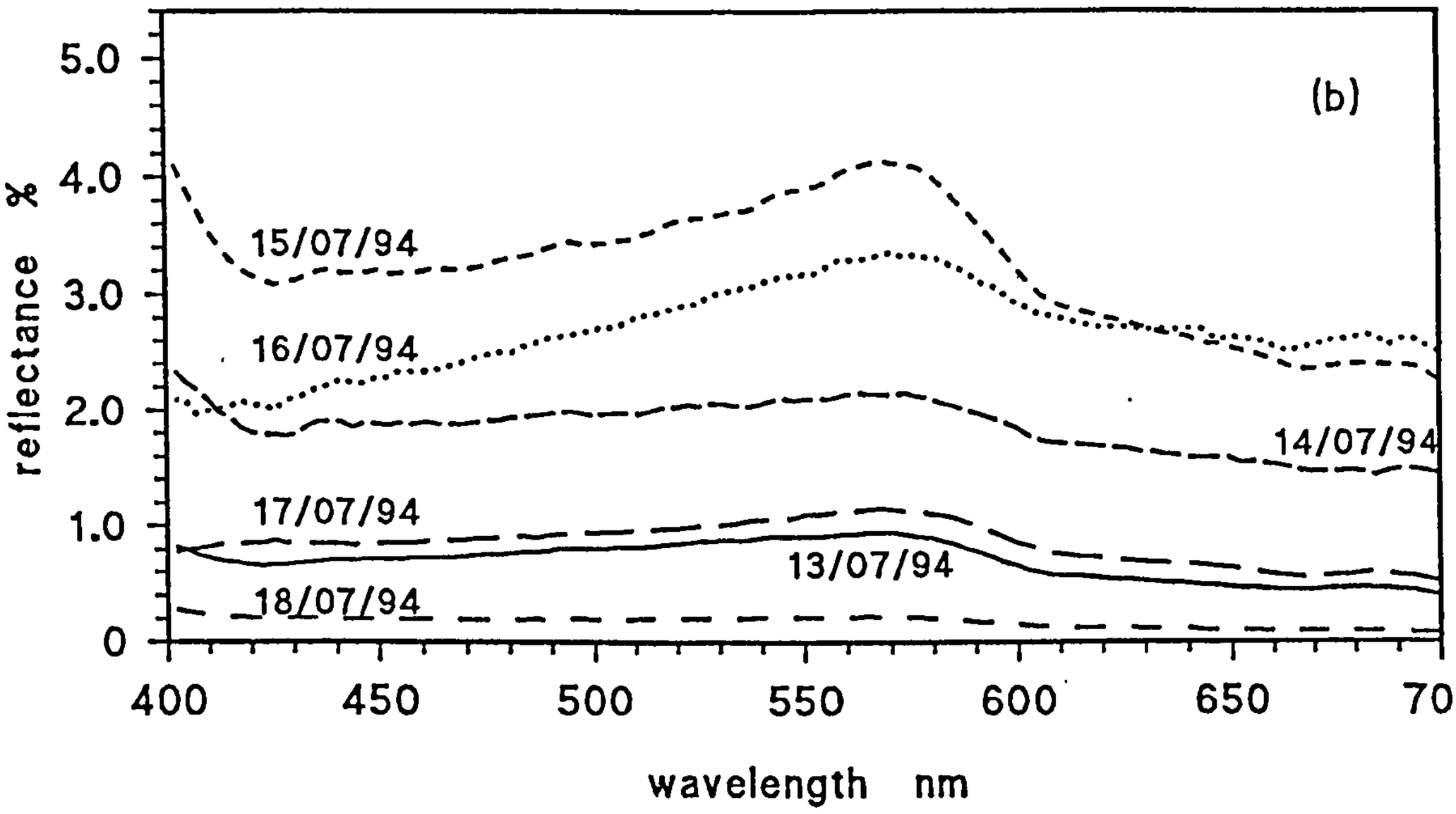
(b)
reflectance %
5.0
4.0
3.0
2.0
1.0
0
15/07/94
16/07/94
14/07/94
17/07/94
13/07/94
18/07/94
400 450 500 550 600 650 700
wavelength nm

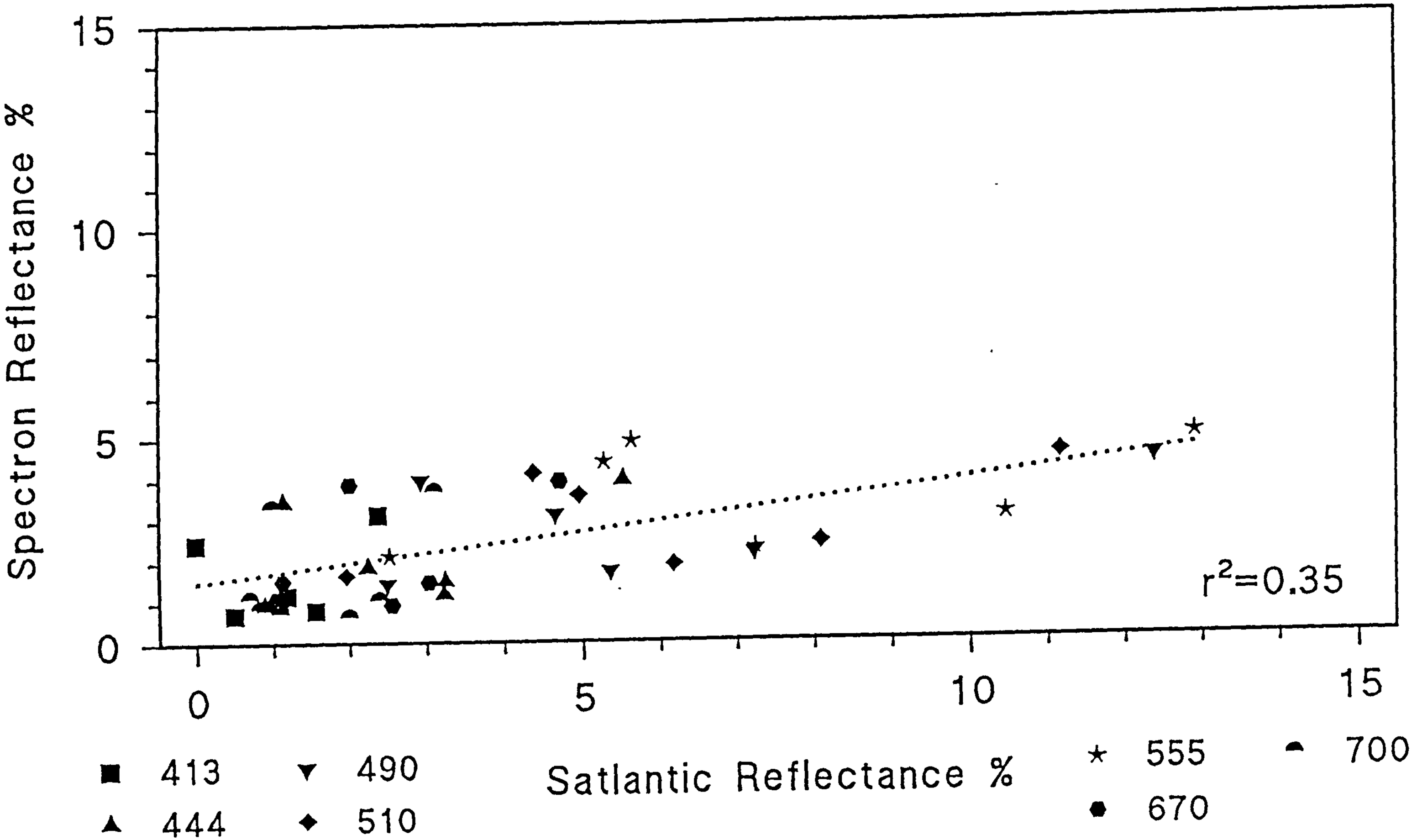

Figure 6.16 Reflectance values for August Pier Survey 1995, Spectron measurements compared with Satlantic measurements

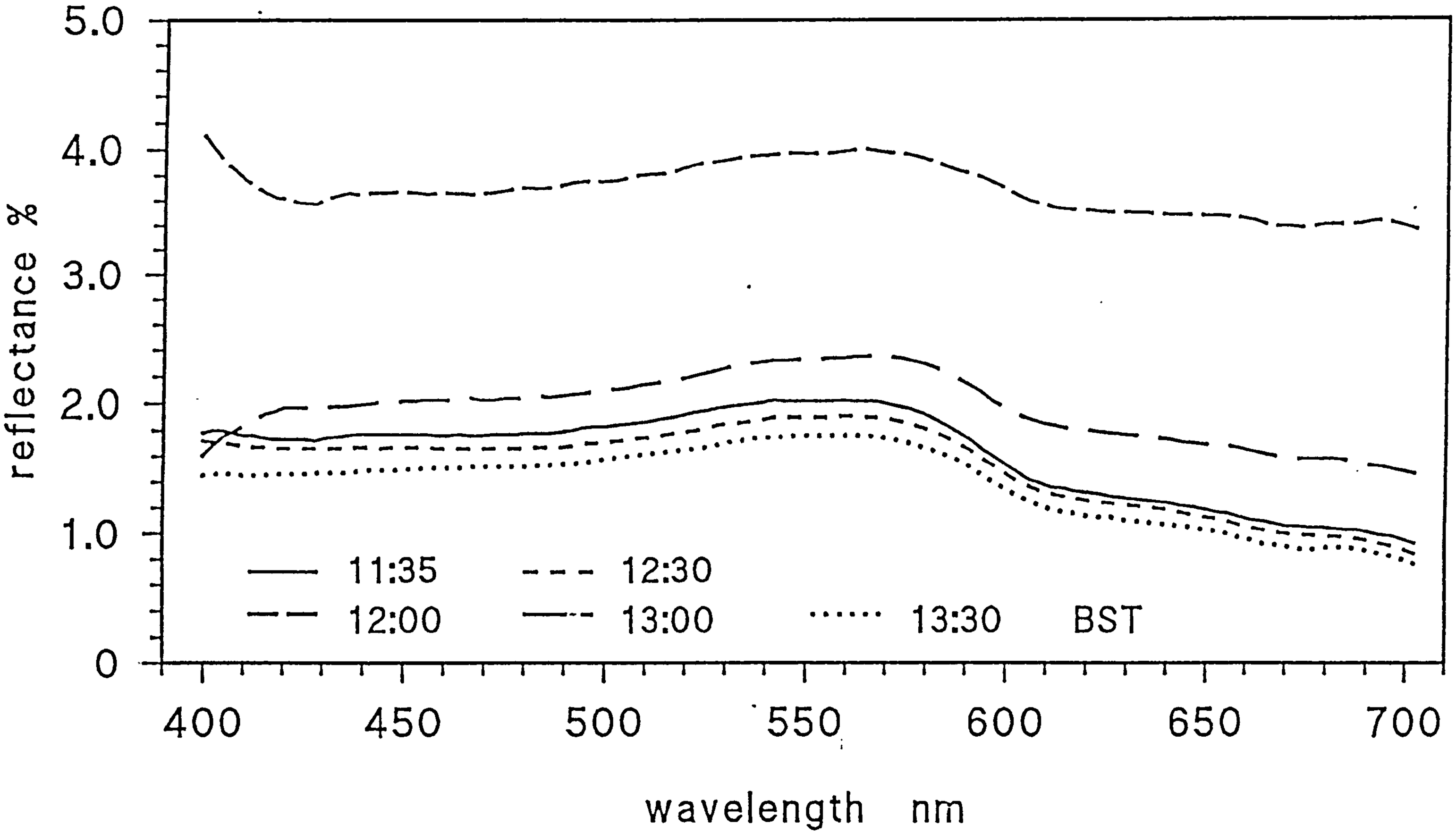

Figure 6.17 Spectron reflectance spectra for Cwmystradllyn [02/08/95]

Figure 6.18 Upwelling signal measured by Satlantic for Cwmystradllyn [31/03/96]
a) upwelling radiance L_u and irradiance E_u
b) ratio between irradiance and radiance

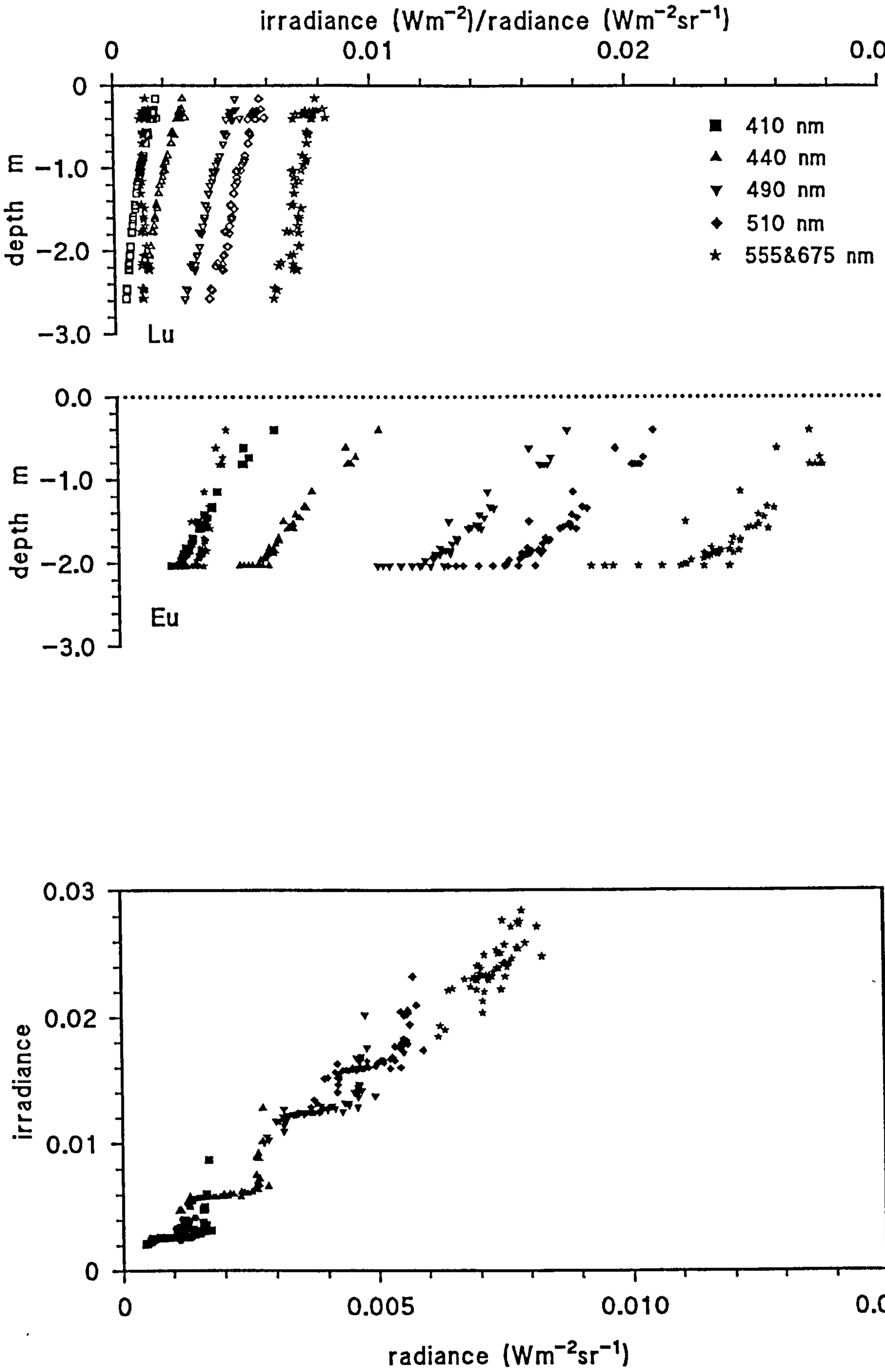
irradiance (Wm^{-2})/radiance (Wm^{-2}sr^{-1})
0
0.01
0.02
0.03
depth m
0
−1.0
−2.0
−3.0
Lu
410 nm
440 nm
490 nm
510 nm
555&675 nm
0.0
−1.0
−2.0
−3.0
depth m
Eu
0.03
0.02
0.01
0
irradiance
0
0.005
0.010
0.01
radiance (Wm^{-2}sr^{-1})

Figure 6.19 Variation of radiance with angle in Cwmystradllyn [31/03/96]
a) tilt/roll angle and radiance over time
b) radiance level against tilt angle

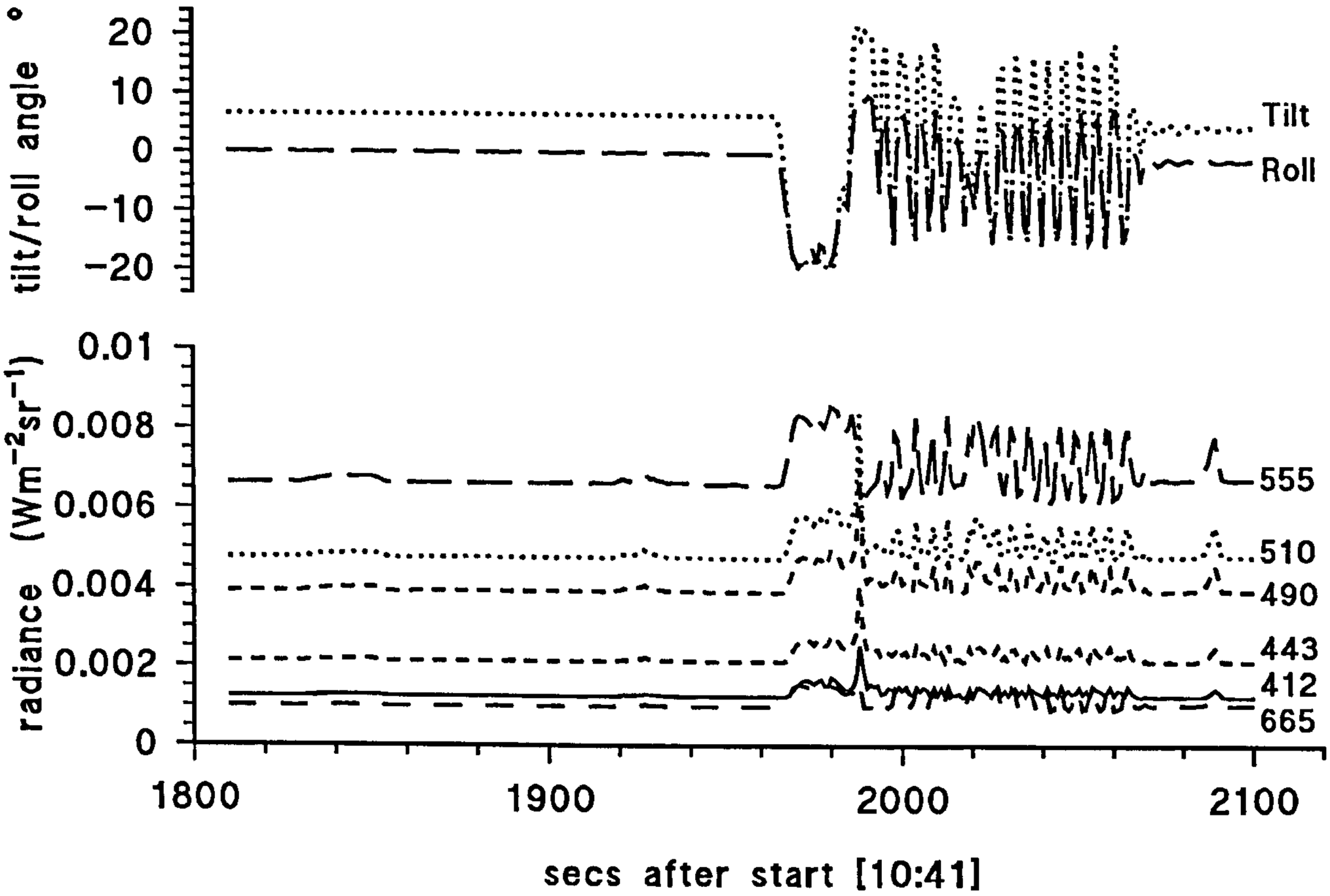
tilt/roll angle °
20
10
0
−10
−20
Tilt
Roll
radiance (Wm⁻²sr⁻¹)
0.01
0.008
0.006
0.004
0.002
0
555
510
490
443
412
665
1800
1900
2000
2100
secs after start [10:41]

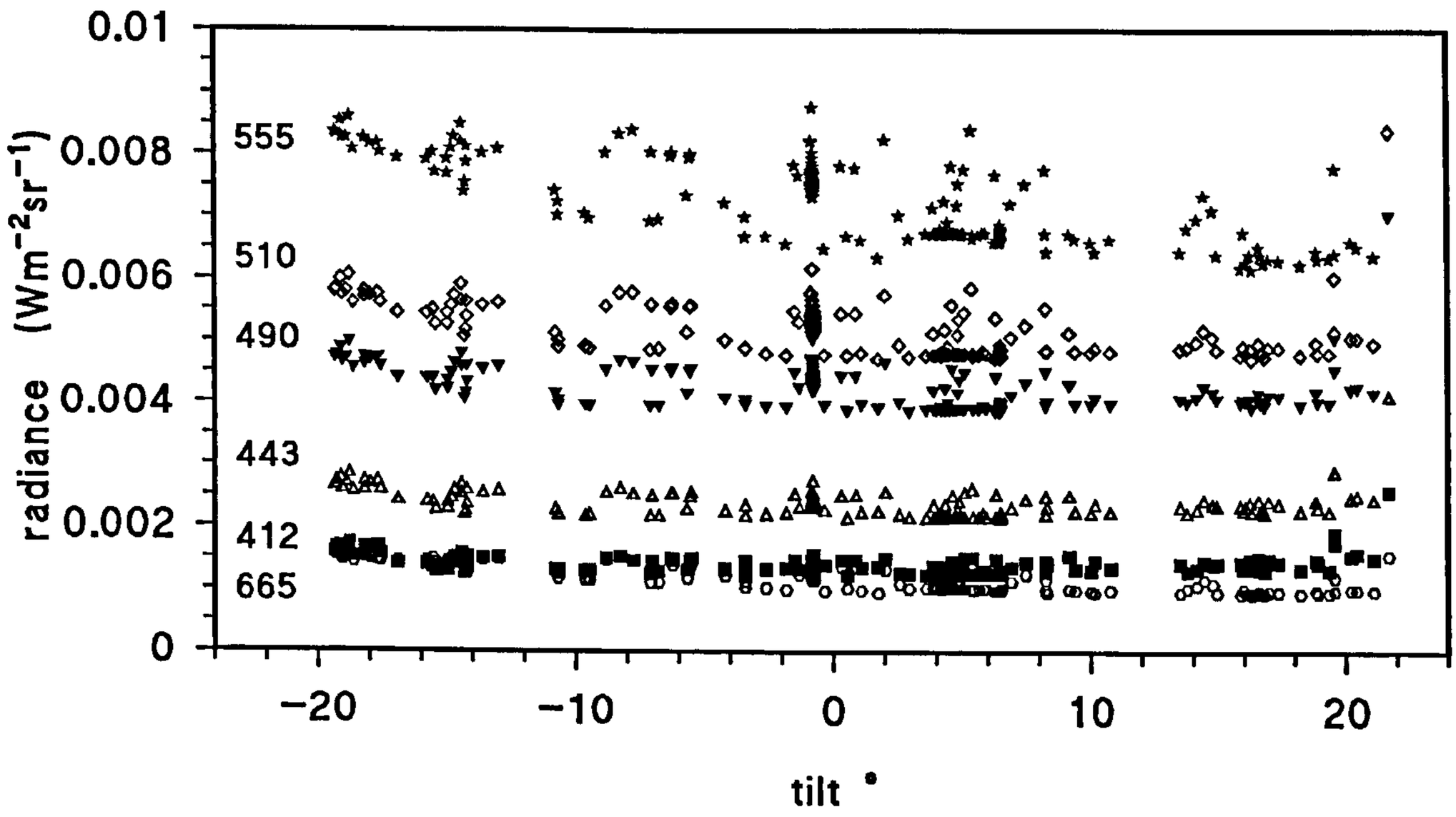
radiance (Wm⁻²sr⁻¹)
0.01
0.008
0.006
0.004
0.002
0
555
510
490
443
412
665
−20
−10
0
10
20
tilt °

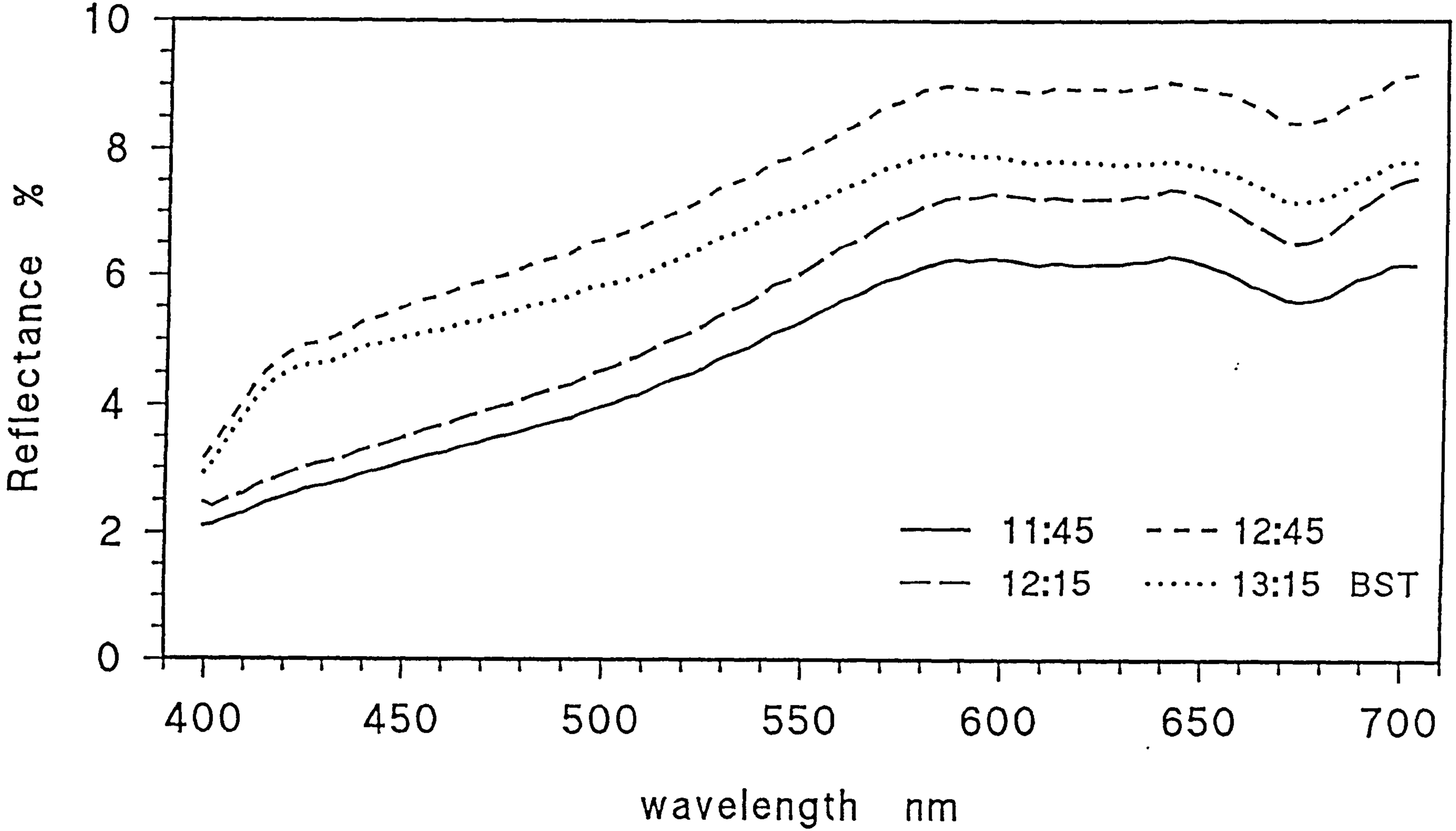

Figure 6.20 Spectron reflectance spectra for Dolgarrog, Conwy [29/07/95]

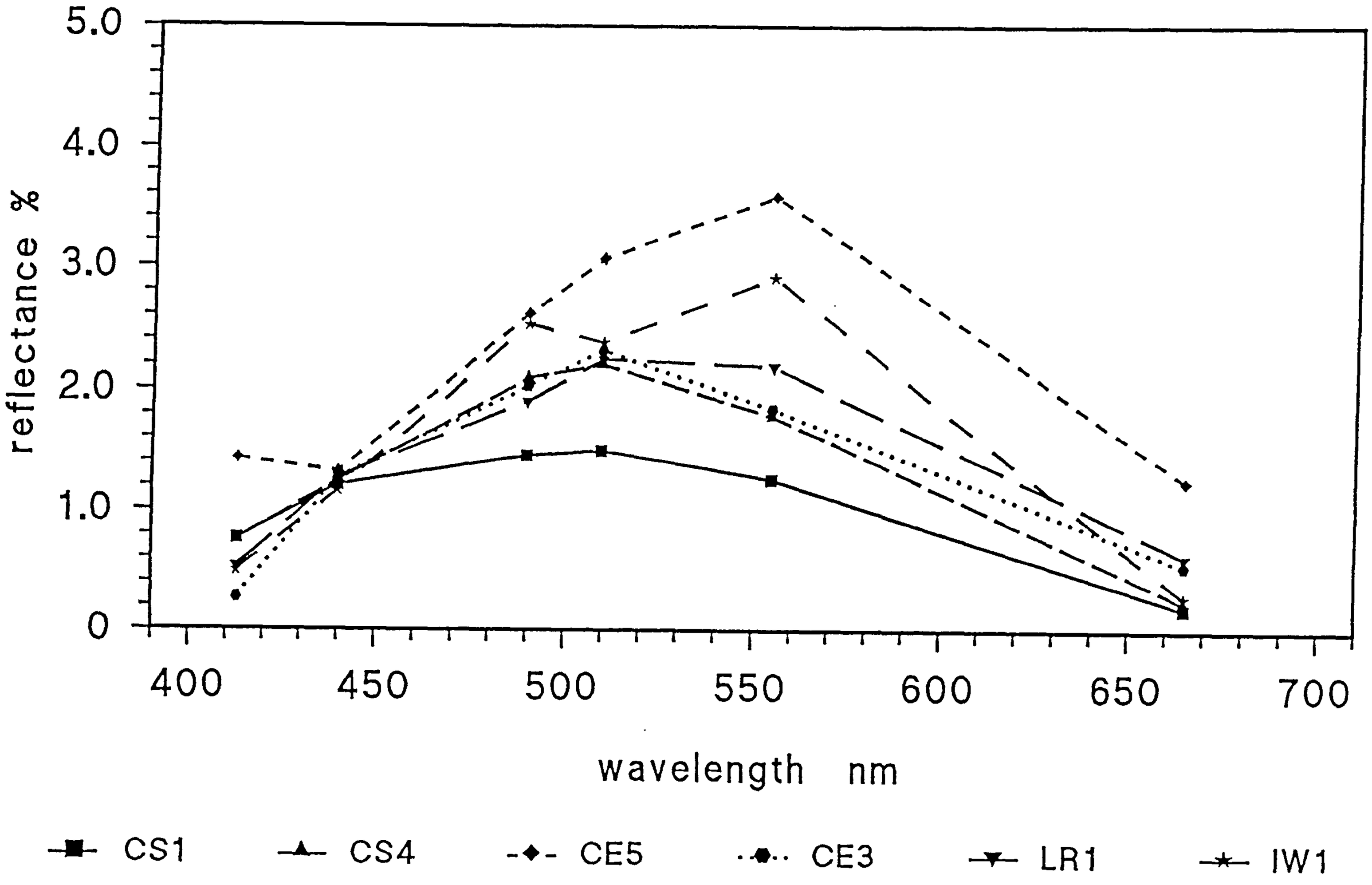

Figure 6.21 PRR-600 reflectance spectra for Clyde Survey 1996, showing increase in reflectance, with a shift in the peak towards the red as constituent concentrations increase

Figure 6.22 Effect of bottom albedo in reflectance profiles, assumes $E=L\pi$

a) Cwmystradllyn 31/03/96: 412 nm, 443 nm, 490 nm
b) Cwmystradllyn 31/03/96: 510 nm, 555 nm, 665 nm
c) Dolgarrog 26/03/96: 412 nm, 443 nm, 490 nm
d) Dolgarrog 26/03/96: 510 nm, 555 nm, 665 nm

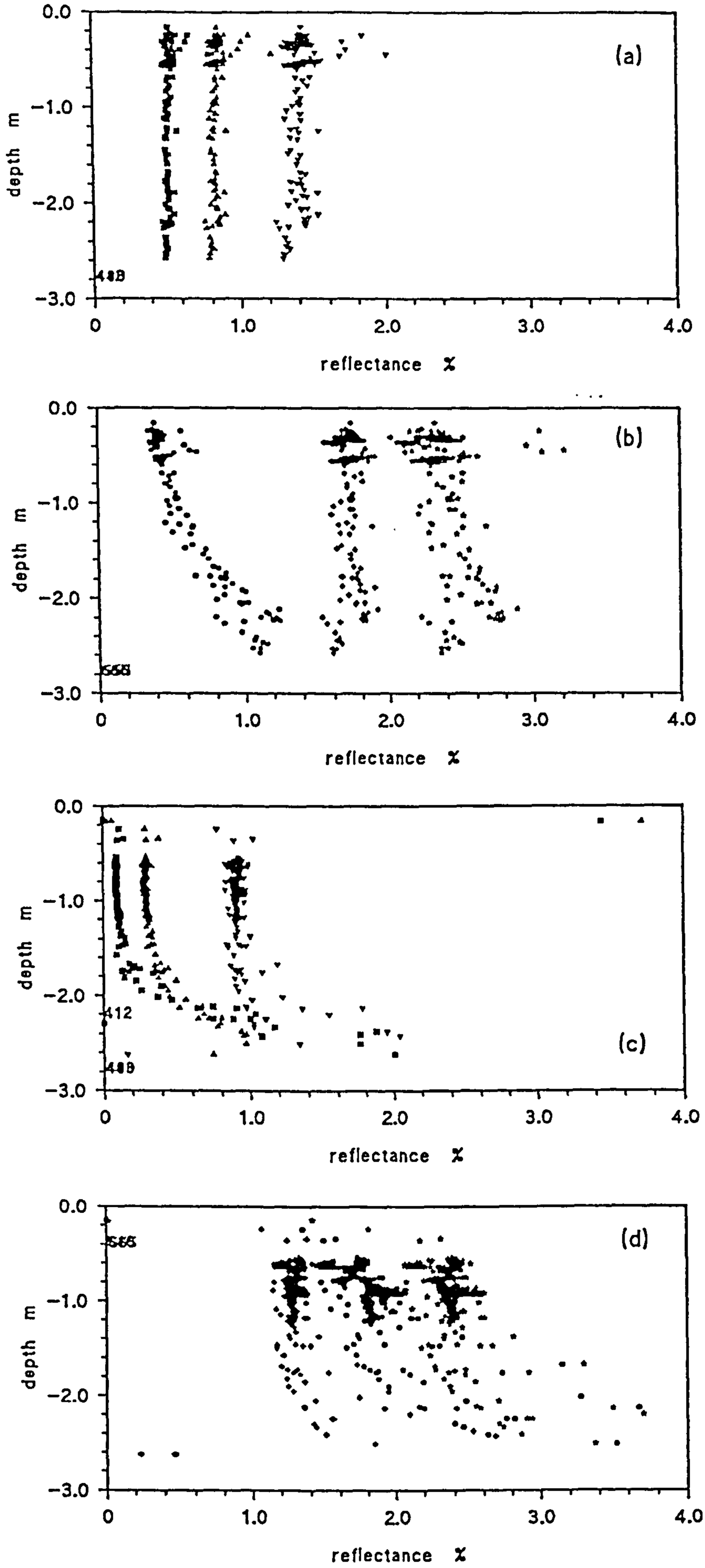
0.0
−1.0
−2.0
−3.0
depth m
0
1.0
2.0
3.0
4.0
reflectance %
(a)
(b)
(c)
(d)

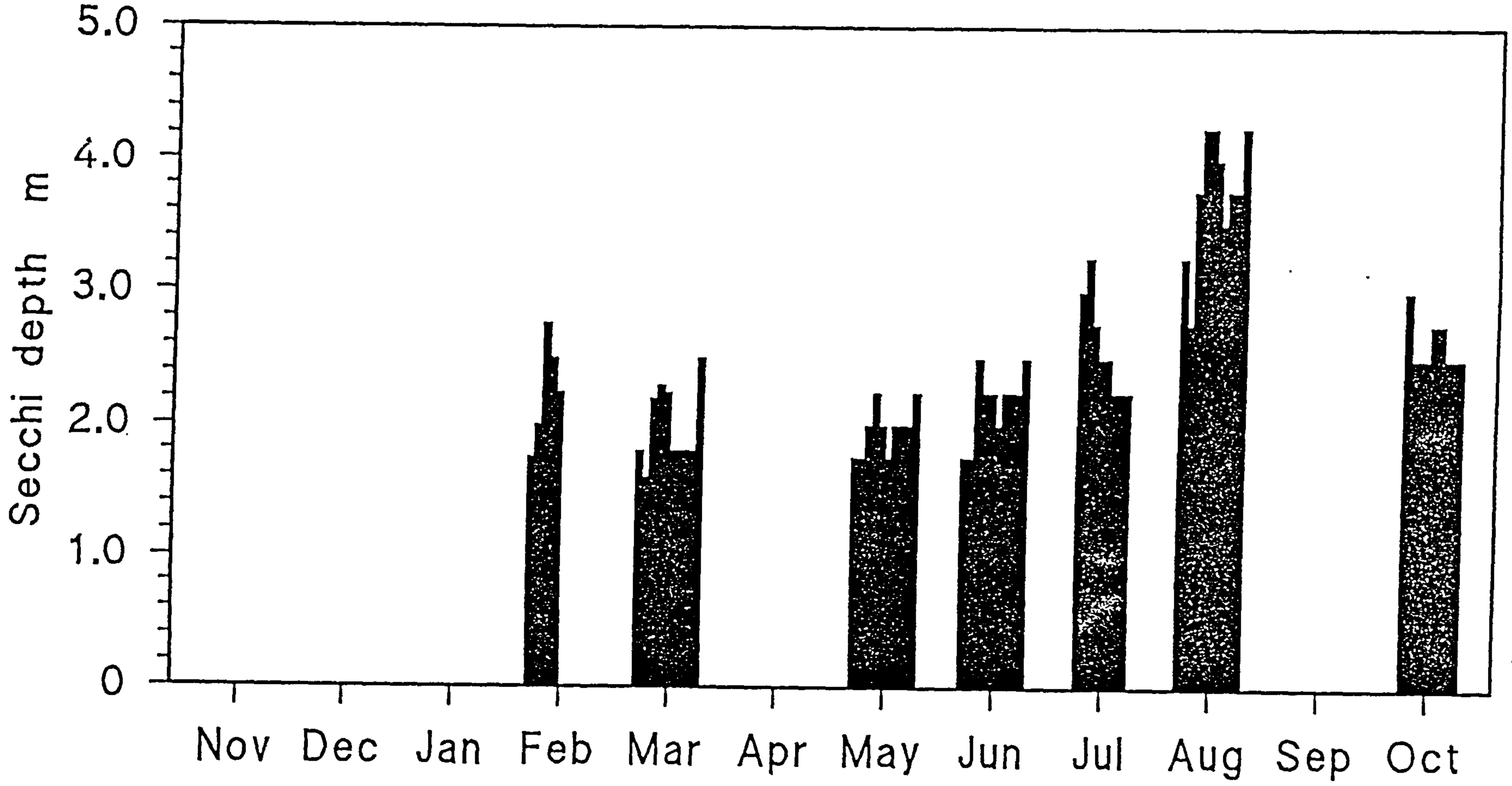

Figure 6.23 Secchi depth measured through the Menai Strait Survey 1993-1994

Figure 6.24 Secchi depth measured through the July Pier Survey 1994

a) Daily value at midday with tidal height

b) Hourly value through 24 hour period 21-22 July, with tidal height

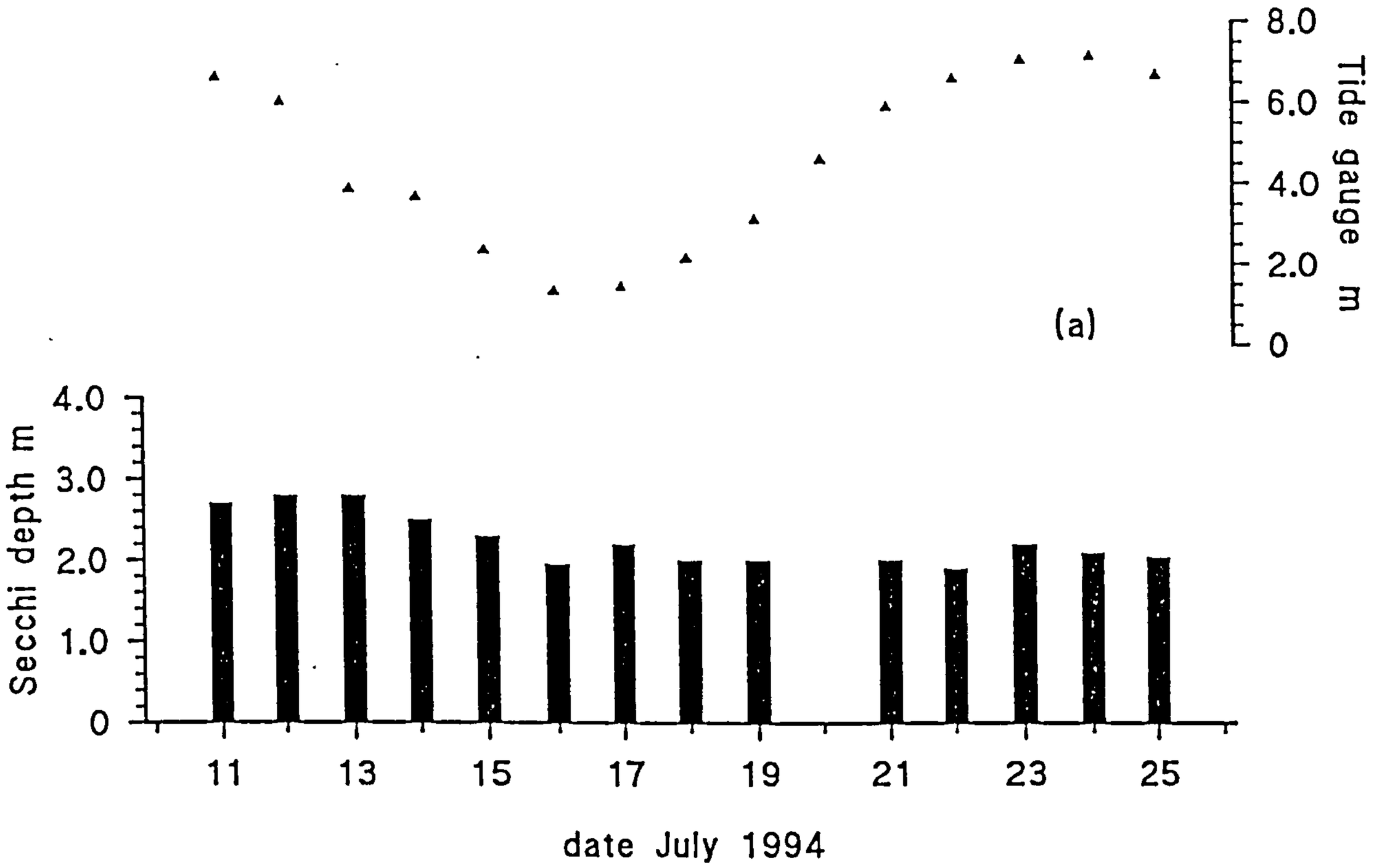
(a)
8.0
6.0
4.0
2.0
0
Tide gauge m
4.0
3.0
2.0
1.0
0
Secchi depth m
11
13
15
17
19
21
23
25
date July 1994
(b)
8.0
6.0
4.0
2.0
0
Tide gauge m
4.0
3.0
2.0
1.0
0
Secchi depth m
08
12
16
20
06
time 21–22 July 1994

Figure 6.25 Secchi depth measured through the August Pier Survey 1995

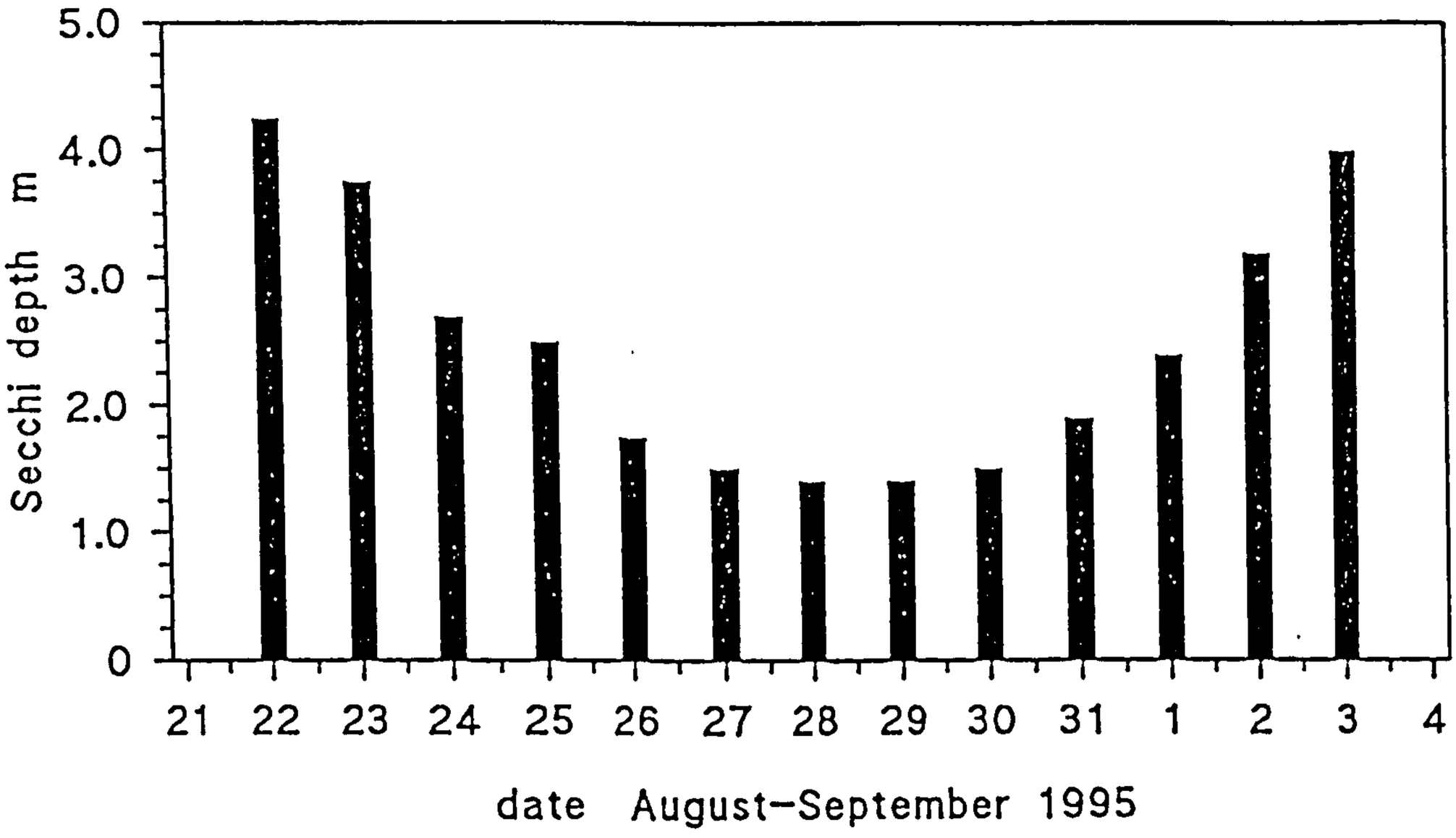
Secchi depth m
5.0
4.0
3.0
2.0
1.0
0
21 22 23 24 25 26 27 28 29 30 31 1 2 3 4
date August–September 1995

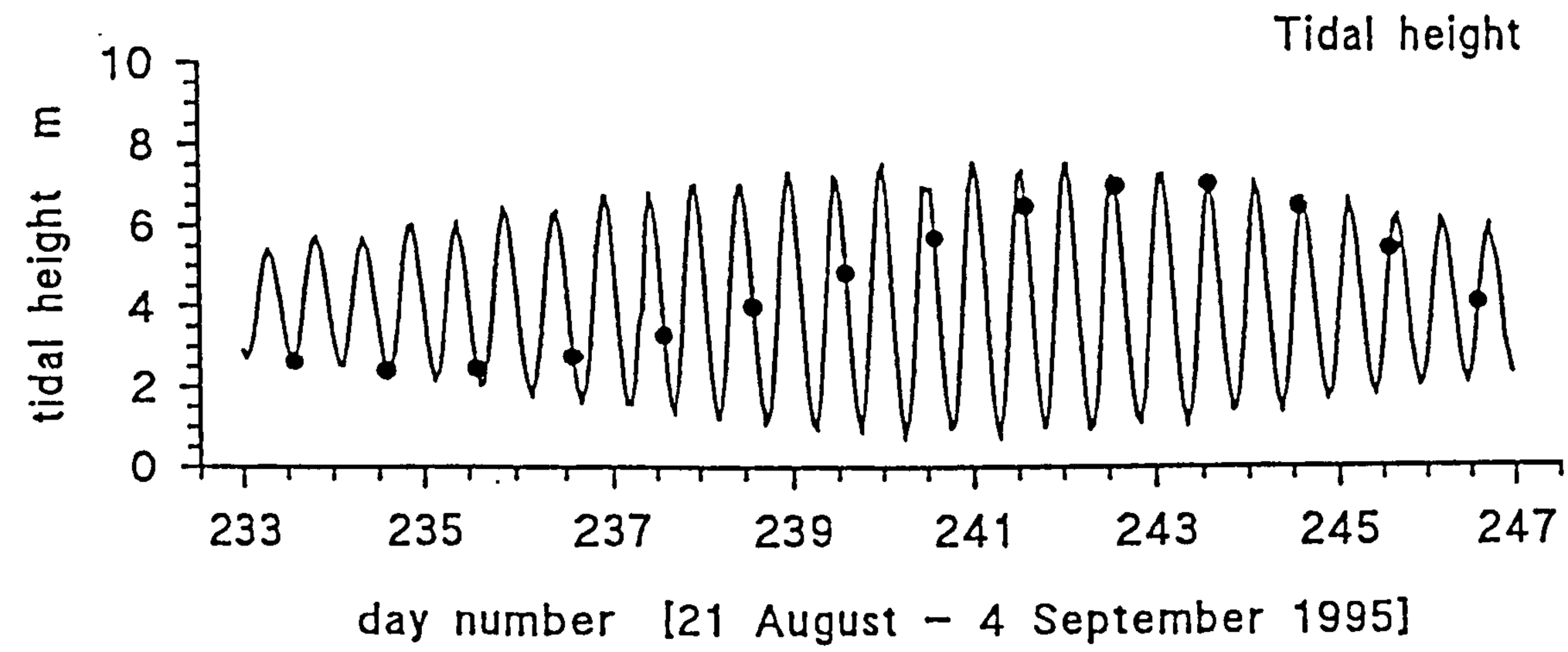
Tidal height
tidal height m
10
8
6
4
2
0
233 235 237 239 241 243 245 247
day number [21 August – 4 September 1995]

Figure 6.26 Transmissometer readings through tidal cycle, July Pier Survey 1994

a) beam attenuation

b) temperature

c) tidal height

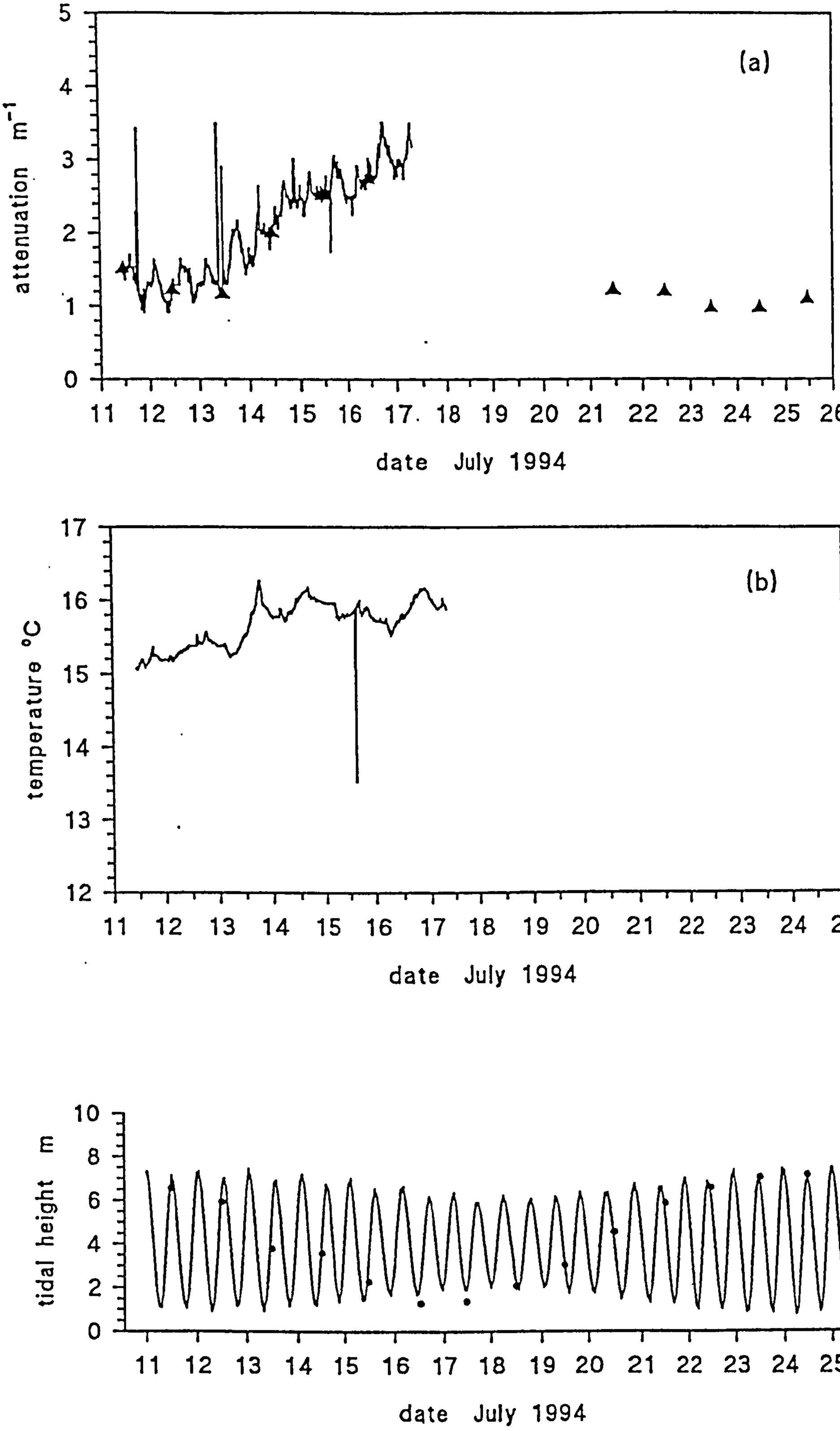
(a)
attenuation m^{-1}
0
1
2
3
4
5
11 12 13 14 15 16 17. 18 19 20 21 22 23 24 25 26
date July 1994
(b)
temperature °C
12
13
14
15
16
17
11 12 13 14 15 16 17 18 19 20 21 22 23 24 25
date July 1994
tidal height m
0
2
4
6
8
10
11 12 13 14 15 16 17 18 19 20 21 22 23 24 25
date July 1994

Figure 6.27 Transmissometer readings through tidal cycle, August Pier Survey 1995

a) beam attenuation: all readings

b) beam attenuation: de-spiked and averaged per hour

c) tidal height

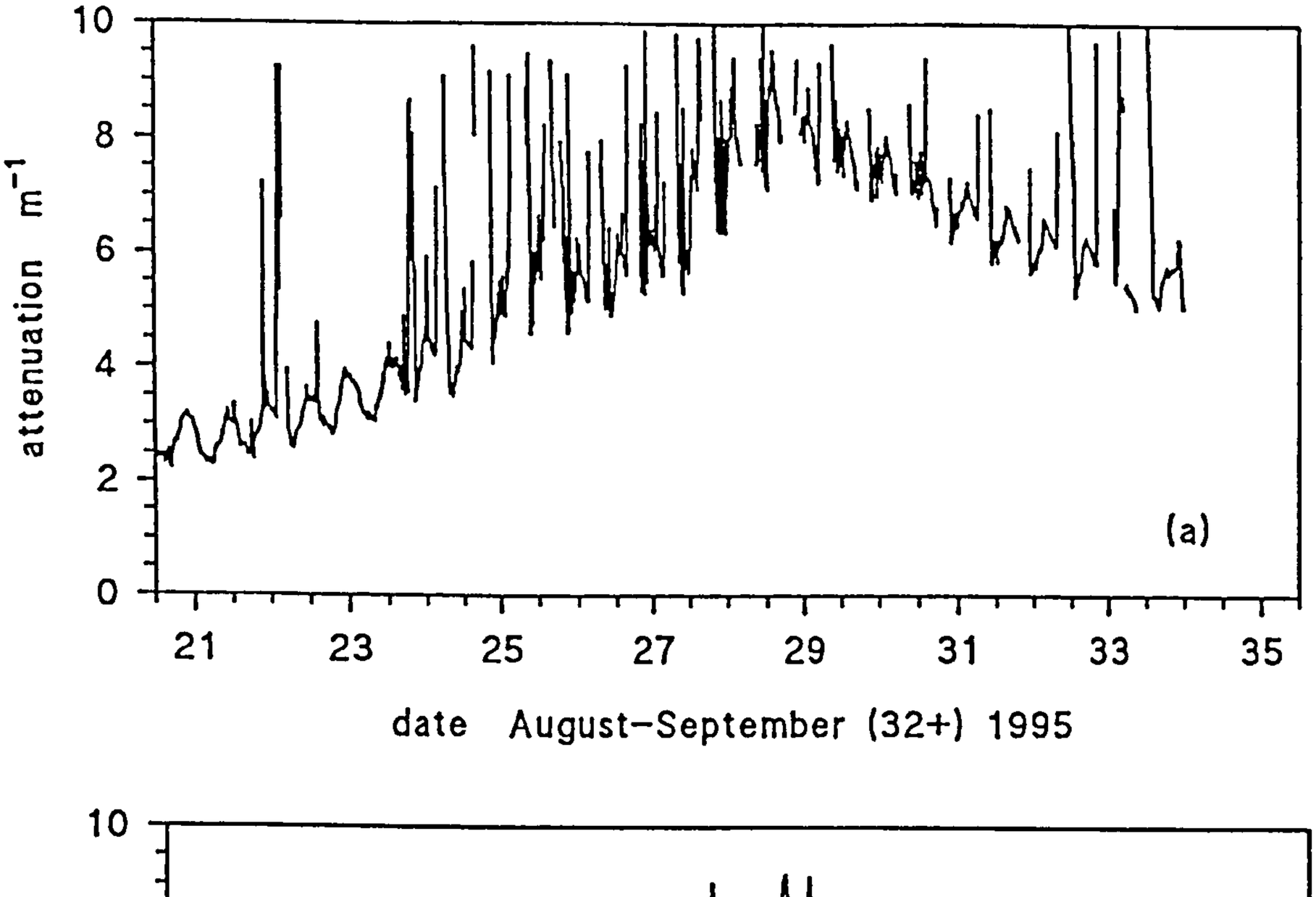
attenuation m^{-1}
10
8
6
4
2
0
21
23
25
27
29
31
33
35
date August–September (32+) 1995
(a)
attenuation m^{-1}
10
8
6
4
2
0
21
23
25
27
29
31
33
35
date August–September (32+) 1995
(b)

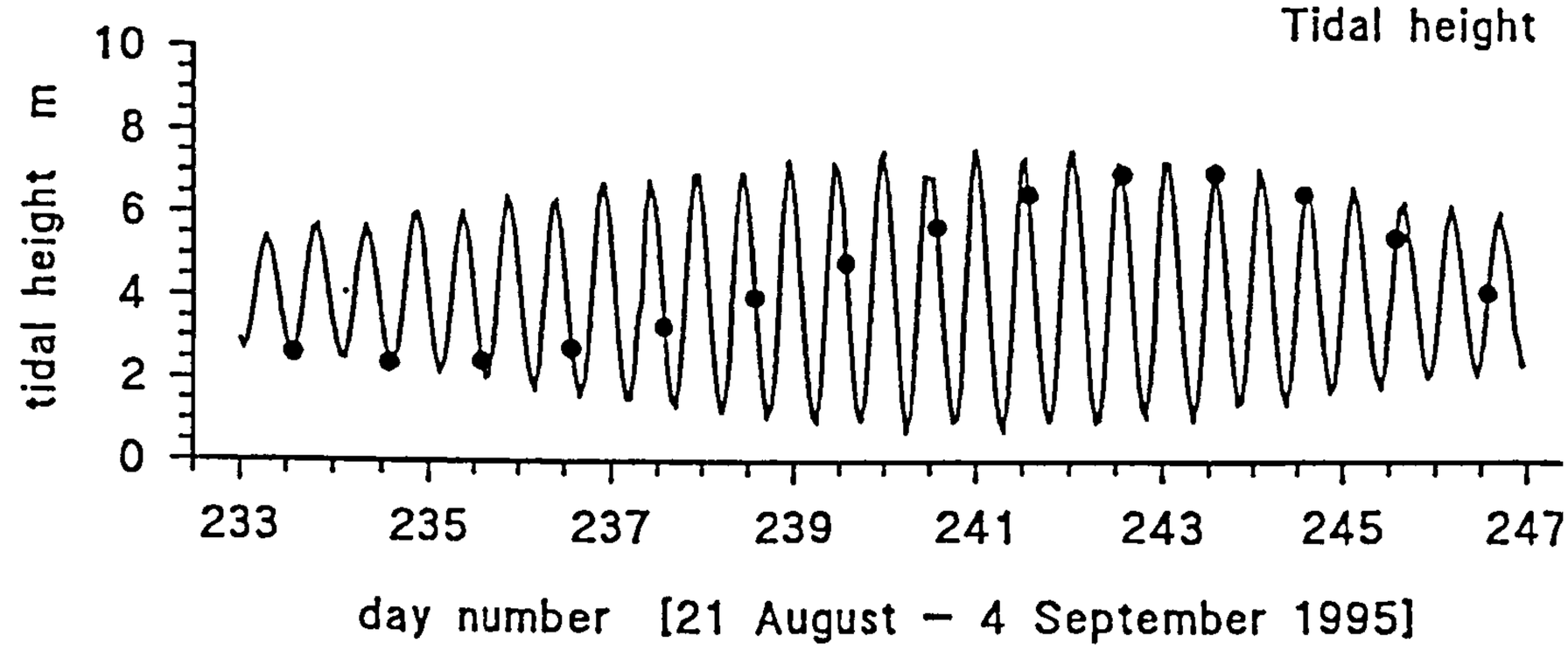
Tidal height
tidal height m
10
8
6
4
2
0
233
235
237
239
241
243
245
247
day number [21 August – 4 September 1995]

Figure 6.28 Transmissometer readings through flooding tide at Dolgarrog, Conwy

a) beam attenuation
b) salinity
c) temperature
d) depth of sensor

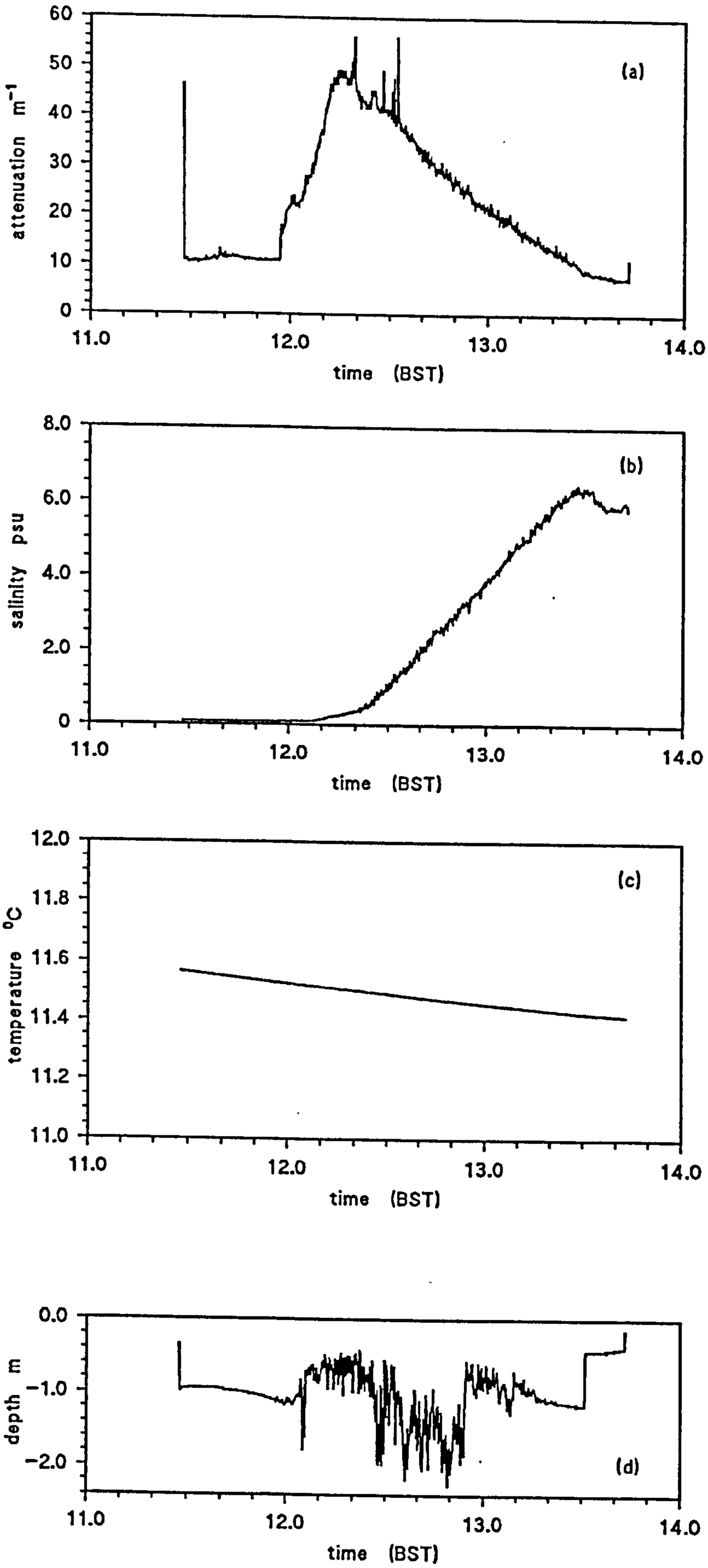
attenuation m⁻¹
60
50
40
30
20
10
0
(a)
11.0
12.0
13.0
14.0
time (BST)
salinity psu
8.0
6.0
4.0
2.0
0
(b)
11.0
12.0
13.0
14.0
time (BST)
temperature °C
12.0
11.8
11.6
11.4
11.2
11.0
(c)
11.0
12.0
13.0
14.0
time (BST)
depth m
0.0
−1.0
−2.0
(d)
11.0
12.0
13.0
14.0
time (BST)

Figure 6.29 Absorption and scatter derived from IRM1 readings for Menai Strait Survey using Kirk's (1985) algorithms

a-e) absorption coefficient 444 nm, 521 nm, 552 nm, 596 nm and 670 nm

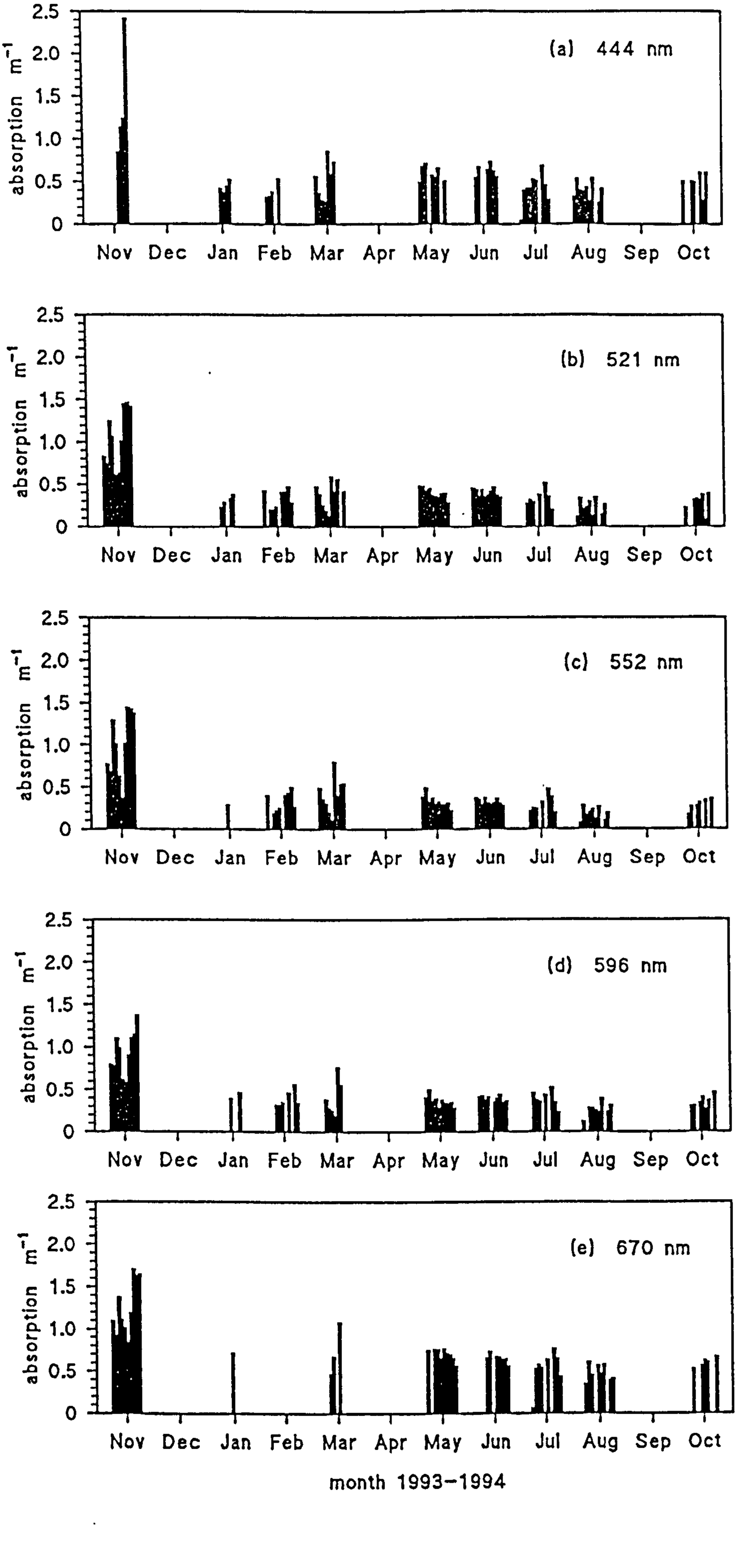
(a) 444 nm
(b) 521 nm
(c) 552 nm
(d) 596 nm
(e) 670 nm
absorption m-1
2.5
2.0
1.5
1.0
0.5
0
Nov Dec Jan Feb Mar Apr May Jun Jul Aug Sep Oct
month 1993–1994

Figure 6.29 Absorption and scatter derived from IRM1 readings for Menai Strait Survey using Kirk's (1985) algorithms

f-j) scattering coefficient 444 nm, 521 nm, 552 nm, 596 nm and 670 nm

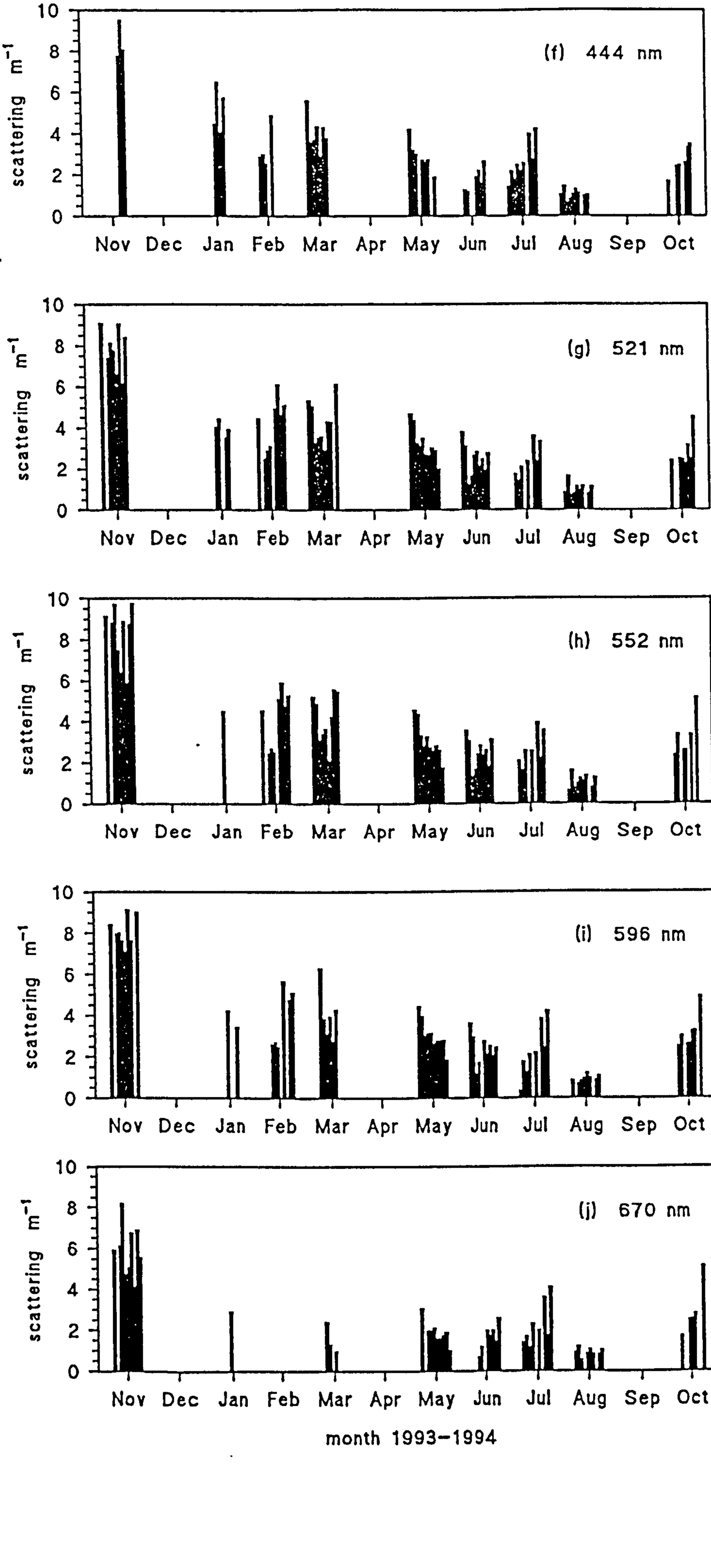
(f) 444 nm
(g) 521 nm
(h) 552 nm
(i) 596 nm
(j) 670 nm
scattering m^{-1}
0
2
4
6
8
10
Nov Dec Jan Feb Mar Apr May Jun Jul Aug Sep Oct
month 1993–1994

Figure 6.30 Absorption and scatter derived from colour sensor readings for July Pier Survey 1994 using Kirk's (1985) algorithms

a) absorption from colour sensor readings all day
b) scatter from colour sensor readings all day
c) absorption from colour sensor readings 12:00-14:00 GMT
d) scatter from colour sensor readings 12:00-14:00 GMT

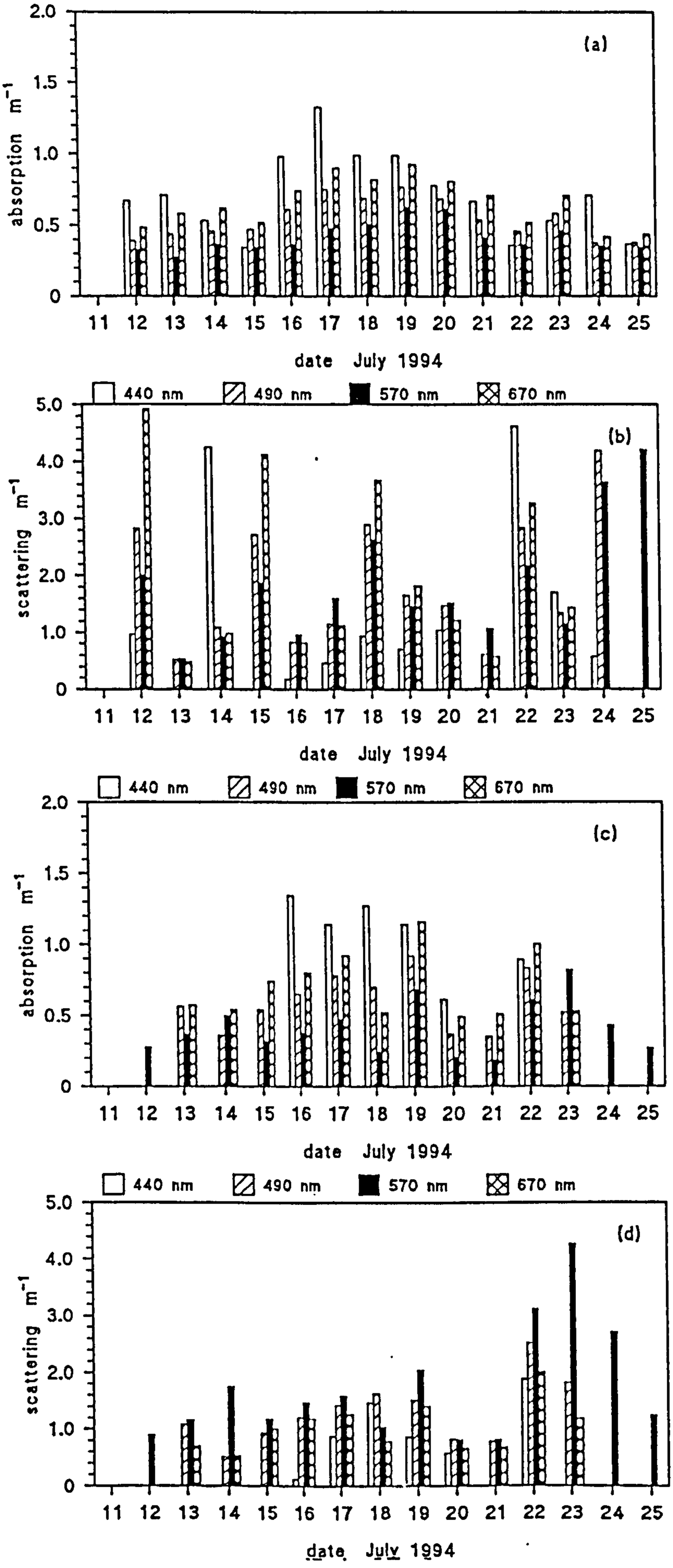
(a)
absorption m^{-1}
2.0
1.5
1.0
0.5
0
11 12 13 14 15 16 17 18 19 20 21 22 23 24 25
date July 1994
440 nm
490 nm
570 nm
670 nm
(b)
scattering m^{-1}
5.0
4.0
3.0
2.0
1.0
0
11 12 13 14 15 16 17 18 19 20 21 22 23 24 25
date July 1994
440 nm
490 nm
570 nm
670 nm
(c)
absorption m^{-1}
2.0
1.5
1.0
0.5
0
11 12 13 14 15 16 17 18 19 20 21 22 23 24 25
date July 1994
440 nm
490 nm
570 nm
670 nm
(d)
scattering m^{-1}
5.0
4.0
3.0
2.0
1.0
0
11 12 13 14 15 16 17 18 19 20 21 22 23 24 25
date July 1994

Figure 6.31 Comparison of beam attenuation with the sum of the in situ derived absorption and scatter for the Pier Surveys
a) July Pier Survey 1994
b) August Pier Survey 1995, using Spectron and Satlantic readings

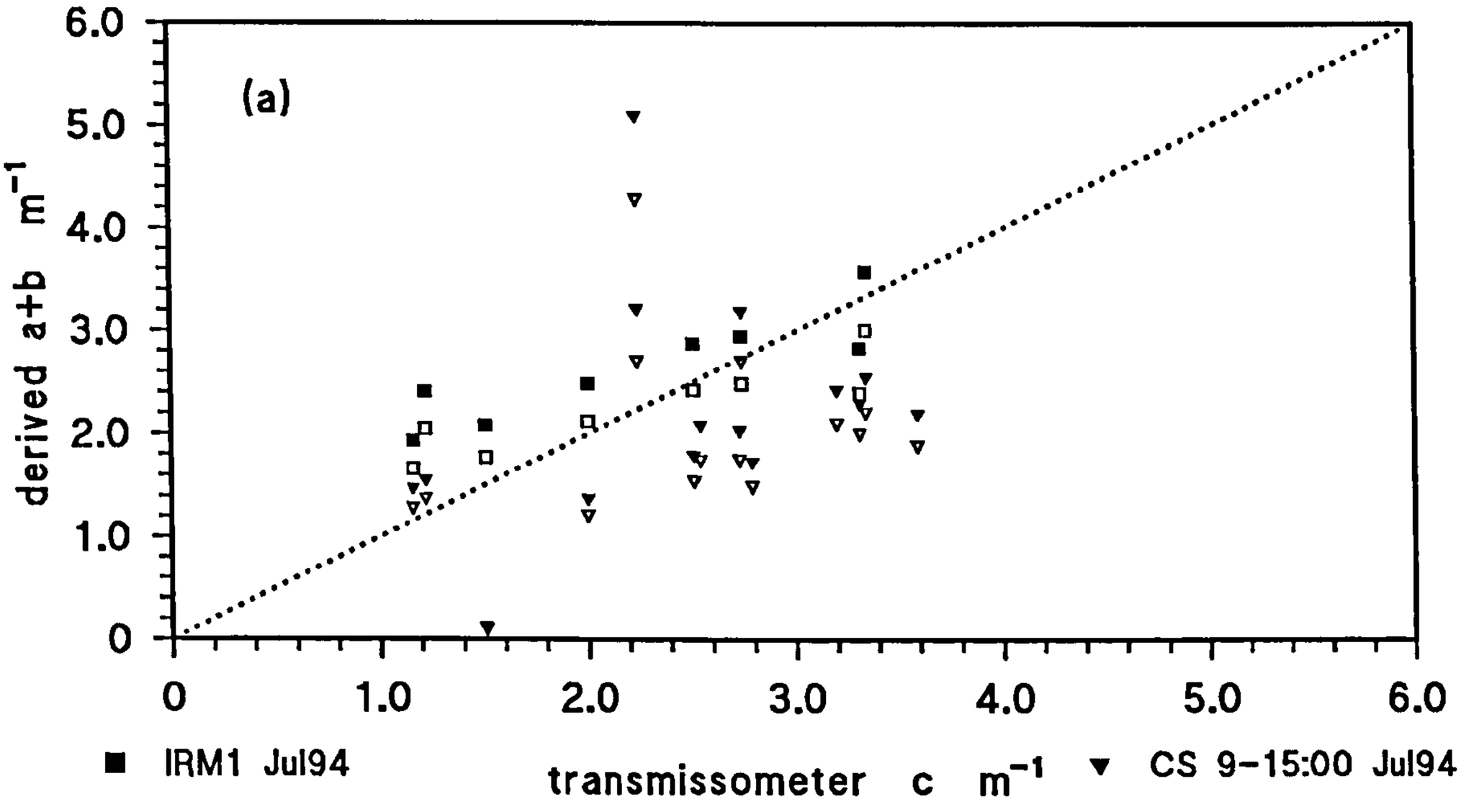

solid shapes use 0.33 b_b/a, open use Kirk

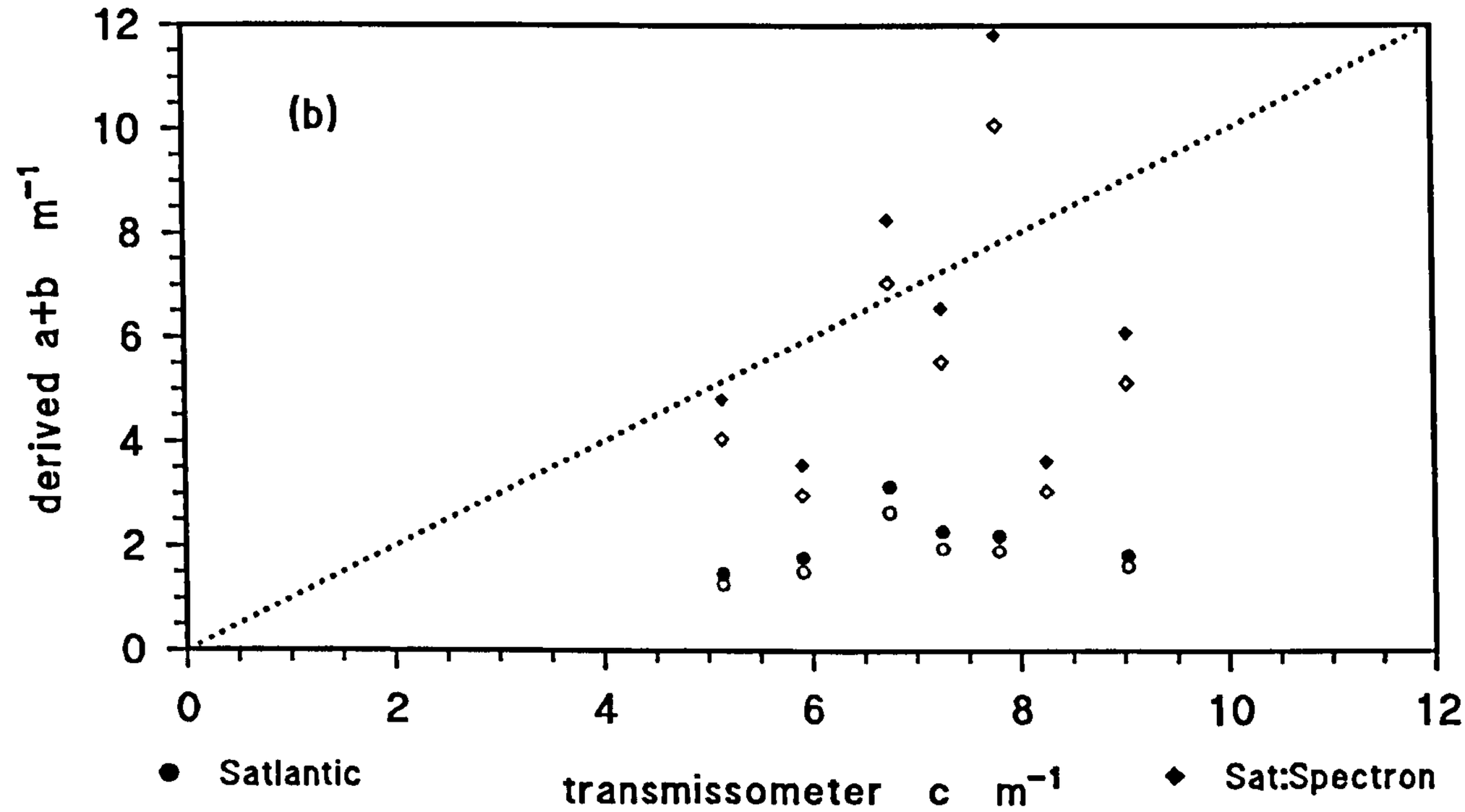

solid shapes use 0.33 b_b/a, open use Kirk

Figure 6.32 Diffuse attenuation curves, averaged over survey

a) Satlantic measurements: Conwy 1996, August Pier Survey 1995, Cwmystradllyn 1996 and Vestfjorden 1994

b) UCNW Irradiance meter: Clyde 1994, Loch Striven 1994, Cardigan Bay 1994 and July Pier Survey 1994

c) UCNW Irradiance meter: Menai Strait Survey 1993-1994 monthly surveys

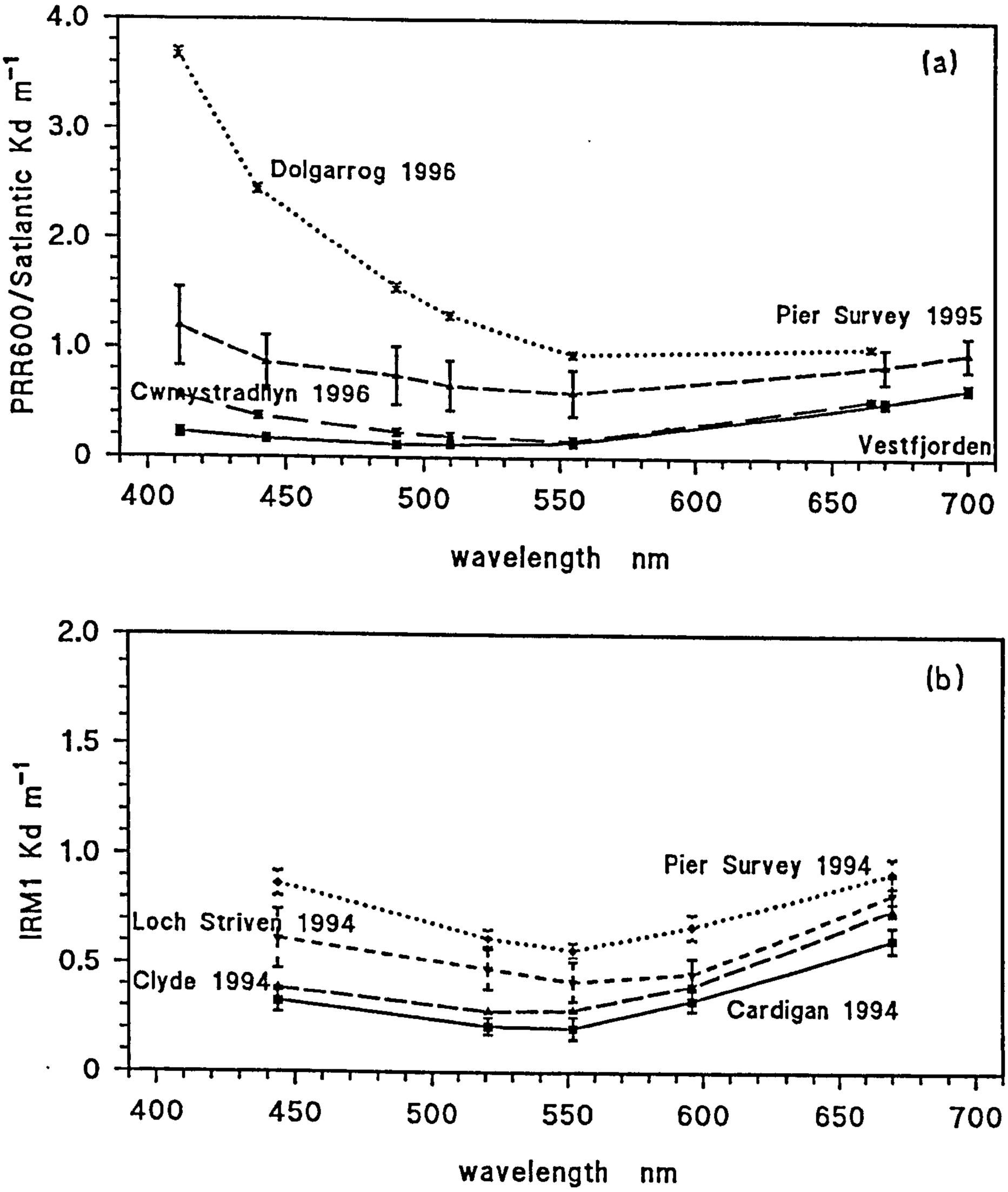
(a)
PRR600/Satlantic Kd m-1
4.0
3.0
2.0
1.0
0
Dolgarrog 1996
Pier Survey 1995
Cwmystradllyn 1996
Vestfjorden
400
450
500
550
600
650
700
wavelength nm
(b)
IRM1 Kd m-1
2.0
1.5
1.0
0.5
0
Pier Survey 1994
Loch Striven 1994
Clyde 1994
Cardigan 1994
400
450
500
550
600
650
700
wavelength nm
(c)
IRM1 Kd m-1
4.0
3.0
2.0
1.0
0
400
450
500
550
600
650
700
wavelength nm

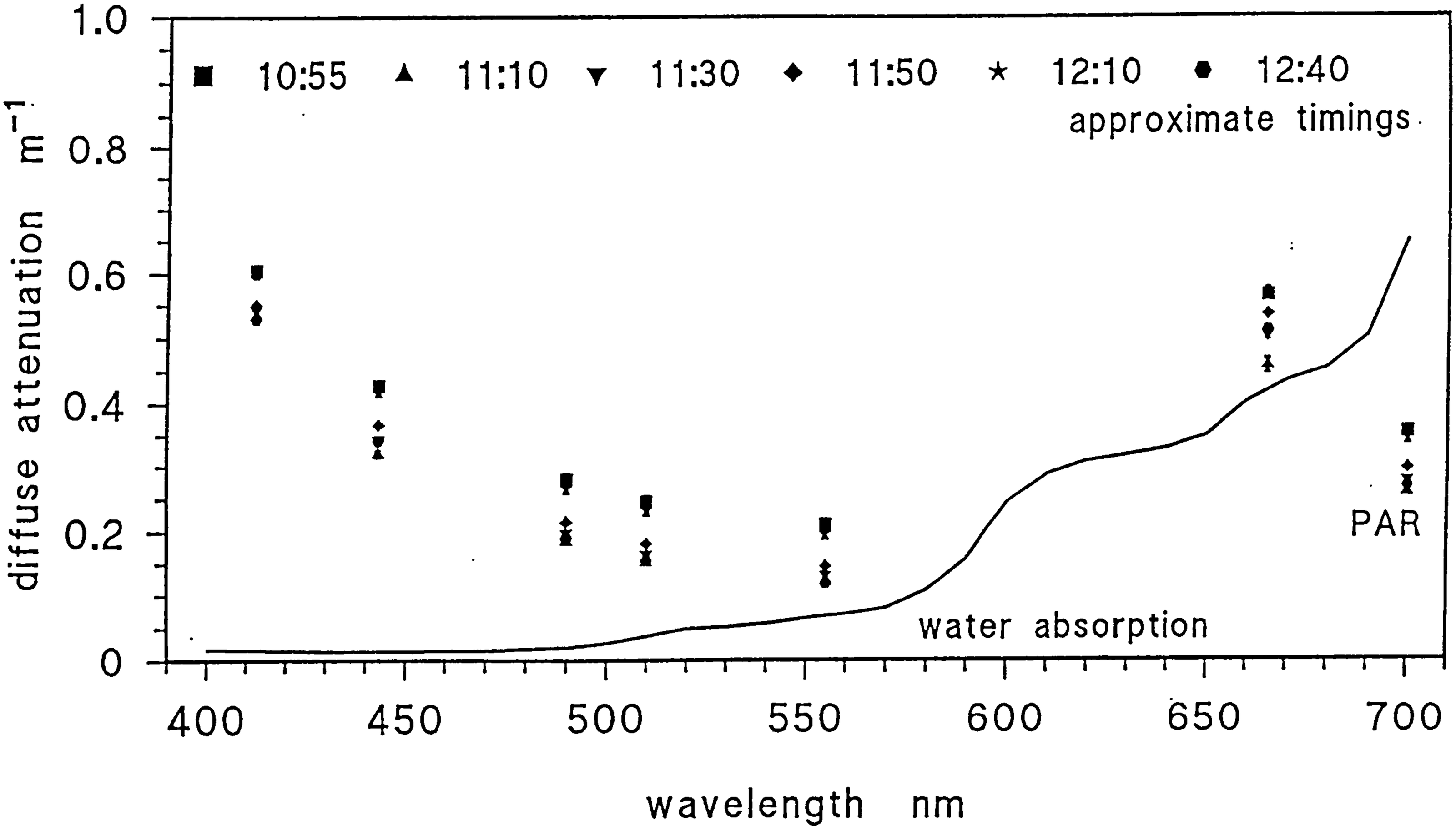

Figure 6.33 Cwmystradllyn [31/03/96] diffuse attenuation of irradiance, with high attenuation at shorter wavelengths due to dissolved organics, compared with water absorption spectrum

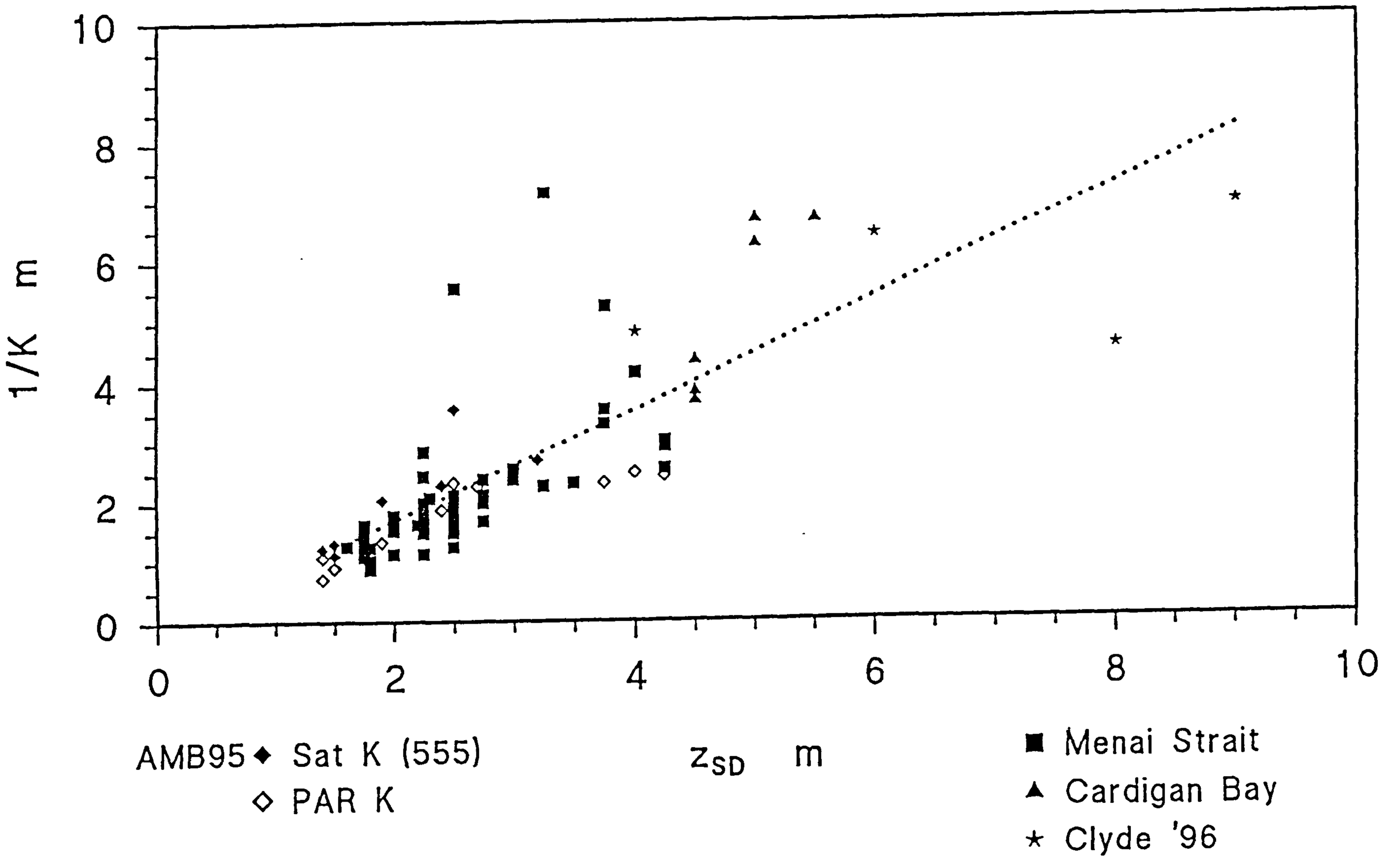

Figure 6.34 $1/K_d$ compared with Secchi depth for various surveys

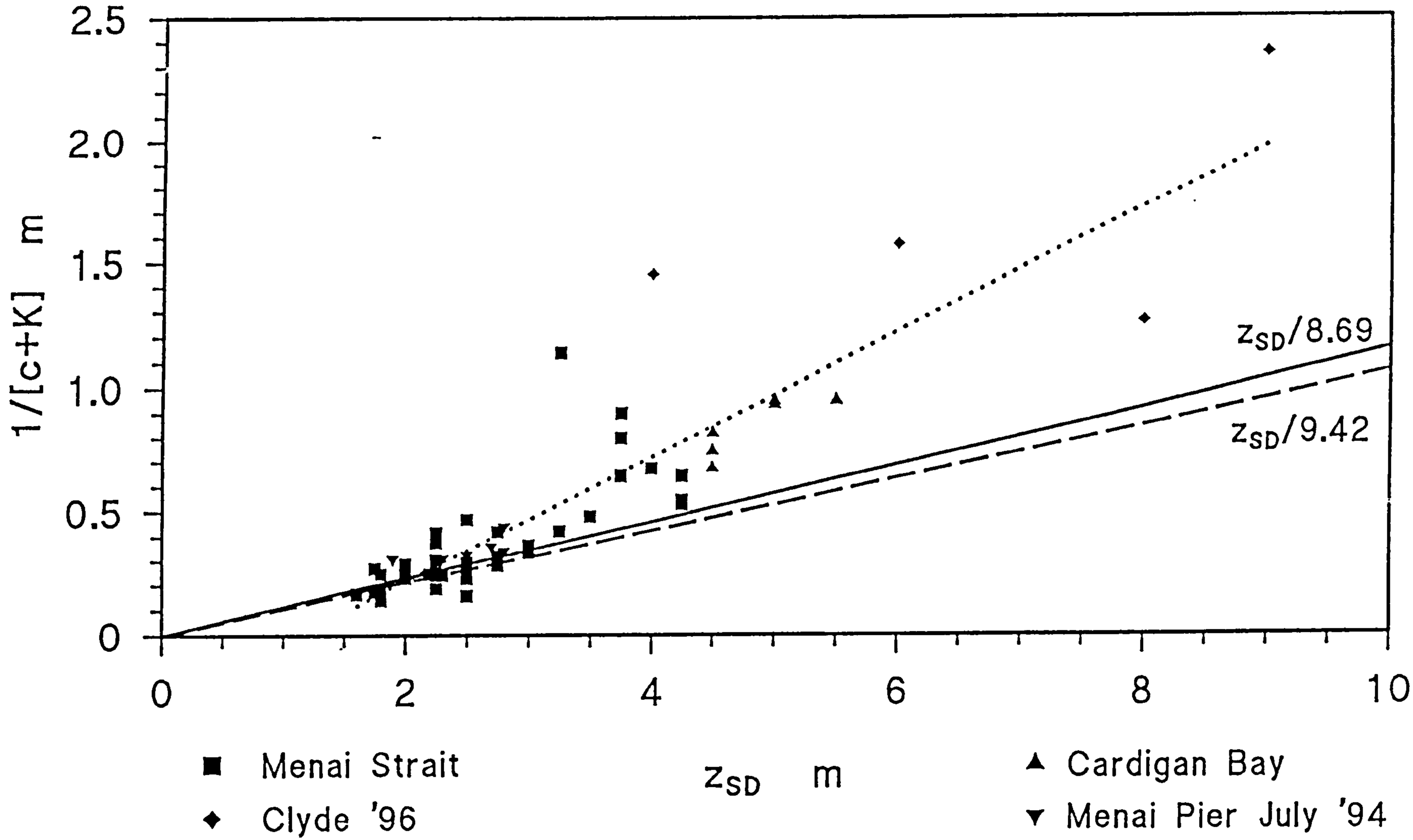

Figure 6.35 $1/(c+K_d)$ compared with Secchi depth, where c is derived from R and K by Kirk algorithms, at 552 nm

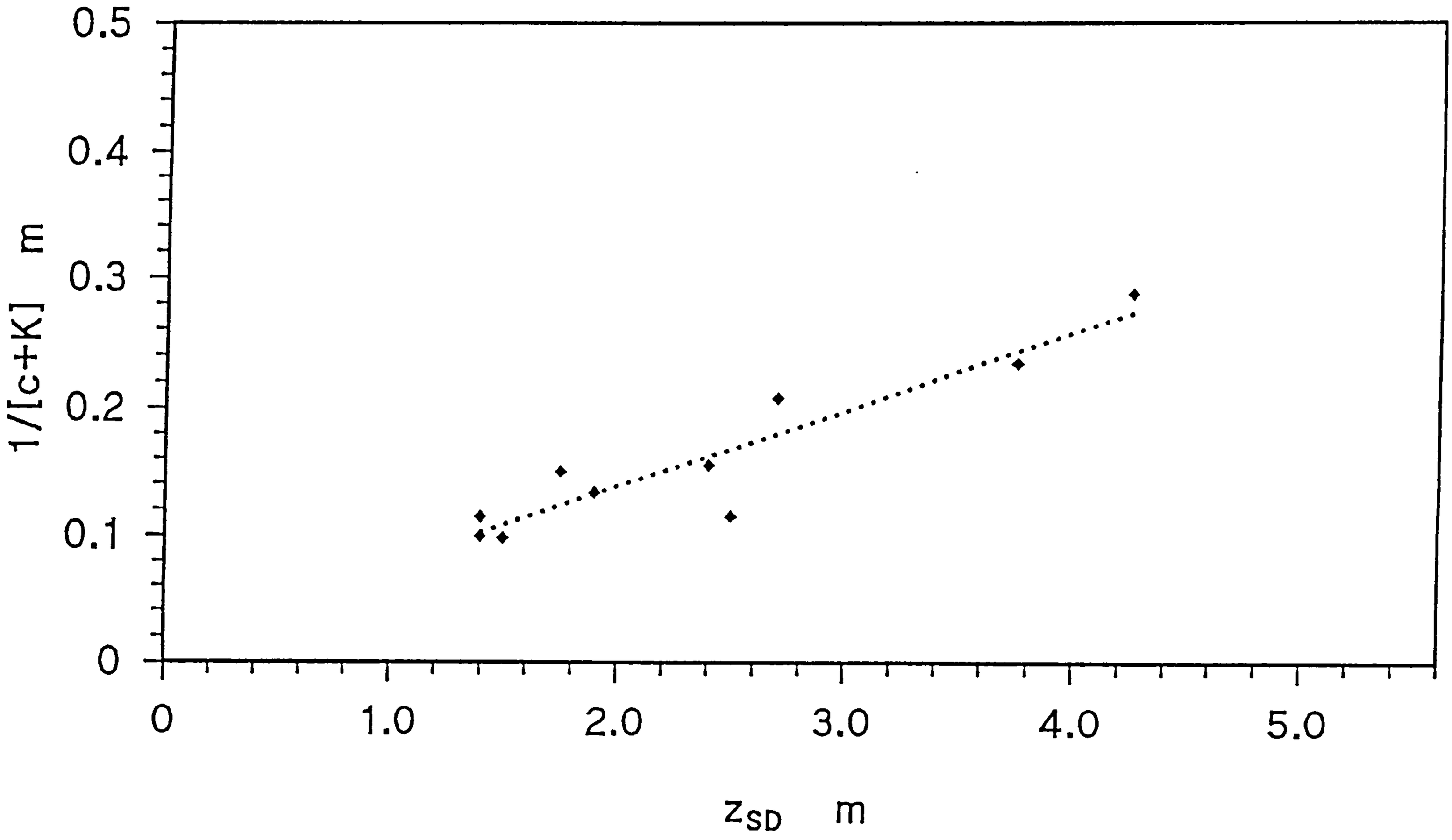

Figure 6.36 $1/(c+K_d)$ compared with Secchi depth, where K_d is for PAR during the August Pier Survey 1995

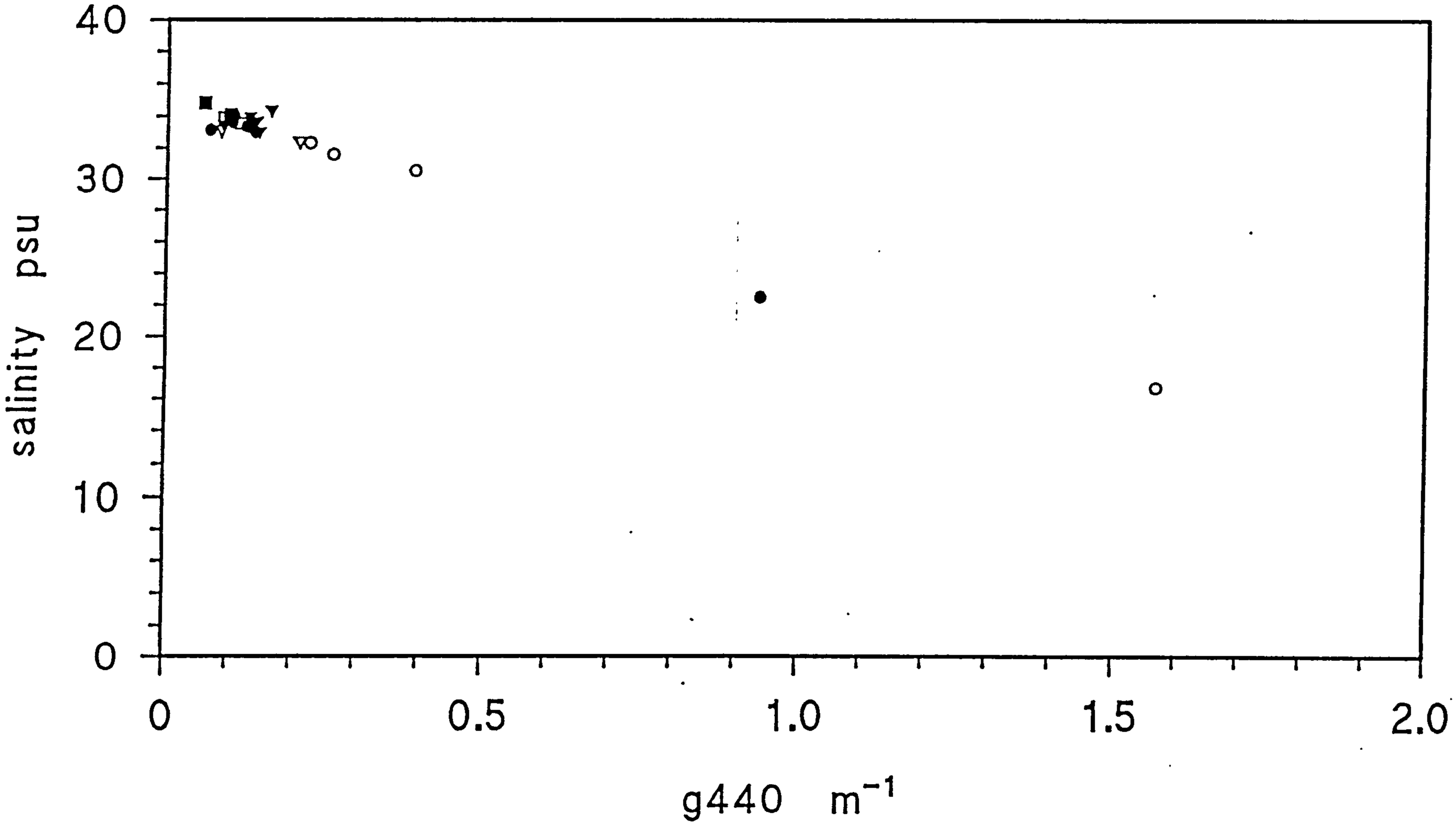

Figure 6.37 Salinity compared with yellow substance concentration (g440) in the Clyde Survey 1996. Open symbols are surface values.

7. LABORATORY RESULTS

7.1 SPECTRA

All absorption spectra decreased from the blue wavelengths to the red wavelengths, with water samples and yellow substance following an exponential decay, as did the furnaced filters. The average values for furnaced particles and yellow substance were very similar, with the errors overlapping. The exponents for all **Menai Strait** spectra, without the application of a pathlength correction, are shown in Appendix VIII, and are summarized in Table 7.1. Once a β correction of 2 has been applied to the furnaced particle spectra, the exponent is closer to that of the water sample.

	water	yellow substance	inorganic
minimum	-0.0016	-0.0084	-0.0098
maximum	-0.0118	-0.0170	-0.0146
mean	-0.007	-0.0110	-0.0120
standard deviation	0.002	0.0019	0.0008

Table 7.1 Exponents for spectra from the **Menai Strait**, regression of ln values of zeroed spectra where $r^2>0.9$

There was little variation in the cell water spectra throughout the year which suggests that the concentrations of the constituents in the cell were too low to show clearly, and the absorbance measured was a general background level, mainly due to yellow substance.

The 'fresh' filter spectra (and the dried filters) did not show an exponential curve as the mineral particles do (Fig. 7.1), indicating that the organic fraction dominates the spectral shape of absorption.

7.2 INTERCOMPARISON BETWEEN WATER PROPERTIES

To extract the signal due to a particular constituent the absorption curves can be regressed on the concentrations at each wavelength. This identifies the specific absorption curve for the constituent considered. This method is only valid where the constituents are totally independent of each other (Whitlock *et al*, 1982). The relationships between the concentrations in the **Menai Strait** are shown in Table 7.2.

y = mx + c								
y	x	m	± S.E.	c	± S.E.	r^2	n	p
Strait Survey 1993-1994								
YS	Chl	-0.0009	0.003	0.308	0.016	0.002	77	0.719
YS	MSS	0.0022	0.002	0.289	0.019	0.014	77	0.304
MSS	Chl	-0.448	0.129	8.819	0.832	0.140	77	0.0008
Pier Survey July 1995								
YS	Chl	0.0086	0.0095	0.234	0.078	0.060	15	0.380
YS	MSS	-0.0174	0.0142	0.307	0.076	0.104	15	0.242
MSS	Chl	-0.0517	0.1095	4.269	0.900	0.632	15	0.0004
Pier Survey August 1995								
YS	Chl	0.028	0.019	0.056	0.054	0.116	18	0.166
YS	MSS	0.0004	0.002	0.117	0.057	0.003	18	0.831
MSS	Chl	2.432	2.940	1.227	8.149	0.041	18	0.420
without two high MSS values								
YS	MSS	-0.0075	0.004	0.146	0.054	0.190	16	0.091
MSS	Chl	0.997	1.279	0.937	3.388	0.042	16	0.449

Table 7.2 Correlation between constituents for the **Menai Strait,** omitting spurious values in May and June, and the **Menai Pier Surveys**

7.3 SPECIFIC SPECTRA

7.3.1 Phytoplankton

Fig. 7.2 shows the variation of the specific curve for **JMB94,** using the Cleveland & Weidemann (1993) correction and $\beta = 2$. This highlights the difference resulting from the method of correction. When the 'fresh' spectra are regressed on Chl concentrations (using $\beta = 2$) for **June 1994, JMB94** and **AMB95** (Fig. 7.3) the resultant spectra differ, showing that there is variation in the phytoplankton signal. However, all are in general agreement with Gallegos *et al*, 1990. **AMB95** shows the least variation with wavelength as there was a limited range in pigment concentration over the survey to produce a clear signal in a regression. Both **June** and **JMB94** have similar magnitudes to that in Gallegos *et al* (1990), but the "noise" in **June,** as a result of very low absorbance values, masks any clear signal. The **JMB94** spectra are the clearest, and in good agreement with Gallegos *et al.* However, the red peak in this survey occurred at a lower wavelength (675 nm) than Gallegos *et al*, **June** and **AMB95** (683 nm).

The 'constant' generated by these regressions follows an approximate exponential decay, in agreement with measurements taken of the dried filters, between 400 and 550 nm. At longer wavelengths the regression constant shows a peak characteristic of phytoplankton. This suggests that some pigments were not associated with the chlorophyll concentration in the regression, which is due to the similarity in the trend of the phytoplankton and inorganic concentrations. However, in general the dried filters gave an indication of the inorganic and detrital constituents (Fig. 7.4).

7.3.2 Mineral Solids

Similarly, regression can be used to calculate the specific absorption curve for MSS through the **Menai Strait** survey. Fig. 7.5 shows the curve calculated across the whole year, but when split into 'summer' and 'winter' the curves are slightly different, with a more uniform spectrum occurring during the summer. This method of deriving the specific spectrum through regression gives good agreement with the observed spectra of the furnaced particles (Fig. 7.6). This confirms that furnacing the particles at 500 °C does not change the optical properties of the minerals themselves (Bowers

et al, 1996).

The specific mineral spectra calculated from **AMB95** are higher than those from the **Menai Strait Survey,** although the shape closely follows that from the summer months, as would be expected. The shape of the curves can most easily be compared by normalising all spectra to the value at 440 nm, this emphasizes the relative difference across the visible spectrum rather than the absolute magnitude. Such measurements of inorganic particles from **Cardigan Bay** and **Cwmystradllyn** are surprisingly similar to those in the **Menai Strait** with the error bars overlapping. However, the site-specific nature of this measurement is shown by comparing these spectra with that derived from the **Conwy** data (Fig. 7.7).

The constant from these regressions gives a curve of similar shape to that of specific chlorophyll, indicating that that the appropriate constituents had been identified (Fig.7.8). The higher values at shorter wavelengths may represent a detrital component, forming an exponential curve upon which the pigments are superimposed.

7.4 ERROR DUE TO SCATTER

It is apparent that the pathlength amplification factor used on filters can greatly affect the magnitude of the calculated absorption spectrum. It therefore seems better to use spectra of suspensions. However, if particle concentrations are low there is an insufficient concentration within a 100 mm cell to produce a recognisable spectrum, as shown with the water spectra, whereas if concentrations are high, there is a possibility of particles settling while the spectrum is taken. In addition, there is scattering from the cell which is registered as loss due to absorption. This last problem can be improved by using an integrating sphere. Where this is not available the scattering component is reduced by placing a diffuser between the cell and the receiver, so that light scattered at low forward angles will be redirected towards the sensor. This is not ideal as there will still be light scattered at greater angles, but it does produce a quantifiable reduction.

This technique was employed on kaolin samples (which are theoretically pure

scatterers), and then on the second **Conwy** and **Cwmystradllyn** surveys. Increasing weights of kaolin were suspended in distilled water in the 100 mm cells and the spectrum taken, then a sheet (2 mm thickness) of white perspex inserted between the cell and the receiver and the spectrum re-taken, having shaken the cell to ensure the particles had not settled. The difference between the spectra (Fig. 7.9a), of the order of 50%, indicates the amount of scattered light which was redirected towards the sensor. Unfortunately, this cannot be converted into a percentage as the proportion which is still scattered out of the cell is unknown.

This difference can equally be seen in the **Conwy** data (Fig. 7.9b), although the concentrations at **Cwmystradllyn** were too low to make any appreciable difference (and so are not shown). It is apparent that the diffuser makes a marked difference when there is a significant concentration of particles within the cell and therefore is a good method for gauging the scale of the scattering, even though it does not give the total value. In both the above cases, the contribution from forward scattering is independent of wavelength, confirming the work of Kullenberg (1968). The kaolin results imply that scattering at greater angles increases with decreasing wavelength as the remaining "absorbance" must be due to scatter at greater angles.

However, when taking the kaolin spectra a mistake was initially made and the diffuser placed between the source and the cell, this gave very similar results at higher concentrations to those when the diffuser was in the correct position. This casts doubt on the effectiveness of the perspex, as when placed before the cell it should not have an appreciable effect, and there seems no apparent reason why the same results should be produced.

7.5 DISCUSSION

The specific absorption curve for MSS has not previously been defined, even though much work has been done on mineral reflection (*e.g.* Hunt, 1977; Hunt & Ashley, 1979; Hunt & Salisbury, 1976, Curran & Novo, 1988). However, the optical properties of glass have been defined, and the absorption curve which is derived from the optical attenuation follows an exponential curve with exponent -0.055. Glass is

formed using quartz minerals, which are predominant in the **Menai Strait.** This value for glass suggests that the derived mineral spectrum is realistic as the observed exponent derived for minerals is also -0.055.

It has therefore been shown that the use of regression of the spectra from filter and solution measurements on the constituent concentrations can identify the specific absorption curves for each constituent. This method is only appropriate when the constituents themselves are independent *i.e.* the technique could not be used when yellow substance was purely the derivative of phytoplankton. However, the only limitation in these datasets is the lack of variation in the different constituent concentrations for any particular survey, for example the small range of yellow substance throughout the **Menai Strait Survey,** and the lack of pigment variation in the **August Pier Survey.**

Even with these limitations it has been possible to classify each constituent optically, giving results which are compatible with those previously found in the literature, *e.g.* Gallegos *et al* (1990) for phytoplankton and Tassan (1988) for yellow substance, and establishing a characterisitic spectrum for inorganic sediments.

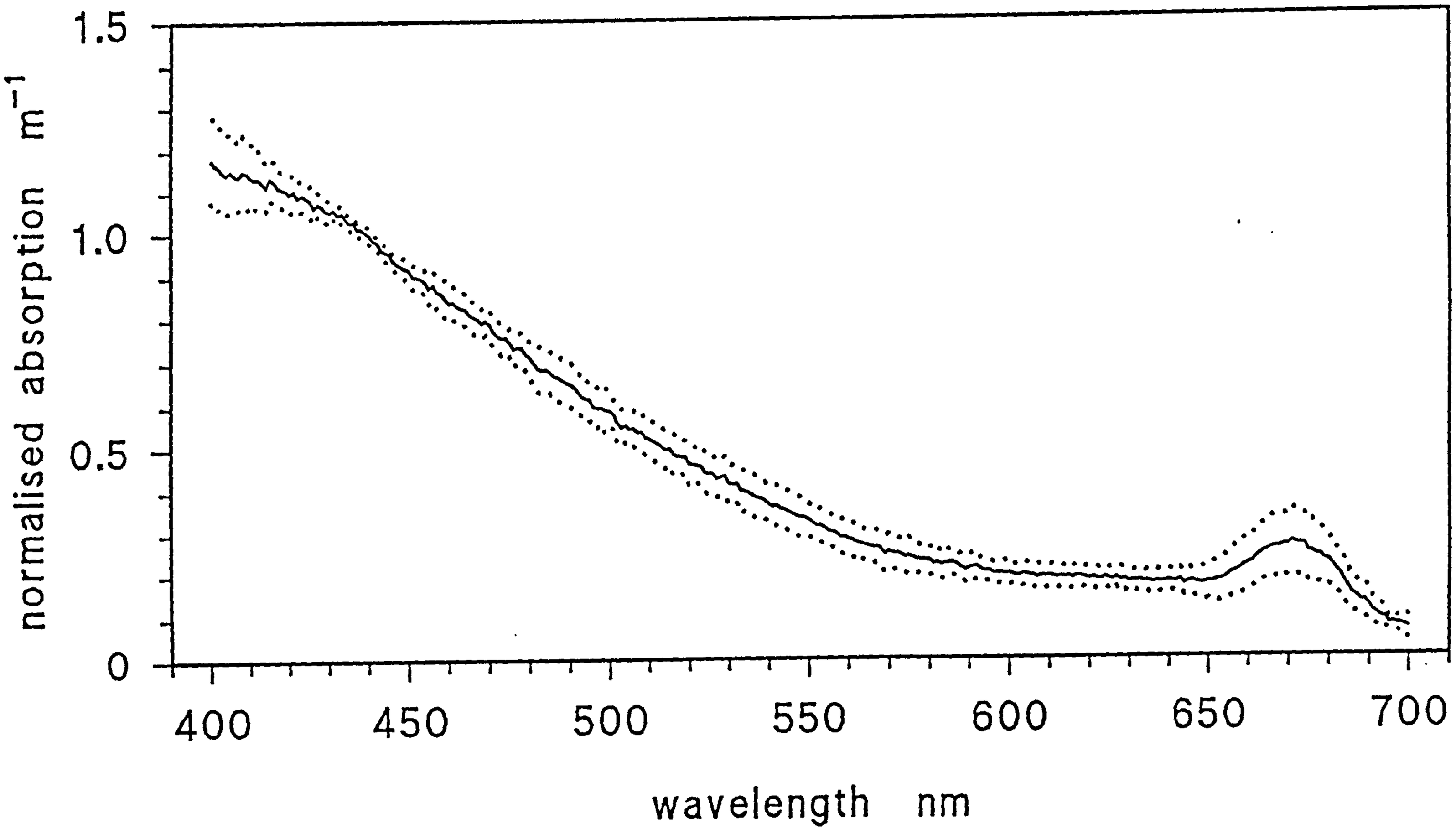

Figure 7.1 Average of fresh filter spectra from Pier Surveys normalised at 440 nm, with standard error

Figure 7.2 Specific chlorophyll spectra calculated with different pathlength amplification corrections, compared with Gallegos et al, 1990

Figure 7.3 Specific chlorophyll spectra, calculated with $\beta = 2$, for June 1994, the Pier Surveys for July 1994 and August 1995

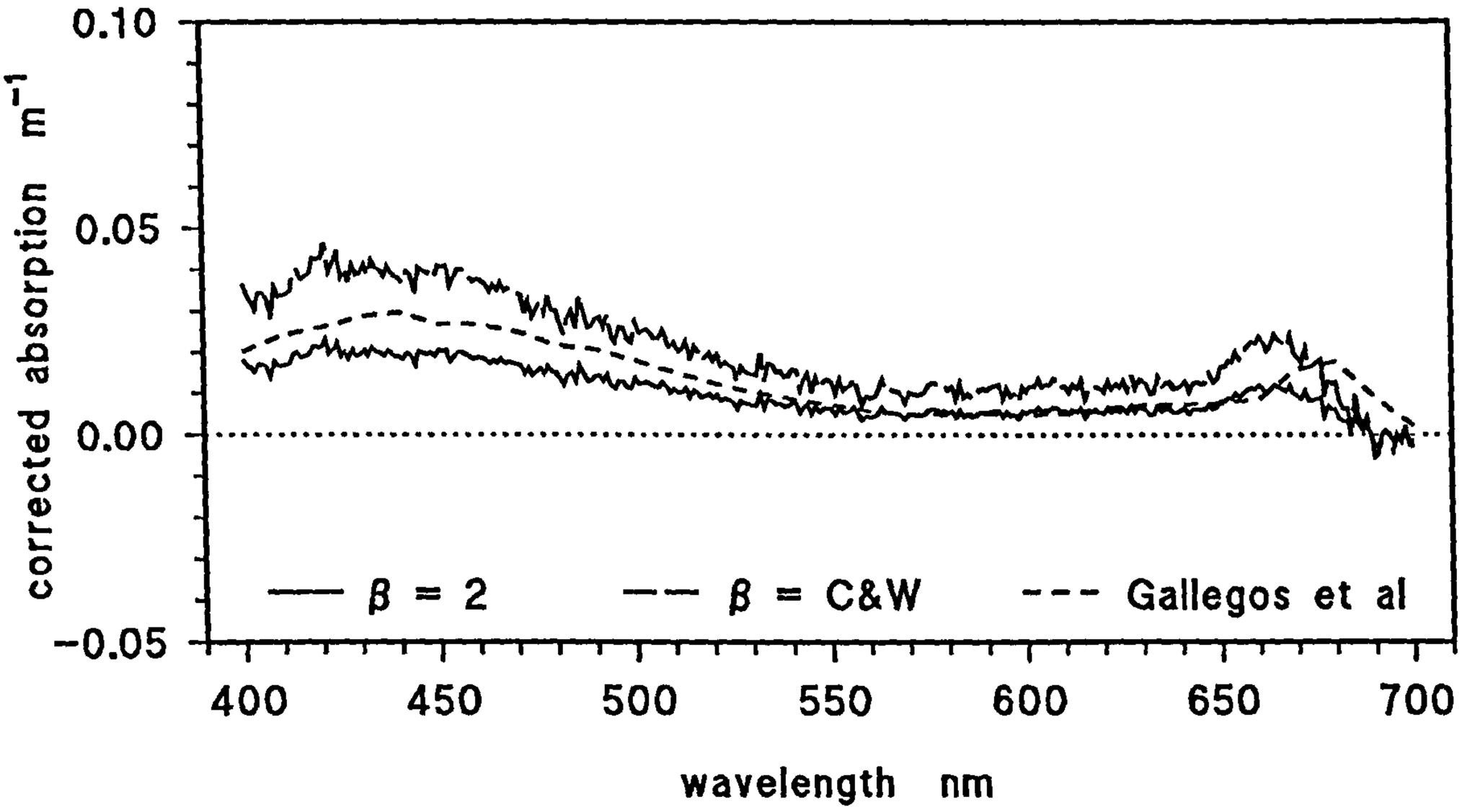
0.10
0.05
0.00
−0.05
corrected absorption m⁻¹
β = 2
β = C&W
Gallegos et al
400
450
500
550
600
650
700
wavelength nm

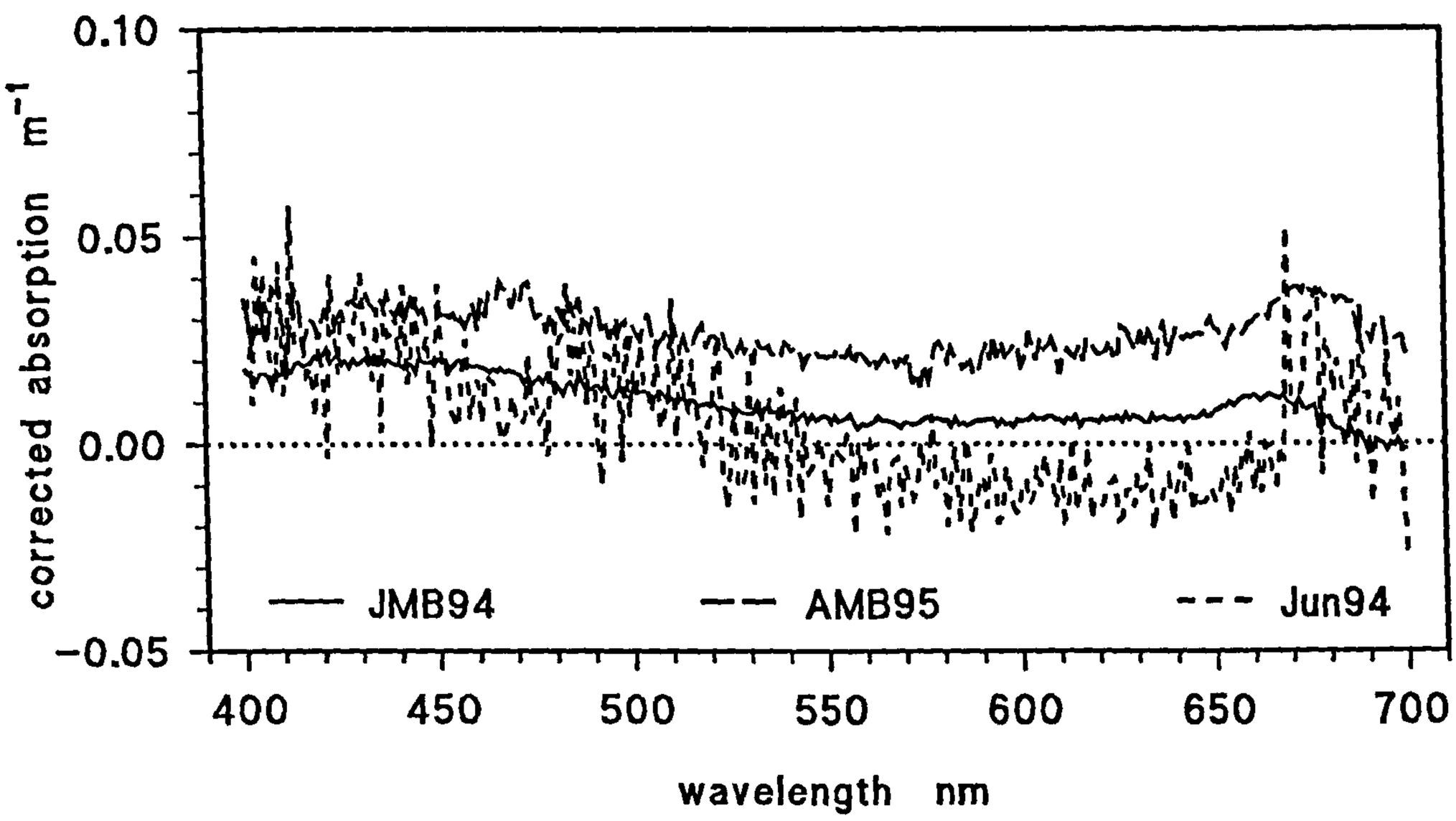
0.10
0.05
0.00
−0.05
corrected absorption m⁻¹
JMB94
AMB95
Jun94
400
450
500
550
600
650
700
wavelength nm

Figure 7.4 "Constant" from July regression, with average of dried particle spectra
a) values with standard error
b) normalised at 440nm

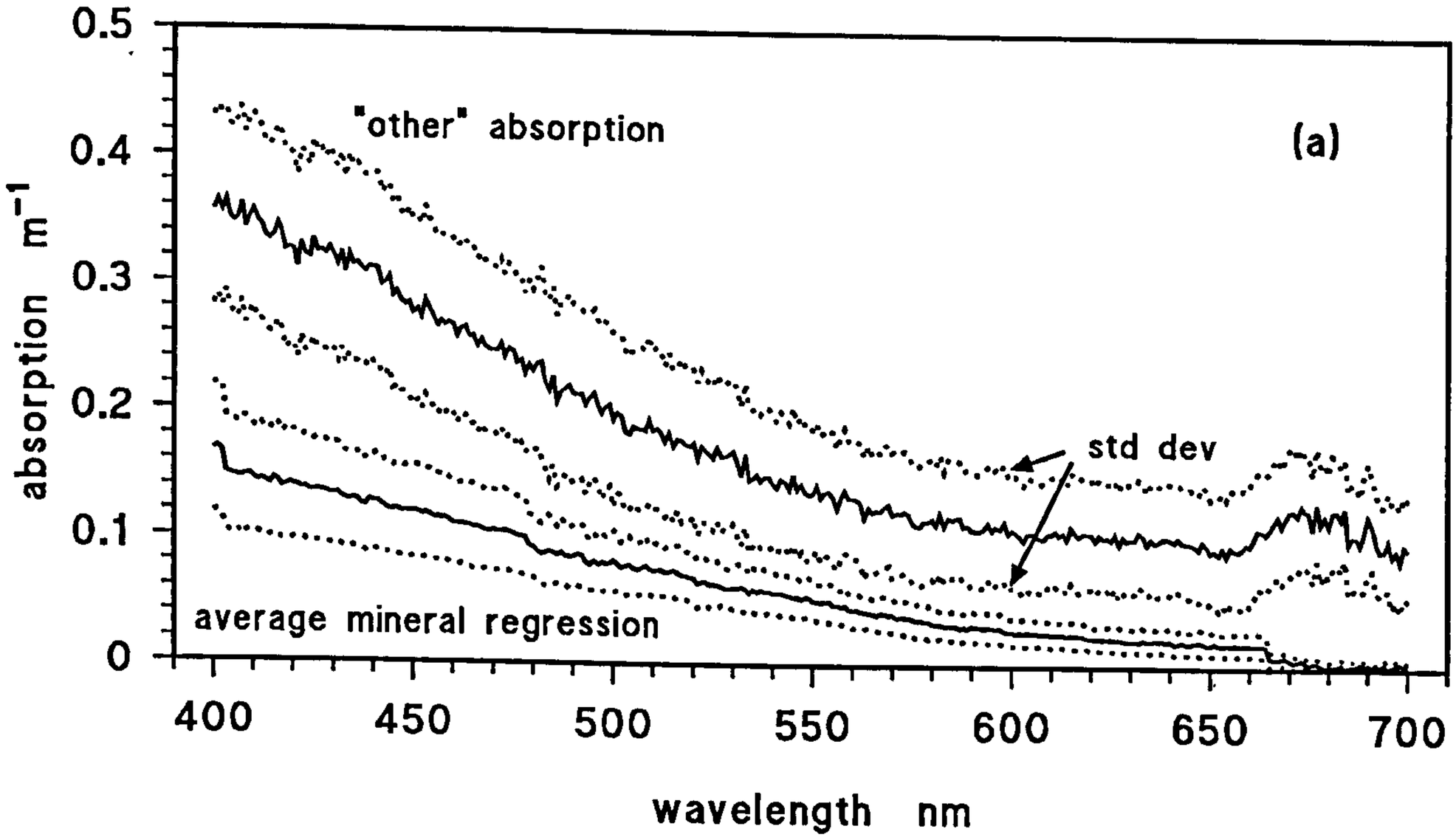
0.5
0.4
0.3
0.2
0.1
0
absorption m-1
"other" absorption
(a)
std dev
average mineral regression
400
450
500
550
600
650
700
wavelength nm

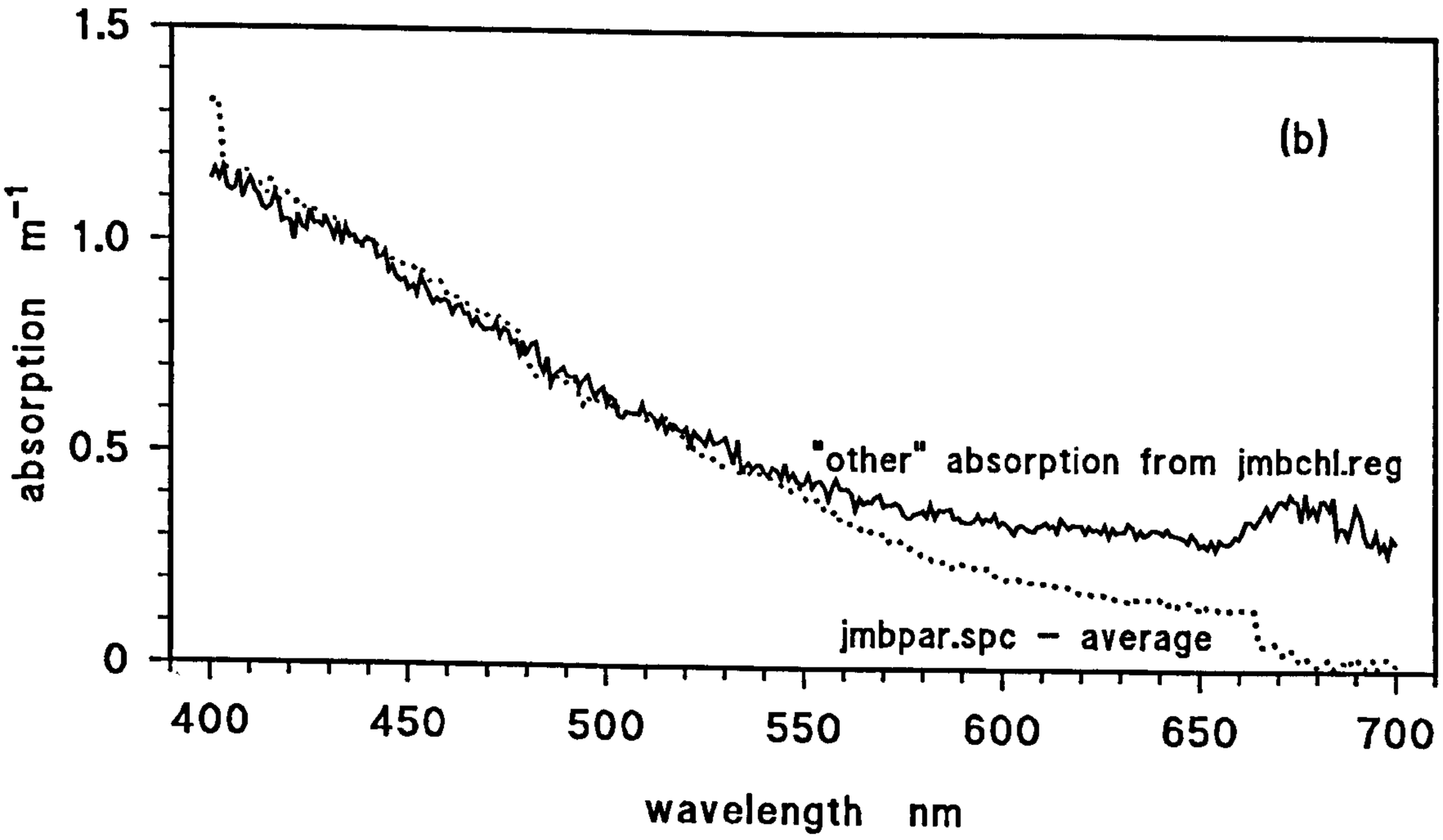
1.5
1.0
0.5
0
absorption m-1
(b)
"other" absorption from jmbchl.reg
jmbpar.spc – average
400
450
500
550
600
650
700
wavelength nm

Figure 7.5 Specific inorganic spectra from Menai Pier Surveys. Filters are not zeroed, correction $\beta=1$.

Figure 7.6 Specific inorganic spectrum with average furnace spectrum for August normalised at 440nm. Filters are not zeroed.

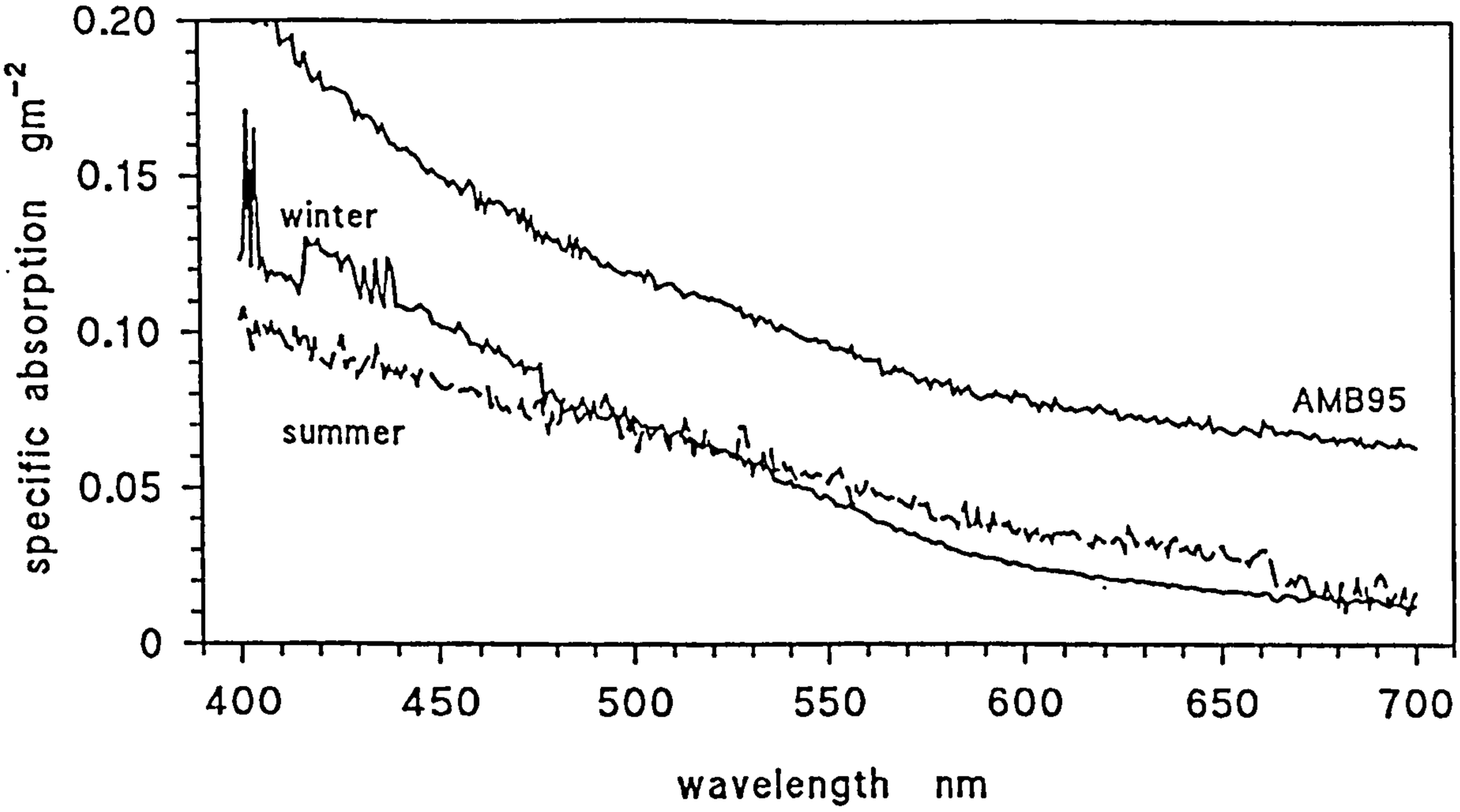
specific absorption gm^{-2}
0.20
0.15
0.10
0.05
0
winter
summer
AMB95
400
450
500
550
600
650
700
wavelength nm

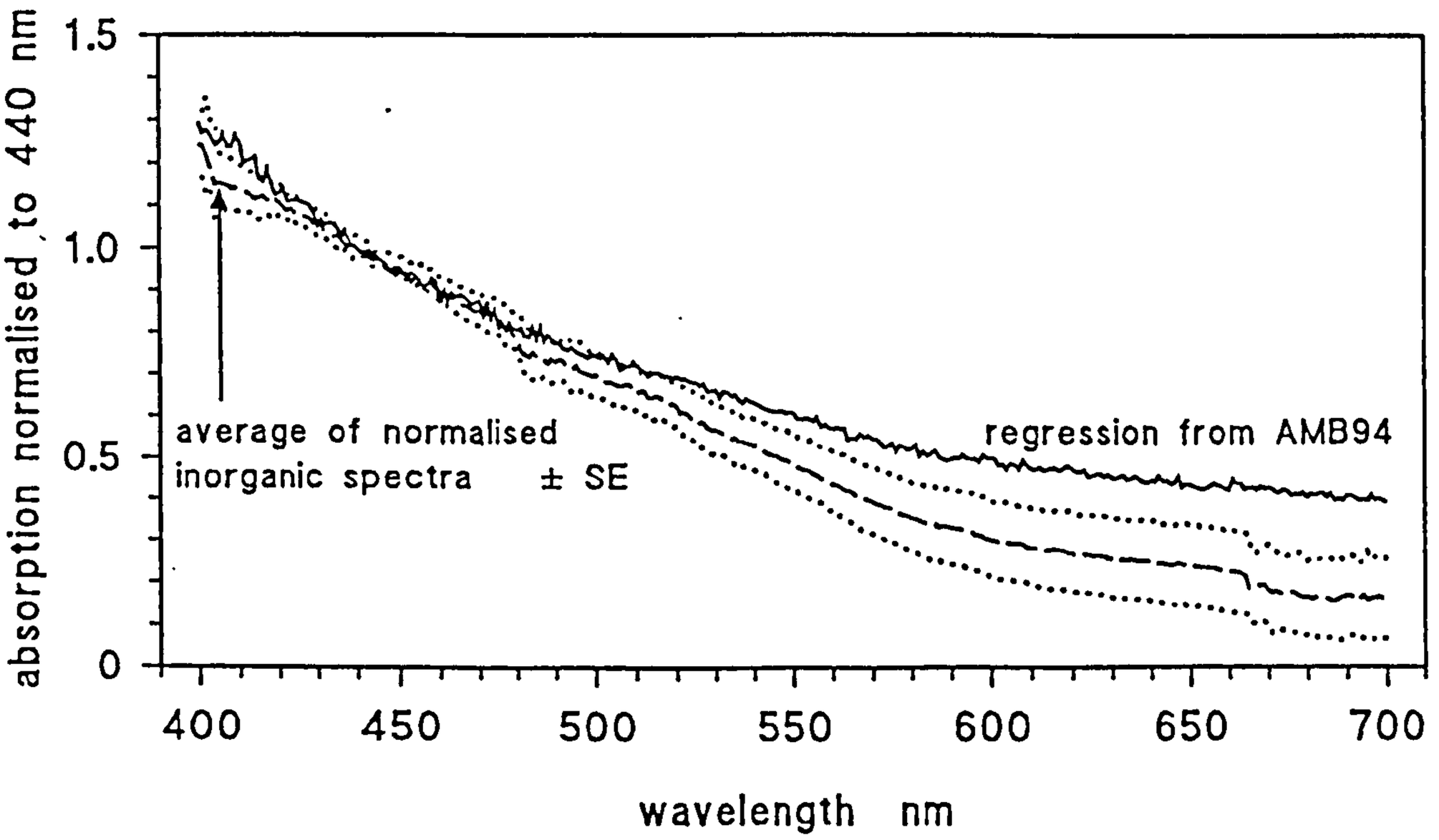
absorption normalised to 440 nm
1.5
1.0
0.5
0
average of normalised
inorganic spectra ± SE
regression from AMB94
400
450
500
550
600
650
700
wavelength nm

Figure 7.7 Average of normalised spectra for various sites
a) furnaced spectra
b) dried spectra

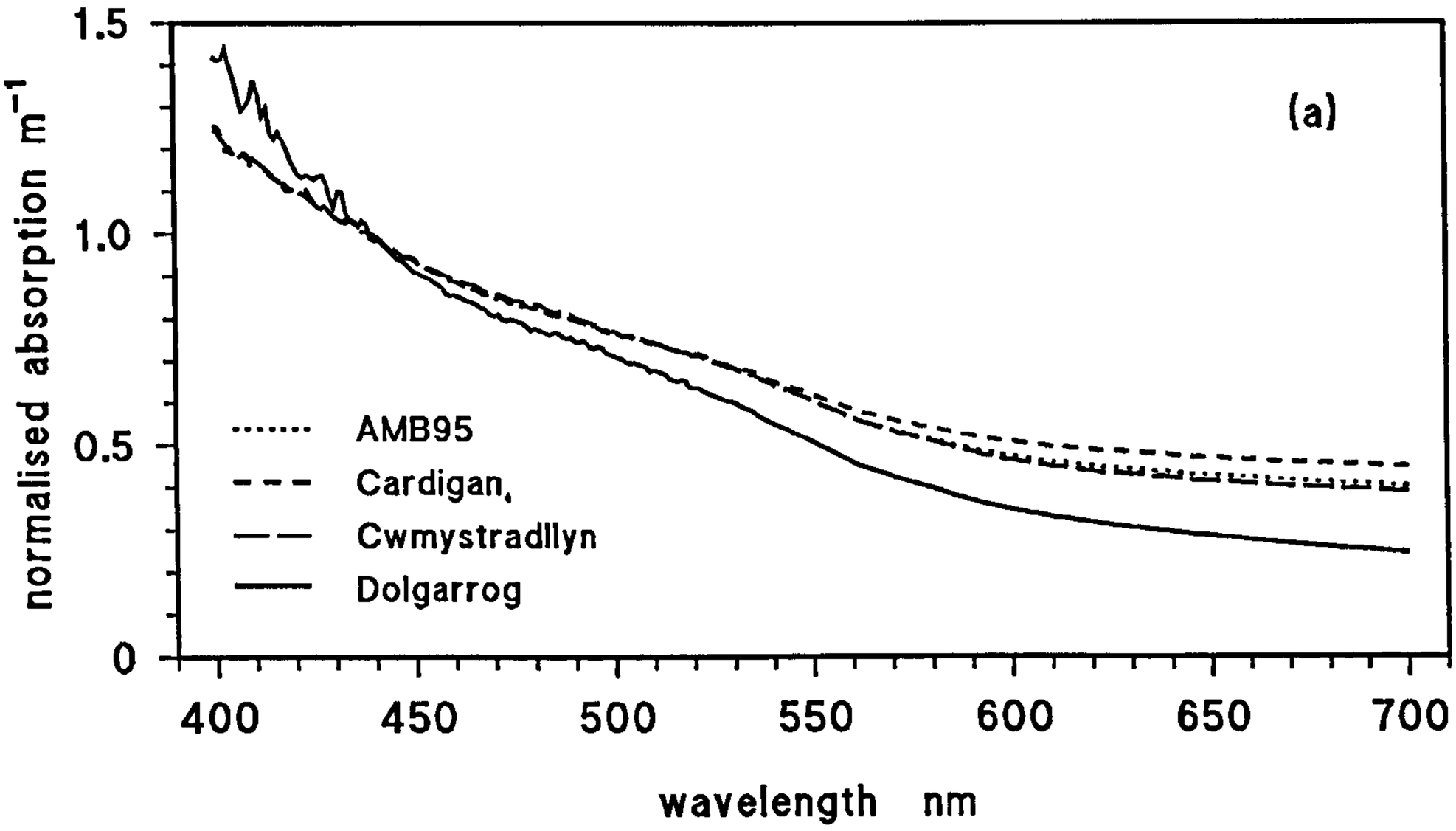
(a)
normalised absorption m-1
1.5
1.0
0.5
0
AMB95
Cardigan,
Cwmystradllyn
Dolgarrog
400
450
500
550
600
650
700
wavelength nm

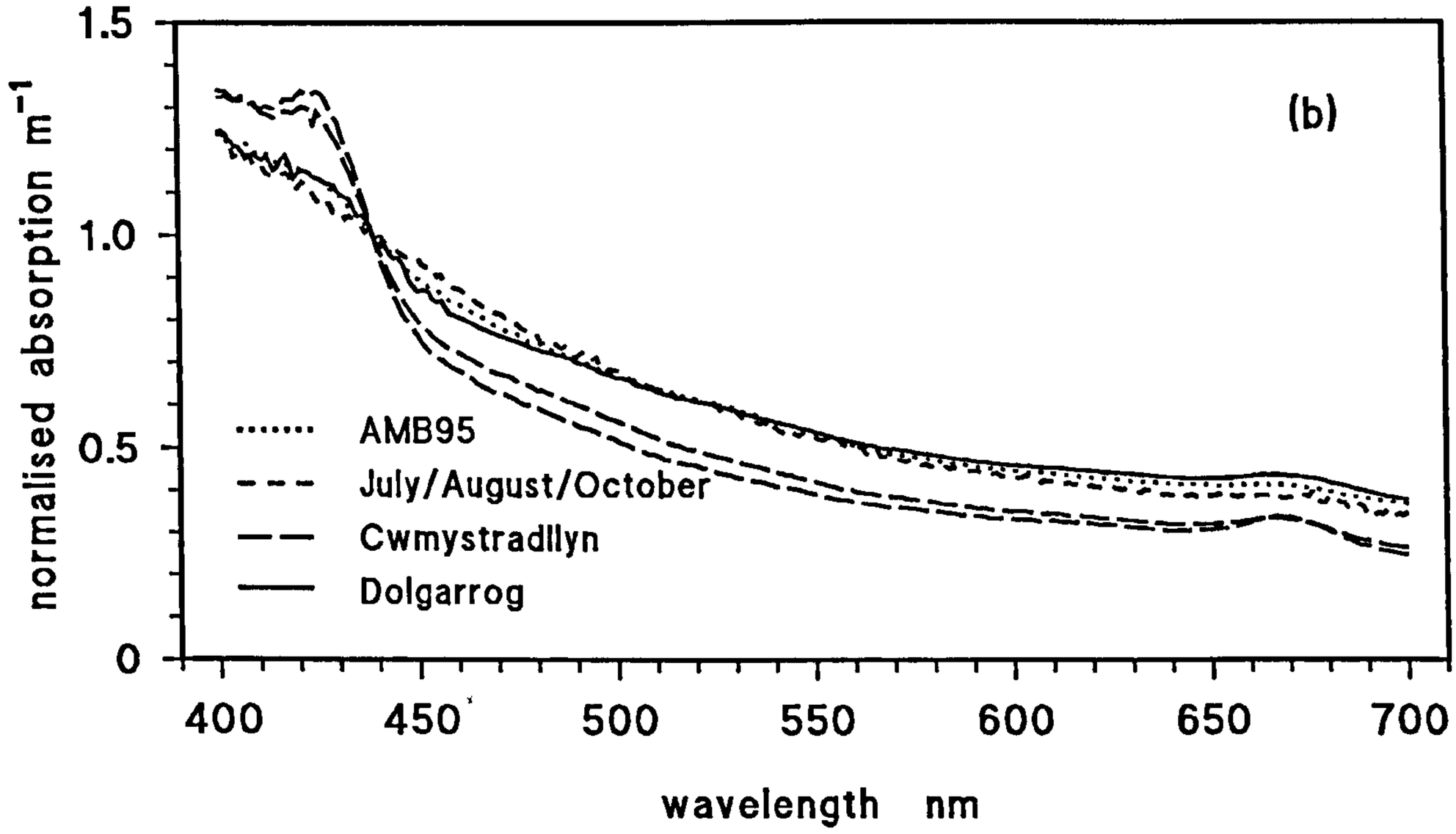
(b)
normalised absorption m-1
1.5
1.0
0.5
0
AMB95
July/August/October
Cwmystradllyn
Dolgarrog
400
450
500
550
600
650
700
wavelength nm

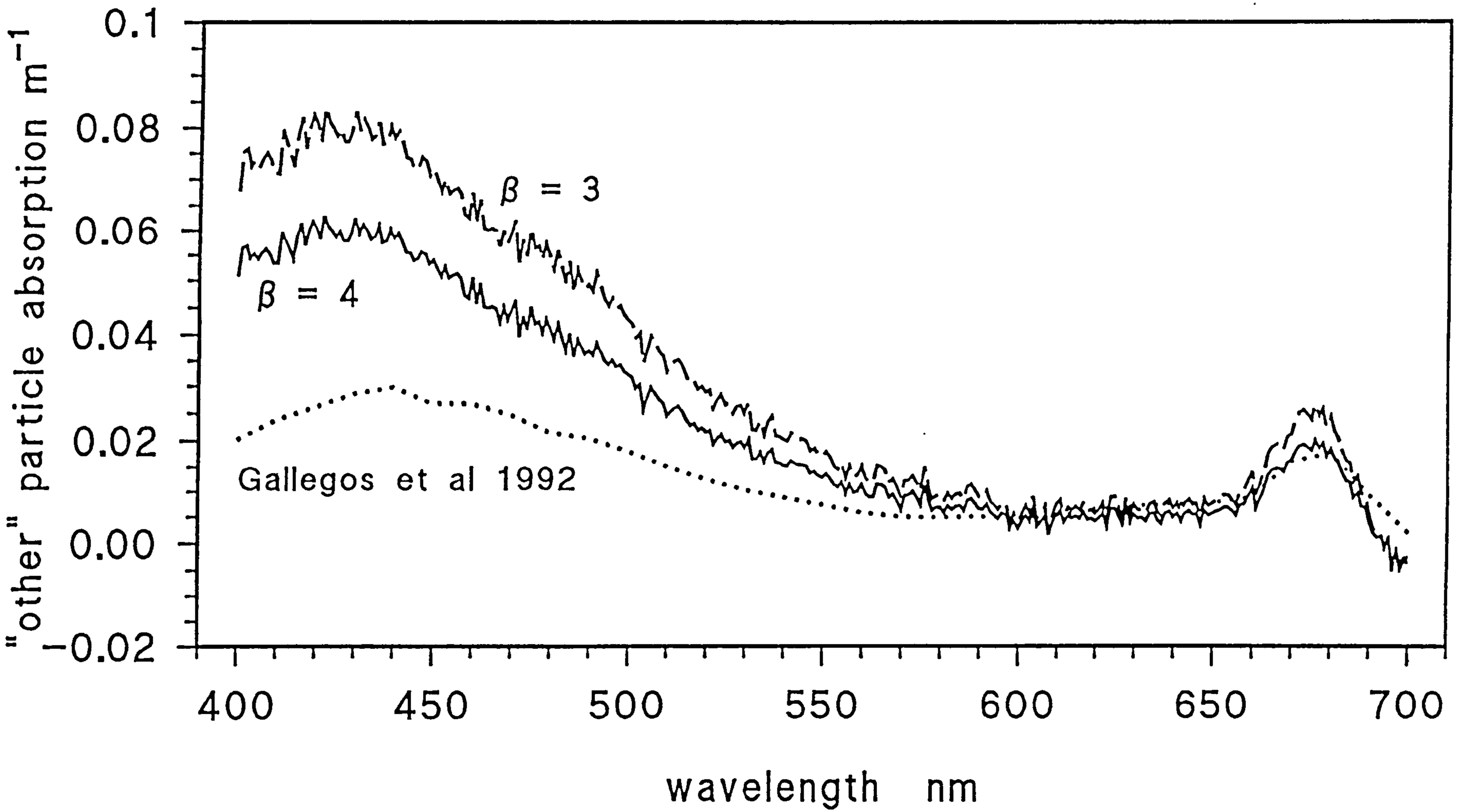

Figure 7.8 "Constant" from August regression of fresh spectra on inorganic concentration

Figure 7.9 Average of spectra with and without diffuser
a) kaolin
b) Conwy survey

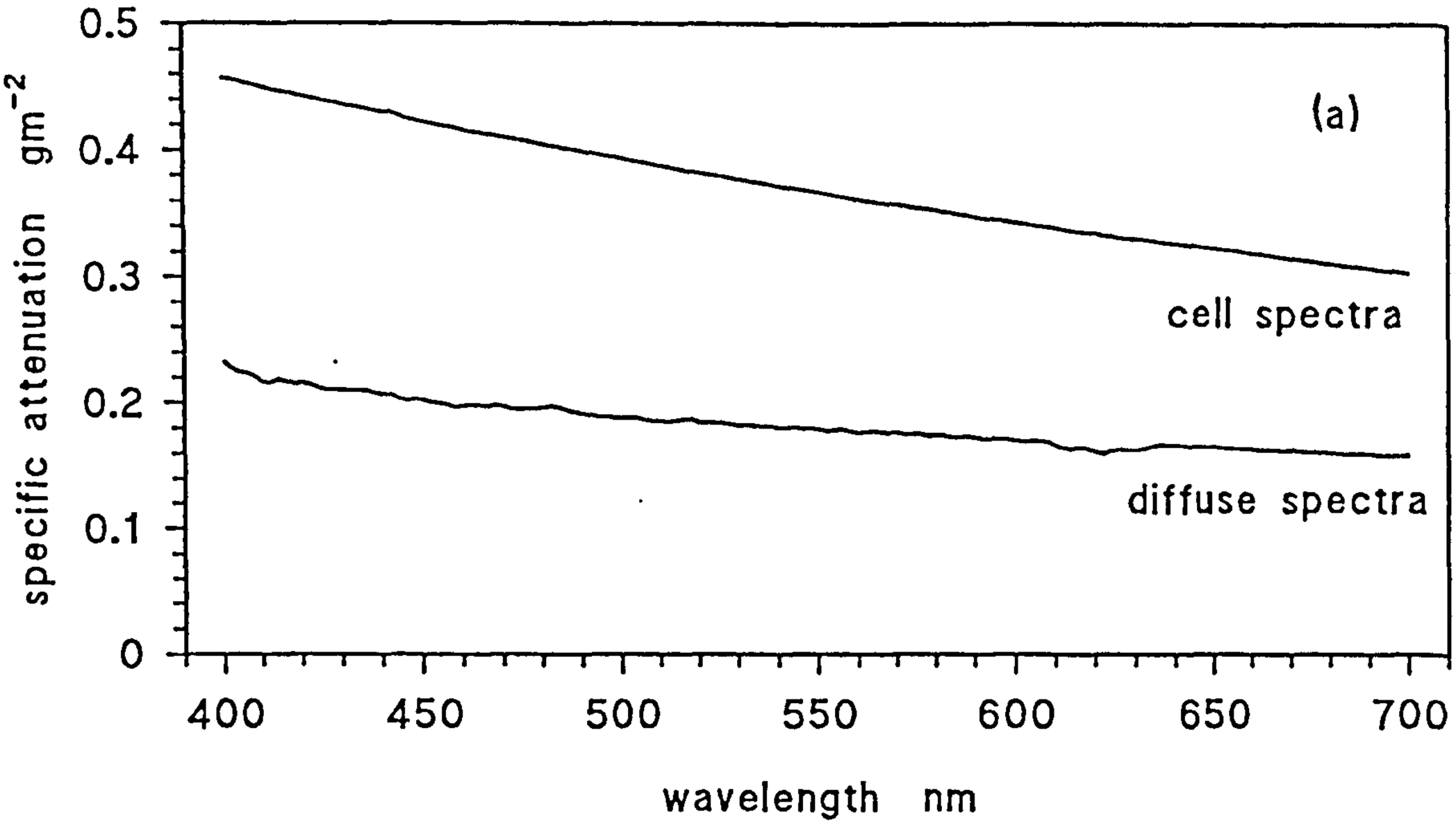
0.5
0.4
0.3
0.2
0.1
0
specific attenuation gm^{-2}
(a)
cell spectra
diffuse spectra
400
450
500
550
600
650
700
wavelength nm

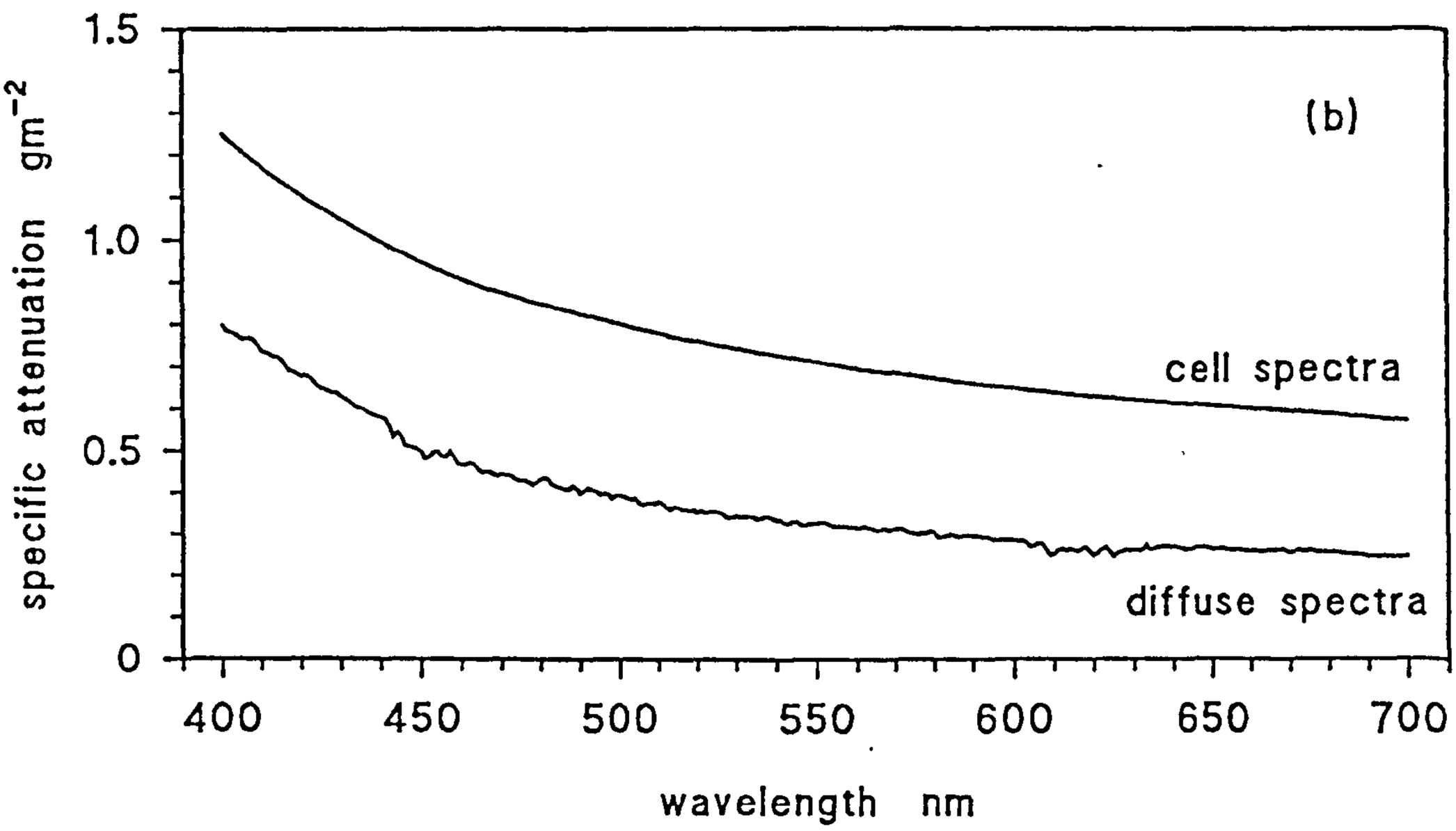
1.5
1.0
0.5
0
specific attenuation gm^{-2}
(b)
cell spectra
diffuse spectra
400
450
500
550
600
650
700
wavelength nm

8. COMPARISON BETWEEN LABORATORY AND FIELD MEASUREMENTS

In order to test the consistency of the measurements, the specific values for absorption and scattering derived from the *in situ* data can be compared with those measured in the laboratory. This comparison can be made in three ways: a) by comparing the derived absorption from the light sensor with the total absorption from the laboratory, and the derived scattering with the difference between the transmissometer attenuation and the laboratory absorption (§8.1); b) by relating the measured values of reflectance and diffuse attenuation with the ratio between b and a, calculated from the beam attenuation and the laboratory absorption (§8.2); c) by calculating the specific absorption values for each constituent from both the field and laboratory measurements and comparing these (§8.3 - the technique for regressing optical properties on concentrations to extract the specific values was described in §6.7).

8.1 ABSORPTION AND SCATTERING

Kirk's (1985) algorithms for deriving a and b from R and K were tested with the field measurements in §6.6, when the beam attenuation coefficient from the transmissometer was compared with the sum of a and b. As an alternative, the total laboratory absorption (the "fresh" filter spectra plus water and yellow substance) can be used as an independent value of absorption, and then subtracted from the transmissometer c to determine b, and hence test the derived values of a and b from the field separately.

The use of Kirk's algorithm (1994) for diffuse attenuation depends greatly on the influence of G. The value of G used was 0.256 as calculated for San Diego Bay. This is unrealistic for the Menai Strait which would have greater turbidity and therefore a lower value of G. It is also apparent that the value of G would change between the various sites visited. However, more suitable values of G were not available and consequently this standard value was used. Kirk (1994) relates G to the solar altitude as well as the scattering phase function. In this respect, the values for the Menai Strait survey are unlikely to change as most surveys were undertaken with cloudy conditions and therefore a diffuse ambient light field, with little dependence

on solar variation.

The comparison between absorption values for the **July Pier Survey** is shown in Fig. 8.1a-d - Fig. 8.1 a and b use $\beta=2$ correction on the particle spectra whereas, c and d use Cleveland & Weidemann (1993). The colour sensor values were calculated from the readings between 10:00 and 16:00; the extended time interval may explain the bias of the absorption to higher values relative to those in the laboratory as attenuation would be greater when the sun was lower. The values from the IRM1 are closer to the laboratory values; this was also observed with the field comparison as the profiles were taken at the same time as the water samples and the transmissometer readings. The difference between the methods of calculation, *i.e.* Kirk compared with $R=0.33b_b/a$, are small with respect to the scatter of points about a 1:1 line.

The scattering comparison can only be shown at 670 nm, the wavelength of the transmissometer (Fig. 8.2). The values calculated from the IRM1 readings show the same trend as (c-a) but are consistently too high (by ~0.4 m^{-1}). In contrast, the colour sensor values are more scattered, but predominantly too low.

In the **August Pier Survey,** the values of reflectance from the Satlantic were considered dubious, and when using these, the scattering values were much lower than those estimated with the transmissometer (as shown in Fig. 5.24). In the field data, the combined absorption and scattering were in much better agreement with attenuation when using the Spectron reflectance. This improvement is also apparent with the scattering measurements (Fig. 8.3), those calculated from the Satlantic data alone being less than 3 m^{-1}, whereas (c-a) ranges from 4.5 to 8.5 m^{-1}. However, the absorption calculated from the Satlantic data shows good agreement with laboratory, whereas the Satlantic-Spectron values have a tendency to be too high, although in the correct range (Fig. 8.4a-d). This bias is most apparent when the Cleveland & Weidemann (1993) correction is used (Fig. 8.4d). Once again, the difference when using Kirk's algorithms is minor compared with the overall scatter.

8.2 b/a RELATIONSHIPS

A more direct test of Kirk's algorithms is to correlate R and K/a with b/a. Kirk (1994) relates these as:

$$R = (0.975 - 0.629\mu_0)\frac{b_b}{a}$$

where $b_b = 0.019\ b$

and

$$\frac{K_d}{a} = \frac{1}{\mu_0}\left[1 + (0.425\mu_0 - 0.19)\frac{b}{a}\right]^{1/2}$$

where K_d is the downward diffuse attenuation averaged over the euphotic zone

If μ_0 is assumed to equal 0.85 (Petzold, 1972), these become:

$$R = 0.837\frac{b}{a} \quad \% \qquad \textit{eqn.}\ 8.1$$

and

$$\left[\frac{K_d}{a}\right]^2 = 1.384 + 0.237\frac{b}{a}$$

Reflectance and attenuation values were directly taken from sensor measurements, absorption was taken from the laboratory (as above), while scattering was calculated from transmissometer readings and is assumed constant over the visible wavelength range.

Fig. 8.5 shows the clear relationship between IRM1 R and b/a from observations during the July 1994 Pier Survey, producing a significant correlation:

$$R = 0.871\frac{b}{a} + 0.985 \qquad r^2 = 0.725 \quad p < 0.001 \quad n = 30$$

When forced through zero this becomes:

$$R = 1.149 \frac{b}{a}$$

If scattering is not considered constant with wavelength, the comparison can only be made for 670 nm:

$$R = 0.411 \frac{b}{a} + 0.952 \qquad r^2 = 0.816 \quad p < 0.001 \quad n = 6$$

which becomes

$$R = 0.839 \frac{b}{a}$$

This constant agrees well with that in equation 8.1.

In these equations the correlations should theoretically pass through zero, but the initial relationships fitted to the data have an intercept significantly different from zero, and therefore the zeroed relationship should not be used as a good fit.

It is apparent from Fig. 8.5 that the observations do not follow Kirk exactly, but have a greater gradient, although the values at 670 nm are similar.

The values for the **August 1995 Pier Survey** are shown in Fig. 8.6, using the reflectance from the Spectron. Three distinct relationships can be seen. The lowest relationship applies to only one day (23 August) and so has been considered invalid, as the low reflectance values may be due to shadowing effects. Most data points follow a relationship similar to that of Kirk, correlating as:

$$R = 0.556 \frac{b}{a} - 0.092 \qquad r^2 = 0.736 \quad p < 0.001 \quad n = 36$$

However, the values for 28-31 August follow a different relationship:

$$R = 1.864 \frac{b}{a} - 2.015 \qquad r^2 = 0.759 \quad p < 0.001 \quad n = 18$$

For both these relationships the intercept is not significantly different from zero.

These three days cover the spring tide, where total suspended sediment concentrations were highest (max. 10.25 mgl^{-1}). This suggests that the relationship between *b/a* and reflectance may vary with the dominant source of reflectance. The greater slope is associated with the higher mineral concentrations and may indicate a higher backscatter ratio, consistent with the higher scattering contribution from harder particles.

Fig. 8.7 represents the $[K_d/a]^2$ to *b/a* relationship for the **July Pier Survey.** Fig. 8.7a uses the Cleveland & Weidemann (1993) correction for the absorption spectra, while Fig. 8.7b uses $\beta=2$. In both cases there is wide scatter. Similarly, Fig 8.8 a&b show the data for the **August Pier Survey,** excluding the points for 25 August due to their anomalously low values compared with the rest of the survey. The correlations for these are shown in Table 8.1. The equations for 670 nm only are included as this is the wavelength at which scattering was calculated. Although regression coefficients improve in the **July** data when only 670 is considered, the relationship is less significant (indicated by the higher p values) which suggests that scattering can be considered constant over the visible range.

$[K_d/a]^2 = m[b/a] + c$					
description	m	c	r^2	p	n
JMB β=C&W	0.432	1.499	0.337	<0.001	43
670 nm	0.463	1.208	0.618	0.0041	11
JMB β=2	0.362	1.664	0.277	<0.001	43
670 nm	0.441	1.178	0.610	0.0046	11
AMB β=C&W	0.256	-0.564	0.891	<0.001	36
670 nm	0.230	-0.208	0.338	0.226	6
AMB β=2	0.215	0.087	0.785	<0.001	36
670 nm	0.270	-0.646	0.492	0.120	6

Table 8.1 Correlations between K_d/a and *b/a* for the **Pier Surveys**

All these graphs also show the relationship suggested by Kirk (1994), using $\mu_0 = 0.85$. For the **JMB94** data the Kirk relationship is too low, and appears to delimit a lower boundary to the observed data. However, in the **AMB95** survey the Kirk relationship is higher than the observations, though follows the same trend.

8.3 SPECIFIC SPECTRA

The laboratory values for phytoplankton pigment (described in §5.2.4) are within the error bars of the instrument derived (Fig. 8.9), showing general agreement.

The IRM1 derived absorption values change slightly from winter to summer, the MSS absorption being slightly greater in winter (Fig. 8.10). This trend is not observed in the laboratory spectra, where the winter furnaced spectra appear to have a steeper exponential curve with less variation between the spectra, but are not greater in overall magnitude. The zeroed MSS spectra (*i.e.* the value at 750 nm was subtracted from all absorbances) were initially compared with the field data (Fig. 8.11) exhibiting a steeper exponential and lower values than observed in the field. However, if the spectra are not zeroed at 750 nm the more uniform absorption across the spectrum is in better agreement with the field data. This is most apparent when comparing the summer spectra with the IRM1 and those from **AMB95** with the Satlantic data (Fig. 8.12). When all the **Menai Strait** values are combined the specific curve is lower than other measurements, but is the same shape as that derived from **AMB95.**

These spectra can be used to calculate a wavelength dependent value of β, by comparing the **Menai Strait** derived absorption with that measured in the laboratory. Initially, the *in situ* derived absorption was compared with β values of 2, 3 and 4 (Fig. 8.13), appearing to agree most closely with $\beta=3$. However, when the Satlantic data were used, $\beta=3$ produced a curve which was too low at longer wavelengths. Conversely, $\beta=2$ gave correct values at longer wavelengths but was too high in the blue. Fig. 8.14 shows the higher absorption towards shorter wavelengths which may be due to increased scatter that can be incorporated in β. When curves are fitted to the observations, and the ratio calculated (Fig. 8.15), the resultant equation for β is:

$$\beta = 2.0 + 0.75\exp[-0.009(\lambda - 400)] \qquad \textit{eqn.}\ 8.2$$

The successful comparison of these optical properties leads to the construction of the *in situ* readings from the laboratory measurements (Fig. 8.16-8.18), following the basic equations for total absorption in §2.3.1. These figures show the wet particles plus yellow substance and water for the **Pier Surveys** and the **Clyde** compared with the sensor absorption, while the **Menai Strait** comparison is the inorganic particle spectra, plus yellow substance, water and the chlorophyll concentration multiplied by the specific spectrum (corrected as per Cleveland & Weidemann, 1993) derived from the **July Pier Survey.** The series of three figures compares the corrections of Cleveland & Weidemann (1993), β=2 and β=(2+scattering) [*i.e.* equation 8.2]. The laboratory values match the *in situ* measurements best when the correction β=(2+scattering) is used (Fig. 8.18), allowing for change across the spectrum. Fig. 8.19 uses the three methods of correction for the surface spectra and compares this with the *in situ* absorption. However, Fig. 8.20 uses the spectra for the middle sample, taken at approximately 3 optical depths. It is apparent that this sample gives better agreement with the instruments. This implies that optical measurements should be used with the average concentration throughout the euphotic zone and not just from surface measurements, unless these are representative of the upper part of the column.

8.4 AVERAGE COSINE

The combination of the laboratory and field measurements can be used to determine the average cosine μ in the **Menai Strait** and how it varies throughout the year. This is calculated as the ratio between the laboratory absorption and the *in situ* diffuse attenuation. Fig. 8.21 shows the slight increase in all wavelengths into the summer, as the signal from the sun becomes stronger and higher in the sky. This is illustrated by the variation in the cosine receiver used with the IRM1 (Fig. 6.14).

8.5 SUMMARY

Within the different surveys, the variation due to the use of different reflectance equations appears minor in relation to the overall scatter. Consequently, this does not clarify whether the use of Kirk's (1985) algorithms is appropriate for these types of

environment.

The comparison between the regression on the derived values from the *in situ* measurements and the regressions on the laboratory measurements are in good agreement when organic particles dominate *i.e.* in the summer months. However, the relationship between R and b/a may change with the nature of the particles, giving a steeper correlation when mineral particles dominate. It has been shown that the correction of mineral particles to zero at 750 nm is inappropriate, as there is a component of absorption as well as scattering in the spectrum measured in the infra-red. An alternative pathlength amplification correction has also been suggested which is applicable to mineral particles with higher values of absorption than those previously calculated for phytoplankton. This correction was determined through the comparison of field and laboratory measurements and includes a wavelength dependency for scatter. When this correction is used, measurements from other surveys are in better agreement indicating that this correction is more applicable than the others used in this context.

Figure 8.1 Total laboratory absorption (water+yellow substance+fresh filter) compared with *in situ* absorption, for JMB94

a) colour sensor
b) UCNW irradiance meter
c) colour sensor using C&W (1993) filter correction
d) UCNW irradiance meter using C&W (1993) filter correction

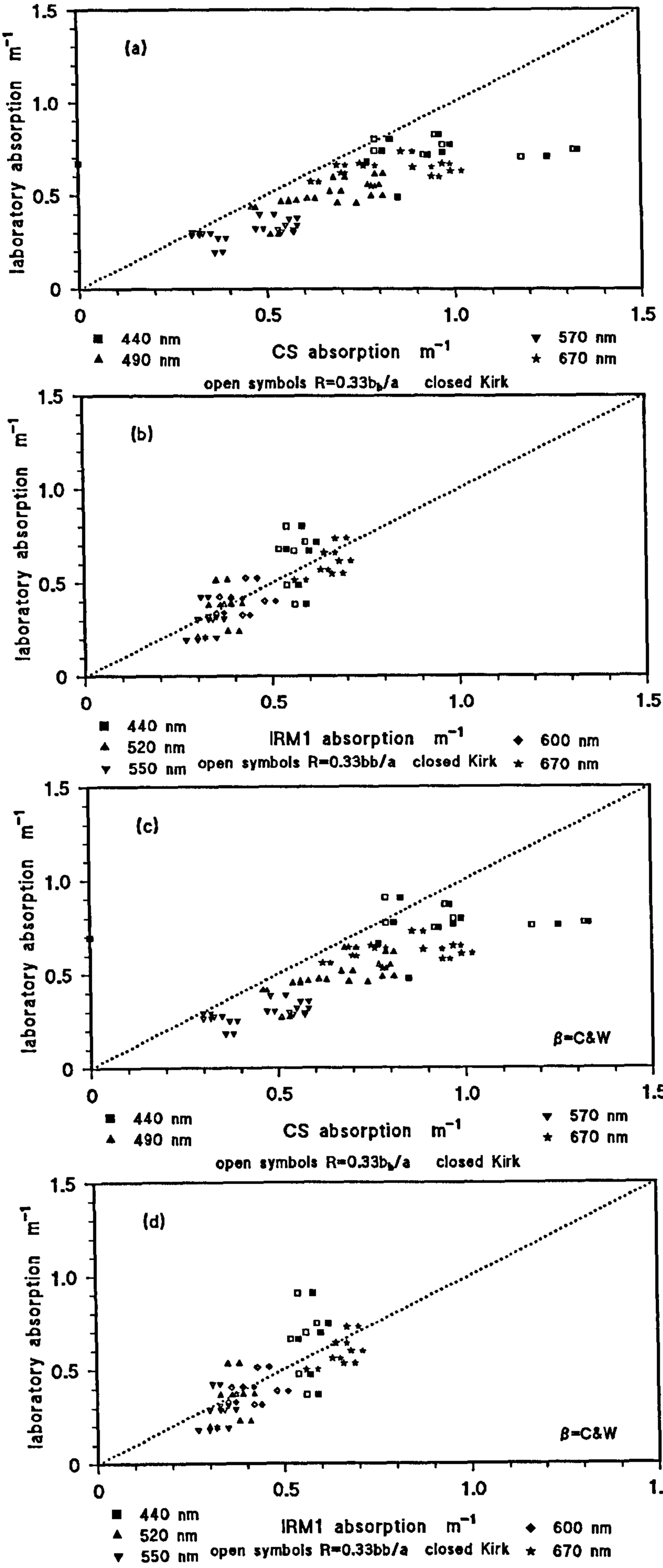
(a)
laboratory absorption m⁻¹
CS absorption m⁻¹
■ 440 nm
▲ 490 nm
▼ 570 nm
★ 670 nm
open symbols R=0.33b_b/a closed Kirk
(b)
IRM1 absorption m⁻¹
■ 440 nm
▲ 520 nm
▼ 550 nm
◆ 600 nm
★ 670 nm
open symbols R=0.33bb/a closed Kirk
(c)
β=C&W
(d)
0
0.5
1.0
1.5

Figure 8.2 Difference between transmissometer *c* and laboratory absorption compared with *in situ* scatter for JMB94, 670nm

Figure 8.3 Difference between transmissometer *c* and laboratory absorption compared with *in situ* scatter for AMB95, 670nm. The use of $\beta=2$ or C&W (1993) does not make an observable difference.

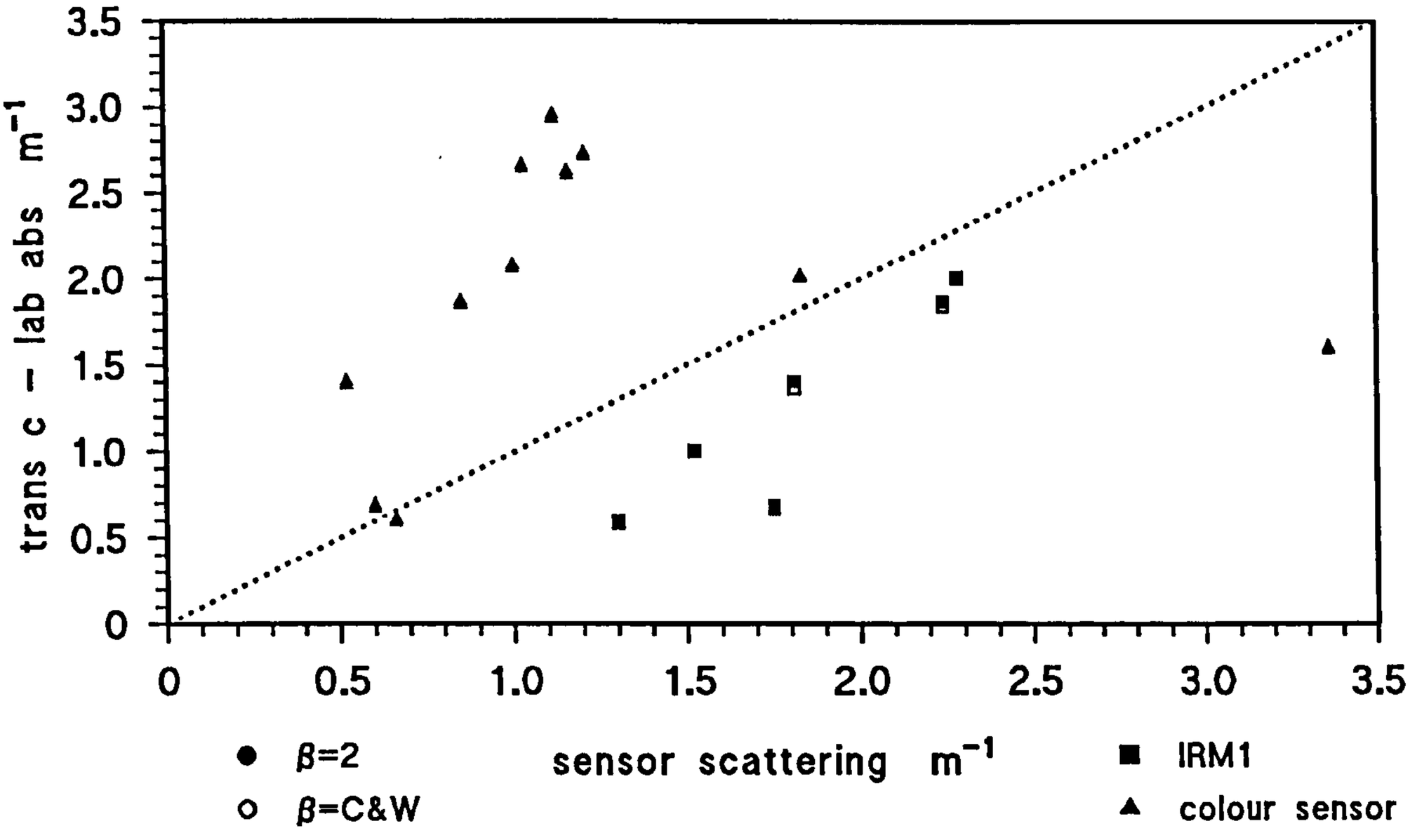
trans c – lab abs m⁻¹
3.5
3.0
2.5
2.0
1.5
1.0
0.5
0
0
0.5
1.0
1.5
2.0
2.5
3.0
3.5
sensor scattering m⁻¹
β=2
β=C&W
IRM1
colour sensor

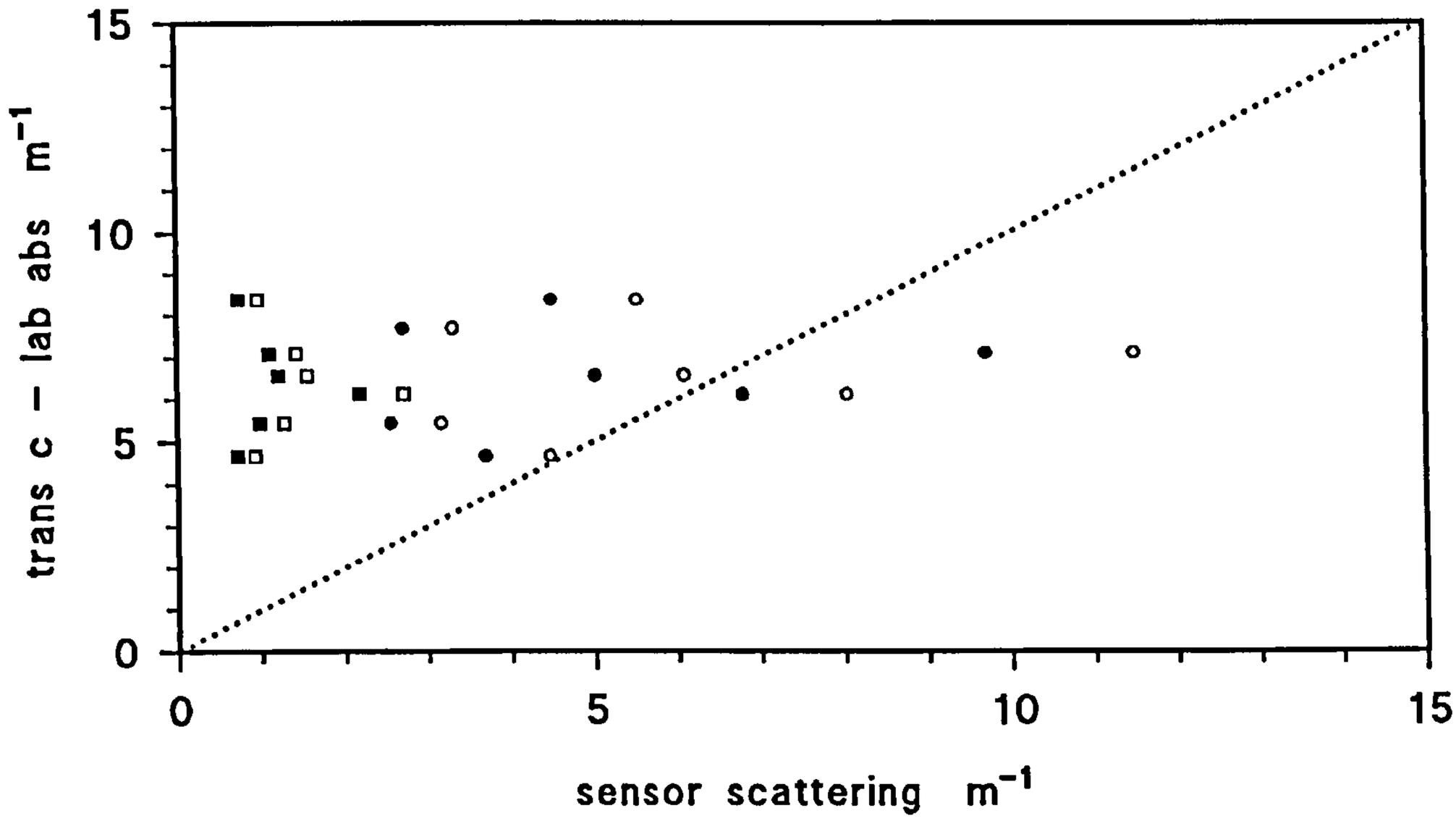
trans c – lab abs m⁻¹
15
10
5
0
0
5
10
15
sensor scattering m⁻¹
uses Satlantic and Spectron
uses Satlantic K and R
closed use Kirk open R=0.33b_b/a

Figure 8.4 Total laboratory absorption (water+yellow substance+fresh filter) compared with *in situ* absorption, for AMB95

a) Satlantic

b) combined Satlantic and Spectron

c) Satlantic with Cleveland & Weidemann (1993) correction used for laboratory spectra

d) combined Satlantic and Spectron with Cleveland & Weidemann (1993) correction used for laboratory spectra

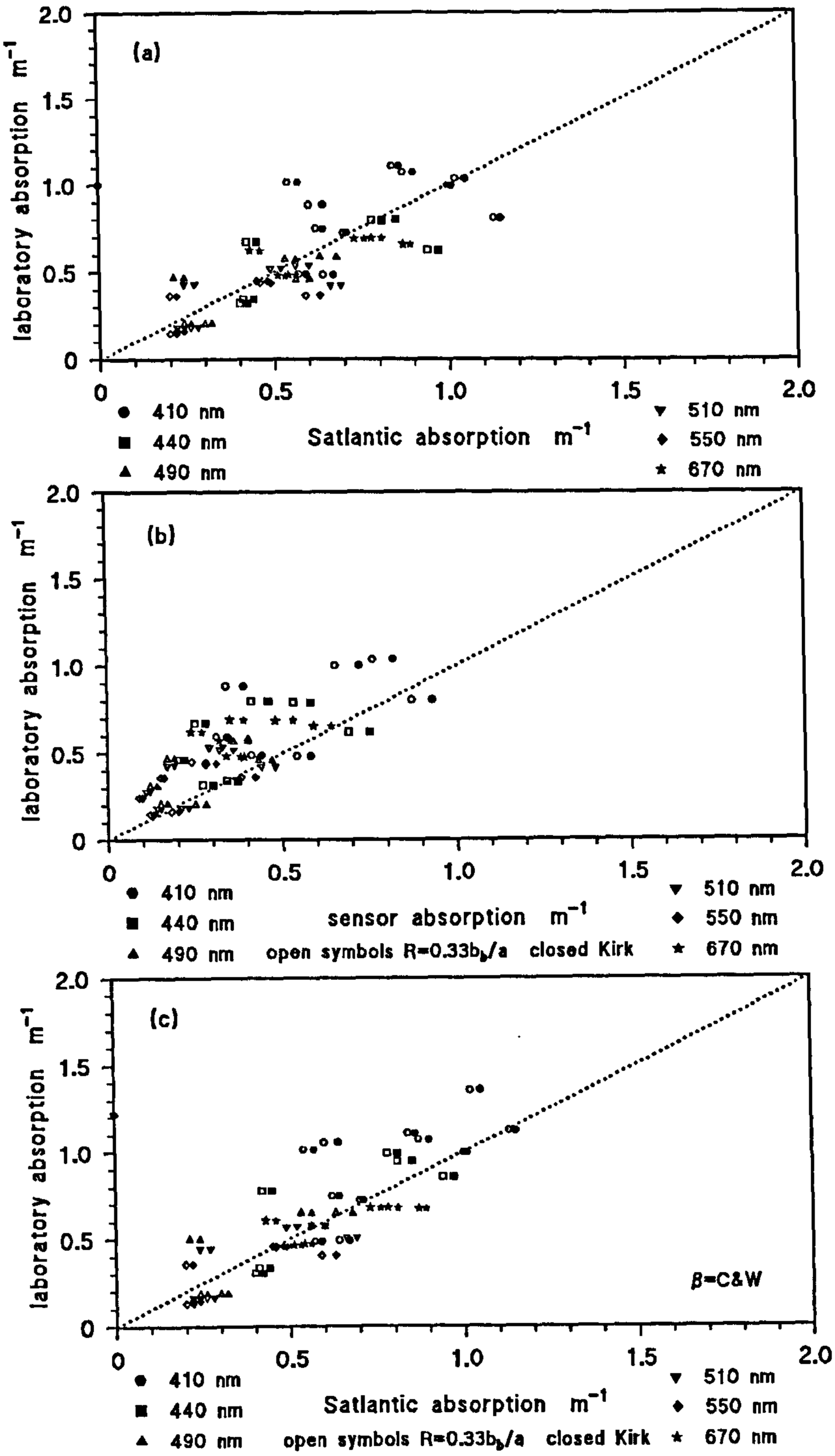
(a)
laboratory absorption m^{-1}
Satlantic absorption m^{-1}
410 nm
440 nm
490 nm
510 nm
550 nm
670 nm
(b)
laboratory absorption m^{-1}
sensor absorption m^{-1}
410 nm
440 nm
490 nm
open symbols R=0.33b$_b$/a closed Kirk
510 nm
550 nm
670 nm
(c)
laboratory absorption m^{-1}
β=C&W
Satlantic absorption m^{-1}
410 nm
440 nm
490 nm
open symbols R=0.33b$_b$/a closed Kirk
510 nm
550 nm
670 nm
(d)
laboratory absorption m^{-1}
β=C&W
sensor absorption m^{-1}
410 nm
440 nm
490 nm
open symbols R=0.33b$_b$/a closed Kirk
510 nm
550 nm
670 nm

Figure 8.5 Irradiance meter reflectance compared with the ratio between scatter and absorption, where b=c-a, for JMB94

Figure 8.6 Spectron reflectance compared with the ratio between scatter and absorption, where b=c-a, for AMB95.
Open symbols indicate data points which were omitted from the regression: 28-31 August 1995.

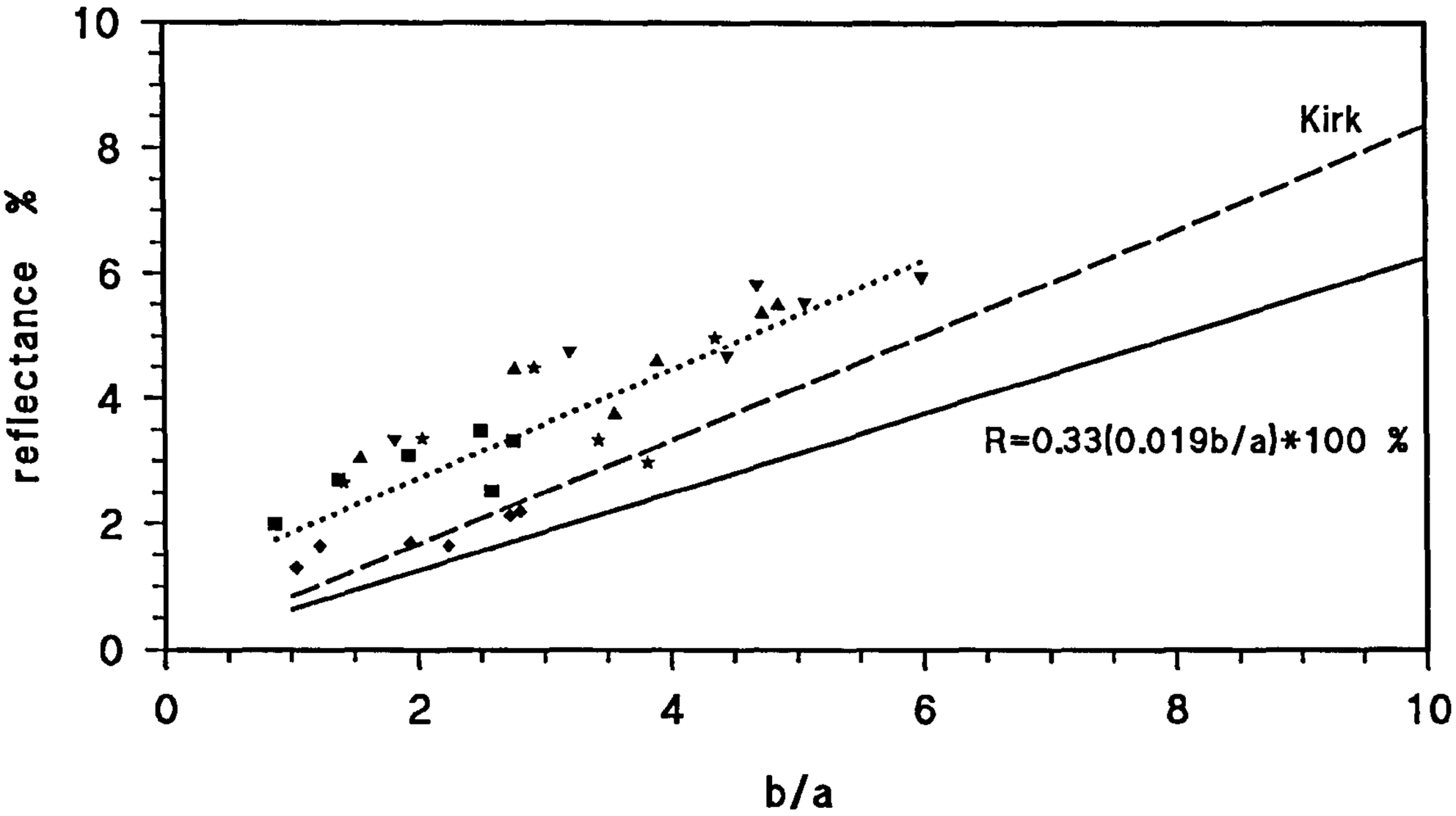
reflectance %
10
8
6
4
2
0
0
2
4
6
8
10
b/a
Kirk
R=0.33(0.019b/a)*100 %

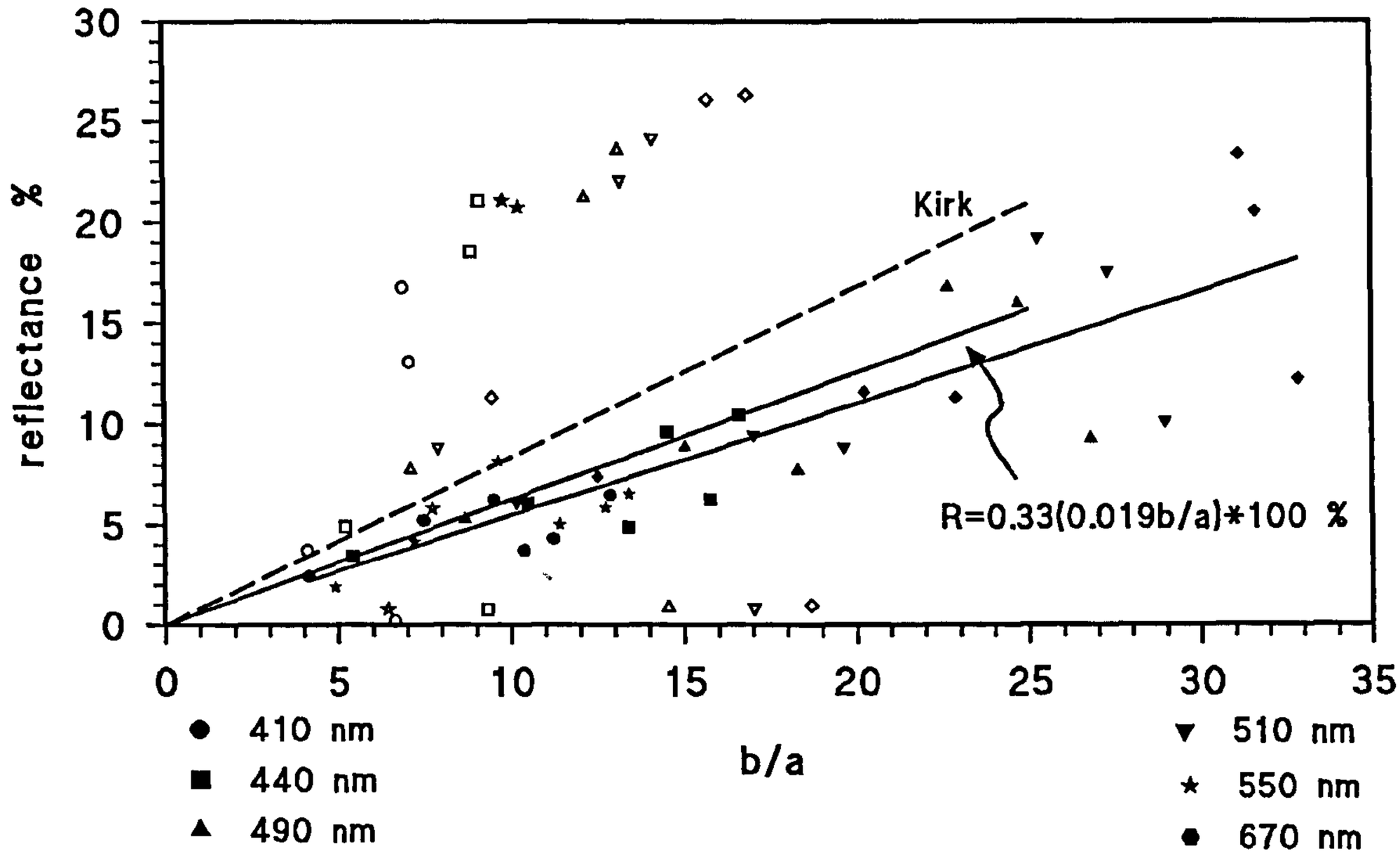
reflectance %
30
25
20
15
10
5
0
0
5
10
15
20
25
30
35
b/a
Kirk
R=0.33(0.019b/a)*100 %
410 nm
440 nm
490 nm
510 nm
550 nm
670 nm

Figure 8..7 $(K_d/a)^2$ compared with b/a, where K_d is from the colour sensor between 09:00 and 15:00, for JMB94 (a=water+yellow substance+fresh filter)

a) Cleveland & Weidemann (1993) absorption correction

b) $\beta=2$ absorption correction

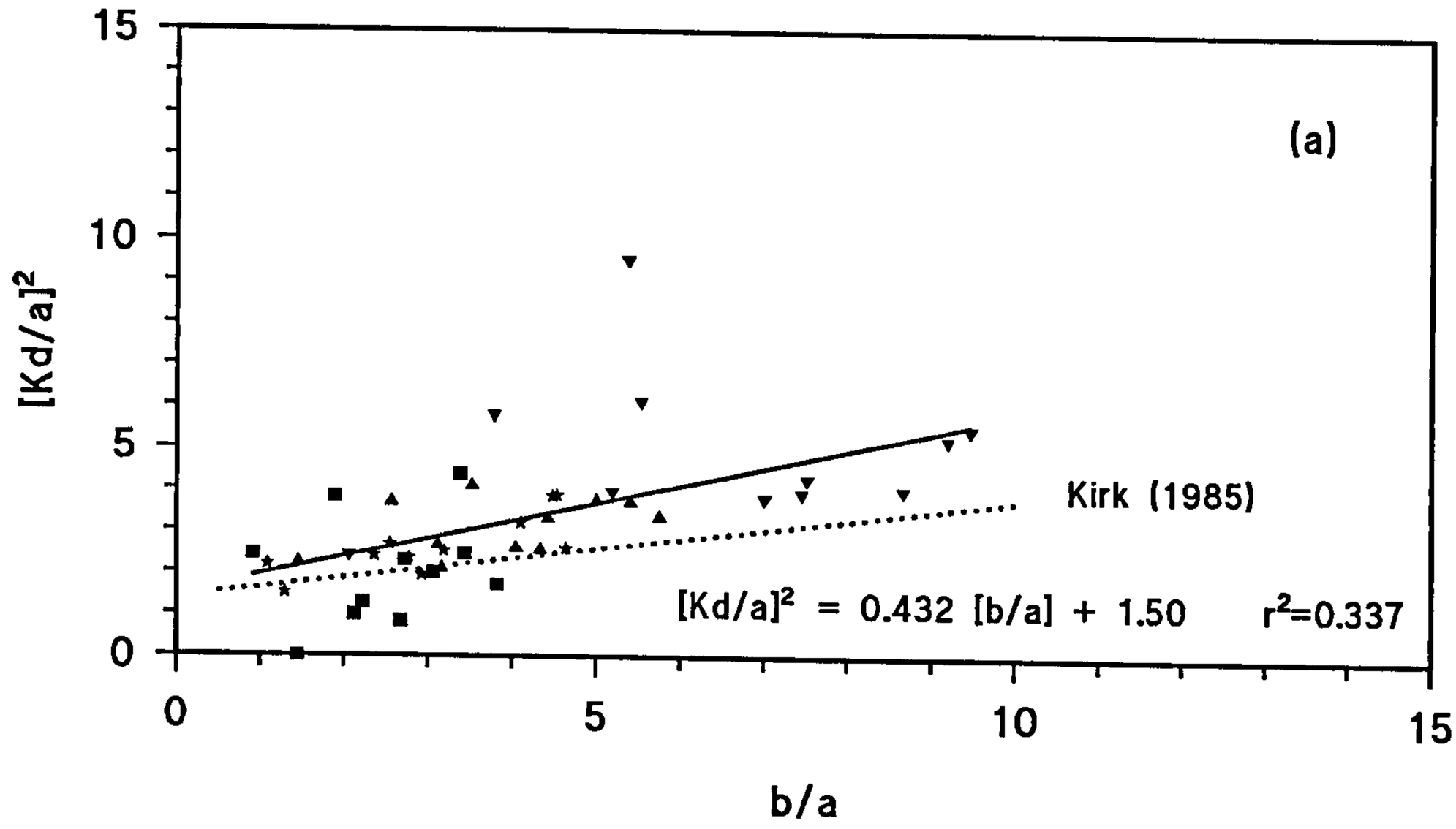
(a)
15
10
5
0
[Kd/a]²
0
5
10
15
b/a
Kirk (1985)
[Kd/a]² = 0.432 [b/a] + 1.50
r²=0.337

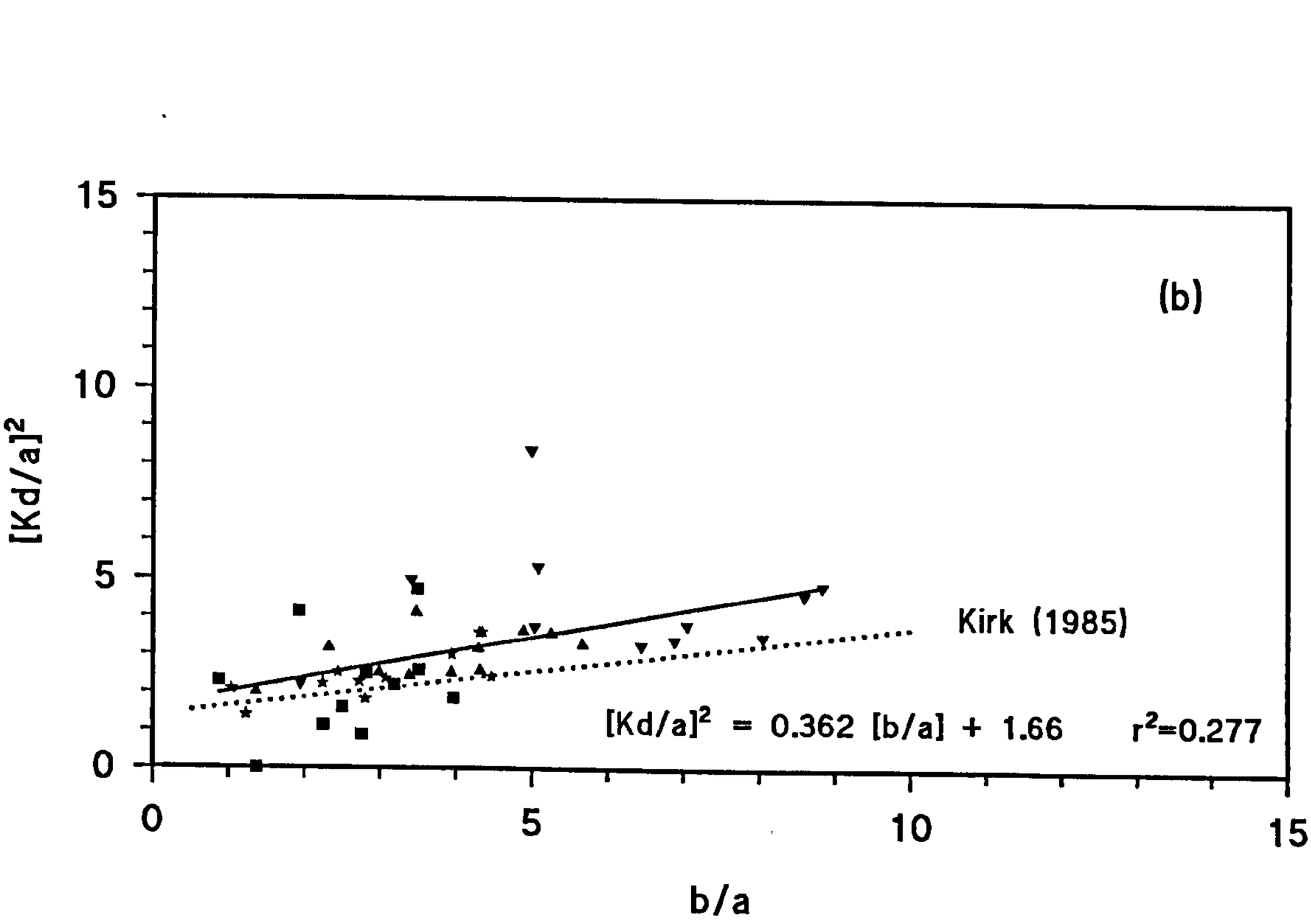
(b)
15
10
5
0
[Kd/a]²
0
5
10
15
b/a
Kirk (1985)
[Kd/a]² = 0.362 [b/a] + 1.66
r²=0.277

Figure 8.8 $(K_d/a)^2$ compared with b/a, where K_d is from the Satlantic, for AMB95
a) Cleveland and Weidemann (1993) pathlength amplification correction
b) $\beta = 2$ correction

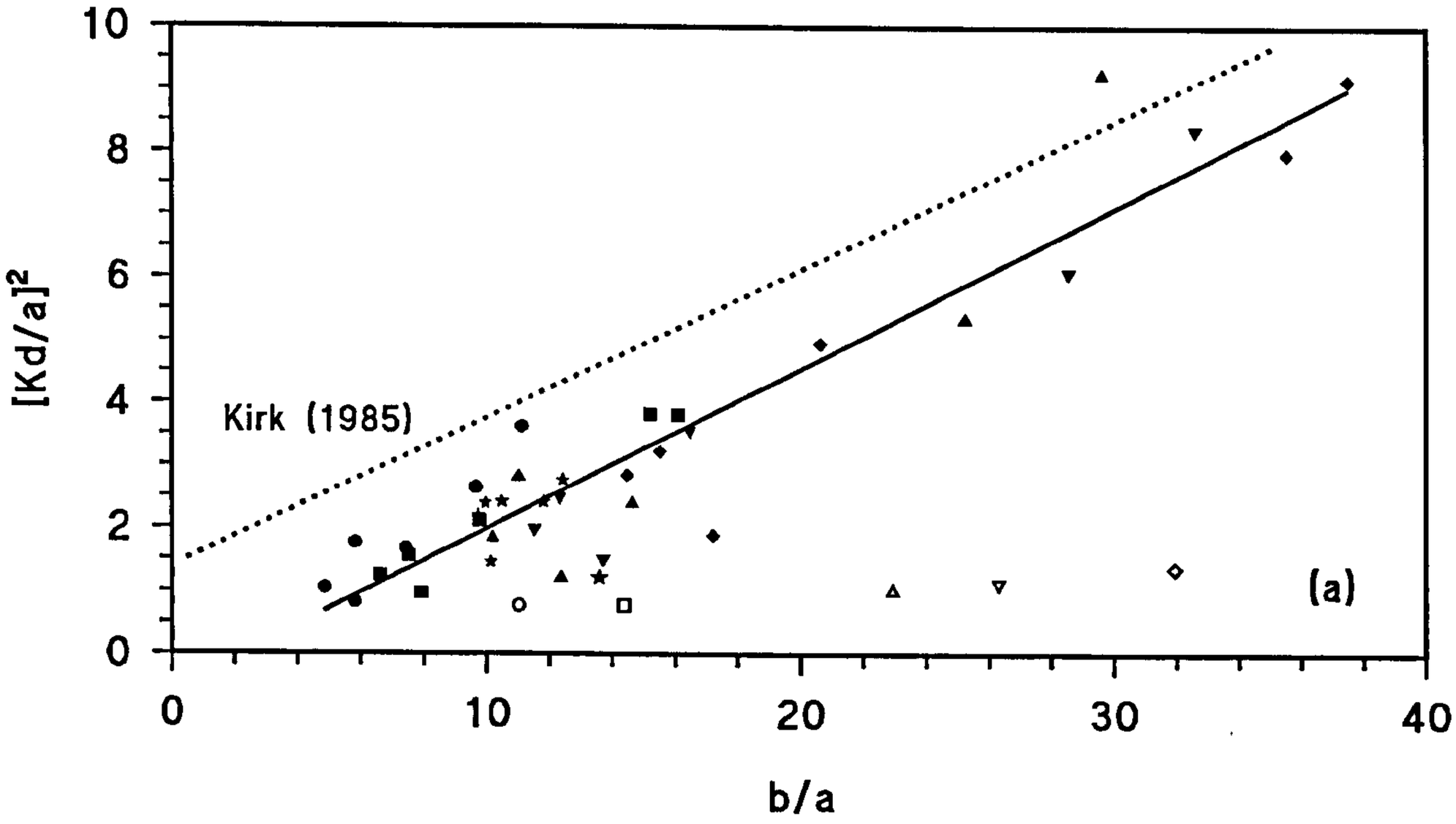
10
8
6
4
2
0
[Kd/a]²
Kirk (1985)
(a)
0
10
20
30
40
b/a

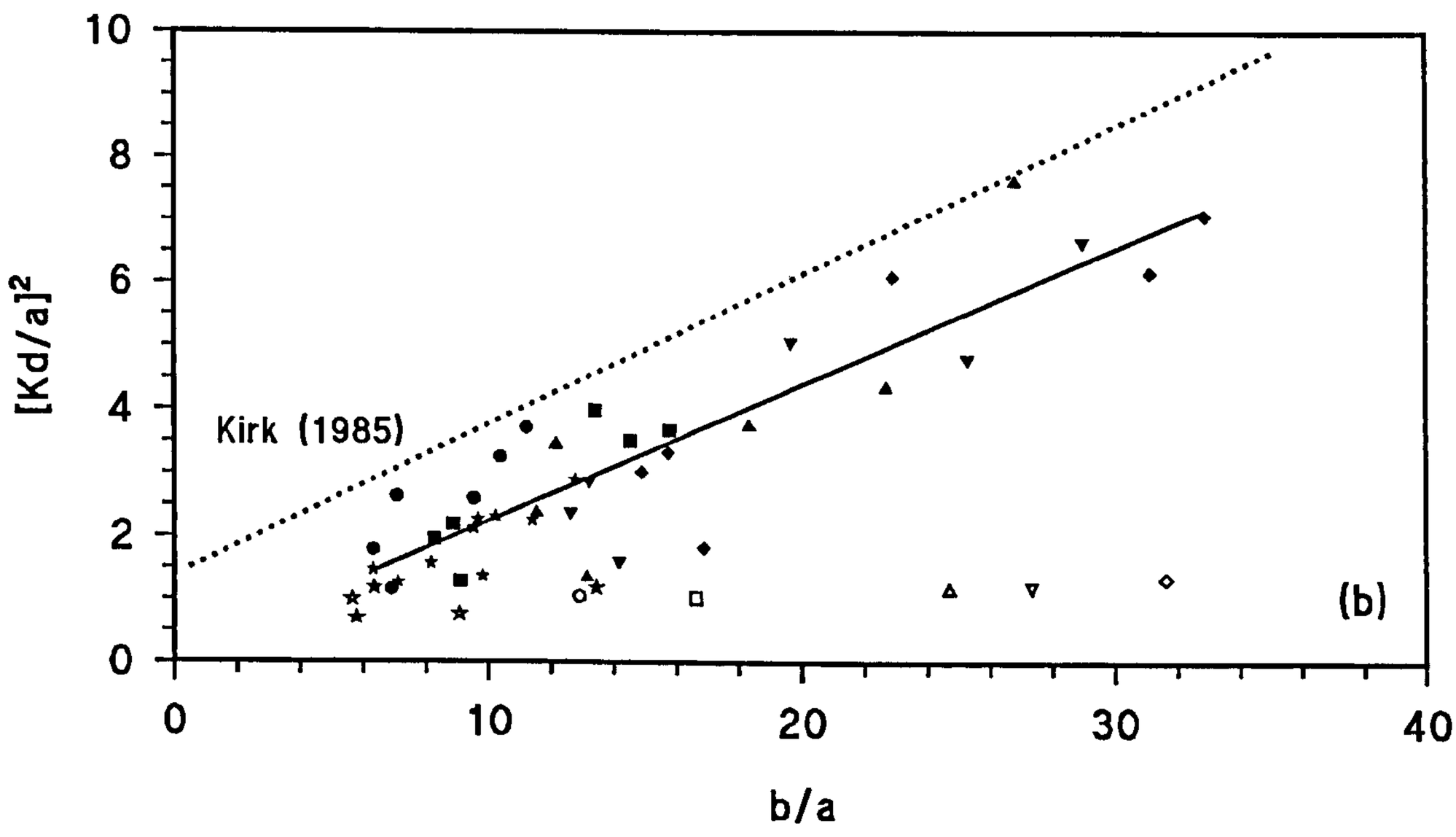
10
8
6
4
2
0
[Kd/a]²
Kirk (1985)
(b)
0
10
20
30
40
b/a

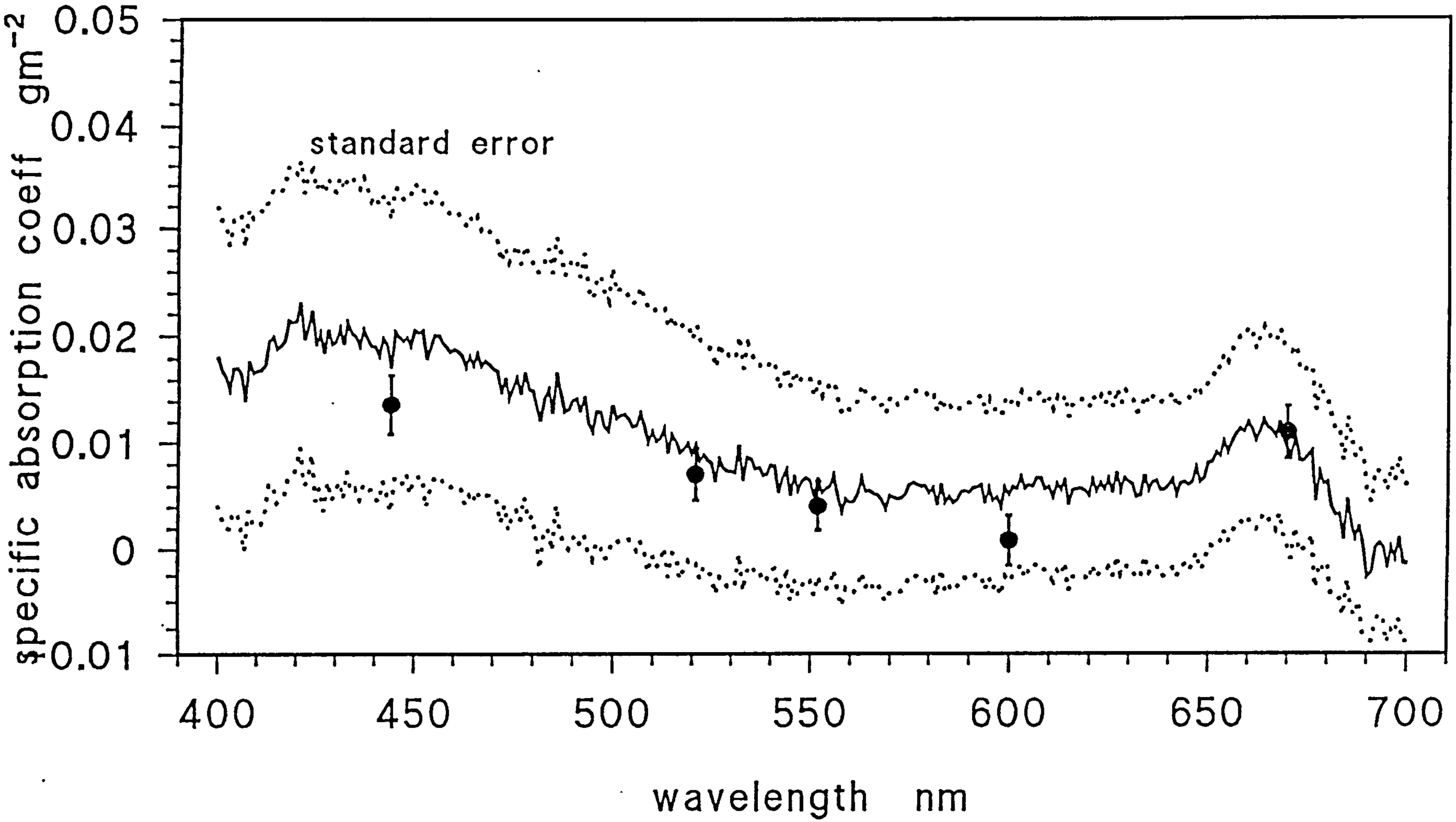

Figure 8.9 Phytoplankton spectrum derived from "fresh" spectra and in situ measurements

Figure 8.10 Furnaced spectra for Menai Strait Survey 1993-1994. Filters not zeroed, $\beta=2$

a) average of all spectra
b) average of winter spectra (Nov93-Mar94, Oct94)
c) average of summer spectra (May94-Aug94)

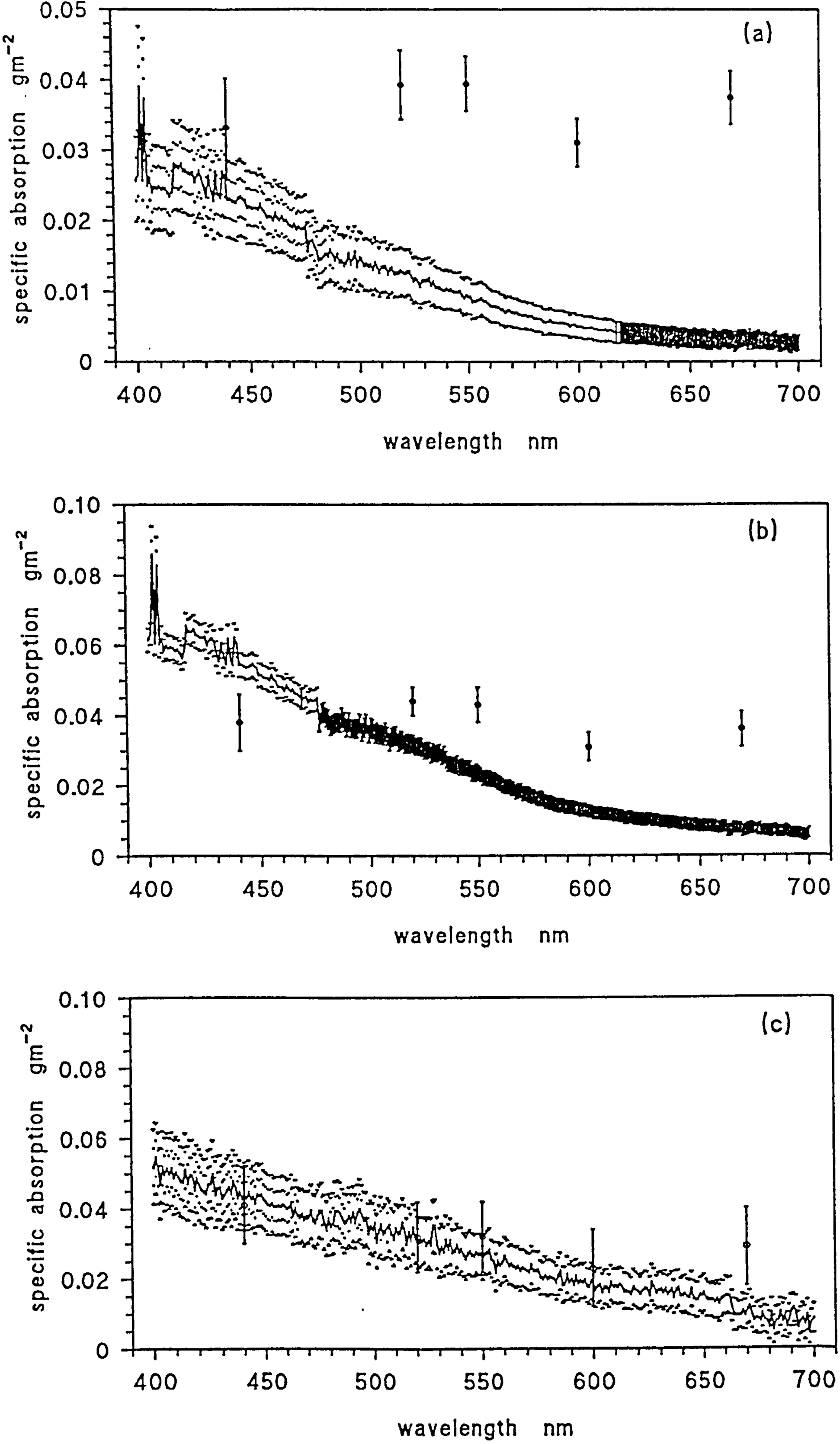
(a)
specific absorption gm^{-2}
0.05
0.04
0.03
0.02
0.01
0
400
450
500
550
600
650
700
wavelength nm
(b)
specific absorption gm^{-2}
0.10
0.08
0.06
0.04
0.02
0
400
450
500
550
600
650
700
wavelength nm
(c)
specific absorption gm^{-2}
0.10
0.08
0.06
0.04
0.02
0
400
450
500
550
600
650
700
wavelength nm

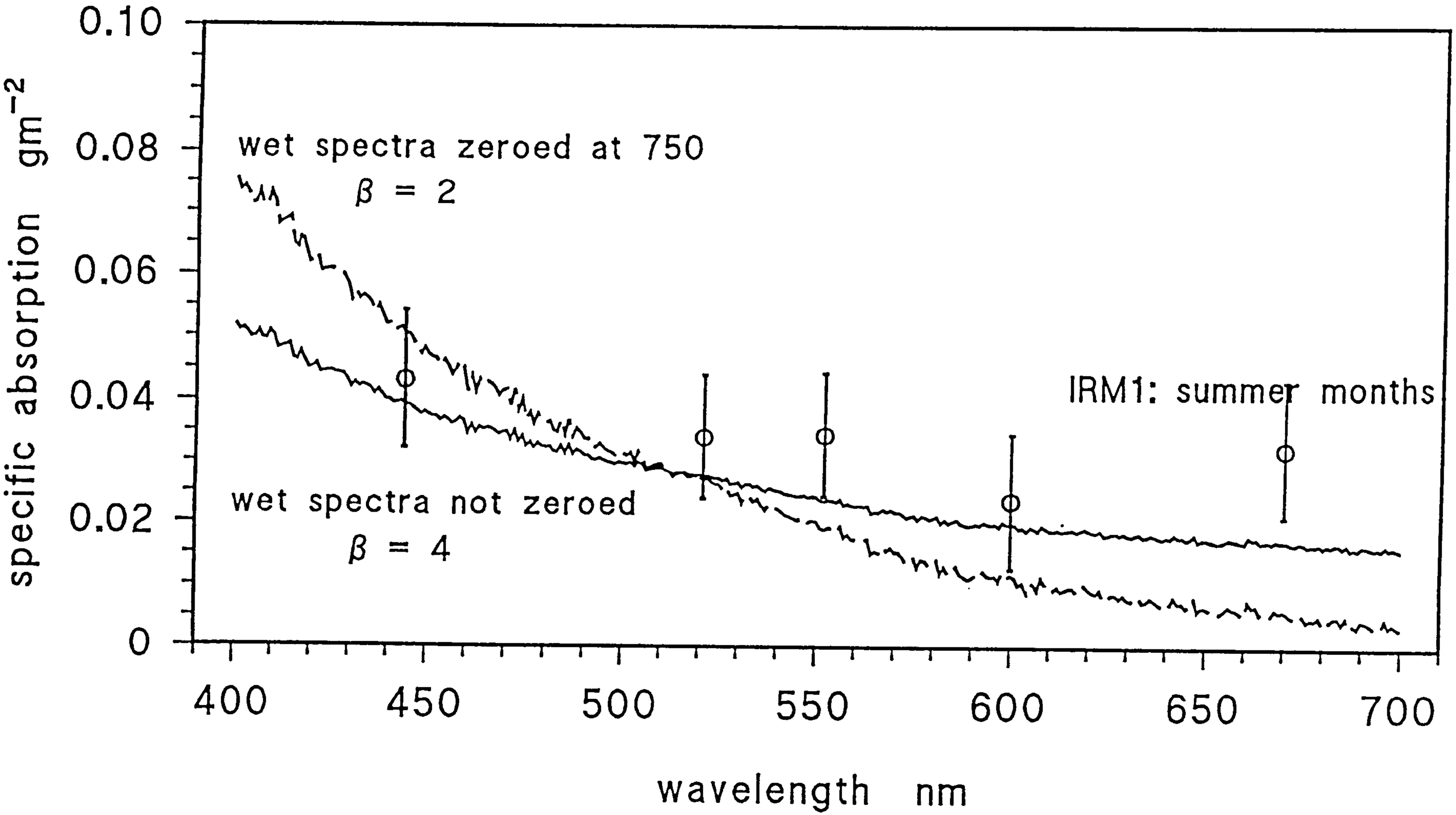

Figure 8.11 Furnaced spectra compared with in situ derived inorganic spectrum

Figure 8.12 Sensor derived inorganic spectrum compared with fresh filter derived spectrum

a) Satlantic

b) Irradiance meter (summer)

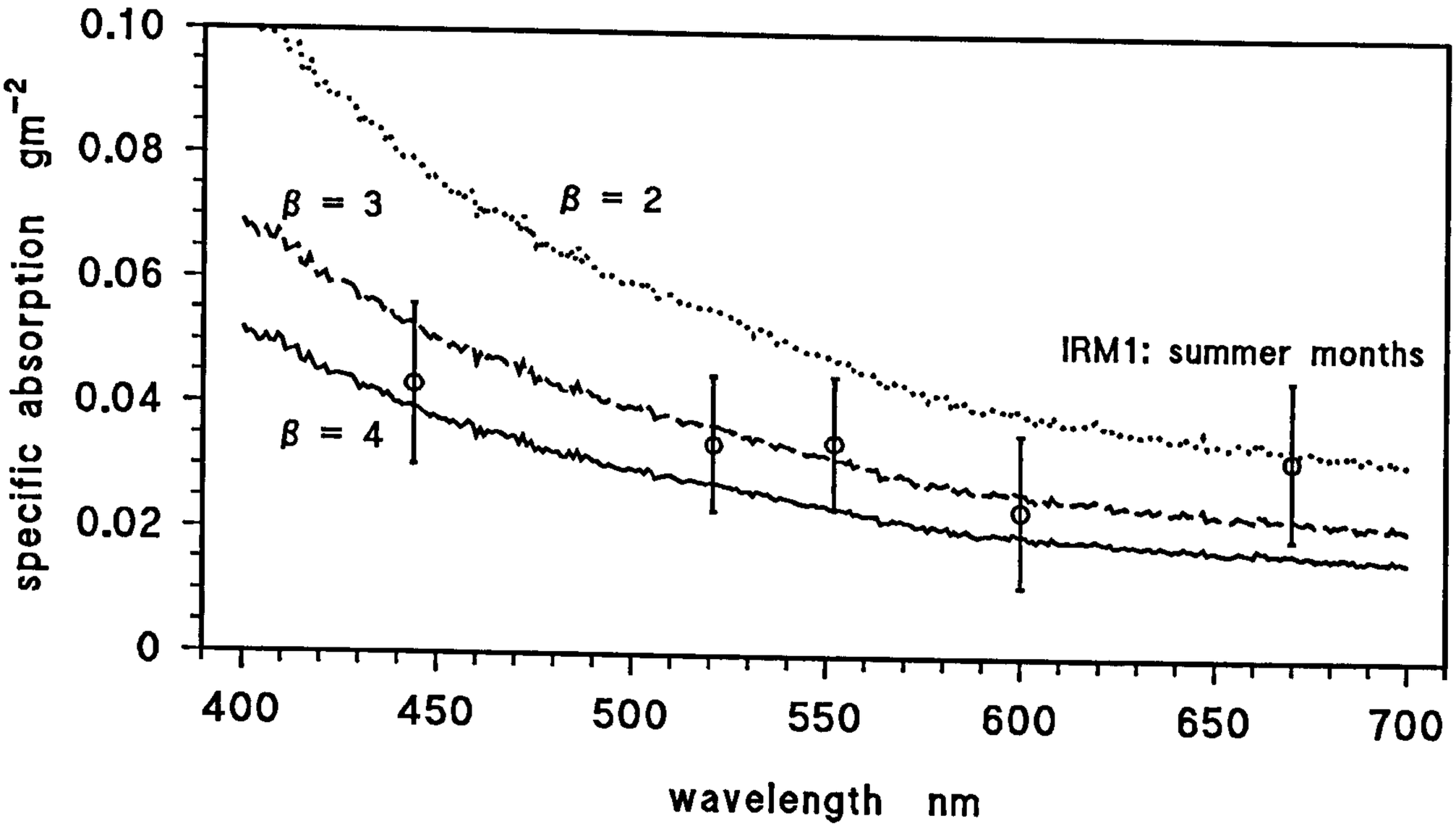
0.10
0.08
0.06
0.04
0.02
0
specific absorption gm^{-2}
β = 3
β = 2
β = 4
IRM1: summer months
400
450
500
550
600
650
700
wavelength nm

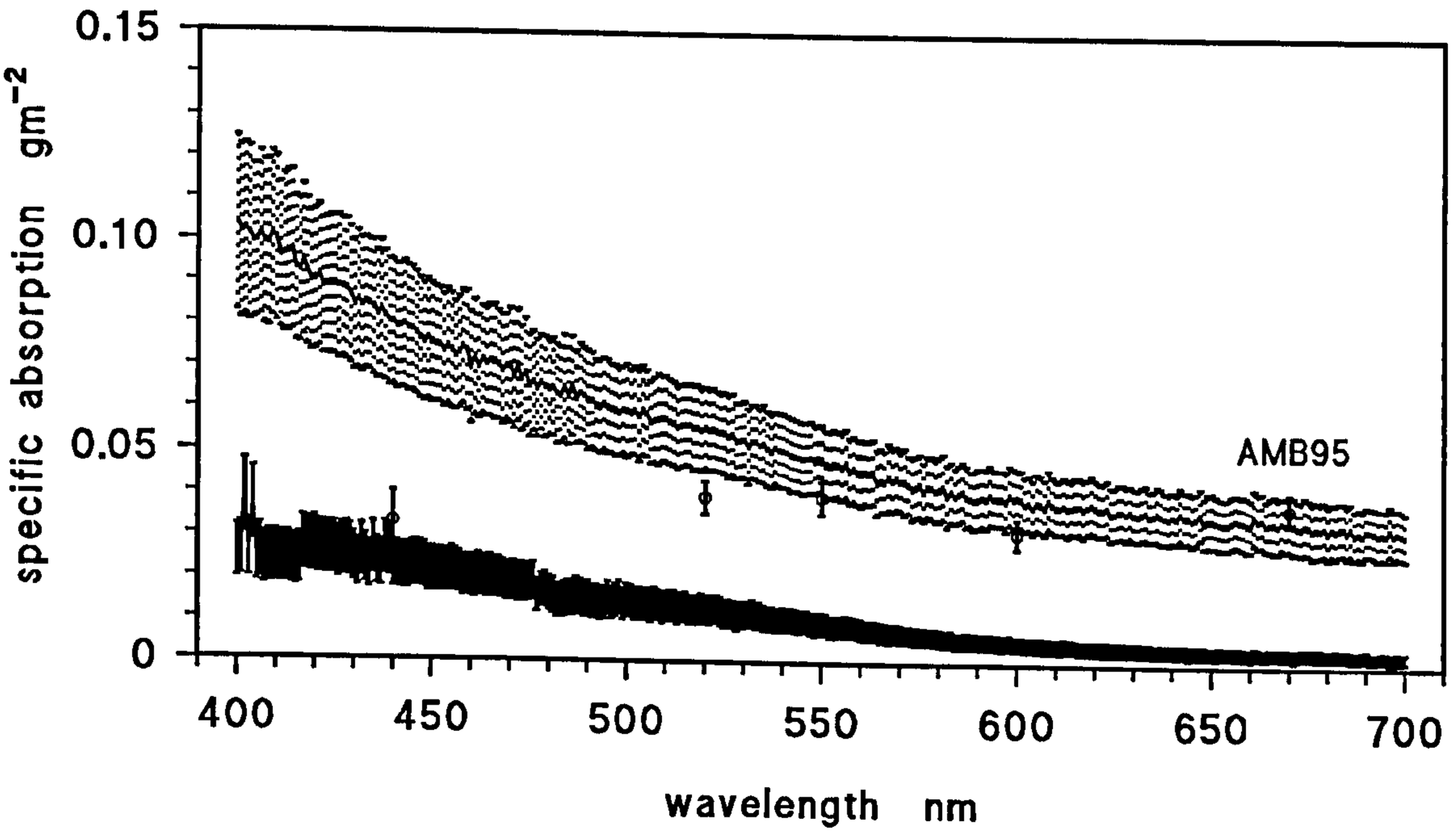
0.15
0.10
0.05
0
specific absorption gm^{-2}
AMB95
400
450
500
550
600
650
700
wavelength nm

Figure 8.13 *In situ* inorganic absorption derived from Satlantic data compared with laboratory spectrum, derived from "fresh" filter spectra with $\beta=2$ and $\beta=3$

Figure 8.14 Comparison of smoothed laboratory derived spectrum ($\beta=2$) with *in situ* Satlantic spectrum from AMB95

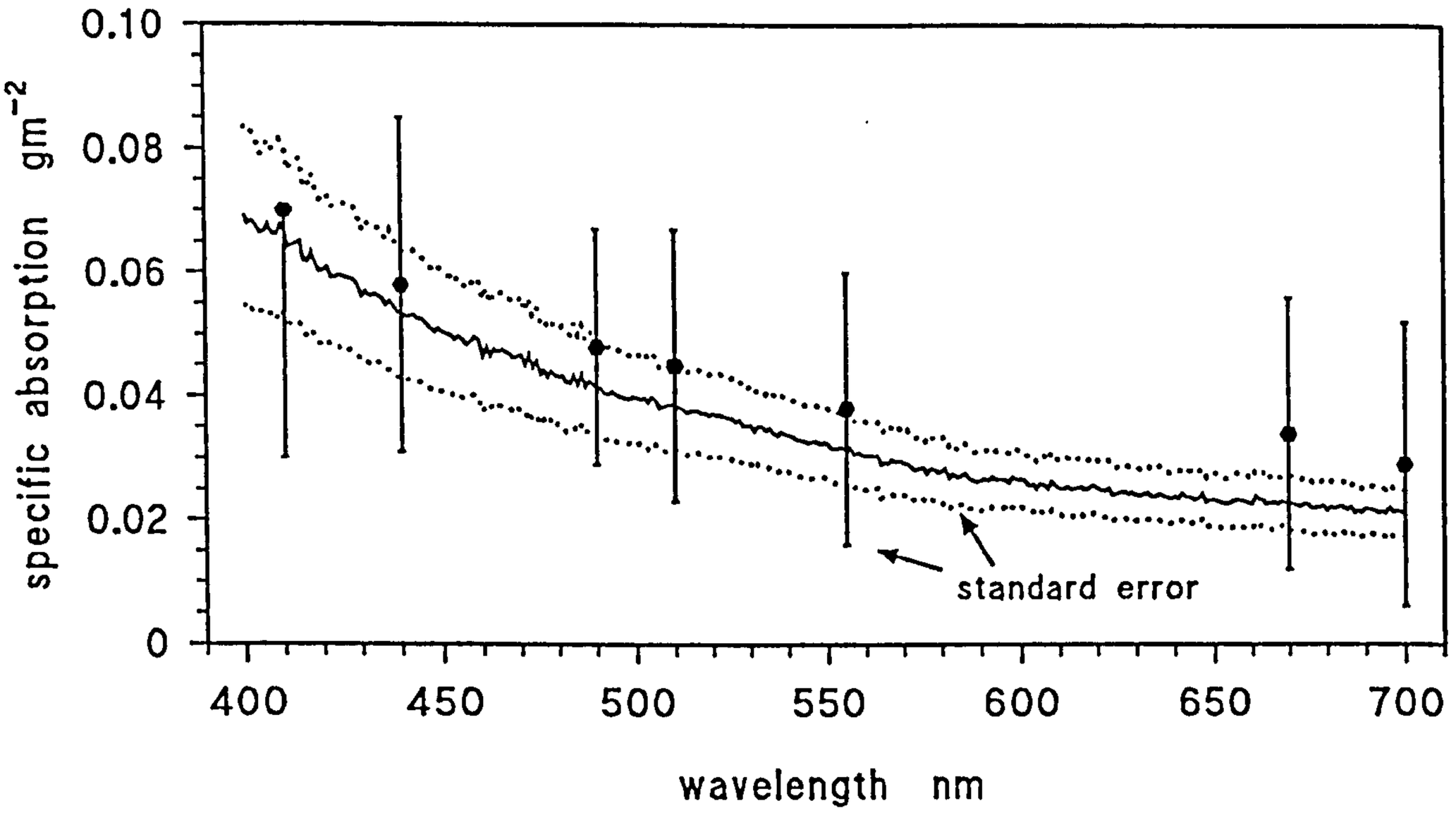
0.10
0.08
0.06
0.04
0.02
0
specific absorption gm^{-2}
400
450
500
550
600
650
700
wavelength nm
standard error

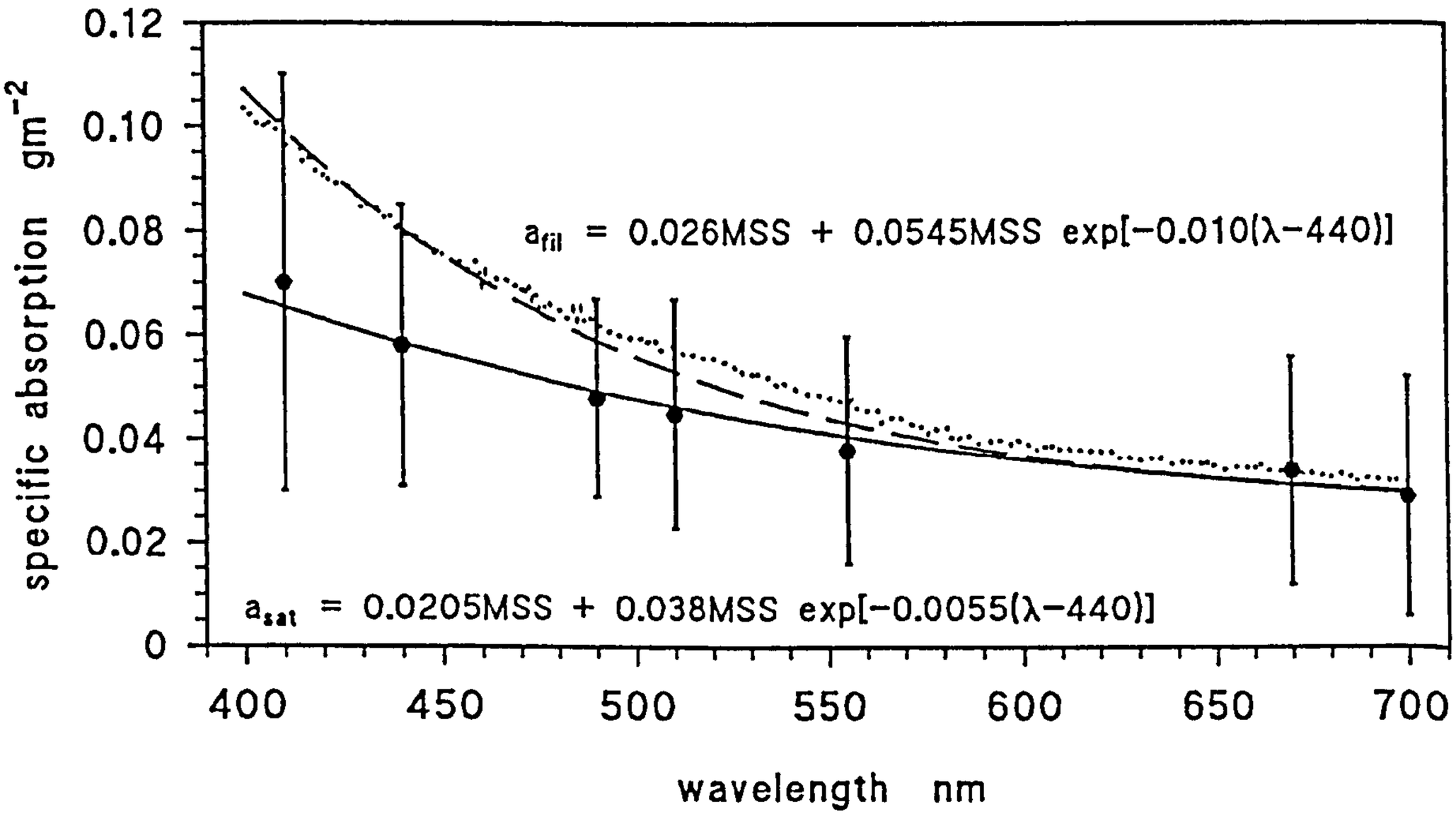
0.12
0.10
0.08
0.06
0.04
0.02
0
specific absorption gm^{-2}
a_{fil} = 0.026MSS + 0.0545MSS exp[−0.010(λ−440)]
a_{sat} = 0.0205MSS + 0.038MSS exp[−0.0055(λ−440)]
400
450
500
550
600
650
700
wavelength nm

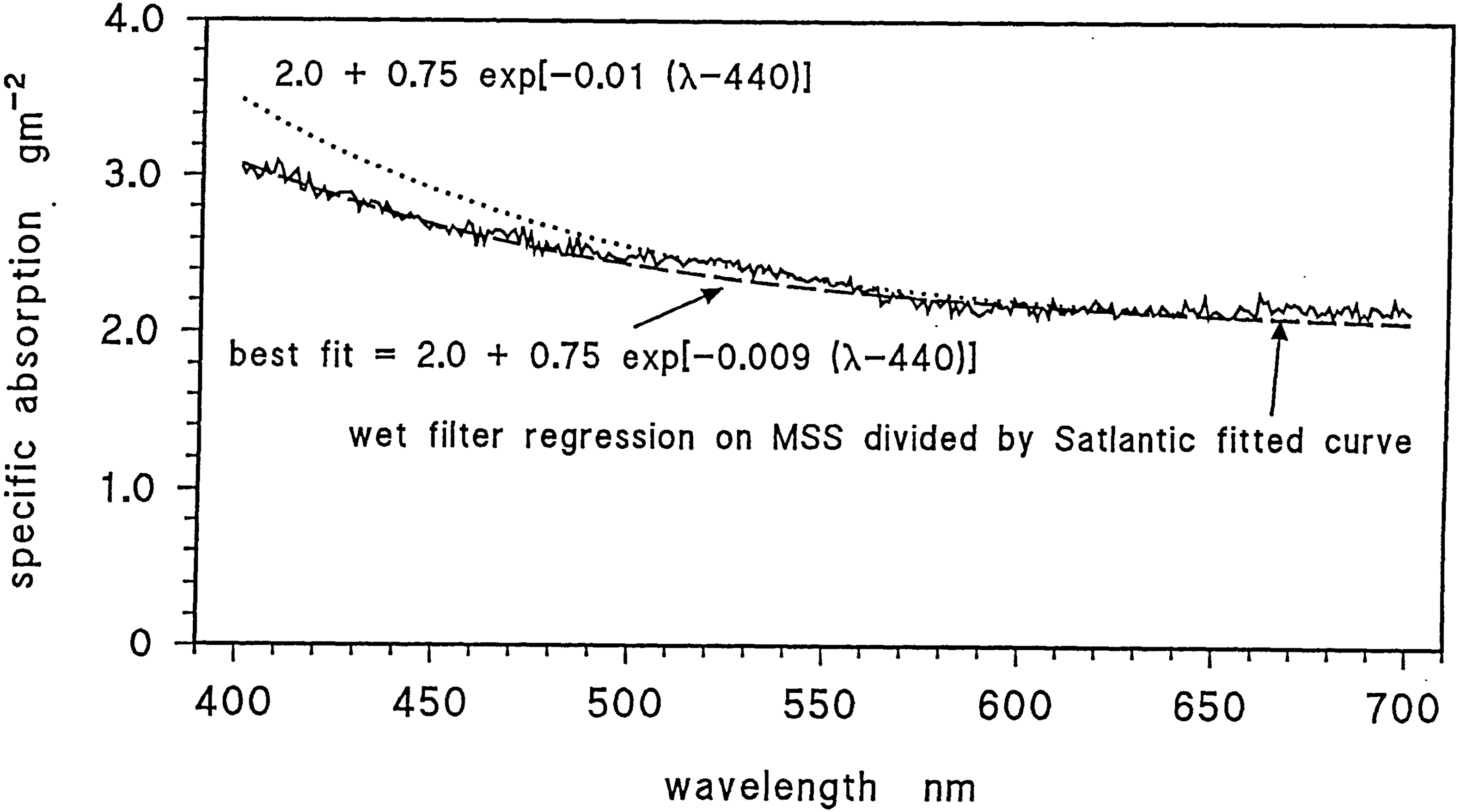

Figure 8.15 Ratio between regressed spectrum from fresh filters and Satlantic derived curve for inorganic matter

8.16 Comparison between total absorption calculated in the laboratory and in situ where filter spectra are corrected as Cleveland & Weidemann (1993)

a) Menai Strait Survey: furnaced spectrum + YS + water + Chl concentration multiplied by spectrum derived from JMB94

b) July Pier Survey: fresh filter spectrum + YS + water

c) August Pier Survey: fresh filter spectrum + YS + water

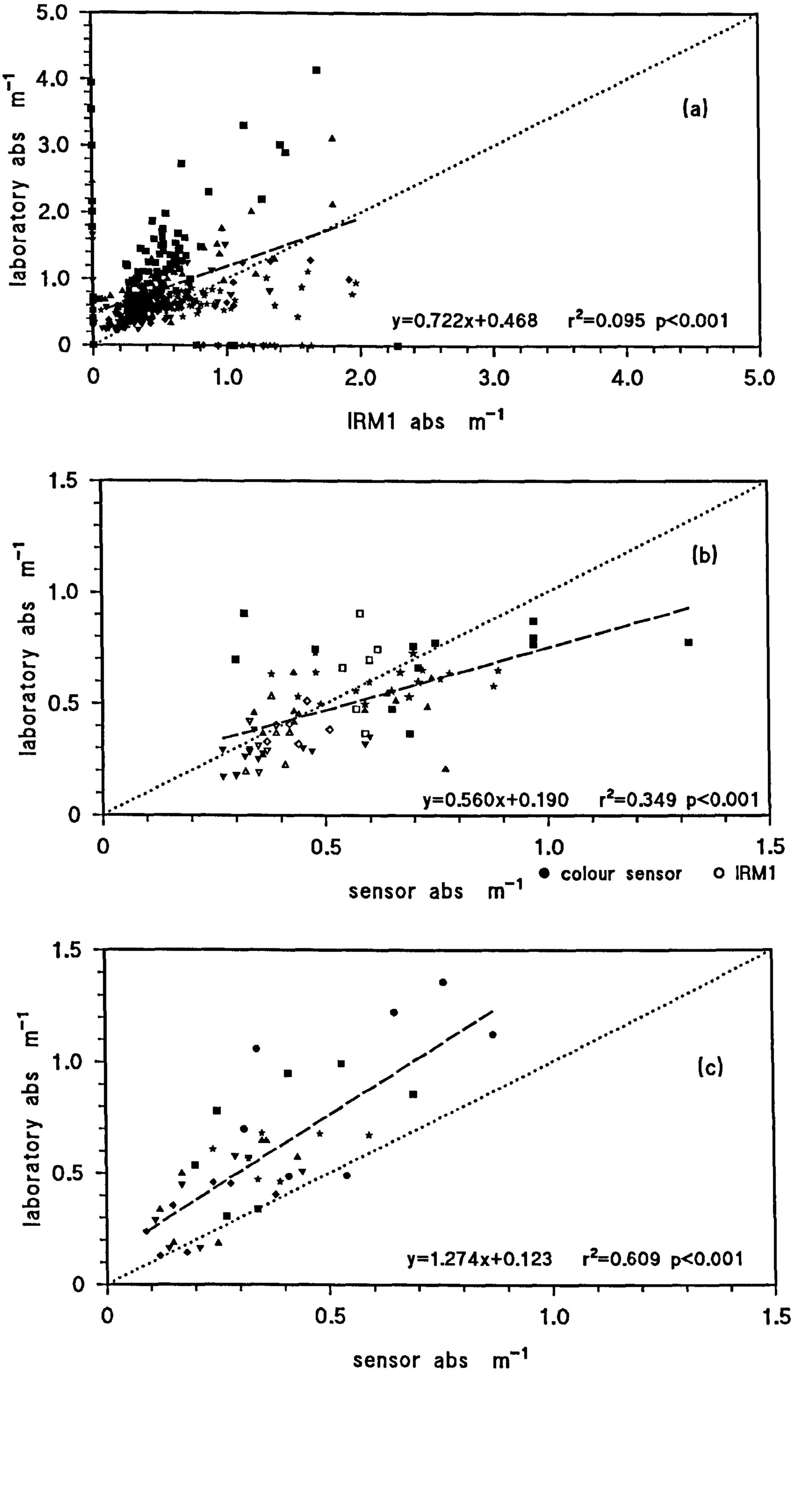
(a)
laboratory abs m⁻¹
IRM1 abs m⁻¹
y=0.722x+0.468 r²=0.095 p<0.001
0
1.0
2.0
3.0
4.0
5.0
(b)
laboratory abs m⁻¹
sensor abs m⁻¹
y=0.560x+0.190 r²=0.349 p<0.001
0
0.5
1.0
1.5
● colour sensor ○ IRM1
(c)
laboratory abs m⁻¹
sensor abs m⁻¹
y=1.274x+0.123 r²=0.609 p<0.001

Figure 8.17 Comparison between total absorption calculated in the laboratory and *in situ* where filter spectra are corrected with $\beta=2$

a) Menai Strait Survey: furnaced spectrum + YS + water + Chl concentration multiplied by spectrum derived from JMB94

b) July Pier Survey: fresh filter spectrum + YS + water

c) August Pier Survey: fresh filter spectrum + YS + water

Values below the theoretical minimum for absorption are excluded from the regression.

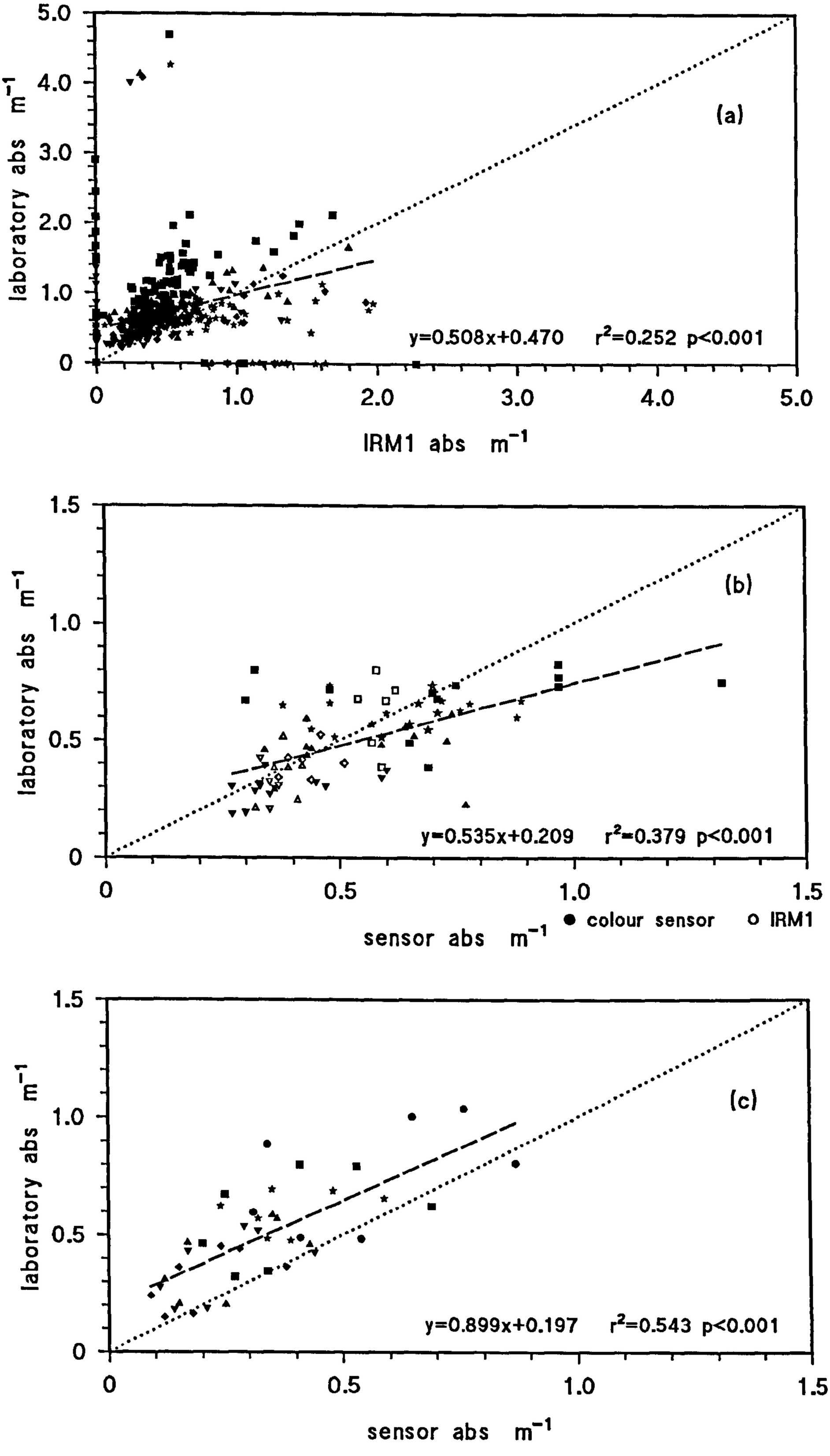
(a)
laboratory abs m⁻¹
IRM1 abs m⁻¹
y=0.508x+0.470 r²=0.252 p<0.001
0
1.0
2.0
3.0
4.0
5.0
(b)
laboratory abs m⁻¹
sensor abs m⁻¹
y=0.535x+0.209 r²=0.379 p<0.001
● colour sensor ○ IRM1
0
0.5
1.0
1.5
(c)
laboratory abs m⁻¹
sensor abs m⁻¹
y=0.899x+0.197 r²=0.543 p<0.001

Figure 8.18 Comparison between total absorption calculated in the laboratory and *in situ* where filter spectra are corrected with $\beta=2+0.75 \exp[-0.009(\lambda-440)]$

a) Menai Strait Survey: furnaced spectrum + YS + water + Chl concentration multiplied by spectrum derived from JMB94

b) July Pier Survey: fresh filter spectrum + YS + water

c) August Pier Survey: fresh filter spectrum + YS + water

Values below the theoretical minimum for absorption are excluded from the regression.

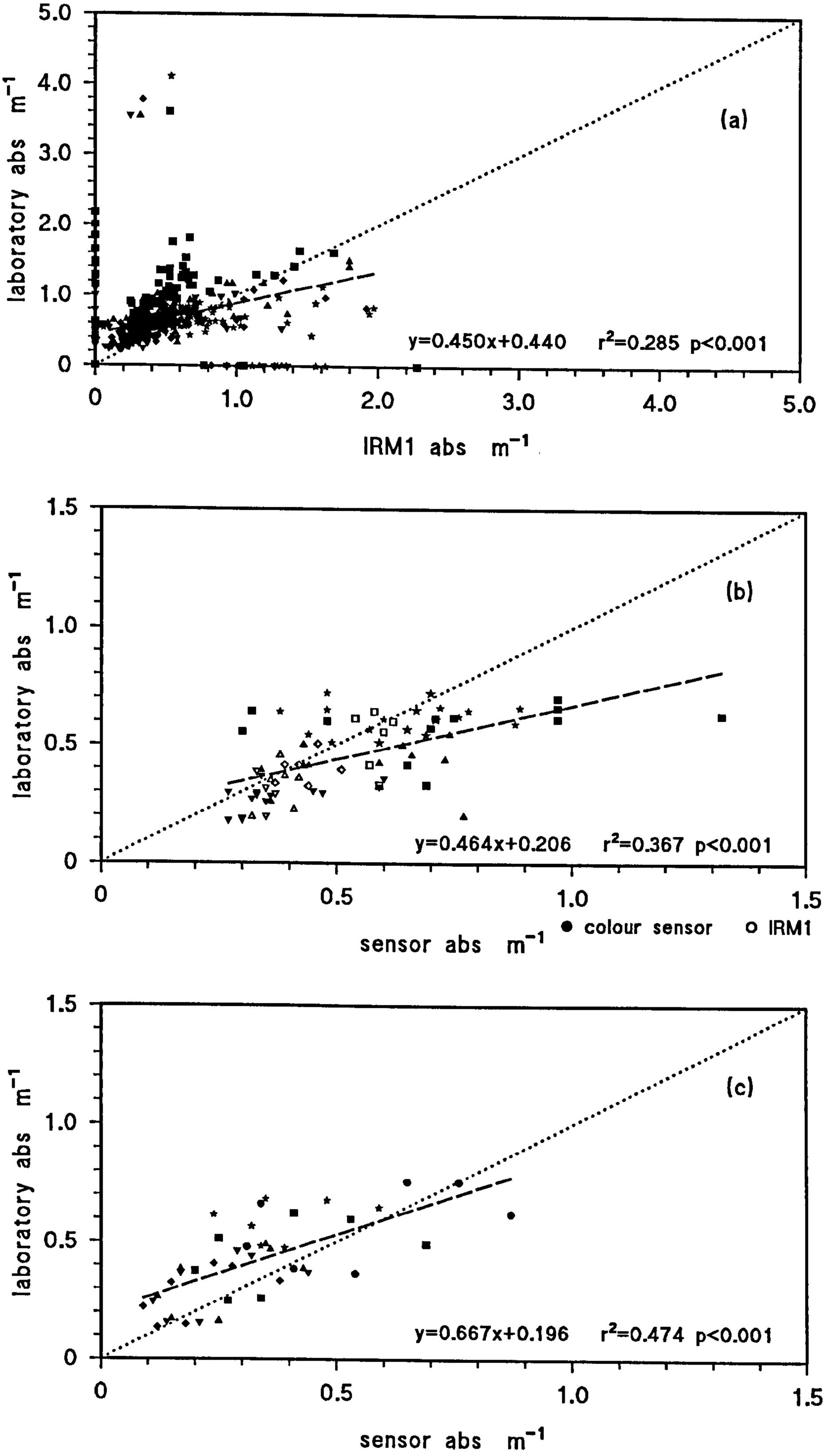
(a)
laboratory abs m⁻¹
IRM1 abs m⁻¹
y=0.450x+0.440 r²=0.285 p<0.001
0
1.0
2.0
3.0
4.0
5.0
(b)
laboratory abs m⁻¹
sensor abs m⁻¹
y=0.464x+0.206 r²=0.367 p<0.001
0
0.5
1.0
1.5
● colour sensor ○ IRM1
(c)
laboratory abs m⁻¹
sensor abs m⁻¹
y=0.667x+0.196 r²=0.474 p<0.001

Figure 8.19 Comparison between total absorption calculated in the laboratory and *in situ* for Clyde 1996 Survey: fresh filters + YS + water
data from surface samples

a) filter spectra corrected as Cleveland & Weidemann (1993)
b) filter spectra corrected with $\beta = 2$
c) filter spectra corrected with $\beta = 2+0.75 \exp[-0.009(\lambda-440)]$

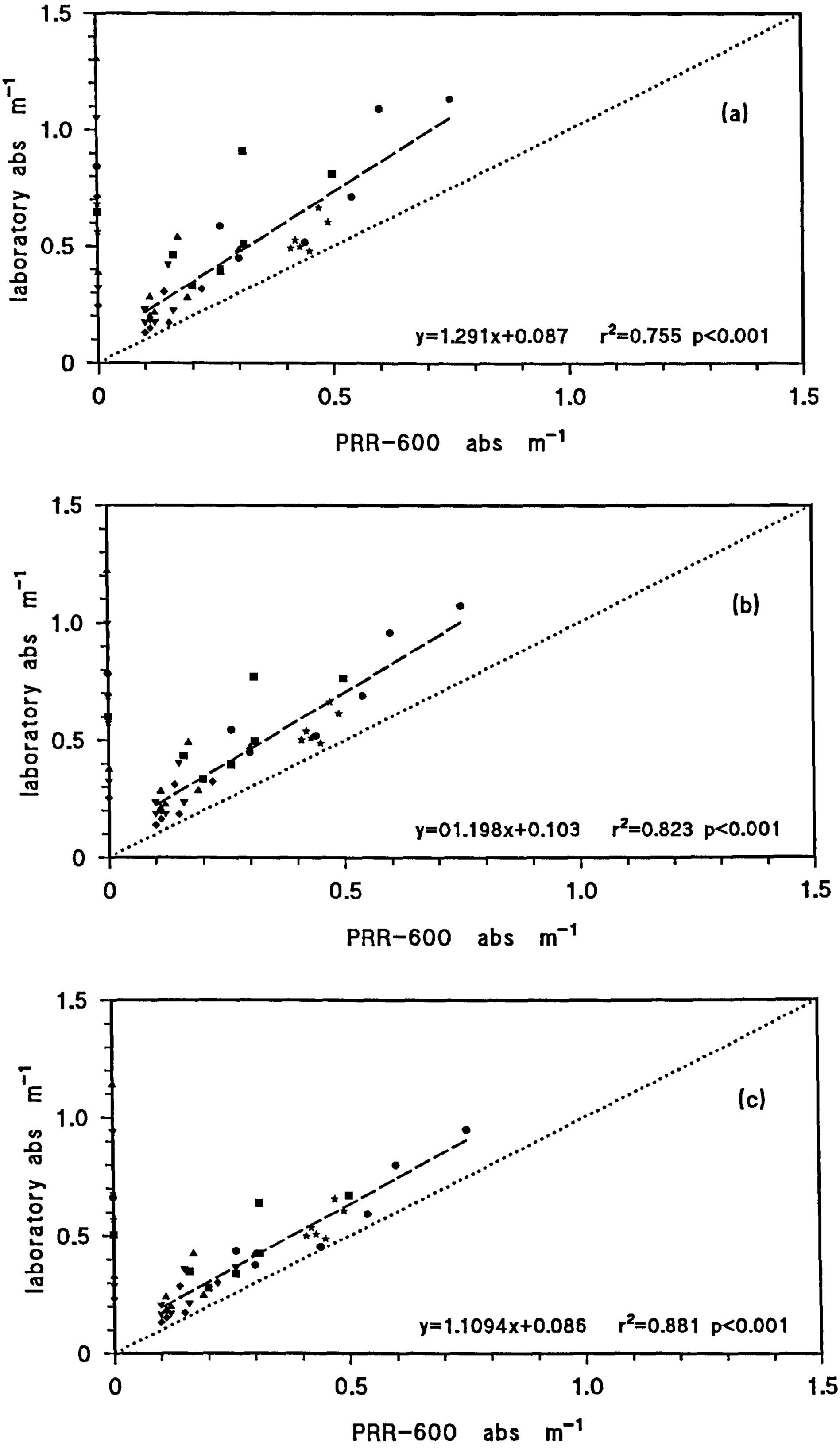
laboratory abs m^{-1}
PRR-600 abs m^{-1}
(a)
y=1.291x+0.087 r^2=0.755 p<0.001
(b)
y=01.198x+0.103 r^2=0.823 p<0.001
(c)
y=1.1094x+0.086 r^2=0.881 p<0.001
0
0.5
1.0
1.5

Figure 8.20 Comparison between total absorption calculated in the laboratory and *in situ* for Clyde 1996 Survey: fresh filters + YS + water
data from mid-euphotic zone samples

a) filter spectra corrected as Cleveland & Weidemann (1993)
b) filter spectra corrected with $\beta = 2$
c) filter spectra corrected with $\beta = 2+0.75 \exp[-0.009(\lambda-440)]$

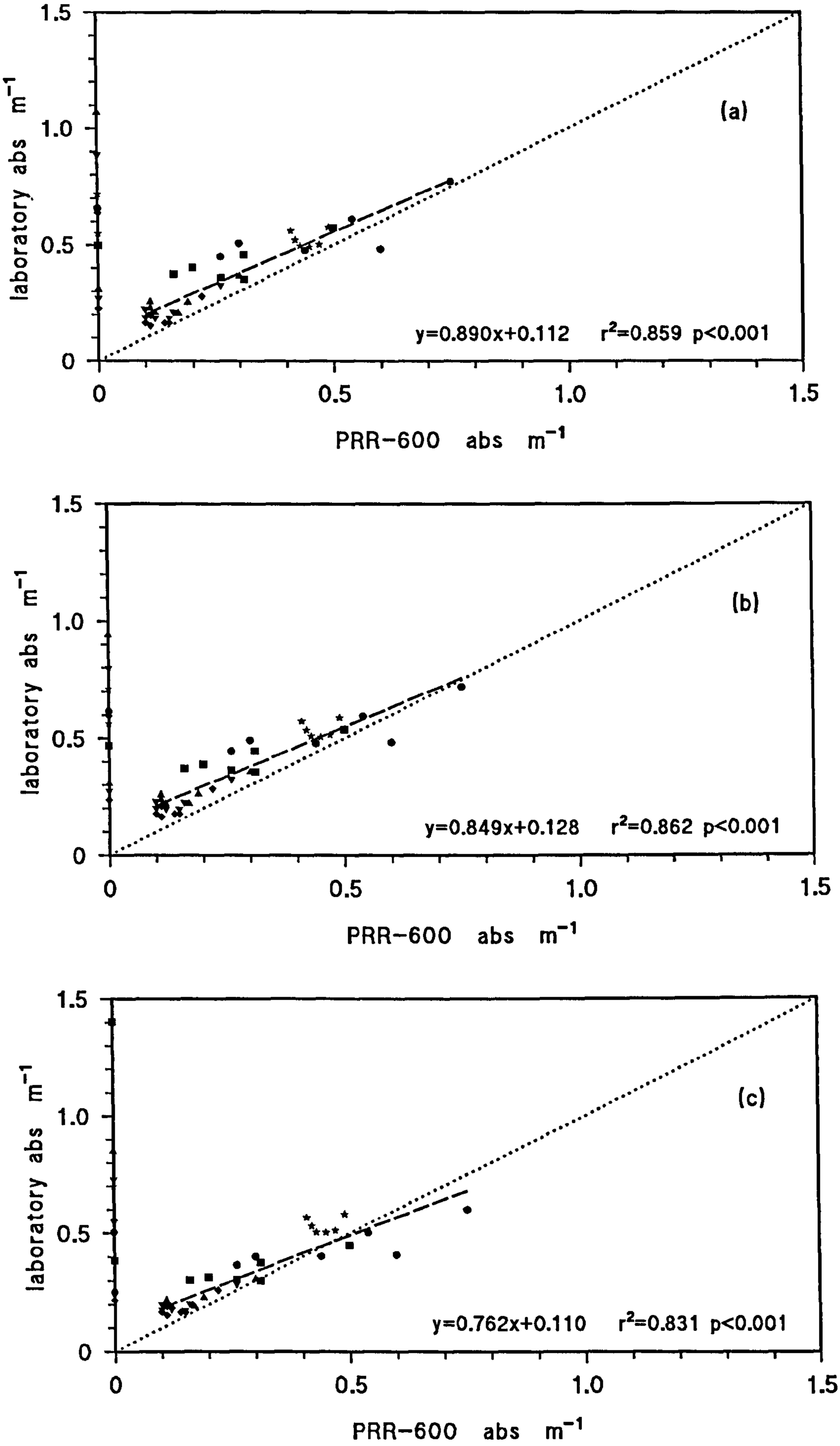
(a)
laboratory abs m^{-1}
PRR-600 abs m^{-1}
y=0.890x+0.112 r^2=0.859 p<0.001
(b)
laboratory abs m^{-1}
PRR-600 abs m^{-1}
y=0.849x+0.128 r^2=0.862 p<0.001
(c)
laboratory abs m^{-1}
PRR-600 abs m^{-1}
y=0.762x+0.110 r^2=0.831 p<0.001
0
0.5
1.0
1.5

Figure 8.21 Average cosine (a/K) calculated for Menai Strait Survey where absorption is total calculated in laboratory

a) filter spectra corrected as Cleveland & Weidemann (1993)

b) filter spectra corrected with $\beta = 2$

c) filter spectra corrected with $\beta = 2+0.75 \exp[-0.009(\lambda-440)]$

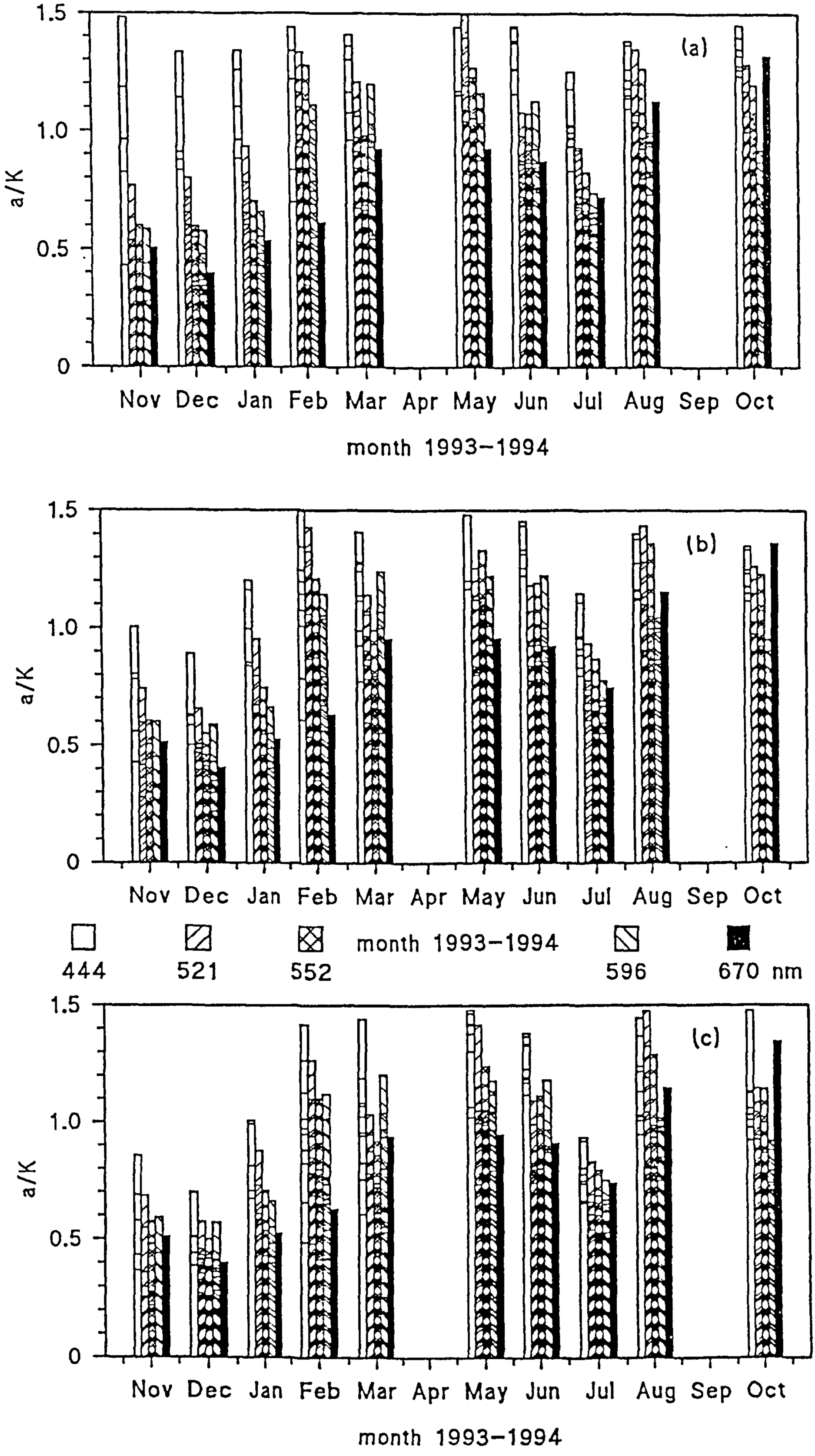
1.5
1.0
0.5
0
a/K
(a)
Nov Dec Jan Feb Mar Apr May Jun Jul Aug Sep Oct
month 1993–1994
(b)
(c)
444
521
552
596
670 nm

9. OCEAN COLOUR MODEL

Using the comparisons from laboratory and field work, a model was developed to predict diffuse attenuation and reflectance from the constituent concentrations. This was achieved by calculating the absorption and scattering for each substance, computing from these the total absorption, scattering and backscattering, and then substituting these values into the Kirk (1994) equations to calculate K_d and R. Initially, the model was based on yellow substance, phytoplankton and mineral particles, as these are the dominant contributors in the Menai Strait, however, detrital particles were subsequently added, so that the model could be applied to other areas.

9.1 CALCULATION OF PROPERTIES

The model requires two input files (pure water and phytoplankton) which cover the visible spectrum. It is possible to change these files to accommodate different phytoplankton curves.

Inputs: files - water absorption and scattering spectrum at 10 nm intervals
- Smith & Baker, 1981
specific chlorophyll absorption at 10 nm intervals,
e.g. Gallegos *et al*, 1990
concentrations of chlorophyll, mineral and detrital suspended solids,
plus the absorption of yellow substance at 440 nm (g440)

9.1.1 Calculation of absorption coefficient:

It is assumed that the absorption terms are additive (Gordon *et al*, 1988):

$$a(\lambda) = a_w(\lambda) + a_y(\lambda) + a_c^*(\lambda)C + a_d(\lambda)OSS + a_m(\lambda)MSS$$

where a is absorption coefficient, λ is wavelength, C is chlorophyll concentration, OSS is the organic detrital concentration and MSS is mineral suspended solids concentration. Subscripts w, c, y, d and m are water, chlorophyll, yellow substance, detritus and minerals respectively.

The absorption curves for water and chlorophyll are contained within the input files, while yellow substance is assumed to follow (as Bricaud *et al*, 1981):

$$a_g(\lambda) = g440 \exp[-0.014(\lambda - 440)]$$

Detrital absorption follows the dried laboratory spectra, having removed the contribution from minerals. This gives an exponential curve:

$$a_d(\lambda) = 0.113\,OSS + 0.012\,OSS \exp[-0.015(\lambda - 440)]$$

Originally, mineral absorption followed the exponential curve from the laboratory. However, when the zeroed exponential spectra were used, the value in the blue was much too high; consequently, the UCNW meter readings, which gave a wavelength independent absorption, were more appropriate. The constant used was derived by regressing the MSS concentrations on the absorption calculated from the meter readings. This gives:

$$a_d = 0.05\ MSS$$

Although this works well with the data from the Menai Strait Survey, other observations did give a slightly higher value in the blue, so that the model was adapted to include an exponential curve plus a uniform baseline for absorption, as derived from non-zeroed laboratory spectra and the Satlantic data:

$$a_m(\lambda) = 0.0205\,MSS + 0.038\,MSS \exp[-0.0055(\lambda - 440)]$$

In both particulate absorption curves, the constants and exponent can be altered to reflect local conditions as required. Thus wavelength independent mineral absorption can be substituted if appropriate.

9.1.2 Calculation of scattering and backscatter coefficients:

Scattering was initially divided into three components - water, chlorophyll and minerals. Values for water are contained in the input file from Smith and Baker (1982). Chlorophyll scattering followed Morel (1988):

$$b_c = 0.12\ C^{0.63}$$

where b_c is the scattering coefficient for chlorophyll

Mineral scattering was assumed to be dominated by MSS, employing a magnitude constant determined by Prieur & Sathyendranath (1981), and a wavelength dependency from Tassan (1994):

$$b_d(\lambda) = 0.42\ MSS\ (550/\lambda)$$

These three factors were added to give total scattering.

Backscatter was then calculated by multiplying the total scattering coefficient by the backscatter ratio (b_b'). A constant value of 0.019 was used unless the chlorophyll concentration was less than 0.1 mgm^{-3} where a wavelength dependency was introduced (Gordon *et al*, 1988):

$$b_b' = 0.019\ (560/\lambda)$$

However, these relationships were empirically derived from various studies in different conditions, and were therefore deemed inflexible. Consequently, the scattering curves were then changed - Anomalous Diffraction Theory (Kirk, 1994) was used to calculate b for the phytoplankton, detrital and mineral particles. This is an approximation to Mie Theory, and requires the density, refractive index and size of the particles. These parameters can all be interactively changed to local parameters, or default settings used if the nature of the particles is unknown.

The default values are based on values from the literature to give 'typical' characteristics of the particles. Thus, for phytoplankton the radius is 0.25 μm, the density is 1.1 gcm^{-3}, and the refractive index 1.05 (Boney, 1975); for detrital particles, the radius is 2.5 μm, the density is 1.2 gcm^{-3}, and the refractive index 1.1; while for minerals, the radius is 1.5 μm, the density is 2.2 gcm^{-3}, and the refractive index 1.2. Table 9.1 shows the refractive index for different minerals.

mineral	index in air	index in water
Kaolinite	1.56-1.60	1.17-1.20
Montmarillonite	1.50-1.53	1.13-1.15
Illite	1.57-1.61	1.18-1.21
Quartz	1.54	1.16
Feldspar	1.54	1.16
Calcite	1.66	1.25

Table 9.1 Refractive indices for different minerals

The effect of using different radii is shown in Fig. 9.1. This figure illustrates the variation due to changes in the radius of mineral particles, while detrital particle, phytoplankton and yellow substance concentrations remain constant. This indicates the model's sensitivity to variation within the natural environment, as the radii observed will cover a wide range whereas only one value is used in the model. This will add significant error in the calculation of scatter due to the efficiency of the different particle sizes (Baker & Lavelle, 1984) as can be seen in the range of curves given in the figure. The variation due to radius is similar in the blue, green and red wavelengths, spanning a K_d range of approximately 4 m^{-1} when MSS=50 mgl^{-1}. However, the combined effect with PAR increases the range of error, with a variation of 7.5 m^{-1} caused at a concentration of 50 mgl^{-1}. The parameters of density and refractive index will also change, but these changes will be more marked between sites, or periods, where the nature of the particles changes, whereas size variation will be present at all times.

As well as altering the calculation of *b*, the backscatter ratios were changed, so that each constituent is treated individually. Hence, 0.019 is still used for minerals, while 0.5 is used for water, 0.005 is used for phytoplankton and 0.01 is used for organic detritus. These values allow for the variation in the refractive index between the particles, and their absorption properties; they may all be changed by the user. Backscattering is then considered additive to give the total value.

9.1.3 Reflection and Attenuation

The above coefficients may then be entered into equations suggested by Kirk (1981) to calculate *R* and *Kd*:

$$R(\lambda) = (0.975 - 0.629\mu_0)\frac{b_b(\lambda)}{a(\lambda)}$$

$$Kd(\lambda) = \frac{a(\lambda)}{\mu_0}[1 + (0.425\mu_0 - 0.19)\frac{b_b(\lambda)}{a(\lambda)}]^{1/2}$$

where μ_0 is the average cosine

Although the average cosine is given a default value of 0.85, it can be changed to describe the specific light field more closely.

Alternatively, the basic reflectance equation can be used:

$$R(\lambda) = 0.33\frac{b_b(\lambda)}{a(\lambda)}$$

9.2 MODEL MODES

The model is designed to be used for three main purposes:

i) to observe how the attenuation and reflectance change as the constituent concentrations change

ii) to give attenuation and reflectance curves for known concentrations

iii) to show and output to a file the predicted attenuation and reflectance values for a large dataset of concentrations

Therefore the model has three "modes" of operation.

The first screen asks the user whether they want to change the settings for calculating the optical characteristics. If yes, the model shows the names of the files used to input the chlorophyll and water values, plus the various equations used in the model, listing the constants within these, and the default values. These can then be

interactively changed. After these, the equations for reflectance and attenuation are shown, with an option to choose either the basic reflectance equation or that from Kirk (1994). Finally, the settings for the axes of the screen graphs are given and can be changed for unusually clear or turbid waters.

Once set, another menu is given, to choose the "mode" required.

Mode 1

Each constituent can be chosen to increase or decrease by a set amount so that the reflectance curves can be seen as a constituent concentration changes. This can occur while the other constituents remain at zero, or at higher values.

Mode 2

A particular value is input for each constituent, so that a combination of concentrations can be observed. This is designed to study cases of specific interest. The results can be printed to five files. The user inputs the stem of the filename, and extensions are added: .abs, .sct, .bma, .att and .ref.

Mode 3

An input file is required with the constituent concentrations; this should have header line for general information, then the number of sites on the next line. Subsequent lines should have the MSS, OSS, Chl and g440 concentrations separated by spaces. The optical properties are printed to five files (if wanted), all of which contain the concentrations, and then:

colout.abs	- total absorption
colout.sct	- total scattering
colout.att	- diffuse attenuation
colout.ref	- reflectance as %
colout.bma	- beam attenuation

The output data can be printed at 10 nm intervals, or at ten wavelengths:

410 440 490 510 520 550 570 600 670 700

which cover most optical sensor wavebands.

9.3 APPLICABILITY OF THE MODEL

To test the model the concentrations from all surveys were used, excluding those where there was doubt about the accuracy of the measurement. The model predictions have not been compared with laboratory measurements, as these were the basis for the model.

Fig. 9.2 shows the comparison between *in situ* derived absorption and the model, using default values. The predictions are close for all wavelengths although there is a tendency to overestimate absorption, and at two points from the Conwy estuary the model predicts very high values due to high concentrations, which are not apparent in the optical observations. The same pattern is observed in the diffuse attenuation values (Fig. 9.3).

The scattering values, although following the same trend have a high degree of error (Fig. 9.4). This error is compounded in the reflectance values (Fig. 9.5), producing a wide region of scatter with an upper limit to the model predictions. This upper limit is governed by the b_b:a ratio for mineral solids. The higher reflectance values are mainly due to mineral solids, so the b_b:a ratio is dominated by the minerals, and thus reflectance, which is proportional to this ratio. Consequently, the model will always reach a limit above which it will not predict, although the value of this will change with the nature of the particles. Such a limit in reflectance has been observed by Curran & Novo (1988), although the measurements in the **Menai Strait** exceed this predicted limit. High reflectance values would be expected in lakes which have very fine, white particles (such as glacial flour, as observed in Lake Tekapo, New Zealand, where the PAR reflectance can exceed 35%, Davies-Colley pers. comm.) where the particles would have a very high scattering coefficient and very low absorbance. Values in the **Menai Strait** would be expected to be much lower than this due to the organic fraction of particles and the type of sediment in the area.

It was only possible to compare beam attenuation predictions for the **Pier Surveys** (Fig. 9.6). The higher values are from **AMB95** while the cluster at lower values is from **JMB94.** The uniformity in the model results shows the effect of increasing

phytoplankton with decreasing minerals so maintaining an approximately constant level of $a+b$ whereas the observations of c mirror the trend in minerals. This suggests that the minerals dominate the attenuation signal in this survey. Once again, the degree of error could be attributed to the variability of the scatter.

The error in the scattering prediction is thought to be due to the use of default values for the particle characteristics, as the particles would change throughout the year and would be a mixture of different types. However, although a particle analysis was undertaken twice to study the particle characteristics (Appendix IX), the instrument was not available for most of the surveys, so that the accuracy of these parameters cannot be improved. The resolution for the size measurements only extended to 2 μm which did not cover the range necessary for the model input. There is a peak of smaller particles below this diameter which sugget that the model estimates of 1.5 μ_0 are realistic. It was originally intended that a parameter for particle size distribution could be incorporated within the model, and so use these measurements further. However, this development was not possible within the time constraints of the work although would be an interesting development for future modifications.

The effect of increasing each constituent separately is shown in Fig. 9.7 a-d. The reflectance of water alone shows the clear blue spectrum expected. An increase in chlorophyll produces a gradual change from blue to green, as is observed in a phytoplankton bloom, while pivoting around the value at 505 nm as previously observed (Bukata *et al*, 1983). The yellow substance decreases the level of reflectance, while the spectrum becomes more uniform; this agrees with observations of lakes with high humic concentrations which appear almost black due to the high absorption. Conversely, the minerals increase the reflectance, particularly in the red which gives the water a bright brown appearance, as observed in the Conwy estuary (Fig. 9.8).

To extend the usefulness of the model to more general ecological studies, the value for PAR diffuse attenuation and reflectance have been added. These can be used for light limit levels, used in plant species studies in freshwater lakes, where the

succession is dependent on the level of PAR reaching the bed (Schwarz, pers.comm.).

A listing of the model is given in Appendix X.

9.4 MODEL INVERSION

The ultimate aim in many such studies is to invert the model in order to estimate the concentrations from the optical signal. The model indicates that reflectance can vary greatly with relatively minor changes in the particle characteristics. It is therefore better to use inherent optical properties which are directly related to the particles, to estimate the concentrations. Scattering can also change greatly with variations in the particulates rather than the concentrations. Thus, the most effective method is to use the absorption. Although variable, in coastal waters with varying concentrations of constituents this is the most consistent optical property.

The use of absorption for an inverse model restricts its applicability to *in situ* observations where absorption can be measured, or calculated. The equation for total absorption has four variables (the concentrations) assuming that the specific absorption coefficients are known. Therefore, with *in situ* measurements at four or more wavelengths the concentrations can be calculated, as the unknowns are overdetermined. The most efficient method of calculation would be through matrices. However, for ease of determination, simultaneous equations can also be used, and are more flexible if the number of channels (or equations) are not known in advance. Consequently, a second program was written to obtain the concentrations from the absorption coefficients, using the specific coefficients given in Table 9.2.

This inversion is limited by the use of the specific absorption values, which may be incorrect for the particular location. However, Fig. 9.9 shows the concentrations of mineral solids extracted from the absorption values for the Menai Strait. Although scattered, the concentrations give an approximation to the conditions within the water.

$a_T = a_w + a_y + a_{ph} + a_m$				
wavelength nm	Water	Yellow Substances	Phytoplankton	Mineral Solids
440	0.0145	1	0.0298	0.0585
520	0.0477	0.326	0.0125	0.0450
550	0.0638	0.214	0.0074	0.0413
600	0.244	0.106	0.0049	0.0363
670	0.430	0.040	0.0159	0.0312

Table 9.2 An example of specific absorption values for each constituent at five wavelengths as used in the model. Sources: water (Smith & Baker 1983), yellow substance (Tassan, 1988), phytoplankton (Gallegos *et al*, 1990) and mineral solids from observations

For an independent test, absorption values from Palmer (1985) were used in the model, giving a better result for the mineral concentrations predicted (Fig. 9.10). However, although these were able to estimate the inorganic concentrations the values for chlorophyll and yellow substance were very inaccurate (Table 9.3), which suggests that only the dominant concentration can be estimated with any confidence.

9.5 SUMMARY

The predictive model uses semi-analytical techniques to predict inherent and apparent optical properties from constituent concentrations. The equations used within this are defined but each constant can be changed as appropriate to any particular location. When using the default values derived from observations in the Menai Strait, it seems possible to predict absorption and diffuse attenuation closely, but the error involved in the scatter predictions becomes more marked in the reflectance signal giving a poor fit for both these parameters.

Observations			Predictions		
M.S.S. mgl^{-1}	Y.S. g440 m^{-1}	Chl mgm^{-3}	M.S.S. mgl^{-1}	Y.S. m^{-1}	Chl mgm^{-3}
4.69	0.012	-	3.15	0.13	9.24
3.57	0.010	-	5.57	0.05	6.76
3.91	0.011	-	7.19	0.05	4.02
7.92	0.021	2.59	7.64	0.24	-5.19
8.48	0.008	3.74	4.02	0.15	3.31
8.38	0.012	3.18	4.68	-0.18	15.02
4.15	0.011	2.06	3.24	0.09	5.20
-	0.010	2.99	4.41	0.13	3.43
-	0.018	3.55	4.35	0.11	5.14
7.05	0.018	4.30	6.99	-0.01	6.27
6.20	0.016	3.55	9.17	-0.04	7.57
12.96	0.019	3.55	14.00	0.08	-0.16
13.51	0.019	3.55	10.93	0.46	-8.53
14.39	0.019	4.49	12.27	0.09	5.04
12.48	0.019	4.30	14.29	0.02	2.97
5.92	0.027	3.74	6.65	0.15	3.44
6.97	0.027	4.11	6.74	0.15	6.33
13.28	0.023	5.05	13.73	0.13	2.24
8.60	0.020	3.55	10.91	-0.02	6.38
12.01	0.019	4.30	12.49	0.05	2.44
9.03	0.019	-	9.23	0.14	1.98
5.20	0.020	2.62	3.59	0.19	0.87
4.95	0.020	2.24	3.10	0.15	2.64
3.67	0.022	2.24	5.03	-0.08	7.18
3.57	0.021	4.86	3.49	0.06	7.22
4.33	0.022	4.49	1.37	0.39	0.55
20.51	0.024	6.54	23.30	-0.12	9.25
39.65	0.021	7.85	41.10	-0.08	-3.52
24.14	0.022	5.42	29.01	-0.26	7.58

Table 9.4 Results from inversion program: Menai Strait observations, Palmer (1985)

Figure 9.1 Diffuse attenuation calculated by the model for different radii of inorganic particles

a) 440 nm
b) 550 nm
c) 670 nm
d) PAR

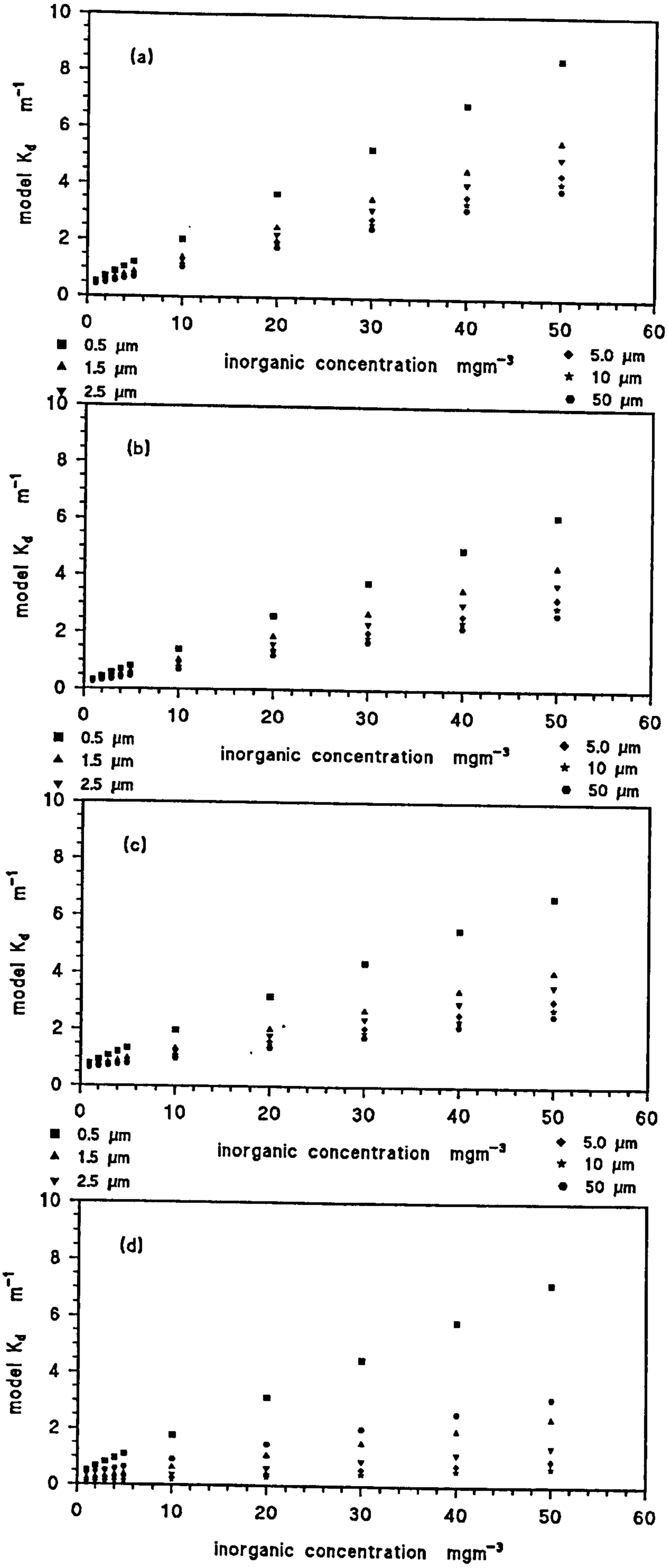
(a)
(b)
(c)
(d)
model K_d m^{-1}
inorganic concentration mgm^{-3}
0
10
20
30
40
50
60
0
2
4
6
8
10
0.5 µm
1.5 µm
2.5 µm
5.0 µm
10 µm
50 µm

Figure 9.2 Model absorption compared with observed absorption for all surveys
a) 440 nm
b) 490-520 nm
c) 550-570 nm
d) 670 nm

Anomalous values and those below the theoretical minimum are excluded from the regression.

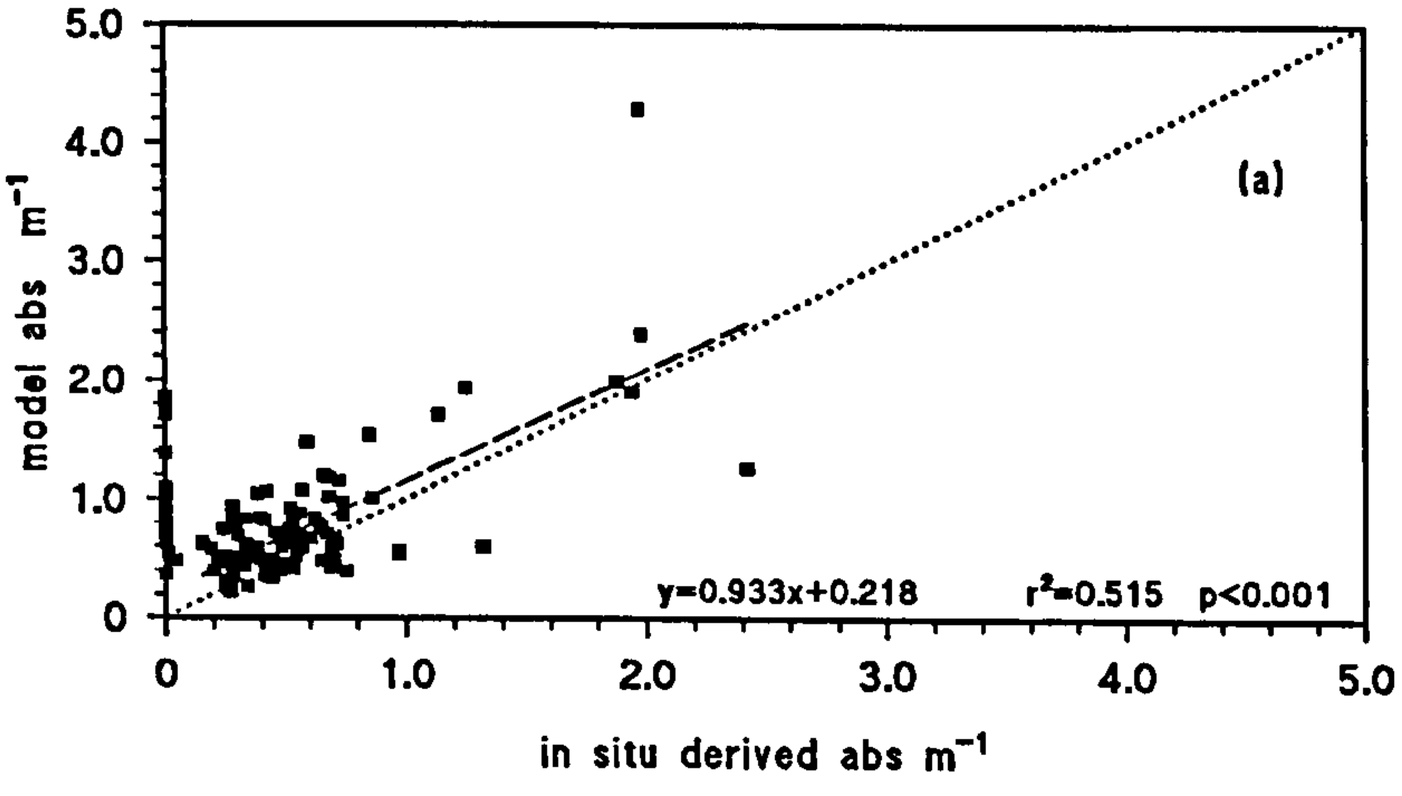
model abs m^{-1}
in situ derived abs m^{-1}
(a)
y=0.933x+0.218 r^2=0.515 p<0.001
490 nm y=0.810x+0.046 r^2=0.557 p<0.001
510 nm y=1.153x+0.060 r^2=0.886 p<0.001
520 nm y=0.758x+0.188 r^2=0.689 p<0.001
(b)
550 nm y=0.737x+0.152 r^2=0.723 p<0.001
570 nm y=−0.268x+0.326 r^2=0.387 p=0.01
(c)
(d)
y=0.559x+0.308 r^2=0.606 p<0.001

Figure 9.3 Model diffuse attenuation compared with observed attenuation for all surveys

a) 440 nm
b) 490-520 nm
c) 550-570 nm
d) 670 nm

Anomalous values and those below the theoretical minimum are excluded from the regression.

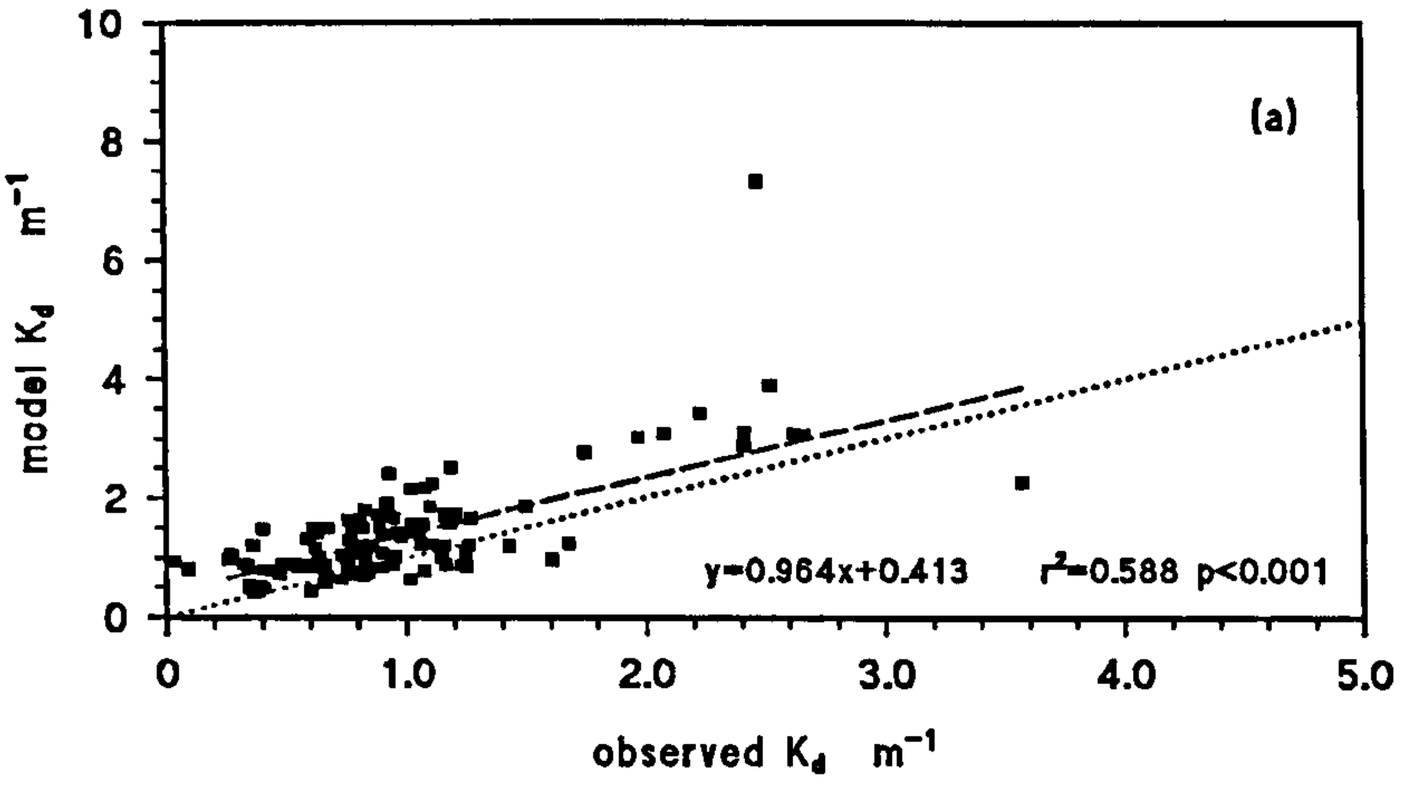
model K_d m^{-1}
observed K_d m^{-1}
(a)
y=0.964x+0.413 r^2=0.588 p<0.001

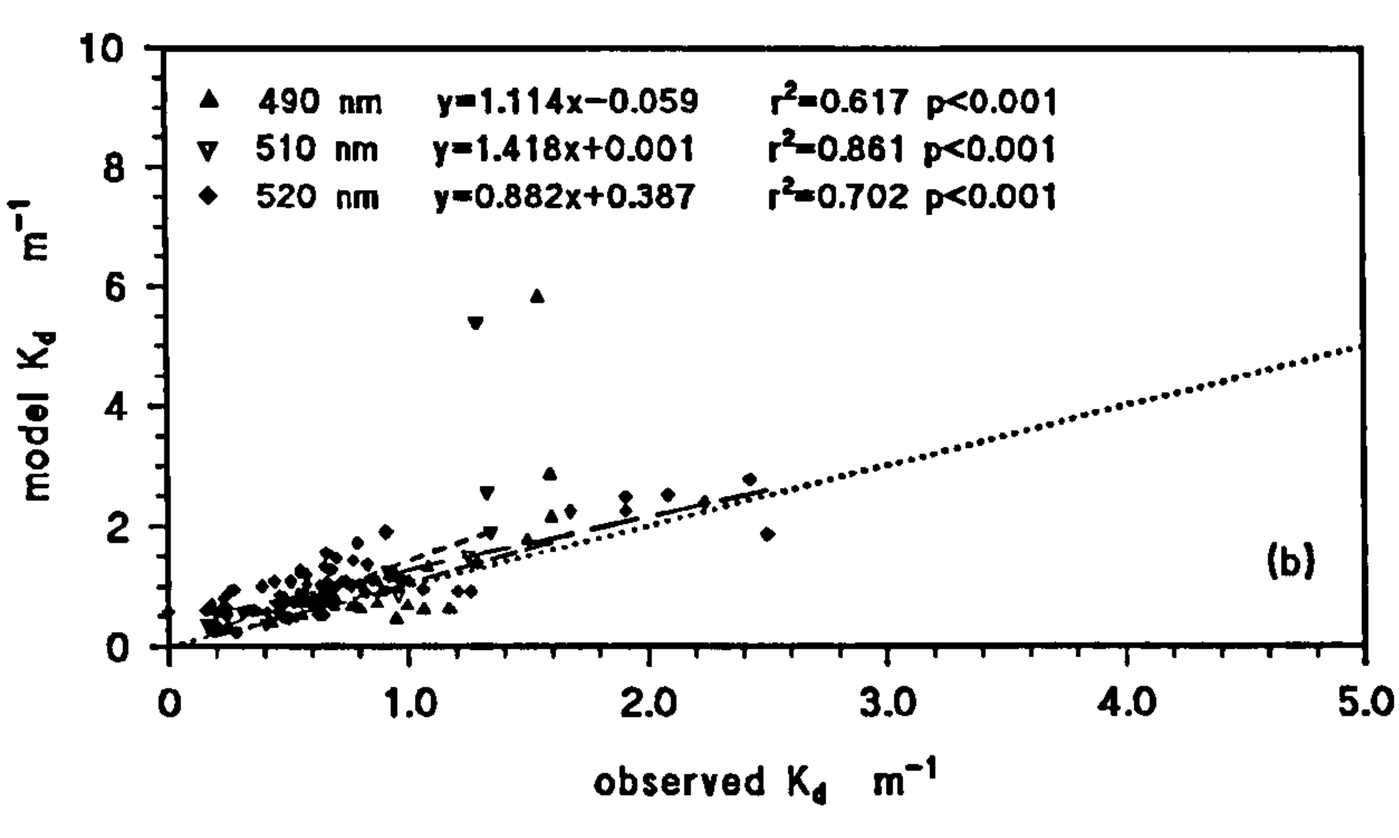
model K_d m^{-1}
observed K_d m^{-1}
490 nm y=1.114x−0.059 r^2=0.617 p<0.001
510 nm y=1.418x+0.001 r^2=0.861 p<0.001
520 nm y=0.882x+0.387 r^2=0.702 p<0.001
(b)

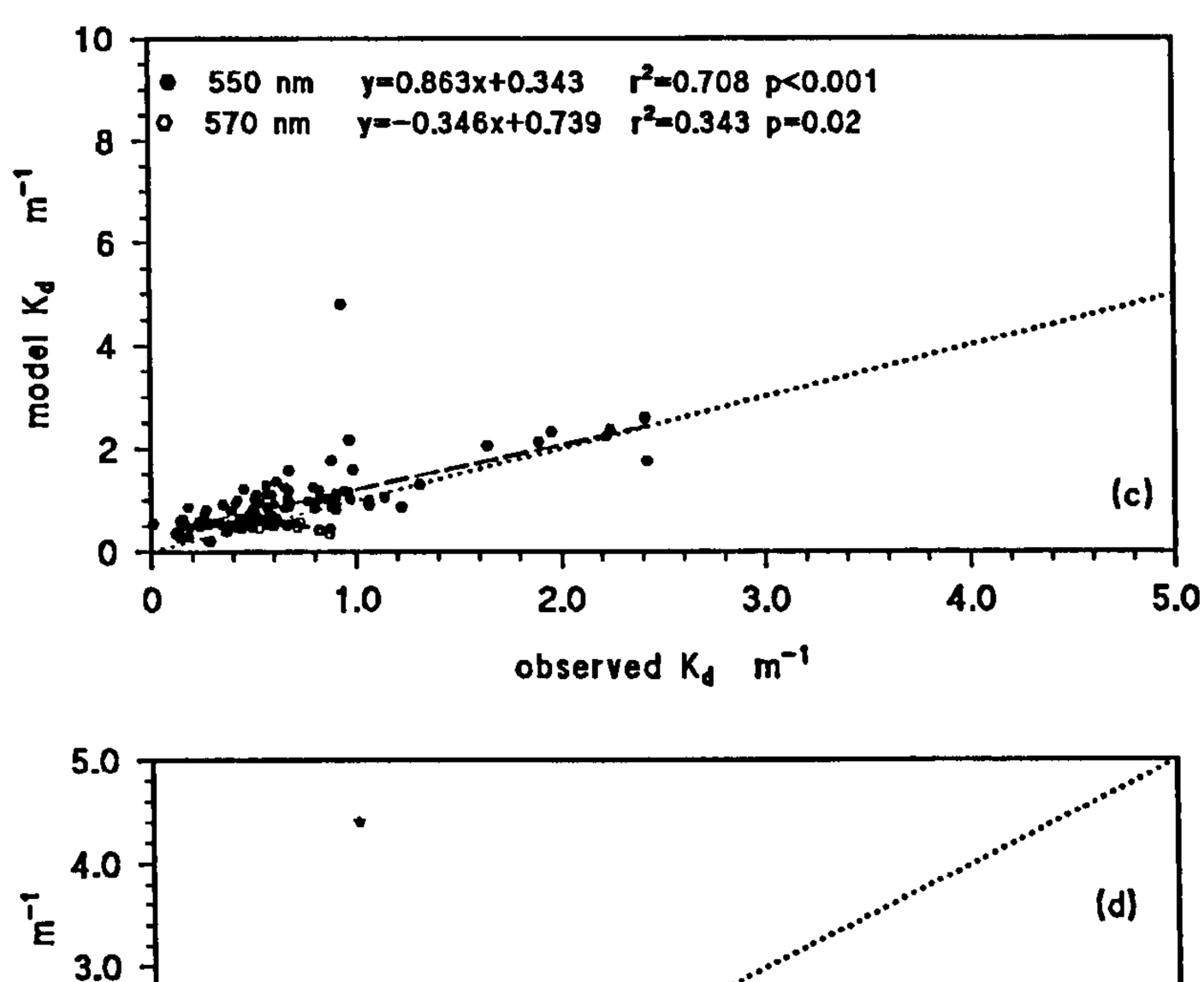
model K_d m^{-1}
observed K_d m^{-1}
550 nm y=0.863x+0.343 r^2=0.708 p<0.001
570 nm y=−0.346x+0.739 r^2=0.343 p=0.02
(c)

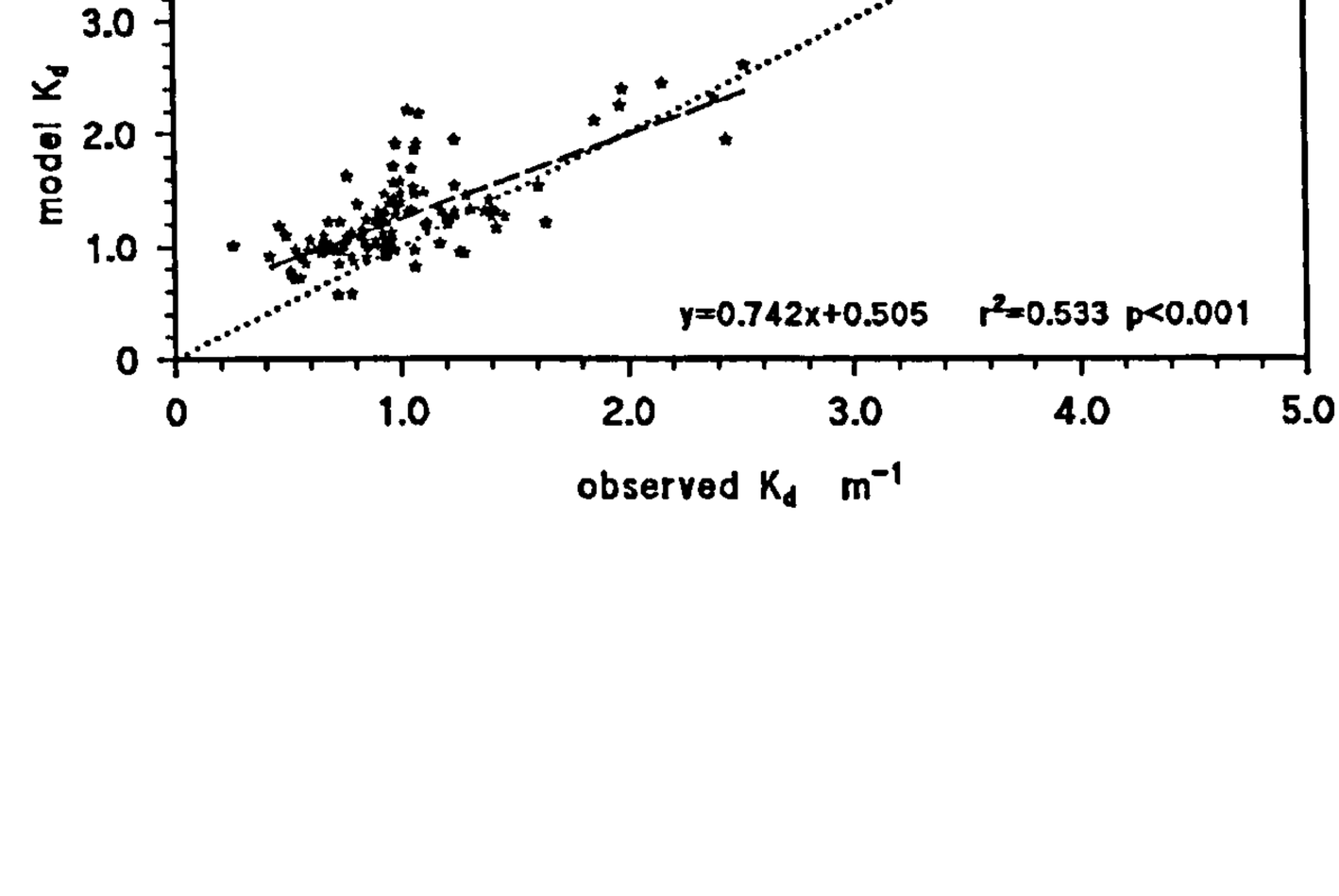
model K_d m^{-1}
observed K_d m^{-1}
(d)
y=0.742x+0.505 r^2=0.533 p<0.001

Figure 9.4 Model scatter compared with observed scatter for all surveys
a) 440 nm
b) 490-520 nm
c) 550-570 nm
d) 670 nm

Anomalous values and those below the theoretical minimum are excluded from the regression.

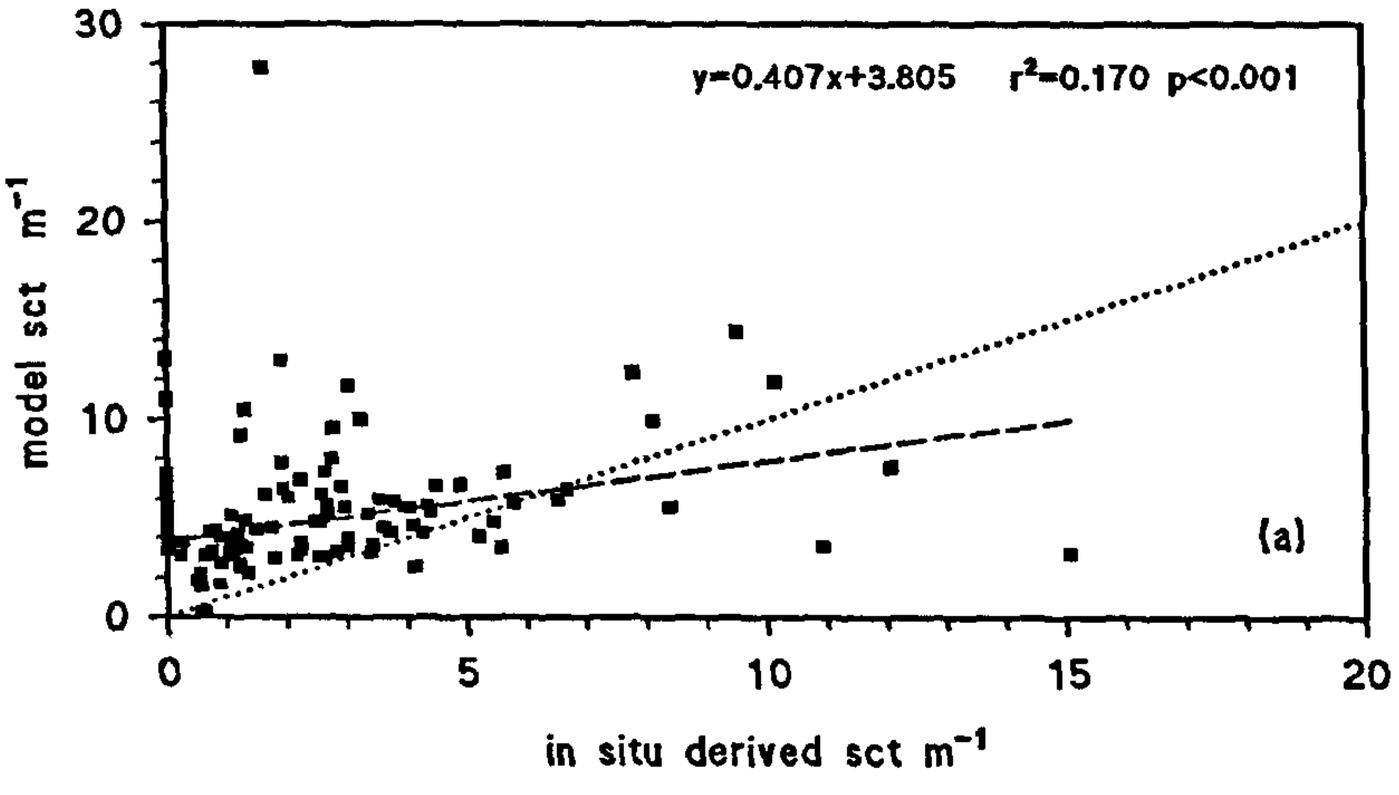
y=0.407x+3.805 r²=0.170 p<0.001
(a)
model sct m⁻¹
in situ derived sct m⁻¹
▲ 490 nm y=0.435x+2.700 r²=0.195 p=0.01
▽ 510 nm y=0.626x+2.785 r²=0.261 p=0.05
◆ 520 nm y=0.893x+3.307 r²=0.489 p<0.001
(b)
● 550 nm y=0.790x+3.464 r²=0.405 p<0.001
○ 570 nm y=−0.056x+3.842 r²=0.037 p=0.49
(c)
y=0.448x+4.663 r²=0.15 p=0.001
(d)

Figure 9.5 Model reflectance compared with observed reflectance for all surveys
a) 440 nm
b) 490-520 nm
c) 550-570 nm
d) 670 nm

Anomalous values and those below the theoretical minimum are excluded from the regression.

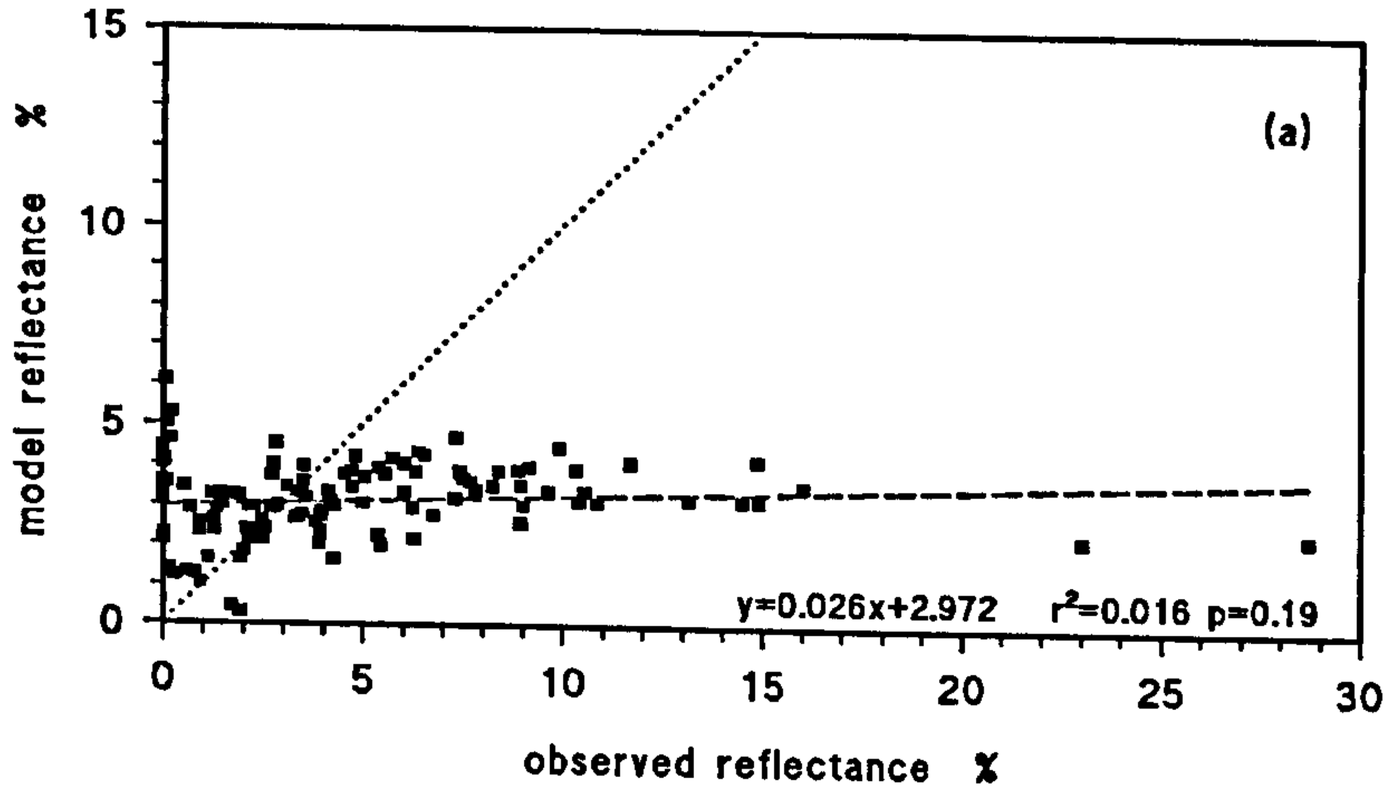
model reflectance %
observed reflectance %
(a)
y=0.026x+2.972 r²=0.016 p=0.19
▲ 490 nm y=−0.074x+4.105 r²=0.028 p=0.39
▽ 510 nm y=−0.987x+6.702 r²=0.749 p<0.001
◆ 520 nm y=0.051x+5.109 r²=0.056 p=0.03
(b)
● 550 nm y=0.070x+5.636 r²=0.069 p=0.01
○ 570 nm y=0.094x+4.803 r²=0.194 p=0.10
(c)
y=0.122x+2.918 r²=0.075 p=0.005
(d)

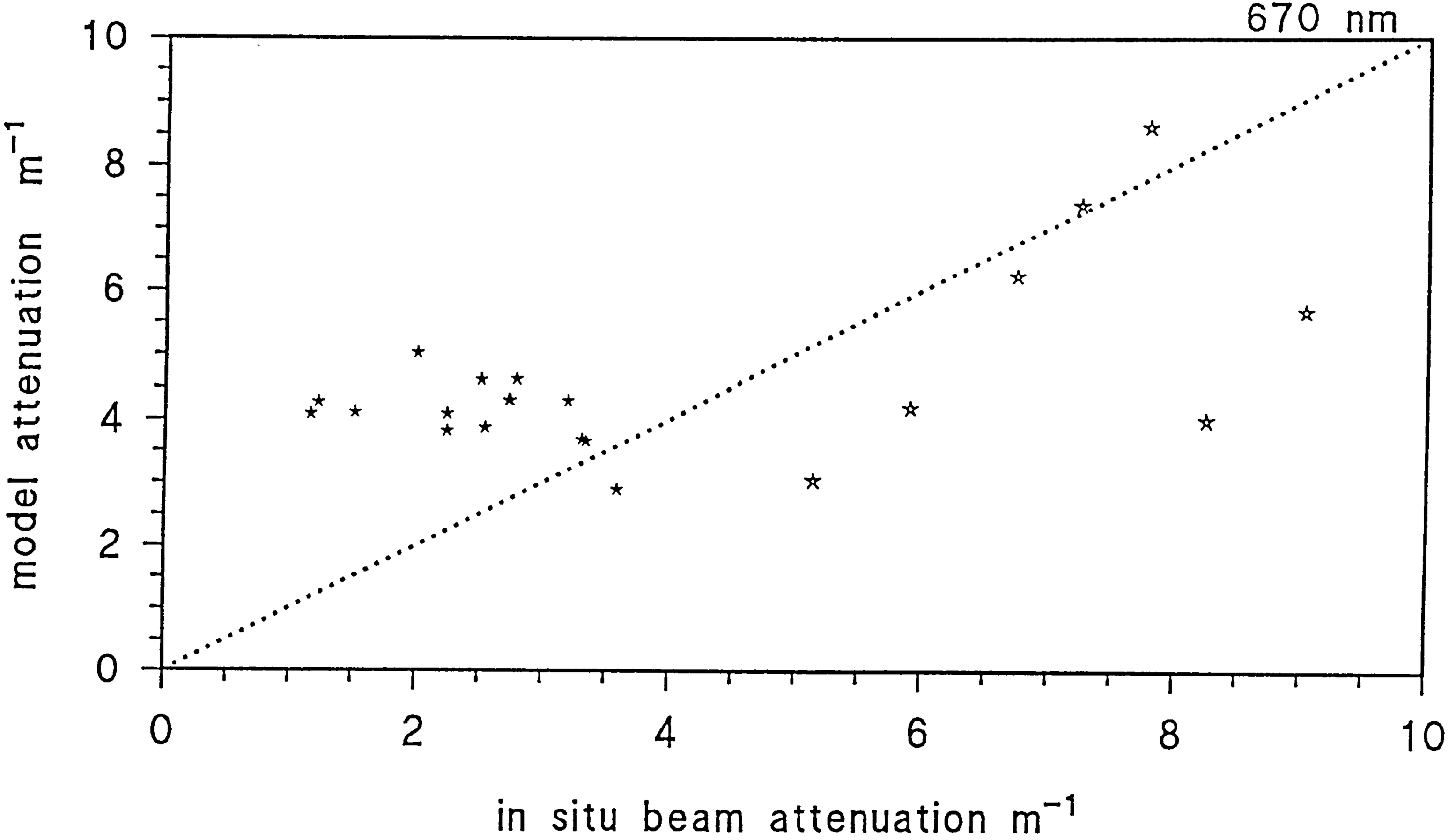

Figure 9.6 Model beam attenuation compared with the sum of observed absorption and scatter for the Pier Surveys

Figure 9.7 Model reflectance for different constituents

a) pure water
b) increasing chlorophyll concentration
c) increasing yellow substance
d) increasing inorganic particle concentration

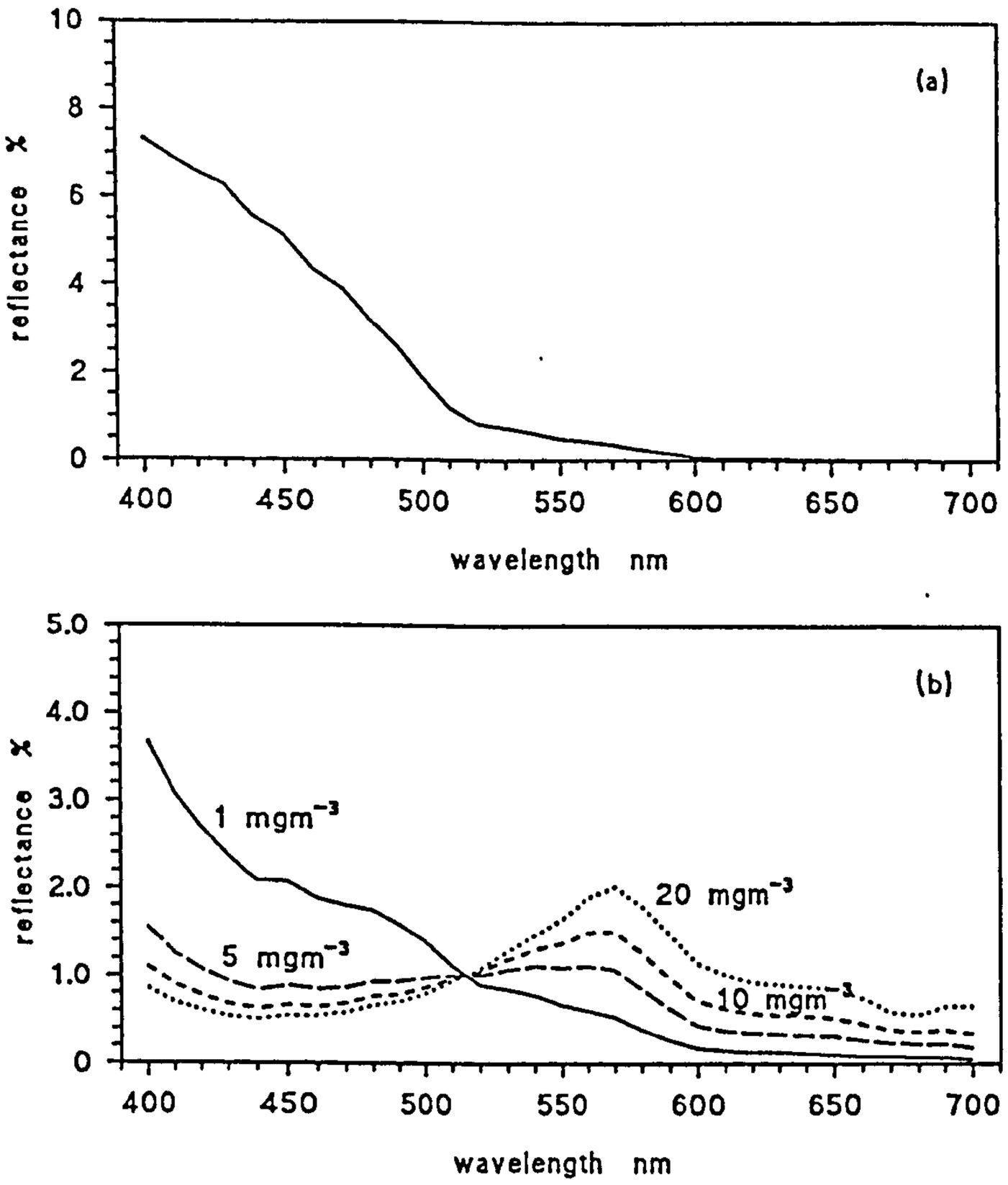
(a)
reflectance %
wavelength nm
(b)
1 mgm⁻³
5 mgm⁻³
20 mgm⁻³
10 mgm⁻³
(c)
0.2 m⁻¹
0.5 m⁻¹
1.0 m⁻¹
2.0 m⁻¹
(d)
50 mgl⁻¹
20 mgl⁻¹
10 mgl⁻¹
1 mgl⁻¹

Figure 9.8 Conwy estuary at Dolgarrog

Figure 9.9 Inversion model compared with measurements of mineral substances in the Menai Strait Survey

Figure 9.10 Inversion model compared with measurements of mineral substances in a Menai Strait Survey by Palmer 1985

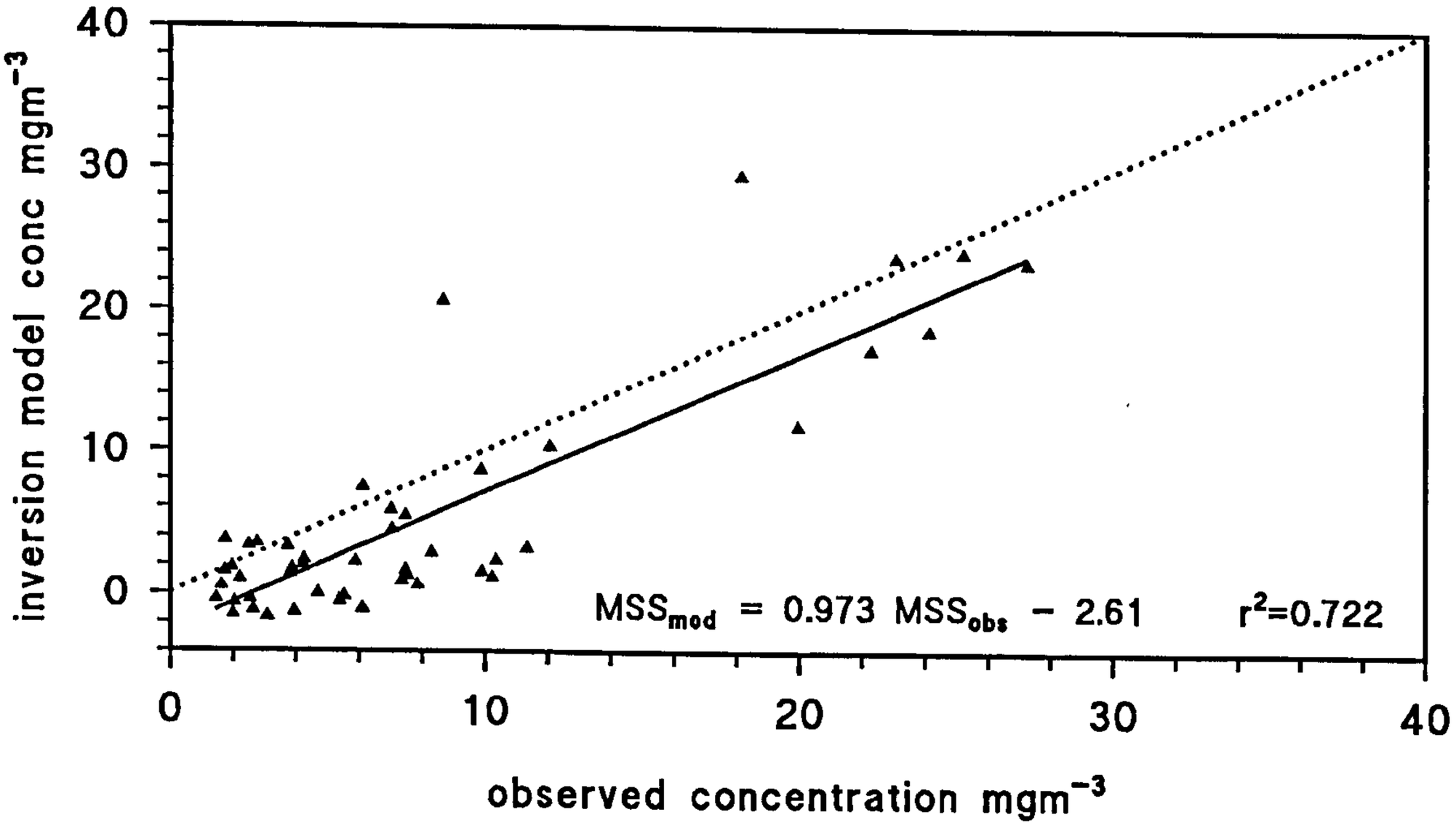
40
30
20
10
0
inversion model conc mgm^{-3}
0
10
20
30
40
observed concentration mgm^{-3}
MSS_{mod} = 0.973 MSS_{obs} − 2.61
r^2=0.722

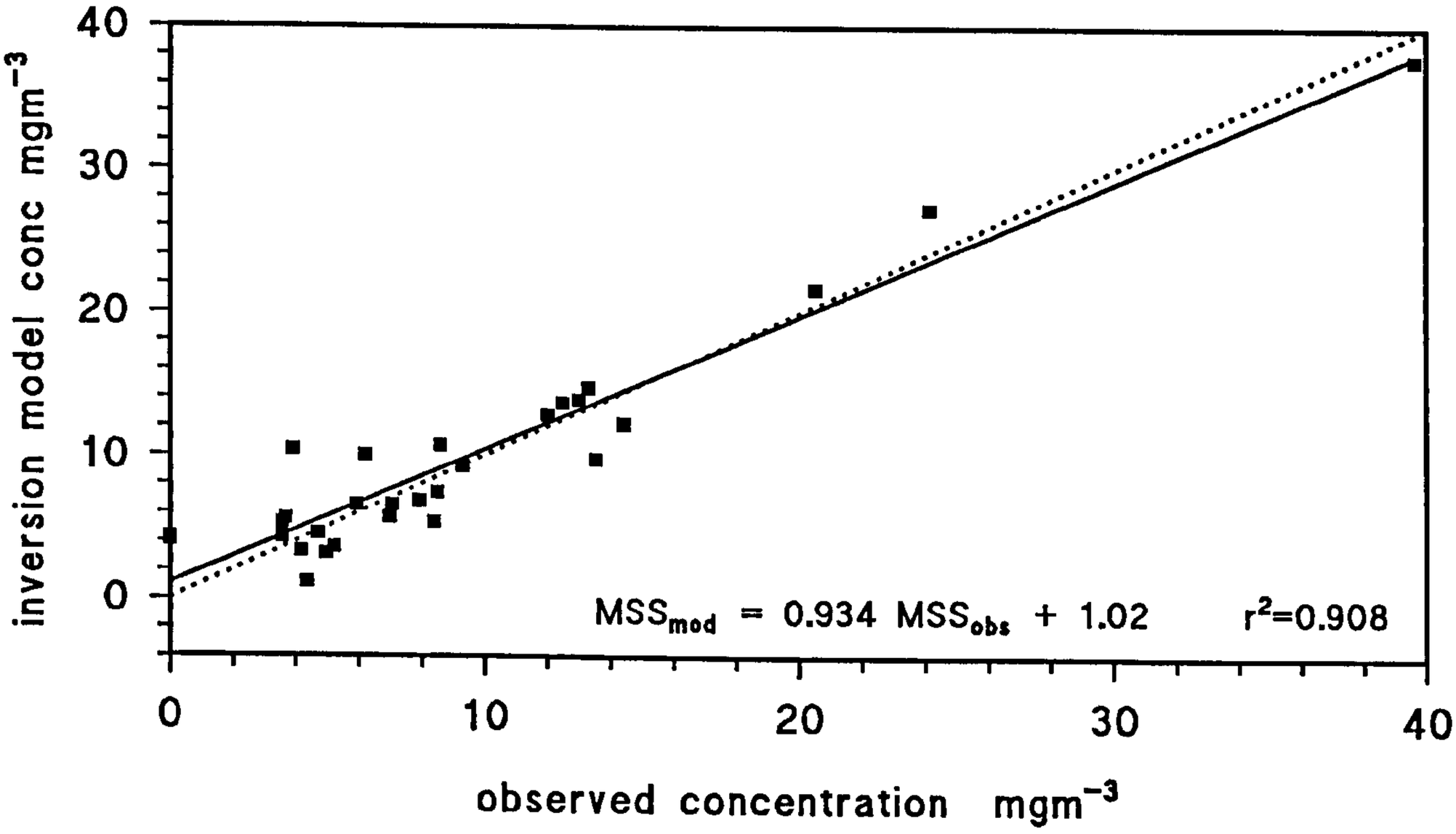
40
30
20
10
0
inversion model conc mgm^{-3}
0
10
20
30
40
observed concentration mgm^{-3}
MSS_{mod} = 0.934 MSS_{obs} + 1.02
r^2=0.908

10. DISCUSSION

Observations at different sites over time have highlighted that the optical characteristics of the water constituents change spatially and temporally. Although models can be constructed from general observations, which are then useful in approximating the overall optical properties, it is necessary to know local conditions for a more detailed and accurate prediction (Ivanov & Kumeysha, 1993). Other studies have tried to distinguish different species of phytoplankton from the optical signal and have demonstrated that species and stage of development have a significant effect on the 'colour' of the water. However, it is also necessary to consider any changes in the yellow substance and mineral particles, particularly in Case 2 waters. As the geology changes with site so will the dominant particles within the water. For surface studies in relatively deep coastal water, the size and density of the mineral particles will be limited, as they remain in suspension and must therefore have a low settling velocity. However, in water bodies where there is a high degree of mixing and resuspension, such as estuaries, the particle composition can be much more varied, and thus the interpretation must encompass this.

The observed values in the Menai Strait for diffuse attenuation and reflectance are in good agreement with other studies which range from 0.06 m^{-1} to 2.9 m^{-1} for K_d in non-estuarine, coastal waters (Kirk, 1994). The absorption values measured in the laboratory and derived from the *in situ* measurements are comparable to spectra observed by others for yellow substance (*e.g.* Bricaud *et al*, 1981) and phytoplankton (Gallegos *et al*, 1990). The observed values for K_d and R covered a greater range than those measured in the equivalent study by Weidemann & Bannister (1986) who found ranges of 0.8-1.2 m^{-1} and 3-6% respectively. They also derived absorption and scattering from these values to give ranges of 0.44-0.83 m^{-1} for absorption and 1.8-5.0 m^{-1} for scattering - smaller ranges than in the Menai Strait but of a comparable magnitude. That study also found an independent estimate of absorption to be in reasonable agreement with the derivation through the Kirk (1985) algorithms.

The other sites used in this study were mainly to provide a contrast to test the model

which was developed. However, the reflectance spectra from Llyn Cwmystradllyn agree well with the Type 3 lake discussed by Vertucci & Likens (1989) although they do not comment on the general environmental implications of the colour.

There were several possible sources of error within both the field and laboratory measurements. It was unfortunate, but unavoidable, that different instruments were used throughout the survey so that consistency could not be maintained. Although the various instruments were compared, the problems of particular sensors failing to download, or other malfunctions, led to ambiguity within the comparisons.

The *in situ* measurements of K_d were limited with the UCNW instruments by the amount of time necessary to measure the light level at each depth. This also affected the reflectance measurements, although there were further errors in this property due to self-shading for the K_u values used to calculate R and the time lag between upwelling and downwelling observations. With the PRR-600 and the Satlantic, reflectance was affected by the conversion used to calculate upwelling irradiance from the radiance value. This indicates that the diffuse attenuation results were more robust and should be given more import in the analysis. There was thus greater confidence in this parameter when constructing the model. Even though the observations of K_d are acceptable, the lack of incorporating the influence of the volume scattering function through using a variable G (as discussed in §2.4.2) will increase the error in the derivation of a and b.

The concentration measurements were limited by the lack of replicates taken during the Menai Strait Survey, making it difficult to determine the precision. In later studies the pigment concentrations are consistent within 10% (Appendix VII). Yellow substance measurements in relatively stable environments are consistent to 0.01 m^{-1} - 1% of the total absorption. However, in dynamic environments such as the Conwy Estuary on the flood-tide this error increases to 10%. The sediment concentrations, when three replicates were taken agree to within 0.1 mgl^{-1} for the filters without a blank beneath, when the total concentrations were of the order of 20 mgl^{-1}. The third filter (used with a blank) consistently had a higher concentration which suggests that

the error was increased by this technique. For non-blank measurements, this implies that the error was of the order of 1%.

In the laboratory, the main source of error was due to scattering as discussed in §7.4. This is particularly important with the inorganic particles where scatter dominates the optical signal and may alter with wavelength, as is suggested through the measurements using a diffuser. Given the uncertainties within the optical properties of the sediment it is difficult to distinguish between the absorption and scattering contribution. This is particularly important when determining the best value for the pathlength amplification factor. Although studies have been undertaken to calculate the best β for phytoplankton studies, there has been little work including inorganic particles. Thus, it was necessary to derive a new value for β from the *in situ* and laboratory measurements, which improves comparisons in this study and suggests that more work should be done to investigate this variable.

The inability to measure scatter accurately in the laboratory led to limitations in modelling this parameter within the final model, resulting in high variation with the scatter coefficients derived.

For future studies which investigate the links between the apparent and inherent optical properties with an aim to predict the colour from the constituent concentrations, it is most important to take more accurate measurements of the particle concentrations, through the use of more replication and greater volumes of water. This is logistically difficult but would improve the confidence that can be given to the final results. In addition, the optical measurements should be replicated so that several profiles are done at any one time to ensure that brief fluctuations are not incorporated when they may have no relation to the water samples taken.

The comparison between inherent and apparent properties will only be truly achievable when *in situ* measurements of absorption and scattering can be taken. The development of such absorption-scatter meters is now occurring and should be used to understand the links between these properties as it is the inherent optical properties

which will lead to more accurate predictions of concentrations.

At present, the model can only reproduce observed conditions where the parameters are specified for each site. This suggests that any inverse model, which estimates concentrations from the optical signals will also be site specific, and should incorporate as much local information as possible. Without detailed information, about the minerals in particular, the ability to distinguish the constituent signals from the optics is limited. Further information may be gained by extending the measurements beyond the visible part of the spectrum, as it may be possible to quantify mineral concentrations in the infrared portion of the spectrum, or use red-infrared ratios for phytoplankton (Quibell, 1991; Han *et al*, 1994). However, these techniques need further investigation.

Satellite algorithms are particularly restricted, as the only information available is the upwelling radiance, which limits interpretation to the reflectance signal alone. For example, the upward radiance in the blue may be dominated by yellow substance fluorescence (Spitzer & Dirks, 1985) which would increase the signal above that expected with the concentrations present. The image may also be influenced by surface foam, and wind roughening (Tassan, 1994) which increase the level of the signal, plus other scattering effects at the air-sea interface (Carter & Duncan, 1993), and atmospheric effects (Viollier *et al*, 1980). Remote optical sensors are therefore more useful in conjunction with other types of images, *i.e.* those from fluorescence sensors (Gower & Borstad, 1981; Mitchell & Kiefer, 1988a) or infra-red sensors (Stramska & Dickey, 1993). Combined images can then be used to locate areas of pollution (Clark, 1993; King *et al*, 1993), and algal blooms with association to physical structure (Mitchelson, 1984).

It may be possible to employ remote sensors in monitoring physical features which are strongly linked to optically prominant constituents. For example, yellow substance appears to be conservative and gives a good correlation with salinity in the River Clyde. However, the extent of this correlation is surprising given that the source of the yellow substance will change when beyond the river itself. In the deeper water

of the Clyde Sea, the expected source would be phytoplankton detritus rather than terrestrial humic acids, and consequently there seems no logical reason why the inverse relationship with salinity should be maintained. In a closed system with a terrestrial source, the change in salinity is due to dilution of fresh water with salt water, so that the optical signal becomes a reliable indicator of salinity. This relationship is dependent on the signature of the humic acids remaining constant and identifiable for the specific location. The use of yellow substance as a tracer is most appropriate for estuaries, which are, unfortunately, the most complex areas for distinguishing the different optical signals, usually bearing high phytoplankton and mineral loads, and thus complicating the determination of the yellow substance concentration from the colour.

Inherent optical properties are more accurate for monitoring constituents as they are directly linked to the constituents themselves. This necessitates *in situ* monitoring, and is thus suitable for buoy deployments over time. However, the validity of buoy measurements is dependent on the rate of fouling. Estimates of the constituent concentrations will improve with the amount of information available, so that if absorption and scattering can be measured the estimates will be more accurate. This can be achieved by using a transmissometer in conjunction with a nephelometer, or an absorption-scattering meter if available. The accuracy would be improved with additional information about the nature of the particles, such as particle size analysis from acoustic backscatter (Lynch *et al*, 1994). When only general radiance/irradiance meters are used the error is increased as the inherent properties must then be derived from reflectance and attenuation, and the relationships between these can be dependent on local conditions. As shown, the scattering depends on the nature of the particle and the total cross-sectional area (Owen, 1973), but it also varies with the light intensity, and can be more dependent on this than an increase in concentration (Ackleson *et al*, 1993). This emphasizes the importance of several types of sensor being used together.

Further studies on the relationships between the optical properties and the constituents may improve the accuracy of predictions and enable models to be used more widely.

However, it is also important to consider the effect of the laboratory techniques upon the results within any particular study. The use of spectra is particularly sensitive as the temperature of the water blank compared with the sample is important (Pegau & Zaneveld, 1993), the subtraction of the value at 750 nm is widely used and may not be applicable, particularly in studying mineral particles. In addition, the correction for the pathlength amplification factor is highly variable. There is also error added by using the absorbance measured with a spectrophotmeter as proportional to absorption, given that scattering of particles in cells and on filters may make a significant contribution. Even the use of an integrating sphere or diffuser system will not eradicate scattering completely. Consequently, there must always be a margin of error accepted within such results; although not perfect these methods are the most effective that can be widely employed.

It is debatable whether more extensive studies at a greater number of sites would produce algorithms for global use. Optical models are useful in identifying the dominant constituent within the water column, and the presence of other substances, but may not achieve precise concentrations with the instruments and knowledge available at present. In shallow water, the use of optical sensors may be a good method for relatively rapid coverage of bed composition, giving an indication of the sediment type and degree of vegetation cover. Limitations will occur from the field of view of the sensor, particularly in areas of highly diverse coverage, and identification of individual species, but may still be useful for monitoring gross change.

In general, optics can be used as a relatively cheap and simple method of monitoring over wide areas, with remote sensing, or over long time periods, with buoy deployment. It is not yet possible to use such data to estimate concentrations or species of phytoplankton accurately but the information is useful to gauge the general condition and any change which occurs. Further studies in the more optically complex areas such as estuaries and Case 2 waters will enhance the knowledge and understanding of optical characteristics and may hopefully extend optical use to more precise applications.

LIST OF REFERENCES

Ackleson, S. G., J. J. Cullen, J. Brown and M. Lesser (1993). Irradiance induced variability in light scatter from marine phytoplankton in culture, *Journal of Plankton Research* 15, 737-759.

Ackleson, S. G., W. M. Balch and P. M. Holligan (1994). Response of water-leaving radiance to particulate calcite and chlorophyll a concentrations: A model for Gulf of Maine coccolithophore blooms, *Journal of Geophysical Research* 99, 7483-7499.

Agnew, M. (1983). Bio-optical measurements in coastal waters, *MSc Thesis, UCNW Bangor.*

Ahn, Y.-H., A. Bricaud and A. Y. Morel (1992). Light backscattering efficiency and related properties of some phytoplankters, *Deep Sea Research* 39, 1835-1855.

Aiken, J., G. Moore, C. C. Trees, S. B. Hooker and D. K. Clark (1995). NASA Technical Memorandum 104566, Vol.29, *SeaWiFS Technical Report Series*, Ocean Optics Protocols for SeaWiFS Validation, Editors: S. B. Hooker, E. R. Firestone, and J. G. Acker, Goddard Space Flight Centre, Greenbelt, Maryland.

Anderson, F. P., L. V. Shannon, S. A. Mostert, N. M. Walters and O. G. Malan (1981). A South African ocean colour experiment, *Oceanography from Space* 381-386, pp. 978.

Asghar, A. (1992). Sedimentological, geophysical and oceanic studies of postglacial and contemporary sedimentary processes of the north east Menai Strait and Conwy Bay (Wales, UK), *PhD Thesis, UCNW Bangor,* pp.214.

Atlas, D. and T. T. Bannister (1980). Dependence of mean spectral extinction coefficient of phytoplankton on depth, water colour and species, *Limnology and Oceanography* 25, 157-159.

Austin, R. W. (1970). Transmittance, scattering and ocean colour, in Tyler (ed.) *Light in the Sea*, 125-133.

Austin, R. W. (1991). Optical Remote Sensing of the Oceans: BC (Before CZCS). and AC (After CZCS), in Barale & Schlittenhardt *Ocean Colour: Theory and Applications in a decade of CZCS experience,* 1-16.

Austin, R. W. and T. J. Petzold (1981). The determination of the diffuse attenuation coefficient of sea water using the Coastal Zone Colour Scanner, *Oceanography from Space* 239-256, pp. 978.

Babin, M., J. C. Therriault, L. Legendre and A. Condal (1993). Variations in the specific absorption coefficient for natural phytoplankton assemblages: Impact on estimates of primary production, *Limnology and Oceanography* 38, 154-177.

Bader, R. G., D. W. Hood and J. B. Smith (1960). Recovery of dissolved organic matter in sea-water and organic sorption be particulate material, *Geochimica et Cosmochimica Acta* 19, 236-243.

Baker, T. T. and J. W. Lavelle (1984). The effect of particles size on the light attenuation coefficient of natural suspensions, *Journal of Geophysical Research* 89, 8197-8203.

Balch, W. M. and K. A. Kilpatrick (1982). Particulate reflectance measurements of phytoplankton, *Journal of Plankton Research* 14, 721-735.

Balsam, W. L. and B. C. Deaton (1991). Sediment dispersal in the Atlantic Ocean: evaluation by visible light spectra, *Review of Aquatic Sciences* 4, 411-477.

Balsam, W. L. and R. J. Wolhart (1993). Sediment dispersal in the Argentine Basin: evidence from visible light spectra, *Deep Sea Research* 40, 1001-1031.

Barale, V. and P. M. Schlittenhardt (1991). *Ocean Colour: Theory and Applications in a decade of CZCS Experience* Kluwer Academic Publishers, Dordrecht, The Netherlands, pp. 367.

Beardsley, G. F., H. Pak, K. L. Carder and B. Lundgren (1970). Light scattering and suspended particles in the Eastern equatorial Pacific Ocean, *Journal of Geophysical Research* 75, 2837-2845.

Bhargava, D. S. and D. W. Mariam (1990). Spectral reflectance relationships to turbidity generated by different clay materials, *Photogrammetric Engineering and Remote Sensing* 56, 225-229.

Blough, N. V., O. C. Zafiriou and J. Bonilla (1993). Optical absorption spectra of waters from the Orinoco River outflow: terrestrial input of coloured organic matter to the Caribbean, *Journal of Geophysical Research* 98, 2271-2278.

Bohren, C. F. and D. R. Huffman (1983). *Absorption and scattering of light by small particles,* John Wiley & Sons, New York, pp. 530.

Boney, A. D. (1975). Phytoplankton, *Studies in Biology* no.52, pp. 116.

Bowers, D. G., G. E. L. Harker and B. Stephan (1996). Absorption spectra of inorganic particles in the Irish Sea and their relevance to remote sensing of chlorophyll, *International Journal of Remote Sensing* 17, 2449-2460.

Bricaud, A., A. Morel and L. Prieur (1981). Absorption by dissolved organic matter of the sea (yellow substance). in the UV and visible domains, *Limnology and Oceanography* 26, 43-53.

Bricaud, A. and A. Y. Morel (1986). Light attenuation and scattering by phytoplanktonic cells: a theoretical model, *Applied Optics* 25, 571-580.

Bricaud, A,. C. Roesler and J. R. V. Zaneveld (1995). In situ methods for measuring the inherent optical properties of ocean waters, *Limnology and Oceanography* 40, 393-410.

Brown, J. and J. H. Simpson (1990). The radiometric determination of total pigment and seston and its potential use in shelf seas, *Estuarine, Coastal and Shelf Science* 31, 1-9.

Browne, D. P. (1993). Studies of ERS-1 Synthetic Aperture Radar Imagery of the Cardigan Bay Front, *MSc Thesis, UCNW Bangor,* pp.31.

Bukata, R. P., J. E. Bruton, J. H. Jerome, S. C. Jain and H. H. Zwick (1981a). Optical water quality model of Lake Ontario 1: Determination of the optical cross sections of organic and inorganic particulates in Lake Ontario, *Applied Optics* 20, 1696-1703.

Bukata, R. P., J. E. Bruton, J. H. Jerome, S. C. Jain and H. H. Zwick (1981b). Optical water quality model of Lake Ontario 2: Determination of chlorophyll-a and suspended mineral concentration of natural waters from submersible and low altitude optical sensors, *Applied Optics* 20, 1704-1714.

Bukata, R. P., J. E. Bruton and J. H. Jerome (1983). Use of chromaticity in remote measurements of water quality, *Remote Sensing of Environment* 13, 161-177.

Campbell, D. E. and R. W. Spinrad (1987). The relationship between light attenuation and particle characteristics in a turbid estuary, *Estuarine, Coastal and Shelf Science* 25, 53-65.

Carder, K. L., S. L. Hawes, K. A. Baker, R. C. Smith, R. G. Steward and B. G. Mitchell (1991). Reflectance model for quantifying chlorophyll-a in the presence of productivity degradation products, *Journal of Geophysical Research* 96, 20599-20611.

Carder, K. L., R. G. Steward, G. R. Harvey and P. B. Ortner (1989). Marine humic and fulvic acids: their effects on remote sensing of oceanic chlorophyll, *Limnology and Oceanography* 34, 68-81.

Carder, K. L., R. G. Steward, J. H. Paul and G. H. Vargo (1986). Relationships between chlorophyll and ocean colour constituents as they affect remote sensing reflectance models, *Limnology and Oceanography* 31, 403-413.

Carter, W. H. and D. D. Duncan (1993). Scattering of a light beam from waves at an air-sea interface, *Applied Optics* 32, 3286-3294.

Clark, C. D. (1993). Satellite remote sensing for marine pollution investigations, *Marine Pollution Bulletin* 36, 357-368.

Clark, D. K. (1981). Phytoplankton pigment algorithms for the Nimbus-7, *Oceanography from Space,* 227-237, pp. 978.

Cleveland, J. S. and A. D. Weidemann (1993). Quantifying absorption by aquatic particles: A multiple scattering correction for glass-fibre filters, *Limnology and Oceanography* 38, 1321-1327.

Curran, P. J. and E. M. M. Novo (1988). The relationship between suspended sediment concentration and remotely sensed spectral radiance: a review, *Journal of Coastal Research* 4, 351-368.

Davies-Colley, R. J. (1983). Optical properties and reflectance spectra of 3 shallow lakes obtained from a spectrophotometric study, *New Zealand Journal of Marine and Freshwater Research* 17, 445-459.

Davies-Colley, R. J. (1988). Measuring water clarity with a black disc, *Limnology and Oceanography* 33. 616-623.

Davies-Colley, R. J. (1992). Yellow substance in coastal and marine waters round the South Island, New Zealand, *New Zealand Journal of Marine and Freshwater Research* 26, 311-322.

Davies-Colley, R. J. and M. E. Close (1990). Water colour and clarity of new Zealand rivers under baseflow conditions, *New Zealand Journal of Marine and Freshwaater Research* 24, 357-365.

Davies-Colley, R. J. and D. G. Smith (1995). Optically pure waters in Waikoropupu ('Pupu'). Springs, Nelson, New Zealand, *New Zealand Journal of Marine and Freshwater Research* 29, 251-256.

Deaton, B. and W. L. Balsam (1991). Visible spectroscopy - a rapid method for determining hematite and geothite concentration in geological materials,, *Journal of Sedimentary Petrology* 61, 628-632.

Di Toro, D. M. (1978). Optics of turbid estuarine waters: approximations and applications, *Water Research* 12, 1059-1068.

Doerffer, R. (1980). Applications of a two-flow model for remote sensing of substances in water, *Boundary Layer Meteorology* 18, 221-232.

Doerffer, R. and J. Fischer (1994). Concentrations of chlorophyll, suspended matter, and Gelbstoff in Case II waters derived from satellite coastal zone colour scanner data with inverse modelling methods, *Journal of Geophysical Research* 99, 7457-7466.

Duysens, L. N. M. (1956). The flattening of the absorption spectrum of suspensions, as compared to that of solutions, *Biochemica et Biophysica Acta* 19, 1-12.

Edmondson, W. T. (1980). Secchi disk and chlorophyll, *Limnology and Oceanography* 25, 378-379.

Embleton, C. (1964). The deglaciation of Arfon and Southern Anglesey, and the origin of the Menai Straits, *Proceedings of the Geological Association* 75, 407-427.

Estep, L. (1994). Bottom influence on the estimation of chl concentration in water from remotely sensed data, *International Journal of Remote Sensing* 15, 205-214.

Fry, E. S. and G. W. Kattawar (1988). Measurement of the absorption coefficient of ocean water using isotropic illumination, *SPIE Ocean Optics IX* 925, 142-148.

Fry, E. S., G. W. Kattawar and R. M. Pope (1992). Integrating cavity absorption meter, *Applied Optics* 31, 2055-2065.

Gaffey, S. J. (1985). Reflectance spectroscopy in the visible and near-infrared (0.35-2.55 microns): Applications in carbonate petrology, *Geology* 13, 270-273.

Gallegos, C. L., D. L. Correll and J. W. Pierce (1990). Modelling spectral diffuse attenuation, absorption, and scattering coefficients in a turbid estuary, *Limnology and Oceanography* 35, 1486-1502.

Gallie, E. A. and P. A. Murtha (1992). Specific absorption and backscattering spectra for suspended minerals and chlorophyll-a in Chilko Lake, British Columbia, *Remote Sensing of Environment* 39, 103-118.

Ganf, G. G., R. L. Oliver and A. E. Walsby (1989). Optical properties of gas-vacuolate cells and colonies of microcystis in relation to light attenuation in a turbid, stratified reservoir (Mount Bold Reservoir, South Australia), *Australian Journal of Marine and Freshwater Research* 40, 595-611.

Ge, Y., H. R. Gordon and K. J. Voss (1993). Simulation of inelastic scattering contributions to the irradiance field in the ocean: variation in Fraunhofer line depths, *Applied Optics* 32, 4028-4037.

Giannini, L. (1981). Differential spectroscopy for the coastal water quality identification by remote sensing, *Oceanography from Space,* 395-402, pp.978.

Gitelson, A. (1992). The peak near 700 nm on radiance spectra of algae and water: relationships of its magnitude and position with chlorophyll concentration, *International Journal of Remote Sensing* 13, 3367-3373.

Gitelson, A. A. and G. P. Keydan (1990). Remote sensing of Inland Surface Water Quality - Measurements in the Visible Spectrum, *Acta Hydrophysica* 34, 5-27.

Goodin, D. G., L. Han, R. M. Fraser, D. C. Rundquist and W. Stebbins (1993). Analysis of suspended solids in water using remotely sensed high resolution derivative spectra, *Photogrammetric Engineering and Remote Sensing* 59, 505-510.

Gordon, H. R. (1979). Diffuse reflectance of the ocean: the theory and augmentation by chlorophyll-a fluorescence at 685 nm, *Applied Optics* 18, 1161-1166.

Gordon, H. R. (1980). Irradiance attenuation coefficient in a stratified ocean: a local property of the medium, *Applied Optics* 19, 2092-1094.

Gordon, H. R. (1988). Influence of vertical stratification on the distribution of irradiance at the sea surfacefrom a point source in the ocean, *Applied Optics* 27, 2643-2645.

Gordon, H. R. (1989). Dependence of the diffuse reflectance of natural waters on sun angle, *Limnology and Oceanography* 34, 1484-1489.

Gordon, H. R. (1991). Absorption and scattering estimates from irradiance measurements: Monte Carlo simulations, *Limnology and Oceanography* 36, 769-777.

Gordon, H. R. (1992). Diffuse reflectance of the ocean: influence of non-uniform phytoplankton pigment profile, *Applied Optics* 31, 2116-2129.

Gordon, H. R. (1993). Sensitivity of radiative transfer to small angle scattering in the ocean: quantitative assessment, *Applied Optics* 32, 7505-7511.

Gordon, H. R., J. W. Brown and R. H. Evans (1988). Exact Rayleigh scattering calculations for use with the Nimbus-7 Coastal Zone Colour Scanner, *Applied Optics* 27, 862-871.

Gordon, H. R. and O. B. Brown (1972). A theoretical model of light scattering by Sargasso Sea particulates, *Limnology and Oceanography* 17, 826-832.

Gordon, H. R., O. B. Brown, R. H. Evans, J. W. Brown, R. C. Smith, K. S. Baker and D. K.Clark (1988). A semianalytic radiance model of ocean colour, *Journal of Geophysical Research* 93, 10909-10924.

Gordon, H. R., D. K. Clark, J. L. Mueller and W. A. Hovis (1980). Phytoplankton pigments from the Nimbus-7 Coastal Zone Colour Scanner: comparisons with surface measurements, *Science* 210, 63-66.

Gordon, H. R. and K. Y. Ding (1992). Self-shading of in-water optical instruments, *Limnology and Oceanography* 37, 491-500.

Gordon, H. R. and A. Y. Morel (1983). *Remote assessment of ocean colour for interpretation of satellite visible imagery: A review.*

Gower, J. F. R. and G. Borstad (1981). Use of *in vivo* fluorescence line at 685 nm for remote sensing surveys of surface chlorophyll-a, *Oceanography from Space* 313-320, pp. 978.

Han, L. and D. C. Rundquist (1994). The response of both surface reflectance and the underwater light field to variouslevels of suspended sediments: preliminary results, *Photogrammetric Engineering and Remote Sensing* 60, 1463-1471.

Han, L., D. C. Rundquist, L. L. Liu, R. N. Fraser and J. F. Scahalles (1994). The spectral responses of algal chlorophyll in water with varying levels of suspended sediment, *International Journal of Remote Sensing* 15, 3707-3718.

Han, L. and D. C. Rundquist (1996). Spectral characterization of suspended sediments generated from two texture classes of clay soil, *International Journal of Remote Sensing* 17, 643-649.

Harvey, J. G. (1968). The Flow of Water Through the Menai Straits, *Geophysical Journal of the Royal Astronomical Society* 15, 517-528.

Hochman, H. T., F. E. Muller-Karger and J. J. Walsh (1994). Interpretation of the coastal zone colour scanner signature of the Orinoco River plume, *Journal of Geophysical Research* 99, 7443-7455.

Hochman, H. T., J. J. Walsh and K. L. Carder (1995). Analysis of ocean color components within stratified and well-mixed waters of the western English Channel, *Journal of Geophysical Research* 100, 10777-10787.

Hoepffner, N. and S. Sathyendranath (1992). Bio-optical characteristics of coastal waters: absorption spectra of phytoplankton and pigment distribution in the Western North Atlantic, *Limnology and Oceanography* 37, 1660-1679.

Højerslev, N. K. (1980). Water colour and its relation to primary production, *Boundary Layer Meteorology* 18, 203-220.

Højerslev, N. K. (1981). Assessment of some suggested algorithms on sea colour and surface chlorophyll, *Oceanography from Space*, 347-354, pp.978.

Højerslev, N. K. (1994). A history of early optical oceanic instrument design in Scandinavia, in Sprinrad et al.(eds). *Ocean Optics* 118-147.

Holmes, R. W. (1970). The Secchi disk in turbid coastal waters, *Limnology and Oceanography* 15, 688-694.

Holyer, R. J. (1978). Toward universal multispectral suspended sediment algorithms, *Remote Sensing of Environment* 7, 323-338.

Hunt, G. R. (1977). Spectral signatures of particulate minerals in the visible and near infrared, *Geophysics* 42, 501-513.

Hunt, G. R. and R. P. Ashley (1979). Spectra of altered rocks in the visible and near infrared, *Economic Geology* 74, 1613-1629.

Hunt, G. R. and J. W. Salisbury (1976). Visible and near infrared spectra of minerals and rocks: XI. Sedimentary rocks, *Modern Geology* 5, 211-217.

Ivanoff, A., N. Jerlov and T. H. Waterman (1961). A comparative study of irradiance, beam transmittance and scattering in the sea near Bermuda, *Limnology and Oceanography* 6, 451-456.

Ivanov, A. R. and A. A. Kumeysha (1993). The specifics of optical structure and the relationships between the characteristics of light scattering in the Atlantic Ocean, *Oceanology* 33, 156-160.

Jain, S. C. and J. R. Miller (1976). Subsurface water parameters: optimization approach to their determination from remotely sensed water colour data, *Applied Optics* 15, 886-890.

Jerlov, N. G. (1968). *Optical Oceanography,* Elsevier, Netherlands, pp.194.

Jerlov, N. G. and E. S. Nielson (1974). *Optical Aspects of Oceanography*, pp. 494.

Jonasz, M. and H. Prandke (1986). Comparison of measured and computed light scattering in the Baltic, *Tellus* 38, 144-157.

Jones, S. J. (1978). The sedimentary history of Gallows Point in the Menai Strait, *MSc Thesis, UCNW Bangor,* pp.47.

Kalle, K. (1966). The problem of Gelbstoff in the sea, *Oceanography and Marine Biology Annual Review* 4, 91-104.

Kattawar, G. W. and G. N. Plass (1972). Monte Carlo calculations of radiative transfer in theEarth's atmosphere-ocean system: Radiance in the atmosphere and ocean, *Journal of Physical Oceanography* 2, 146-156.

King, M. D., L. F. Radke and P. V. Hobbs (1993). Optical properties of marine stratocumulus clouds modified by ships, *Journal of Geophysical Research* 98, 2729-2739.

Kirk, J. T. O. (1981a). Monte Carlo study of the nature of the underwater light field in, and therelationships between optical properties of, turbid yellow waters, *Australian Journal of Marine and Freshwater Research* 32, 517-532.

Kirk, J. T. O. (1981b). Estimation of the scattering co-efficient of natural waters using underwaterirradiance measurements, *Australian Journal of Marine and Freshwater Research* 32, 533-539.

Kirk, J. T. O. (1984). Dependence of relationship between inherent and apparent optical properties ofwater on solar altitude, *Limnology and Oceanography* 29, 350-356.

Kirk, J. T. O. (1985). Effects of suspensoids (turbidity). on penetration of solar radiation in aquatic ecosystems, *Hydrologia* 125, 195-208.

Kirk, J. T. O. (1989). The upwelling light stream in natural waters, *Limnology and Oceanography* 34, 1410-1425.

Kirk, J. T. O. (1992). Monte Carlo modelling of the performance of a reflectance tube absorption meter, *Applied Optics* 31, 6463-6468.

Kirk, J. T. O. (1994). *Light and Photosynthesis in aquatic ecosystems, Second edition* Cambridge University Press, Cambridge, pp.401.

Kirk, J. T. O. and R. L. Oliver (1995). Optical closure in an ultraturbid lake, *Journal of Geophysical Research* 100, 13221-13225.

Kitchen, J. C. and J. R. V. Zaneveld (1992). A three-layered sphere model of the optical properties of phytoplankton, *Limnology and Oceanography* 37, 1680-1690.

Koepke, P. (1985). The reflectance factors of a rough ocean with foam - comment on 'Remote sensing of the sea state using the 0.8-1.1 micron spectra band' by L. Wald and J.M.Monget, *International Journal of Remote Sensing* 6, 787-799.

Kullenberg, B. (1953). Absolute chronology of deep-sea sediments and the deposition of clay on the ocean floor, *Tellus* 5, 302-305.

Kullenberg, G. (1968). Scattering of light by Sargasso Sea water, *Deep Sea Research* 15, 423-432.

Kullenberg, G. (1974). Observed and computed scattering functions, *Optical Aspects of Oceanography* 25-49.

Lynch, J. F., J. D. Irish, C. R. Sherwood and Y. C. Agrawal (1994). Determining suspended sediment particle size information from acoustical and optical backscatter measurements, *Continental Shelf Research* 14, 1139-1165.

Maffione, R. A., K. J. Voss and R. C. Honey (1993). Measurement of the spectral absorption co-efficient in the ocean with an isotropic source, *Applied Optics* 32, 3273-3279.

Man'kovskiy, V. I. (1978). Empirical formula for estimating the light attenuation coefficient in sea water from Secchi disk readings, *Oceanology* 18, 493-494.

Maritorena, S., A. Morel and B. Gentili (1994). Diffuse reflectance of oceanic shallow waters: influence of water depth and bottom albedo, *Limnology and Oceanography* 39, 1689-1703.

Marshall, B. R. and R. C. Smith (1990). Raman scattering and in-water ocean optical properties, *Applied Optics* 29, 71-84.

McNeil, W. R., K. P. B. Thomsom and J. Jerome (1976). The application of remote spectral measurements to water quality monitoring, *Canadian Journal of Remote Sensing* 2, 48-58.

Mitchell, B. G. and D. A. Kiefer (1988). Chlorophyll-a specific absorption and fluorescence excitation spectra for light-limited phytoplankton, *Deep Sea Research* 35, 639-663.

Mitchelson, E. G. (1984). Phytoplankton and suspended sediment distributions in relation to physical structure and water leaving colour signals, *PhD Thesis, UW Bangor,* pp.126.

Mittenzwey, K.-H., S. Ullrich, A. A. Gitelson and K. Y. Kondratiev (1992). Determination of chlorophyll-a of inland waters on the basis of spectral reflectance, *Limnology and Oceanography* 37, 147-149.

Mobley, C. D., B. Gentili, H. R. Gordon, A. Jin, G. W. Kattatwar, A. Morel, P. Reinersman, K.Stamnes, and R. H. Stavn (1993). Comparison of numerical mdoels for computing underwater light fields, *Applied Optics* 32, 7484-7503.

Morel, A. Y. (1980). In-water and remote measurements of ocean colour, *Boundary Layer Meteorology* 18, 177-202.

Morel, A. Y. (1987). Chlorophyll specific scattering co-efficient of phytoplankton. A simplified theoretical approach, *Deep Sea Research* 34, 1093-1105.

Morel, A. Y. (1988). Optical modelling of the upper ocean in relation to its biogenous matter content, *Journal of Geophysical Research* 93, 10749-10768.

Morel, A. Y. and A. Bricaud (1981). Theoretical results concerning light absorption in a discrete medium, and application to specific absorption of phytoplankton, *Journal of Geophysical Research* 28, 1375-1393.

Morel, A. Y. and A. Bricaud (1981). Theoretical results concerning the optics of phytoplankton with special reference to remote sensing applications, *Oceanography from Space,* 313-327, pp.978.

Morel, A. and B. Gentili (1991). Diffuse reflectance of oceanic waters: its dependence on sun angle as influenced by the molecular scattering contribution, *Applied Optics* 30, 4427-4438.

Morel, A. Y. and L. Prieur (1977). Analysis of variations in ocean colour, *Limnology and Oceanography* 22, 709-722.

Morel, A. and R. C. Smith (1982). Terminology and units in optical oceanography, *Marine Geodesy* 5, 335-349.

Moritorena, S. and N. Guiliocheau (1996). Optical properties of water and spectral light absorption by living and non-living particles and by yellow substances in coral reef waters of French Polynesia, *Marine Ecology Progress Series* 131, 245-255.

Munday, J. C. and T. T. Alfoldi (1979). LANDSAT test of diffuse reflectance models for aquatic suspended solids measurement, *Remote Sensing of Environment* 14, 225-239.

Nanu, L. and C. Robertson (1993). The effect of suspended sediment depth distribution on coastal water spectral reflectance: theoretical simulation, *International Journal of Remote Sensing* 14, 225-239.

Neuymin, G. G., L. A. Zemlyanaya, O. V. Martynov and M. V. Solov'yev (1982). Estimate of the chlorophyll concentration from measurements of the colour index in different regions of the ocean, *Oceanology* 22, 280-283.

Novo, E. M. M., J. D. Hansom and P. J. Curran (1989). The effect of sediment type on the relationship between reflectance and suspended sediment concentration, *International Journal of Remote Sensing* 10, 1283-1289.

Ochakovsky, Y. Y. (1966). On the comparison of measured and calculated scattering indicatrices of sea water, *Report - US Department of Commerce Joint Publishing Research Service* 36, 98-105.

Owen, R. W. (1973). The effect of particles on light scattering in the sea, *Journal of Oceanographic Society of Japan* 29, 171-184.

Pak, H., G. F. Beardsley, G. R. Heath and H. Curl (1970). Light scattering vectors of some marine particles, *Limnology and Oceanography* 15, 683-387.

Palmer, R. D. (1985). Optical properties and internal environment of the Menai Straits, *MSc thesis.*

Parslow, J. S. (1991). An efficient algorithm for estimating chlorophyll from Coastal Zone Colour Scanner data, *International Journal of Remote Sensing* 12, 2065-2072.

Parsons, T. R., Y. Maita and C. M. Lalli (1984). *A Manual of Chemical and Biological methods for Seawater Analysis,* Pergamon Press, pp.173.

Pegau, W. S. and J. R. V. Zaneveld (1993). Temperature-dependent absorption of water in the red and near-infrared portions of the spectrum, *Limnology and Oceanography* 38, 188-192.

Petzold, T. J. (1977). Volume scattering functions for selected ocean water, in Tyler (ed.) *Light in the Sea,* 152-174.

Plass, G. N., T. J. Humphreys and G. W. Dattar (1981). Ocean colour calculations, *Oceanography from Space*, 377-380, pp. 978.

Plass, G. N. and G. W. Kattawar (1972). Monte Carlo calculations of radiative transfer in the Earth's atmosphere-ocean system: I Flow in the atmosphere and ocean, *Journal of Physical Oceanography* 2, 139-145.

Preisendorfer, R. W. (1959). Theoretical proof of the existence of characteristic diffuse light in natural waters, *Sears Foundation Journal of Marine Research* 18, 1-9.

Preisendorfer, R. W. (1986a). Theoretical proof of the existence of characteristic diffuse light in natural waters, *Sears Foundation, Journal of Marine Research* 18, 1-9.

Preisendorfer, R. W. (1986b). Secchi disk science: visual optics of natural waters, *Limnology and Oceanography* 31, 909-926.

Preisendorfer, R. W. and C. D. Mobley (1984). Direct and inverse irradiance models in hydrologic optics, *Limnology and Oceanography* 29, 903-929.

Prieur, L. and S. Sathyendranath (1981). An optical classification of coastal and oceanic waters based on the specific spectral absorption curves of phytoplankton pigments, dissolved organic matter, and other particulate materials, *Limnology and Oceanography* 26, 671-689.

Quibell, G. (1991). The effect of suspended sediment on reflectance from freshwater algae, *International Journal of Remote Sensing* 12, 177-182.

Sathyendranath, S., F. E. Hoge, T. Platt and R. N. Swift (1994). Detection of phytoplankton pigments from ocean colour, *Applied Optics* 33, 1081-1089.

Sathyendranath, S., T. Platt, V. Stuart, B. D. Irwin, M. J. W. Veldhuis, G. W. Kraay and W. G. Harrison (1996). Some bio-optical characteristics of phytoplankton in the NW Indian Ocean, *Marine Ecology Progress Series* 132, 299-311.

Schiebe, F. R., J. A. Jarrington and J. C. Ritchie (1992). Remote sensing of suspended sediments: the Lake Chicot, Arkansas Project, *International Journal of Remote Sensing* 13, 1487-1509.

Setiapermana, D. (1990). Quantum yield of phytoplankton photosynthesis in relation to nutrient status, *PhD Thesis, UW Bangor.*

Simpson, J. H. and J. Brown (1987). The interpretation of visible band imagery of turbid shallow seas in terms of the distribution of suspended particulates, *Continental Shelf Research* 7, 1307-1313.

Smith, D. G., G. F. Croker & K. McFarlane (1995a). Human perception of water appearance 1. Clarity and colour for bathing and aesthetics, *New Zealand Journal of Marine and Freshwater Research* 29, 29-43.

Smith, D. G., G. F. Croker & K. McFarlane (1995b). Human perception of water appearance 2. Colour judgement, and the influence of perceptual set on perceived water suitability for use, *New Zealand Journal of Marine and Freshwater Research* 29, 45-50.

Smith, R. C. (1981). Remote sensing and depth distribution of ocean colour, *Marine Ecology Progress Series* 5, 359-361.

Smith, R.C. and K. S. Baker (1981). Optical properties of the clearest natural water (200-800 nm), *Applied Optics* 20, 177-184.

Smith, R. C. and K. S. Baker (1982). Oceanic chlorophyll concentrations as determined by satellite (Nimbus-7 Coastal Zone Colour Scanner), *Marine Biology* 66, 269-279.

Smith, R. C. and W. H. Wilson (1981). Ship and satellite bio-optical research in the California Bight, *Oceanography from Space,* 281-294, pp. 978.

Spinrad, R. W., K. L. Carder & M. S. Parry (eds) (1994). *Ocean Optics* Oxford University Press Inc., New York, pp. 283.

Spinrad, R. W., J. R. V. Zaneveld and J. C. Kitchen (1983). A study of the optical characteristics of the suspended particles in the benthis nepheloid layer of the Scotian Rise, *Journal of Geophysical Research* 88, 7641-7645.

Spitzer, D. and R. W. J. Dirks (1985). Contamination of the reflectance of natural waters by solar induced fluorescence of dissolved organic matter, *Applied Optics* 21, 444-445.

Stavn, R. H. (1993). Effects of Raman scattering across the visible spectrum in clear ocean water: a Monte Carlo study, *Applied Optics* 32, 6853-6863.

Stavn, R. H. and A. D. Weidemann (1989). Shape functions, two-flow models and the problem of irradiance inversion in estimating optical parameters, *Limnology and Oceanography* 34, 1426-1441.

Stramska, M. and T. D. Dickey (1993). Phytoplankton bloom and the vertical thermal structure of the upper ocean, *Journal of Marine Research* 51, 819-842.

Stramski, D. and D. A. Kiefer (1991). Light scattering by microorganisms in the open ocean, *Progress in Oceanography* 28, 343-383.

Sturm, B. (1981). Ocean colour remote sensing and quantitative retrieval of surface chlorophyll in coastal waters using Nimbus CZCS data, *Oceanography from Space*, 267-280, pp. 978.

Sydor, M. (1980). Remote sensing of particulate concentration in water, *Applied Optics* 19, 2794-2800.

Tassan, S. (1981). The influence of wind in the remote sensing of chlorophyll in the sea, *Oceanography from Space,* 371-375, pp.978.

Tassan, S. (1988). The effect of dissoved 'yellow substance' on the quantitative retrieval of chlorophyll and total suspended sediment concentration from remote measurements of water colour, *International Journal of Remote Sensing* 9, 787-797.

Tassan, S. (1994). Local algorithms using SeaWiFS data for the retrieval of phytoplankton, pigments, suspended sediment, and yellow substance in coastal waters, *Applied Optics* 33, 2369-2378.

Tett, P. (1990). Plankton, in Baker & Wolff (eds) *Biological Surveys of Estuaries and Coasts,* 291-341.

Thomas, J. P. (1981). Large area marine productivity - pollution experiments (LAMPEX). - a series of studies being developed to hasten the operational use of remote sensing for living marine resources and environmental quality, *Oceanography from Space,* 403-409, pp.978.

Thompson, M. J., L. E. Gilliland and L. K. Rosenfeld (1979). Light scattering and extinction in a highly turbid coastal inlet, *Estuaries* 2, 164-171.

Topliss, B. J. (1986). Spectral variations in upwelling radiant intensity in turbid coastal waters, *Estuarine, Coastal and Shelf Science* 22, 395-414.

Topliss, B. J., L. A. Payzant, P. C. F. Hurley, J. R. Miller and J. Freemantle (1991). Interpretation of multi-season, multi-year colour imagery for a continental shelf region, *Oceanologica Acta* 14, 533-547.

Trowbridge, J. H., B. Butman and R. Limburner (1994). Characteristics of the near-bottom suspended sediment field over the continental shelf off northern California based on optical attenuation measurements during STRESS and SMILE, *Continental Shelf Research* 14, 1257-1272.

Tyler, J. E. (1961). Scattering properties of distilled and natural waters, *Limnology and Oceanography* 6, 451-456.

Tyler, J. E. (1968). The Secchi disk, *Limnology and Oceanography* 13, 1-6.

Tyler, J. E. (1977) ed. *Light in the Sea,* Dowden, Hutchinson & Ross, Pennsylvania.

Ulloa, O., S. Sathyendranath and T. Platt (1994). Effect of particle size distribution on the backscatter ratio in seawater, *Applied Optics* 33, 7070-7077.

Ulloa, O., S. Sathyendranath, T. Platt and R. A. Quiñones (1992). Light scattering by marine heteorotrophic bacteria, *Journal of Geophysical Research* 97, 9619-9629.

Van Stokkom, H. T. C., G. N. M. Stokman and J. W. Hovenier (1993). Quantituative use of passive optical remote sensing over coastal and inland water bodies, *International Journal of Remote Sensing* 14, 541-563.

Vant, W. N. (1991). Underwater light in the northern Manakan Harbour, New Zealand, *Estuarine, Coastal and Shelf Science* 33, 291-307.

Vasil'kov, A. P. and O. V. Kopenevich (1982). Reasons for the appearance of the maximum near 700 nm in the radiance spectrum emitted by the ocean layer, *Oceanology* 22, 697-701.

Vertucci, F. A. and G. E. Likens (1989). Spectral reflectance and water quality of Adirondack mountain region lakes, *Limnology and Oceanography* 34, 1656-1672.

Viollier, M. and B. Sturm (1984). CZCS data analysis in turbid coastal water, *Journal of Geophysical Research* 89, 4977-4985.

Viollier, M., D. Tanre and P. Y. Deschamps (1980). An algorithm for remote sensing of water colour from space, *Boundary Layer Meteorology* 18, 247-267.

Voss, K. J. (1989). Use of the radiance distribution to measure the optical absorption co-efficient in the ocean, *Limnology and Oceanography* 34, 1614-1622.

Voss, K. J. (1992). A spectral model of the beam attenuation coefficient in the ocean and coastal areas, *Limnology and Oceanography* 37, 501-509.

Walne, A. W. (1993). A modelling study of nitrogen cycling in the Firth of Clyde, *PhD Thesis, UCNW Bangor.*

Waters, K. J. (1995). Effects of Raman scattering on the water-leaving radiance, *Journal of Geophysical Research* 100, 13151-13161.

Weidemann, A. D. and T. T. Bannister (1986). Absorption and scattering co-efficients in Irondequoit Bay, *Limnology and Oceanography* 31, 567-583.

Whitlock, C. H., C. Y. Kuo and S. R. LeCroy (1982). Criteria for the use of regression analysis for remote sensing of sediment and pollutants, *Remote Sensing of Environment* 12, 151-168.

Williams, J. (1970). *Optical properties of the sea*, United States Naval Institute, Annapolis, Maryland, pp. 125.

Wilson, W. H. and D. A. Kiefer (1979). Reflectance spectroscopy of marine phytoplankton Part 2. A simple model of ocean colour, *Limnology and Oceanography* 24, 673-682.

Zaneveld, J. R. V., D. M. Roach and H. Pak (1974). The determination of the index of refraction distribution of oceanic particulates, *Journal of Geophysical Research* 79, 4091-4095.

Zwick, H. H., S. C. Jain and J. R. Miller (1981). Modelling aspects of water quality estimated by remote sensing, *Oceanography from Space,* 355-363, pp. 978.

APPENDIX I

Optical Models in the Literature

Examples of models

	author	date	comments
Radiative transfer function			
	Jain & Miller	1976	spectral albedo interpreted by optimization
	Gordon	1979	included fluorescence
	Doerffer	1980	backscattered radiation field
	Preisendorfer & Mobley	1984	inverse model
	Stavn & Weidemann	1989	investigates inversion for scattering
	Marshall & Smith	1990	Raman scattering & fluorescence
	Gordon	1993	irradiance can be estimated with abs & vol scat function only
	Maffione et al	1993	vector irradiance generated by isotropic source
	Ackleson et al	1994	iterative inversion
	Doerffer & Fischer	1994	inverse model with CZCS
Empirical			
	Bukata et al	1988 a&b	five component model
	Carder et al	1986	covariation of concentrations
	Gordon	1988	mean concentration determines E(0) not vertical distribution
	Gallegos et al	1990	YS & inorganic spectra similar
	Gitelson & Keydan	1990	determines Chl, MSS & YS from diffusely scattered radiation
	Carder et al	1991	two refl ratios used to estimate Chl

Monte Carlo			
	Kattawar & Plass	1972	min lu function of nadir angle of observation
	Plass & Kattawar	1972	includes orders of multiple scattering
	Kirk	1981	relationship between K and a & b
	Kirk	1984	dependence on sun angle
	Stavn & Weidemann	1988	Raman contribution
	Gordon	1989	refl dependence on sun angle & vol scat function
	Kirk	1989	upward scattering
	Gordon	1991	estimates a, b & bb from c, R & Kd
	Morel & Gentili	1991	refl dependence on sun angle
	Gordon	1992	separate phytoplankton and detrital a & b
	Gordon & Ding	1992	self-shading effect
	Kirk	1992	refl tube absorption meter
	Ge et al	1993	Fraunhofer line separates elastic and inelastic scat
	Stavn	1993	Raman contribution
	Waters	1995	Raman contribution
Other			
	Gordon & Brown	1972	Mie theory with two phytoplankton species
	Wilson & Kiefer	1979	refl based on water and phytoplankton
	Jonasz & Prandke	1981	Mie theory
	Morel & Bricaud	1981a	Mie theory variation in specific abs
		1981b	Mie theory scattering efficiencies
	Plass et al	1981	Ld decreases when sun out of "critical cone"
	Vasil'kov & Kopelevich	1982	refl min at 665 nm, max at 685 due to fluorescence
	Koepke	1985	effect of foam on refl
	Bricaud & Morel	1986	Mie-Lorenz model of phytoplankton
	Gordon et al	1988a	Rayleigh radiance and atmos correction
		1988b	variation in radiance due to backscat
	Tassan	1988	importance of YS
	Setiapermana	1990	phytoplankton photosynthesis
	Kitchen & Zaneveld	1992	properties of individual phytoplankton
	Voss	1992	attenuation model
	Nanu & Robertson	1993	Mie theory spectral reflectance
	Stavn	1993	Raman scat
	Tassan	1994	algorithms different when Chl<1 mg/m3
	Ulloa et al	1994	Mie theory bb ratio dependent on submicrometer parts
Reviews			
	Zwick et al	1981	reviews four types of model
	Mobley et al	1993	comparison of seven models

APPENDIX II

Definitions of

Basic Optical Properties

BASIC DEFINITIONS

To consider the physics and interacting processes within a light field, it is necessary to define the standard concepts and properties.

Visible radiation from the sun is divided into quanta of energy, known as photons; the time rate of flow of this radiant energy is termed the radiant flux (Φ). The strength of this energy is measured as the radiant intensity (I) - "the radiant flux emitted by a point source, or by an element of an extended source, in an infinitesimal cone containing the given direction, divided by that element of solid angle":

$$I = \frac{d\Phi}{d\omega}$$

The most commonly studied parameters of the underwater light field are radiance and irradiance -

radiance is "the radiant flux per unit solid angle per unit projected area of a surface":

$$L(\theta,\phi) = \frac{d^2\Phi}{dA\cos\theta\, d\omega}$$

where Φ is radiant flux, θ is the zenith angle, ϕ is the azimuth angle, ω is the solid angle and A is area

while irradiance is "the radiant flux incident on an infinitesimal element of surface containing the point under consideration, divided by the area of that element" (Jerlov, 1968):

$$E = \frac{d\Phi}{dA}$$

Energy which enters the water from above and is transmitted downwards is known as *downward irradiance*, while photons which travel upwards, having been diverted from their downward path, produce *upward irradiance*.

Scalar irradiance E_0 is the integral of the radiance distribution at a point over all directions about the point. The ratio of the net downward irradiance to scalar irradiance is known as the average cosine:

$$\bar{\mu} = \frac{E_d - E_u}{E_0}$$

The ratio between the reflected and the incident radiant flux is termed the *reflectance*, a special case of which is the *irradiance ratio*, the ratio most often referred to:

$$R = \frac{E_u}{E_d}$$

The vertical gradient of the logarithm (natural) of radiance, or irradiance, is known as the vertical attenuation coefficient:

$$K = -\frac{d \ln (X)}{dz} = -\frac{1}{X}\frac{dX}{dz}$$

where X can be either radiance or irradiance and z is depth

The directional nature of the radiant energy is determined by the volume scattering function [$\beta(\theta)$] - "the radiant intensity, from a volume element in a given direction, per unit of irradiance on the cross-section of the volume and per unit volume (V)":

$$\beta(\theta) = \frac{dI(\theta)}{EdV}$$

The change in radiance over a certain length consists of loss by attenuation (c) and gain by scattering (Jerlov, 1968):

$$\frac{dL(z,\theta,\phi)}{dr} = -cL(z,\theta,\phi) + L^*(z,\theta,\phi)$$

where L is radiance, r is distance between source and receiving point,
c is the beam attenuation coefficient, θ is angle from the zenith, and
ϕ is azimuth angle

The latter term [$L^*(z,\theta,\phi)$] is known as the path function, being the double integral of the product of the radiance and the volume scattering function; it decreases with depth at the rate of the diffuse attenuation coefficient:

$$L^*(z,\theta,\phi) = \int_{\phi'=0}^{2\pi} \int_{\theta'=0}^{\pi} \beta(\theta,\phi;\theta',\phi')\, L(z,\theta',\phi') \sin\theta' d\theta' d\phi'$$

For an optically uniform medium this can be integrated along (z,θ,ϕ,r) to give the apparent radiance:

$$L^*(z,\theta,\phi) = L_0(z_t,\theta,\phi)\, e^{-cr} + \int_0^r L^*(z',\theta,\phi)\, e^{-c(r-r')} dr'$$

which becomes:

$$L_r(z,\theta,\phi) = L_0(z_t,\theta,\phi)\, e^{-cr} + \frac{L^*(z,\theta,\phi)}{c + K\cos\theta}\left(1 - e^{-(c+K\cos\theta)r}\right)$$

For a path directed at zenith, this gives:

$$L(z) = L_0 e^{-cz} + \frac{L^*(z)}{c-K}(1 - e^{-(c-K)z})$$
$$= L_0 e^{-cz} + \frac{L^*(0)\, e^{-kz}}{c-K}(1 - e^{-(c-K)z})$$

As depth increases below the surface, the amount of light present decreases. This decrease can be quantified as the ratio of the radiant flux lost from a beam to the incident flux, which is known as *attenuance*. If the attenuating processes are uniform in all directions, the rate of decrease of upward irradiance is equal to that of downward irradiance, although at a lower level of energy. This 'loss' is due to both absorption, where photons are effectively extinguished, and scattering, where the photon is redirected. It is generally accepted that attenuation is due only to these two processes, and that they are additive, so that the attenuation coefficient can be defined as the internal attenuance of a infinitesimally thin layer of the medium normal to the beam, divided by the thickness of the layer (Δr):

$$c = \frac{-\Delta\Phi_c / \Phi_0}{\Delta r} = a + b$$

where a is the absorption coefficient and b is the scattering coefficient, both in m^{-1}.

The absorption coefficient (a) is defined as the absorptance (A) of an infinitesimally thin layer of the medium normal to the beam, divided by the thickness of the layer (r),

$$a = -\frac{\Delta A}{\Delta r}$$

while absorptance is the ratio of the radiant flux lost from a beam by means of absorption (Φ_a), to the incident flux (Φ_o).

$$A = \frac{\Phi_a}{\Phi_o}$$

Scatterance (B) is the radiant flux scattered from a beam (Φ_b), to the incident flux:

$$B = \frac{\Phi_b}{\Phi_o}$$

Thus, the total scattering coefficient (b) if the scatterance of an infinitesimally thin layer of the medium normal to the beam, divided by the thickness of the layer.

$$b = \frac{\Delta B}{\Delta r}$$

Preisendorfer (1959) categorized optical properties as either *apparent* or *inherent*. Apparent properties are those which are affected by changes in the radiance distribution, while inherent properties are independent of this. Thus, attenuation, absorption and scattering coefficients are all inherent properties, as is the volume

scattering function, as they are not affected by the direction of the light nor its intensity, while radiance and irradiance are apparent.

The refractive index is "the phase velocity of radiant energy in free space divided by the phase velocity of the same energy in a specified medium".

All definitions are taken from Jerlov (1968), and Morel and Smith (1982).

APPENDIX III

IRM 1 Calibration Curves

Response curves for each channel + diffuser effect

Response curves compensated for the effect of the diffuser

Normalised response curves to allow comparison of half-band widths

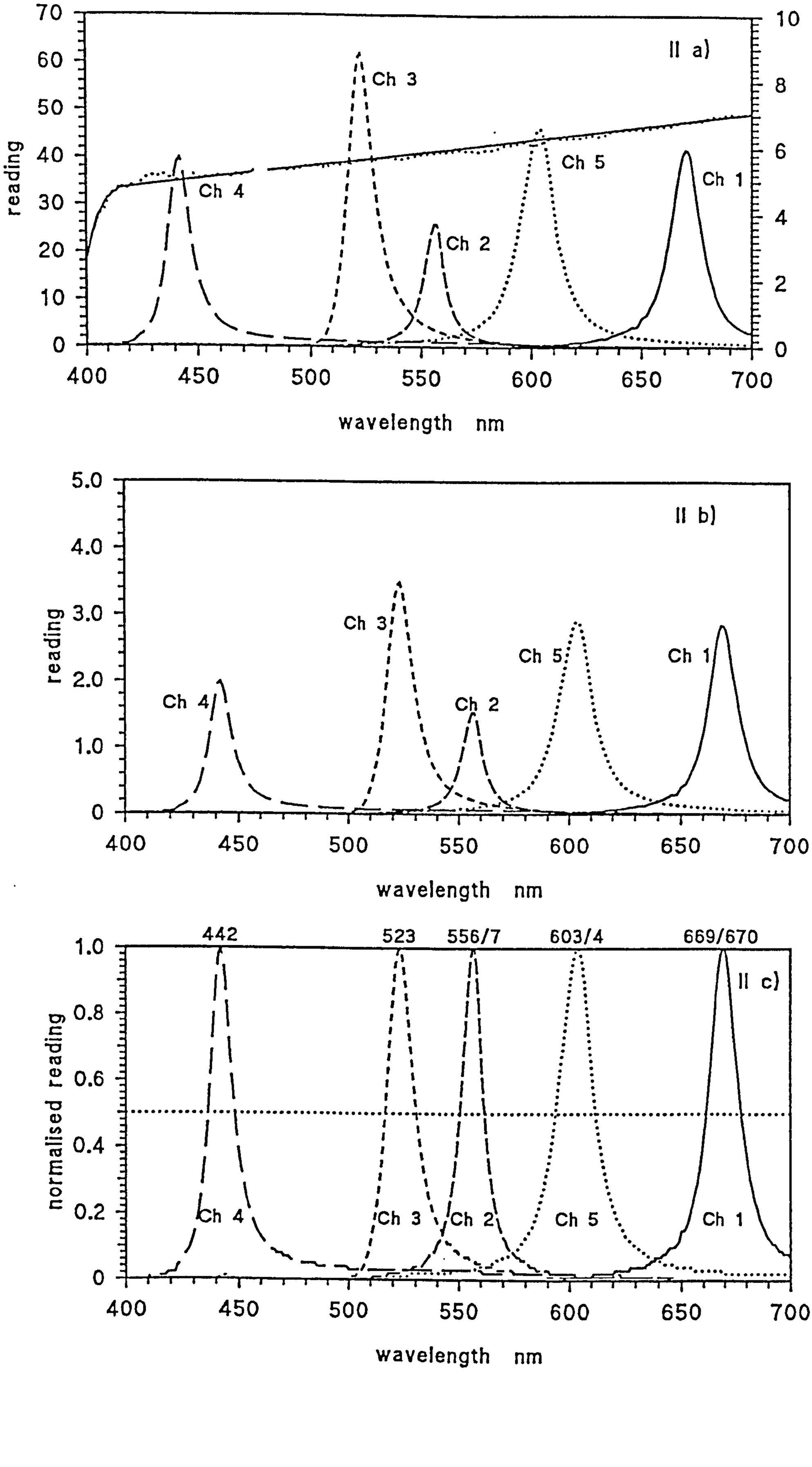
II a)
reading
Ch 3
Ch 4
Ch 2
Ch 5
Ch 1
70
60
50
40
30
20
10
0
10
8
6
4
2
0
400
450
500
550
600
650
700
wavelength nm
II b)
reading
Ch 3
Ch 5
Ch 1
Ch 4
Ch 2
5.0
4.0
3.0
2.0
1.0
0
400
450
500
550
600
650
700
wavelength nm
II c)
normalised reading
442
523
556/7
603/4
669/670
Ch 4
Ch 3
Ch 2
Ch 5
Ch 1
1.0
0.8
0.6
0.4
0.2
0
400
450
500
550
600
650
700
wavelength nm

APPENDIX IV

Comparison of Spectron Data

taken With and Without a Pipe

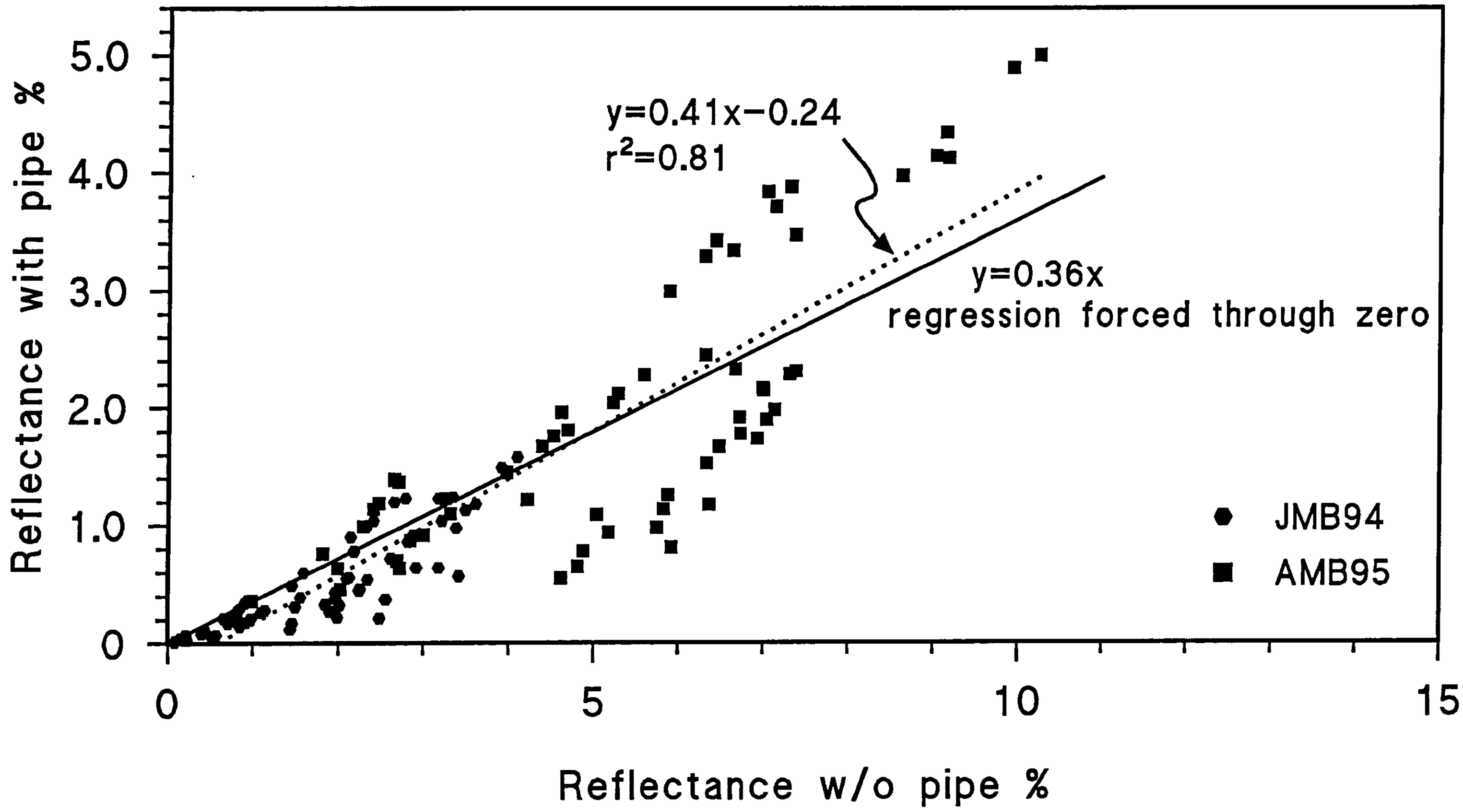
y=0.41x−0.24
r²=0.81
y=0.36x
regression forced through zero
JMB94
AMB95
Reflectance with pipe %
Reflectance w/o pipe %
0
1.0
2.0
3.0
4.0
5.0
0
5
10
15

APPENDIX V

Comparison of Yellow Substance

Measurements using a Membrane Filter

or a GF/F Filter

These measurements were taken on water
samples from the Conwy River

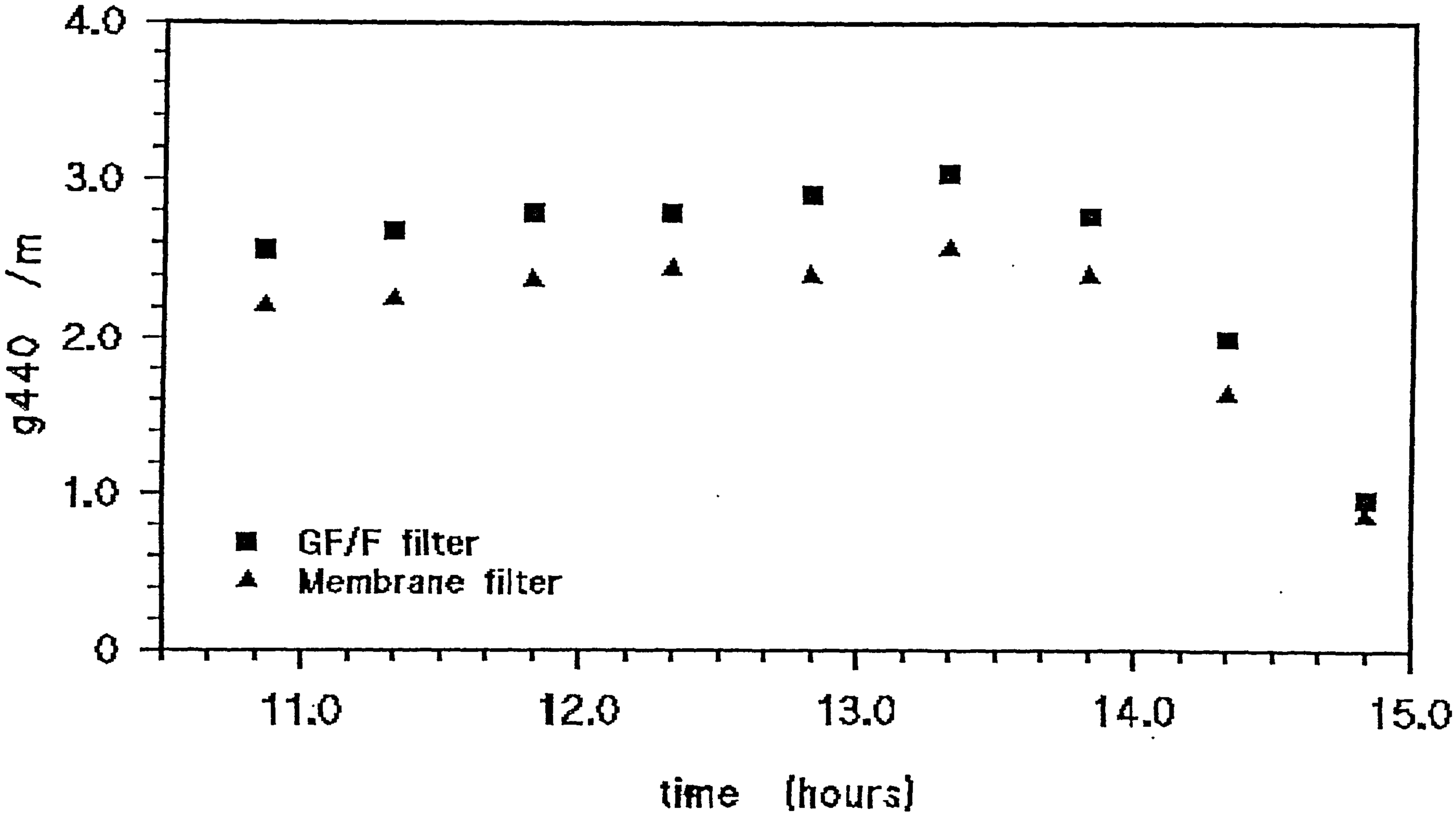
4.0
3.0
2.0
1.0
0
g440 /m
GF/F filter
Membrane filter
11.0
12.0
13.0
14.0
15.0
time (hours)

APPENDIX VI

Comparison of Spectra

with Filter over Spectrophotometer

Source or Receptor

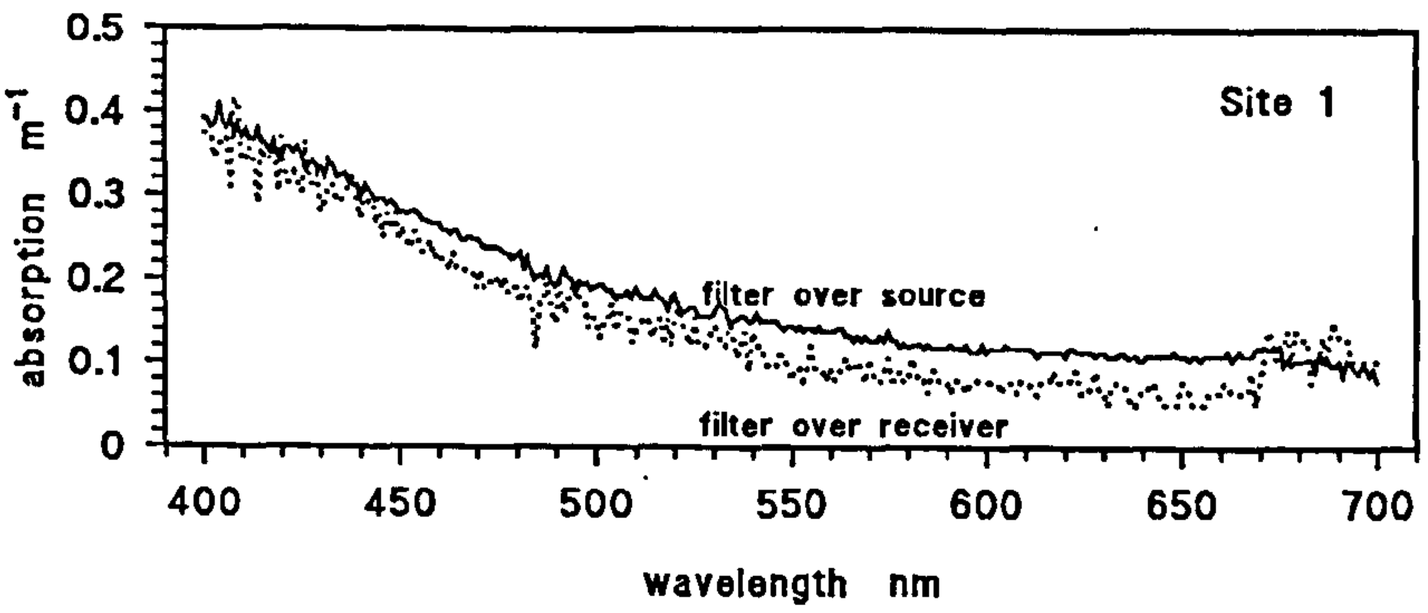
Site 1
filter over source
filter over receiver
absorption m⁻¹
0.5
0.4
0.3
0.2
0.1
0
400
450
500
550
600
650
700
wavelength nm

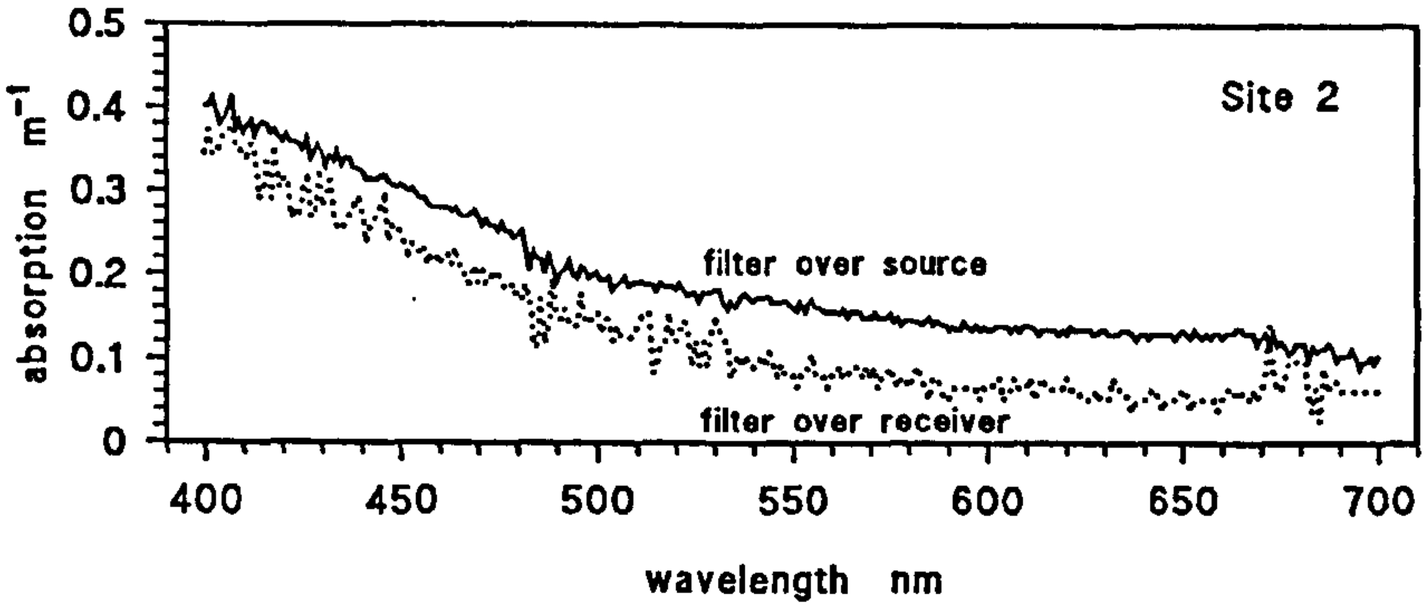
Site 2
filter over source
filter over receiver
absorption m⁻¹
0.5
0.4
0.3
0.2
0.1
0
400
450
500
550
600
650
700
wavelength nm

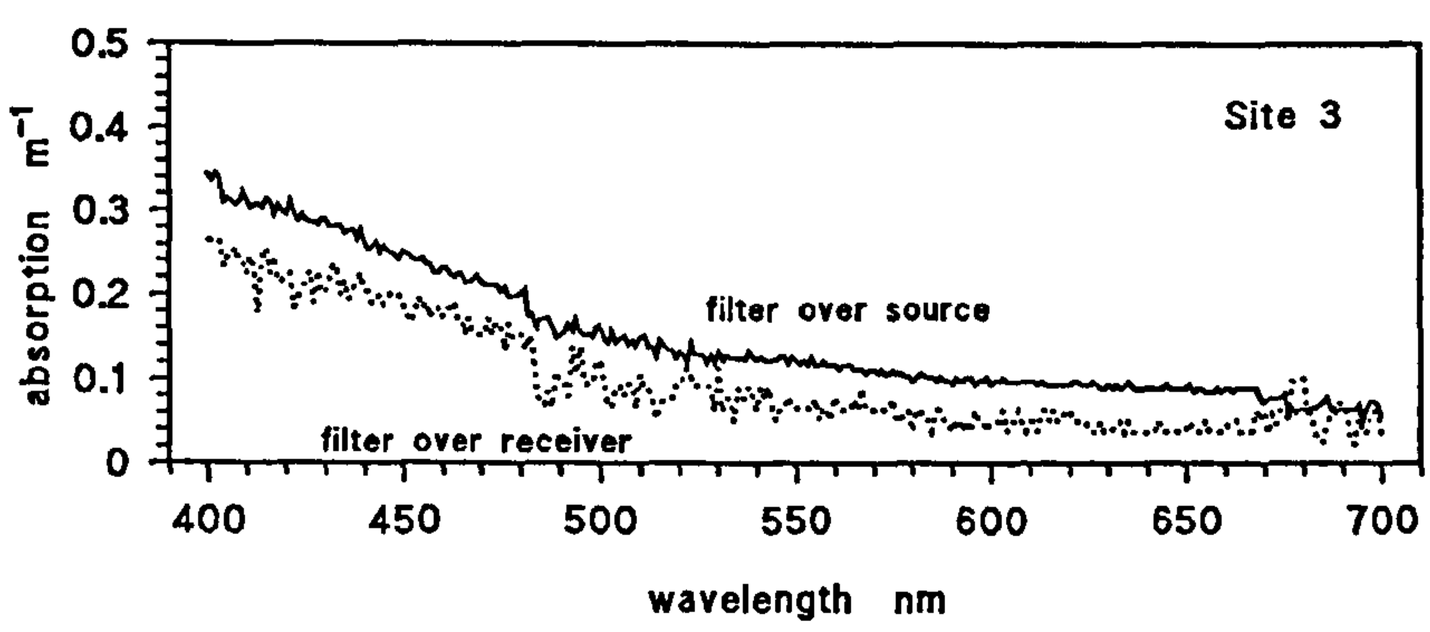
Site 3
filter over source
filter over receiver
absorption m⁻¹
0.5
0.4
0.3
0.2
0.1
0
400
450
500
550
600
650
700
wavelength nm

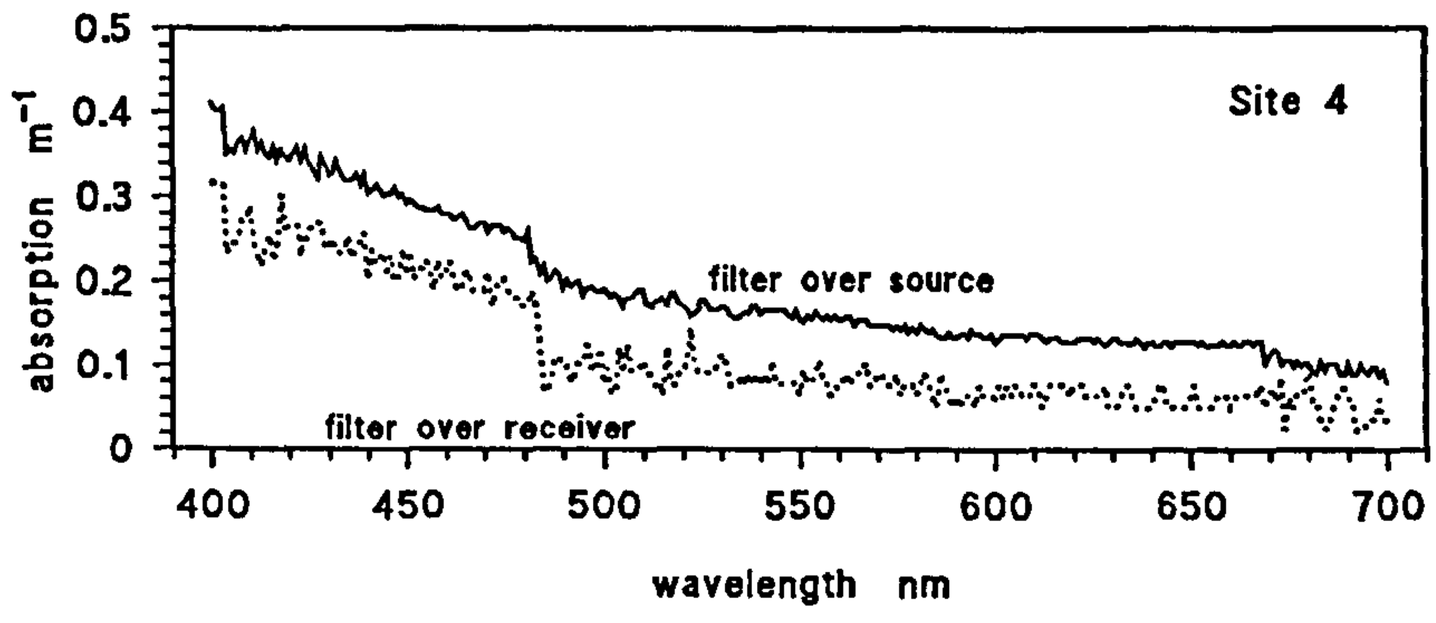
Site 4
filter over source
filter over receiver
absorption m⁻¹
0.5
0.4
0.3
0.2
0.1
0
400
450
500
550
600
650
700
wavelength nm

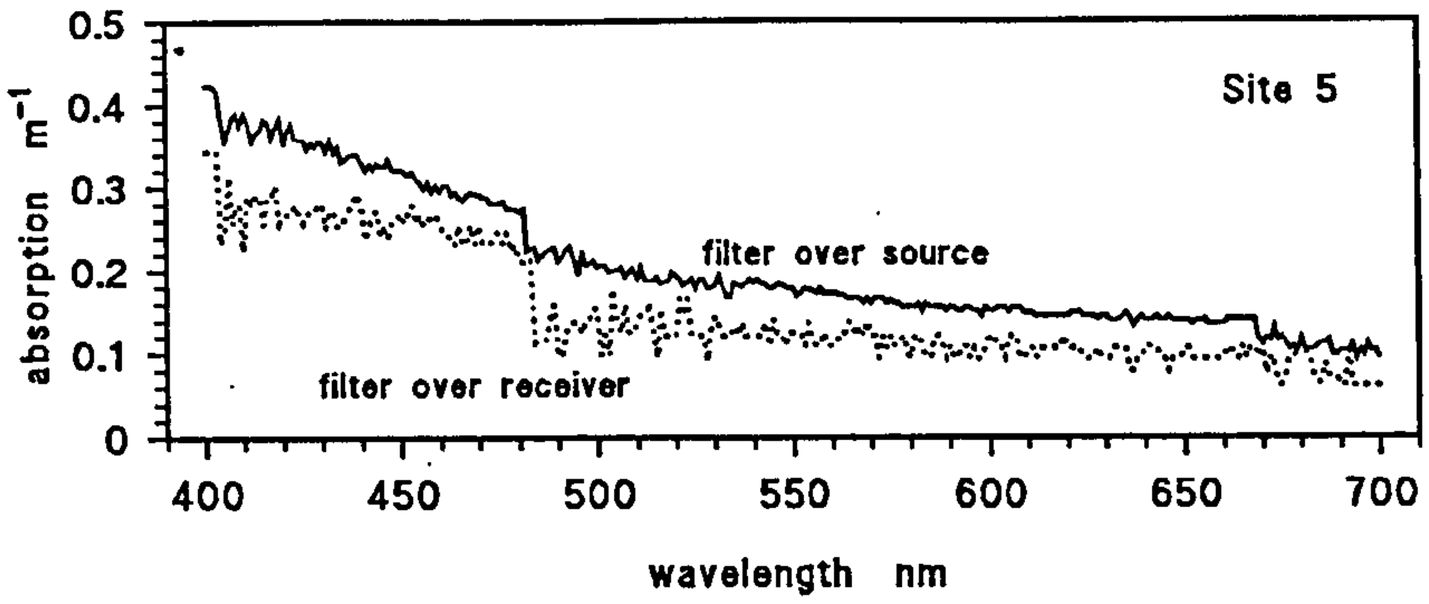
Site 5
filter over source
filter over receiver
absorption m⁻¹
0.5
0.4
0.3
0.2
0.1
0
400
450
500
550
600
650
700
wavelength nm

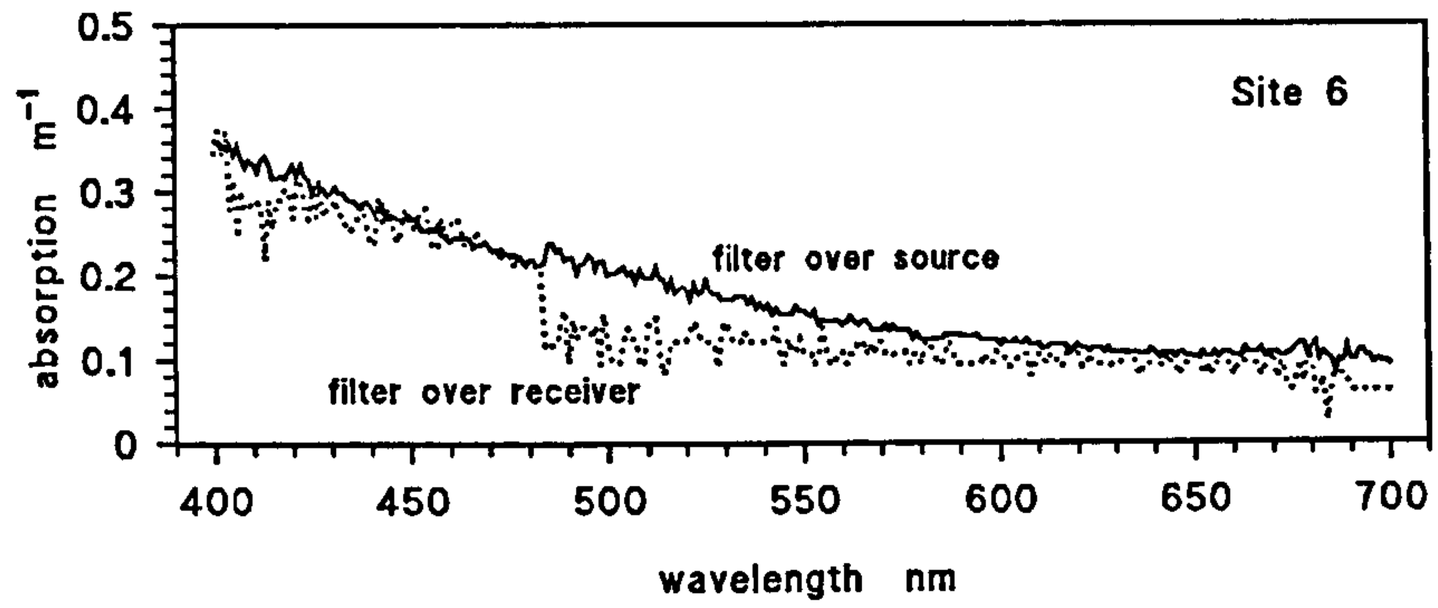
Site 6
filter over source
filter over receiver
absorption m⁻¹
0.5
0.4
0.3
0.2
0.1
0
400
450
500
550
600
650
700
wavelength nm

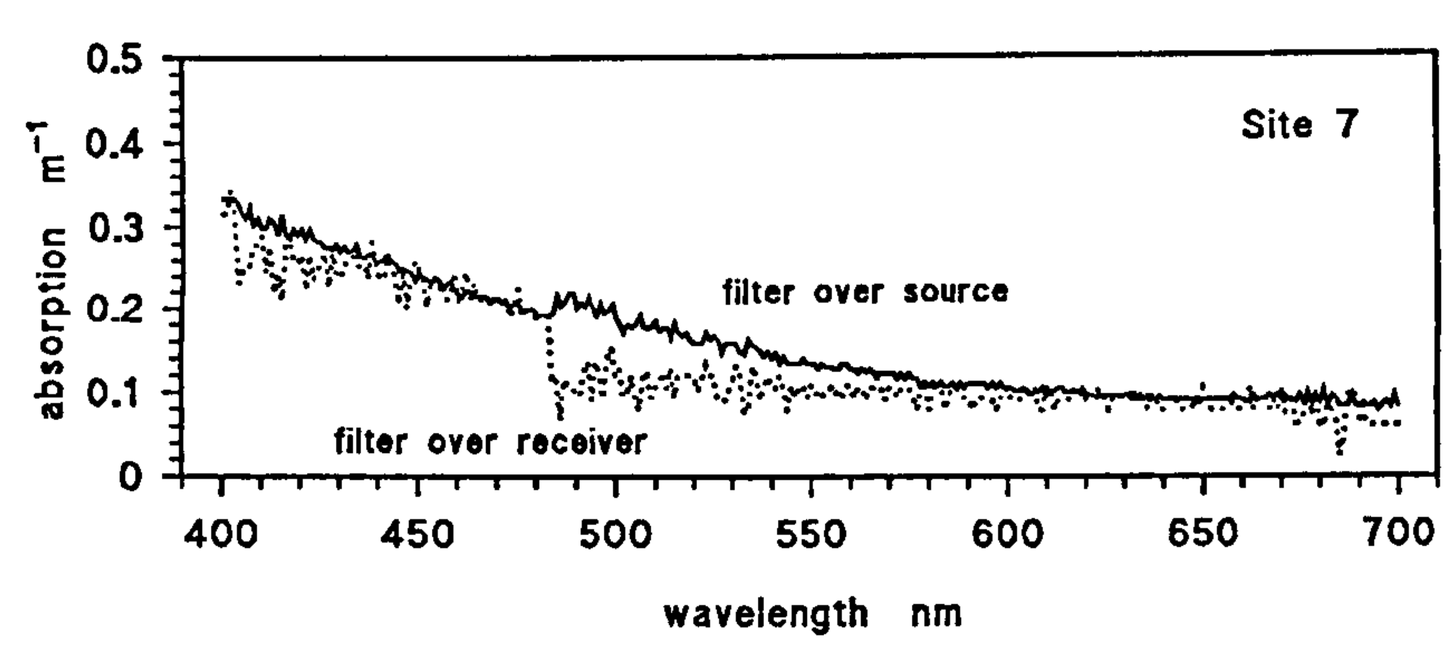
Site 7
filter over source
filter over receiver
absorption m⁻¹
0.5
0.4
0.3
0.2
0.1
0
400
450
500
550
600
650
700
wavelength nm

Site 8
filter over source
filter over receiver
absorption m⁻¹
0.5
0.4
0.3
0.2
0.1
0
400
450
500
550
600
650
700
wavelength nm

APPENDIX VII

Raw Data

Menai Strait: Constituent Concentrations
Diffuse attenuation and Reflectance

Other Sites: Constituent Concentrations
Diffuse attenuation and Reflectance

MENAI STRAIT SURVEY 1993-1994

MINERAL SUSPENDED SOLIDS

	1	2	3	4	5	6	7	8	9	10	ave	std dev	% std dev
November		19.95	25.22	24.13	12.07	7.54	22.27	23.07	27.23	18.16	19.958	6.079	30.46
December	35.43	18.16	14.05	16.56	25.23	22.69	22.37	23.35	20.38	33.19	23.139	6.445	27.86
January				12.00	11.33	9.64	7.70	9.41			10.017	1.516	15.13
February	8.57	15.89	7.36	4.22	8.30	6.91	7.48	9.64	9.88	9.90	8.813	2.865	32.51
March	7.34	10.35	3.88	5.53	6.85	8.68	6.13	7.08	7.33	7.63	7.079	1.652	23.33
May	24.05	14.43	4.69	10.22	3.08	7.48	1.62	6.10	40.85	3.95	11.648	11.602	99.61
June	16.68	15.19	-1.13	4.26	-6.58	-2.43	-4.54	1.96	-1.96	-4.48	1.697	7.727	455.30
July	1.40	1.75	1.74	2.21	3.65	2.51	2.68	7.03	2.76	4.45	3.016	1.597	52.94
August	1.77	3.69	1.46	2.55	2.00	1.05	3.82	2.64	1.47	2.04	2.247	0.881	39.21
October		5.38	8.31	7.50	7.86	3.76	5.18	5.88	6.15	7.06	6.341	1.385	21.83

TOTAL SUSPENDED SOLIDS

	1	2	3	4	5	6	7	8	9	10	ave	std dev	% std dev
November		23.93	29.04	28.47	15.07	8.90	26.07	27.14	31.89	21.94	23.606	6.932	29.36
December	39.34	21.81	18.03	19.67	28.43	26.62	26.64	27.41	24.46	38.80	27.118	6.792	25.05
January				13.82	14.41	12.79	10.03	12.44			12.699	1.509	11.89
February	12.52	23.82	13.69	8.13	13.16	11.61	14.13	15.46	13.91	15.44	14.185	3.789	26.71
March	11.19	15.02	8.82	8.65	11.03	11.87	11.82	12.23	12.54	12.75	11.591	1.771	15.28
May	32.26	22.85	14.67	19.16	9.12	11.59	9.38	14.27	53.45	11.36	19.811	13.098	66.11
June	18.91	26.68	5.79	14.30	5.47	9.54	8.42	9.79	8.47	7.14	11.451	6.376	55.68
July	6.26	6.42	5.72	5.77	7.45	5.86	6.71	11.39	6.44	8.67	7.069	1.671	23.65
August	8.77	7.58	6.95	7.21	5.02	6.00	7.90	5.78	5.76	6.45	6.742	1.092	16.19
October		9.08	14.78	12.12	10.22	9.80	10.05	11.54	10.83	12.41	11.204	1.637	14.61

GELBSTOFF													
	1	2	3	4	5	6	7	8	9	10	ave	std dev	% std dev
November	0.151	0.634	0.195	0.280	0.335	0.267	0.181	0.313	0.294	0.163	0.281	0.133	47.31
December	0.294	0.301	0.163	0.405	0.095	0.360	0.981	0.240	0.256	0.202	0.330	0.234	70.84
January				0.200	0.361	0.437	0.241	0.223			0.292	0.091	31.18
February	0.256	0.421	0.353	0.309	0.316	0.215	0.413	0.356	0.420	0.332	0.339	0.066	19.37
March	0.566	0.368	0.282	0.291	0.393	0.459	0.280	0.509	0.158	0.517	0.382	0.124	32.41
May	0.385	0.183	0.361	0.054	0.310	0.562	0.278	0.323	0.122	0.072	0.265	0.150	56.77
June	0.531	0.359	0.341	0.350	0.299	0.337	0.339	0.347	0.387	0.283	0.357	0.064	17.95
July	0.184	0.184	0.184	0.138	0.253	0.207	0.161	0.184	0.184	0.184	0.187	0.028	15.07
August	0.184	0.230	0.184	0.230	0.207	0.253	0.230	0.253	0.276	0.253	0.230	0.029	12.65
October		0.366	0.338	0.370	0.417	0.424	0.411	0.424	0.357	0.387	0.388	0.030	7.69

CHLOROPHYLL AND ASSOCIATED PIGMENTS													
	1	2	3	4	5	6	7	8	9	10	ave	std dev	% std dev
November	0.06	1.01	1.02	1.22	0.99	1.17	1.33	1.15	0.92	0.65	0.950	0.347	36.49
December	1.03	0.86	0.63	0.80	0.92	1.11	0.92	0.84	0.81	1.07	0.899	0.139	15.44
January				0.73	0.66	0.69	0.55	0.49			0.623	0.088	14.16
February	1.20	0.79	0.93	0.86	0.86	0.56	0.57	0.72	0.58	0.90	0.798	0.189	23.64
March	2.35	2.67	2.08	1.89	1.16	0.93	0.70	1.07	1.05	0.97	1.486	0.657	44.21
May	14.83	18.69	17.67	16.32	14.65	15.57	16.40	16.52	14.25	14.11	15.900	1.432	9.01
June	12.91	12.84	11.78	13.54	12.49	11.65	13.57	12.84	11.82	9.67	12.311	1.096	8.91
July	1.93	2.01	1.46	1.89	1.37	1.61	1.33	1.55	1.23	1.17	1.554	0.284	18.28
August	4.77	4.99	5.31	3.31	5.40	3.48	3.29	3.43	2.78	2.95	3.971	0.970	24.42
October		1.76	2.19	1.81	1.10	0.91	1.14	1.60	1.00	0.96	1.386	0.435	31.36

			Chlorophyl pigment g/m3	Yellow Substance /m	TSS mg/l	MSS mg/l	Secchi Depth m
Cardigan Bay							
24/06/94		1	0.899	0.420	5.119	2.085	5
		2	0.994	0.452	6.135	2.100	5
30/06/94		1	0.092	0.372	7.904	4.100	5.5
		2	0.503	0.259	6.472	3.300	5
		3	0.325	0.248	8.064	4.665	5
		4	0.597	0.253	7.194	3.810	4.5
		5	0.671	0.588	9.138	5.290	4.5
		6	0.766	0.429	8.377	4.675	4.5
Clyde Sea							
22/02/94		1	0.905	0.301	0.293	0.097	
24/02/94		2	0.757	0.393	0.206	0.023	
Clyde Sea and Estuary							
	CS1		0.890	0.089	2.180	1.027	
	CS4		0.350	0.115	3.540	2.493	
	CE6		1.740	1.570	7.220	4.550	
	CE5		0.550	0.393	4.280	2.830	
	CE4		1.470	0.225	2.980	1.933	4.5
	CE3		3.150	0.268	3.847	2.560	4
	LR1		1.320	0.209	4.547	2.020	8
	IW1		1.740	0.163	2.500	0.467	6
Pier Survey - July 1994							
11/07/94	surface		1.827	0.165	6.850	3.280	2.7
12/07/94	surface		2.685	0.202	6.670	3.050	2.8
13/07/94	surface		3.072	0.405	6.030	1.890	2.8
14/07/94	surface		4.723	0.257	6.970	3.100	2.5
15/07/94	surface		6.691	0.211	5.030	1.410	2.3
16/07/94	surface		8.364	0.275	3.420	0.070	1.95
17/07/94	surface		8.511	0.327	3.300	0.130	2.2
18/07/94	surface		6.516	0.326	3.180	0.000	2
19/07/94	surface		6.385	0.333	3.300	0.310	2
20/07/94	surface		3.844	0.265	3.180	0.030	
21/07/94	surface		3.600	0.391	6.790	3.300	2
22/07/94	surface		3.294	0.193	6.360	3.200	1.9
23/07/94	surface		2.851	0.200	5.650	2.790	2.2
24/07/94	surface		3.300	0.200	5.910	3.100	2.1
25/07/94	surface		2.300	0.345	6.030	3.220	2.05
21/08/95	surface		1.375	0.184	1.715	-0.595	
21/08/95	mid		1.451	0.184	2.635	0.120	
22/08/95	surface		2.953	0.230	2.163	-0.817	4.25
23/08/95	surface		3.026	0.150	32.835	24.860	3.75
23/08/95	mid		2.971	0.161	6.220	2.805	
24/08/95	surface		3.062	0.092	5.703	2.230	2.7
25/08/95	surface		2.734	0.138	6.047	2.857	2.5
26/08/95	surface		3.062	0.138	9.007	5.593	1.75
27/08/95	surface		2.515	0.115	9.583	6.660	1.5
28/08/95	surface		2.679	0.092	12.600	9.030	1.4
29/08/95	surface		2.060	0.161	38.817	29.180	1.4
29/08/95	mid		2.406	0.138	15.640	10.245	
30/08/95	surface		2.406	0.046	13.177	8.463	1.5
31/08/95	surface		1.330	0.069	11.450	6.720	1.9
31/08/95	mid		1.604	0.069	8.650	5.020	
01/09/95	surface		1.422	0.023	7.223	3.257	2.4
02/09/95	surface		1.422	0.046	4.900	2.077	3.2
03/09/95	surface		1.877	0.115	4.730	1.087	4

			Chlorophy pigment g/m3	Yellow Substance /m	TSS mg/l	MSS mg/l
Cwmystadllyn						
		11:35	1.244	0.341	2.490	0.000
		11:35	1.299	0.334	2.180	0.000
		11:35	1.271	0.338	2.060	0.000
		12:00	1.449	0.368	1.320	0.000
		12:00	1.476	0.281	2.605	0.000
		12:30	1.230	0.346	1.650	0.000
		12:30	2.012	0.379	2.200	0.000
		13:00	1.750	0.402	3.027	0.000
		13:00	1.947	0.401	4.047	0.747
		13:30	1.728	0.298	3.013	0.120
		13:30	2.165	0.354	3.287	0.000
	31/03/96	11:00	0.950	0.181	3.890	1.513
		11:00	1.945	0.162	2.730	0.560
		11:30	1.945	0.161	2.730	0.573
		11:30	1.282	0.165	2.560	0.320
		12:00	1.282	0.170	2.830	0.833
		12:00	0.664	0.170	2.910	0.753
		12:30	1.284	0.198	3.520	0.730
		12:30	1.041	0.198	3.900	0.750
		12:30	1.163	0.198	5.170	1.920
		13:00	1.616	0.230	1.790	0.000
		13:00	1.900	0.230	2.990	0.000
		13:00	1.758	0.230	3.360	0.180
Dolgarrog						
		11:45	14.135	2.146	18.050	12.100
		11:45	10.368	3.826	19.420	12.360
		11:45	12.649	3.510	20.350	12.610
		12:15	53.899	2.418	160.340	135.860
		12:15	27.994	3.130	151.880	122.720
		12:15	26.266	2.826	163.720	135.360
		12:45	15.552	1.725	109.120	85.160
		12:45	56.104	2.157	124.840	100.160
		12:45	43.419	2.167	113.080	88.160
		13:15	46.789	1.830	67.720	49.160
		13:15	44.237	1.708	67.480	47.960
		13:15	43.865	1.881	63.600	45.120
	26/03/96	14:30	5.435	1.361	51.300	40.160
		14:30	7.202	1.453	73.850	58.730
		14:30	11.840	1.407	50.000	35.540
		15:00	3.798	1.307	25.880	9.750
		15:00	2.850	1.307	18.160	6.960
		15:00	3.798	1.307	18.240	7.280
		15:30	5.435	1.318	36.320	23.280
		15:30	6.254	1.318	21.840	9.640
		15:30	6.254	1.318	19.120	11.920
		16:00	4.610	2.102	13.180	3.760
		16:00	7.754	1.258	9.200	0.000
		16:00	4.617	1.258	9.020	3.180
Vestfjorden						
	29/09/94	V2121	0.128	0.051	4.070	-
		V2125	0.103	0.000	1.560	-
		V2129	0.179	0.166	1.465	-
	30/09/94	M1606	0.065	0.340	1.870	-
		M1506	0.085	0.140	1.600	-
		M1406	0.090	0.087	1.780	-
	01/10/94	M2506	0.058	0.030	1.120	-
		M2306	0.103	0.027	1.515	-
		M2206	0.108	0.020	2.070	-
		M2106	0.121	0.000	1.285	-
	02/10/94	M1906	0.066	0.052	1.400	-
		M1906	0.074	0.073	2.750	-
	03/10/94	M1906	0.126	0.200	1.905	-
		M1908	0.091	0.132	2.375	-
		M1909	0.099	0.037	1.845	-

			Diffuse attenuation Kd /m										Reflectance %									
	Date	Station/time	412	444	490	510	521	552	570	596	670	PAR/700	412	444	490	510	521	552	570	596	670	PAR	Instrument
Pier Survey	11/07/94		-	0 86	-	-	0.55	0.51	-	0.61	0.80	-	-	2.53	-	-	5.37	5.55	-	4.50	1.69	-	IRM1
July 1994	12/07/94		-	0.84	-	-	0.66	0.58	-	0.68	0.94	-	-	2.72	-	-	4.47	4.78	-	3.37	1.65	-	
	13/07/94		-	0.76	-	-	0.59	0.53	-	0.61	0.88	-	-	2.00	-	-	3.03	3.36	-	2.67	1.30	-	
	14/07/94		-	0.94	-	-	0.66	0.61	-	0.78	0 97	-	-	3.10	-	-	3.75	4.71	-	3.35	1.66	-	
	15/07/94		-	0.91	-	-	0.62	0.57	-	0.66	0.95	-	-	3.34	-	-	5.50	5.97	-	4 99	2.20	-	
	18/07/94		-	0.87	-	-	0.52	0.43	-	0.41	0.68	-	-	5.45	-	-	10.77	13.88	-	10.10	5 50	-	
	19/07/94		-	0.58	-	-	0.27	0.17	-	0.24	0.42	-	-	6.98	-	-	13.13	17.40	-	12.58	8.43	-	
	22/07/94		-	0.89	-	-	0.62	0.58	-	0.69	0.99	-	-	3.49	-	-	4.61	5.85	-	3.00	2.14	-	
Pier Survey	11/07/94		-	1.07	1.17	-	-	-	0.70	-	0.98	-	-	2.71	2.43	-	-	-	14.70	-	6.76	-	CS
July 1994	12/07/94		-	0.88	0.69	-	-	-	0.55	-	0.94	-	-	1.20	6.00	-	-	-	5.12	-	8.52	-	
calculated	13/07/94		-	0.83	0.57	-	-	-	0.39	-	0.74	-	-	0.01	0.98	-	-	-	1.61	-	0.70	-	
over whole	14/07/94		-	0.96	0.65	-	-	-	0.52	-	0.82	-	-	6.77	1.96	-	-	-	2.07	-	1.33	-	
day	15/07/94		-	0.94	0.78	-	-	-	0.56	-	0.94	-	-	23.01	4.84	-	-	-	4.55	-	6.64	-	
	16/07/94		-	1.17	0.79	-	-	-	0.53	-	0.95	-	-	0.15	1.13	-	-	-	2.15	-	0.91	-	
	17/07/94		-	1.61	1.00	-	-	-	0.71	-	1.17	-	-	0.29	1.28	-	-	-	2.80	-	1.05	-	
	18/07/94		-	1.25	1.06	-	-	-	0.82	-	1.28	-	-	0.78	3.52	-	-	-	4.35	-	3.77	-	
	19/07/94		-	1.23	1.06	-	-	-	0.87	-	1.26	-	-	0.59	1.79	-	-	-	1.96	-	1.63	-	
	20/07/94		-	1.01	0.95	-	-	-	0.87	-	1.06	-	-	1.12	1.78	-	-	-	2.06	-	1.26	-	
	21/07/94		-	0.79	0.69	-	-	-	0.60	-	0.89	-	-	0.02	0.95	-	-	-	2.12	-	0.67	-	
	22/07/94		-	0.75	0.78	-	-	-	0.61	-	0.89	-	-	10.87	5.14	-	-	-	4.97	-	5.22	-	
	23/07/94		-	0.78	0.81	-	-	-	0.66	-	0.97	-	-	2.67	1.93	-	-	-	2.08	-	1.68	-	
	24/07/94		-	0.90	0.76	-	-	-	0.70	-	0.92	-	-	0.66	9.26	-	-	-	8.45	-	12.08	-	
	25/07/94		-	1.15	0.87	-	-	-	0.72	-	1.06	-	-	28.70	13.65	-	-	-	10.04	-	15.73	-	
Pier Survey	11/07/94		-	0.00	0.00	-	-	-	0.06	-	0.07	-	-	0.00	0.00	-	-	-	2.61	-	0.91	-	CS
July 1994	12/07/94		-	1.01	0.69	-	-	-	0.53	-	0.99	-	-	0.03	1.03	-	-	-	2.23	-	0.63	-	
calculated	13/07/94		-	0.90	0.63	-	-	-	0.45	-	0.81	-	-	0.02	1.33	-	-	-	2.22	-	0.86	-	
over midday	14/07/94		-	1.11	0.72	-	-	-	0.58	-	0.89	-	-	0.16	0.97	-	-	-	2.25	-	0.61	-	
	15/07/94		-	0.99	0.76	-	-	-	0.49	-	0.92	-	-	0.00	1.33	-	-	-	3.10	-	1.01	-	
	16/07/94		-	1.17	0.83	-	-	-	0.52	-	1.00	-	-	0.17	1.34	-	-	-	2.72	-	1.08	-	
	17/07/94		-	1.61	1.07	-	-	-	0.71	-	1.24	-	-	0.29	1.34	-	-	-	2.55	-	1.01	-	
	18/07/94		-	1.25	1.08	-	-	-	0.84	-	1.31	-	-	0.78	1.57	-	-	-	2.83	-	1.00	-	
	19/07/94		-	1.19	1.07	-	-	-	0.83	-	1.27	-	-	0.55	1.19	-	-	-	2.17	-	0.87	-	
	20/07/94		-	1.04	0.96	-	-	-	0.86	-	1.04	-	-	0.91	1.81	-	-	-	2.92	-	1.19	-	
	21/07/94		-	0.87	0.69	-	-	-	0.62	-	0.88	-	-	0.06	1.67	-	-	-	3.24	-	1.03	-	
	22/07/94		-	1.14	1.05	-	-	-	0.81	-	1.22	-	-	1.79	2.67	-	-	-	3.72	-	1.71	-	
	23/07/94		-	1.77	0.93	-	-	-	0.83	-	1.13	-	-	2.25	2.12	-	-	-	2.85	-	1.97	-	
	24/07/94		-	1.77	1.16	-	-	-	0.95	-	1.41	-	-	2.25	3.80	-	-	-	4.75	-	2.98	-	
	25/07/94		-	1.77	0.59	-	-	-	0.74	-	0.70	-	-	2.25	2.95	-	-	-	4.14	-	2.11	-	

			Diffuse attenuation Kd /m										Reflectance %										
	Date	Station/time	412	444	490	510	521	552	570	596	670	PAR/700	412	444	490	510	521	552	570	596	670	PAR	Instrument
Pier Survey	27/08/95		1.49	1.28	0.87	0.99	-	0.88	-	-	1.17	1.29	0.50	0.90	2.49	1.97	-	2.52	-	-	1.04	0 83	Satlantic
August 1995	29/08/95		1.57	1.28	1.08	0.94	-	0.85	-	-	1.09	1.21	0.00	1.14	2.94	4.38	-	5.64	-	-	2.01	0.99	
Satlantic	30/08/95		1.37	1.14	0.87	0.85	-	0.76	-	-	1.03	1.15	1.09	3.25	7.23	8.10	-	10.47	-	-	3.04	2.39	
Kd and R	31/08/95		0.96	0.75	0.53	0.55	-	0.49	-	-	0.73	0.86	2.38	5.52	12.38	11.17	-	12.91	-	-	4.71	3.11	
	01/09/95		0.91	0.70	0.55	0.48	-	0.44	-	-	0.73	0.86	1.56	3.23	5.36	6.19	-	7.25	-	-	2.55	1.99	
	02/09/95		0.78	0.60	0.43	0.40	-	0.37	-	-	0.73	0.88	1.19	2.24	4.66	4.96	-	5.28	-	-	1.12	0.70	
Pier Survey	25/08/95		0.61	0.47	0.33	0.31	-	0.28	-	-	0.62	0.72	6.52	10.47	15.97	17.57	-	20.51	-	-	6.57	3.42	Satlantic/
August 1995	27/08/95		1.45	1.25	0.88	0.96	-	0.90	-	-	1.12	1.25	3.74	4.91	7.75	8.92	-	11.32	-	-	5.88	4.65	Spectron
Spectron R	29/08/95		1.62	1.18	1.08	0.91	-	0.82	-	-	1.05	1.17	13.09	18.54	21.21	22.12	-	26.12	-	-	20.73	17.84	
	30/08/95		1.39	1.11	0.88	0.80	-	0.76	-	-	1.00	1.10	5.24	7.91	11.65	12.98	-	16.24	-	-	7.98	5.72	
	31/08/95		0.96	0.76	0.54	0.55	-	0.49	-	-	0.73	0.85	16.77	21.05	23.56	24.20	-	26.34	-	-	21.05	19.87	
	01/09/95		0.93	0.68	0.56	0.48	-	0.44	-	-	0.72	0.84	4.33	6.30	9.29	10.15	-	12.23	-	-	5.02	3.47	
	02/09/95		0.79	0.60	0.43	0.40	-	0.37	-	-	0.73	0.88	6.25	9.67	16.77	19.23	-	23.34	-	-	8.17	5.93	
Vestfjorden	29/09/94	V2121	0.21	0.14	0.10	0.10	-	0.12	-	-	0.51	0.59	0.66	0.75	0.93	0.87	-	0.61	-	-	0.13	0.22	Satlantic
		V2125	0.23	0.16	0.12	0.12	-	0.13	-	-	0.53	0.67	0.68	0.79	0.94	0.87	-	0.65	-	-	0.14	0.20	
		V2129	0.25	0.18	0.14	0.14	-	0.15	-	-	0.54	0.68	0.59	0.66	0.79	0.75	-	0.61	-	-	0.14	0.23	
	30/09/94	M1606	0.18	0.14	0.10	0.11	-	0.12	-	-	0.51	0.64	0.83	0.93	1.12	1.06	-	0.70	-	-	0.11	0.20	
		M1506	0.16	0.12	0.08	0.08	-	0.10	-	-	0.46	0.58	0.95	1.11	1.48	1.43	-	0.95	-	-	0.19	0.33	
		M1406	0.15	0.12	0.08	0.09	-	0.10	-	-	0.44	0.58	1.00	1.08	1.25	1.16	-	0.74	-	-	0.15	0.25	
	01/10/94	M2506	0.20	0.13	0.09	0.09	-	0.10	-	-	0.48	0.61	0.72	0.86	1.13	1.07	-	0.71	-	-	0.13	0.17	
		M2306	0.20	0.14	0.09	0.09	-	0.10	-	-	0.40	0.53	0.72	0.88	1.12	1.06	-	0.77	-	-	0.23	0.37	
		M2206	0.23	0.17	0.12	0.12	-	0.14	-	-	0.51	0 67	0.63	0.74	0.89	0.81	-	0.58	-	-	0.09	0.13	
	02/10/94	M1906	0.32	0.27	0.21	0.21	-	0.23	-	-	0.57	0.68	0.62	0.68	0.95	0.90	-	0.64	-	-	0.23	0.35	
		M1806	0.26	0.19	0.14	0.14	-	0.16	-	-	0.55	0.72	0.62	0.75	0.99	0.90	-	0.65	-	-	0.10	0.15	
	03/10/94	M1906	0.26	0.18	0.13	0.13	-	0.14	-	-	0.55	0.66	0.57	0.61	0.97	0.91	-	0.66	-	-	0.12	0.19	
		M1907	0.23	0.17	0.13	0.13	-	0.14	-	-	0.51	0.65	0.63	0.73	0.88	0.79	-	0.54	-	-	0.09	0.13	
		M1908	0.22	0.16	0.12	0.12	-	0.14	-	-	0.50	0 64	0.75	0.87	1.04	0.93	-	0.65	-	-	0.13	0.19	
		M1909	0.23	0.16	0.11	0.12	-	0.13	-	-	0.48	0.59	0.62	0.75	0.97	0 88	-	0.59	-	-	0.16	0.31	

			Diffuse attenuation Kd /m										Reflectance %									
	Date	Station/time	412	444	490	510	521	552	570	596	670	PAR/700	412	444	490	510	521	552	570	596	670	PAR	Instrument
Cardigan	24/06/93	1	-	0.32	-	-	0.20	0.15	-	0.31	0.58	-	-	5.44	-	-	8 64	9.30	-	4.49	1.38	-	IRM1
		2	-	0.26	-	-	0.15	0.16	-	0.30	0.56	-	-	6.27	-	-	9.38	8.38	-	4.68	1.02	-	
	30/06/93	1	-	0.27	-	-	0.18	0.15	-	0.27	0.53	-	-	6.22	-	-	9.20	9.06	-	4.87	0.87	-	
		2	-	0.09	-	-	0.00	0.01	-	0.14	0.42	-	-	14.90	-	-	22.97	21.84	-	11.55	1.44	-	
		3	-	0.03	-	-	-0.08	-0.11	-	0.02	0.26	-	-	16.01	-	-	28.58	30.13	-	14.35	2.80	-	
		4	-	0.34	-	-	0.25	0.23	-	0.32	0.68	-	-	4.13	-	-	5.24	5.22	-	3.12	0.66	-	
		5	-	0.40	-	-	0.26	0 27	-	0.40	0.66	-	-	2.41	-	-	5.50	5.58	-	2.32	0.80	-	
		6	-	0.36	-	-	0.23	0.26	-	0.38	0.66	-	-	3.36	-	-	6.20	4.97	-	2.48	0.76	-	
Clyde	22/02/93	CS1	-	0.38	-	-	0.28	0.29	-	0.41	0.78	-	-	1.71	-	-	2.71	2.18	-	3.61	-	-	IRM1
	24/02/93	CS4	-	0.39	-	-	0.28	0.28	-	0.39	0.72	-	-	1.92	-	-	2.24	2.90	-	3.30	-	-	
	18/06/96	CS1	0.33	0.22	0.15	0.15	-	0.14	-	-	0.51	0.16	0.76	1.21	1.48	1.50	-	1.26	-	-	0.19	1.52	PRR-600
		CS4	0.39	0.27	0.16	0.15	-	0.15	-	-	0.50	0.17	0.75	1.24	2.09	2.20	-	1.79	-	-	0.24	2 00	
	19/06/96	CE6	2.65	2.26	1.61	1.40	-	1.13	-	-	1.13	1.15	-	-	-	-	-	-	-	-	-	-	
		CE5	1.04	0.68	0.46	0.42	-	0.37	-	-	0.67	0.43	1.42	1.32	2.62	3.06	-	3.58	-	-	1.25	3.26	
		CE4	0.74	0.52	0.30	0.27	-	0.23	-	-	0.58	0.32	-	-	-	-	-	-	-	-	-	-	
		CE3	0.73	0.42	0.24	0.23	-	0.21	-	-	0.60	0.23	0.27	1.27	2.03	2.31	-	1.85	-	-	0.55	1.68	
	20/06/96	LR1	0.68	0.43	0.27	0.25	-	0.22	-	-	0.54	0.25	0.53	1.27	1.91	2.24	-	2.19	-	-	0.62	2.34	
		LW1	0.55	0.34	0.19	0.18	-	0.16	-	-	0.55	0.18	0.49	1.16	2.53	2.38	-	2.91	-	-	0.29	2 84	
Cwmystradllyn	31/03/96	10:50	0.61	0.43	0.29	0.25	-	0.22	-	-	0.57	-	1.42	1.91	2.69	3.04	-	3.68	-	-	0.88	-	PRR-600
		11:00	0.53	0.35	0.20	0.17	-	0.13	-	-	0.51	-	0.86	1.26	2.02	2.38	-	3.05	-	-	0.46	-	
		11:30	0.55	0.36	0.21	0.17	-	0.14	-	-	0.53	-	0.86	1.28	2.03	2.39	-	3.12	-	-	0.50	-	
		12:00	0.55	0.37	0.21	0.18	-	0.15	-	-	0.53	-	0.87	1.29	2.03	2.38	-	3.07	-	-	0.49	-	
		12:15	0.58	0.40	0.25	0.22	-	0.18	-	-	0.56	-	1.53	2.01	2.78	3.12	-	3.78	-	-	0.89	-	
		12:30	0.53	0.34	0.19	0.16	-	0.12	-	-	0.51	-	0.91	1.35	2.12	2.49	-	3.21	-	-	0.52	-	
Dolgarrog	26/03/96	14:30	3.73	2.47	1.55	1.29	-	0.93	-	-	1.00	-	0.44	0.52	1.36	1.80	-	3.06	-	-	1.82	-	PRR-600
		14:50	3.74	2.41	1.60	1.34	-	0.98	-	-	1.05	-	0.44	0.91	1.22	2.63	-	4.52	-	-	2.74	-	
		15:20	3.70	2.52	1.59	1.33	-	0.97	-	-	1.03	-	0.48	0.90	1.97	2.57	-	4.00	-	-	2.51	-	
		15:50	3.61	2.41	1.50	1.25	-	0.90	-	-	0 97	-	0.51	0.91	2.11	2.68	-	3.99	-	-	2.54	-	
		16:10	3.64	2.44	1.51	1.28	-	0.91	-	-	0.99	-	0.49	0.90	2.09	2.62	-	3.91	-	-	2.54	-	
Loch Striven	19/04/94	1	-	0.55	-	-	0.40	0.35	-	0.41	0.73	-	-	0.00	-	-	0.00	0.00	-	1.59	0.00	-	IRM1
		2	-	0.75	-	-	0.47	0.40	-	0.46	0.88	-	-	0.00	-	-	2.23	3.49	-	2.40	0.75	-	
		M2	-	0.38	-	-	0.30	0.25	-	0.30	0.76	-	-	0.00	-	-	3.11	4.61	-	3.14	3.73	-	
	20/04/94	3	-	0.81	-	-	0.52	0.46	-	0.50	0.89	-	-	0.00	-	-	1.30	0.71	-	1.11	0.71	-	
		4	-	0.74	-	-	0.51	0.43	-	0.48	0.87	-	-	0.00	-	-	1.57	2.76	-	2.21	1.49	-	
		M4	-	0.50	-	-	0.42	0.37	-	0.44	0.66	-	-	2.83	-	-	2.36	3.16	-	2.33	1.43	-	
	21/04/94	M5	-	0.64	-	-	0.60	0.51	-	0.54	0.93	-	-	6.88	-	-	1.45	2.97	-	1.84	0.84	-	
		M6	-	0.53	-	-	0.58	0.57	-	0.53	0.84	-	-	1.83	-	-	1.50	1.56	-	2.00	1.11	-	

APPENDIX VIII

Exponents of Spectra from

Menai Strait Survey

Filter Spectra:

All particles

Inorganics

Cell Spectra

Water samples

Yellow Substance

		INORGANIC				
		slp	std err	const	std err	rsq
NOV17	2	-0.0127	0.00014	0.61592	0.20287	0.967
NOV17	3	-0.0123	0.00012	0.86155	0.18291	0.972
NOV17	4	-0.0124	0.00013	0.86259	0.18901	0.97
NOV18	5	-0.0132	0.00015	0.56956	0.22533	0.963
NOV18	6	-0.0146	0.00028	-0.1728	0.41724	0.903
NOV18	7	-0.0122	0.00011	1.34321	0.16006	0.978
NOV18	8	-0.0124	0.00012	1.00307	0.17889	0.973
NOV18	9	-0.0123	0.00011	1.20306	0.16823	0.976
NOV18	10	-0.0128	0.00013	0.70442	0.19995	0.969
DEC16	1	-0.0113	0.00011	1.57413	0.16708	0.972
DEC16	2	-0.0121	0.00014	1.05346	0.20763	0.962
DEC16	3	-0.0123	0.00014	0.98782	0.21586	0.961
DEC16	4	-0.0123	0.00015	0.90617	0.22162	0.959
DEC16	5	-0.011	0.00013	1.19433	0.18931	0.962
DEC16	6	-0.0115	0.00012	1.12507	0.18585	0.967
DEC16	7	-0.0115	0.00014	1.1644	0.20682	0.959
DEC16	8	-0.0117	0.00014	1.21804	0.21016	0.959
DEC16	9	-0.0112	0.00013	1.20222	0.19131	0.963
DEC16	10	-0.0114	0.00014	1.47267	0.20638	0.958
JAN25	4	-0.0125	0.00018	0.15583	0.26582	0.944
JAN25	5	-0.0128	0.00015	0.48843	0.22648	0.96
JAN25	6	-0.0128	0.0002	0.43828	0.30022	0.932
JAN25	7	-0.013	0.0002	0.44018	0.30758	0.931
JAN25	8	-0.0134	0.00022	0.53699	0.32433	0.928
FEB09	1	-0.011	0.00016	-0.0695	0.24381	0.939
FEB09	2	-0.0129	0.00025	0.69793	0.37081	0.902
FEB09	3	-0.0119	0.00024	0.00781	0.35298	0.895
FEB09	4	-0.0137	0.00042	0.11384	0.61567	0.785
FEB09	5	-0.0116	0.00028	0.48792	0.39041	0.869
FEB09	6	-0.012	0.00027	0.2707	0.40491	0.87
FEB09	7	-0.0121	0.00026	0.43616	0.3959	0.878
FEB09	8	-0.0119	0.00024	0.48283	0.36012	0.891
FEB09	9	-0.0123	0.00031	0.58514	0.47178	0.837
FEB09	10	-0.0121	0.00027	0.5161	0.40945	0.868
MAR10	1	-0.0115	0.00016	0.3351	0.23881	0.948
MAR10	2	-0.0121	0.00016	0.53401	0.24613	0.948
MAR10	3	-0.0129	0.00022	0.07667	0.33651	0.917
MAR10	4	-0.0132	0.00024	-0.0729	0.34504	0.91
MAR10	5	-0.0131	0.00023	0.2324	0.33993	0.918
MAR10	6	-0.0129	0.00028	0.33011	0.42339	0.874
MAR10	7	-0.0128	0.00025	0.251	0.37104	0.898
MAR10	8	-0.0124	0.0002	0.46566	0.30603	0.925
MAR10	9	-0.0133	0.00028	0.4049	0.42411	0.881
MAR10	10	-0.0125	0.00022	0.36511	0.3246	0.918
MAY18	1	-0.0109	0.00011	0.68369	0.16468	0.97
MAY18	2	-0.0115	0.00023	0.0338	0.35001	0.891
MAY18	3	-0.0114	0.00028	0.04347	0.3992	0.85
MAY18	4	-0.0118	0.00027	0.16618	0.37527	0.871
MAY18	5	-0.0117	0.00031	0.06307	0.43031	0.836
MAY18	6	-0.0119	0.00043	0.30107	0.62323	0.727
MAY18	7	-0.0105	0.00019	-0.1903	0.2473	0.916
MAY18	8	-0.0122	0.00045	-0.0874	0.63684	0.72
MAY18	9	-0.0129	0.00034	-0.1342	0.48372	0.836
MAY18	10	-0.0124	0.00036	-0.1187	0.48773	0.81
JUN10	1	-0.0114	0.00027	-0.5071	0.40381	0.858
JUN10	2	-0.0098	0.00018	-0.2369	0.26755	0.91
JUN10	3	-0.0092	0.00019	-0.8398	0.26714	0.892
JUN10	4	-0.008	0.00033	-0.6446	0.42685	0.687
JUN10	5	-0.0053	0.00038	-1.0254	0.51597	0.407
JUN10	6	-0.0107	0.00024	-0.234	0.33478	0.876
JUN10	7	-0.0106	0.00023	-0.3404	0.33807	0.877
JUN10	8	-0.0244	0.00093	-0.6553	0.9979	0.764
JUN10	9	-0.0105	0.00028	-0.6114	0.38739	0.835
JUN10	10	-0.0147	0.00041	-0.4755	0.56214	0.823
JUL27	1	-0.0121	0.00019	-0.238	0.27989	0.934
JUL27	2	-0.0132	0.00021	-0.1782	0.29977	0.934
JUL27	3	-0.0128	0.00019	-0.3061	0.27233	0.941
JUL27	4	-0.0115	0.00017	-0.1342	0.25676	0.938
JUL27	5	-0.0119	0.00017	-0.0545	0.25844	0.941
JUL27	6	-0.012	0.0002	-0.1309	0.30066	0.923
JUL27	7	-0.013	0.00026	-0.191	0.37869	0.895
JUL27	8	-0.0111	0.00016	0.29259	0.23472	0.944
JUL27	9	-0.0121	0.00028	-0.1144	0.42624	0.859
JUL27	10	-0.0119	0.0002	0.00771	0.29853	0.924
AUG16	1	-0.0109	0.00014	-0.6858	0.2078	0.953
AUG16	2	-0.0118	0.00028	-0.1511	0.38721	0.875
AUG16	3	-0.0118	0.00024	-0.6585	0.35102	0.894
AUG16	4	-0.0113	0.00015	-0.9016	0.22042	0.951
AUG16	5	-0.0114	0.00019	-0.7627	0.27126	0.927
AUG16	6	-0.0118	0.0002	-0.7584	0.29619	0.922
AUG16	7	-0.0116	0.00016	-0.0667	0.24309	0.945
AUG16	8	-0.0125	0.00026	-0.6909	0.3889	0.885
AUG16	9	-0.0111	0.00018	-0.8269	0.27273	0.926
AUG16	10	-0.0118	0.00027	-0.6183	0.40186	0.867
OCT24	2	-0.012	0.0002	0.05643	0.2935	0.926
OCT24	3	-0.0118	0.00018	0.21858	0.26793	0.936
OCT24	4	-0.0121	0.00019	0.23824	0.27929	0.934
OCT24	5	-0.0123	0.00021	0.06098	0.31872	0.92
OCT24	6	-0.0143	0.00043	-0.0119	0.64335	0.788
OCT24	7	-0.0127	0.00021	0.03295	0.30919	0.925
OCT24	8	-0.0114	0.00015	0.17264	0.2225	0.952
OCT24	9	-0.0113	0.00014	0.19955	0.21482	0.954
OCT24	10	-0.0117	0.00015	0.31328	0.22468	0.953

		TOTAL PARTS				
		slp	std err	const	std err	rsq
NOV17	2					
NOV17	3					
NOV17	4					
NOV18	5					
NOV18	6					
NOV18	7					
NOV18	8					
NOV18	9					
NOV18	10					
DEC16	1					
DEC16	2					
DEC16	3					
DEC16	4					
DEC16	5					
DEC16	6					
DEC16	7					
DEC16	8					
DEC16	9					
DEC16	10					
JAN25	4					
JAN25	5					
JAN25	6					
JAN25	7					
JAN25	8					
FEB09	1					
FEB09	2					
FEB09	3					
FEB09	4					
FEB09	5					
FEB09	6					
FEB09	7					
FEB09	8					
FEB09	9					
FEB09	10					
MAR10	1					
MAR10	2					
MAR10	3					
MAR10	4					
MAR10	5					
MAR10	6					
MAR10	7					
MAR10	8					
MAR10	9					
MAR10	10					
MAY18	1					
MAY18	2					
MAY18	3					
MAY18	4					
MAY18	5					
MAY18	6					
MAY18	7					
MAY18	8					
MAY18	9					
MAY18	10					
JUN10	1	-0.0063	0.00013	-0.8769	0.18812	
JUN10	2	-0.0066	0.00025	-0.7508	0.36916	
JUN10	3	-0.0054	0.00015	-0.1808	0.22931	
JUN10	4	-0.0055	0.00022	0.33875	0.3355	
JUN10	5	-0.0048	0.00027	0.00572	0.41047	
JUN10	6	-0.0043	0.00023	0.09686	0.34843	
JUN10	7	-0.005	0.00028	0.13803	0.40875	
JUN10	8	-0.0057	0.00031	0.31413	0.45509	
JUN10	9	-0.0047	0.00033	0.10333	0.49476	
JUN10	10	-0.0047	0.00028	0.13238	0.42214	
JUL27	1	-0.0091	0.00012	-0.4848	0.17373	
JUL27	2	-0.0085	0.00012	-0.4494	0.18116	
JUL27	3	-0.0085	0.00012	-0.5351	0.18125	
JUL27	4	-0.0087	0.00017	-0.4315	0.2618	
JUL27	5	-0.0081	0.00013	-0.3803	0.20014	
JUL27	6	-0.0089	0.0001	-0.5229	0.14276	
JUL27	7	-0.0096	9E-05	-0.5917	0.13673	
JUL27	8	-0.0097	9E-05	-0.1395	0.12955	
JUL27	9					
JUL27	10	-0.0095	9E-05	-0.4361	0.14118	
AUG18	1	-0.0091	0.00016	-0.67	0.24098	
AUG18	2	-0.0096	0.00016	-0.8621	0.24557	
AUG18	3	-0.0098	0.00014	-0.6246	0.21183	
AUG18	4	-0.0094	0.0001	-0.336	0.14384	
AUG18	5	-0.0094	0.00012	-0.524	0.181	
AUG18	6	-0.0095	0.00014	-0.7383	0.20451	
AUG18	7	-0.0089	8E-05	-0.3134	0.12483	
AUG18	8	-0.0094	0.00013	-0.7764	0.19041	
AUG18	9	-0.0103	0.00015	-0.797	0.22794	
AUG18	10	-0.0095	0.00014	-0.7574	0.20997	
OCT24	2	-0.0092	8E-05	-0.3476	0.11514	
OCT24	3	-0.0096	0.0001	-0.1942	0.15706	
OCT24	4	-0.009	9E-05	-0.202	0.13095	
OCT24	5	-0.0093	9E-05	-0.3962	0.13865	
OCT24	6	-0.0095	0.00011	-0.3614	0.16778	
OCT24	7	-0.0094	0.00012	-0.2514	0.1734	
OCT24	8	-0.0091	0.0001	-0.0891	0.1448	
OCT24	9	-0.0092	0.00013	-0.1564	0.19094	
OCT24	10	-0.0089	0.00011	-0.044	0.17001	

		WATER SAMPLE				
		slp	std err	const	std err	rsq
NOV17	2					
NOV17	3					
NOV17	4					
NOV18	5					
NOV18	6					
NOV18	7					
NOV18	8					
NOV18	9					
NOV18	10					
DEC16	1	-0.0045	8E-05	0.44546	0.08841	0.952
DEC16	2	-0.0008	5E-05	1.87924	0.05529	0.611
DEC16	3	-0.0028	0.0001	0.0075	0.1117	0.828
DEC16	4	-0.004	8E-05	0.35998	0.08157	0.947
DEC16	5	-0.0022	7E-05	0.59658	0.06952	0.885
DEC16	6	-0.0032	5E-05	0.64289	0.05695	0.96
DEC16	7	-0.0037	0.00011	0.45968	0.117	0.881
DEC16	8	-0.0021	6E-05	0.43567	0.0596	0.906
DEC16	9	-0.0036	8E-05	0.40395	0.08993	0.925
DEC16	10	-0.0016	4E-05	0.94746	0.04625	0.901
JAN25	4	-0.0078	0.0002	-0.2817	0.21815	0.908
JAN25	5	-0.0073	0.00036	-0.3918	0.37789	0.737
JAN25	6	-0.0086	0.00024	0.30678	0.25434	0.897
JAN25	7	-0.008	0.00018	-0.1042	0.1922	0.93
JAN25	8	-0.0078	0.00025	-0.1935	0.26326	0.868
FEB09	1	-0.0096	0.00038	-0.6199	0.40647	0.81
FEB09	2	-0.0082	0.00035	-0.278	0.36567	0.793
FEB09	3	-0.0084	0.00042	-0.5281	0.44448	0.73
FEB09	4	-0.0078	0.00037	-0.6779	0.39395	0.748
FEB09	5	-0.008	0.00023	-0.0328	0.24942	0.887
FEB09	6	-0.0092	0.00079	-1.0068	0.76011	0.493
FEB09	7	-0.0064	0.00061	-1.5091	0.60151	0.444
FEB09	8	-0.0112	0.0007	-1.2447	0.73444	0.647
FEB09	9	-0.0118	0.00026	-1.5374	0.25908	0.937
FEB09	10	-0.0127	0.00064	-1.3852	0.6135	0.741
MAR10	1	-0.0078	0.00018	0.1732	0.19648	0.923
MAR10	2	-0.0078	0.00026	0.27126	0.27178	0.855
MAR10	3	-0.0083	0.00031	-0.4264	0.3312	0.826
MAR10	4	-0.007	0.00027	-0.2378	0.29079	0.816
MAR10	5	-0.0086	0.00039	-0.4256	0.4072	0.773
MAR10	6	-0.0081	0.00024	-0.3144	0.25245	0.887
MAR10	7	-0.0072	0.00023	-0.1516	0.24059	0.873
MAR10	8	-0.0073	0.00033	0.04175	0.35146	0.764
MAR10	9	-0.0071	0.00029	0.14339	0.30839	0.801
MAR10	10	-0.0077	0.00028	0.09653	0.30286	0.829
MAY18	1	-0.0101	0.00064	-0.2501	0.64129	0.636
MAY18	2	-0.0058	0.00067	-1.2942	0.62877	0.364
MAY18	3	-0.0075	0.00059	-0.7474	0.5681	0.544
MAY18	4	-0.0065	0.00067	-0.9798	0.63498	0.418
MAY18	5	-0.0096	0.00064	-0.4588	0.61877	0.617
MAY18	6	-0.008	0.00024	-0.2742	0.25183	0.885
MAY18	7	-0.0081	0.00024	-0.4831	0.25445	0.884
MAY18	8	-0.0077	0.00037	-0.4472	0.39174	0.742
MAY18	9	-0.0083	0.00019	-0.1076	0.20546	0.925
MAY18	10	-0.0077	0.00021	-0.3958	0.22025	0.902
JUN10	1	-0.0075	0.00039	0.21123	0.41445	0.711
JUN10	2	-0.0081	0.00051	-0.012	0.51675	0.641
JUN10	3	-0.0077	0.00052	-0.3155	0.50041	0.618
JUN10	4	-0.007	0.00043	-0.5479	0.40952	0.659
JUN10	5	-0.0085	0.00063	-0.0989	0.63579	0.557
JUN10	6	-0.0074	0.00022	-0.4332	0.23048	0.888
JUN10	7	-0.0072	0.00016	-0.3342	0.17276	0.929
JUN10	8	-0.0075	0.00024	-0.4822	0.25679	0.866
JUN10	9	-0.0073	0.00015	-0.3169	0.16384	0.938
JUN10	10	-0.0064	0.00029	-0.4955	0.30522	0.77
JUL27	1					
JUL27	2					
JUL27	3					
JUL27	4					
JUL27	5					
JUL27	6					
JUL27	7					
JUL27	8					
JUL27	9					
JUL27	10					
AUG16	1					
AUG16	2					
AUG16	3					
AUG16	4					
AUG16	5					
AUG16	6					
AUG16	7					
AUG16	8					
AUG16	9					
AUG16	10					
OCT24	2	-0.0081	4E-05	-0.2233	0.08536	0.992
OCT24	3	-0.0083	6E-05	-0.0575	0.09295	0.984
OCT24	4	-0.0082	4E-05	-0.2502	0.05966	0.993
OCT24	5	-0.0093	6E-05	-0.2736	0.08835	0.988
OCT24	6	-0.0089	6E-05	-0.0163	0.0908	0.986
OCT24	7	-0.0083	4E-05	-0.0917	0.06183	0.993
OCT24	8	-0.0083	4E-05	-0.1027	0.06643	0.992
OCT24	9	-0.0085	6E-05	0.01922	0.09209	0.985
OCT24	10	-0.0084	5E-05	0.0444	0.07612	0.989

		YELLOW SUBSTANCE				
		slp	std err	const	std err	rsq
NOV17	2					
NOV17	3					
NOV17	4					
NOV18	5					
NOV18	6					
NOV18	7					
NOV18	8					
NOV18	9					
NOV18	10					
DEC16	1	-0.0158	0.00195	-2.0583	0.85586	0.497
DEC16	2	-0.0028	9E-05	-0.4683	0.10048	0.853
DEC16	3	-0.0037	0.0005	-1.3454	0.50526	0.284
DEC16	4	-0.0064	0.00037	-0.7608	0.39105	0.669
DEC16	5	-0.002	0.00027	-1.5148	0.28862	0.273
DEC16	6	-0.0153	0.00053	-1.3094	0.3286	0.893
DEC16	7	-0.0058	0.00036	-0.8794	0.36678	0.648
DEC16	8	-0.0032	0.00021	-0.8938	0.22375	0.606
DEC16	9	-0.0023	0.0001	-0.2785	0.10124	0.794
DEC16	10	-0.0141	0.00126	-2.1107	0.78002	0.563
JAN25	4	-0.0097	0.00044	-1.5075	0.46587	0.763
JAN25	5	-0.0102	0.00029	-0.9029	0.29887	0.897
JAN25	6	-0.0105	0.0002	-0.7566	0.21313	0.948
JAN25	7	-0.0099	0.0004	-1.3136	0.40835	0.809
JAN25	8	-0.0113	0.00059	-1.465	0.59377	0.726
FEB09	1	-0.0153	0.0008	-1.2827	0.60632	0.822
FEB09	2	-0.0115	0.00046	-0.7545	0.48072	0.811
FEB09	3	-0.0082	0.00047	-0.9581	0.48865	0.68
FEB09	4	-0.0099	0.00053	-1.0041	0.55549	0.702
FEB09	5	-0.0109	0.0004	-1.0604	0.41373	0.837
FEB09	6	-0.0102	0.00077	-1.4818	0.713	0.571
FEB09	7	-0.01	0.00048	-0.7707	0.49241	0.75
FEB09	8	-0.011	0.00031	-0.9759	0.32506	0.896
FEB09	9	-0.0099	0.00035	-0.7699	0.36879	0.843
FEB09	10	-0.0102	0.00032	-1.0752	0.34141	0.871
MAR10	1	-0.0101	0.00048	-0.3874	0.49803	0.753
MAR10	2	-0.0073	0.00068	-0.8397	0.68993	0.443
MAR10	3	-0.0102	0.00077	-1.2039	0.74539	0.561
MAR10	4	-0.0086	0.00035	-1.1579	0.37077	0.804
MAR10	5	-0.0084	0.00024	-0.8712	0.251	0.895
MAR10	6	-0.0103	0.00041	-0.6681	0.42978	0.813
MAR10	7	-0.014	0.00077	-1.1028	0.76882	0.7
MAR10	8	-0.0099	0.00034	-0.5555	0.35914	0.853
MAR10	9	-0.0071	0.00104	-2.0491	0.74509	0.289
MAR10	10	-0.0097	0.00032	-0.5562	0.33753	0.881
MAY18	1	-0.0117	0.00025	-0.8127	0.26869	0.935
MAY18	2	-0.017	0.00044	-1.5991	0.41914	0.915
MAY18	3	-0.0107	0.00041	-0.9103	0.43256	0.822
MAY18	4	0.00031	0.00122	-2.881	1.09554	0.001
MAY18	5	-0.0118	0.00021	-1.088	0.21925	0.957
MAY18	6	-0.012	0.00021	-0.4505	0.22265	0.958
MAY18	7	-0.0134	0.00037	-1.1283	0.36328	0.904
MAY18	8	-0.0133	0.00056	-0.9532	0.55649	0.799
MAY18	9	-0.0034	0.00127	-2.4306	1.1735	0.068
MAY18	10	-2E-05	0.0013	-2.8547	1.16664	0
JUN10	1	-0.0101	0.00016	-0.5225	0.16597	0.966
JUN10	2	-0.0138	0.00059	-0.8359	0.61771	0.789
JUN10	3	-0.0108	0.00024	-0.9939	0.25346	0.931
JUN10	4	-0.0105	0.00027	-0.9575	0.27985	0.913
JUN10	5	-0.011	0.00039	-1.1302	0.41601	0.84
JUN10	6	-0.0126	0.0003	-0.945	0.31552	0.922
JUN10	7	-0.0125	0.0003	-0.9385	0.3102	0.924
JUN10	8	-0.0122	0.00033	-0.9224	0.3423	0.905
JUN10	9	-0.0114	0.00026	-0.8174	0.26741	0.931
JUN10	10	-0.0128	0.00031	-1.1542	0.31613	0.923
JUL27	1					
JUL27	2					
JUL27	3					
JUL27	4					
JUL27	5					
JUL27	6					
JUL27	7					
JUL27	8					
JUL27	9					
JUL27	10					
AUG16	1					
AUG16	2					
AUG16	3					
AUG16	4					
AUG16	5					
AUG16	6					
AUG16	7					
AUG16	8					
AUG16	9					
AUG16	10					
OCT24	2	-0.0091	9E-05	-1.0324	0.14128	0.969
OCT24	3	-0.009	8E-05	-1.0798	0.12068	0.977
OCT24	4	-0.0093	8E-05	-0.9419	0.11954	0.978
OCT24	5	-0.0084	6E-05	-0.8386	0.09679	0.983
OCT24	6	-0.0098	7E-05	-0.775	0.10934	0.984
OCT24	7	-0.0093	7E-05	-0.8524	0.11035	0.982
OCT24	8	-0.0099	7E-05	-0.7905	0.10896	0.984
OCT24	9	-0.0105	0.00011	-0.9699	0.16424	0.969
OCT24	10	-0.0093	8E-05	-0.9184	0.12289	0.977

APPENDIX IX

Particle Analysis

VOLUME DISTRIBUTION TABLE (PERCENT)

SAMPLE NAME : MENAI STRAIT G1
FILE NAME : Data Not Saved.

DATE	: 24/03/1995	ACQ. RANGE	: 2-600	COUNTS	: 133607
TIME	: 14:44	ACQ. MODE	: SAMPLE	S.N.F.	: 0.39
CONFIG.	: 2 (0.5 A)	ACQ. TIME	: 482 SEC	S.D.U.	: 167
CELL TYPE	: LQFLOW	SAMPLE SIZE	: 4	CONCENTR.	: 5.2E+05 #/m
SAMPLE TYPE	: SPECIAL /L	REQ. CONF.	: None	SOLIDS	: 3.5E-03 %

UNDER(%)	SIZE (microns)	OVER(%)
10	3.50	90
40	5.82	60
55	7.76	45
60	9.23	40
65	11.74	35
70	14.51	30
75	16.17	25
80	19.62	20
85	24.82	15
90	36.95	10
95	55.21	5
97	58.27	3
100	118.00	0

G A L A I - C I S - 1 0 0

Computerized Inspection System

NUMBER DISTRIBUTION TABLE (RANGES)

SAMPLE NAME : MENAI STRAIT G1
FILE NAME : GMS1.DAT

DATE : 24/03/1995	ACQ. RANGE : 2-600	COUNTS : 133607
TIME : 14:44	ACQ. MODE : SAMPLE	S.N.F. : 0.39
CONFIG. : 2 (0.5 A)	ACQ. TIME : 482 SEC	S.D.U. : 167
CELL TYPE : LQFLOW	SAMPLE SIZE : 4	CONCENTR.: 5.2E+05 #/ml
SAMPLE TYPE : SPECIAL /L	REQ. CONF. : None	SOLIDS : 3.5E-03 %

RANGE (microns)	LOCAL (%)	UNDER(%)-CUMULATIVE-OVER(%)
0.0 - 4.0	63.04	63.04 36.96
4.0 - 8.0	35.06	98.10 1.90
8.0 - 12.0	1.26	99.37 0.63
12.0 - 18.0	0.52	99.88 0.12
18.0 - 24.0	0.07	99.95 0.05
24.0 - 30.0	0.03	99.98 0.02
30.0 - 40.0	0.01	99.99 0.01
40.0 - 50.0	0.00	100.00 0.00
50.0 - 60.0	0.00	100.00 0.00
60.0 - 70.0	0.00	100.00 0.00
70.0 - 80.0	0.00	100.00 0.00
80.0 - 100.0	0.00	100.00 0.00
100.0 - 120.0	0.00	100.00 0.00
120.0 - 140.0	0.00	100.00 0.00
140.0 - 160.0	0.00	100.00 0.00
160.0 - 180.0	0.00	100.00 0.00
180.0 - 200.0	0.00	100.00 0.00
200.0 - 250.0	0.00	100.00 0.00
250.0 - 300.0	0.00	100.00 0.00
300.0 - 600.0	0.00	100.00 0.00

G A L A I - C I S - 1 0 0

Computerized Inspection System

SAMPLE NAME : MENAI STRAIT G1
FILE NAME : Data Not Saved.

DATE	: 24/03/1995	ACQ. RANGE	: 2-600	COUNTS	: 133607
TIME	: 14:44	ACQ. MODE	: SAMPLE	S.N.F.	: 0.39
CONFIG.	: 2 (0.5 A)	ACQ. TIME	: 482 SEC	S.D.U.	: 167
CELL TYPE	: LQFLOW	SAMPLE SIZE	: 4	CONCENTR.	: 5.2E+05 #/ml
SAMPLE TYPE	: SPECIAL /L	REQ. CONF.	: None	SOLIDS	: 3.5E-03 %

PROBABILITY VOLUME DENSITY GRAPH

Name: MENAI STRAIT G1
3.5E-05 cc/ml(100.0%)
Mode at 5.00 µm
Mean(nv): 5.03µm
S.D.(nv): 2.03µm
Median : 7.04µm
Mean(vm): 14.46µm
S.D.(vm): 17.73µm
Conf(vm):100.00 %
<< SCALE RANGE (µm): ADJUSTED >>

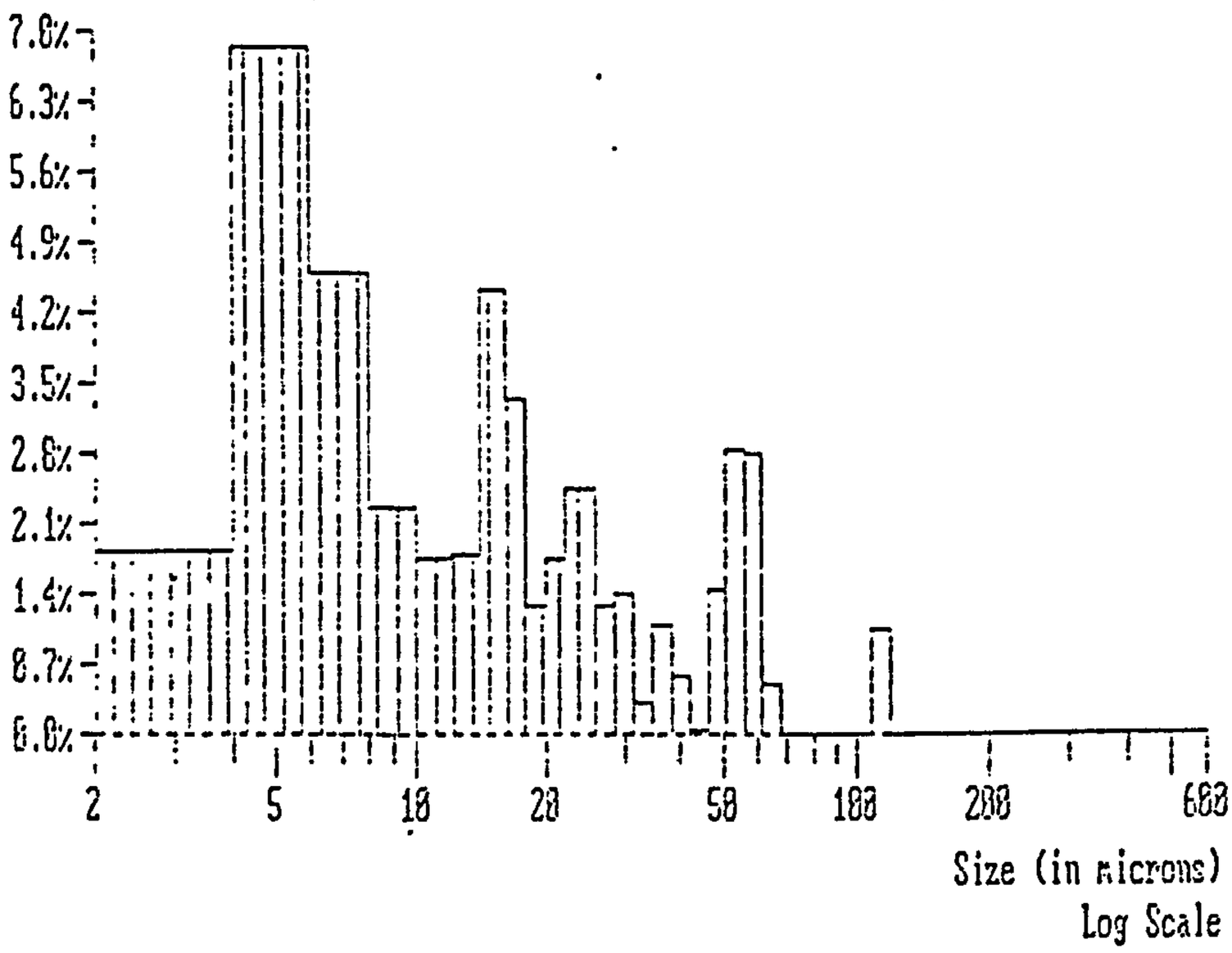

SAMPLE NAME : MENAI STRAIT G1
FILE NAME : Data Not Saved.

DATE	: 24/03/1995	ACQ. RANGE	: 2-600	COUNTS	: 133607
TIME	: 14:44	ACQ. MODE	: SAMPLE	S.N.F.	: 0.39
CONFIG.	: 2 (0.5 A)	ACQ. TIME	: 482 SEC	S.D.U.	: 167
CELL TYPE	: LQFLOW	SAMPLE SIZE	: 4	CONCENTR.	: 5.2E+05 #/m³
SAMPLE TYPE	: SPECIAL /L	REQ. CONF.	: None	SOLIDS	: 3.5E-03 %

PROBABILITY VOLUME DISTRIBUTION

Name: MENAI STRAIT G1
3.5E-05 cc/m³(100.0%)

Mean(nv): 5.03µm
S.D.(nv): 2.03µm

Median : 7.84µm
Mean(vm): 14.46µm
S.D.(vm): 17.73µm
Conf(vm):100.00 %

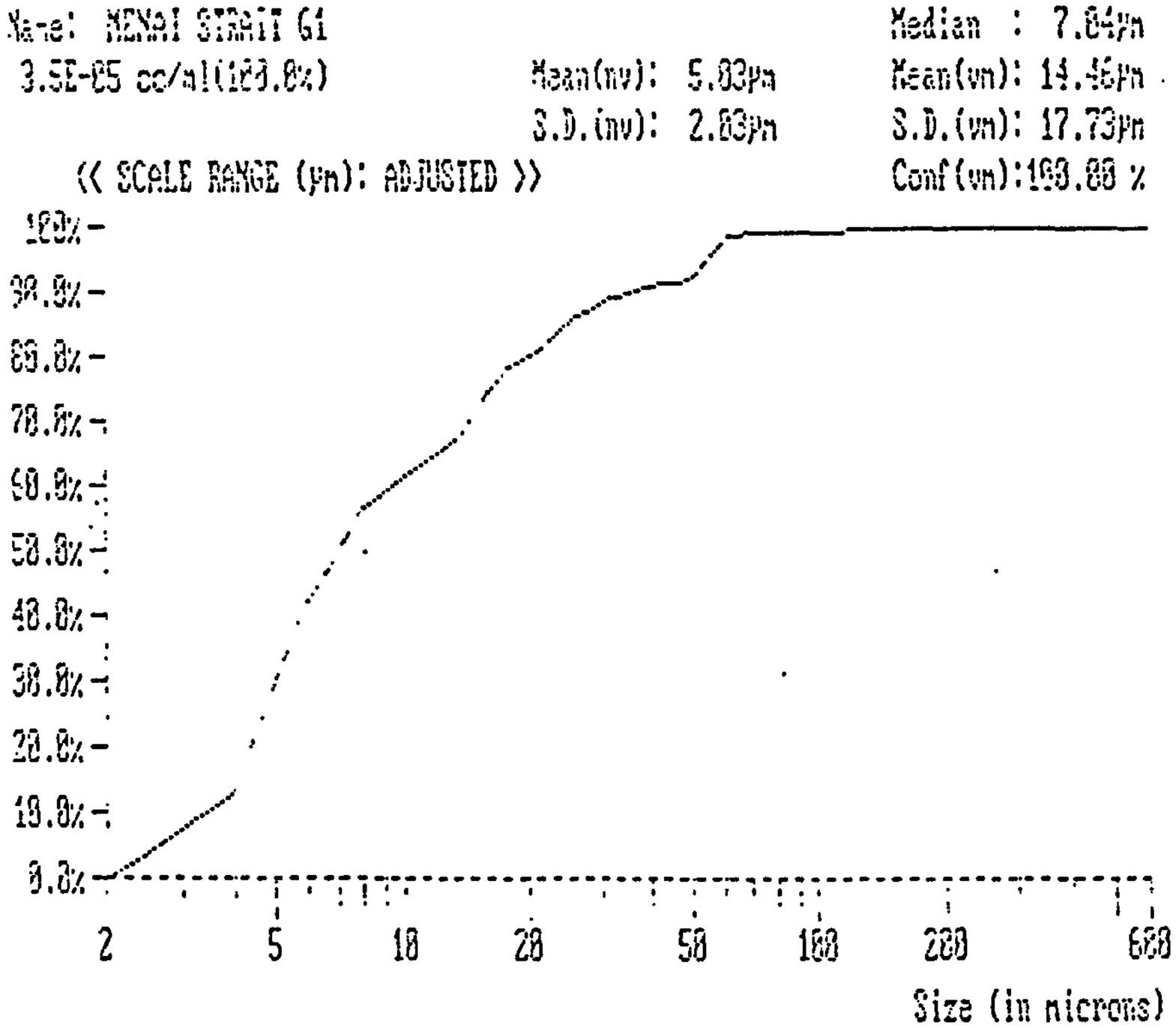

VOLUME DISTRIBUTION TABLE (PERCENT)

SAMPLE NAME : MENAI STRAIT G2
FILE NAME : Data Not Saved.

DATE : 24/03/1995	ACQ. RANGE : 2-600	COUNTS : 358295
TIME : 15:06	ACQ. MODE : SAMPLE	S.N.F. : 0.82
CONFIG. : 2 (0.5 A)	ACQ. TIME : 930 SEC	S.D.U. : 589
CELL TYPE : LQFLOW	SAMPLE SIZE : 5 (ABORTED)	CONCENTR. : 2.0E+05 #/ml
SAMPLE TYPE : SPECIAL /L	REQ. CONF. : None	SOLIDS : 2.2E-03 %

UNDER(%)	SIZE (microns)	OVER(%)
5	3.29	95
20	5.43	80
30	7.16	70
35	8.52	65
40	11.25	60
50	15.90	50
55	19.19	45
60	26.02	40
65	36.40	35
70	44.91	30
75	52.49	25
80	84.81	20
85	94.81	15
90	108.12	10
97	115.38	3
100	122.00	0

VOLUME DISTRIBUTION TABLE (PERCENT)

SAMPLE NAME : MENAI STRAIT G2
FILE NAME : Data Not Saved.

DATE	: 24/03/1995	ACQ. RANGE	: 2-600	COUNTS	: 358295
TIME	: 15:06	ACQ. MODE	: SAMPLE	S.N.F.	: 0.82
CONFIG.	: 2 (0.5 A)	ACQ. TIME	: 930 SEC	S.D.U.	: 589
CELL TYPE	: LQFLOW	SAMPLE SIZE	: 5 (ABORTED)	CONCENTR.	: 2.0E+05 #/ml
SAMPLE TYPE	: SPECIAL /L	REQ. CONF.	: None	SOLIDS	: 2.2E-03 %

UNDER(cc/ml)	SIZE (microns)	OVER(cc/ml)
1.120E-06	3.29	2.128E-05
4.479E-06	5.43	1.792E-05
6.719E-06	7.16	1.568E-05
7.838E-06	8.52	1.456E-05
8.958E-06	11.25	1.344E-05
1.120E-05	15.90	1.120E-05
1.232E-05	19.19	1.008E-05
1.344E-05	26.02	8.958E-06
1.456E-05	36.40	7.838E-06
1.568E-05	44.91	6.719E-06
1.680E-05	52.49	5.599E-06
1.792E-05	84.81	4.479E-06
1.904E-05	94.81	3.359E-06
2.016E-05	108.12	2.240E-06
2.172E-05	115.38	6.719E-07
2.240E-05	122.00	6.157E-13

NUMBER DISTRIBUTION TABLE (RANGES)

SAMPLE NAME : MENAI STRAIT G2
FILE NAME : GMS2.DAT

DATE	: 24/03/1995	ACQ. RANGE	: 2-600	COUNTS	: 358295
TIME	: 15:06	ACQ. MODE	: SAMPLE	S.N.F.	: 0.82
CONFIG.	: 2 (0.5 A)	ACQ. TIME	: 930 SEC	S.D.U.	: 589
CELL TYPE	: LQFLOW	SAMPLE SIZE	: 5 (ABORTED)	CONCENTR.	: 2.0E+05 #/ml
SAMPLE TYPE	: SPECIAL /L	REQ. CONF.	: None	SOLIDS	: 2.2E-03 %

RANGE (microns)	LOCAL (%)	UNDER(%)-CUMULATIVE-OVER(%)
0.0 - 4.0	61.89	61.89 38.11
4.0 - 8.0	35.24	97.14 2.86
8.0 - 12.0	1.81	98.94 1.06
12.0 - 18.0	0.84	99.78 0.22
18.0 - 24.0	0.13	99.91 0.09
24.0 - 30.0	0.04	99.95 0.05
30.0 - 40.0	0.03	99.98 0.02
40.0 - 50.0	0.01	99.99 0.01
50.0 - 60.0	0.00	99.99 0.01
60.0 - 70.0	0.00	100.00 0.00
70.0 - 80.0	0.00	100.00 0.00
80.0 - 100.0	0.00	100.00 0.00
100.0 - 120.0	0.00	100.00 0.00
120.0 - 140.0	0.00	100.00 0.00
140.0 - 160.0	0.00	100.00 0.00
160.0 - 180.0	0.00	100.00 0.00
180.0 - 200.0	0.00	100.00 0.00
200.0 - 250.0	0.00	100.00 0.00
250.0 - 300.0	0.00	100.00 0.00
300.0 - 600.0	0.00	100.00 0.00

G A L A I - C I S - 1 0 0

Computerized Inspection System

SAMPLE NAME : MENAI STRAIT G2
FILE NAME : Data Not Saved.

DATE	: 24/03/1995	ACQ. RANGE	: 2-600	COUNTS	: 358295
TIME	: 15:06	ACQ. MODE	: SAMPLE	S.N.F.	: 0.82
CONFIG.	: 2 (0.5 A)	ACQ. TIME	: 930 SEC	S.D.U.	: 589
CELL TYPE	: LQFLOW	SAMPLE SIZE	: 5 (ABORTED)	CONCENTR.	: 2.0E+05 #/ml
SAMPLE TYPE	: SPECIAL /L	REQ. CONF.	: None	SOLIDS	: 2.2E-03 %

PROBABILITY VOLUME DENSITY GRAPH

Name: MENAI STRAIT G2
2.2E-05 cc/ml(100.0%)
Mode at 113.80 µm

Mean(nv): 6.80µm
S.D.(nv): 2.87µm

Median : 15.90µm
Mean(vm): 35.63µm
S.D.(vm): 37.91µm
Conf(vm): 95.10 %

<< SCALE RANGE (µm): ADJUSTED >>

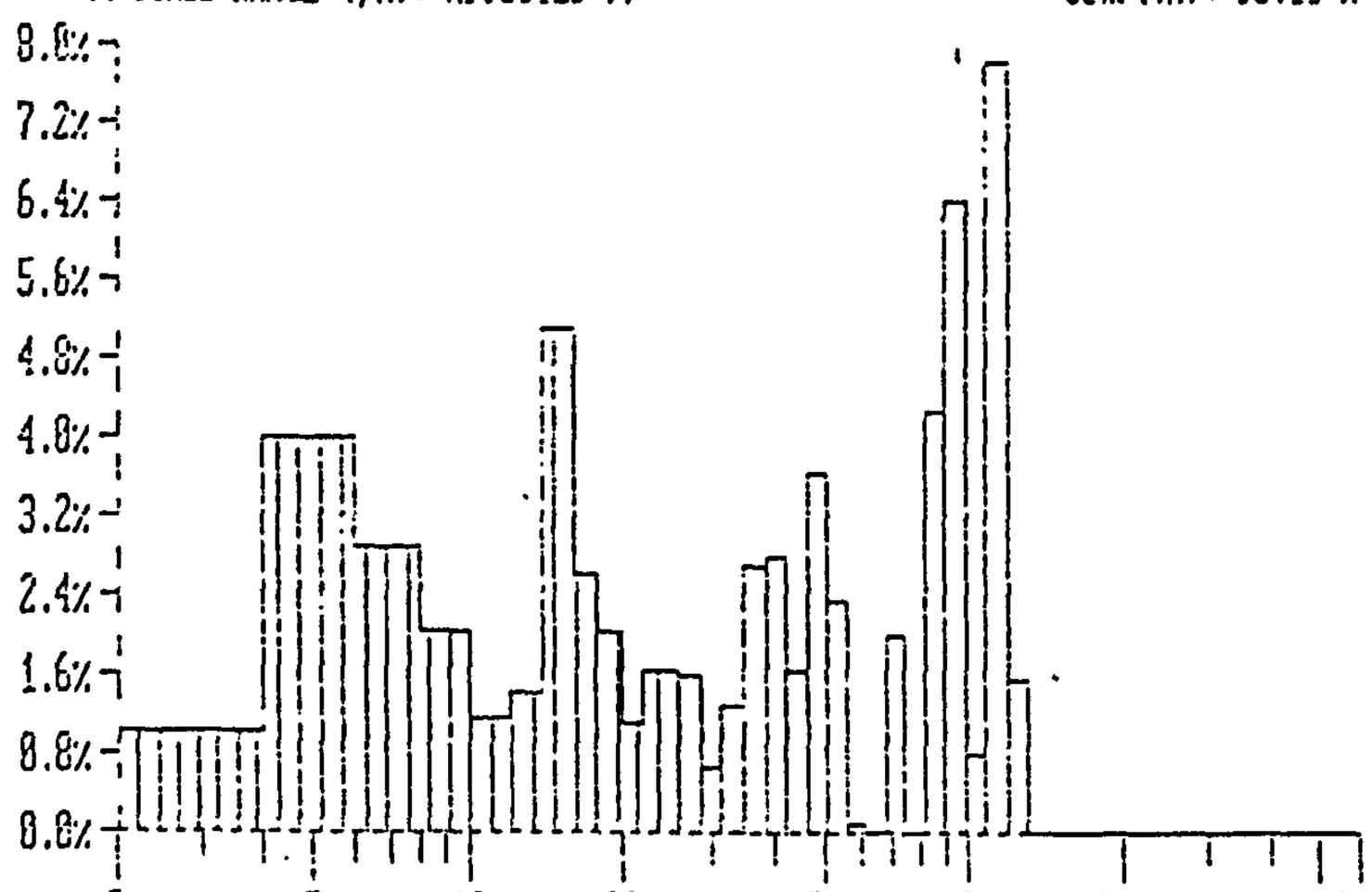

SAMPLE NAME : MENAI STRAIT G2
FILE NAME : Data Not Saved.

DATE	: 24/03/1995	ACQ. RANGE	: 2-600	COUNTS	: 358295
TIME	: 15:06	ACQ. MODE	: SAMPLE	S.N.F.	: 0.82
CONFIG.	: 2 (0.5 A)	ACQ. TIME	: 930 SEC	S.D.U.	: 589
CELL TYPE	: LQFLOW	SAMPLE SIZE	: 5 (ABORTED)	CONCENTR.	: 2.0E+05 #/ml
SAMPLE TYPE	: SPECIAL /L	REQ. CONF.	: None	SOLIDS	: 2.2E-03 %

PROBABILITY VOLUME DISTRIBUTION

Name: MENAI STRAIT G2
2.2E-05 cc/ml(100.0%)

Mean(mv): 6.80µm
S.D.(mv): 2.87µm

Median : 15.98µm
Mean(vm): 35.63µm
S.D.(vm): 37.91µm
Conf(vm): 95.10 %

<< SCALE RANGE (µm): ADJUSTED >>

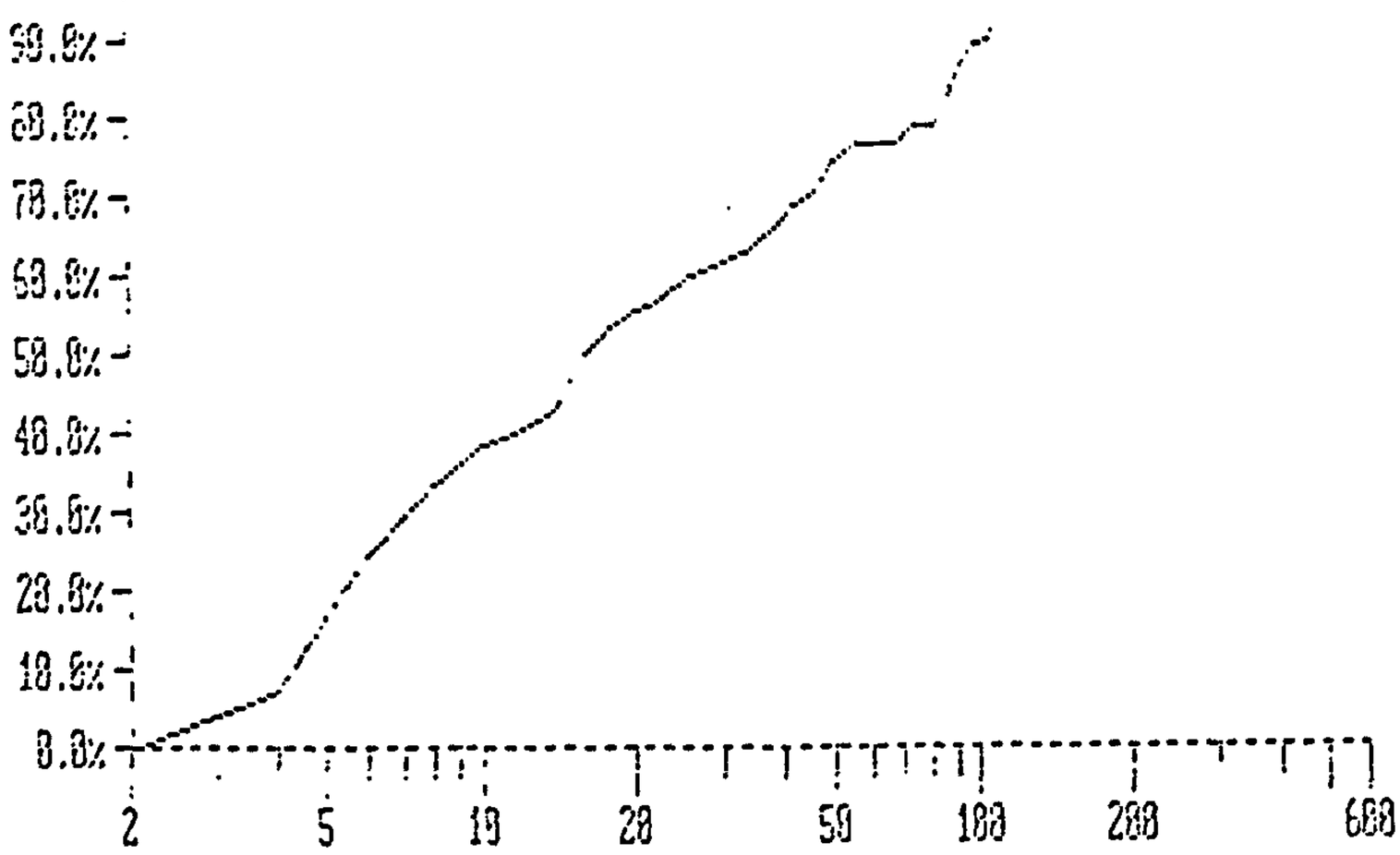

Size (in microns)
Log Scale

G A L A I - C I S - 1 0 0
Computerized Inspection System

SAMPLE NAME : MSTRAIT1
FILE NAME : Data Not Saved.

DATE	: 28/03/1995	ACQ. RANGE	: 2-600	COUNTS	: 79955
TIME	: 14:44	ACQ. MODE	: SAMPLE	S.N.F.	: 0.65
CONFIG.	: 2 (0.5 A)	ACQ. TIME	: 161.3 SEC	S.D.U.	: 206
CELL TYPE	: LQFLOW	SAMPLE SIZE	: 5 (ABORTED)	CONCENTR.	: 6.0E+04 £/ml
SAMPLE TYPE	: SPECIAL /L	REQ. CONF.	: None	SOLIDS	: 8.3E-04 %

PROBABILITY VOLUME DENSITY GRAPH

Name: MSTRAIT1
9.3E-06 cc/ml(100.0%)
Mode at 77.80 µm
<< SCALE RANGE (µm): ADJUSTED >>

Mean(nv): 6.44µm
S.D.(nv): 3.13µm

Median : 28.18µm
Mean(um): 31.69µm
S.D.(um): 28.41µm
Conf(um): 95.38 %

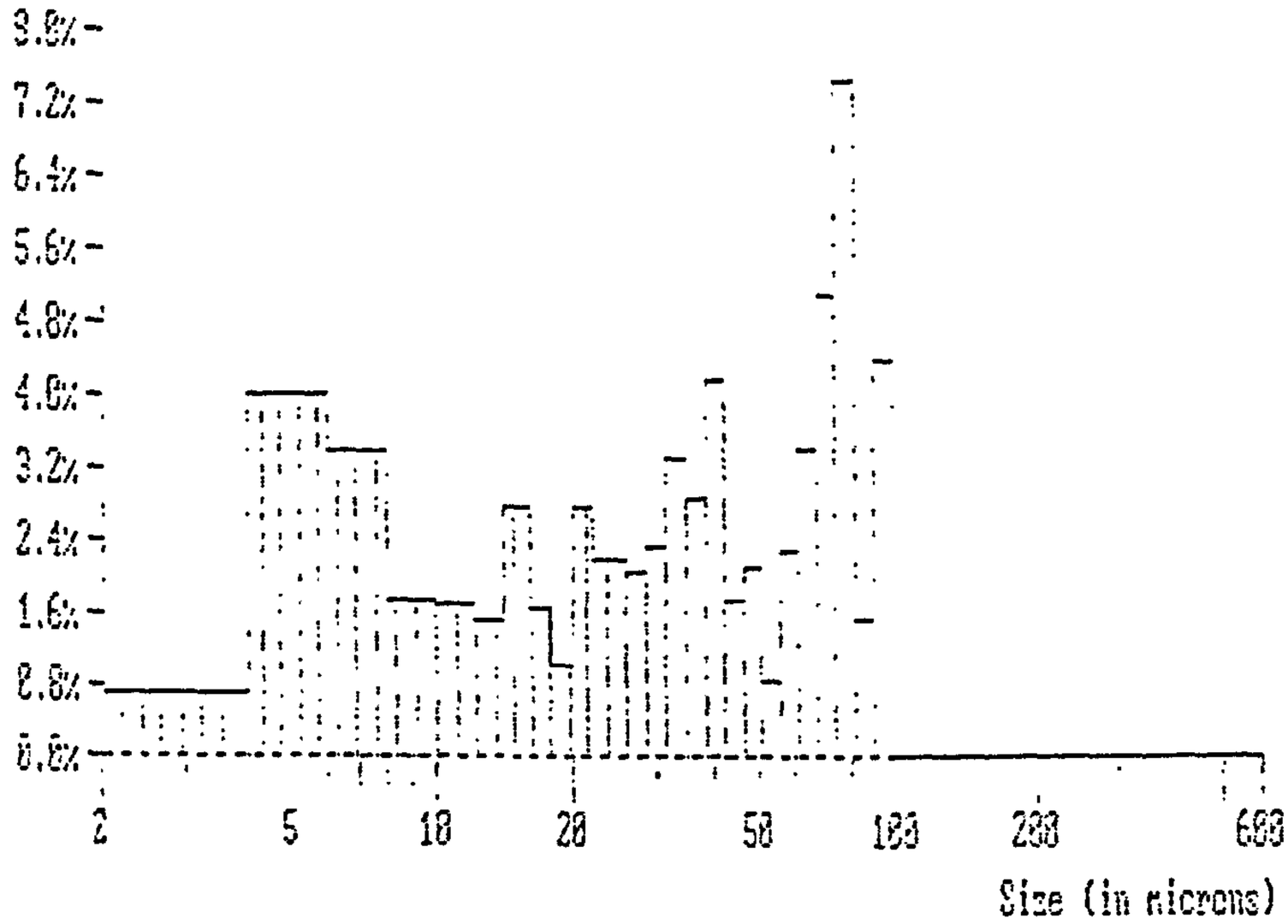

G A L A I – C I S 1 0 0 0

Computerized Inspection System

UCNW Particle Shape Analysis

SAMPLE NAME : cbtest4
FILE NAME : MSTRAIT1

DATE & TIME	: 28/03/1995 ,14:36	Area	:	0.000	- 1968398
MAGNIFICATION	: 2.737 ,Lens [DW]	Perimeter	:	0.000	- 718334
CALIBRATION	: 2.740	Shape factor	:	0.000	- 1.000
ACQ. TIME	: 1744 Seconds	Specific len.	:	0.000	- 718334
REQ. PARTICLES	: 2000	Aspect ratio.	:	0.000	- 1.000
COUNT	: 1343	User param.	:	0.000	- 1000000000

Bar Histogram of Shape factor

Units: None No.of pictures: 467 Average : 0.7572 ± 0.0087
Total objects: 1343 Object density: 3.69E+02/Cm²

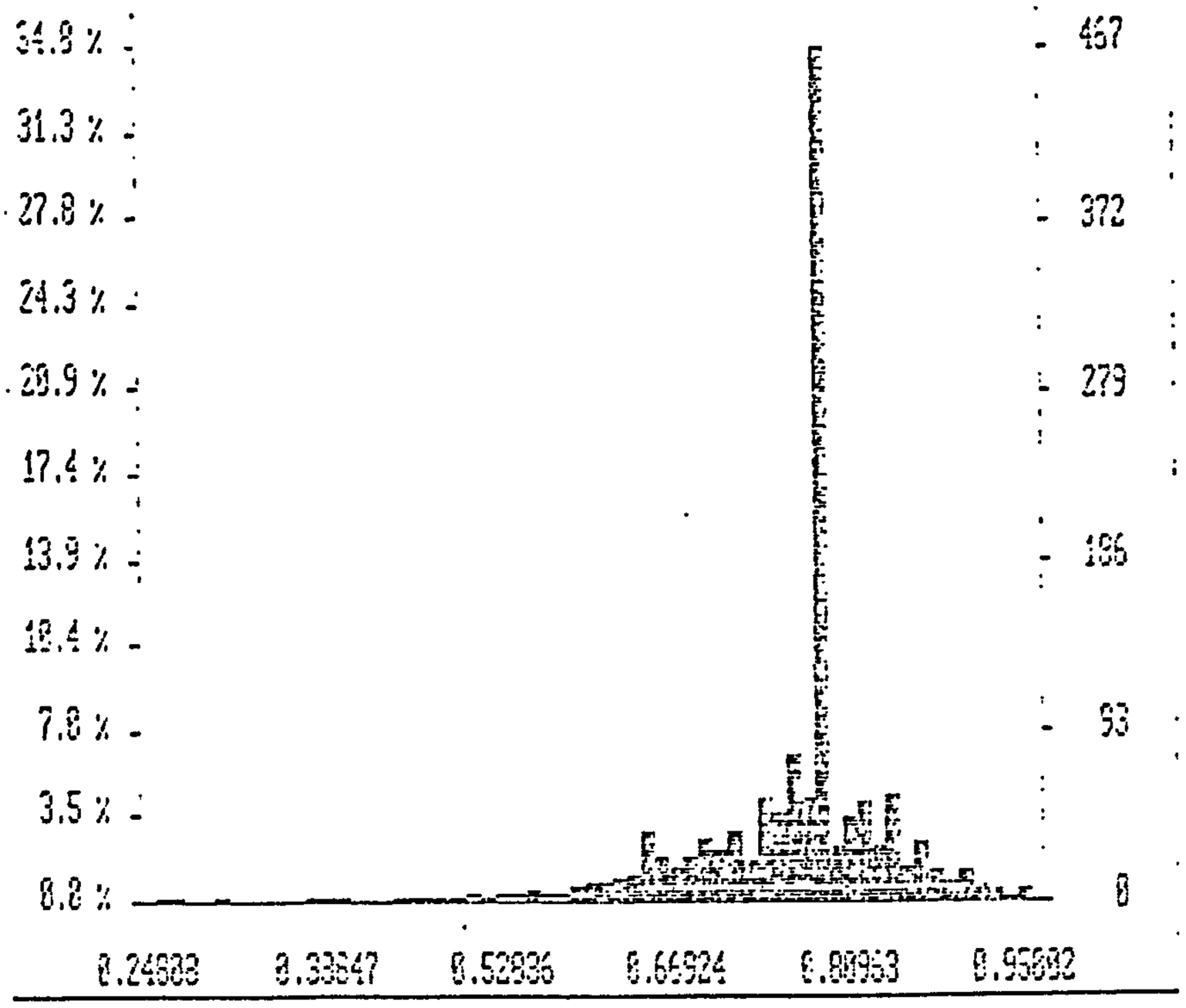

APPENDIX X

Listing of

Ocean Colour Model

```
'colallss - colour model modified 11/95 to include mss higher abs **********
'also 19/01/96 to use Mie scat for chl: needs chlcoef.dat for input ********
'20/07/96 includes detrital absn as well as MSS ******************************
'24/09/96 calcs PAR attenuation and reflectance ******************************
'calcs scat by anomalous diffractive theory (kirk p90) ***********************
'andinput - interactive creation of input file for colour model ************

DECLARE SUB inposprn (xpt!, ypt!, txt$, num!)
DECLARE SUB inpostxt (xpt!, ypt!, file$)
DECLARE SUB posprn (xpt!, ypt!, txt$)
DECLARE SUB posprncl (xpt!, ypt!, txt$, c!)
DECLARE SUB optprop (i, chl, glb, mss, oss, wvl(), wabs(), wsct(), phab(), spbc(), spbm(),
spbo(), glbcn, mssval, msscon, mssexp, ossval, osscon, ossexp, chlrad, cmass, mmass,
mssrad, mssdens, omass, ossrad, ossdens, cbrat, mbrat, obrat, mu0, a(), _
b(), att(), Kd(), Ref(), reftyp, parktot, parrtot)
DECLARE SUB bksct (b!(), bw, wvl!(), bksc!(), bchl!, bmss, boss, i!)
DECLARE SUB modinp ()
DECLARE SUB printout (nw!, mss!, oss, chl!, glb!, wvl(), a!(), b!(), att(), Kd!(), Ref!(), park,
parr)
DECLARE SUB printall (nw!, mss!, oss, chl!, glb!, wvl!(), a!(), b!(), att!(), Kd!(), Ref!(), park,
parr)
DECLARE SUB filetitl (head$, outpt$)
DECLARE SUB printfil ()
DECLARE SUB axes (x0!, xh!, y0!, yh!)
DECLARE SUB label (x0!, xh!, y0!, yh!, yln!, xln!)
DECLARE SUB conprn (mss!, oss, chl!, glb!)
DECLARE SUB grplt (nw!, wvl!(), Ref!(), Kd!(), rupper!, kupper!, park, parr)
DECLARE SUB filnum (filn!)
DECLARE SUB pntfilx (out$)
DECLARE SUB pntoutn (nw!, mss!, oss, chl!, glb!, wvl!(), a!(), b!(), att(), Kd!(), Ref!(), park,
parr)
DECLARE SUB filopen (fileout$)

nw = 31: nlin = 32
DIM wvl(nw), wabs(nw), wsct(nw), phab(nw)
DIM qsct(nw), mqsct(nw), spbc(nw), spbm(nw), oqsct(nw), spbo(nw)
DIM SHARED a(nw), b(nw), bksc(nw), att(nw), Kd(nw), Ref(nw)

ON ERROR GOTO 555
SCREEN 12

CLS

' instructions to restart or stop using F2 and F1 ****************************
ON KEY(1) GOSUB 200
KEY(1) ON
10  ON KEY(2) GOSUB 10
KEY(2) ON

pi = 3.141593
' calc level of PAR energy ***************************************************
 FOR x = 400 TO 700 STEP 10
   paren = 1 / x + paren
 NEXT x
'
**********************************************************************************
***

' first screen - instructions to stop, option to change settings ************
30 VIEW: WINDOW: CLS
LINE (70, 320)-(530, 440), 15, B
```

```
posprn 25, 24, "Press F1 to QUIT at any time"
posprn 32, 25, "F2 to RESTART"


LINE (70, 20)-(530, 140), 15, B
LINE (72, 22)-(528, 138), 15, B

posprncl 16, 5, "Edit input file for equation constants (Y/N) ", 11

DO: ans$ = UCASE$(INKEY$)
LOOP UNTIL ans$ = "Y" OR ans$ = "N"
CLS
IF ans$ = "Y" THEN modinp
IF ans$ = "N" THEN eqfile$ = "andinpos.dat" ELSE eqfile$ = "colinpos.dat"
```

```
'input equation constants ***************************************************
45  OPEN eqfile$ FOR INPUT AS #1
INPUT #1, watfl$, chlfl$
INPUT #1, glbcn, mssval, msscon, mssexp, ossval, osscon, ossexp
INPUT #1, chlrad, chldens, chlref, mssrad, mssdens, mssref, ossrad, ossdens, ossref
INPUT #1, cbrat, mbrat, obrat
INPUT #1, reftyp, mu0
INPUT #1, rupper, kupper
CLOSE #1

'***************************************************************************
' Mie scat for chl: calc number of partls in conc ***************************
' and m=1.05-0.001i **********************************************************
' mass calc in mg ************************************************************
49
  cmass = 4 / 3 * pi * (chlrad * .000001) ^ 3 * chldens * 1E+09
  mmass = 4 / 3 * pi * (mssrad * .000001) ^ 3 * mssdens * 1E+09
  omass = 4 / 3 * pi * (ossrad * .000001) ^ 3 * ossdens * 1E+09

'cnum:  mg/m3 / mg **********************************************************
'cnum is *1000 as phyto mass is pigment *1000 *******************************
'mnum: [g/m3*1000 = mg/m3] / mg *********************************************
  cnum = 40 / cmass
  mnum = 1000 / mmass
  onum = 1000 / omass

'***************************************************************************
55 OPEN watfl$ FOR INPUT AS #201
 OPEN chlfl$ FOR INPUT AS #202

 FOR h = 1 TO 2
  LINE INPUT #201, head$
  LINE INPUT #202, head2$
 NEXT h

95 FOR i = 1 TO nw
  INPUT #201, wvl(i), wabs(i), wsct(i)
  INPUT #202, wv, phab(i)

  croe = 4 * pi * (chlrad * .000001) / (wv * 1E-09) * chlref
  mroe = 4 * pi * (mssrad * .000001) / (wv * 1E-09) * mssref
  oroe = 4 * pi * (ossrad * .000001) / (wv * 1E-09) * ossref
  qsct(i) = 2 - (4 / croe * SIN(croe)) + (4 / croe ^ 2) * (1 - COS(croe))
  mqsct(i) = 2 - (4 / mroe * SIN(mroe)) + (4 / mroe ^ 2) * (1 - COS(mroe))
  oqsct(i) = 2 - (4 / oroe * SIN(oroe)) + (4 / oroe ^ 2) * (1 - COS(oroe))
```

```
 spbc(i) = pi / 4 * qsct(i) * cnum * ((chlrad * 2 * .000001) ^ 2)
 spbm(i) = pi / 4 * mqsct(i) * mnum * ((mssrad * 2 * .000001) ^ 2)
 spbo(i) = pi / 4 * oqsct(i) * onum * ((ossrad * 2 * .000001) ^ 2)

NEXT i

CLOSE #201: CLOSE #202

'menu screen**********************************************************************
60 VIEW: WINDOW
CLS
LINE (30, 20)-(600, 350), 15, B
LINE (32, 22)-(598, 348), 15, B

posprn 18, 7, "Choose method to control concentration values"
posprn 12, 10, " 1 - Alter values by increase/decrease keys and watch change "
posprn 12, 12, " 2 - Input exact values for each constituent "
posprn 12, 14, " 3 - Read all concentrations from a file "

posprn 25, 17, "[Press F1 to QUIT at any time]"
posprn 32, 18, "[F2 to RESTART]"

DO: menan$ = INKEY$
LOOP UNTIL menan$ = "1" OR menan$ = "2" OR menan$ = "3"

IF menan$ = "1" GOTO 250
IF menan$ = "2" GOTO 350
IF menan$ = "3" GOTO 450

' calculate reflectance ***************************************************
' option 1: increase/decrease concentrations ***********************************
250 VIEW: WINDOW
CLS
LINE (20, 10)-(580, 85), 15, B
LINE (20, 87)-(580, 87), 15
cch$ = "S"
posprn 6, 1, " Constituent concentrations "
posprn 15, 3, " MSS, mg/l    OSS, mg/l    Chl, mg/m3    g440, /m "

conprn mss, oss, chl, glb
posprn 4, 2, " To change, press M for MSS, O for OSS, C for Chl and G for Gelbstoff"
posprn 5, 5, " +/- increase/decrease   TAB,/  multiply, divide increment by 10"
posprn 5, 6, " ESC to stop "
posprn 21, 6, " R to return to menu "
posprn 45, 6, " Z to set all conc to zero "

xpt = 24: ypt = 4: value = mss
IF cch$ = "S" THEN GOTO 275

270
DO: sign$ = INKEY$
 IF sign$ = CHR$(43) OR sign$ = CHR$(45) GOTO 516
 incch$ = UCASE$(sign$)
 IF incch$ = "R" GOTO 60
 IF incch$ = "M" THEN cch$ = "M"
 IF incch$ = "O" THEN cch$ = "O"
 IF incch$ = "C" THEN cch$ = "C"
 IF incch$ = "G" THEN cch$ = "G"
 IF incch$ = "Z" THEN cch$ = "Z"
```

```
LOOP UNTIL incch$ = "M" OR incch$ = "O" OR incch$ = "C" OR incch$ = "G" OR incch$
= "Z"

IF cch$ = "M" THEN xpt = 18: ypt = 4: inc = .5: value = mss
IF cch$ = "O" THEN xpt = 31: ypt = 4: inc = .5: value = oss
IF cch$ = "C" THEN xpt = 45: ypt = 4: inc = .5: value = chl
IF cch$ = "G" THEN xpt = 58: ypt = 4: inc = .05: value = glb
IF cch$ = "Z" THEN
  mss = 0: oss = 0: chl = 0: glb = 0
  conprn mss, oss, chl, glb
  cch$ = "S"
  GOTO 275
END IF

505 DO: posprn xpt, ypt, STR$(value)
  sign$ = INKEY$
LOOP UNTIL sign$ = CHR$(43) OR sign$ = CHR$(45) OR sign$ = CHR$(27) OR sign$ =
CHR$(9) OR sign$ = CHR$(47)
IF sign$ = CHR$(9) THEN
  inc = inc * 10
  GOTO 505
END IF
IF sign$ = CHR$(47) THEN
  inc = inc / 10
  GOTO 505
END IF

IF sign$ = CHR$(27) GOTO 500

515 DO
  sign2$ = INKEY$
  IF sign2$ = CHR$(27) OR sign2$ = CHR$(9) OR sign2$ = CHR$(47) OR sign2$ =
CHR$(43) OR sign2$ = CHR$(45) GOTO 520

516  IF sign$ = CHR$(43) THEN
    value = value + inc
  END IF
  IF sign$ = CHR$(45) THEN
    value = value - inc
  END IF
 IF value < 0 THEN value = 0
  posprn xpt, ypt, STR$(value) + "      "

 IF cch$ = "M" THEN mss = value
 IF cch$ = "O" THEN oss = value
 IF cch$ = "C" THEN chl = value
 IF cch$ = "G" THEN glb = value

275                    'calculation of a, b, K and R **************
 FOR i = 1 TO nw
  optprop i, chl, glb, mss, oss, wvl(), wabs(), wsct(), phab(), spbc(), spbm(), spbo(), glbcn,
mssval, msscon, mssexp, ossval, osscon, ossexp, chlrad, cmass, mmass, mssrad, mssdens,
omass, ossrad, ossdens, cbrat, mbrat, obrat, mu0, a(), b(), att(), _
Kd(), Ref(), reftyp, parktot, parrtot
 NEXT i
 park = parktot / paren: parktot = 0
 parr = parrtot / paren: parrtot = 0

 grplt nw, wvl(), Ref(), Kd(), rupper, kupper, park, parr

 SLEEP 1
```

```
 IF cch$ = "S" THEN GOTO 270

510 LOOP

500
GOTO 270

350             ' option 2: input exact concentrations **********************
' whether to print to a file ***************************************************
pntfilx out$

' input conc values from keyboard **********************************************
VIEW: WINDOW
CLS
LINE (20, 10)-(580, 85), 15, B
LINE (20, 87)-(580, 87), 15
cch$ = "I"

posprn 6, 1, " Constituent concentrations "
posprn 15, 3, " MSS, mg/l    OSS, mg/l    Chl, mg/m3    g440, /m "

LOCATE 4, 18: INPUT mss
LOCATE 4, 31: INPUT oss
LOCATE 4, 45: INPUT chl
LOCATE 4, 58: INPUT glb

posprn 4, 5, " To change, press M for MSS, O for OSS, C for Chl and G for Gelbstoff"
posprn 20, 6, " R to return to menu, P to print to file "

370  FOR i = 1 TO nw
   optprop i, chl, glb, mss, oss, wvl(), wabs(), wsct(), phab(), spbc(), spbm(), spbo(), glbcn,
mssval, msscon, mssexp, ossval, osscon, ossexp, chlrad, cmass, mmass, mssrad, mssdens,
omass, ossrad, ossdens, cbrat, mbrat, obrat, mu0, a(), b(), att() _
, Kd(), Ref(), reftyp, parktot, parrtot
  NEXT i
  park = parktot / paren: parktot = 0
  parr = parrtot / paren: parrtot = 0

posprn 9, 7, "                                                    "
grplt nw, wvl(), Ref(), Kd(), rupper, kupper, park, parr

375 DO: cch$ = UCASE$(INKEY$)
LOOP UNTIL cch$ = "M" OR cch$ = "O" OR cch$ = "C" OR cch$ = "G" OR cch$ = "R" OR
cch$ = "P"

IF cch$ = "P" THEN
  posprn 9, 7, "                                                      "
  COLOR 12: LOCATE 7, 10: INPUT "Filename: ", fileout$: COLOR 15
  filopen fileout$
  pntoutn nw, mss, oss, chl, glb, wvl(), a(), b(), att(), Kd(), Ref(), park, parr
  posprn 30, 7, ".............................completed"
  CLOSE #31: CLOSE #32: CLOSE #33: CLOSE #34: CLOSE #35
  GOTO 375
END IF
```

```
IF cch$ = "M" THEN
  posprn 18, 4, "      "
  LOCATE 4, 18: INPUT mss
ELSEIF cch$ = "O" THEN
  posprn 31, 4, "      "
  LOCATE 4, 31: INPUT oss
ELSEIF cch$ = "C" THEN
  posprn 45, 4, "      "
  LOCATE 4, 45: INPUT chl
ELSEIF cch$ = "G" THEN
  posprn 58, 4, "      "
  LOCATE 4, 58: INPUT glb
ELSEIF cch$ = "R" THEN GOTO 60
END IF
GOTO 370

'option 3: input values from a file ***************************************
450 VIEW: WINDOW
CLS
LINE (30, 20)-(600, 350), 15, B
LINE (32, 22)-(598, 348), 15, B

posprn 35, 5, " INPUT FILE "
posprn 7, 8, " The ASCII file should have one header line for general comments, "
posprn 11, 9, " followed by the number of sites/samples on the next line. "
posprn 9, 11, " The successive lines should each represent one site/sample"
posprn 32, 12, " in the form  "
posprn 24, 13, " mss     oss     chl     glb "
posprn 23, 14, " with spaces between each value "

LOCATE 16, 28: INPUT " Input file: ", infile$

455 OPEN infile$ FOR INPUT AS #31
LINE INPUT #31, head$
INPUT #31, nst

posprncl 23, 18, " Output values to a file (Y/N): ", 11

DO: out$ = UCASE$(INKEY$)
LOOP UNTIL out$ = "Y" OR out$ = "N"

posprn 20, 18, "                              "

IF out$ = "Y" THEN
 printfil

 DO: outpt$ = UCASE$(INKEY$)
 LOOP UNTIL outpt$ = "T" OR outpt$ = "A"
END IF

458
posprn 28, 18, " Number of stations: " + STR$(nst)

posprncl 18, 20, " Move through automatically or manually (A/M): ", 11
DO: page$ = UCASE$(INKEY$)
LOOP UNTIL page$ = "A" OR page$ = "M"

LINE (30, 390)-(600, 410), 15, B
posprn 6, 25, " Press ESC to continue "
```

```
DO: LOOP UNTIL INKEY$ = CHR$(27)

IF out$ = "Y" THEN filetitl head$, outpt$

CLS
LINE (20, 10)-(580, 85), 15, B
LINE (20, 87)-(580, 87), 15

posprn 6, 1, " Constituent concentrations "
posprn 17, 3, " MSS, mg/l    OSS, mg/l     Chl, mg/m3    g440, /m "
IF page$ = "M" THEN posprn 27, 5, " Press ESC to continue "
posprn 25, 6, " R to return to input menu "
posprn 4, 2, " Input file: " + infile$
posprn 60, 2, " total: " + STR$(nst)
posprn 35, 2, "row of data: "

460 FOR s = 1 TO nst
  INPUT #31, mss, oss, chl, glb
  IF mss < 0 THEN mss = 0
  conprn mss, oss, chl, glb
  posprn 47, 2, STR$(s) + "   "

  FOR i = 1 TO nw
   optprop i, chl, glb, mss, oss, wvl(), wabs(), wsct(), phab(), spbc(), spbm(), spbo(), glbcn,
mssval, msscon, mssexp, ossval, osscon, ossexp, chlrad, cmass, mmass, mssrad, mssdens,
omass, ossrad, ossdens, cbrat, mbrat, obrat, mu0, a(), b(), att() _
, Kd(), Ref(), reftyp, parktot, parrtot
  NEXT i

  park = parktot / paren: parktot = 0
  parr = parrtot / paren: parrtot = 0

  grplt nw, wvl(), Ref(), Kd(), rupper, kupper, park, parr

  IF out$ = "Y" AND outpt$ = "T" THEN printout nw, mss, oss, chl, glb, wvl(), a(), b(), att(),
Kd(), Ref(), park, parr
  IF out$ = "Y" AND outpt$ = "A" THEN printall nw, mss, oss, chl, glb, wvl(), a(), b(), att(),
Kd(), Ref(), park, parr

  IF page$ = "M" THEN
    DO: cont$ = UCASE$(INKEY$)
    LOOP UNTIL cont$ = CHR$(27) OR cont$ = "R"
    IF cont$ = "R" THEN GOTO 470
  END IF
  IF page$ = "A" THEN IF UCASE$(INKEY$) = "R" THEN GOTO 470
NEXT s

IF page$ = "A" THEN DO: LOOP UNTIL UCASE$(INKEY$) = "R"
470 CLOSE #31: CLOSE #101: CLOSE #102: CLOSE #103: CLOSE #104: CLOSE #105
GOTO 60
```

```
'*************************************************************************
520  SELECT CASE sign2$
CASE IS = CHR$(27)
GOTO 500
CASE IS = CHR$(9)
inc = inc * 10
GOTO 510
CASE IS = CHR$(47)
inc = inc / 10
GOTO 510
CASE IS = CHR$(43)
sign$ = CHR$(43)
GOTO 510
CASE IS = CHR$(45)
sign$ = CHR$(45)
GOTO 510

END SELECT

555          'identify and print type of error ***************************
VIEW: WINDOW
posprn 38, 27, " ************************************ "
posprn 45, 28, " Error: " + STR$(ERR) + " on line " + STR$(ERL) + "   "

SELECT CASE ERR
CASE IS = 53
LOCATE 18, 15: INPUT " File not found, please try again:  ", infile$
posprn 15, 18, "                                          "
RESUME 455
END SELECT
STOP
'*************************************************************************

200 VIEW: WINDOW
CLS
LINE (60, 140)-(540, 194), 15, B
LINE (58, 138)-(542, 196), 15, B

posprn 30, 11, " THAT'S ALL FOLKS!! "
END

SUB axes (x0, xh, y0, yh)
' plot axes of graphs ***************************************************

xint = (xh - x0) / 6: ylen = xint / 5
yint = (yh - y0) / 5: xlen = yint / 20

FOR xln = x0 TO xh STEP xint
  LINE (xln, y0 + xlen)-(xln, y0)
NEXT xln

FOR yln = y0 TO yh STEP yint
  LINE (x0, yln)-(x0 - ylen, yln)
NEXT yln


END SUB
```

```
SUB bksct (b(), bw, wvl(), bksc(), bchl, bmss, boss, i)

'calculate backscatter coeff ***************************************************

bconst = .019
bcons = bconst

'Gordon et al, 1988 to allow for wavelength dependency below 0.1 mg/m3
'IF chl < .1 THEN
  'bcons = (560 / wvl(i)) * .019
'END IF

' chl bkscatter Morel&Bricaud 1981 ***********************************************
bbchl = bchl * .002
bbmss = bmss * .019
bboss = boss * .01

bksc(i) = bbchl + bbmss + bboss + bw * .5


END SUB

SUB conprn (mss, oss, chl, glb)

'print values of concentrations *************************************************

posprn 18, 4, STR$(mss) + "    "
posprn 31, 4, STR$(oss) + "    "
posprn 45, 4, STR$(chl) + "    "
posprn 58, 4, STR$(glb) + "        "

END SUB

SUB filetitl (head$, outpt$)

' print title in output files ***************************************************

  PRINT #101, " ABS "; head$
  PRINT #102, " SCT "; head$
  PRINT #103, " ATT "; head$
  PRINT #104, " REF "; head$

IF outpt$ = "T" THEN
  PRINT #101, "  mss   oss   chl   glb     410   440   490   510   520   550   570
600   670   700 "
  PRINT #102, "  mss   oss   chl   glb     410   440   490   510   520   550   570
600   670   700 "
  PRINT #103, "  mss   oss   chl   glb     410   440   490   510   520   550   570
600   670   700   PAR "
  PRINT #104, "  mss   oss   chl   glb     410   440   490   510   520   550   570
600   670   700   PAR "
ELSE
  PRINT #101, _
"  mss   oss   chl   glb    400   410   420   430   440   450   460   470   480   490
500   510   520   530   540   550   560   570   580   590   600   610   620   630
640   650   660   670   680   690   700 "
  PRINT #102, _
"  mss   oss   chl   glb    400   410   420   430   440   450   460   470   480   490
500   510   520   530   540   550   560   570   580   590   600   610   620   630
640   650   660   670   680   690   700 "
```

```
 PRINT #103, _
" mss   oss   chl   glb    400   410   420   430   440   450   460   470   480   490
500   510   520   530   540   550   560   570   580   590   600   610   620   630
640   650   660   670   680   690   700   PAR " _

 PRINT #104, _
" mss   oss   chl   glb    400   410   420   430   440   450   460   470   480   490
500   510   520   530   540   550   560   570   580   590   600   610   620   630
640   650   660   670   680   690   700   PAR " _

END IF

END SUB

SUB filopen (fileout$)
' open files for option 2 ***********************************************

31  OPEN fileout$ + ".abs" FOR OUTPUT AS #31
32  OPEN fileout$ + ".sct" FOR OUTPUT AS #32
33  OPEN fileout$ + ".att" FOR OUTPUT AS #33
34  OPEN fileout$ + ".ref" FOR OUTPUT AS #34
35  OPEN fileout$ + ".bma" FOR OUTPUT AS #35

END SUB

SUB grplt (nw, wvl(), Ref(), Kd(), rupper, kupper, park, parr)
'plot graphs of attenuation and reflectance ***********************************
form$ = "& ##.##"

posprn 55, 8, " REFLECTANCE "
posprn 47, 18, " DIFFUSE ATTENUATION "

VIEW (75, 127)-(525, 267), , 15
WINDOW (400, rupper)-(700, 0)
CLS 1
axes 400, 700, 0, rupper
label 400, 700, 0, rupper, 5, 18
LOCATE 10, 50: PRINT ; USING form$; "PAR R = "; parr

FOR i = 1 TO nw
 IF wvl(i) > 400 THEN
   LINE (wvl(i), Ref(i))-(wvl(i - 1), Ref(i - 1)), 15
 END IF
NEXT i

VIEW: WINDOW

280
 VIEW (75, 289)-(525, 429), , 15
 WINDOW (400, kupper)-(700, 0)
 CLS 1
 axes 400, 700, 0, kupper
 label 400, 700, 0, kupper, 5, 28

 LOCATE 20, 50: PRINT ; USING form$; "PAR K = "; park
 FOR i = 1 TO nw
  IF wvl(i) > 400 THEN
    LINE (wvl(i), Kd(i))-(wvl(i - 1), Kd(i - 1)), 15
  END IF
 NEXT i
END SUB
```

```
SUB inposprn (xpt, ypt, txt$, num)
' input values, showing defaults ***********************************************

whltxt$ = txt$ + STR$(num) + "): "

LOCATE ypt, xpt
PRINT whltxt$;
INPUT inp$

IF inp$ = "" THEN
  num = num
ELSE
  num = VAL(inp$)
END IF

END SUB

SUB inpostxt (xpt, ypt, file$)
' input text, showing defaults ***********************************************

whltxt$ = "(" + file$ + "): "

LOCATE ypt, xpt
PRINT whltxt$;
INPUT inp$

IF inp$ = "" THEN
  file$ = file$
ELSE
  file$ = inp$
END IF

END SUB

SUB label (x0, xh, y0, yh, yln, xln)
'label graph axes ***********************************************************

IF xln = 18 GOTO 600
posprn yln + 2, xln, STR$(x0)
posprn yln + 60, xln, STR$(xh)
600
posprn yln, xln - 9, STR$(yh)
posprn yln, xln - 1, STR$(y0)

END SUB

SUB modinp

' input default values from file *********************************************
OPEN "andinpos.dat" FOR INPUT AS #1
INPUT #1, watfl$
INPUT #1, chlfl$
INPUT #1, glbcn, mssval, msscon, mssexp, ossval, osscon, ossexp
INPUT #1, chlrad, chldens, chlref, mssrad, mssdens, mssref, ossrad, ossdens, ossref
INPUT #1, cbrat, mbrat, obrat
INPUT #1, reftyp, mu0
INPUT #1, rupper, kupper
CLOSE #1
```

```
LINE (15, 20)-(360, 425), 15, B

posprn 65, 3, "1 out of 3"
posprn 4, 4, "ABSORPTION"
posprn 5, 6, "Input files at 10 nm intervals 400-700nm"
posprn 6, 8, "water has 2 header lines,"
posprn 7, 9, "then wvl, abs and scat on each line"
posprn 6, 11, "chlorophyll file has 2 header lines,"
posprn 7, 12, "then wvl and specific abs on each line"

posprn 5, 14, "Gelbstoff equation"
posprn 6, 15, "a = g440 exp(m * (wvl-440))"
posprn 5, 18, "Mineral suspended solids"
posprn 6, 19, "a = l*MSS + p*MSS*exp(n * (wvl-440))"
posprn 5, 22, "Other suspended solids"
posprn 6, 23, "a = j*OSS + k*OSS*exp(h * (wvl-440))"

LINE (380, 20)-(620, 425), 15, B
posprn 50, 5, "Default values in brackets"
posprn 51, 6, "Press RETURN if correct"

50
posprn 50, 8, "water file"
inpostxt 51, 9, watfl$
posprn 50, 11, "chlorophyll file"
inpostxt 51, 12, chlfl$

inposprn 55, 15, " m (", glbcn
inposprn 55, 18, " l (", mssval
inposprn 55, 19, " p (", msscon
inposprn 55, 20, " n (", mssexp
inposprn 55, 22, " j (", ossval
inposprn 55, 23, " l (", osscon
inposprn 55, 24, " h (", ossexp

LINE (15, 440)-(620, 460), 15, B

posprncl 6, 28, " Are all values correct?  (Y/N) ", 11

DO: ans$ = UCASE$(INKEY$)
LOOP UNTIL ans$ = "Y" OR ans$ = "N"
IF ans$ = "N" GOTO 50

'*****************************************************************************
CLS
LINE (15, 20)-(360, 425), 15, B

posprn 4, 4, "SCATTERING"
posprn 5, 8, "Chlorophyll based on Mie: ref index cm"
posprn 6, 9, "radius x "
posprn 6, 10, "density y (1.03-1.10 g/cm3)"
posprn 5, 11, "backscattering ratio bbc "
posprn 5, 14, "Mineral suspended solids: ref index mm"
posprn 6, 15, "radius w "
posprn 6, 16, "density z"
posprn 5, 17, "backscattering ratio bbm "
posprn 5, 20, "Other suspended solids: ref index om"
posprn 6, 21, "radius v "
posprn 6, 22, "density u"
posprn 5, 23, "backscattering ratio bbo "
```

```
LINE (380, 20)-(620, 425), 15, B
posprn 50, 5, "Default values in brackets"
posprn 51, 6, "Press RETURN if correct"
posprn 65, 3, "2 out of 3"

70 inposprn 55, 8, " cm (", chlref
inposprn 55, 9, " x (", chlrad
inposprn 55, 10, " y (", chldens
inposprn 55, 11, " bbc (", cbrat
inposprn 55, 14, " mm (", mssref
inposprn 55, 15, " w (", mssrad
inposprn 55, 16, " z (", mssdens
inposprn 55, 17, " bbm (", mbrat
inposprn 55, 20, " om (", ossref
inposprn 55, 21, " v (", ossrad
inposprn 55, 22, " u (", ossdens
inposprn 55, 23, " bbo (", obrat

LINE (15, 440)-(620, 460), 15, B

posprncl 6, 28, " Are all values correct?  (Y/N) ", 11

DO: ans$ = UCASE$(INKEY$)
LOOP UNTIL ans$ = "Y" OR ans$ = "N"
IF ans$ = "N" GOTO 70

'
**********************************************************************************
***
CLS
LINE (15, 20)-(620, 400), 15, B

posprn 65, 3, "3 out of 3"

posprn 8, 4, "Calculation of Kd and R using Kirk's algorithms:"
posprn 11, 6, "DIFFUSE ATTENUATION"
posprn 12, 7, " Kd = (a/mu0) * (1 + 0.256*b/a)^0.5 "

posprn 11, 10, "REFLECTANCE"
posprn 12, 11, " 1.     R = 0.33 * bb/a "
posprn 12, 12, " 2.     R = (0.975 - 0.629 mu0) * bb/a "
80 inposprn 11, 13, "Reflectance equation (", reftyp

inposprn 21, 16, "mu0 (", mu0
posprn 12, 19, "Upper values for y-axes on graphs (lower is zero) "
inposprn 23, 20, " R (", rupper
inposprn 23, 21, " K (", kupper

LINE (15, 440)-(620, 460), 15, B

posprncl 6, 28, " Are all values correct?  (Y/N) ", 11

DO: ans$ = UCASE$(INKEY$)
LOOP UNTIL ans$ = "Y" OR ans$ = "N"
IF ans$ = "N" GOTO 80
```

```
OPEN "colinpos.dat" FOR OUTPUT AS #11
PRINT #11, watfl$
PRINT #11, chlfl$
PRINT #11, glbcn
PRINT #11, mssval
PRINT #11, msscon
PRINT #11, mssexp
PRINT #11, ossval
PRINT #11, osscon
PRINT #11, ossexp
PRINT #11, chlrad
PRINT #11, chldens
PRINT #11, chlref
PRINT #11, mssrad
PRINT #11, mssdens
PRINT #11, mssref
PRINT #11, ossrad
PRINT #11, ossdens
PRINT #11, ossref
PRINT #11, cbrat
PRINT #11, mbrat
PRINT #11, obrat
PRINT #11, reftyp
PRINT #11, mu0
PRINT #11, rupper
PRINT #11, kupper
CLOSE #11

END SUB

SUB optprop (i, chl, glb, mss, oss, wvl(), wabs(), wsct(), phab(), spbc(), spbm(), spbo(), glbcn,
mssval, msscon, mssexp, ossval, osscon, ossexp, chlrad, cmass, mmass, mssrad, mssdens,
omass, ossrad, ossdens, cbrat, mbrat, obrat, mu0, a(), b(), _
att(), Kd(), Ref(), reftyp, parktot, parrtot)
' calculate absorption, scattering, attenuation and reflectance ************

  achl = phab(i) * chl
  aglb = glb * EXP(glbcn * (wvl(i) - 440))
  amss = mssval * mss + msscon * mss * EXP(mssexp * (wvl(i) - 440))
  omss = ossval * oss + osscon * oss * EXP(ossexp * (wvl(i) - 440))
  a(i) = achl + aglb + amss + wabs(i)

  bchl = spbc(i) * chl
  bmss = spbm(i) * mss
  boss = spbo(i) * oss

'  IF wvl(i) > 600 THEN bmss = bmss * (600 / wvl(i)) ^ 2
  b(i) = bmss + bchl + boss
  bw = wsct(i)

'calculate attenuation
  att(i) = b(i) + a(i)

'calculate backscatter
  bksct b(), bw, wvl(), bksc(), bchl, bmss, boss, i

'reflectance coeffs [*100 to convert to percentages]:

  IF reftyp = 2 THEN Ref(i) = ((.975 - .629 * mu0) * bksc(i) / a(i)) * 100
  IF reftyp = 1 THEN Ref(i) = .33 * bksc(i) / a(i) * 100
```

```
  Kd(i) = (1 / mu0) * (1 + (.425 * mu0 - .19) * b(i) / a(i)) ^ .5 * a(i)
  IF wvl(i) < 701 AND wvl(i) > 399 THEN
    parktot = parktot + Kd(i) * 1 / wvl(i)
    parrtot = parrtot + Ref(i) * 1 / wvl(i)
  END IF

END SUB

SUB pntfilx (out$)
'option to print to file, and details, for option 3 ************************

VIEW: WINDOW
CLS
LINE (20, 20)-(580, 125), 15, B
LINE (20, 127)-(580, 127), 15

filn = 1
posprncl 7, 3, "Print to file (Y/N) ", 11

DO: out$ = UCASE$(INKEY$)
LOOP UNTIL out$ = "Y" OR out$ = "N"

IF out$ = "N" THEN GOTO 320

posprn 11, 5, " Type P when you wish to print the values to a file "
posprn 8, 6, " There will be a prompt to enter the stem of the filename "
posprn 6, 7, " The extensions .abs, .sct, .bma, .att and .ref will be added "


LINE (30, 390)-(600, 410), 15, B
posprn 6, 25, " Press ESC to continue "

DO: LOOP UNTIL INKEY$ = CHR$(27)

320 END SUB

SUB pntoutn (nw, mss, oss, chl, glb, wvl(), a(), b(), att(), Kd(), Ref(), park, parr)
' print option 2 files at 10 nm intervals ************************************

formd$ = " ###   ###.## "

PRINT #31, " MSS = "; mss, " OSS = "; oss, " Chl = "; chl, " g440 = "; glb
PRINT #32, " MSS = "; mss, " OSS = "; oss, " Chl = "; chl, " g440 = "; glb
PRINT #33, " MSS = "; mss, " OSS = "; oss, " Chl = "; chl, " g440 = "; glb
PRINT #34, " MSS = "; mss, " OSS = "; oss, " Chl = "; chl, " g440 = "; glb
PRINT #35, " MSS = "; mss, " OSS = "; oss, " Chl = "; chl, " g440 = "; glb

PRINT #33, " PAR K = "; USING formd$; park
PRINT #34, " PAR R = "; USING formd$; parr

FOR i = 1 TO nw
  PRINT #31, USING formd$; wvl(i); a(i)
  PRINT #32, USING formd$; wvl(i); b(i)
  PRINT #33, USING formd$; wvl(i); Kd(i)
  PRINT #34, USING formd$; wvl(i); Ref(i)
  PRINT #35, USING formd$; wvl(i); att(i)
NEXT i

END SUB
```

```
SUB posprn (xpt, ypt, txt$)
' print text ************************************************************

LOCATE ypt, xpt
PRINT txt$

END SUB

SUB posprncl (xpt, ypt, txt$, c)
' print coloured text ***************************************************

COLOR c
LOCATE ypt, xpt
PRINT txt$
COLOR 15

END SUB

SUB printall (nw, mss, oss, chl, glb, wvl(), a(), b(), att(), Kd(), Ref(), park, parr)
' print option 3 files at 10 nm intervals ********************************

formc$ = " ###.## ##.## ##.## "
forms$ = " ##.## "

PRINT #101, USING formc$; mss; oss; chl; glb;
PRINT #102, USING formc$; mss; oss; chl; glb;
PRINT #103, USING formc$; mss; oss; chl; glb;
PRINT #104, USING formc$; mss; oss; chl; glb;
PRINT #105, USING formc$; mss; oss; chl; glb;

FOR i = 1 TO nw
 PRINT #101, USING forms$; a(i);
 PRINT #102, USING forms$; b(i);
 PRINT #103, USING forms$; Kd(i);
 PRINT #104, USING forms$; Ref(i);
 PRINT #105, USING forms$; att(i);
NEXT i

PRINT #101, : PRINT #102, : PRINT #103, park: PRINT #104, parr: PRINT #105,
END SUB

SUB printfil
' information about option 3 files *************************************
CLS 2

LINE (30, 20)-(600, 350), 15, B
LINE (32, 22)-(598, 348), 15, B

posprn 15, 7, " Four files will be made with the trunk: colout "
posprn 17, 8, " and the extensions: .abs, .sct, .att, .ref "
posprn 23, 10, " The concentrations will be printed "
posprn 14, 11, " and then the optical properties at 10 wavelengths (T): "
posprn 15, 13, " 410  440  490  510  520  550  570  600  670  700 "
posprn 23, 15, " or at 10 nm intervals (A)"
posprncl 55, 15, "T or A: ", 11

OPEN "colout.abs" FOR OUTPUT AS #101
OPEN "colout.sct" FOR OUTPUT AS #102
OPEN "colout.att" FOR OUTPUT AS #103
OPEN "colout.ref" FOR OUTPUT AS #104
OPEN "colout.bma" FOR OUTPUT AS #105
```

```
END SUB

SUB printout (nw, mss, oss, chl, glb, wvl(), a(), b(), att(), Kd(), Ref(), park, parr)
'print option 3 files at 10 wavelengths **********************************

formc$ = " ###.## ##.## ##.## "
forms$ = " ###.## "

PRINT #101, USING formc$; mss; oss; chl; glb;
PRINT #102, USING formc$; mss; oss; chl; glb;
PRINT #103, USING formc$; mss; oss; chl; glb;
PRINT #104, USING formc$; mss; oss; chl; glb;
PRINT #105, USING formc$; mss; oss; chl; glb;

FOR i = 1 TO nw
IF wvl(i) = 410 THEN
  PRINT #101, USING forms$; a(i);
  PRINT #102, USING forms$; b(i);
  PRINT #103, USING forms$; Kd(i);
  PRINT #104, USING forms$; Ref(i);
  PRINT #105, USING forms$; att(i);
END IF

IF wvl(i) = 440 THEN
  PRINT #101, USING forms$; a(i);
  PRINT #102, USING forms$; b(i);
  PRINT #103, USING forms$; Kd(i);
  PRINT #104, USING forms$; Ref(i);
  PRINT #105, USING forms$; att(i);
END IF

IF wvl(i) = 490 THEN
  PRINT #101, USING forms$; a(i);
  PRINT #102, USING forms$; b(i);
  PRINT #103, USING forms$; Kd(i);
  PRINT #104, USING forms$; Ref(i);
  PRINT #105, USING forms$; att(i);
END IF

IF wvl(i) = 510 THEN
  PRINT #101, USING forms$; a(i);
  PRINT #102, USING forms$; b(i);
  PRINT #103, USING forms$; Kd(i);
  PRINT #104, USING forms$; Ref(i);
  PRINT #105, USING forms$; att(i);
END IF

IF wvl(i) = 520 THEN
  PRINT #101, USING forms$; a(i);
  PRINT #102, USING forms$; b(i);
  PRINT #103, USING forms$; Kd(i);
  PRINT #104, USING forms$; Ref(i);
  PRINT #105, USING forms$; att(i);
END IF

IF wvl(i) = 550 THEN
  PRINT #101, USING forms$; a(i);
  PRINT #102, USING forms$; b(i);
  PRINT #103, USING forms$; Kd(i);
```

```
  PRINT #104, USING forms$; Ref(i);
  PRINT #105, USING forms$; att(i);
END IF

IF wvl(i) = 570 THEN
  PRINT #101, USING forms$; a(i);
  PRINT #102, USING forms$; b(i);
  PRINT #103, USING forms$; Kd(i);
  PRINT #104, USING forms$; Ref(i);
  PRINT #105, USING forms$; att(i);
END IF

IF wvl(i) = 600 THEN
  PRINT #101, USING forms$; a(i);
  PRINT #102, USING forms$; b(i);
  PRINT #103, USING forms$; Kd(i);
  PRINT #104, USING forms$; Ref(i);
  PRINT #105, USING forms$; att(i);
END IF

IF wvl(i) = 670 THEN
  PRINT #101, USING forms$; a(i);
  PRINT #102, USING forms$; b(i);
  PRINT #103, USING forms$; Kd(i);
  PRINT #104, USING forms$; Ref(i);
  PRINT #105, USING forms$; att(i);
END IF

IF wvl(i) = 700 THEN
  PRINT #101, USING forms$; a(i)
  PRINT #102, USING forms$; b(i)
  PRINT #103, USING forms$; Kd(i);
  PRINT #104, USING forms$; Ref(i);
  PRINT #105, USING forms$; att(i)
END IF
NEXT i

PRINT #103, USING forms$; park
PRINT #104, USING forms$; parr

END SUB
```

APPENDIX XI

Symbol Explanation

SYMBOLS

a	absorption coefficient
a_c,a_p	absorption due to chlorophyll and particles respectively
a_d,a_m	absorption due to detritus and minerals respectively
a_w,a_y	absorption due to pure water and yellow substance respectivel
a^*	specific absorption
A_c	constant of absorption due to chlorophyll
b	scattering coefficient
b_b	backscatter coefficient
b_b	backscatter ratio
b_c,b_w	scatter due to chlorophyll and pure water respectively
B_c	constant of scatter due to chlorophyll
c	beam attenuation coefficient
C	≡ chl chlorophyll concentration mgm^{-3}
D	diameter of particles
E	irradiance
E_d,E_u	downward and upward irradiance
E_0	scalar irradiance
F(d)	particle size distribution function
g(z)	attenuation weighting factor
g_{440}	≡ A_y (440) absorption of yellow substance at 440 nm
I	radiant intensity
I_T	total scattered radiation
K	beam attenuation coefficient
K_d	diffuse attenuation coefficient
K_E	vertical attenuation for net downward irradiance E_d - E_u
K_f	efficiency factor or effective area coefficient
L	radiance
L^*	path function
L_r,L_u	apparent and upward radiance
L_0	scalar radiance
m	complex refractive index
n	refractive index for purely scattering particles
N	number of particles per unit volume
Q_c	efficiency factor for attenuation due to chlorophyll
r	distance between radiance source and receiving point (m)
R	reflectance (%)
SM	suspended minerals (gm^{-3})
V	volume (m^{-3})
z	depth (m)
z_u	mid-point of euphotic zone
z_q(1%)	depth at which 99% of irradiance has been attenuated
z_{90}	depth at which 90% of irradiance has been attenuated
β	pathlength amplification factor
β_v	volume scattering function
λ	wavelength (nm)
μ	average cosine
θ, Φ	zenith and azimuthal angles
∑	total suspended solids concentration mgl^{-1}
ξ	ratio expression
ω	solid angle
ω_0	scattering albedo

ACRONYMS

AMB95	August Menai Bridge 1995 (Pier Survey)
CS	Colour Sensor (UCW)
CZCS	Coastal Zone Colour Scanner
IRM1	Irradiance Meter (UCW)
JMB94	July Menai Bridge 1994 (Pier Survey)
MSS	Mineral Suspended Solids
PAR	Photosynthetically Active Radiation
TSS	Total Suspended Solids
UCW	University of Wales
YS	Yellow Substance